THE LUBRICATION OF NORMAL HUMAN ANKLE JOINTS

by

JOHN B. MEDLEY

A thesis submitted in fulfilment of the
requirements for the degree of
Doctor of Philosophy

Department of Mechanical Engineering
The University of Leeds
Leeds
England

November 1981

VOLUME CONTAINS CLEAR OVERLAYS

OVERLAYS SCANNED SEPERATELY AND OVER THE RELEVANT PAGE.

ABSTRACT

The geometry, friction and lubrication of normal human ankle joints have been investigated. The joints exhibited converging-diverging surfaces in the direction of motion. The cylindrical form of the measured surface contours indicated that a reduced radius of about 0.35 m gave a good representation of the ankle joint geometry.

Human ankle joint specimens were tested in a joint simulator. Although considerable difficulties were encountered in the measurement of the very small coefficient of friction between the cartilage surfaces, an upper limit of about 0.01 was identified for this important tribological feature of synovial joints.

An equivalent bearing to represent the ankle joint was proposed which consisted of a rigid cylinder covered with a compliant layer sliding on a rigid plane. The dimensions for this geometry were based on the measurements of the present study. Theoretical models were developed to estimate the cyclic variation in elastohydrodynamic film thickness and coefficient of friction for the ankle during walking.

Theoretical minimum film thicknesses of about 1 μm were estimated along with coefficients of friction up to 0.001. The theoretical predictions of the cyclic variation of film thickness remained small compared with the magnitude of the film thickness itself. Furthermore, the theoretical film thicknesses were smaller than the measured Ra roughnesses for cartilage which appear in the literature. When a very considerable increase in the bulk viscosity of the lubricant was introduced into the calculations

film thicknesses of about 18 μm and coefficients of friction up to 0.01 were estimated. This value for film thickness was sufficient to separate the surface asperities of healthy articular cartilage.

Unless thin film mechanisms, such as an increased lubricant viscosity or micro-elastohydrodynamic lubrication act, the present study indicated that full fluid film lubrication cannot be sustained. However, the predicted film thicknesses were not much smaller than the surface roughness of cartilage and the ability to generate and preserve fluid films was found to be greatly enhanced by the entraining and squeeze film action. Thus, the modes of lubrication for normal human ankle joints must include a significant contribution from elastohydrodynamic lubrication.

ACKNOWLEDGEMENTS

I would like to express my appreciation to my thesis supervisors, Professors Duncan Dowson and Verna Wright, for their guidance and helpful discussions.

The financial support provided by the British Council and the permission of Professor B.N. Cole to pursue this research in his laboratories are gratefully acknowledged.

Mr. Devon Darby provided superb technical support in the experimental part of this thesis. In addition, he showed great interest and knowledge concerning the experimental strategy and thus provided valuable advice on numerous occasions.

Various members of the academic staff were most helpful in providing insight for particular aspects of this project. They include Dr. Jude Dowling, Dr. Rosemary Creasey, Dr. Bahaa Seedhom, Dr. David Newland, Dr. Chris Taylor, Dr. Brian Ruddy, Mr. Robin Sharp and Mr. Brian Jobbins.

Thanks are due to Mr. Steve Burridge and Miss Helen Hills for producing the photographs, Mr. Hugh Jones for assisting in measuring the ankle profiles, Mr. Balba Randhawa for helping in design changes on the simulator apparatus and Mr. Arthur Moreton for obtaining the synovial fluid. The members of the Department of Surgery of Leeds General Infirmary are also thanked for obtaining the ankle specimens.

Mrs. Marguerite Hall typed this manuscript with great precision and speed whilst using miraculous talent in interpreting the rough draft.

A special acknowledgement is merited by Dr. Jude Dowling for her assistance in proof-reading and assembling this thesis.

Finally, I would like to thank my fellow research students for their cheerful advice and good humour at all times.

John B. Medley

CONTENTS

PAGE

NOMENCLATURE

The following notation was used throughout the thesis. Special notation, or notation which was confined to a particular section only, has been defined in the text.

a	Half length of dry contact area when surface tractions are neglected.
b	Half length of equivalent bearing (Figure 5.2.1).
β	Twist angle (Figure B.1).
d	Effective elastic layer thickness (Figure 5.2.1).
δ	Surface deformation (Figure 7.2.1).
E	Elastic modulus.
E'	Reduced modulus.
η	Dynamic viscosity.
F	Load.
F'	Load per unit width.
F_A'	Time averaged load per unit width for one cycle.
$f(x)$	Profile for the steady state solution from Section 7.6 at a particular time.
h	Film thickness.
h_c	Central film thickness excluding surface deformation in Sections 7.2 and 7.6.
h_c	Central film thickness at a particular time in Section 7.7.
h_o	Minimum film thickness at a particular time.
θ	Twist angle (Figure B.1).
L	Length for plane inclined surface bearing model (Figure 6.3.1).
M	Slope for plane inclined surface bearing model (Figure 6.3.1).

μ	Coefficient of friction.
p	Film pressure.
p_D	Dry contact stress for the contrained column model.
R	Reduced radius.
R_1	Talus radius.
R_2	Tibia radius.
Ra	Centre line average deviation of surface.
r_c	True cylinder radius.
r_m	Measured profile radius for ankle.
r_s	Joint component radius for equation 4.4.1.
σ	Composite surface roughness.
T	Torque in Chapter 4.
T_D	Dynamic torque.
T_S	Static torque.
T_f	Frictional torque.
t	Time.
t_p	Period of cycle.
U_1	Lower surface velocity (Figure 5.2.1).
U_2	Upper surface velocity (Figure 5.2.1).
u	Entrainment velocity, $\frac{U_1 + U_2}{2}$
u_A	Time averaged entrainment velocity.
ν	Poisson's ratio.
V	Relative surface velocity.
x_e	Exit boundary point (Figure 7.6.1).

Dimensionless Groups

B	Starvation factor, $\frac{b}{R}$
D	Layer thickness, $\frac{d}{R}$
H	Film thickness, $\frac{h}{R}$
H_0	Minimum film thickness, $\frac{h_o}{R}$
P	Pressure, $\frac{p}{E'}$
S	Squeeze factor, $\frac{E't_p}{\eta}$
T	Time, $\frac{t}{t_p}$
U	Speed, $\frac{\eta u_A}{E'R}$
W	Load, $\frac{F_A'}{E'R}$
X	Co-ordinate in direction of surface motion, $\frac{x}{R}$

CHAPTER 1

INTRODUCTION

The human ankle joint is a bearing system of considerable sophistication. Widely varying dynamic loads and velocities are imposed which can result in the severe situation of the highest loads occurring when the entraining velocities are zero. The synovial fluid which acts as a lubricant has non-Newtonian characteristics and it also contains boundary lubricating additives. The bearing material consists of a thin layer of cartilage, which is a viscoelastic material having a high porosity and low permeability. It is attached to relatively rigid bone of a trabecular structure. The bearing surfaces are capable of self repair when damaged, but only at a slow rate compared to most other body tissues. Yet the human ankle joint usually has a trouble free service life of about seventy years throughout which it functions with friction forces of about one percent of the normal loading.

However, synovial joints do not always remain healthy and the pain and degeneration associated with various types of arthritis may be considered as a bearing failure. Such failures in engineering bearings are often caused by impaired lubrication. However, this cannot be stated with certainty in relation to synovial joints. There is evidence to suggest that in rheumatoid arthritis the joint failure is related to direct biochemical attack, but in osteoarthrosis mechanical factors such as wear, fatigue of the sub-chondral bone (Radin, 1974) or the articular cartilage (Weightman et al, 1978) are involved. Recently, evidence has been presented which indicates that osteoarthrosis is a mildly inflammatory disease involving hydroxyapatite and pyrophosphate crystals (Huskinson et al, 1979).

Although lubrication failure has not yet been directly linked to the initiation of arthritic disorders, it is clear that inadequate lubrication must play some role in the subsequent degeneration of the joint. The human ankle joint has a low incidence of primary osteoarthrosis compared with the hip and the knee (Stauffer et al, 1977). However, loads (Seireg and Arvikar, 1975; Stauffer et al, 1977) and normal stresses on the surfaces (Greenwald, 1976) appear to be similar to those acting at the hip and the knee. It therefore seems possible that the human ankle may experience better lubrication protection than other highly stressed synovial joints which exhibit a higher incidence of degeneration.

When synovial joint surfaces are severely damaged due to trauma or arthritic disease, a total joint replacement is often inserted. Prosthetic joints, although inferior to natural ones, are themselves remarkable bearings. They have a service life of about two decades with coefficients of friction somewhat higher than those experienced by healthy, natural joints (Unsworth et al, 1975) and some progressive damage to the surfaces (Dowling et al, 1978). The materials used in prosthetic joints are less compliant than the natural tissues. However, some attempts have been made to introduce elastomeric materials having a compliance similar to cartilage (Medley et al, 1980; Unsworth et al, 1980).

The lubrication of human ankle joints has been considered in both experimental and theoretical investigations reported in this thesis. The purpose of these studies is to provide background information for the diagnosis, treatment and possibly the prevention of arthritic disease. Certain aspects are relevant to the development of current and proposed joint replacements. In the general field of Tribology similar analytical and experimental studies arise in such diverse areas as elastomeric seals (Swales et al, 1972; Ruskell, 1980), vehicle tyres (Moore, 1980) and stylus-record contact (Jamison et al, 1978). The normal human ankle joint exhibits a geometry which is more amenable to theoretical analysis than that of other synovial joints. The experiments reported in the present thesis involved dissected human specimens and the parameters for the theoretical studies were chosen with reference to the ankle joint. However, the generality of the investigation must be emphasized.

CHAPTER 2

THE MECHANICS OF NORMAL SYNOVIAL JOINTS

2.1 INTRODUCTION

The study of the lubrication of normal human ankle joints may be considered as part of the more general investigation into the mechanics of normal synovial joints. The literature on this topic is extensive. An over-view is presented in this chapter and used subsequently in both the development and the interpretation of the present research effort. Certain review articles on various aspects of synovial joint mechanics provide background for this chapter (Swanson and Freeman, 1970; Radin and Paul, 1972; Wright et al, 1973; Torzilli, 1976; Higginson, 1978; McCutchen, 1978; Swanson, 1979; Weightman and Kempson, 1979; Dowson, 1980; Wright and Medley, in the press).

Synovial joints permit relative sliding of surfaces with low friction and negligible wear while transmitting loads without damaging any of the structural components. A general model for synovial joints is shown in Figure 2.1.1. Most of the research work reported to date on the mechanics of synovial joints has been focussed on the subchondral bone, articular cartilage, meniscus and the synovial fluid. This may be attributed to the fact that severe dysfunction of a synovial joint occurs when these tissues are damaged either by trauma or a disease process. Thus, as shown in Figure 2.2.1, the present discussion considers only these tissue components. Also, most of the investigations of synovial joint mechanics have dealt with the hip, knee and ankle. Therefore, the present discussion concentrates on these joints, although it is expected that similar mechanisms act in other human synovial joints. Before the overall mechanical functions of synovial

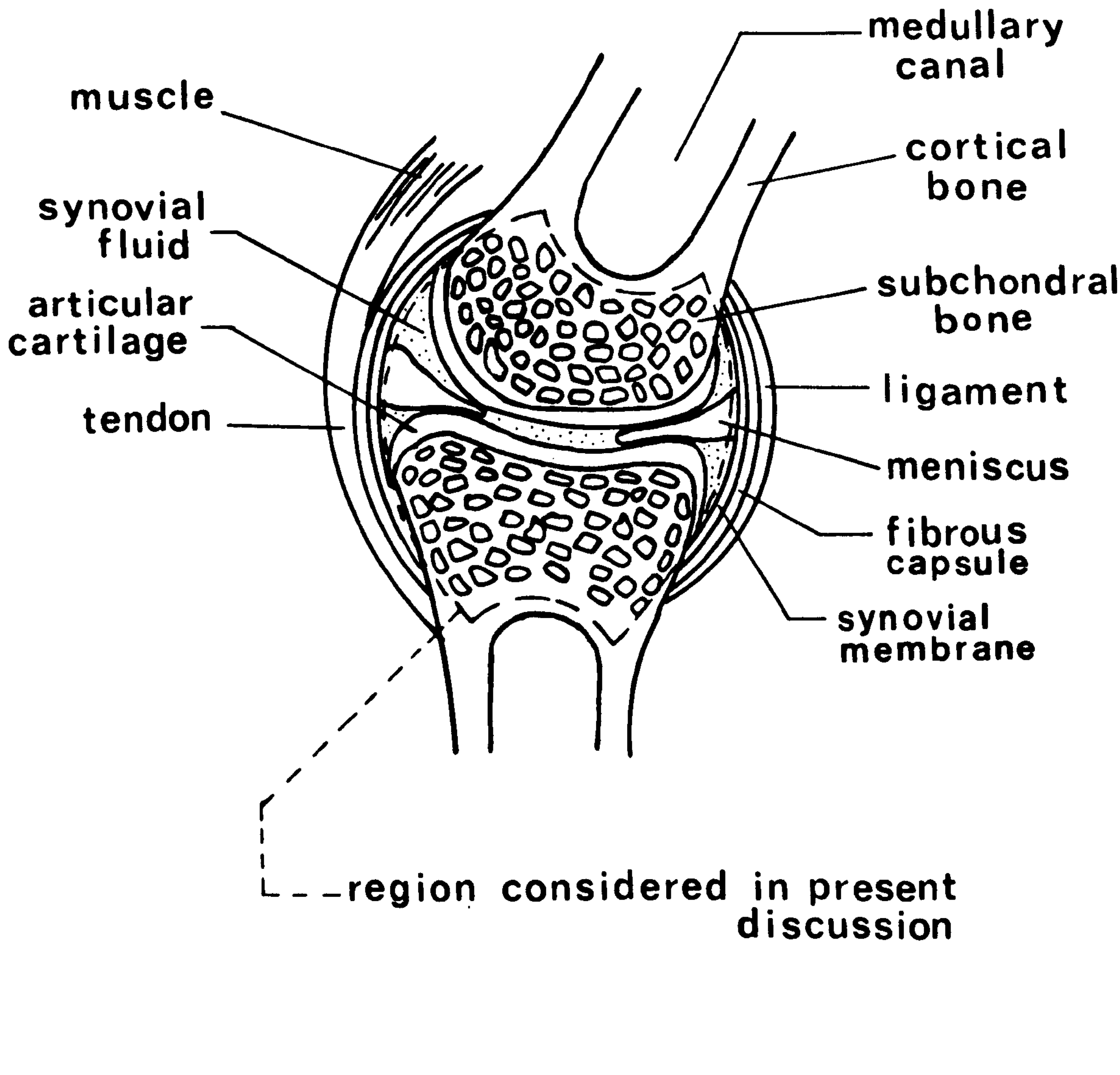

Figure 2.1.1. : A general mechanical model for synovial joints.

joints, such as sliding and load transmission, are considered, a detailed examination of the intrinsic mechanical properties of each tissue component is presented.

2.2 SYNOVIAL JOINT COMPONENTS

Subchondral Bone:

The bone found directly underneath the articular cartilage has a trabecular structure with a thin covering plate as shown in Figure 2.2.1. The internal cavities contain red and yellow marrow and interconnect through the structure. The thickness of the subchondral bone plate, the width of the individual trabeculae and the cavity dimensions are all of the order of 1 mm (Swanson and Freeman, 1966).

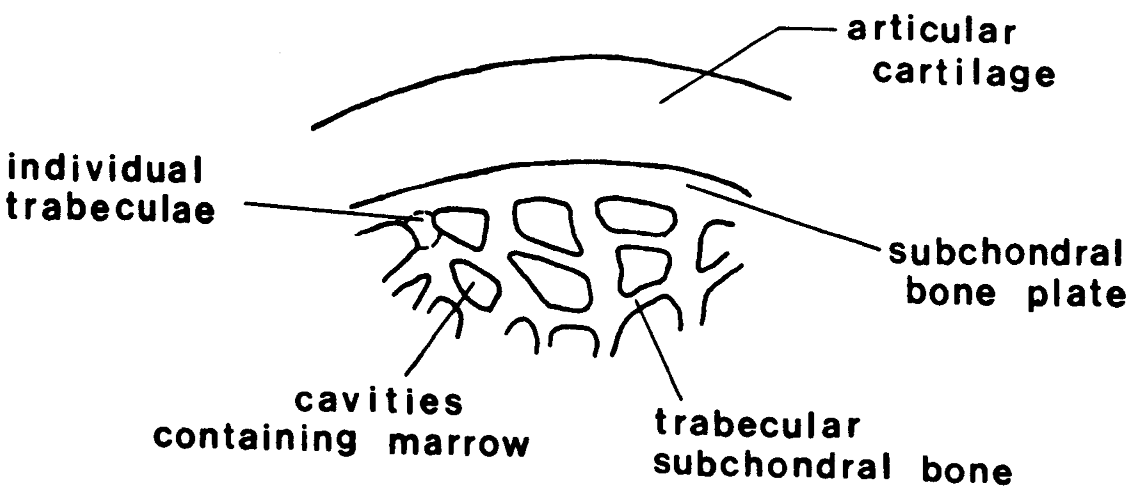

Figure 2.2.1 : Subchondral bone structure.

Bulk subchondral bone behaves elastically under ordinary in vivo conditions (Swanson and Freeman, 1966; Pugh et al, 1973a, 1973b). Small specimens of bulk subchondral bone have compressive elastic moduli approximately one order of magnitude lower than that of cortical bone (Radin et al, 1970b). Tests on individual trabeculae (Townsend et al, 1975) indicate that the trabeculae have an elastic modulus of approximately the same value as that of cortical bone. Thus the web-like structure of trabecular bone accounts for its low bulk elastic modulus by allowing more deflection compared to a solid bone mass as shown in Figure 2.2.2.

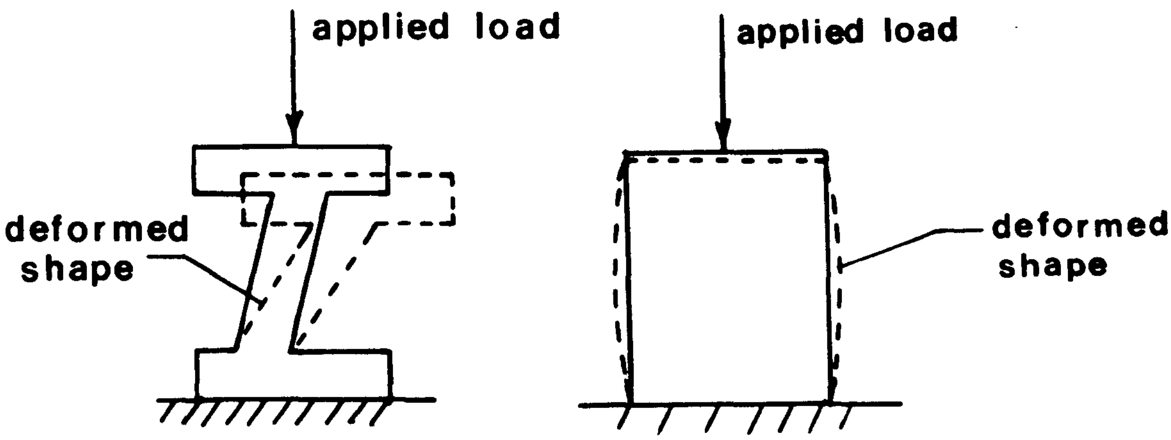

(a) A single trabecular specimen

(b) An equivalent sized cortical bone specimen

Figure 2.2.2 : Deformation of a single trabecula compared to cortical bone of equivalent size for the same applied load.

It follows that the compressive strength increases with the bulk density (Behrens et al, 1974; Ducheyne et al, 1977). However, plugs of bone with the same bulk density may have different compressive strengths due to their internal trabecular architecture (Behrens et al, 1974; Pugh et al, 1973b). The marrow apparently does not play a significant role in the response to ordinary in vivo loads (Swanson and Freeman, 1966). However, in rapid plastic deformation involving large scale fracture of the trabeculae the marrow does resist a significant portion of the imposed load (Hayes and Carter, 1976). Occasionally individual trabeculae are fractured in vivo (Radin et al, 1973b) but this does not significantly affect the overall mechanical properties of bulk subchondral bone (Ducheyne et al, 1977).

Articular Cartilage:

A detailed description of articular cartilage has been published recently (Freeman, 1979). A layer of articular cartilage, about 2.5 mm thick, covers the subchondral bone, as shown in Figure 2.2.3. It is composed of 60 - 80% by weight water apparently divided approximately equally between the cells, proteoglycan gel and the free interstitial fluid (Linn and Sokoloff, 1965). The remaining tissue is approximately 40% by weight chondrocytes, 35% by weight collagen and 25% by weight proteoglycans.

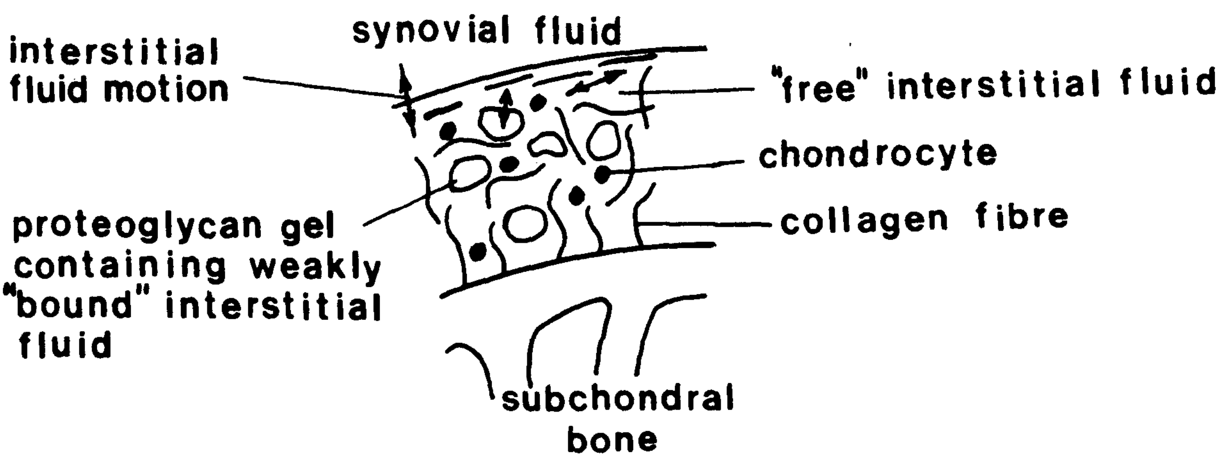

Figure 2.2.3 : Articular cartilage structure.

The surfaces of articular cartilage appear smooth to the naked eye but light and electron microscope studies have shown surface depressions 20 - 40 μm in diameter and 0.3 - 15 μm deep (Clarke, 1973). Using profile measuring devices Ra surface roughnesses in the range of 2 - 6 μm have been measured

(Walker et al, 1968; Clarke, 1973; Sayles et al, 1979, Thomas et al, 1980).

The interstitial fluid in articular cartilage is composed of water and positively charged solutes. It is able to move within and across the surface of cartilage as shown in Figure 2.2.3. The proteoglycan gel is composed of a protein core which has glycosaminoglycan branches containing fixed negatively charged groups. The interstitial fluid, containing positively charged solutes, is bound by weak electrostatic forces to these fixed negatively charged groups. The chondrocytes or cartilage cells synthesize the protein for the proteoglycans and the collagen. The collagen fibres are in the order of 1 μm diameter and form a fine mesh network with specific orientations at various locations within the cartilage.

The collagen fibre network apparently entangles and immobilizes the proteoglycan gels. Thus cartilage stiffness is a result of the proteoglycan gels pushing against the collagen fibre network. When cartilage deforms under load the permeability of the proteoglycan gel allows the weakly bound interstitial fluid to be mechanically squeezed out to join the free interstitial fluid. The free interstitial fluid can move within the cartilage, away from the loaded regions, and across the cartilage surface into the synovial fluid. This fluid motion is impeded, and thus deformation resisted, by the small size of the pores within the proteoglycan gel and between the collagen fibres.

Further resistance to deformation and flow results from the osmotic pressure within the proteoglycans. The osmotic pressure is caused by the outflow of the interstitial fluid with its positively charged solutes. This leaves the fixed negative charged groups in close proximity, resulting in forces of electrostatic repulsion (Edwards, 1967). Also the collagen fibre network begins to stretch and possibly re-orientate (McCall, 1969) to resist the imposed forces, causing tensile stress in the fibres. This complicated response to loading is shown in Figure 2.2.4. Osmotic pressure may also be considered to act on a larger scale across the cartilage surface as interstitial fluid is expressed into the synovial fluid and proteoglycan gels of net negative charge repel each other.

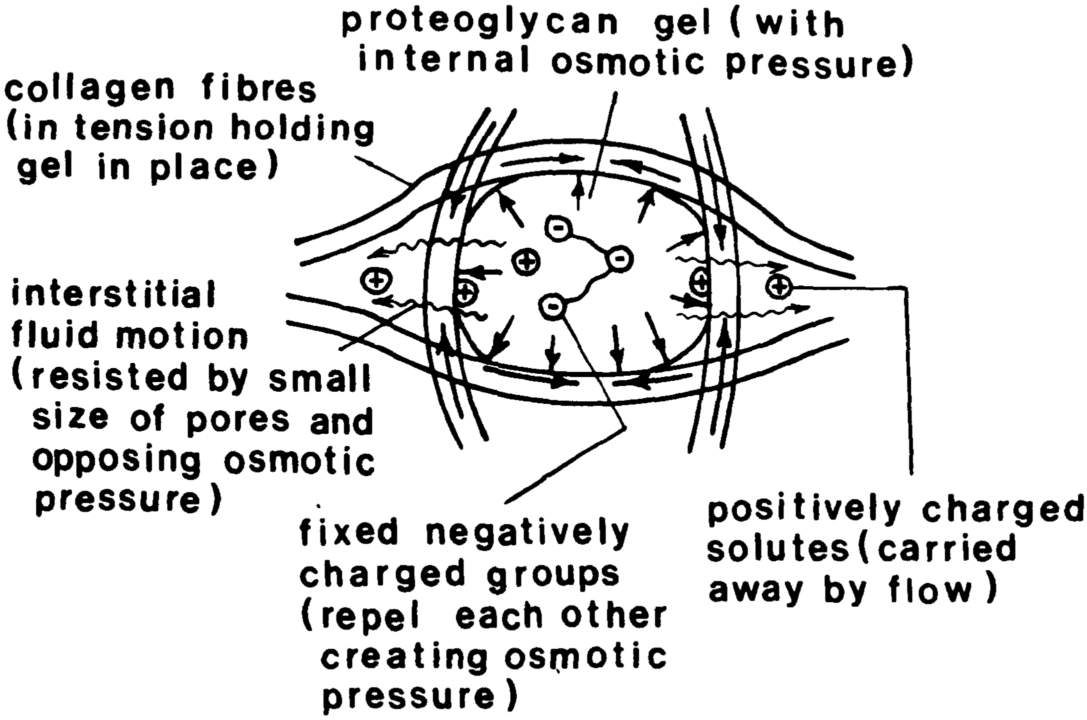

Figure 2.2.4 : Internal mechanisms resisting cartilage deformation.

Upon removal of the load, collagen fibres relax and osmotic pressure pulls fluid into the cartilage and ultimately into the proteoglycan gels. This behavior makes cartilage a viscoelastic material, since its behaviour is time dependent and recoverable as shown in Figure 2.2.5. It is interesting to note that interstitial fluid can be pulled in from the synovial fluid but differs from it by the absence of certain molecules in synovial fluid which are apparently too large to enter the cartilage pores.

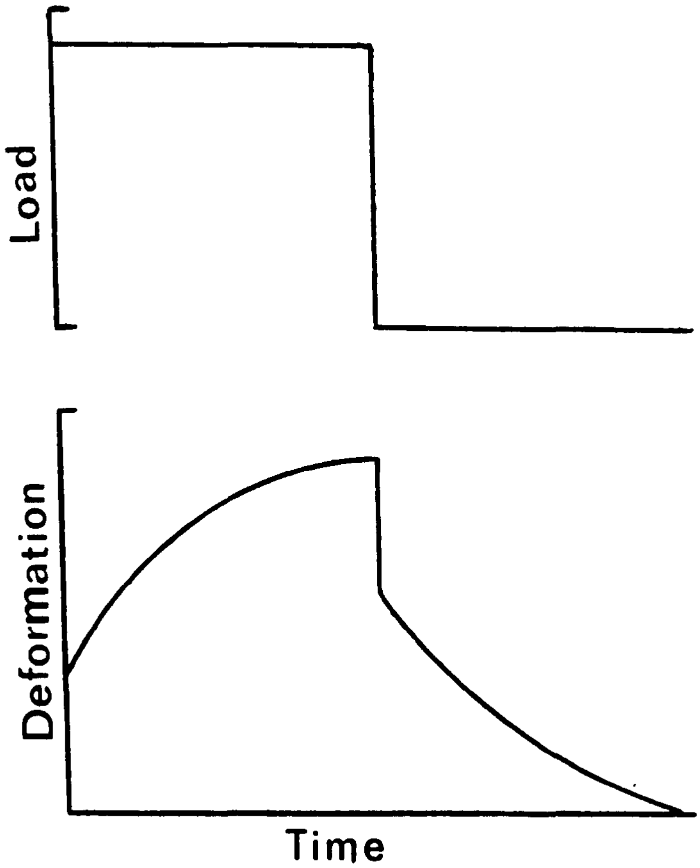

Figure 2.2.5 : Time dependent cartilage deformation.

A number of recent studies have sought to determine the complex microscopic interaction of collagen fibre tension, osmotic pressure and resistance to interstitial fluid flow when cartilage deforms under various load patterns. These studies have used or developed theory for small specimens of articular cartilage from humans and animals.

A generalized viscoelastic model for the deformation of cartilage with an indentor has been developed recently (Parsons and Black, 1977). This formulation extended and combined previous models for cartilage viscoelasticity (Hayes and Mockros, 1971) and indentation testing (Hayes et al, 1972; Hori and Mockros, 1976). It was used to show that, in a normal ionic environment, collagen fibres in the surface regions of cartilage are not pre-stressed under no load conditions (Parsons and Black. 1979).

Recent studies have also attempted to model both interstitial fluid flow and matrix deformation separately (Higginson et al, 1976; Mansour and Mow, 1977; Mow et al, 1980). Such models are sensitive to the decrease in permeability which occurs as cartilage is compressed (Maroudas et al, 1968; Mansour and Mow, 1976). Thus, it is very difficult to separate the various internal mechanisms of cartilage deformation. However, flow independent viscoelastic properties of cartilage with its surface layer removed have been measured for small shear strains (Hayes and Bodine, 1978). This study showed that, for a given load, collagenase digestion or proteoglycan depletion each gave characteristic increases in deformation while increasing the cross-linking of the collagen fibres decreased deformation

Further complications in the detailed study of cartilage mechanics result from the changes in collagen fibre orientation and proteoglycan distribution from the surface to the bone interface. This tissue variation has been studied mechanically by a number of groups (Kempson et al, 1968, 1973; Maroudas and Bullough, 1968; Cameron et al, 1975; Woo et al, 1976, 1979). The significant differences in mechanical properties reported by each of these groups indicate that models which assume a homogeneous isotropic cartilage layer must be applied with caution.

The investigations of the intrinsic mechanical properties of cartilage begin to show potential in detecting pathogenic physico-chemical changes. Unfortunately, their use in characterising the overall response of cartilage to in vivo loading patterns has not been realized as yet. However, some studies have examined the behaviour of small cartilage specimens subject to cyclic compressive stress patterns similar to those believed to act in vivo (Johnson et al, 1977; Higginson and Snaith, 1979). After the first few cycles the cartilage response was essentially elastic with a very small amount of non-recoverable creep occurring during each cycle. Eventually a final cyclic steady state was reached as shown in Figure 2.2.6. A model was introduced which considered the non-recoverable creep accumulated during previous cycles to be part of the specimen's history. Instantaneous elastic moduli were evaluated at various creep strains. Then, with the measured rate of creep, cartilage response was characterized. As expected, the instantaneous elastic modulus was found to increase with increasing creep strain.

Menisci:

The menisci are present in the knee but not the hip or ankle joints. The two menisci in the knee are half-moon shaped fibro-cartilage structures having approximately triangular cross-sections as shown in Figure 2.2.7. The thickness at the joint periphery is in the order of 5 mm, which is approximately equal to the combined thickness of the articular cartilage layers.

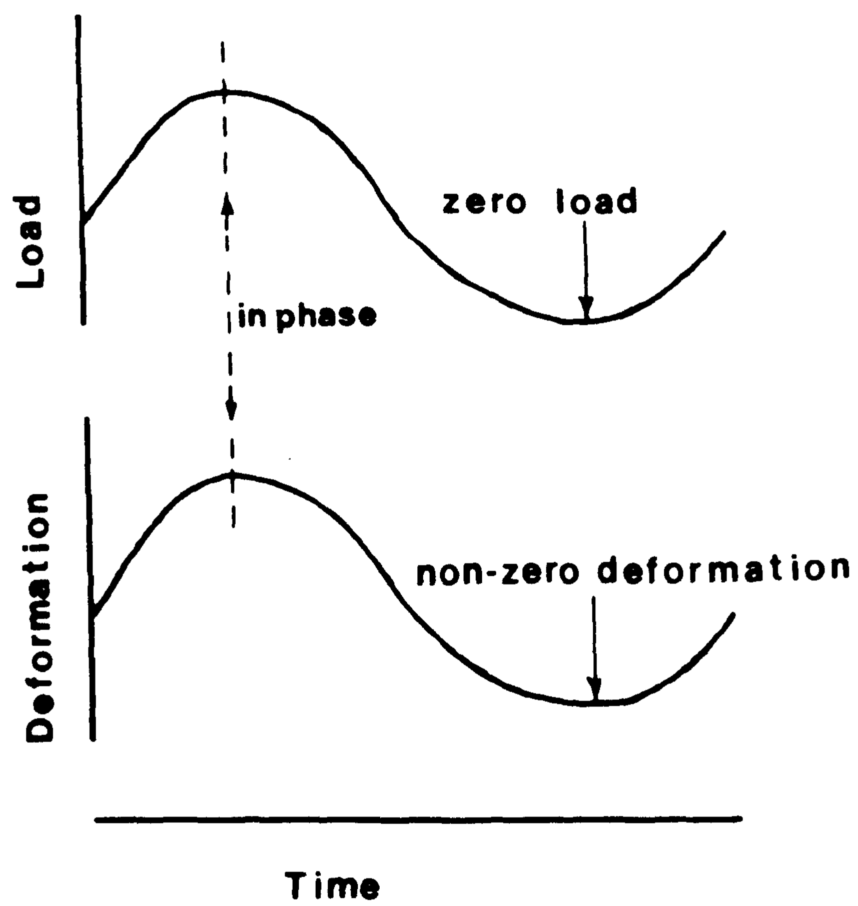

Figure 2.2.6 : The steady state response of cartilage to cyclic loading.

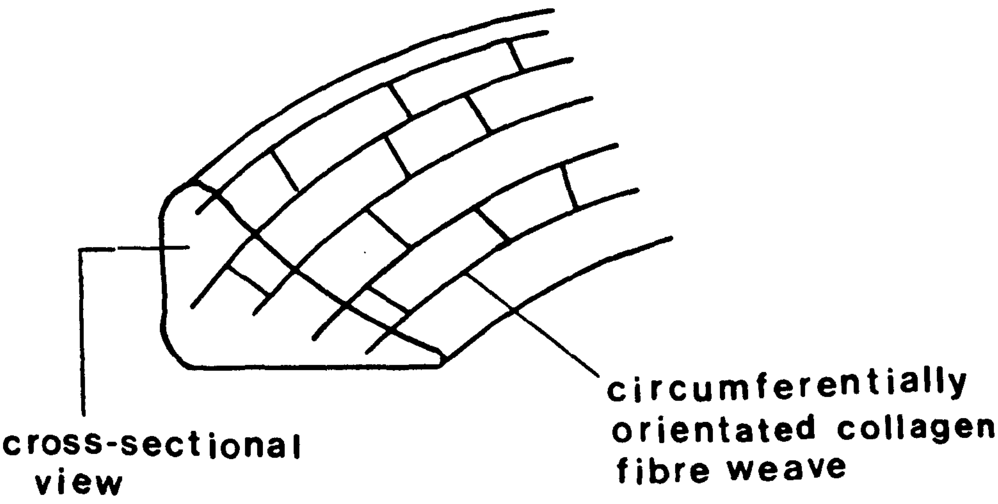

Figure 2.2.7 : Menisci structure.

The menisci are approximately 70% by weight water with collagen comprising about 75% by weight of the remaining tissue (Peters and Smillie, 1972). With its high collagen content the meniscus is similar to a ligament in composition rather than articular cartilage. The collagen fibres exhibit significant circumferential orientation with some radial links between them (Cameron and Macnab, 1972) as shown in Figure 2.2.7.

The tensile strength (Bullough et al, 1970) and tensile elastic modulus (Uezaki et al, 1979) of the menisci are in the same range as those of articular cartilage, with fairly wide variations depending on collagen fibre orientation. The response to tensile forces is mainly elastic, as opposed to viscoelastic, and probably results from changes in collagen fibre orientation (Uezaki et al, 1979).

Synovial Fluid:

Synovial fluid is a light yellowish liquid contained within synovial joints in the region bounded by the synovial membrane and the articular cartilage surfaces as shown in Figure 2.2.8. It is essentially a dialysate of blood plasma with the addition of approximately 3 mg/ml hyaluronate macromolecules. These macromolecules are believed to be added to the plasma component by the synovial membrane and may combine directly with protein elements in the fluid or interact only mildly when in solution (Wright et al, 1973). By including water within their domain, hyaluronate macromolecules are believed to assume an approximately spherical shape in synovial fluid with a radius of about 1 μm. Synovial fluid also contains a smaller glycoprotein molecule which may be involved in lubrication of the cartilage surfaces (Swann, 1978).

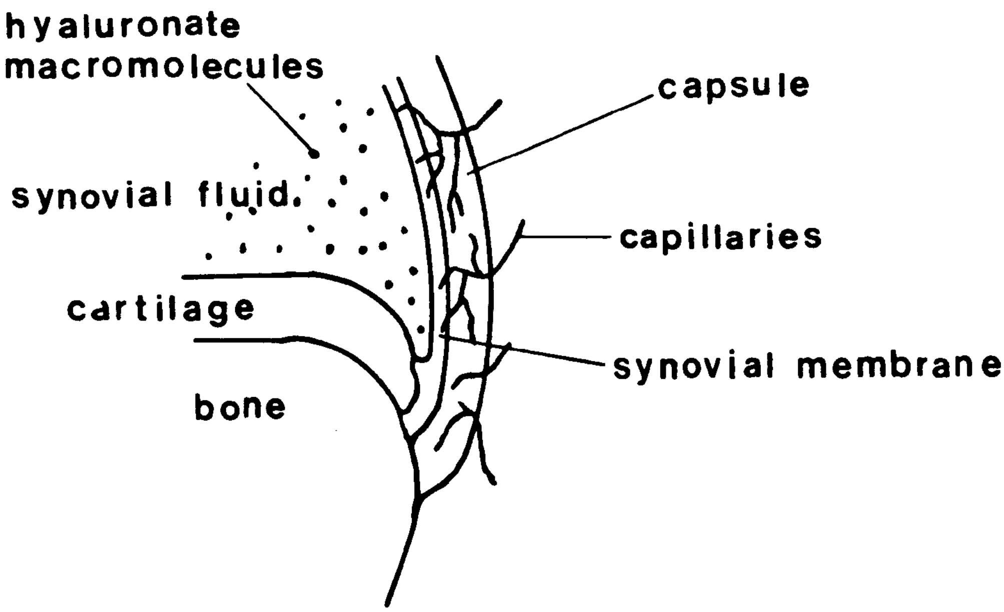

Figure 2.2.8 : Synovial fluid structure.

Synovial fluid, like many polymer solutions, recovers to some extent after being deformed or, in other words, it exhibits some elasticity. If synovial fluid is sheared, but not compressed, between two surfaces in relative motion, it imposes resisting shear and normal forces on the surfaces as shown in Figure 2.2.9 (Ogston and Stanier, 1953). The normal forces are very small compared to the physiological loads estimated to act through synovial joints. Thus synovial fluid is not believed to resist deformation significantly in vivo due to its elasticity (Ogston and Stanier, 1953; Caygill and West, 1969).

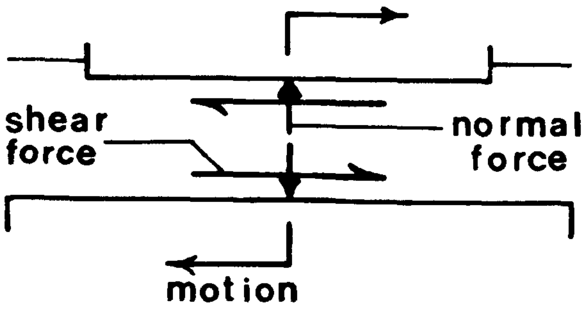

Figure 2.2.9 : Forces on the surfaces caused by tangential motion but not compression of the interposed synovial fluid.

In contrast to its elasticity, the resistance to shear resulting from the fluid viscosity is an important factor, when combined with lubrication mechanics, in the deformation or flow of synovial fluid in vivo. Extensive measurements of the viscosity of synovial fluid for humans and animals have been recorded (Ogston and Stanier, 1953; Davies, 1967; Palfrey and White, 1968; Davies and Palfrey, 1969; Cooke et al, 1978). These studies show reasonable agreement (Swanson, 1979). Viscosity decreases as shear rate increases and eventually approaches a constant value that is somewhat larger than that of water as shown in Figure 2.2.10. This behaviour is believed to be caused by tangling of the macromolecules at low shear rates and eventual separation at higher shear rates (Ogston and Stanier, 1953). For a given shear rate, the viscosity of synovial fluid has also been found to increase with increasing hyaluronate concentration (Ogston and Stanier, 1953; Negami, 1964), or decreasing temperature. (Ogston and Stanier, 1953; Evangelista et al, 1978).

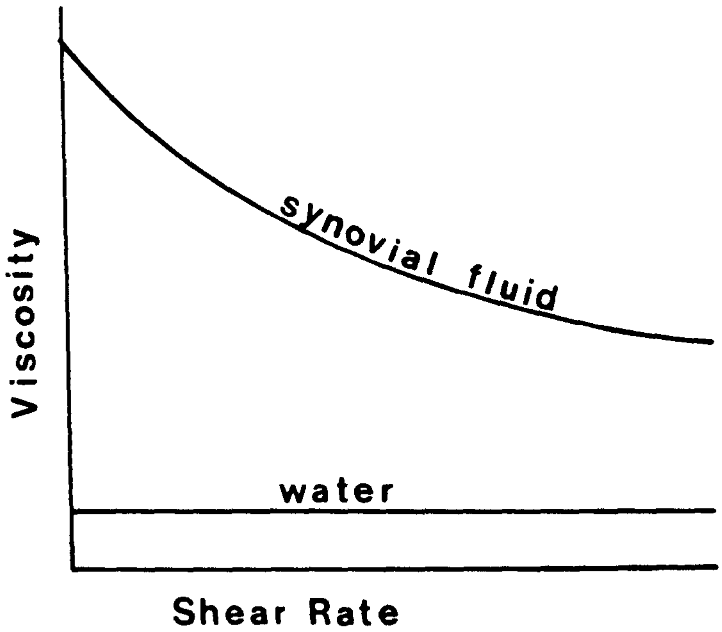

Figure 2.2.10 : The viscosity variation of synovial fluid with shear rate.

The viscosity combined with the elastic behaviour of synovial fluid has led to elaborate viscoelastic models to characterize the deformation and flow of the lubricant (Lai et al, 1977, 1978). However, one difficulty in comprehensive modelling of synovial fluid flow in vivo results from the possibility that the apparent viscosity may not be a property of the fluid alone. Theoretical investigations have been reported of fluid flow through passageways with dimensions similar to those of particles within the fluid. The apparent viscosity of synovial fluid depends on many features, including the extent to which the passageway surfaces inhibit particle spin (Allen and Kline, 1971).

The apparent viscosities of thin layers of synovial fluid sheared between cartilage and glass surfaces have been measured and shown to be two orders of magnitude higher than that of bulk synovial fluid (Walker et al, 1970). In this study, structured layers about 10 μm thick were observed on cartilage surfaces. These layers were believed to be rich in hyaluronate and protein elements of synovial fluid and a theory was developed to explain the formation and the viscosities of these layers (Dowson et al, 1970). Thus, macromolecular interaction with the cartilage surfaces may cause significant changes in the apparent viscosity during thin film flow of synovial fluid.

Concluding Remarks on Synovial Joint Components:

In general, the deformation of synovial tissues subject to external loading depends on local composition and structure as well as the complex behaviour of the various internal elements. However, the deformation can be approximated as elastic in order to gain some insight into the comparative behaviour of the tissues in vivo. Thus, the elastic moduli of various synovial joint tissues are given in Table 2.2.1. along with some common orthopaedic implant materials. Synovial fluid is not included in Table 2.2.1. since its elastic modulus is negligible compared with the more solid tissues. It is noted that the viscosity of bulk synovial fluid at high shear rates is a few times greater than that of water.

Having considered some simplified material constants to describe the load-deformation response of synovial joint tissues, it is important to remember that the exact behaviour and internal mechanisms responsible for this behaviour cannot be ignored. They are essential to many of the larger scale mechanisms of load transmission and lubrication which are discussed subsequently.

Table 2.2.1 : The elastic moduli of synovial joint components and some materials used in joint replacement.

Material	Approximate Elastic Modulus (MPa)
Vitallium	10^5
Cortical bone	10^4
Individual subchondral trabeculae	10^4
Bone cement (PMMA)	10^3
UHMW polyethylene	10^3
Bulk subchondral bone	$10^2 - 10^3$
Articular cartilage	$10 - 10^2$
Meniscus	10

2.3 LOAD TRANSMISSION

Both normal (perpendicular) and tangential forces are transmitted in vivo from one cartilage surface to the other during common activities like walking. The normal forces result from the static and dynamic effects of the body mass plus muscle and ligament tensions. During walking they vary from close to zero up to as much as eight times body weight (Paul, 1967, 1976; Seireg and Arvikar, 1975). The tangential forces result from friction during sliding motions. Since these friction forces are only about 1% of the normal forces they will be ignored in this discussion of load transmission. However, the subject of friction will be considered in a later section on lubrication.

As shown in Table 2.2.1, cartilage and menisci have elastic moduli much lower than bulk subchondral bone, which itself has a much lower modulus than cortical bone. The purpose of this soft structure is apparently to "spread" the transmitted forces and thus reduce peak normal stresses at the cartilage surfaces. This serves to enhance lubrication. However, the joint tissues must be able to withstand the transmitted forces without sustaining progressive damage. This ability is as important to overall joint function as the lubrication of the surfaces.

To examine the way in which loads are transmitted through the joint tissues, it is convenient to consider the transmission of peak loads first and then consider the additional dynamic effects present during the in vivo transmission of these peak loads. This division allows a complete description of the spectrum of mechanisms which act to reduce high local forces in load transmission.

Peak Load Transmission:

The reduction of high local transmitted forces (or stress concentrations) within the joint tissues occurs by what will be termed internal and external mechanisms. High forces transmitted through specific tissue may result from local geometry, such as the bone asperities at the cartilage-subchondral bone interface, or from large scale geometry.

Internal mechanisms may exist within cartilage to reduce transmitted forces (Weightman and Kempson, 1979). Support for the existence of these internal mechanisms results from the observed increase in subchondral bone damage which occurs when the same stresses are imposed on arthritic as on healthy joint surfaces (Freeman et al, 1975). The possible mechanisms of reducing stresses within cartilage include the development of tensile stresses in the collagen fibre network and local flow of interstitial fluid. These mechanisms are shown in Figure 2.3.1.

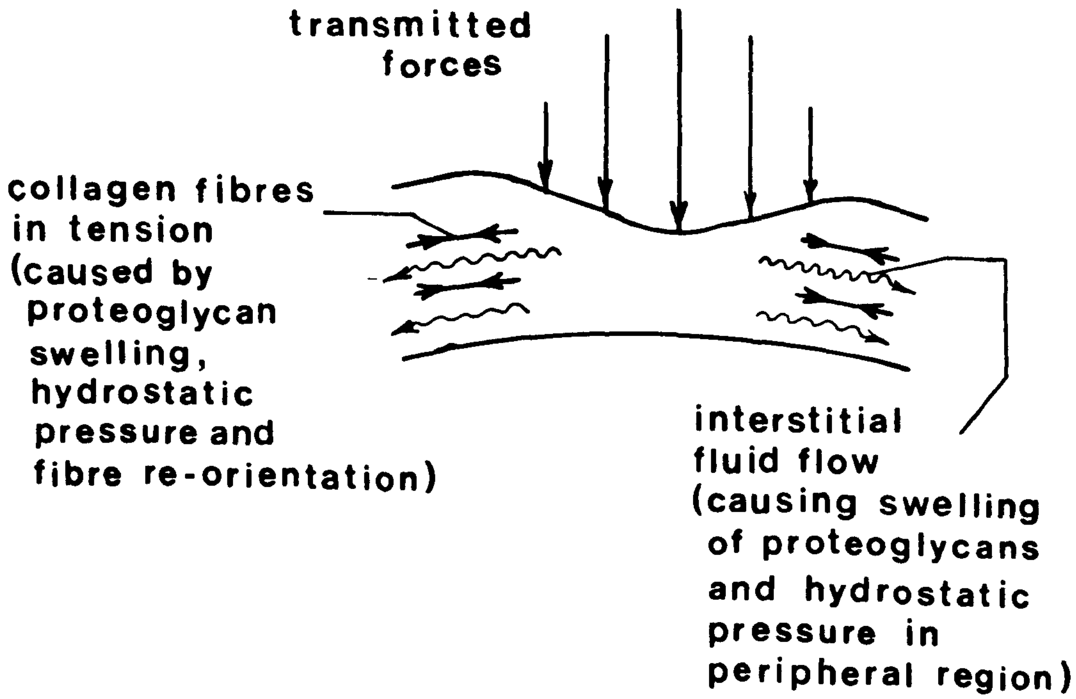

Figure 2.3.1 : Possible internal mechanisms of articular cartilage force spreading.

There is some conflict in the literature concerning the amount by which internal mechanisms in cartilage are capable of reducing transmitted forces. Recent mathematical modelling of cartilage (Askew and Mow, 1978) and subchondral bone (Hayes et al, 1978) suggests that cartilage layers are too thin to accomplish significant internal force spreading.

Internally subchondral bone can spread high normal forces by virtue of its trabecular structure and thickness. Hayes et al, 1978). This is done by inducing tensile stresses in laterally remote trabeculae as shown in Figure 2.3.2.

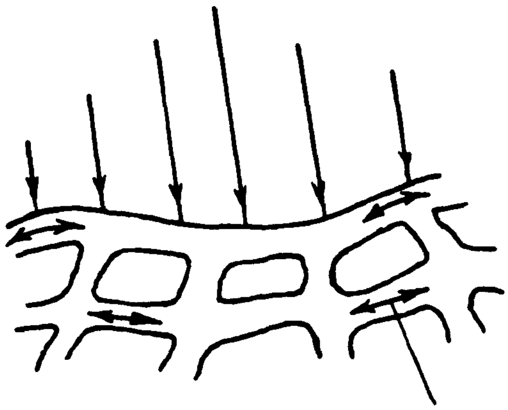

Figure 2.3.2 : Possible internal mechanisms of subchondral bone force spreading.

On a larger scale, certain factors create external force spreading mechanisms. The internal architecture of subchondral bone varies both normally and tangentially to the joint surfaces (Raux et al, 1975; Behrens et al, 1979). These variations may serve to spread transmitted forces evenly from the cortical bone through the subchondral bone (Hayes et al, 1978). Also, it has been suggested that high tensile stresses in the subchondral bone plate may act to reduce compressive stresses in the trabecular subchondral bone (Jacob et al, 1976).

Cartilage itself has property variations across the joint surfaces (Kempson et al, 1971; Cameron et al, 1975), although it has been estimated that such variations do not significantly alter the transmitted forces (Weightman and Kempson, 1979). However, it is generally agreed that cartilage, being much more deformable than subchondral bone, plays a more significant role in increasing the size of contact areas. This reduces normal stresses in both the cartilage and the subchondral bone (Day et al, 1975; Freeman et al, 1975; Weightman and Kempson, 1979). Cartilage visco-elasticity serves to further increase the contact areas and thus enhances this mechanism of load sharing. The ability of cartilage to increase contact areas is shown in Figure 2.3.3. The menisci in the knee also play a significant role in increasing contact areas and spreading transmitted forces (Seedhom et al, 1974; Shrive, 1974; Walker and Erkman, 1975; Maquet et al, 1975; Seedhom, 1979; Seedhom and Hargreaves, 1979).

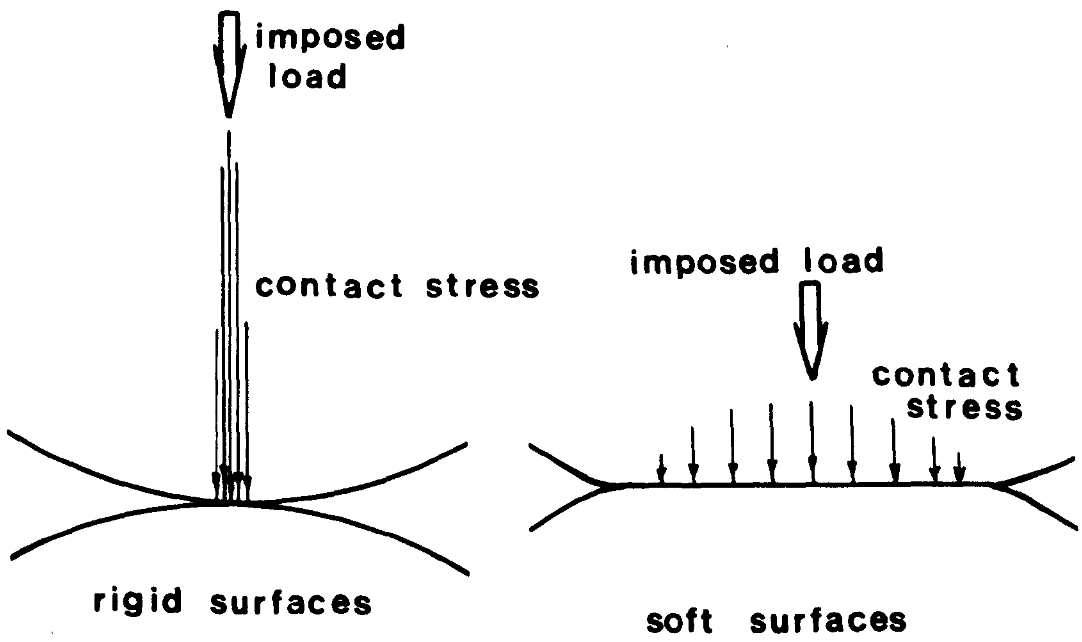

Figure 2.3.3 : The ability of a soft surface to deform which increases contact areas and thus reduces peak contact stress for a given imposed load.

Some synovial joints also appear to reduce peak contact stresses by having a slightly smaller radius of curvature for the concave than for the convex surface (Greenwald et al, 1971, 1976). This mechanism is shown in Figure 2.3.4 and essentially serves to distribute the contact stress more evenly over the joint surface.

The knee joint achieves a similar effect through the presence of the menisci (Seedhom and Hargreaves, 1979). In addition to geometry, this mechanism depends on the deformation of cartilage and menisci to create a conforming joint under peak loading conditions.

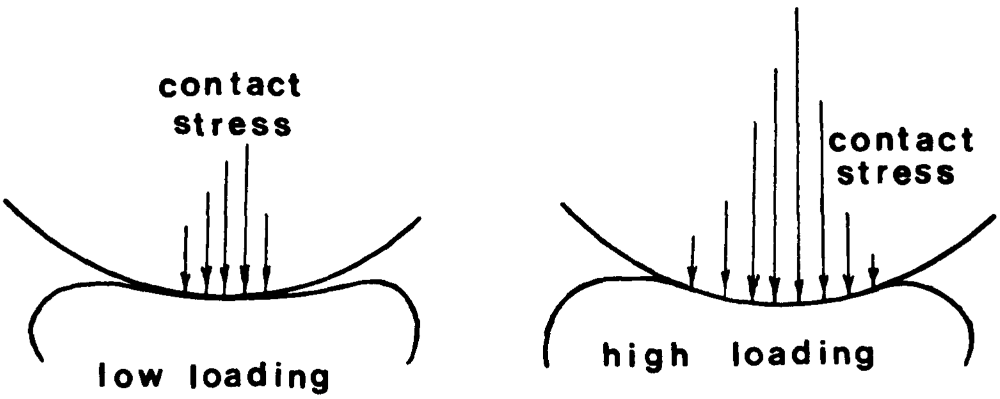

(a) Larger radius of curvature for concave than for convex surface

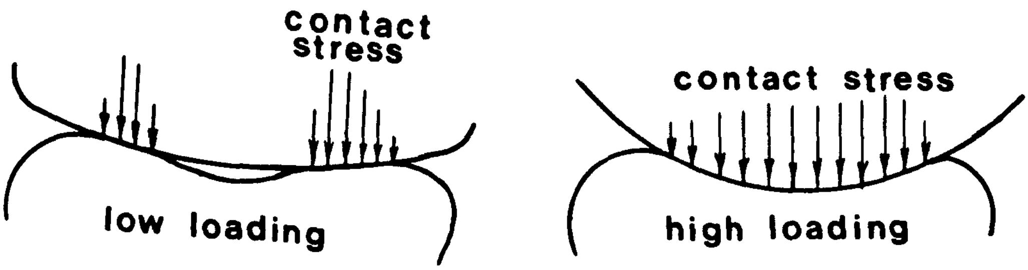

(b) Smaller radius of curvature for concave than for convex surface

Figure 2.3.4 : A method of achieving a more even distribution of contact stress magnitudes.

Dynamic Effects in Peak Loading Transmission:

The magnitude of the transmitted forces, which a particular region of tissue experiences, is reduced by the internal and external mechanisms mentioned previously. Under dynamic loading conditions, additional mechanisms act to reduce transmitted forces.

The creep of the cartilage, due to its viscoelastic properties, may create large contact areas during a period of static loading. The larger contact areas may then help to reduce contact stresses during the rapid application of peak loads.

Subchondral bone plays an important role as a shock absorber. Although cartilage, synovial fluid and the menisci all have intrinsic shock absorbing properties, they are present in layers too thin to achieve significant attenuation of transmitted forces (Radin and Paul, 1969, 1970a). However, subchondral bone, which is not so intrinsically energy-absorbing, is present in much thicker layers. It apparently provides enough deflection to reduce the accelerations of the body mass and thus significantly reduce the dynamic transmitted forces (Radin et al, 1970b; Radin and Paul, 1971a, 1971b, 1973). This mechanism is shown in Figure 2.3.5. Also subchondral bone may prevent the splitting of cartilage under peak dynamic loads by providing constraint at the bone-cartilage interface (Findlay and Repo, 1978).

There is one more mechanism which arises during dynamic load transmission. During dynamic in vivo activities in which both loads and velocities vary, it has been observed that cartilage increases in thickness (Ingelmark and Ekholm, 1948; Ekholm and Ingelmark, 1952). This may enhance the previously mentioned internal mechanisms by which cartilage spreads transmitted forces, since more interstitial fluid would be present. Also the differences in radii of curvature between concave and convex surface curvatures may change such that the contact stress is more evenly distributed (Oberlander, 1978). Finally, having an increased cartilage thickness would allow more cartilage deformation, if required, as load and velocity patterns changed.

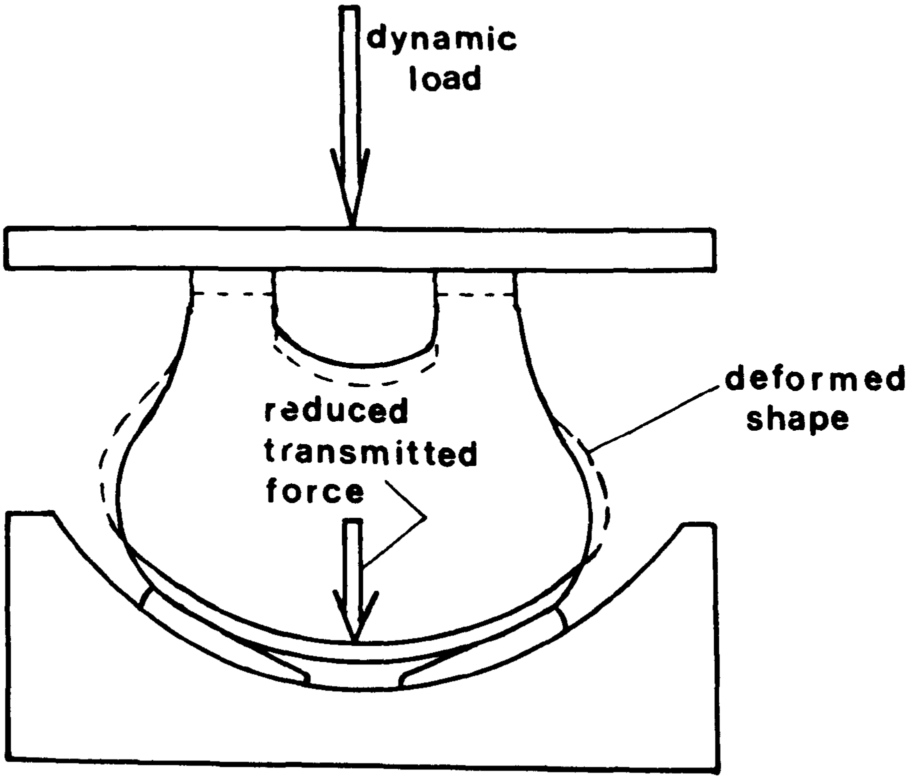

Figure 2.3.5 : Dynamic load attenuation by subchondral bone.

Concluding Remarks on Load Transmission:

In overall load transmission an important function of cartilage and menisci appears to be the ability to deform and create larger contact areas. An important function of subchondral bone appears to be its role as a shock absorber. In all these joint tissues internal force spreading mechanisms and local tissue variations may also influence load transmission. It is difficult to select any one mechanism as being the most important, since changes in any of them may increase stresses to abnormal levels in some region of the synovial joint.

2.4 LUBRICATION MECHANICS

The low friction forces arising during the relative sliding of articular cartilage surfaces may be attributed to effective lubrication. When synovial fluid is removed from a fresh cadaveric joint, oscillation under load produces higher friction and significant damage to the cartilage surfaces in a few hours (Clarke et al, 1975). Thus in vivo joint lubrication appears to depend on synovial fluid or one of its components. The exact way in which this occurs is not yet known. A number of different mechanisms have been suggested in the literature and are discussed separately in this section. However, during routine in vivo activities like walking it is likely that a number of different modes of lubrication act on a given surface region at various times (Dowson, 1967). Little research has been done on the lubrication of intact joints during the specific load and velocity patterns which occur in vivo.

Fluid Film Mechanism:

When a fluid lubricant is present in a bearing, films can be generated by the motion of converging-diverging surfaces. The viscosity of the lubricant causes its layers adjacent to the moving surfaces to "stick" together when shear is imposed by the surface motion. As a result, lubricant is pulled into the "contact" region by an 'entraining' action of the moving surface. If enough lubricant is entrained the surfaces are separated by a thin fluid film. This means that the integral of the pressures in the lubricant film balances the applied load. This mechanism is shown in Figure 2.4.1 for the simplified case when only one surface is in motion.

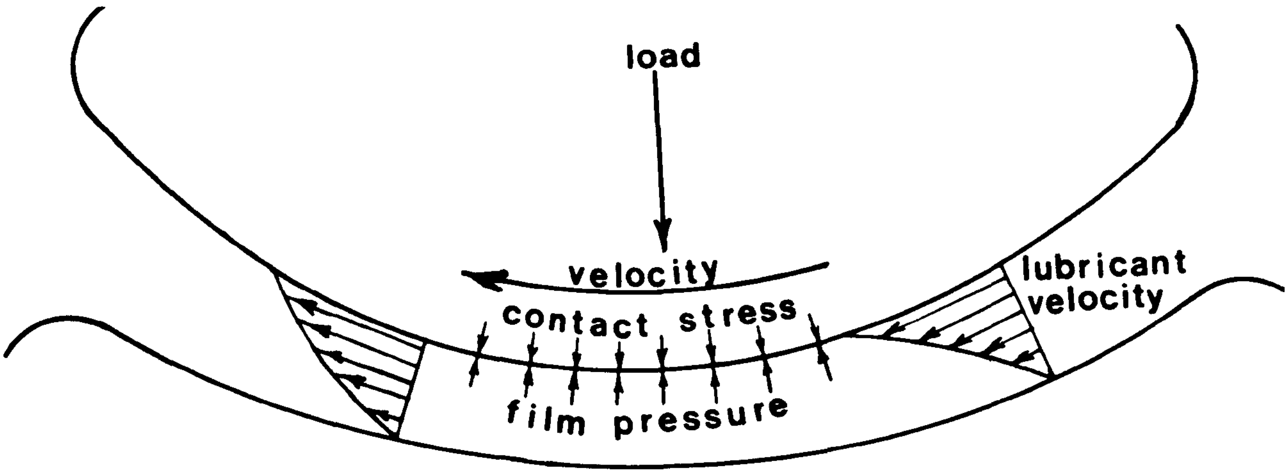

Figure 2.4.1 : An example of fluid film lubrication.

It is common engineering practice to calculate a theoretical lubricant film thickness by assuming that the surfaces are perfectly smooth. If this film is thick enough to separate the real surface asperities it can be predicted that full fluid film lubrication occurs. In engineering applications, experimental techniques may be used to verify these predictions. Effective fluid films can be established which are only a few microns thick.

If the bearing surfaces remain rigid, the process by which fluid films are entrained is known as hydrodynamic lubrication. The lubrication of human finger joints by a hydrodynamic mechanism has been considered (Pagowski et al, 1976). However, when the film pressures are large enough to deform the surfaces the region of contact (close surface proximity) is increased. This reduces the film pressures required to balance the applied load. As a result lubricant can be drawn between the surfaces at higher loads or lower velocities than in hydrodynamic lubrication. This mechanism is called elastohydrodynamic lubrication and is depicted in Figure 2.4.2. The possibility of elastohydrodynamic lubrication of this type occurring in synovial joints has also been examined (Dintenfass, 1963; Tanner, 1966; Higginson, 1978; Dowson, 1967, 1980).

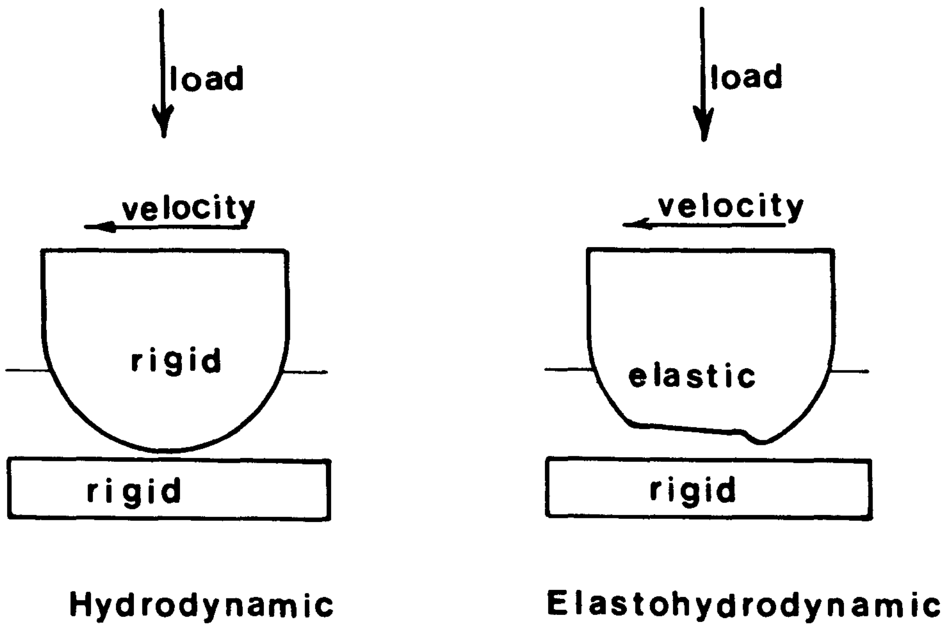

Figure 2.4.2 : A comparison between hydrodynamic and elastohydrodynamic lubrication.

During in vivo activities such as walking, the relative surface velocities are zero for the instants at which the directions of surface motion are reversed. When low or zero velocities occur the fluid film which may have been built up during the higher velocity periods is sqeezed out from between the surfaces as shown in Figure 2.4.3. A high lubricant viscosity extends this process so that films may remain until the surface velocity increases again and more lubricant is entrained between the surfaces. The surface deformation plays an additional role in trapping fluid within the contact region by being less deformed at the periphery as shown in Figure 2.4.3. Squeeze film behaviour has been studied in some detail for synovial joint models (Fein, 1967; Higginson and Norman, 1974a, 1974b; Gaman et al, 1974; Rhode et al, 1976, 1979; Rybicki et al, 1978, 1979).

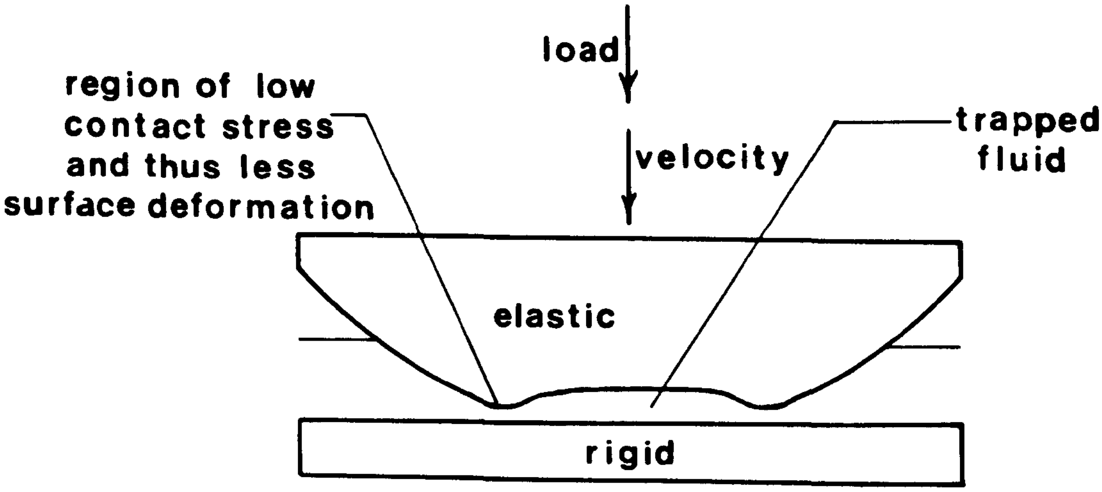

Figure 2.4.3 : Elastohydrodynamic sqeeze film behaviour.

Complete analytical or experimental proof of the existence of adequate fluid films in synovial joints during common in vivo activities has not been achieved. However, current analytical estimates suggest that elastohydrodynamic films are not quite thick enough to prevent surface asperity interactions (Dowson, 1980; Marnell and White, 1980). Experimental work with cadaveric hip joints under in vivo load and velocity patterns have suggested that fluid films exist (O'Kelly et al, 1978) but mechanisms other than elastohydrodynamic may have helped to produce them. In another recent study, statically-loaded cadaveric joints were frozen and sectioned to reveal fluid films much thicker than those predicted by current elastohydrodynamic theory (Terayama et al, 1980).

A number of features of synovial joints have obvious beneficial effects on their potential to develop elastohydrodynamic films. The deformation of cartilage and menisci by definition enhances film formation. The joint geometry is important in creating the required converging-diverging surfaces and in helping to reduce the required film pressures by encouraging large contact areas.

The previously mentioned possibility of slightly smaller radius of curvature for the concave compared with the convex surface may play an important role in enhancing fluid entrapment during squeezing actions. High synovial fluid viscosity would enhance elastohydrodynamic lubrication during both sliding and squeezing. The higher viscosity of synovial fluid at low shear rates may play an enhancing role during squeezing actions (Piotrowski, 1975). On the other hand, gross surface roughness would break up fluid film formation and allow intimate level surface contact. A number of more subtle effects may also contribute to the development of elastohydrodynamic lubrication in synovial joints. Some of these are discussed in the next section as separate mechanisms.

Special Thin Film Lubrication Mechanisms:

Two enhancing mechanisms, which depend to some extent on cartilage porosity, may occur in very thin film lubrication of synovial joints. The first, weeping lubrication, proposes that, once some of the opposing cartilage surface asperities begin to touch, interstitial fluid is expressed from the cartilage into the gap between the cartilage surfaces as shown in Figure 2.4.4 (Lewis and McCutchen, 1959; McCutchen, 1962, 1967, 1969, 1978). Thus more fluid is available for lubrication purposes. This theory further postulates that the contacting asperity tips are protected by boundary lubrication and this concept is discussed in a later section. Weeping lubrication has been criticised on the grounds that the amount of fluid expressed may not be significant (Higginson and Norman, 1974).

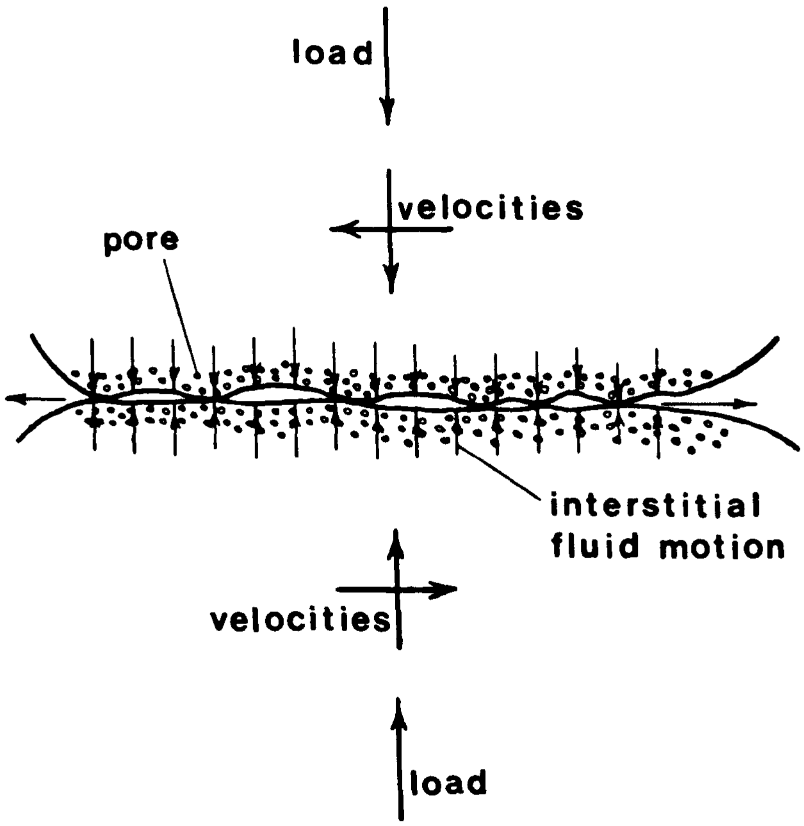

Figure 2.4.4 : Weeping lubrication of synovial joints.

Boosted lubrication, the second mechanism, proposes an alternative behaviour in which fluid passes into the cartilage and laterally between the contacting asperities. The process involves a filtering of synovial fluid films in which the water and small solute components may be forced into the cartilage or laterally out of the contact zone leaving an increased concentration of hyaluronate macromolecules as shown in Figure 2.4.5. (Dowson et al, 1968, 1970; Walker et al, 1968, 1969, 1970; Longfield et al, 1969), The concentrated fluid in the contact zone is postulated to have a much higher viscosity and this enhances fluid film lubrication. This theory also includes the possibility that the filtering occurs through absorbed surface layers of hyaluronate macromolecules (Unsworth, 1972).

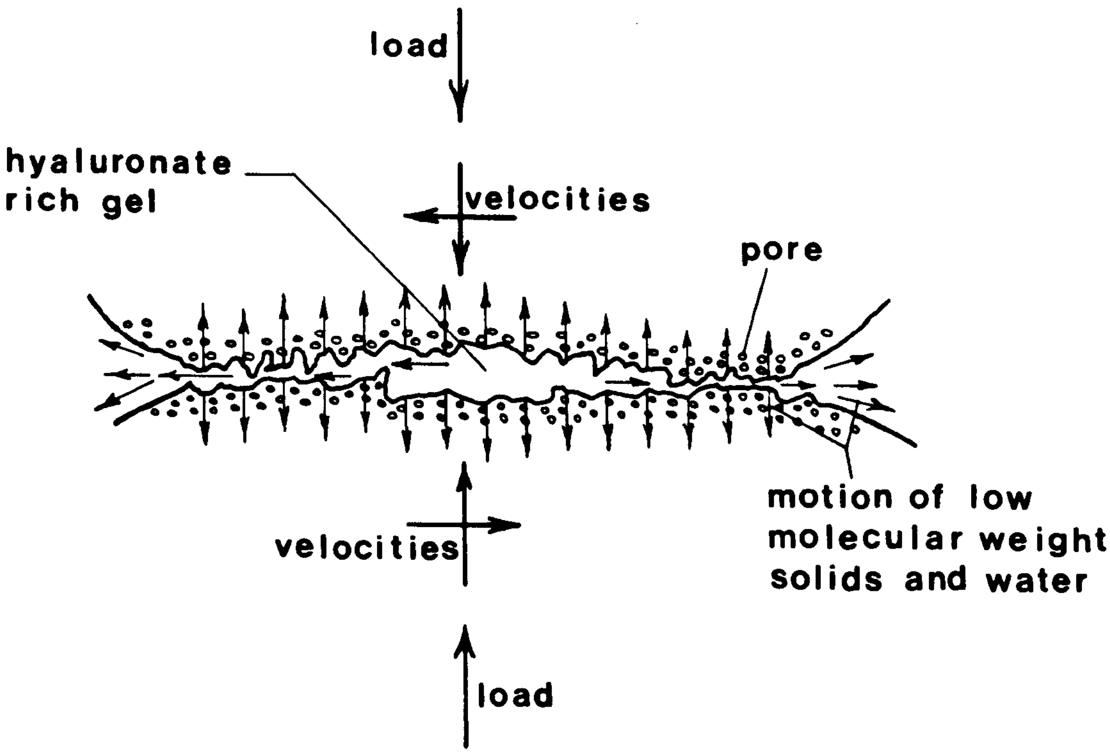

Figure 2.4.5 : Boosted lubrication of synovial joints.

Boosted lubrication has been criticised on the grounds that the calculated film thicknesses are too large for lateral filtering through the surface asperities or for filtering through cartilage to occur (Maroudas, 1979). However, when small cartilage specimens were used in friction experiments and quickly frozen at a time when boosted lubrication theory predicted thick films, such films were observed subsequently using scanning electron microscopy (Walker et al, 1970; Walker and Gold, 1973).

Recent analytical work has suggested that fluid may flow into cartilage at some locations and out of cartilage at other locations within a joint (Ling, 1974; Mansour and Mow, 1977). If so, both boosted and weeping lubrication may occur simultaneously. However, the fluid flow into or out of cartilage is slow compared to physiological loading times and thus may not be a particularly effective mechanism for the lubrication of synovial joints (Higginson, 1978).

A very recent theory, which has not been investigated experimentally, proposes a mechanism by which fluid viscosities higher than those of the bulk lubricant may exist in thin films. Micropolar lubrication models (Allen and Kline, 1971) have been applied to synovial joints (Tandon and Jaggi, 1979). Essentially the theory suggests that the hyaluronate macromolecules tend to spin in a synovial fluid film and this spin is inhibited by the close proximity of the cartilage surfaces. The result is that the effective viscosity is increased in these thin films and this leads to enhanced fluid film lubrication. This concept is illustrated in Figure 2.4.6 along with a possible extension of the theory which predicts that when the cartilage surfaces are moving, the macromolecules may migrate towards them. Such motion of particles to the high velocity regions has been observed in blood flow (Goldsmith, 1971). If this particular mechanism does occur it might contribute to the build up of hyaluronate surface layers which would further increase thin film viscosities.

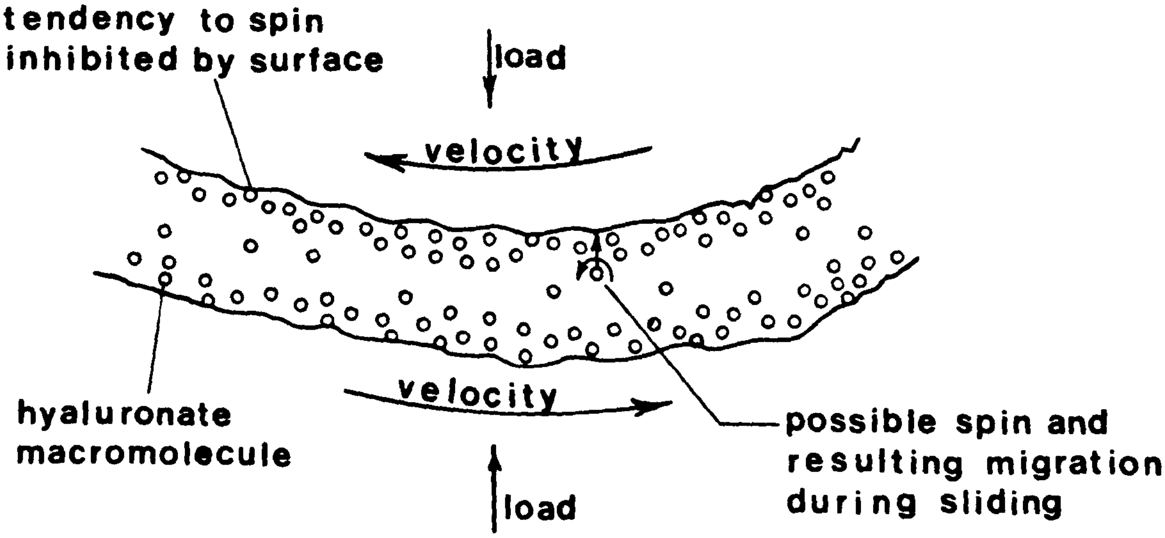

Figure 2.4.6 : Micropolar lubrication of synovial joints.

Boundary Mechanisms:

Boundary lubrication involves the sliding and shearing of adsorbed layers on the surfaces. The adsorbed layers thus protect the underlying surfaces and maintain low friction. This mechanism is illustrated in Figure 2.4.7.

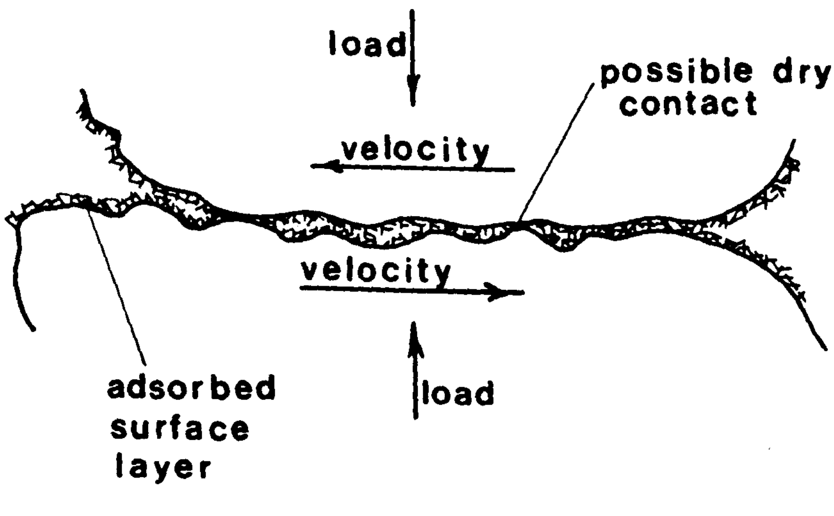

Figure 2.4.7 : Boundary lubrication of synovial joints.

The protein elements in synovial fluid appear to be directly involved in boundary lubrication by attaching themselves to the cartilage surfaces (Linn and Radin, 1968; Wilkins, 1968; Radin et al, 1970c, Swann, 1978; Davies et al, 1979, 1979). Hyaluronate macromolecules (Maroudas, 1967, 1969, 1979) and water molecules (Davies et al, 1979) may also contribute to the surface layers. These layers appear to have internal repulsive electrostatic forces (Roberts, 1971) which create osmotic pressure (McCutchen, 1966; Davies et al, 1979) capable of resisting compression. It has also been suggested that fat within the cartilage may act as a boundary lubricant (Little et al, 1969).

Concluding Remarks on Lubrication Mechanics:

Studies of friction in cadaveric hip joints using cyclic time varying loads and velocities suggests that fluid film lubrication predominates (O'Kelly et al, 1978). Other plausible, though sometimes conflicting, lubrication mechanisms have been suggested. It would appear that the lubrication of synovial joints is a complex process involving a number of mechanisms. Furthermore, it is unlikely that one particular mechanism or combination of mechanisms will operate universally as the loading and sliding conditions are changing continuously in synovial joints. Thus synovial joint lubrication remains an enigma in spite of considerable research effort.

2.5 CONCLUDING REMARKS ON THE MECHANICS OF NORMAL SYNOVIAL JOINTS:

Each mechanism proposed for the various aspects of synovial joint function has been discussed in physical and anatomical terms. Further insight can be gained by considering the major anatomical features of synovial joints and mentioning, for each feature, a number of associated mechanisms.

The size and trabecular structure of the subchondral bone mass aids in spreading transmitted forces. In addition, the large deflections which result from in vivo loading have suggested that subchondral bone is the major shock absorbing tissue in synovial joints.

The articular cartilage layers have low elastic moduli, which allow enough deformation to create large contact areas. In load transmission these contact areas ensure that the contact stresses are maintained at reduced levels. Also, fluid film lubrication is enhanced by large contact areas. The fluid flow within and across the surface of cartilage produces viscoelastic behaviour which may further increase contact areas when high loads are imposed for long periods of time. Fluid flux across cartilage surfaces may contribute to lubrication by boosted or weeping mechanisms. Also, the internal fluid flow, along with the reinforcing collagen fibre network, may act to reduce stress concentrations within cartilage.

Synovial fluid contains protein molecules which are adsorbed onto the cartilage surface and apparently act as a boundary lubricant. The bulk viscosity of synovial fluid is proportional to its concentration of large hyaluronate macromolecules. In thin film flow the concentration of hyaluronate macromolecules may increase resulting in high apparent viscosities. If this occurs fluid film lubrication becomes plausible for a wider range of activities in vivo.

The opposing articular surfaces of synovial joints have slightly different curvatures. In the hip joint, the concave surface apparently has a smaller radius of curvature than the convex surface. This geometry may help to reduce the maximum contact stresses during high loading and to extend the duration of elastohydrodynamic squeeze films which act in synovial joints. The surface incongruity also ensures that regions of converging-diverging geometry exist which provides favourable conditions for fluid film lubrication during sliding.

The experimental verification of the various load transmission and lubrication mechanisms presents immense difficulties. In a living synovial joint there is likely to be a certain tolerance of abnormal motion and loading. Ultimately, studies of the gradual failure processes in synovial joint tissues may determine the clinical relevance of the numerous mechanisms described.

CHAPTER 3

SURFACE GEOMETRY OF THE ANKLE JOINT

3.1 INTRODUCTION

The components of synovial joints and the mechanics of their interactions are described in some detail in the previous chapter. While recognizing that all synovial joints have similar features, the study of the human ankle joint in particular must include some knowledge of the local anatomy.

The bones in the vicinity of the ankle joint are shown in Figures 3.1.1 and 3.1.2. The ankle joint, sometimes referred to as the talocrural joint, permits rotation of the foot in a posterior-anterior plane of vertical orientation. In other words, the simultaneous raising of the toes and lowering of the heel involves flexion of the ankle joint. The side-to-side motion of the foot, or rotation in a medial-lateral plane of horizontal orientation involves the subtalar joint between the talus, navicular and calcaneus bones. The combined motion of the ankle joint and the subtalar joint is analogous to the action of a universal joint. Many activities, including walking, involve this combined motion (Hicks, 1953; Morris, 1977).

Not only do the ankle and subtalar joints move simultaneously, they also have a common ligamentous structure as illustrated in Figures 3.1.3 and 3.1.4. Some of the ligament bands connect tibia and fibula to the talus, while others bypass the talus and connect with the calcaneus and navicular bones.

The ankle joint itself is composed of three pairs of articulating surfaces between:

i) medial malleolus and talus

ii) tibia and talus

iii) lateral malleolus and talus.

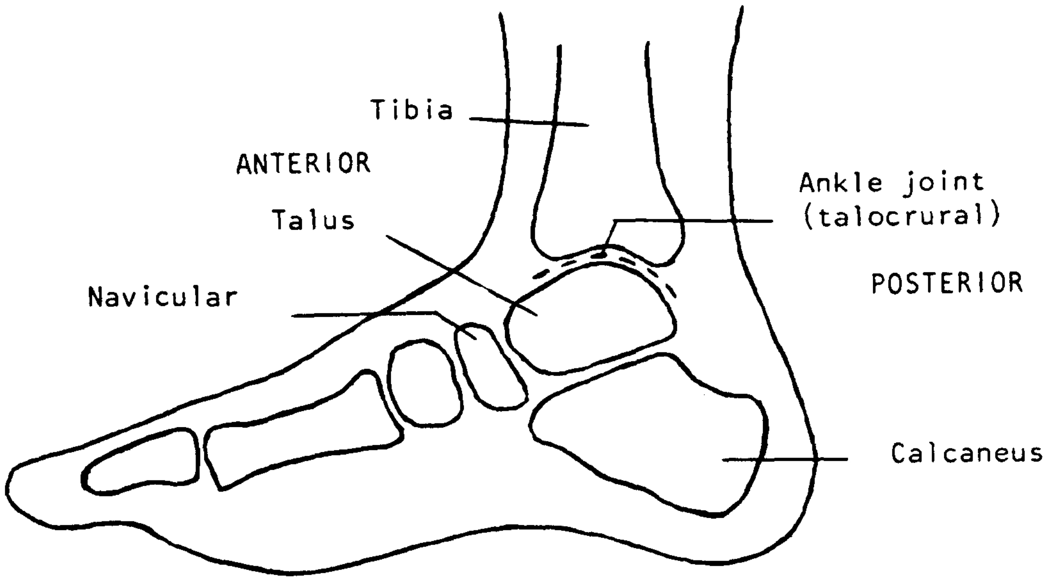

Figure 3.1.1 : Sagittal section of the foot showing bone structure.

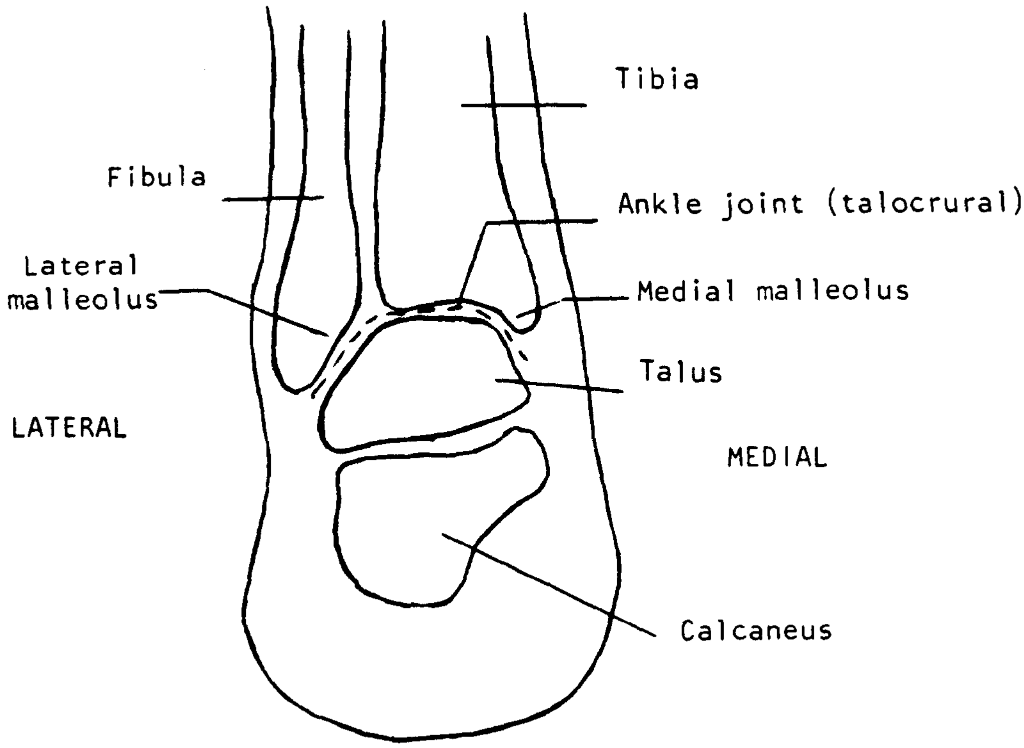

Figure 3.1.2 : Frontal section through the ankle showing bone structure.

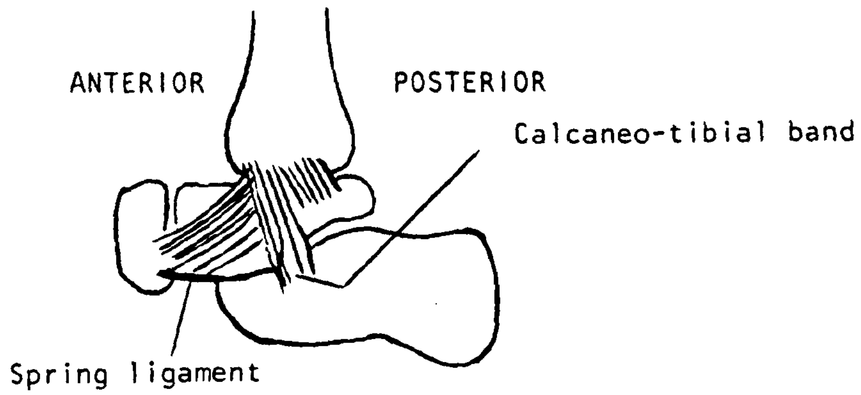

Figure 3.1.3 : Medial ligament of the ankle.

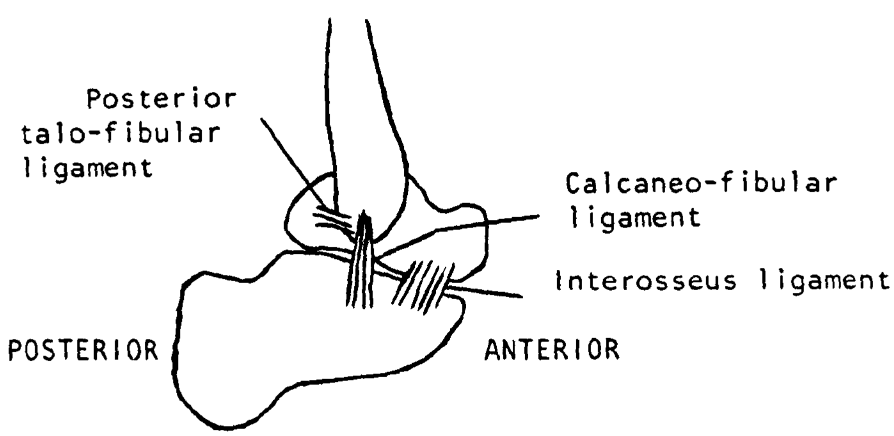

Figure 3.1.4 : Lateral view of the ligaments of the ankle.

The lateral malleolus, formed by the distal end of the fibula, is held in place against the tibia by an interosseus ligament as shown in Figure 3.1.5. This ligament provides some compliance to the lateral constraint imposed by the lateral malleolus on the talus. The articulation between the lateral malleolus and the talus transmits a portion of the normal load on the ankle joint. However, most of the load is transmitted through the tibia-talus articulation (Lambert, 1971).

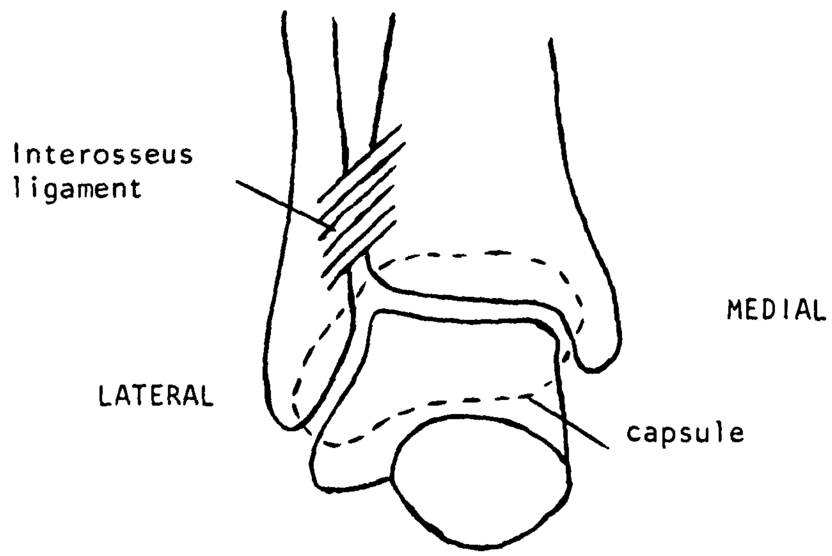

Figure 3.1.5 : Anterior view showing the ankle joint capsule and the interosseus ligament connecting the fibula to the tibia.

A normal ankle joint with the various connecting tissues dissected away is shown in Figure 3.1.6. The articulation between tibia and talus appears at first glance to be simply a contact between two congruent cylindrical surfaces of finite width. However, the talus surface has been described qualitatively by Barnett and Napier (1952) as having three radii of curvature as shown in Figure 3.1.7. This suggests that a changing centre of rotation may occur during ankle joint flexion.

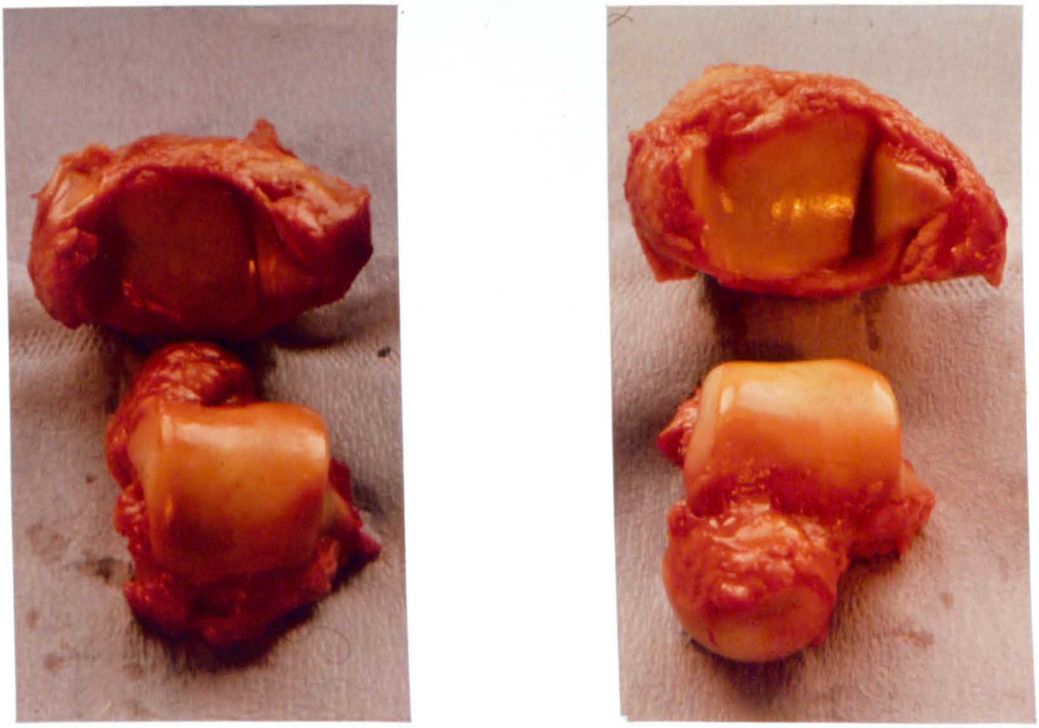

Posterior view Anterior view

Figure 3.1.6 : A dissected human ankle joint. (Joint number I of Table 3.2.1).

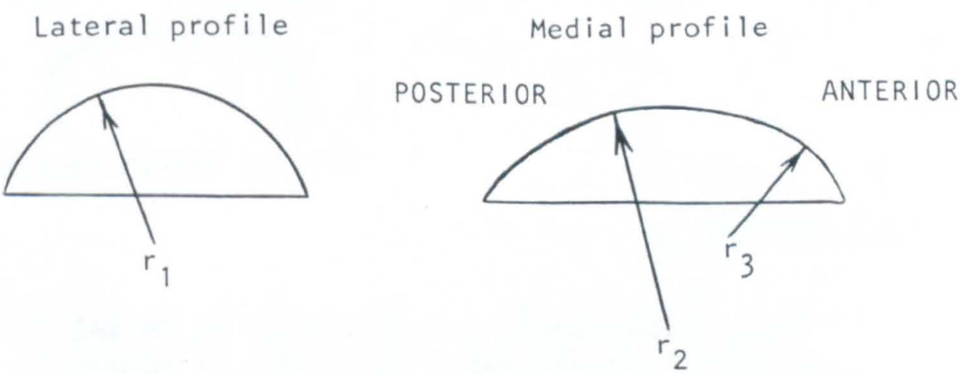

Figure 3.1.7 : Talus surface curvatures according to Barnett and Napier (1952).

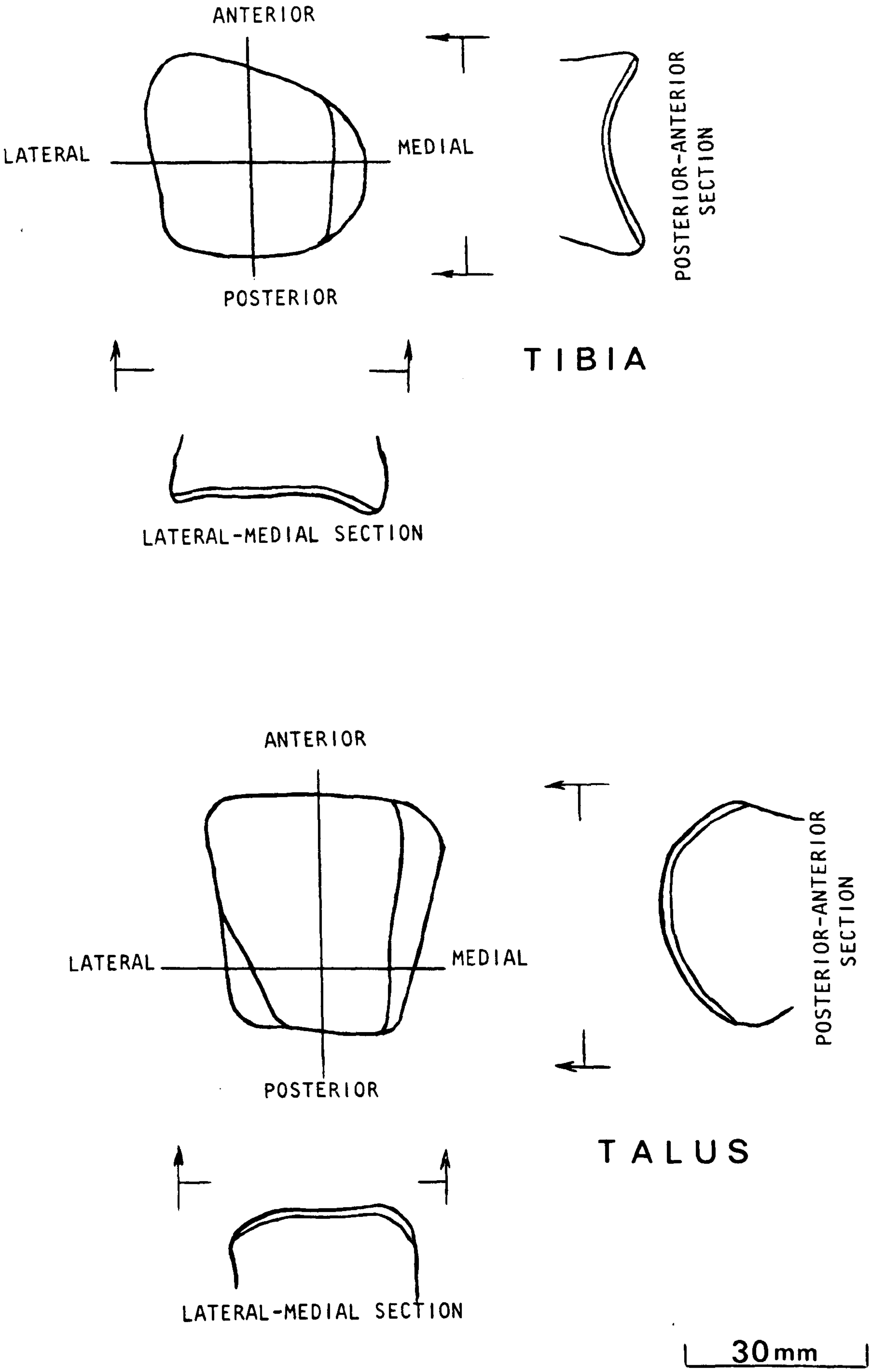

Figure 3.2.3 : Sketch of surface dimensions of ankle joint number 11 (top view, approximately to scale).

Instantaneous centres of rotation have been measured for normal ankles under weight bearing conditions by a number of research groups (Sammarco et al, 1973; Ambrosia et al, 1976; Partasca et al, 1979; Rastegar et al, 1980). In all these investigations the location of the instantaneous centres moved by about 10 mm during ankle flexion. The apparent congruity of the tibia-talus articulation has been challenged by Greenwald et al (1976). They found that under low loads, up to 25 percent of the peak load during walking, separate medial and lateral contact areas exist. As the load was increased these areas merged to give contact over most of the tibial surface.

A number of prosthetic joints have been designed for the human ankle (Kempson et al, 1975; Stauffer, 1976; Pappas et al, 1976). Each of these designs replace the natural geometry with congruent cylindrical surfaces. This gives a single axis of rotation for the prosthetic ankle yet does not appear to affect the gait of the patient.

The functional success of the prosthetic ankle has some important implications. It is apparent that the ligament structure, which is retained in the joint replacement procedure, does not impose motion much different from a fixed axis rotation during walking. Thus, the changing instantaneous centres of rotation for the natural ankle are likely to be caused by the surface contours rather than imposed ligament constraints. Furthermore, these changing centres do not appear essential for normal walking.

The determination of detailed three dimensional characteristics of synovial joint surfaces is a complex procedure. Recently

Scherrer and Hillberry (1979) applied a surface fitting procedure using a network of "patches" to a joint surface. They intended to combine this procedure with mathematics involving spatial linkages to study the relative positions of the joint surfaces during motion.

The purpose of the present study is to evaluate geometrical parameters for both the theoretical and experimental investigation of ankle joint lubrication. Current models of synovial joint lubrication for complete joints under typical in vivo conditions involve many approximations (Dowson, 1980). Thus, it is felt that the following simplifying assumptions can be made without losing the essential geometrical characteristics of ankle joint lubrication:

i) Only the tibia-talus articulation is considered.

ii) The motion is considered to be rotation in a single posterior-anterior plane of approximately vertical orientation.

iii) The central regions of the contact areas have circular profiles when considered in planes parallel to the direction of motion.

The present study uses dissected human specimens. It includes the results from measuring surface curvature and sectioning to examine cartilage thickness.

3.2 Dissection of the Joint Specimens:

Eight ankle joint specimens were dissected in the present study. These specimens were obtained from amputations for severe vascular disease. The operations were performed at Leeds General

Infirmary. As such, the group of patients involved may not have been as active as the general population, especially in the latter stages of the vascular disease. The specimens were collected immediately following amputation and frozen intact until required for dissection. More specific details are given in Table 3.2.1, including the labelling of each joint by number.

Joint	Age (years)	Sex	Body Weight (N)	Comments
I				normal
II				normal
III				pathological
IV	66	Male	510	pathological
V	59	Male	687	pathological
1	48	Male	711	normal
2	52	Male	—	normal
3	67	Female	696	normal

Table 3.2.1 : Details of the ankle joint specimens.

The dissection procedure involved a systematic removal of the soft tissues surrounding the ankle joint. This was performed using a standard scalpel (with frequent blade changes), tweezers and self-gripping clamps. In some cases surgical scissors were used to remove tissue from the edges of the cartilage layers. A bone saw or chisel was used to remove bone in the final stages of the dissection. Surgical gloves were worn at all times to avoid the possibility of contacting disease from the specimens. Physiological saline solution (0.9% NaCl) was available for soaking the joint surfaces to prevent dehydration. The equipment used for dissection is shown in Figure 3.2.1.

The procedure itself began with an incision through the soft tissues surrounding the subtalar joint as shown in Figure 3.2.2. The lower portion of the foot was detached from the talus by cutting all the ligaments attached to the navicular and calcaneus bones. Next the soft tissues surrounding the tibia and fibula were removed. At this point, the talus was still held in place by the posterior talo-fibular ligament and some bands of the medial ligament. The talus was then separated from the tibia and fibula. Upon separation the joint surfaces were covered with tissue paper soaked in saline solution. The interosseus ligament, connecting fibula to tibia, was then severed and the fibula discarded.

The final stage of the dissection involved removing as much tissue as possible from the talus and tibia, excluding the cartilage itself. A test tube clamp attached to a retort stand was often used to hold the joint segments. This stripping of tissue promoted firm fixation when the bones were eventually mounted in tubular holders using plaster of Paris as a fixing agent. For the mounting, it was necessary to trim some part of both the tibia and the talus which were not involved in the ankle articulation.. This was accomplished using a bone saw or chisel.

Throughout the latter part of the dissection procedure, it was considered particularly important to keep the joint surfaces covered with tissue paper soaked in physiological saline solution at all times. This avoided the possibility of structural damage to the cartilage caused by dehydration.

Figure 3.2.1 : The equipment used for the joint dissection.

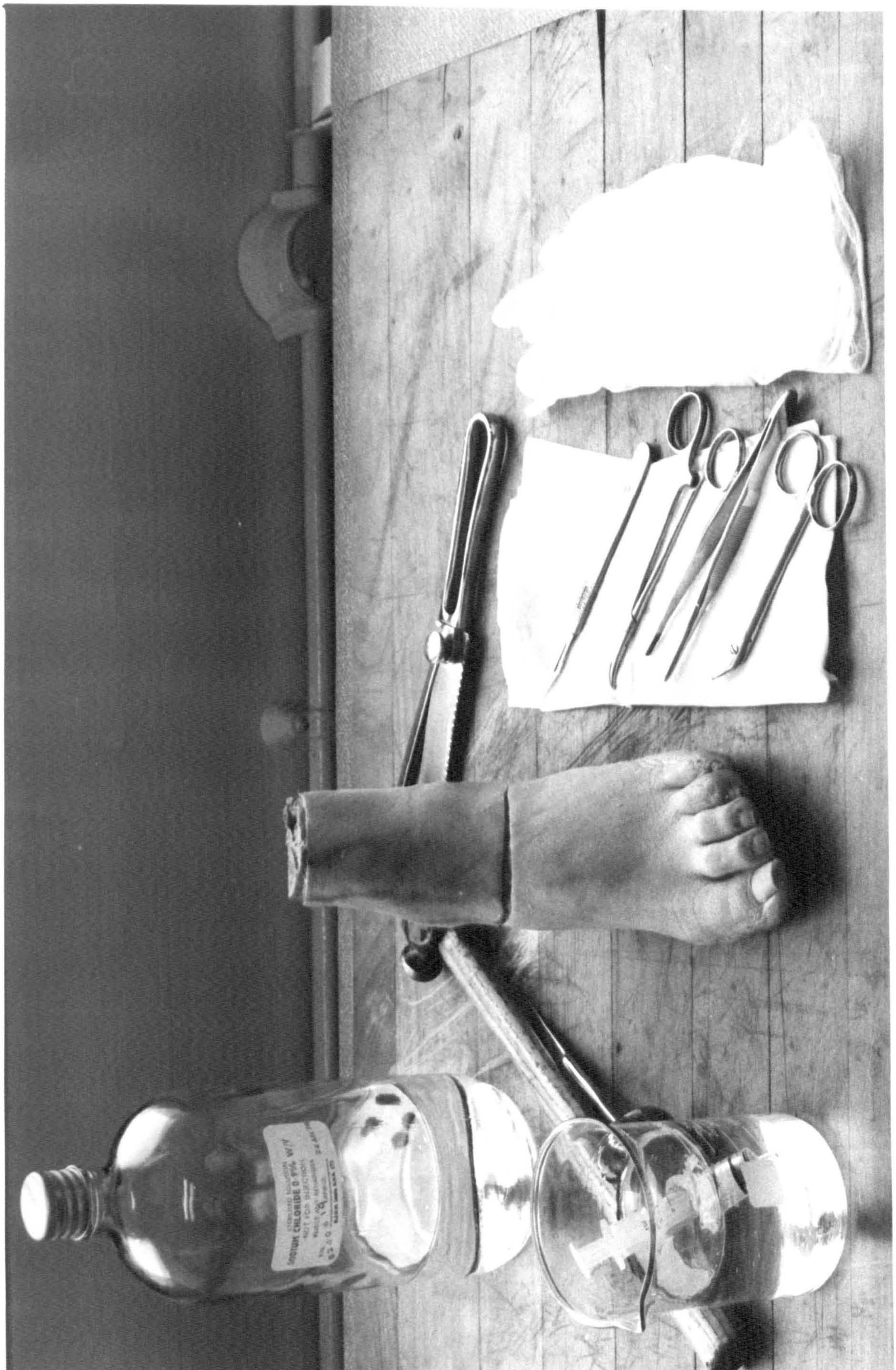

SODIUM CHLORIDE 0·9% W/V

Figure 3.2.2 : The initial incision through the soft tissues for the joint dissection.

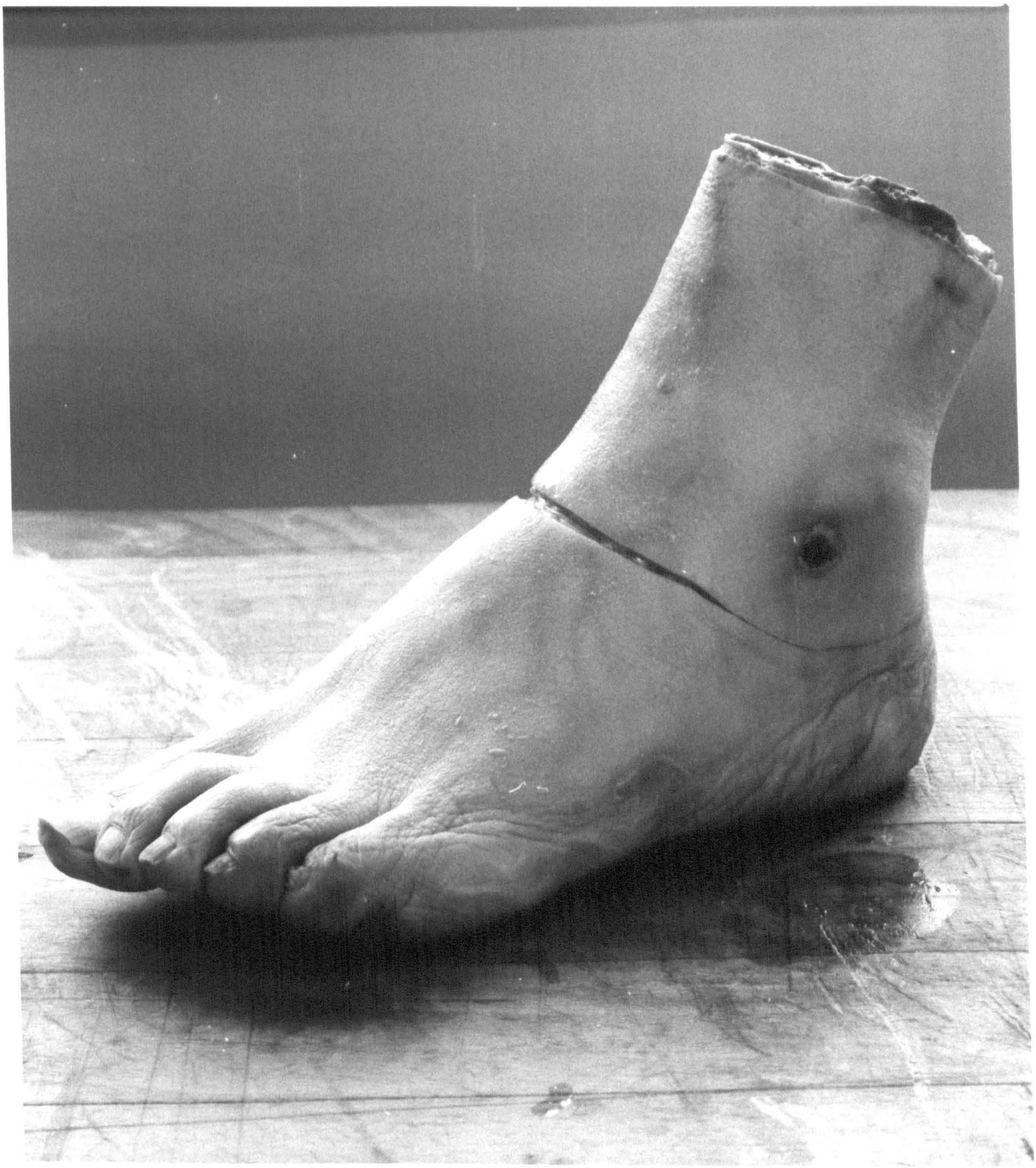

Joint numbers I and II were used for preliminary trials to develop the technique. Figure 3.1.6 of the previous section shows ankle joint number I with fibula still attached to the tibia. The surface dimensions and features of joint number II were recorded in an approximate fashion as shown in Figure 3.2.3.(see pg. 48)

Joint numbers III, IV and V all showed visual evidence of various amounts of pathological surface damage as illustrated by Figures 3.2.4, 3.2.5 and 3.2.6, respectively. The extensive white deposits on the surface of joint number IV completely destroyed the slippery nature of the cartilage surface. This condition apparently did not affect the subtalar joint since it retained a normal surface appearance.

These damaged joints were excluded from the present study of normal ankle joint geometry. They are shown in Figures 3.2.4, 3.2.5 and 3.2.6 for general interest. One observation of some relevance to the present study concerns the parallel scars torn in the surfaces of the joints shown in Figures 3.2.4, 3.2.5 and 3.2.6. These scars appear to be caused by abrasive action during motion. The orientation of some of the scars formed reasonably straight parallel lines when examined in plan view. This suggests that little rotation of the talus about the long axis of the tibia occurred in vivo.

In the present study, joints numbered 1, 2 and 3 were used in a detailed measurement procedure. The cartilage surface of these joints had a smooth shiny appearance similar to that revealed previously by Figure 3.1.6. It was assumed that these joints were normal and healthy enough to provide typical geometrical parameters.

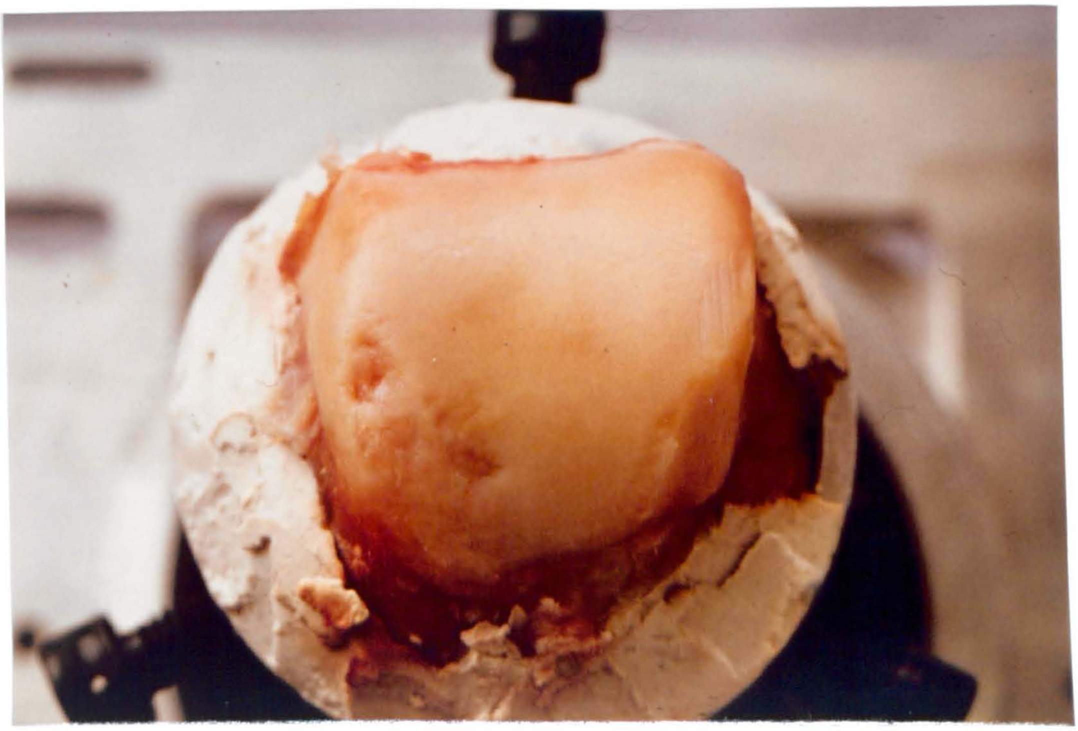

Figure 3.2.4 : Surface appearance of joint number III

Figure 3.2.5 : Surface appearance of joint number IV

Figure 3.2.6 : Surface appearance of joint number V

3.3 Alignment of the Joint Components

Before the surface features of joints numbered 1, 2 and 3 were measured, the talar and tibial components of each were aligned. The orientation of the co-ordinate axes shown in Figure 3.3.1 was chosen for these joints, all of which were left ankles. The alignment technique involved mounting both talus and tibia in tubular holds as shown in Figure 3.3.2 The talus was penetrated by a self-tapping screw attached to a solid metal cylinder. The metal cylinder was gripped by three screws which acted through tapped holes in the wall of the tubular holder. Only two of these screws are revealed by the longitudinal section of Figure 3.3.2. The tibial component was held in a tubular holder of shorter length than the holder for the talus. The internal surface was slightly tapered and once again three screws acted through tapped holes in the tube wall. However, in this case, the shaft of the tibia was gripped directly by the screws. For joint number 2 a screw was inserted into the medullary canal of the tibia. The head of the screw was attached to a disc of larger diameter than the tabular holder. This device helped to hold the tibia in a fixed position.

With both joint components in place, small adjustments were made in their relative positions until the following conditions, illustrated in Figure 3.3.2, were achieved:

i) virtually all of the tibial surface was in nominal contact with the talus;

ii) the talus holder was aligned parallel to the z-axis;

iii) the maximum z co-ordinate for the talus surface was at the centre of its own and the tibial articulating surface with respect to the anterior-posterior length.

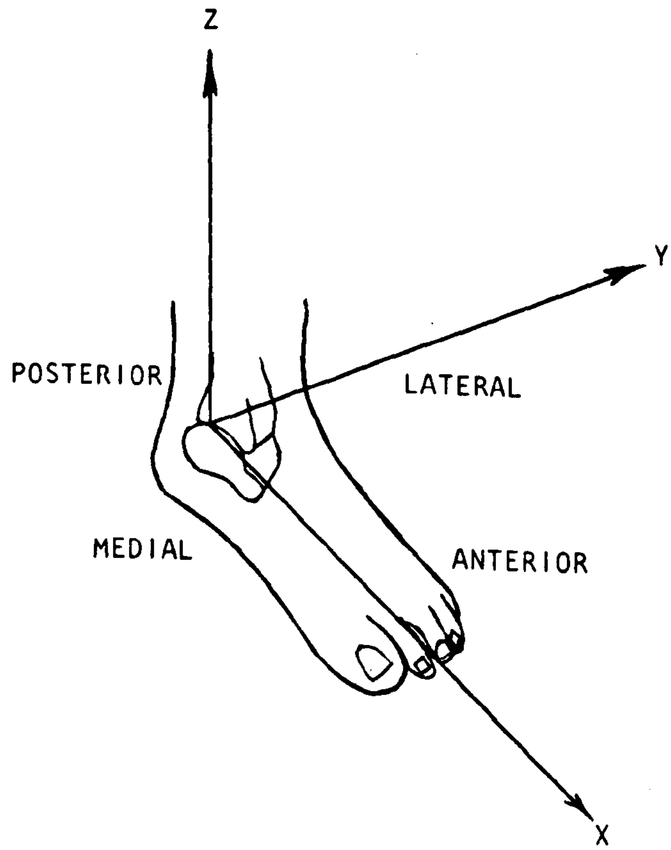

Figure 3.3.1 : The co-ordinate system for ankle joint numbers 1, 2 and 3.

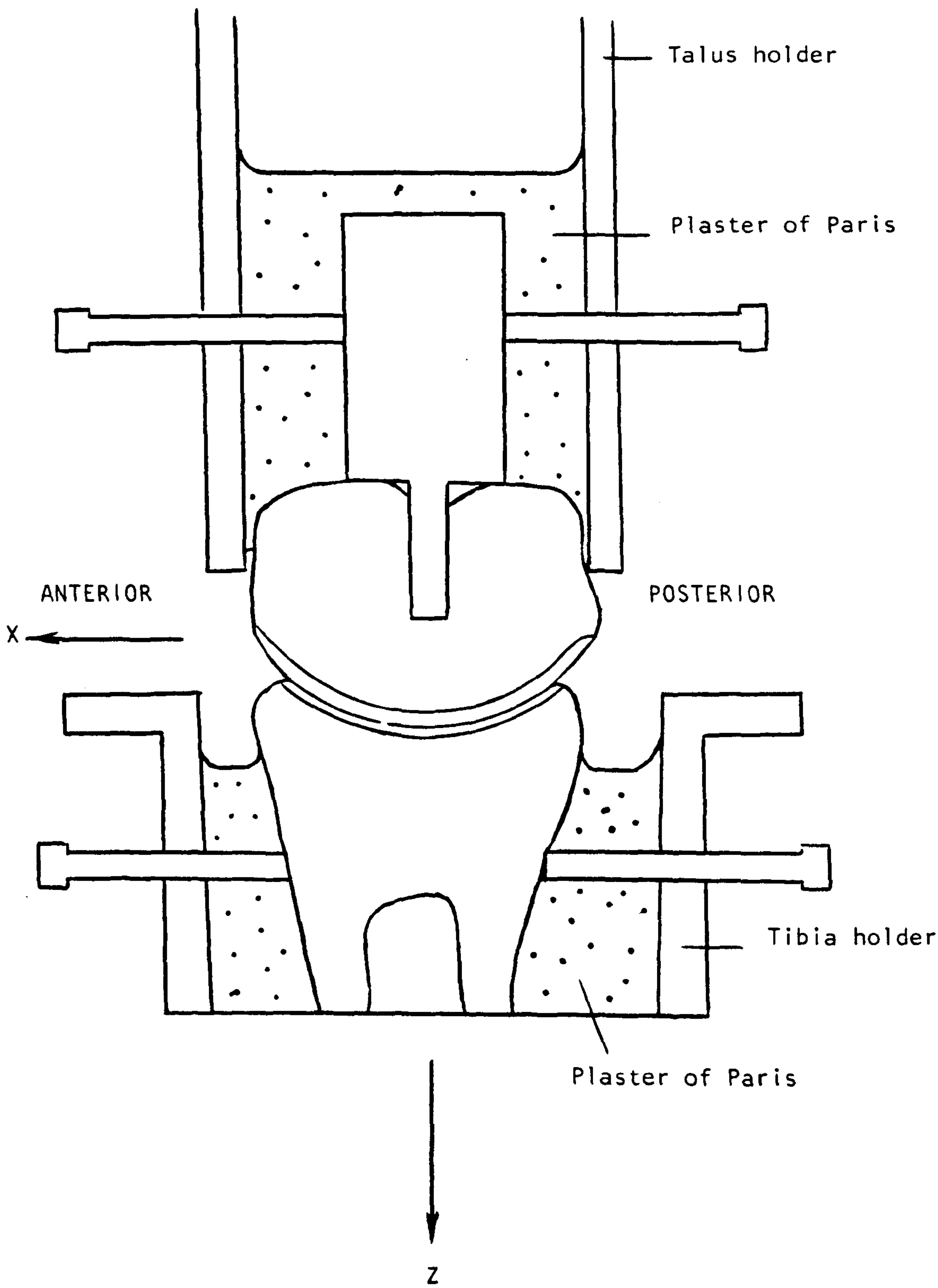

Figure 3.3.2 : Longitudinal section of the joint components in their holders.

iv) rotation of the joint yielded motion principally in the x - z plane.

This positional arrangement was accomplished by using only a set square and visual estimates. The determination of the plane of rotation was aided by the length of the talus holder (175 mm) which was moved while keeping the tibia stationary. Usually the achievement of the specified position for alignment corresponded to a vertical position for most of the talar region which articulated with the lateral malleolus.

Once the joint components were aligned both talus and tibia, including screws and fixtures, were encased in plaster of Paris. In previous trials with joint numbers I, II and III, acrylic bone cement was also employed. However, the moisture at the scraps of tissue still adhering to the bone surface caused the cement to shrink away from the interface. The resulting fixation was somewhat less than optimal. To avoid migration of stray particles onto the cartilage surfaces, a layer of self-curing silicone rubber was placed over the surface of the plaster-of-Paris.

The fixation during alignment was altered for joint number 3. Instead of using three screws to hold the tibial shaft, some thickened plaster of Paris was applied directly. The appropriate adjustments in the positions of both tibia and talus were made before the plaster of Paris could harden. Then with the tibia in the correct position, the plaster of Paris was given time to set before more was added to completely encase the tibial shaft. This procedure required more skill and familiarity with the ankle joint than the one used on joint numbers 1 and 2.

3.4 Measurement of Surface Features:

Considering the co-ordinate system defined in Figure 3.3.1, the joint components were aligned to provide rotation about a line parallel to the y-axis such that motion was in the x - z plane, predominantly in the x-direction. The true shapes of the articulating regions were somewhat irregular as shown in Figure 3.2.3. However, measurements of surface dimensions were recorded in the x - y plane as shown in Figures 3.4.1, 3.4.2 and 3.4.3. The dimensions of equivalent rectangular bearing surfaces are shown in Table 3.4.1.

Joint Number	Width in the y-direction (mm)	Length of Tibia (mm)	Length of Talus (mm)
1	27	31	38
2	26	27	34
3	26	27	34
Average	26	28	35

Table 3.4.1 : Characteristic surface dimensions.

The surface curvatures were measured along the numbered lines of Figures 3.4.1 to 3.4.3 which were oriented in the direction of motion. The lines with the same numbers on tibia and talus for a specific joint touched during articulation. This feature was achieved by carefully marking a touching point on both talus and tibia at the periphery of the contact zone. This common reference

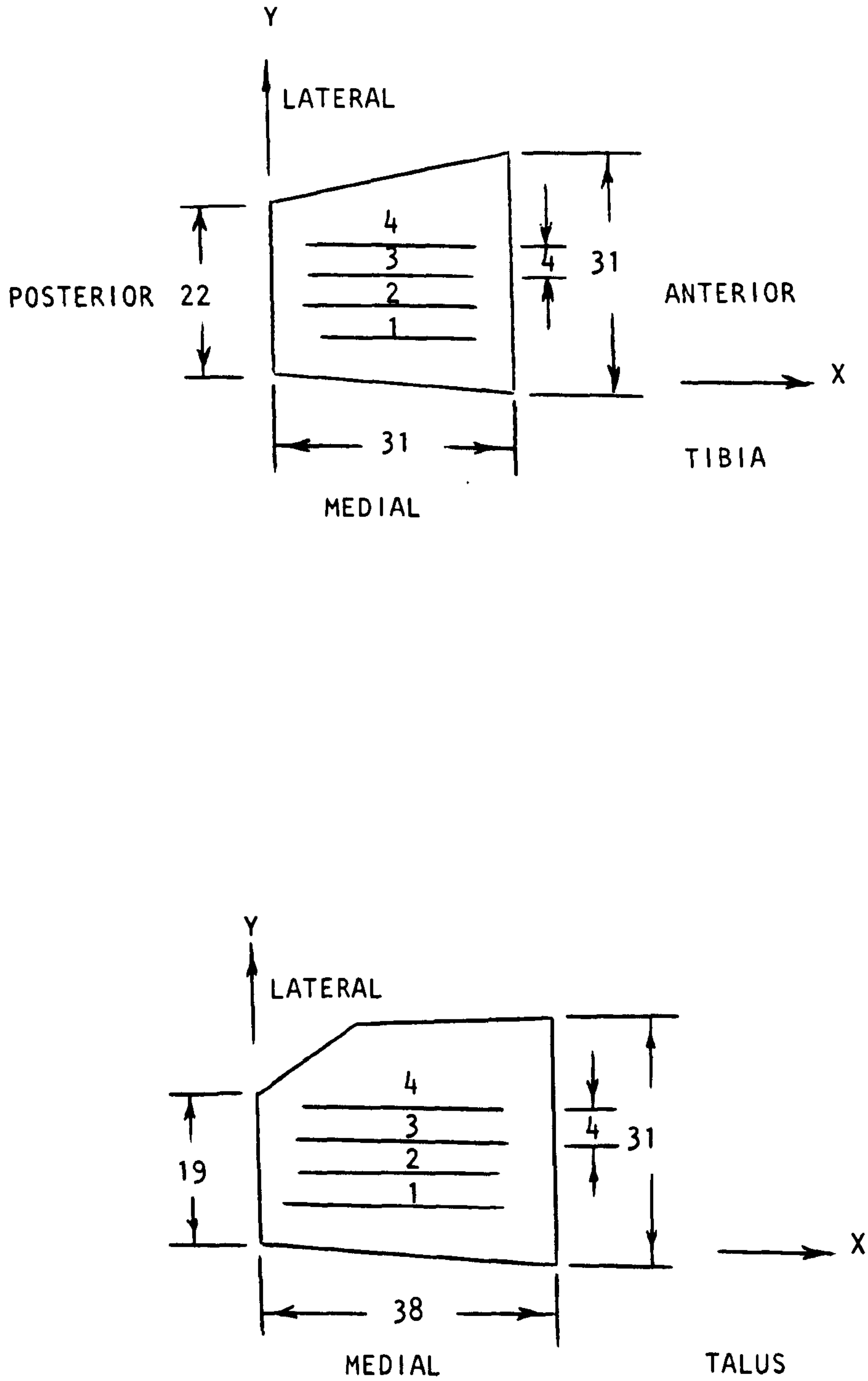

Figure 3.4.1 : Surface dimensions for joint number 1 including the lines (1, 2, 3 and 4) along which the surface profiles were measured.
All dimensions are in mm.

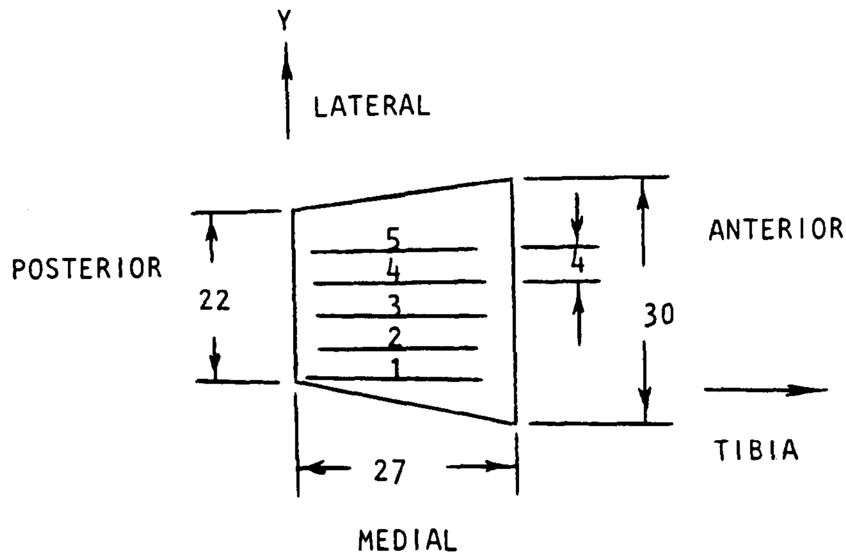

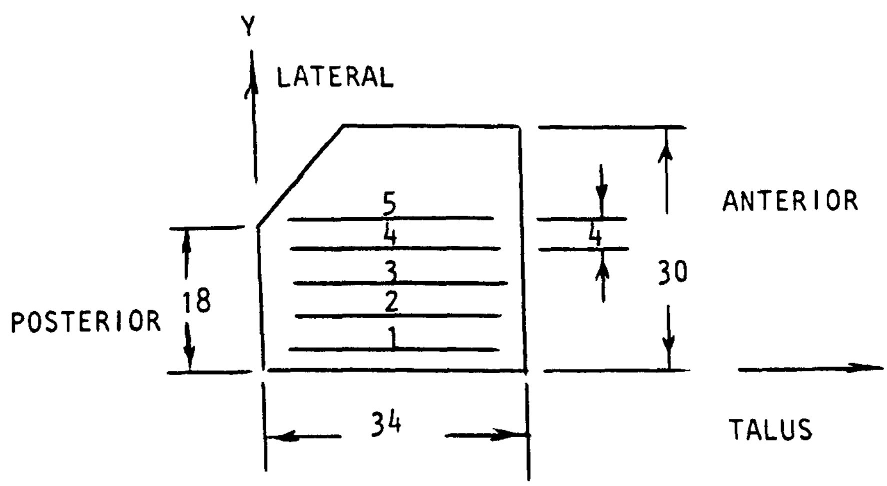

Figure 3.4.2 : Surface dimensions for joint number 2 including the lines (1, 2, 3, 4 and 5) along which surface profiles were measured. All dimensions are in mm.

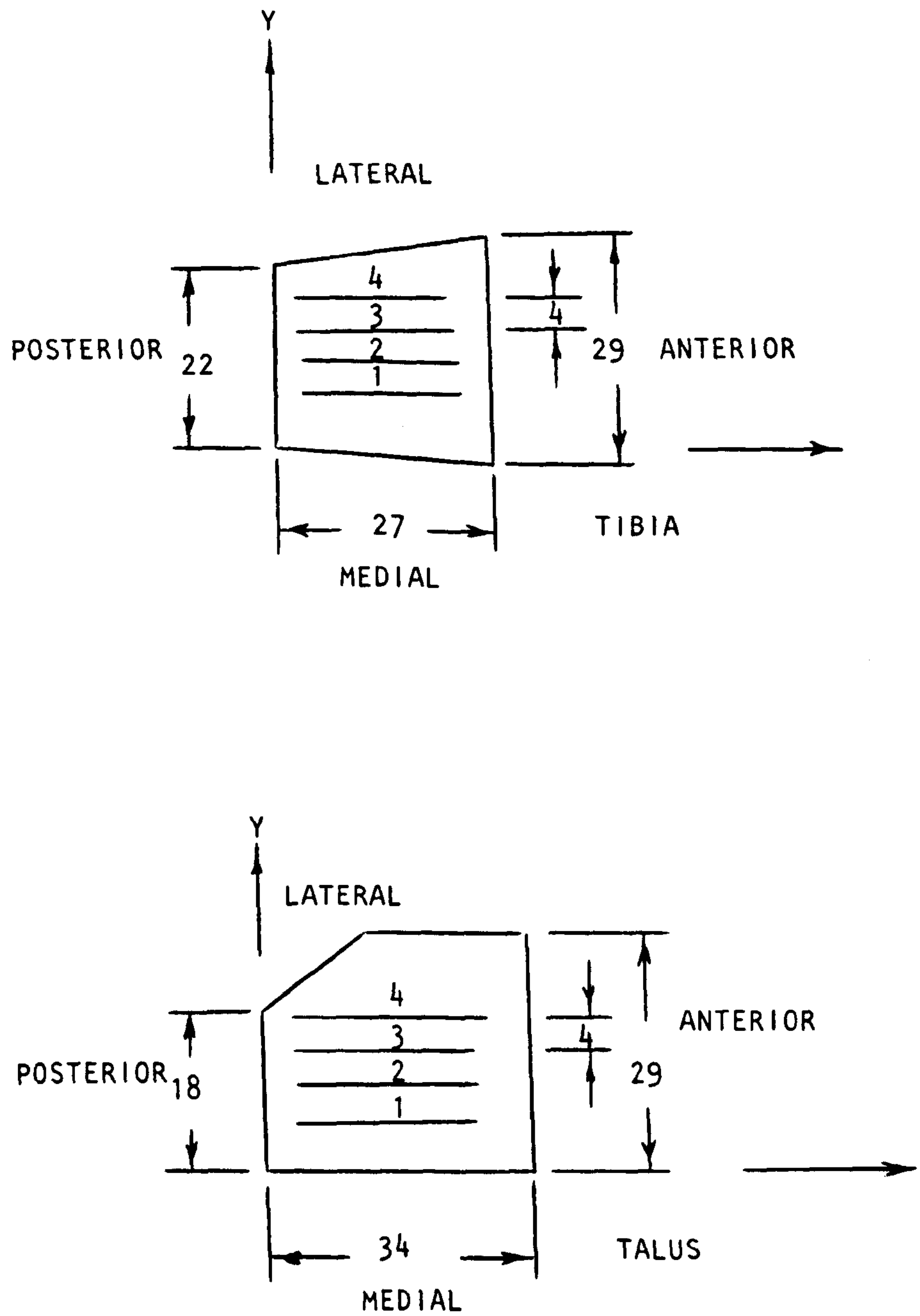

Figure 3.4.3 : Surface dimensions for joint number 3 including the lines (1, 2, 3 and 4) along which the surface profiles were measured. All dimensions are in mm.

point on each surface was extended in the direction of motion to produce two touching lines. During the surface profile measurements, the positions of the other lines were established at 4 mm spacings from the original line using a micrometer controlled specimen table.

A Talycontor instrument made by Rank Taylor Hobson was used to measure the surface profiles. This instrument uses a surface contacting pin attached to a counter-weighted stylus arm. Essentially, it is similar in principle to the more familiar Talysurf instrument, except that large rather than small scale surface features are measured. The standard pin used to contact the surface has a sharp conical point. This reduces pin tip radius effects on the measured profiles. However, a sharp pointed pin could both tear and sink into the soft cartilage surfaces thus producing inaccurate results. This danger was avoided by constructing a special pin with a precision ball glued into a spherical seating to form the tip as shown in Figure 3.4.4. With this pin, the tip radius influenced the measurements and the effect was included in the curve fitting procedure described in the next section.

The cartilage thickness was measured for joints numbered 2 and 3 at certain points along the lines used for the surface profile measurements. The technique involved marking some of these lines on the cartilage surface using a felt tipped pen. A fine-toothed hack saw was then used to cut the joint surfaces along the marked lines. Cartilage thickness was measured with a Profile Projector made by Nikon. This instrument produced an image in colour on a large circular screen, 400 mm in diameter. A photograph of the

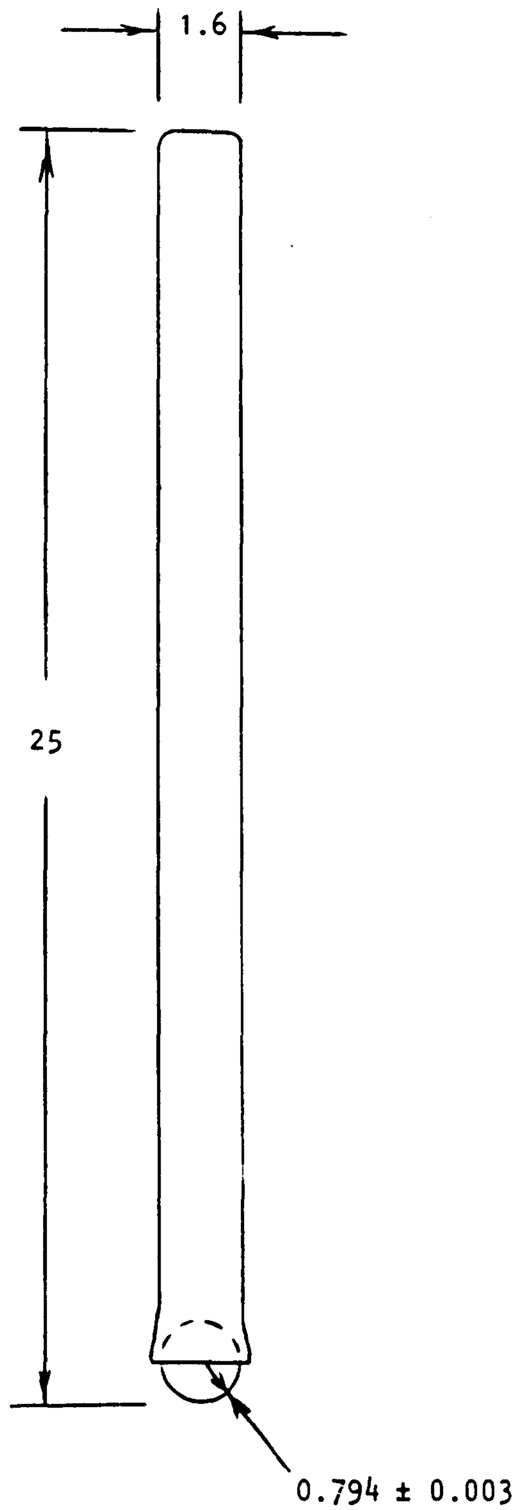

Figure 3.4.4 : The special pin made for the Talycontor. All dimensions are in mm.

screen image is shown in Figure 3.4.5. Reference lines were superimposed on the image and could be moved independently by precision micrometers. These traversing micrometers were connected to a digital display unit. Cartilage thicknesses were measured for each cross-section in a radial direction.

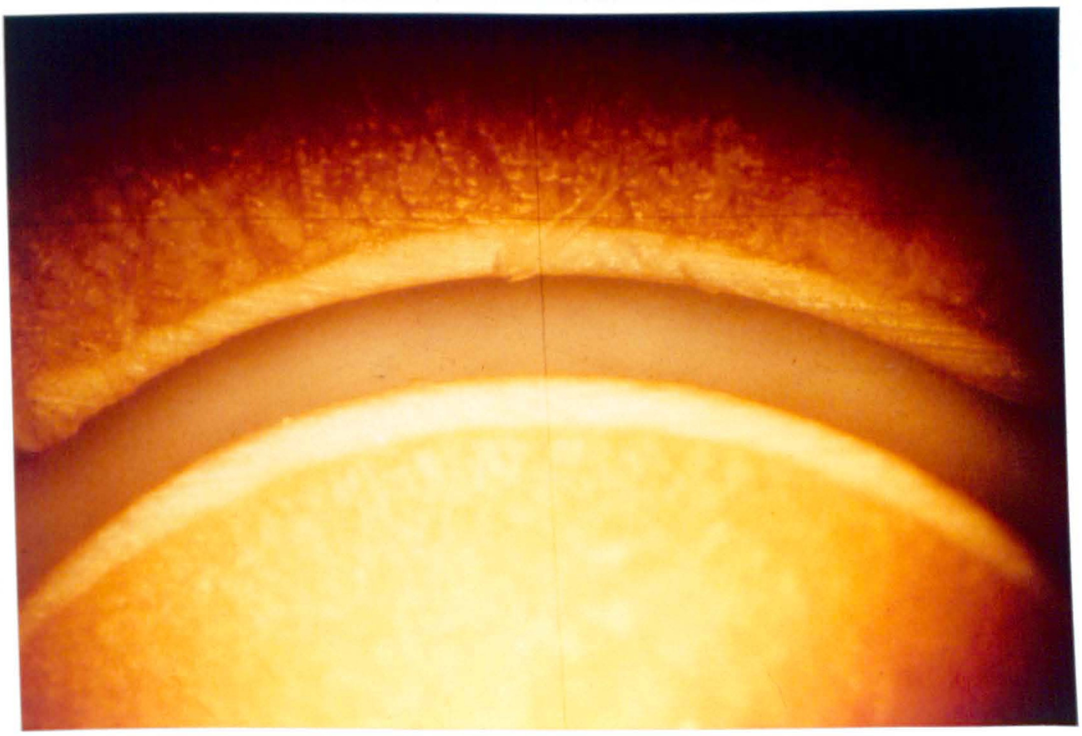

Figure 3.4.5 : The screen image of the Profile Projector showing a posterior-anterior cross-section of an ankle joint.

For the purposes of this study, thickness measurements were performed in the posterior, middle and anterior regions of each cross-section. The resulting values for thickness are listed in Table 3.4.2.

Joint Number	Component	Line	Thickness		
			Posterior (mm)	Middle (mm)	Anterior (mm)
2	Talus	1	1.5	1.7	1.4
		3	1.3	1.4	1.2
		5	1.4	1.3	0.9
	Tibia	1	1.3	1.7	1.5
		3	0.9	1.7	1.1
		5	1.0	1.6	1.3
3	Talus	1	1.1	1.3	0.8
		2	1.2	1.3	1.0
		4	1.3	1.1	0.9
	Tibia	1	1.0	1.1	1.1
		2	1.0	1.0	1.1
		4	1.0	1.2	1.1

Table 3.4.2 : Cartilage thickness measurements.

3.5 Calculation of Surface Radii of Curvature

The Talycontor instrument was used to measure surface profiles of joint numbers 1, 2 and 3. The graphical output from the Talycontor was converted to discrete digital data by hand and entered into computer data files. A curve fitting procedure in which the surface profile was represented by the arc of a circle was developed specifically for ankle joints. However, the curve fitting procedure included provisions for determining the parts of the profile which did not conform to this chosen form. To accomplish this, an estimate of the precision of an individual profile was required. A profile was taken twice consecutively and differences were within 0.25 percent.

The details of the curve fitting procedure are listed as follows:

i) A least squares method was used to obtain a best fit circle based on all the profile data. The mathematical development and the computer programme for this task are included in Appendix A.

ii) Points were excluded from one of the ends of the profile so that an equal number remained on either side of the midpoint of the fitted arc.

iii) Another curve fit was performed using the computer program listed in Appendix A.

iv) If the radius calculated using any single point involved in the circle fit was not within 0.25% of the radius of the fitted circle, then a point from each end of the arc was excluded from the next circle fit.

v) Step numbers ii), iii) and iv) were repeated until all the points involved in the fitted circle had radii within 0.25% of the radius of the fitted circle and were equal in number on either side of the midpoint of the fitted arc.

The curve fitting procedure was applied to the data from the 26 individual profiles shown in Figures 3.4.1, 3.4.2 and 3.4.3. The results showing all the data collected are presented in Figures 3.5.1 to 3.5.6 using symbols defined in Table 3.5.1. It can be seen from these Figures that an arc of a circle provided a good representation of the profile geometry.

Symbol	Description
1, 2, ...	Profile line numbers shown in Figures 3.4.1, 3.4.2 and 3.4.3
M	Medial
L	Lateral
A	Anterior
P	Posterior
□	Points included in least squares fit
x	Points not included in least squares fit
+	Centre of fitted circle
|______|	10 mm
______	arc of fitted circle
--------	Extension of arc of fitted circle

Table 3.5.1 Symbols for Figures 3.5.1 to 3.5.6

The calculated radii of curvature for each profile are given in Table 3.5.2. In lubrication theory, the reduced radius of curvature is a useful parameter. The radii are deemed to be positive for convex and negative for concave surfaces, and hence, for the profiles recorded, the following equation was adopted for the reduced radius of curvature. The resulting values are included in Table 3.5.2.

$$R = \frac{R_1(-R_2)}{R_1+(-R_2)} \qquad (3.5.1)$$

where R_1 = talus radius
R_2 = tibia radius
R = reduced radius

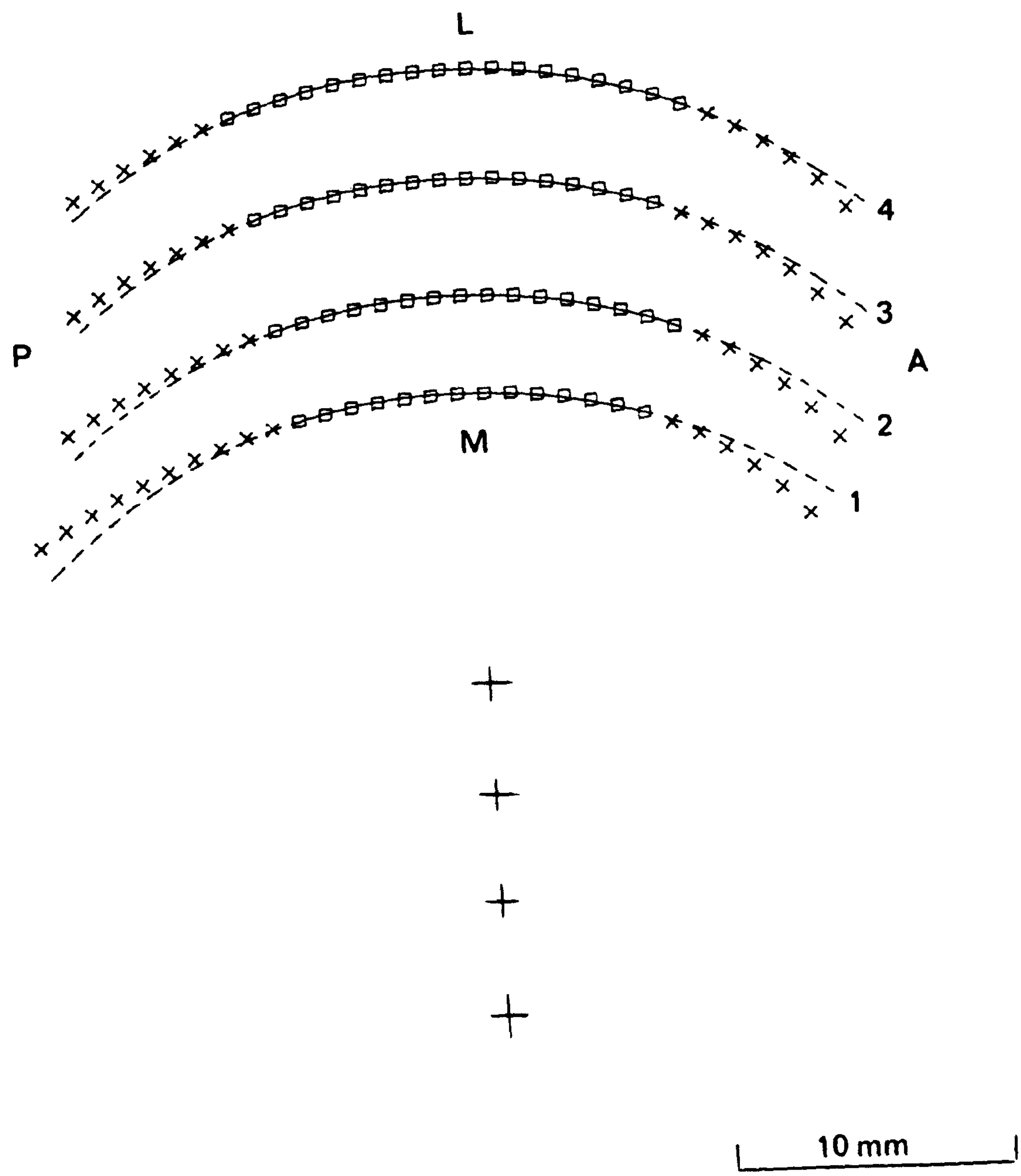

Figure 3.5.1 : The surface profiles for the talus of ankle joint number 1.
(See Table 3.5.1 for definitions of the symbols used above).

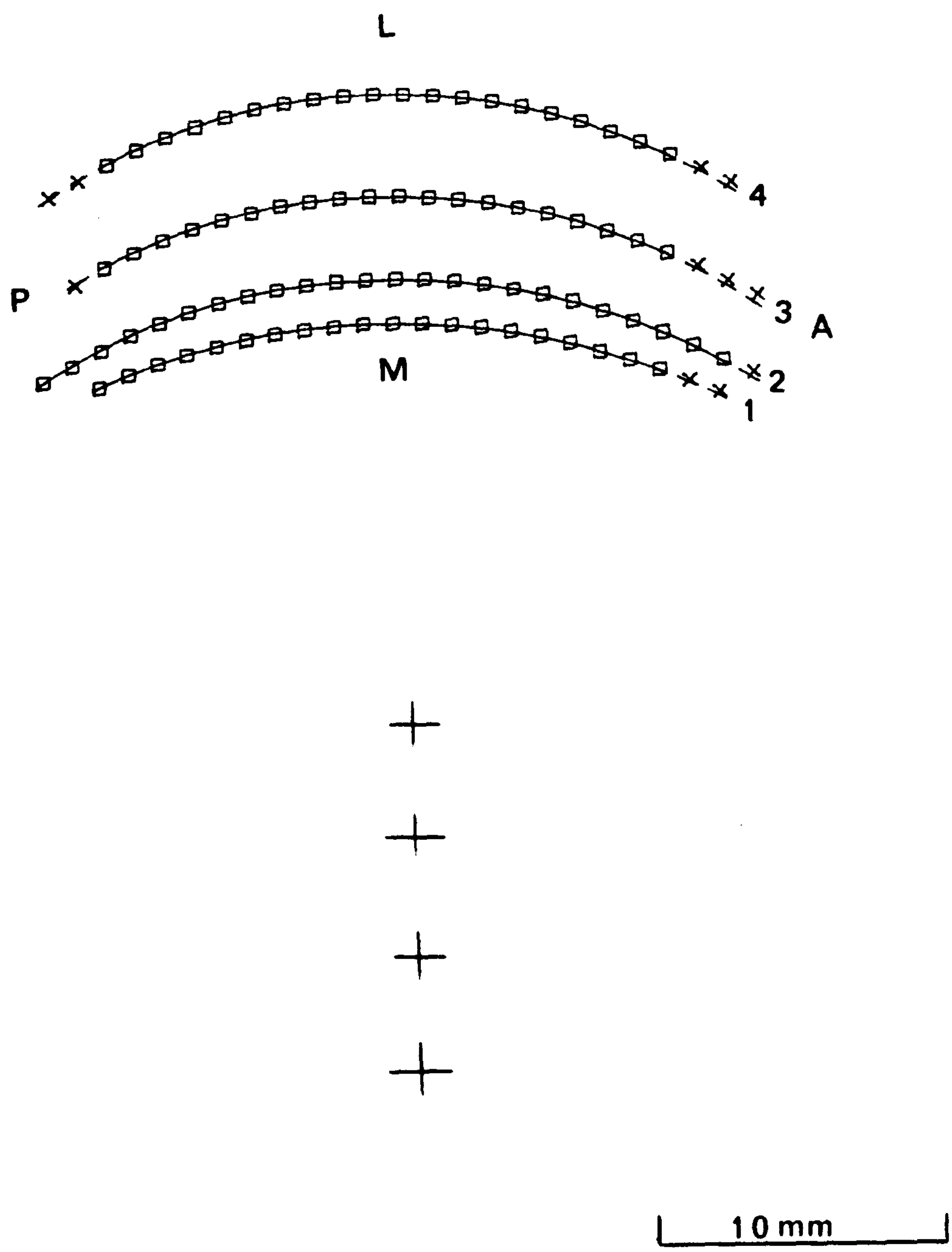

Figure 3.5.2 ; The surface profiles for the tibia of ankle joint number 1. (See Table 3.5.1 for definitions of the symbols used above).

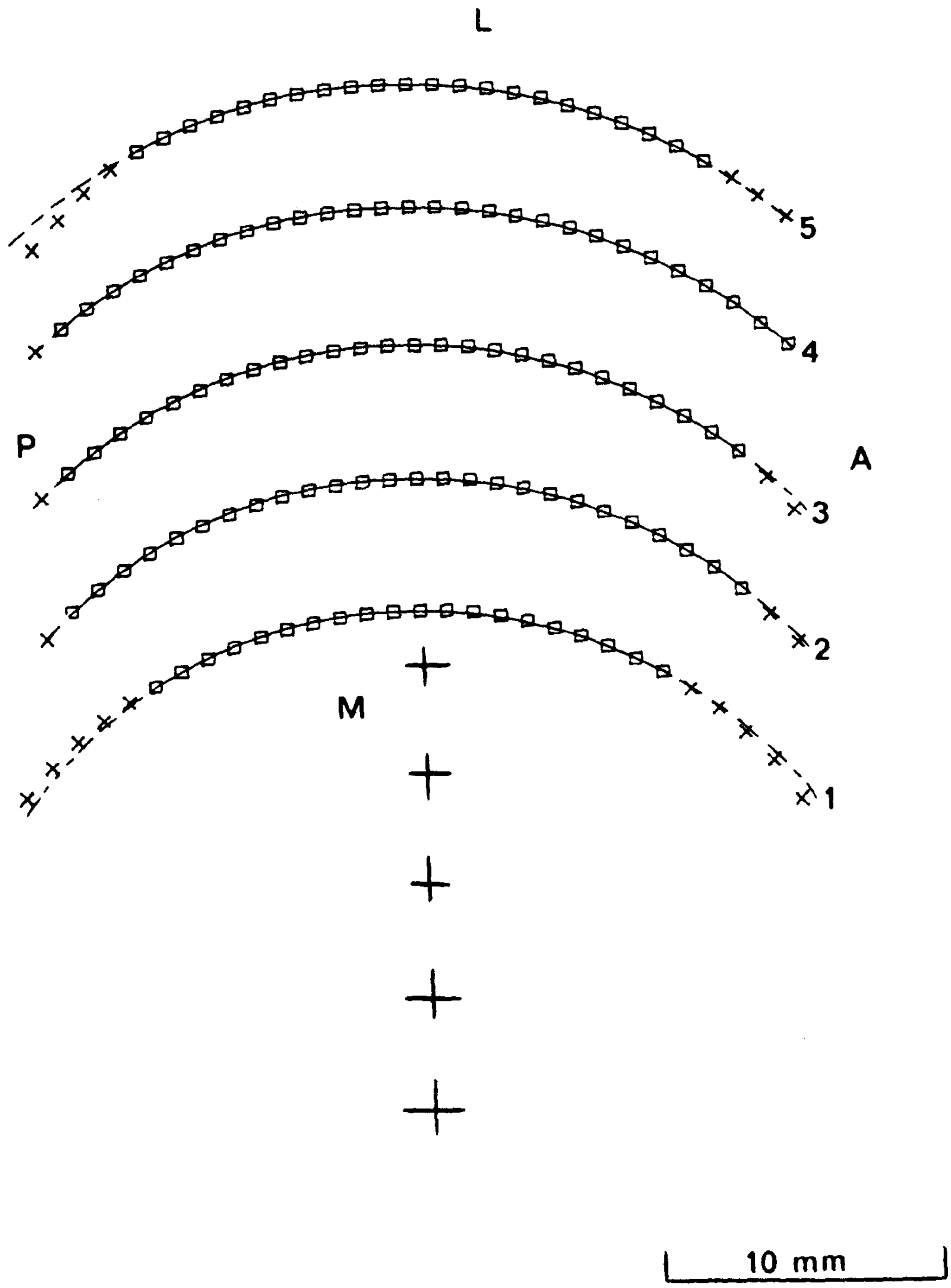

Figure 3.5.3 : The surface profiles for the talus of ankle joint number 2. (See Table 3.5.1 for definitions of the symbols used above).

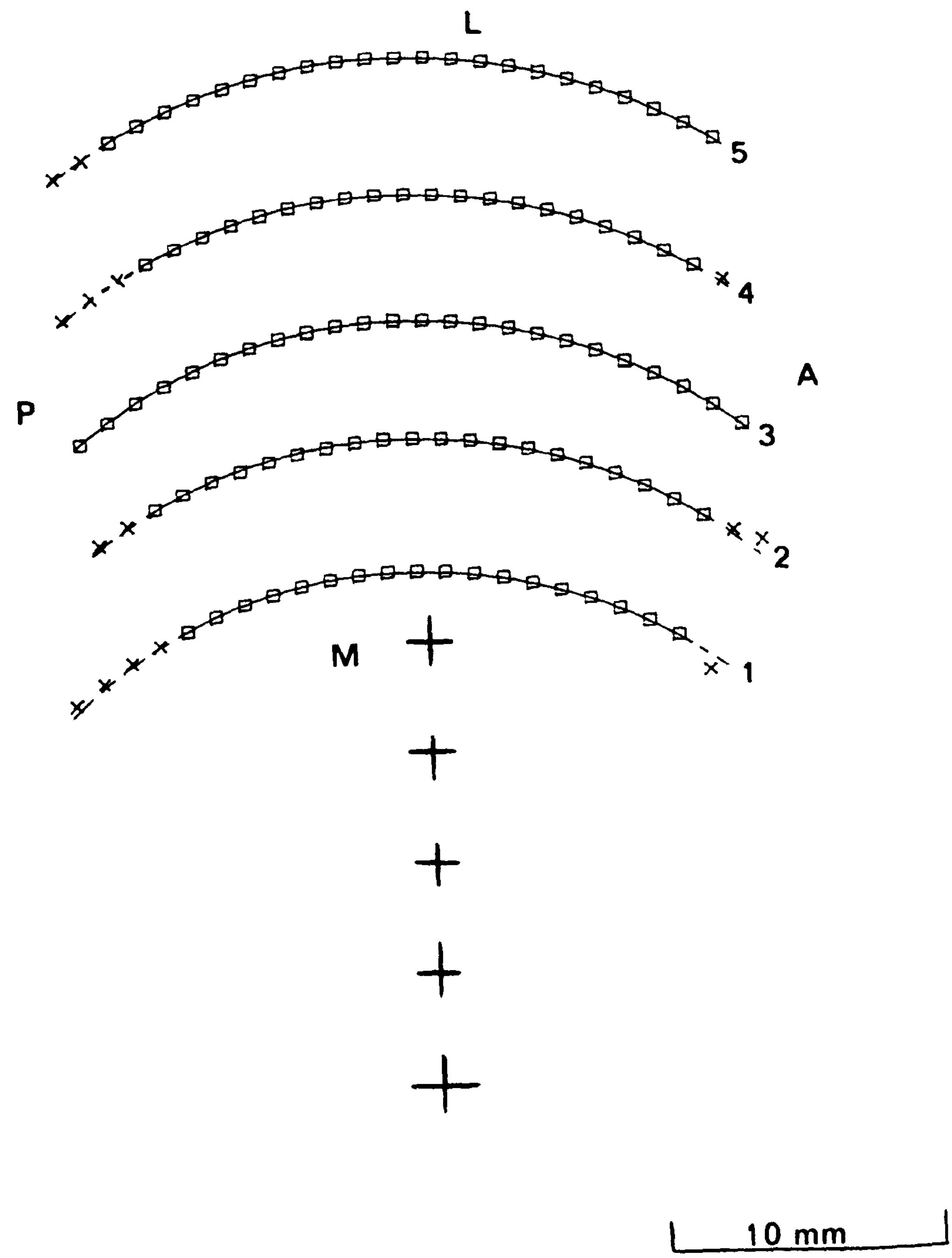

Figure 3.5.4 : The surface profiles for the tibia of the ankle joint number 2. (See Table 3.5.1 for definitions of the symbols used above).

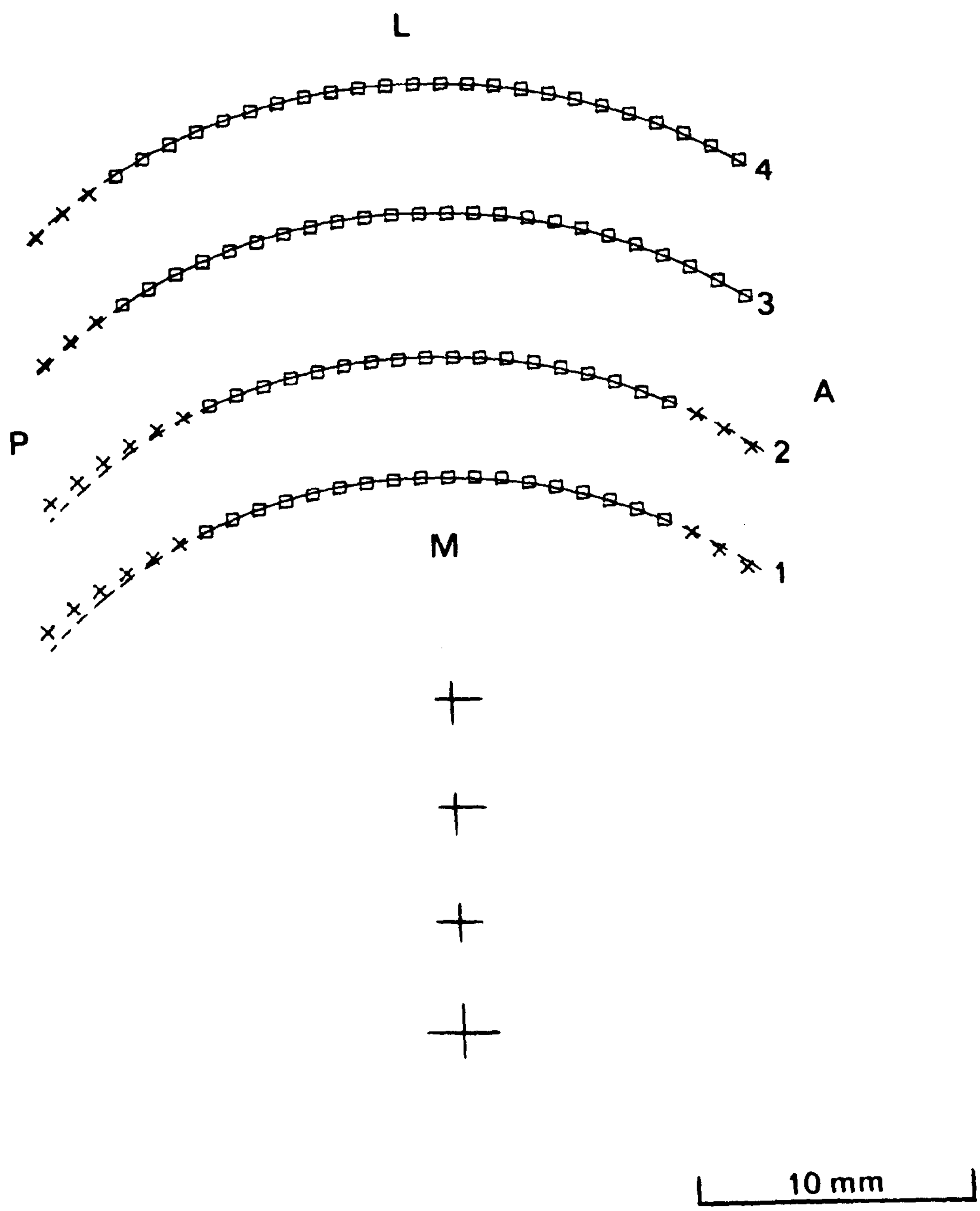

Figure 3.5.5 : The surface profiles for the talus of ankle joint number 3. (See Table 3.5.1 for definitions of the symbols used above).

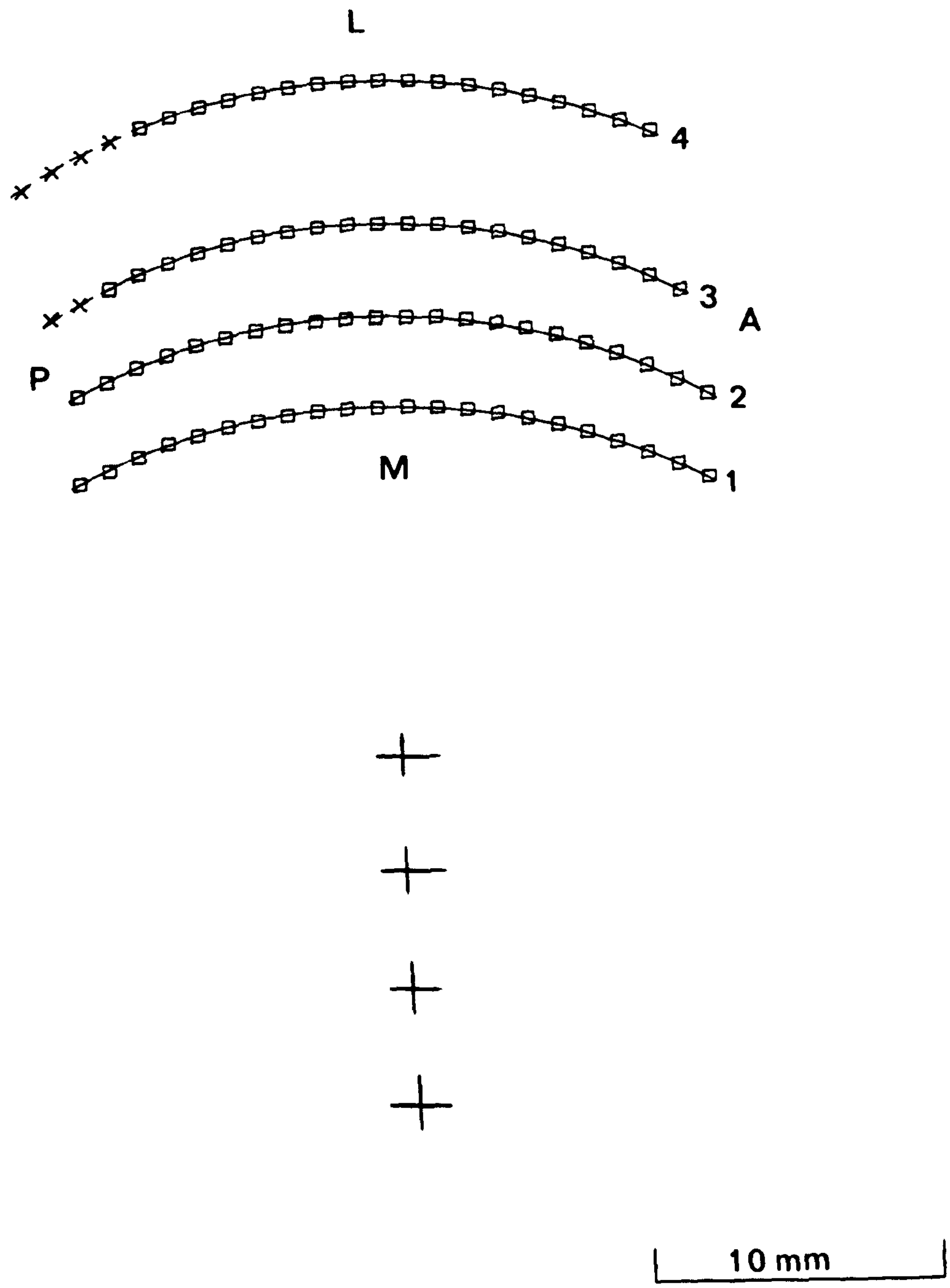

Figure 3.5.6 : The surface profiles for the tibia of ankle joint number 3. (See Table 3.5.1 for definitions of the symbols used above).

Joint Number	Line	Radius for Talus (mm)	Radius for Tibia (mm)	Reduced Radius (m)
1	1	22.5	26.0	0.17
	2	22.0	23.6	0.32
	3	22.3	22.4	2.46
	4	22.3	22.1	*
	Average	22.3	23.5	0.44
2	1	17.8	18.5	0.47
	2	18.6	19.2	0.60
	3	19.3	19.6	1.26
	4	20.3	20.2	*
	5	20.9	21.2	1.48
	Average	19.4	19.7	1.27
3	1	19.7	24.0	0.11
	2	20.0	23.1	0.15
	3	21.2	22.3	0.43
	4	21.8	23.3	0.34
	Average	20.7	23.2	0.19

Table 3.5.2 : Surface curvature values for ankle joint numbers 1, 2 and 3.

* reduced radius undefined.

3.6 Accuracy of the Computed Radii of Curvature

In Section 3.1 the assumption was made that the central regions of the measured profiles were circular. This appeared to be the case as shown in Figures 3.5.1 to 3.5.6 and for each joint small changes occurred in the extent of this central region and the evaluated radius. The radii of curvature have been used to calculate reduced radii of curvature as listed in Table 3.5.2. A small error in a radius curvature could cause a large error in the reduced radius. Thus, a careful examination of the accuracy of the calculation was necessary before the values recorded in Table 3.5.2 could be incorporated into an assessment of the overall geometry of the ankle joint.

The first error to be considered involved the special pin shown in Figure 3.4.4. The spherical tip of the pin had a radius tolerance of ± 0.003 mm. The influence of pin tip radius on the radius of curvature was given by equations (A.20) and (A.21) of Appendix C. Cartilage dehydration was minimized throughout all the experimental procedures by keeping the surfaces soaked in physiological saline solution. However, in the 40 seconds required for a traversal of the Talycontor stylus, dehydration could occur. This may have caused inaccuracy in the determination of the radius of surface curvature by reducing the cartilage thickness. This inaccuracy was estimated as ± 0.02 mm based upon two successive traversals without wetting the surface. The Talycontor mechanism itself had a tolerance which can be estimated from the manufacturers specifications as ±0.08 mm.

The possibility of the pin tip sinking into the soft cartilage was evaluated by using the following Hertzian formula from Timoshenko and Goodier (1951):

$$\frac{d}{R_p} = \left[\frac{3(1 - \nu^2)F}{4E\,R_p^{\,2}}\right]^{2/3}$$

where ν = 0.5 (representative value for Poisson's ratio of cartilage)

E = 12 MPa (representative value of the elastic modulus of cartilage)

F = 0.04 N (maximum stylus load from the manufacturer's specification)

R_p = 0.794 mm (pin tip radius)

The calculated indentation of the pin tip was d = 0.004 mm and from this value a tolerance of ± 0.004 mm was chosen.

The average radius of curvature for all the surfaces was calculated from Table 3.5.2 as 21 mm. The percentage errors associated with various aspects of a profile measurement could thus be estimated using this average radius and the specified error ranges as listed in Table 3.6.2

Possible sources of error	Estimated percentage error
Pin tip radius	0.01
Cartilage dehydration	0.10
Talycontor mechanism	0.38
Pin indentation	0.02

Table 3.6.1 : Some error estimates associated with profile measurements.

In Section 3.3 the alignment procedure adopted in the present study was described. Since much of the alignment was accomplished "by eye", significant inaccuracies may exist in the values listed in Table 3.5.2

In Appendix B two types of misalignment which may arise in the measurement of a cylindrical surface using the Talycontor instrument are described. The measured joint surfaces were approximately cylindrical as indicated in Table 3.5.2. Thus, the equations developed in Appendix B could be used to estimate the errors.

An aligned cylinder would have its horizontal (y) axis perpendicular to both the direction of stylus motion (x) and the z-axis. In Appendix B inclination in the vertical (y - z) plane is described by a tilt angle (θ) while rotation in the horizontal (x - y) plane is described by a twist angle (α).

It was convenient to define the peak point for a profile as the point with maximum z co-ordinate. The co-ordinate system for the ankle is defined in Figure 3.3.1. During the Talycontor measurements, peak point co-ordinates were recorded with respect to arbitrary locations of the origins for each joint component as listed in Table 3.6.2.

The points obtained for each component do not provide a precise representation of the medial-lateral profile. However, if the joint surfaces were cylindrical and aligned perfectly, lines joining the peak points would have zero slope in the ẏ - z and x - y planes. The slopes were calculated using the computer program listed in Appendix C for a linear regression based on a least squares criterion. The evaluated slopes in the y - z and the x - y planes can be used to estimate tilt and twist angles respectively. The peak points, least squares slopes and estimated tilt and twist angles are shown in Figure 3.6.1 for the tibia of joint number 3 and the estimated tilt and twist angles for each joint component are listed in Table 3.6.3

Equation (B.3) is developed in Appendix B to estimate the effects of tilt and twist on the measured radius of a cylinder. Equation (B.3) implies

$$r_c = \frac{2\, r_m}{\cos\theta + \frac{1}{\cos\alpha}} \qquad (3.6.1)$$

Joint Number	Component	Line	Peak Point Co-ordinates		
			x (mm)	y (mm)	z (mm)
1	Talus	1	17.6	0	6.3
		2	16.6	4.0	5.6
		3	16.2	8.0	5.7
		4	16.1	12.0	6.1
	Tibia	1	13.4	0	4.2
		2	13.4	4.0	3.6
		3	13.0	8.0	3.9
		4	13.0	12.0	4.2
2	Talus	1	-	-	-
		2	14.7	4.0	6.9
		3	15.0	8.0	6.2
		4	15.0	12.0	6.2
		5	15.1	16.0	7.3
	Tibia	1	-	-	-
		2	12.1	4.0	5.3
		3	12.7	8.0	4.8
		4	12.9	12.0	5.5
		5	13.1	16.0	4.9
3	Talus	1	15.7	0	6.3
		2	15.7	4.0	5.6
		3	15.3	8.0	5.1
		4	15.6	12.0	5.1
	Tibia	1	11.1	0	3.2
		2	11.4	4.0	2.7
		3	11.7	8.0	2.5
		4	12.7	12.0	2.5

Table 3.6.2 : Peak point co-ordinates with respect to arbitrary origins for each component.

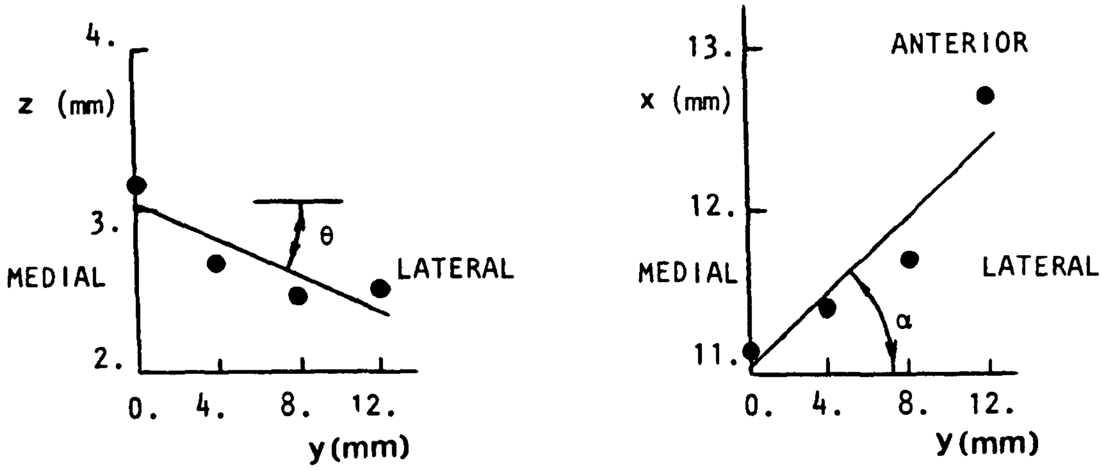

(a) Tilt (b) Twist

Figure 3.6.1 : Peak points, least squares slope and estimated tilt and twist angles for the tibia of joint number 3. (Dimensions are expanded in the x and z directions.)

Joint Number	Component	Average measured radius (mm)	Estimated tilt angle θ (degrees)	Estimated twist angle α (degrees)
1	Talus	22.3	0.9	7.0
	Tibia	23.5	0.4	2.3
2	Talus	19.4	1.8	1.7
	Tibia	19.7	0.8	4.6
3	Talus	20.7	6.1	1.0
	Tibia	23.2	3.1	7.3

Table 3.6.3 : Estimated tilt and twist angles.

where r_m is the measured radius, θ is the tilt angle, α is the twist angle and r_c is the true cylinder radius.

The inaccuracy caused by tilt and twist was estimated by applying equation (3.6.1) to the values of average radius, tilt angles and twist angles listed in Table 3.6.3. The differences between the radius values calculated using equation (3.6.1) and the average measured radii are listed as estimated percentage errors in Table 3.6.4.

Joint Number	Component	Average measured radius (mm)	Estimated percentage error
1	Talus	22.3	0.37
	Tibia	23.5	0.04
2	Talus	19.4	0.003
	Tibia	19.7	0.16
3	Talus	20.7	0.28
	Tibia	23.2	0.34

Table 3.6.4 : Estimated percentage error in the average radius of curvature values caused by misalignment.

The percentage errors from Tables 3.6.1 and 3.6.4 were summed to yield a total error for the average measured radii of each joint component. These errors could themselves be used to estimate the errors in the reduced radii of curvature for each joint. The error in reduced radius of curvature was expressed by applying the following equation

$$R\% = \sqrt{\left(\frac{\partial R}{\partial R_1}\ R_1\%\right)^2 + \left(\frac{\partial R}{\partial R_2}\ R_2\%\right)^2} \qquad (3.6.2)$$

where R%, R_1% and R_2% were estimated percentage errors in the reduced radius of curvature, average measured radius of the talus and the average measured radius of the tibia respectively. Equation (3.6.2) follows from the methods outlined by Kline and McClintock (1953). Equations (3.5.1) and (3.6.2) implied that

$$R\% = R \sqrt{\left(\frac{R_1\%}{R_1}\right)^2 + \left(\frac{R_2\%}{R_2}\right)^2} \quad (3.6.3)$$

The total errors in the average measured radii and the reduced radii of curvature are listed in Table 3.6.5.

Joint Number	Component	Average measured radius		Reduced Radius	
		Value (mm)	Percent error	Value (m)	Percent error
1	Talus	22.3	0.88		
	Tibia	23.5	0.55		
	both			0.44	20
2	Talus	19.4	0.51		
	Tibia	19.7	0.67		
	both			1.27	55
3	Talus	20.7	0.79		
	Tibia	23.2	0.85		
	both			0.19	10

Table 3.6.5 : Total errors in the radii of curvature.

3.7 Selection of a Simple Geometry for Hydrodynamic Lubrication Analysis of the Ankle Joint

The simple geometry of a partial journal bearing with a layered surface was chosen to represent the ankle joint. Values from Tables 3.4.1, 3.4.2 and 3.5.2 were used to specify average dimensions for this simple geometry as shown in Figure 3.7.1.

In the theoretical analysis of joint lubrication presented in this thesis, the reduced radius was a parameter of major importance. For the average dimensions shown in Figure 3.7.1 the reduced radius was 0.35 m.

Some of the average dimensions could be compared to those chosen by Kempson et al (1975) for their standard sized prosthetic ankle joints. The rather close correspondence shown in Table 3.7.1 indicated that these dimensions from the present study can be classified as typical.

The specification of a simple geometry for synovial joint lubrication studies is quite common in the literature. A recent review by Dowson (1980) described the hip as a ball-in-socket with a reduced radius of 0.10 - 1.00 m. In a similar manner ranges for the ankle joint dimensions can be chosen based on the present measurements as listed in Table 3.7.2. The reduced radius of curvature based on average values is 0.35 m with a range of 0.19 to 1.27 m. The range is similar to the range estimated by Dowson (1980) for the hip.

Dimension	Average value from present study	Standard sized ankle joint prosthesis designed by Kempson et al (1975)
Width (mm)	26	25
Tibia length (mm)	28	25
Talus length (mm)	35	34
Tibia radius (mm)	22.1	21
Talus radius (mm)	20.8	21

Table 3.7.1 : Comparison between average dimensions of the present study and those for the ankle joint prosthesis designed by Kempson et al (1975).

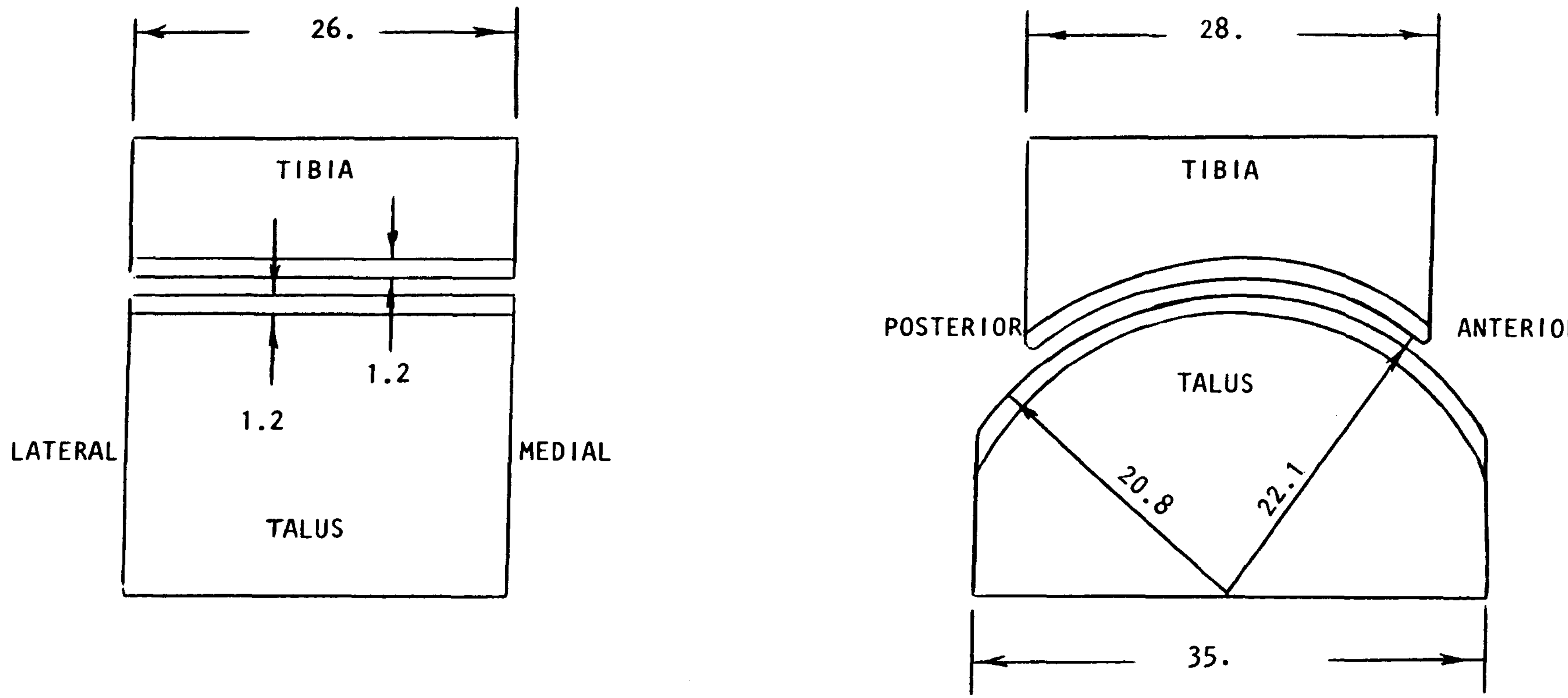

Figure 3.7.1 : The simple ankle joint geometry for lubrication modelling.
All dimensions are in mm.

Dimensions		Average value	Range
Tibia cartilage thickness	(mm)	1.2	0.8 - 1.7
Talus cartilage thickness	(mm)	1.2	0.9 - 1.7
Width	(mm)	26	22 - 31
Tibia length	(mm)	28	27 - 31
Talus length	(mm)	35	34 - 38
Tibia radius	(mm)	22.1	18.5 - 26.0
Talus radius	(mm)	20.8	17.8 - 22.5
Reduced radius	(m)	0.35	0.19- 1.27

Table 3.7.2 : The average values and ranges for the important dimensions representing the geometry of the ankle joint.

3.8 Concluding Remarks

Some general features of the ankle joint surface have been measured in order to specify a simple geometry for subsequent hydrodynamic lubrication analysis. The simple geometry can be discussed in a qualitative manner based on the measurements given in the present study.

In Section 3.1 assumptions were made which reduced the number of features measured. Only the tibia-talus articulation of the ankle was investigated since it transmits most of the joint load (Lambert, 1971). The selection of a single plane of motion was supported by the successful prosthetic replacement for the ankle which had this characteristic (Kempson et al, 1975).

The ankle joint specimens were obtained from a specialized group of patients. Normal healthy joints were selected by visual examination. The chances of this selection procedure failing to detect mildly diseased jointswere lessened somewhat by the low incidence of primary osteoarthrosis in the ankle (Stautter et al, 1977).

The joint surfaces were measured with the cartilage in a relaxed state. However, cartilage creep may occur during in vivo activities which would change the reduced radius of curvature (Higginson, 1978). Ekholm and Ingelmark (1952) measured increases of 5 - 10% in the separation between the femur and tibial plateau as a result of exercise. They claimed that the knee joint cartilages increased in thickness. It is therefore possible that the calculated reduced radii of curvature could have been affected by in vivo activities. However, the measurements of Ekholm and Ingelmark may have included swelling of the menisci. In any case, increases in cartilage thickness can have various effects on surface curvature depending on the region in which it occurs. Thus, it was hoped that the calculated reduced radius of curvature for relaxed cartilage surfaces would provide a satisfactory approximation to that occurring in vivo.

The surface profiles measured in the posterior and anterior regions of the talus deviated by about 0.5 mm from a circular profile. A similar small deviation from circularity was found by Barnett and Napier (1952) and is probably responsible for the changing axis of rotation reported by Sammarco et al (1970) and others. The measured radii of both talus and tibia vary from medial to lateral regions by about five percent, as shown by Table 3.5.2. The overall effect was a considerable variation in reduced radius of curvature for both the medial-lateral direction and as joint flexion occurs. This variation exceeded the maximum error estimated in Table 3.6.5 for the reduced radius of curvature due to errors in measurements.

In spite of the uncertainty in specifying reduced radii of curvature for the ankle joint, there remains strong evidence from the present study to suggest that converging-diverging surfaces are a typical feature of the joint. It is suggested that the simple geometry adopted and the average dimensions deduced adequately represent the ankle joint for subsequent hydrodynamic lubrication analysis.

CHAPTER 4

ANKLE JOINT FRICTION EXPERIMENTS

4.1 INTRODUCTION

A number of experimental approaches have been employed previously in the study of synovial joint lubrication. Some investigators such as McCutchen (1962) and Walker et al (1968) examined the friction between small sections of synovial joint surfaces and glass. Other investigators have used rubber, glass and metal surfaces in various combinations as analogues for particular aspects of synovial joint lubrication (McCutchen, 1966; Higginson and Norman, 1974). Research involving artificial surfaces has assisted the development of understanding the various lubrication mechanisms described in Chapter 2. However, the behaviour of these model experiments may not adequately represent synovial joints in vivo. Thus, it is also necessary to study whole joints under conditions similar to those occurring in vivo.

In general, the friction force at the cartilage surface were measured in the various studies of whole joints. It was hoped that the type of lubrication could be ascertained from these friction measurements. Initially attempts were made to use intact finger joints in friction measuring devices (Jones, 1936; Barnett and Cobbold, 1962). However, the surrounding muscles, ligaments and joint capsule contributed to the measured friction (Wright and Johns, 1960; Barnett and Cobbold, 1962). Thus, most of the measurements of friction directed towards an improved understanding of joint lubrication were usually carried out with dissected synovial joints.

The present study used the dissected human ankle joints described in Chapter 3 in a joint simulator apparatus. Attempts were made to measure the friction between the cartilage surfaces in order to gain insight into the lubrication of ankle joints in vivo.

4.2 Literature Review of Whole Joint Friction Experiments:

The magnitude of the friction between the cartilage surfaces of whole joints was first estimated by Jones (1934). He measured a static coefficient of friction for a dissected knee joint from a horse. Later Charnley (1960) performed a similar experiment on a human knee joint and obtained a range for the static coefficient of friction at various normal loads. This range of friction coefficients included the result obtained by Jones. The details of these early measurements of static friction are listed in Table 4.2.1. Jones did not detect a difference in friction when saline solution was applied to the joint surfaces instead of synovial fluid. However, if the surfaces were allowed to dry, the static coefficient of friction increased dramatically as shown in Table 4.2.1

Free Swinging Pendulums:

Synovial joints are subject to large motions in vivo. Thus, although static friction provides an estimate of whole joint friction behaviour, most subsequent investigations concentrated on measuring the friction forces between moving cartilage surfaces. Various types of apparatus have been used to measure dynamic friction. Possibly the simplest was a pendulum with a synovial joint at the fulcrum. The intention was to determine the coefficient of friction from the rate of decay in pendulum amplitude (Barnett and Cobbold, 1962; Clarke et al, 1975). It was originally thought that the

Table 4.2.1 Measurements of static coefficients of friction for synovial joints

Investigator	Year Published	Joint	Lubricant	Load (N)	Static Coefficient of Friction
Jones	1934	horse knee	synovial	125	0.02
			saline	125	0.02
			dry	125	0.27
Charnley	1960	human knee	synovial	27-2675	0.005-0.023

presence of a lubricant film between the surfaces could also be detected by the rate of decay of the pendulum amplitude (Jones, 1936; Charnley, 1960; Little et al, 1969). However, Barnett and Cobbold (1962) showed experimentally that this was not true in all cases. Furthermore, Unsworth et al (1975) produced analytical estimates which suggested that the presence of fluid film lubrication in synovial joints would be very difficult to detect from the rate of decay in pendulum amplitude. Thus, both Unsworth et al (1975) and O'Kelly et al (1978) measured friction directly without using the rate of decay of the pendulum amplitude.

In spite of these problems, pendulum devices have been widely used. Some details of the investigations using pendulums are listed in Table 4.2.2. The investigations of Clarke et al (1975) and Unsworth et al (1975) showed that the removal of the synovial fluid caused an increase in the coefficient of friction. When Ringer's or buffer solution was used instead of synovial fluid, the coefficient of friction increased in the studies of Little et al (1969) and Clarke et al (1975). In most of the studies included in Table 4.2.2. the coefficient of friction decreased with the increasing load. However, some of the individual experiments of Unsworth et al (1975) showed regions where the coefficient of friction increased with increasing load. Also, Swanson and Freeman (1970) stated that the experiments of Little et al (1969) showed increasing friction with increasing load. At low loads, both Unsworth et al (1975) and O'Kelly et al (1978) obtained some results showing a decrease of friction coefficient with decreasing pendulum velocity.

Table 4.2.2 Studies using a synovial joint at the fulcrum of a free swinging pendulum

Investigator	Year Published	Joint	Lubricant	Load (N)	Initial Angular Displacement (degrees)	Coefficient of Friction
Charnley	1960	human ankle	synovial	134	5	0.014-0.024
Barnett & Cobbold	1962	dog ankle	synovial	4	7.5	0.028
			synovial	11	7.5	0.018
Little et al	1969	human hip	synovial	890	-	0.005-0.012
			ringers	890	-	0.009-0.018
Unsworth et al	1975	human hip	synovial	134	5	0.04-0.01
			synovial	1480	5	0.022-0.015
			dry	134	5	0.125-0.075
			dry	1250	5	0.055-0.018
Clarke et al	1975	human hip	synovial	450	10	0.032
			synovial	1700	10	0.015
			buffer	450	10	0.038
			buffer	2000	10	0.026
			dry	450	10	0.1
			dry	1800	10	0.039
O'Kelly et al	1978	human hip	bovine	100	5-10	0.05-0.08
			synovial	1500	5-10	0.018-0.05

This velocity behaviour, together with the observed decrease of the coefficient of friction with increasing load indicated that some fluid film action was taking place. However, at higher loads and lower velocities these trends were not so pronounced. Thus, all the investigators listed in Table 4.2.2. suggested that a mixture of fluid film and boundary lubrication occurred in their experiments, except Charnley (1960) and Little et al (1969) who proposed boundary lubrication. The increase in friction coefficient when Ringer's or buffer solution was used in place of synovial fluid also supported the view that boundary lubrication prevailed. The Ringer's and buffer solutions had lower viscosity than synovial fluid. Thus, if full fluid film lubrication occurred, a lower coefficient of friction would have been expected for the lower viscosity fluids. In certain experiments O'Kelly et al (1978) found evidence that fluids of lower viscosity than synovial fluid exhibited lower coefficients of friction.

It became increasingly clear that the loads and velocities encountered in the synovial joints tested in free swinging pendulum experiments affected the type of lubrication developed.

Driven Pendulums:

At the same time as work on free swinging pendulums was in progress, some investigators were starting to use driven pendulums. The surface velocities and amplitudes of rotation were much closer to those occurring in common activities in vivo than in the case of free swinging pendulums. However, these devices applied a constant load throughout the cyclic oscillation. Thus, the low loads and high surface velocities which occurred during the swing phase on weight bearing joints were not adequately simulated.

Details of some of the driven pendulum experiments are listed in Table 4.2.3. These investigations showed an increase in the coefficient of friction when saline or buffer solution was used in place of synovial fluid. Contrary to the findings from the free swinging pendulum experiments of Unsworth et al (1975) and O'Kelly et al (1978), the coefficients of friction decreased with increasing velocity in all the investigations, except those of Faber et al (1967). In this study, an increase in the "fluid" component of friction was reported with increasing velocity.

However, they tested intact rabbit's knee joints at high velocities and predicted extremely low film thickness values based upon friction measurements.

Finally, Radin et al (1970) and Radin and Paul (1971) showed an increase in the coefficient of friction with increasing load, while Linn (1968) showed the opposite effect.

Simulators:

An experimental apparatus which applied cyclic time varying loads and velocities was first used on an animal joint by Linn (1967). This joint simulator was a modification of the driven pendulum apparatus used by Linn to generate the results listed in Table 4.2.3. To allow subtraction of torques generated by misalignment of the load axis, the same load pattern was applied for clockwise and counter-clockwise rotation. As a result, the low load, high surface velocity part of the swing phase was not represented. However, low load regions did occur with moderate surface velocities.

Table 4.2.3 Studies using driven pendulum devices

Investigator	Year Published	Joint	Lubricant	Load (N)	Amplitude of Rotation (degrees)	Frequency (cpm)	Coefficient of Friction
Faber et al	1967	rabbit knee	synovial	40-120	± 10	240-600	0.04-0.08
Linn	1967	dog ankle	bovine	180	± 18	5	0.01
			synovial	180	± 18	200	0.004
			saline	180	± 18	5	0.02
			saline	180	± 18	200	0.01
Linn	1968	dog ankle	bovine	90	± 18	5	0.01
				360			0.009
			synovial	90	± 18	200	0.004
				360			0.0035
Radin et al	1970	bovine ankle	synovial	980	-	40	0.006
			synovial	4900	-	40	0.01
			buffer	980	-	40	0.011
			buffer	4900	-	40	0.01
Radin & Paul	1971	bovine ankle	synovial	890	-	40	0.0062
			synovial	4448	-	40	0.0112
			buffer	890	-	40	0.0117
			buffer	4448	-	40	0.0115

Linn (1967) did not follow up his prelimnary work on the simulator apparatus. However, ten years later O'Kelly (1977) published an extensive study using a hip joint simulator. Once again similar load patterns were applied during clockwise and counter-clockwise rotation.

The results of Linn (1967), O'Kelly (1977) and O'Kelly et al (1978) are summarized in Table 4.2.4. A term composed of surface velocity divided by load was used by O'Kelly to correlate with the friction coefficient. If the friction coefficient increased as this term increased then fluid film lubrication predominated. Such behaviour was also demonstrated by Cudworth and Higginson (1976) for a rigid cylinder sliding over a compliant layer under constant load and velocity conditions in the presence of a Newtonian lubricant.

Whether it was correct to assume that the simple correlation reported by Cudworth and Higginson applied to the dynamic conditions imposed by the simulators used by Linn and O'Kelly remained uncertain. However, assuming the correlation was valid, Table 4.2.4 shows that Linn's results indicated boundary or mixed lubrication, while O'Kelly's results supported fluid film lubrication.

Viscosity Effects:

It is not clear from the various studies summarized in Tables 4.2.2, 4.2.3 and 4.2.4 whether fluid film or boundary lubrication predominates in synovial joints during activities such as walking. In an attempt to clarify this situation both Linn (1968) and O'Kelly (1977) conducted experiments with fluids of much greater viscosity than synovial fluid. Representative results are

Table 4.2.4 Studies using joint simulators

Details of Investigation	V (velocity) $(\frac{mm}{s})$	F (load) (N)	$\frac{V}{F}$ $(\frac{mm}{s.N})$	μ (coefficient of friction)
Linn (1967) - dog ankle - talus radius ≃ 8.2 mm - lubricated with saline - motion ± 18.1° at 40 cpm	1.8 10.85	54 165	0.033 0.066	0.021-0.034 0.012
O'Kelly (1977) - human hip -femoral head radius ≃ 26mm - lubricated with saline - motion ± 8° at 37-68 cpm	4-25 13-18 20-26	1271-2383 530 530	0.021-0.01 0.024-0.034 0.039-0.049	0.012-0.031 0.029-0.039 0.039-0.054
O'Kelly et al (1978) - human hip -femoral head radius ≃ 26mm - lubricated with bovine synovial fluid - motion ± 8° at 37-68 cpm	4-25 13-18 20-26	1271-2383 530 530	0.0021-0.01 0.024-0.034 0.039-0.049	0.01-0.05 0.025-0.061 0.035-0.085

summarized in Table 4.2.5. Linn (1968) recorded a decrease in friction with increasing viscosity and O'Kelly measured similar behaviour at low velocities. However, at higher velocities and lower loads O'Kelly measured an increasing friction coefficient with increasing viscosity. Thus, it appeared that fluid film lubrication could be encouraged by introducing high viscosities and velocities along with low loads. The drop in coefficient of friction under higher load and lower velocity conditions may be interpreted as evidence of mixed lubrication. Again a problem exists in determining the appropriate conditions for synovial joints and thus applying these observations to activities in vivo.

Lubricant Constituents:

Another approach to gaining insight into the relative contribution of boundary and fluid film effects in synovial joint lubrication was developed by Radin et al (1970). They tested a bovine ankle in a driven pendulum with a load of 1115 N and a frequency of oscillation of 40 cpm. Constituents of bovine synovial fluid were destroyed biochemically and the resulting friction measurements are summarized in Table 4.2.6. The low friction appeared to depend on the presence of protein. The absence of hyaluronate, which would reduce the synovial viscosity, did not seem to affect the friction. Thus Radin et al concluded that the lubrication of synovial joints was boundary in nature and required the protein constituents in synovial fluid. This result was supported by the more detailed work of Swann et al (1974).

Table 4.2.5 The effect of varying lubricant viscosity

Details of the Investigation	Joint	Lubricant	Viscosity (CP)	Load (N)	Average Velocity (mm/s)	Average Friction Coefficient
Linn (1968) driven pendulum	dog ankle	buffered saline	0.96	178	7	0.0076
		bovine synovial + hyalurondaise	1.2	178	7	0.0037
		bovine synovial	5.2	178	7	0.0037
	dog ankle	buffered saline	0.96	178	7	0.0156
		bovine synovial + hyalurondaise	2	178	7	0.0068
		bovine synovial	6.4	178	7	0.0075
		bovine synovial concentrated	10.7	178	7	0.0059
O'Kelly (1977 simulator	human hip	ringers	1	1964	6	0.018
		ringers + hyaluronic acid	29	1964	6	0.012
		ringers + hyaluronic acid	58	1964	6	0.013
		ringers	1	530	20	0.022
		ringers + hyaluronic acid	29	530	20	0.035
		ringers + hyaluronic acid	58	530	20	0.043

Lubricant	Average Coefficient of Friction
bovine synovial fluid	0.0025
bovine synovial fluid without hyaluronate	0.0026
bovine synovial fluid without protein	0.0051
buffer solution	0.0052

Table 4.2.6 : Experiments on constituents of synovial fluid by Radin et al (1970).

However, the results obtained by O'Kelly et al (1978) did not support this view of the importance of boundary lubrication, since the destruction of the protein element in synovial fluid did not significantly alter friction in their experiments. The destruction of the hyaluronate had only a marginal effect and tended to increase friction.

<u>Concluding Remarks on Previous Whole Joint Friction Experiments:</u>

In whole joint friction experiments a vast number of contradictory findings have been reported. It is of some interest to simply list these findings as shown in Table 4.2.7.

Various joints with different geometries were subject to rather arbitrary ranges of load and velocity. Obviously, this makes it difficult to compare results. Also, since different testing equipment was used and friction forces were small, various types of errors probably distorted the results listed in Table 4.2.7.

Figure 4.2.7 Some contradictory observations in whole joint friction studies

Observation	Supporting	Opposing	Both
Replacing synovial fluid with saline solution increases friction	Linn (1967 Linn (1968 Little et al (1969) Radin et al (1970) Radin & Paul (1971) Clarke et al (1975	--------	O'Kelly et al (1978)
Increasing load reduces friction coefficient	Barnett & Cobbold (1962) Clarke et al (1975) O'Kelly et al (1978)	Swanson & Freeman (1970) Radin et al (1970) Radin & Paul (1971)	Unsworth et al (1975)
Increasing velocity decreases friction	Linn (1967) Linn (1968)	Faber et al (1967) O'Kelly et al (1978)	Unsworth et al (1975)
Increasing velocity divided by load in simulator expt. decreases friction coefficient	Linn (1967)	O'Kelly (1977) O'Kelly et al (1978)	
Increasing viscosity decreases friction	Linn (1967)	--------	O'Kelly (1977)
Removing protein increases friction	Radin et al (1970) Swann et al (1974)	--------	O'Kelly et al (1978)

4.3 General Description of the Ankle Joint Simulator:

The simulator used in the present study was a modified version of the hip joint simulator described by O'Kelly (1977). The hip joint simulator has also been described in two recent publications (O'Kelly et al, 1977, 1978). A sketch of the simulator as used in the present study is shown in Figures 4.3.1 and 4.3.2. The two rolling element bearing and the two hydrostatic bearings shown in Figure 4.3.1 had their centres aligned with the approximate centre of curvature of the talus surface. The upper loading assembly oscillated about this fixed centre in a vertical plane. The lower loading assembly was constrained by eight linear bearings, two for each of four fixed guide pillars, so that only vertical motion could occur. Only two of these eight linear bearings appear in Figure 4.3.1.

The power required to apply the cyclic load and oscillating motion to the joint was supplied by a belt driven from an electric motor with a Kopp variable speed control (Kapak Induction Motor, G.E.C. Machines). The belt drive rotated a steel cam which supplied input to the hydraulic circuit used to load the ankle specimens. The same shaft which drove the cam was also connected to a scotch yoke which converted rotary motion to sinusoidal linear reciprocating motion. This linear motion was applied to a rack and pinion which oscillated the upper loading assembly. A simplified representation of this gearing system is shown in Figure 4.3.1.

The torque assembly shown in Figure 4.3.2 floats on hydrostatic bearings, as shown in Figure 4.3.1, so that any torque about the talus centre was constrained by the Kistler force transducer.

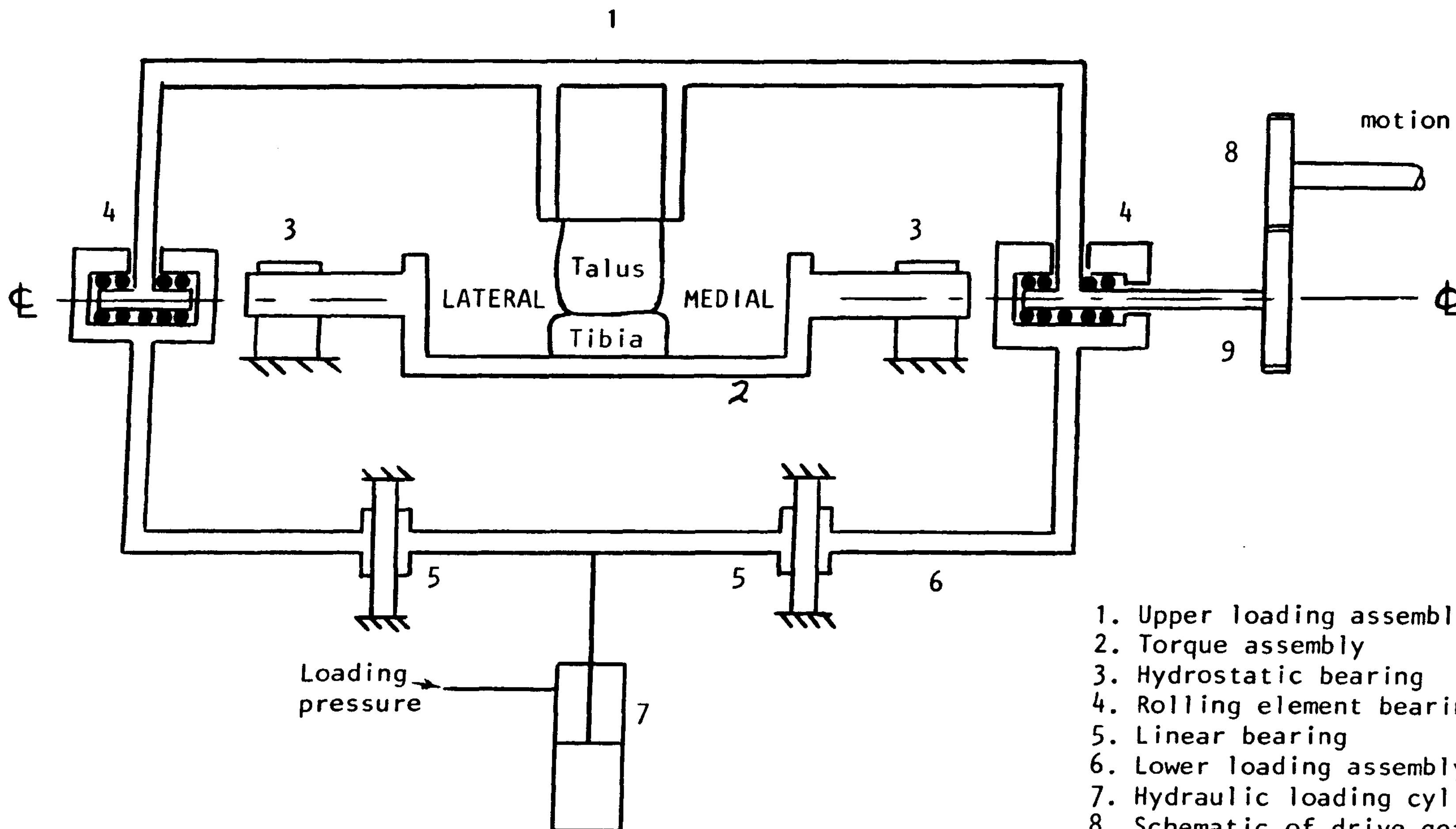

1. Upper loading assembly
2. Torque assembly
3. Hydrostatic bearing
4. Rolling element bearing
5. Linear bearing
6. Lower loading assembly
7. Hydraulic loading cylinder
8. Schematic of drive gear
9. Pinion gear

Figure 4.3.1 : Sketch of a medial-lateral section of the ankle joint simulator apparatus.

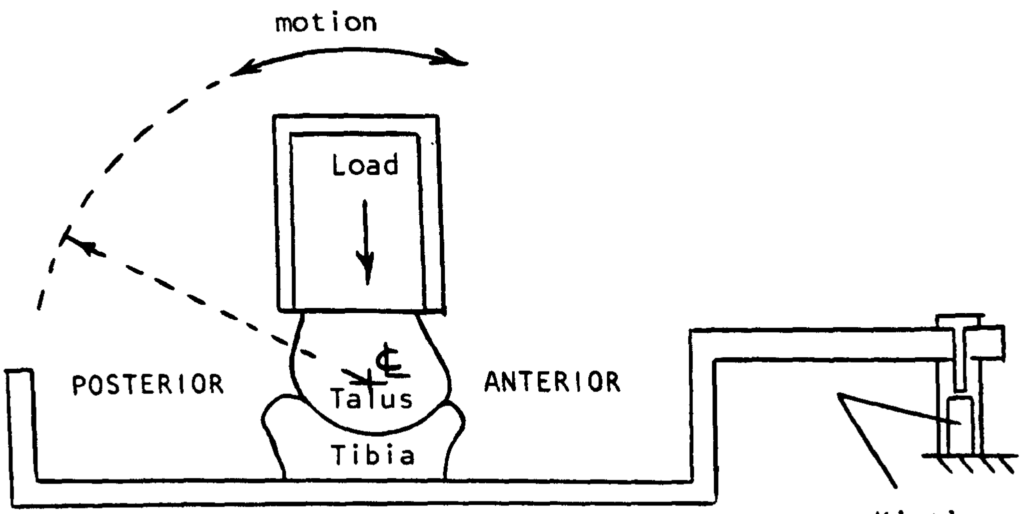

Figure 4.3.2 : Sketch of a posterior-anterior section of the ankle joint simulator apparatus.

The oil used for the hydrostatic bearings (Shell HVI-650) had a viscosity of approximately 2 Pa.s and was supplied by a 0.746 kW Pratts hydraulic pump.

The following modifications were made for the present investigation to the joint simulator used by O'Kelly (1977).

i) A new cam was designed and fabricated to create a load pattern which approximated that encountered in the swing phase of the ankle during walking.

ii) A hydraulic line was replaced with one of larger diameter, fewer bends and shorter length to help the cam follower to stay in contact with the cam.

iii) A limit switch was attached to the simulator to signal the load and friction recording instrumentation at a known angular displacement of the upper loading assembly.

iv) The Kistler force transducer was moved from under the torque assembly to the position shown in Figure 4.3.2.

v) The oil in the hydraulic pump which supplied the hydrostatic bearings was changed to one which was thirty times more viscous.

vi) Styro-foam pads, rubber spacers and flexible tubing were used to help isolate the vibrations of the hydraulic pump from the Kistler force transducer.

vii) Fixtures were made for mounting the ankle specimens that allowed small scale adjustments to be made to the positions of the joint components. Alignment pins were also fabricated.

These modifications will be discussed in detail in subsequent sections of this chapter.

4.4 Load, Displacement and Velocity Imposed by the Simulator:

Considerable data on the displacement of the ankle joint in vivo was presented by Murray et al (1964). Values for the loads on the ankle during walking were estimated analytically by Seireg and Arviker (1975), while Stauffer et al (1977) used both analytical and experimental methods to give displacement and loading of the ankle joint during walking.

In the present study a hardened steel cam was designed to actuate the loading system as described in Appendix D. The heat treatment used to harden the cam was necessary because the stress imposed by the cam follower was sufficient to deform a mild steel cam. In the previous investigations of O'Kelly (1977) difficulty occurred in keeping the cam follower in contact with the cam throughout the loading cycle. As a result the imposed load increased in a series of sharp peaks. This problem did not occur to the same extent in the present study. During a cycle only one rather than two load peaks were imposed. This reduced the maximum rate of change of the cam radius. The shape of the cam was controlled by the theory developed in Appendix D. Also, the hydraulic line from balancing cylinder I to the master cylinder, shown in Figure D.1, was shorter, larger in diameter and had fewer bends than the line used by O'Kelly (1977). This promoted rapid flow of oil from the master cylinder and helped the follower to stay in contact with the cam as the radius descreased. In the operation of the simulator for the present study the cam follower briefly lost contact with the cam at the toe-off position shown in Figure D.2.

The loads imposed by the joint simulator were measured by a force transducer made by applying strain gauges to the walls of a flanged tube which occupied the position normally used for the ankle specimens. This special force transducer, described in detail by O'Kelly (1977), was connected to a bridge amplifier (Tinsley Telcon Ltd.). A low pass filter with a stabilized power supply (Farnell E30/2) was employed to reduce noise in the signal. The voltage output from the bridge amplifer was then recorded during a load cycle with a Tektronix storage oscilloscope. The oscilloscope was triggered by a signal from a limit switch mounted on the simulator and activated when the upper loading assembly reached a known angular displacement.

The voltage output from the oscilloscope was converted to load using the calibration curve shown in Figure 4.4.1. The calibration curve was obtained by placing the force transducer in a Howden testing machine, recording the load required to produce specific voltages and applying the least squares computer program listed in Appendix C. The loads were measured with the pinion gear detached since the special force transducer would not allow oscillatory motion of the upper loading assembly.

The load pattern obtained for the cam used in the present study is shown in Figure 4.4.2 along with the predicted load of Seireg and Arvikar (1975) and Stauffer et al (1977) for a person weighing 440 N. In general, joint loading has been estimated as directly proportional to body weight during walking. It has been shown that both measured and predicted loads for the hip vary,

Figure 4.4.1 : Calibration curve for special force transducer

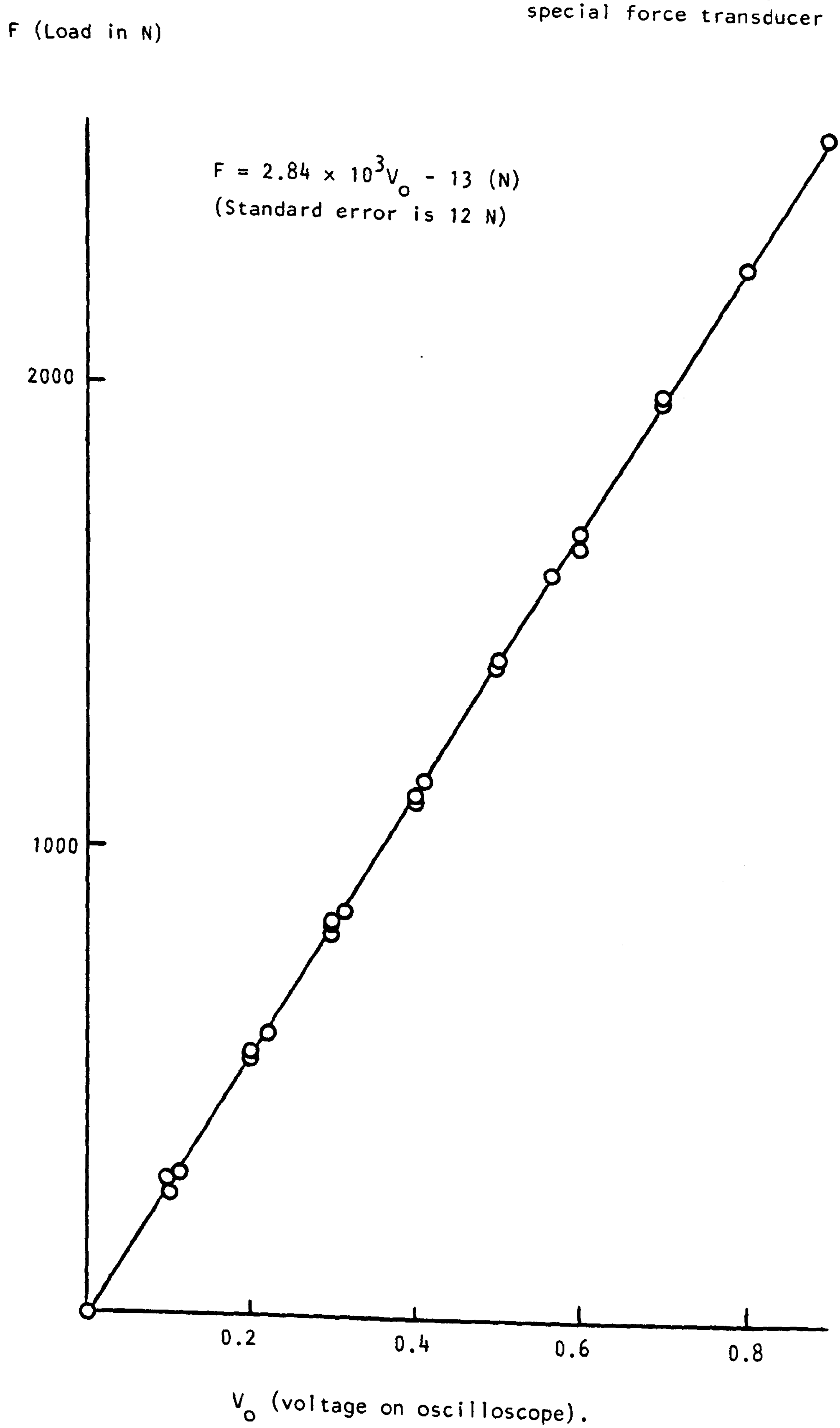

depending on the stride length and walking speed as well as the body weight (Paul, 1976). Such variation must also occur in the ankle joint forces. Thus, the load pattern experienced by a particular ankle specimen during walking can only be approximated.

The load pattern applied by the simulator had a form similar to that predicted by previous investigators for a body weight of 440 N as shown in Figure 4.4.2. Since the loading pattern could not be altered easily (see Appendix D), the same load was applied to each specimen in the present experiments. The value for body weight of 440 N was exceeded by the subjects listed in Table 3.2.1. Thus, peak loads in excess of those predicted during walking were generally avoided. However, the swing phase loads were somewhat larger than those predicted by Seireg and Arvikar (1975) as shown in Figure 4.4.2. This was necessary since low loads could not be imposed or recorded with enough precision by the present apparatus.

The accuracy of the loading system depended on a number of factors. As stated previously, the centres of the roller bearings of the loading assembly had to be aligned with the centres of the hydrostatic bearings of the torque assembly. If the roller bearing centres were lower than the hydrostatic centres, the load at all points in the cycle decreased, since the minimum driving circuit pressure decreased. This occurred to some extent with the mounting of the ankle specimens. A test was conducted with the loading assembly 2.6 mm below the aligned position. The special force transducer recorded a peak load some twenty five percent below the normal level, while the swing phase loads decreased by about fifty percent. The compliance of the specimens also affected the

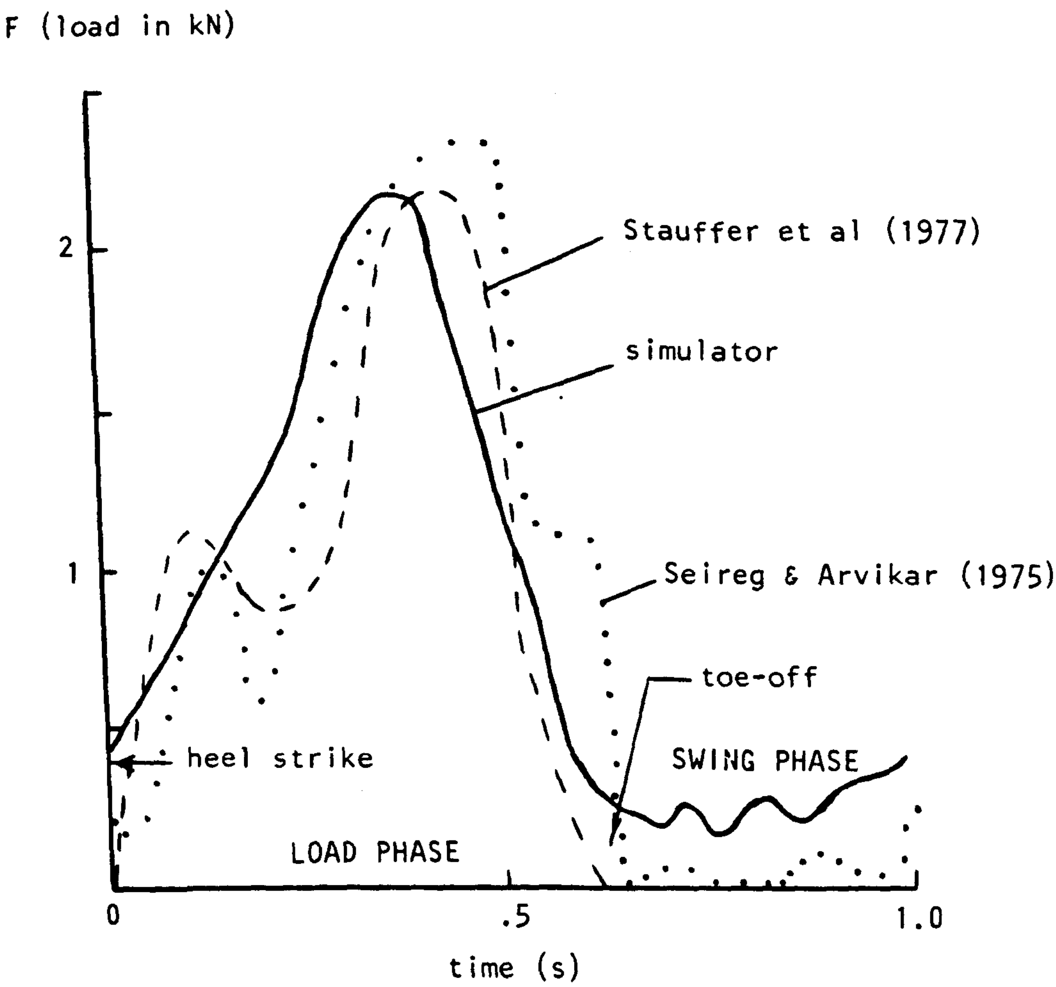

Figure 4.4.2 : The cyclic load pattern imposed on the ankle specimens by the joint simulator and some predicted loads on the ankle during walking for a person weighing 440 N.

imposed load. Tests were conducted with a rubber disc (3.5 mm thick, elastic modulus of about 25 MPa) between various parts of the special force transducer. Variations of about five percent occurred in the peak load while variations of about twenty percent occurred in the swing phase load compared to the loads recorded with the rigid force transducer. In addition to these possible inaccuracies, the calibration curve shown in Figure 4.4.1 produced uncertainties in the imposed forces of about one percent for the peak load and about ten percent for the swing phase loads.

In the present experiments, cycle times of 0.8s and 1.2s were used along with the period of 1.0s recorded in Figure 4.4.2. The changes in loading pattern were small compared with the other inaccuracies involved in the loading system and were thus neglected.

The displacement of the ankle specimens in the simulator was adjusted by changing the radius of the connection point on the scotch yoke mechanism. Sinusoidal displacements were imposed by the scotch yoke and an amplitude of 9° was set for the experiments. O'Kelly (1977) chose an amplitude of 8° for her experiments with hip joints.

The displacement of the ankle during walking has been measured by Murray et al (1964) and Stauffer et al (1977) and their results are shown in Figure 4.4.3, along with the displacements imposed by the simulator. Obviously, the range of motion in the simulator was less than that encountered in vivo, but it was hoped that the lower amplitude of imposed displacement would limit the effects of the changing axis of rotation of the ankle when it was forced to oscillate about a fixed centre by the simulator.

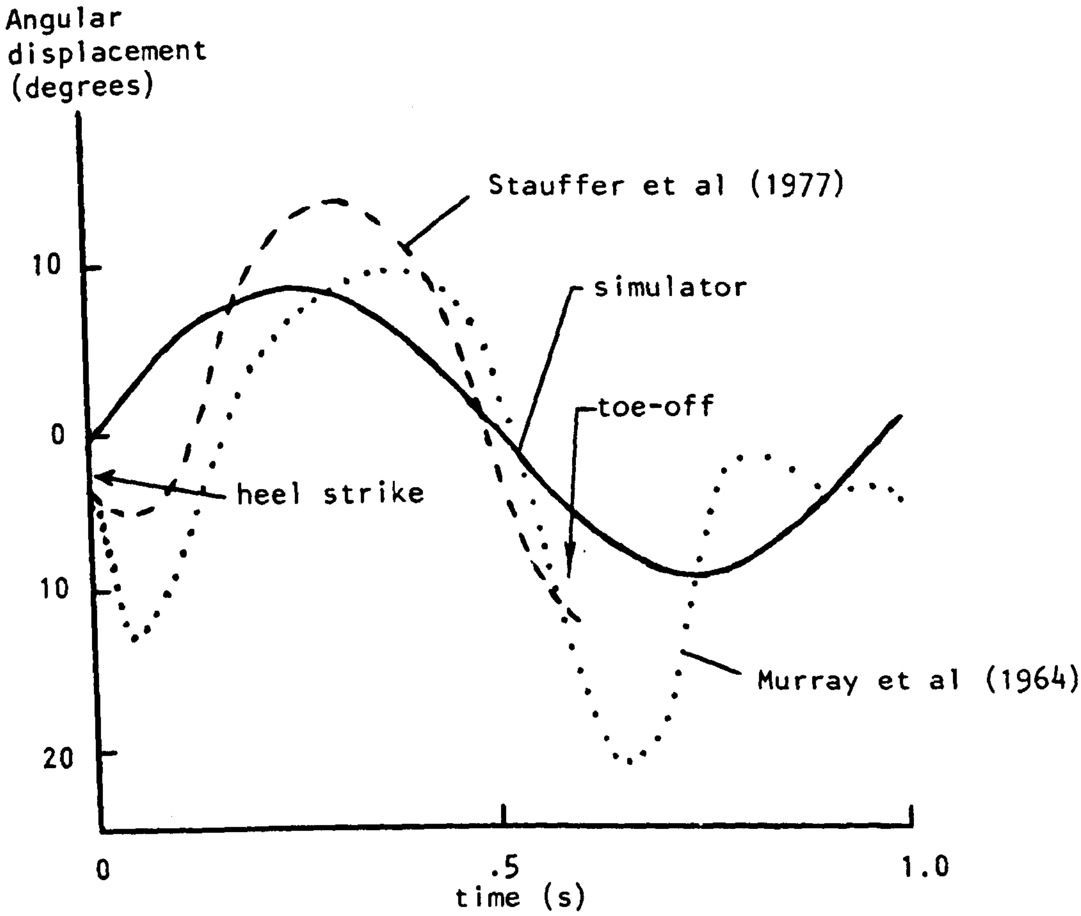

Figure 4.4.3 : The cyclic displacement imposed on the ankle specimens by the joint simulator and some measured displacements on the ankle during walking.

The relative surface velocity of the ankle during walking was estimated from the displacement curves of Murray et al (1964) and Stauffer et al (1977) using an average radius of curvature of 21 mm for the ankle components. These velocity patterns are shown in Figure 4.4.4 with the simulator velocity calculated using the same average radius. It was apparent that higher velocities existed in normal walking than those imposed by the simulator. However, the precision of the calculation of surface velocities during walking depend on estimating slopes of the displacement curves and this was very poor. As a result, values for relative surface velocity during walking were not known with precision for the ankle joint.

The following equation related relative surface velocity in mm/s to the period of oscillation for a component radius of r_s in mm.

$$V = \frac{0.987\ r_s}{t_p} \quad \cos\left(2\pi \frac{t}{t_p}\right) \left(\frac{mm}{s}\right) \qquad (4.4.1)$$

where t_p is the period of oscillation in seconds and t is the time in seconds. The period of oscillation was set to 0.8 , 1.0 and 1.2 s in the course of the present experiments.

4.5 Friction Measurement:

The Kistler force transducer shown in Figure 4.3.2 was connected to a charge amplifier also made by Kistler. The output from the charge amplifier was passed to an ultra-violet recording device made by Southern Instruments. The same limit switch mentioned in Section 4.1 was used to trigger a vertical line on the recording paper at a known angular displacement of the torque

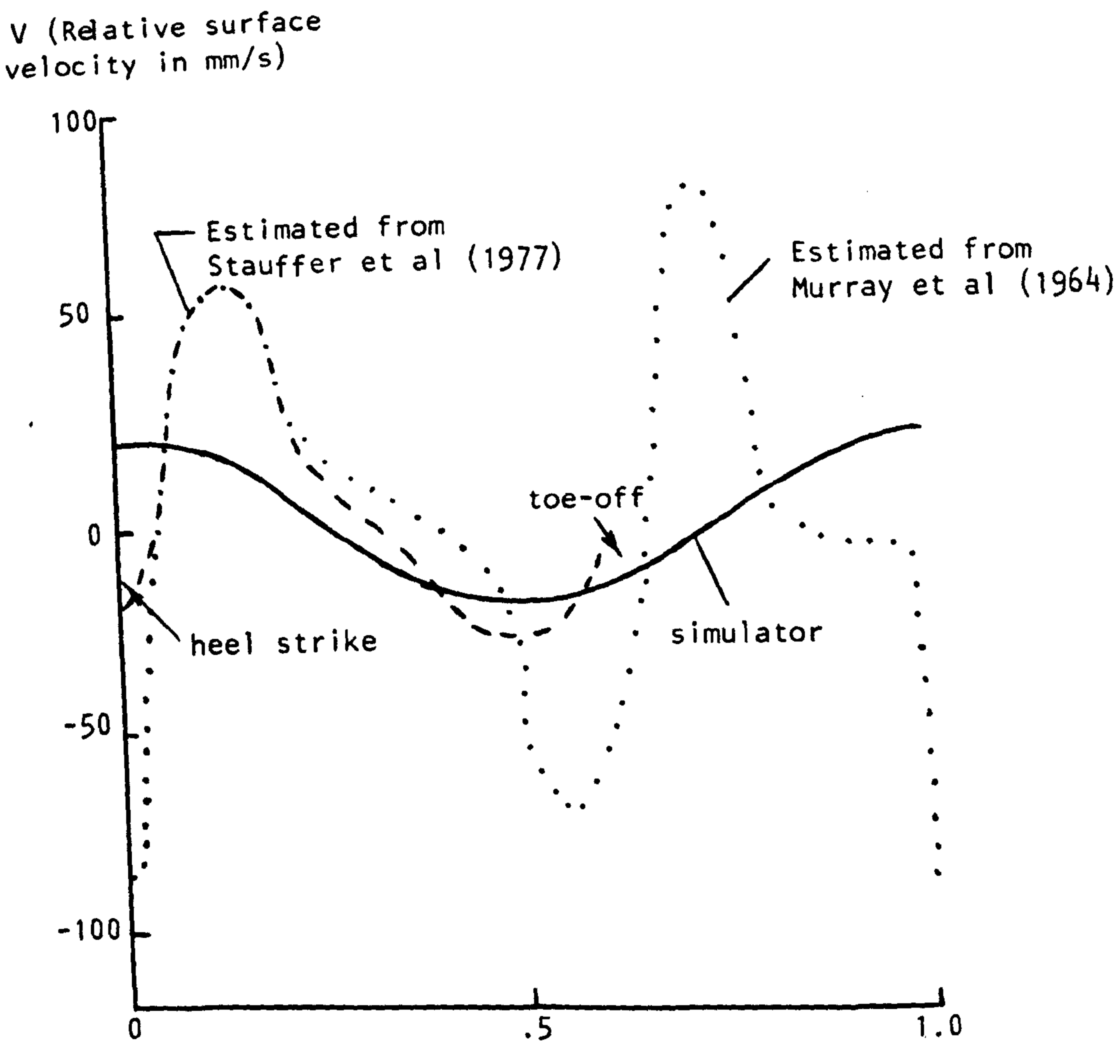

Figure 4.4.4 : The cyclic relative surface velocity imposed on the ankle specimens by the joint simulator and some velocity estimates for the ankle during walking, all for a joint component radius of 21 mm.

assembly. This system measured the torque imposed on the tibia of the ankle specimen during operation of the simulator. The oil supplied to the hydrostatic bearings shown in Figure 4.3.1 was the same as that used by Unsworth et al (1975) in their pendulum apparatus. In the present study and that of Unsworth et al (1975) it was assumed that the resisting torque imposed by the hydrostatic bearings was negligible.

The Kistler force transducer, charge amplifier and the ultra-violet recorder were used previously by both Unsworth et al (1975) and O'Kelly (1977). However, in the hip joint simulator used by O'Kelly the transducer was placed underneath the torque assembly shown in Figure 4.3.2. When increasing torques were applied to the torque assembly with zero normal load imposed, the resulting deflection of the ultra-violet recording instrument increased in a linear fashion. But when the peak normal load was applied statically to the torque assembly, the deflection of the ultra-violet recorder did not achieve a unique value for a specific applied torque. In other words, when a specific torque was applied the recorder gave a specific deflection. However, if the torque was increased and then allowed to return to its previous value, the deflection remained at a higher value than previously. The same "hysteresis" effect ocurred when the specific applied torque was momentarily decreased. One explanation for this behaviour is illustrated in Figure 4.5.1. Bending of the screw which was inserted into the Kistler force transducer may have interfered with the force applied to the transducer. Loosening or tightening the locking nut shown in Figure 4.5.1 did not solve the hysteresis problem. However, the normal load

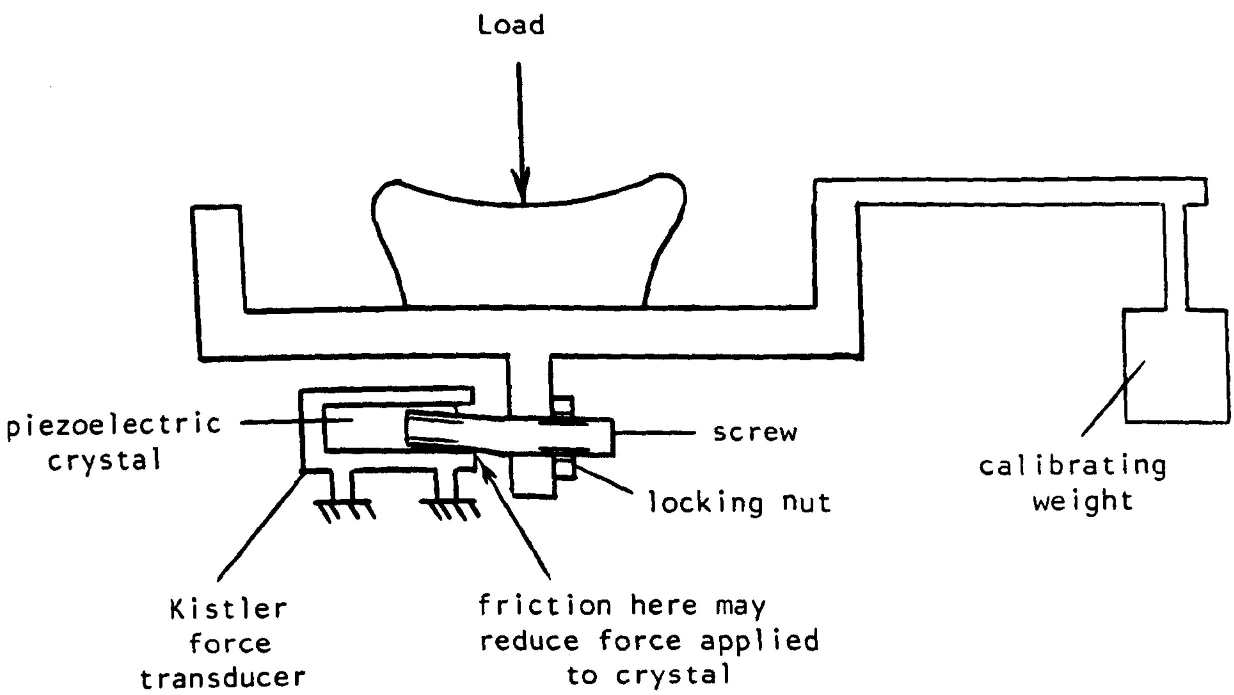

Figure 4.5.1: A possible explanation for the hysteresis observed when calibrating the transducer in the configuration used by O'Kelly (1977).

became significantly coupled with the measured force at the Kistler transducer if the locking nut was not tightened to a specific and critical tension. As a result of these difficulties, the Kistler force transducer was moved from under the torque assembly to the position shown in Figure 4.3.2. The transducer was placed 0.210 m from the centre of rotation. In this position, most of the normal load was carried by the hydrostatic bearings.

A second major problem was encountered with pump vibration. The oil used in the hydraulic pump and supplied to the hydrostatic bearings had a viscosity of about 0.07 Pa.s. At the pressures and flow rates required to support the torque assembly, vibrations from the pump produced significant noise in the Kistler force transducer measurements. The vibrations were reduced by placing the pump on a styro-foam pad, interposing rubber pads where the hydraulic lines touched the simulator frame and replacing a section of the hydraulic line with a reinforced flexible tube. In addition, an oil with a viscosity of 2 Pa.s was used in the pump. The new oil was particularly effective in reducing the vibrations.

The Kistler force transducer was calibrated by applying known torques in both the clockwise and counter-clockwise direction when both swing phase and peak loading was statically imposed. All the results were included as input to the least square computer program listed in Appendix C. The resulting calibration curve is shown in Figure 4.5.2. The scatter in the data used for calibration was mainly a consequence of a rapid drift in the output from the charge amplifier.

In the experiments of O'Kelly (1977) the simulator was used on hip joints. Since the hip was believed to articulate with a

Figure 4.5.2 : Calibration curve for Kistler force transducer.

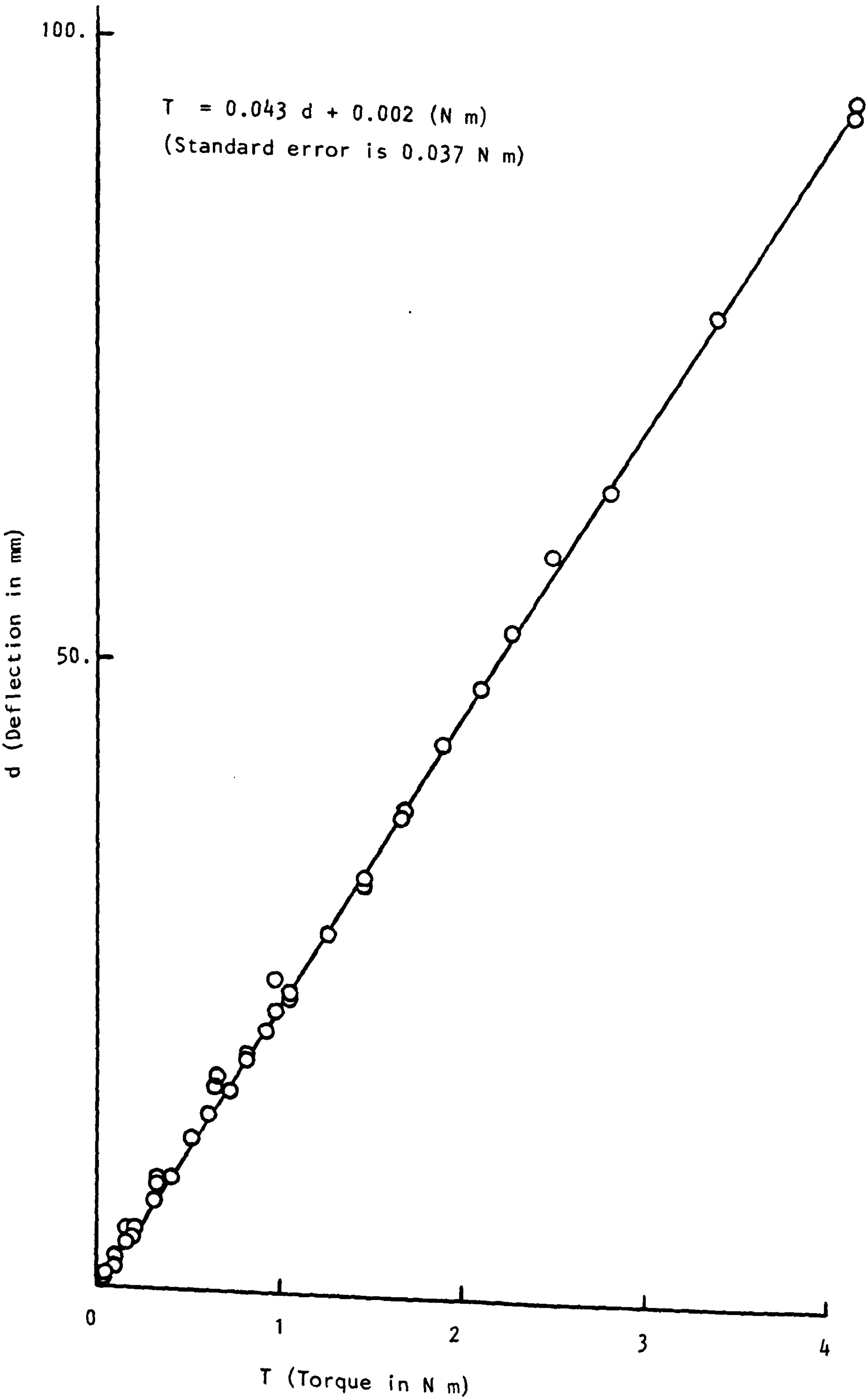

fixed centre of rotation for the applied displacements, the torques measured by the Kistler force transducer were divided by the joint radius to yield the friction force between the cartilage surfaces. However, the ankle has been described by many investigators (Sammarco et al, 1973; Ambrosia et al, 1976: Parlasca et al, 1979; Rastegar et al, 1980) as having a changing axis of rotation. Unfortunately, the simulator oscillates about a fixed centre. The range of motion in the present experiments was thus reduced to about half that measured for the natural ankle during walking. However, it was felt that the assumption of a fixed centre of rotation could not be made.

An analysis of the forces acting on the torque assembly was carried out to determine the influence that a changing centre of rotation would have on the measured torques. If surface deformation is neglected the contact between the talus and tibia can be considered to occur along a single line which is represented as a point C_A in Figure 4.5.3. The motion of the simulator occurred about a fixed centre (C), with a particular angular velocity (ω) at a given instant in time. A radius of curvature (r_1) of the anterior portion of the talus, with a specified centre (C_1) was used to represent the talus surface as shown in Figure 4.5.3. However, the radius of curvature, r_1, changed to r_3 for the posterior surface of the talus as described qualitatively in Chapter 3. In this analysis the radius of curvature of the tibia surface (r_2) remained fixed with centre (C_2) which differed from the fixed centre of oscillation of the simulator.

The action of the load (F) and friction force (F_f) acting on the tibia at C_A is shown in Figure 4.5.4.

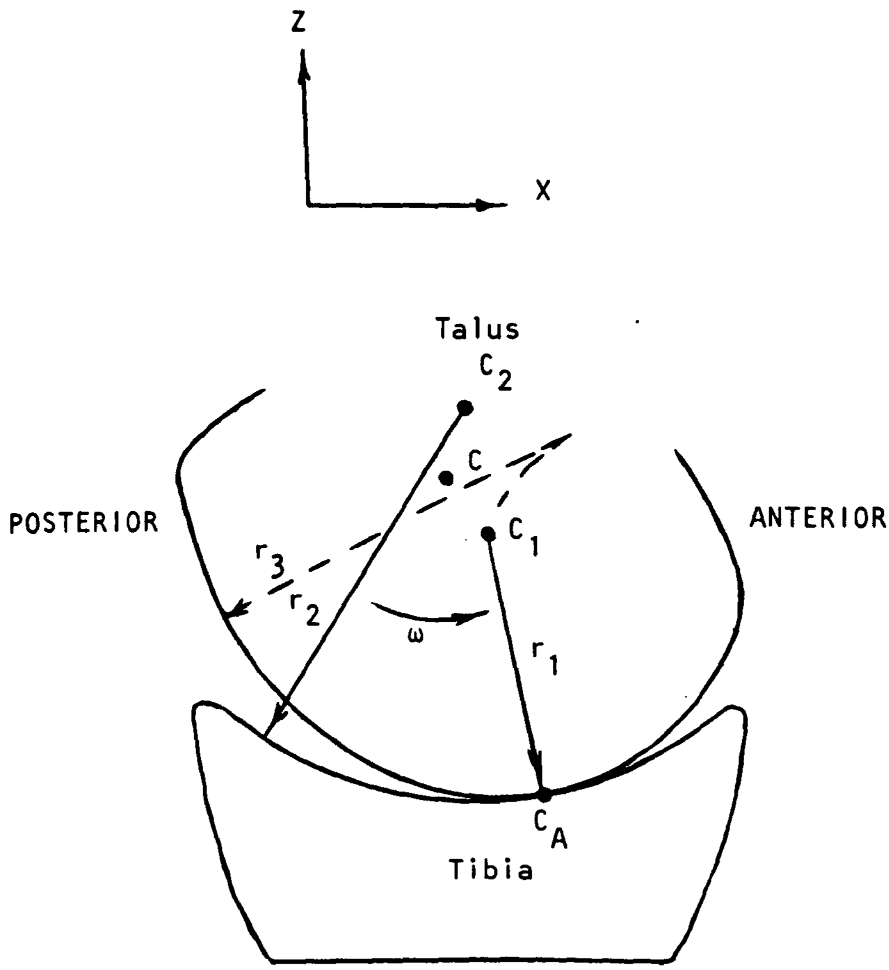

Figure 4.5.3 : The surface interaction of talus and tibia.

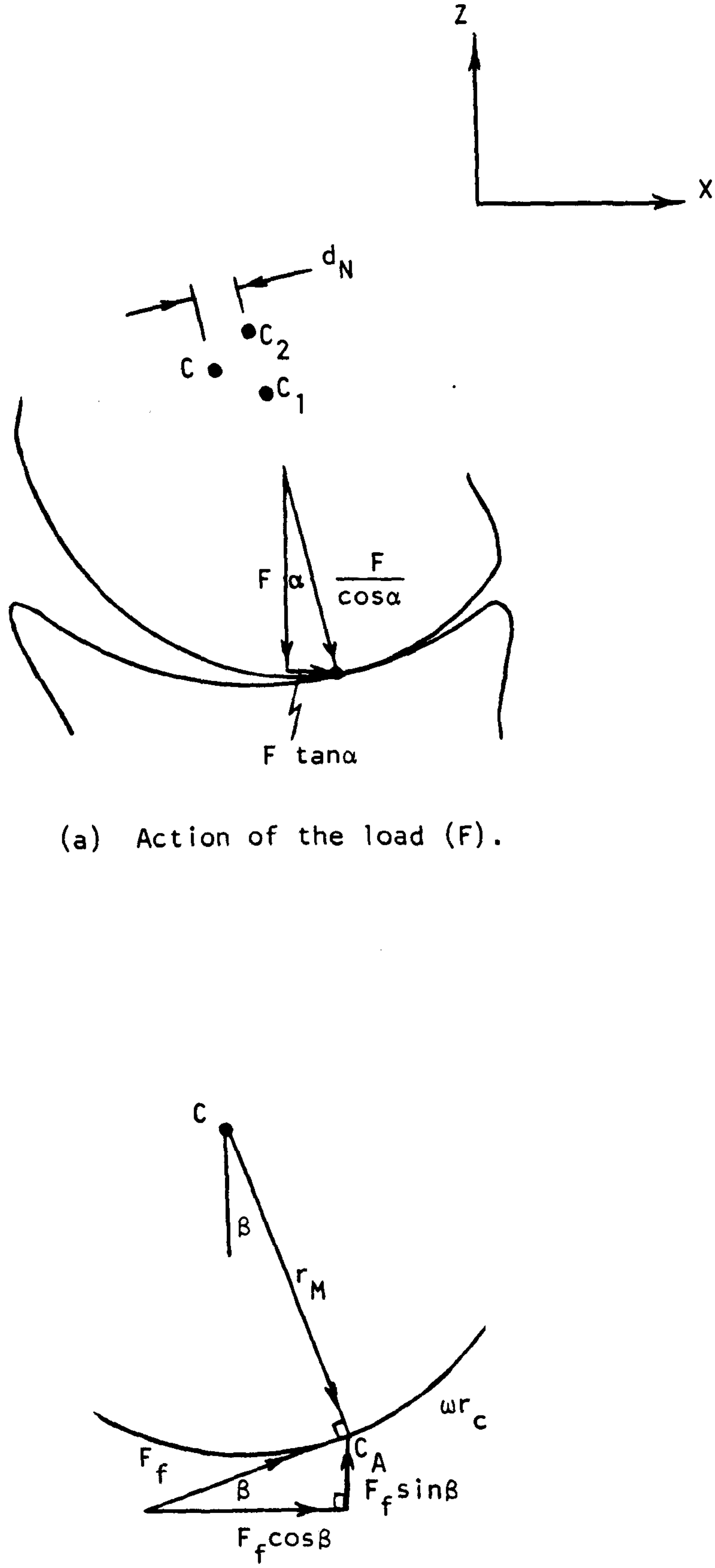

(a) Action of the load (F).

(b) Action of friction force (F_f).

Figure 4.5.4 : The contact forces on the tibia.

Assuming the coefficient of friction between the cartilage surfaces was low, the load acted along the line connecting C_1, C_2 and C_A. This gave rise to the specification of an angle, α, and distance, d_N, in the analysis of the load action. The friction force was assumed to act on the tibia in the direction of motion. Thus, since C_1, C_2 and C were designated as distinct points, a second angle, β, was associated with the action of the friction force.

The torque assembly with associated forces, angles and distances is shown in Figure 4.5.5. The Kistler force transducer was represented as a simple pinned support and the hydrostatic bearings were represented as simple rollers. It was assumed that the forces imposed in the x-direction were resisted by the Kistler force transducer connection (F_{TX}) and that the pressure in the hydrostatic bearings may be represented by a single vertical force (F_{BZ}) acting through the centre (C). The Kistler force transducer measured the force, F_{TZ}, shown in Figure 4.5.5.

Summing the forces on the torque transducer shown in Figures 4.5.4 and 4.5.5 yielded:

$$F \tan \alpha + F_f \cos\beta + F_{TX} = 0 \qquad (4.5.1)$$

and $$- F + F_f \sin\beta + F_{BZ} + F_{TZ} = 0 \qquad (4.5.2)$$

in the X and Z directions respectively. Summing the moments about point C yielded:

$$- \frac{Fd_N}{\cos\alpha} + F_f \, r_M + F_{TZ} \, d_T = 0 \qquad (4.5.3)$$

Since the torque assembly was constrained by the hydrostatic bearings and the Kistler force transducer, dynamic effects were deemed negligible.

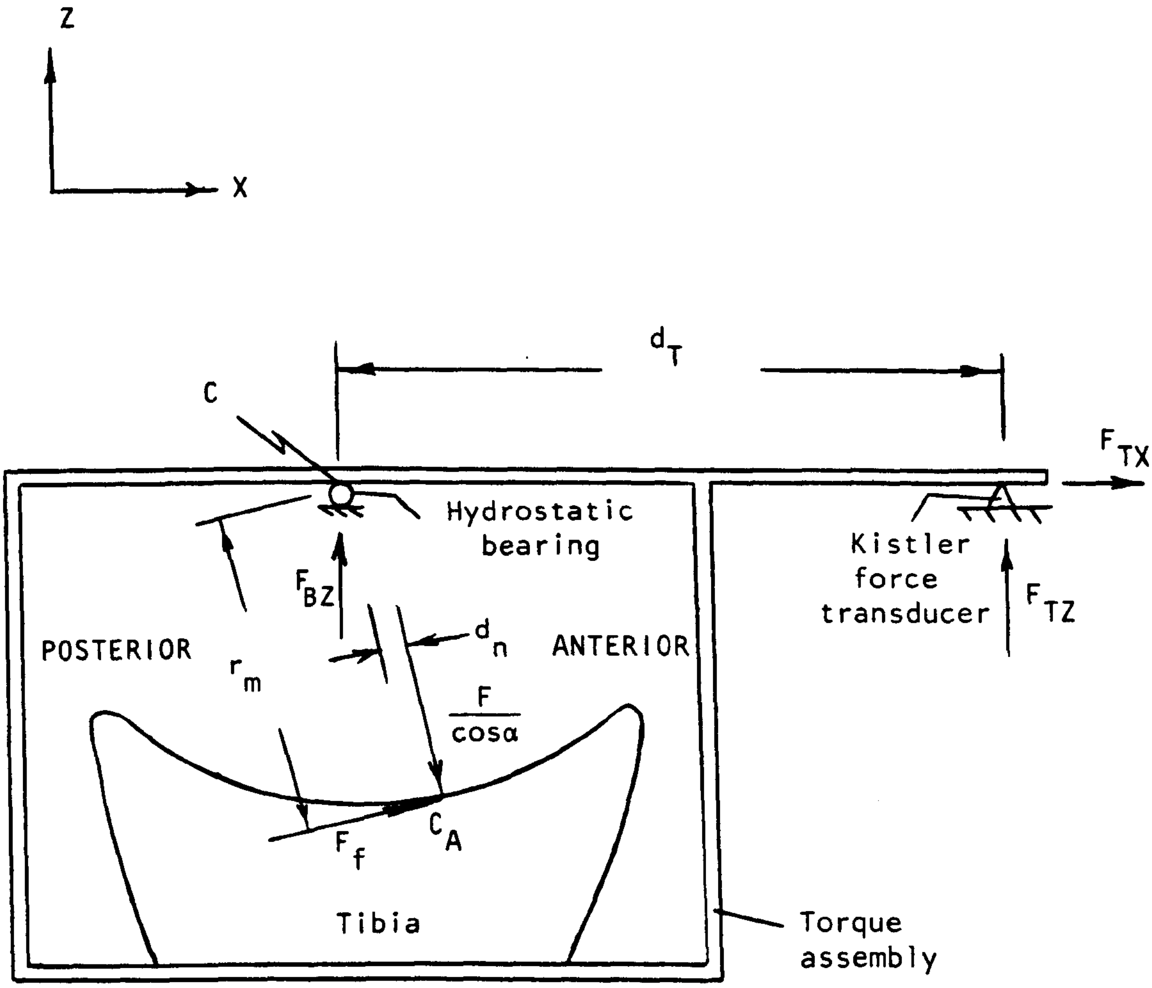

Figure 4.5.5 : The forces on the torque assembly.

It was considered likely that F_f sinβ and F_{TZ} would be small compared to F and this allowed equation (4.5.2) to become,

$$F_{BZ} \cong F$$

However, the terms in equation (4.5.1) and (4.5.3) were of similar magnitude and further reduction was difficult. The values of d_T, F, r_M and F_{TZ} were known in the present experimental design but α, β, F_f, F_{TX} and d_N remained unknown with only equations (4.5.1) and (4.5.3) linking them together. The system was statically indeterminate and thus required further measured values to provide an evaluation of the friction force acting at the cartilage surfaces.

To accomplish this a static loading procedure was included in the experimental design. It was decided to move the upper loading assembly by hand to an equally spaced number of positions in its displacement cycle and to apply the load corresponding to that position. The loads were applied statically, the upper loading assembly being held in position by the pinion gear whilst the lower loading assembly was constrained to have only vertical motion by the eight linear bearings. Thus, it was assumed that equation (4.5.3) applied to this situation with F_f = 0. In other words, the following equation described the static loading situation:

$$\frac{Fd_N}{\cos\alpha} = T_s \qquad (4.5.5)$$

where $T_s = F_{TZ}d_T$ for the static loading conditions. The values of the static torque (T_s) were measured at a number of points in the cycle and since the corresponding dynamic torque ($T_D = F_{TZ}\ d_T$) was known at each particular point, equation (4.5.3) could be used to yield:

$$T_f = T_S - T_D \qquad (4.5.6)$$

where $T_f = F_f \, r_M$

The static loading procedure was accomplished by turning the cam shaft to the appropriate position using a spanner. The positions were identified by markings on the belt drive wheel which had been made with reference to a known position in the simulator cycle. The load which the cam applied statically through the hydraulic circuit was different from the dynamic load as described in Appendix D. However, a calibration procedure was performed using the special force transducer described in Section 4.4. The driving circuit pressure was altered using the hand pump shown in Figure D.1, until the oscilloscope voltage attained the value which corresponded to the dynamic load for that position in the cycle. The least squares computer program in Appendix C was used to yield the calibration curve shown in Figure 4.5.6.

When an ankle joint specimen was used in the simulator, the dynamic torques were recorded with the Kistler force transducer. The static loading procedure was then performed. Once the appropriate pressure existed in the driving circuit, the upper loading assembly was raised manually with a lever and allowed to sink back into contact with the torque assembly. This was intended to introduce a squeeze film between the surfaces so that excessive static friction did not occur between the cartilage surfaces as the loading assembly settled into position. The tendency of the loading assembly to shift laterally was prevented by the pinion gear and the eight linear bearings. Thus, static friction forces which would require the possibility of lateral

Figure 4.5.6 : Calibration curve for the static loading procedure.

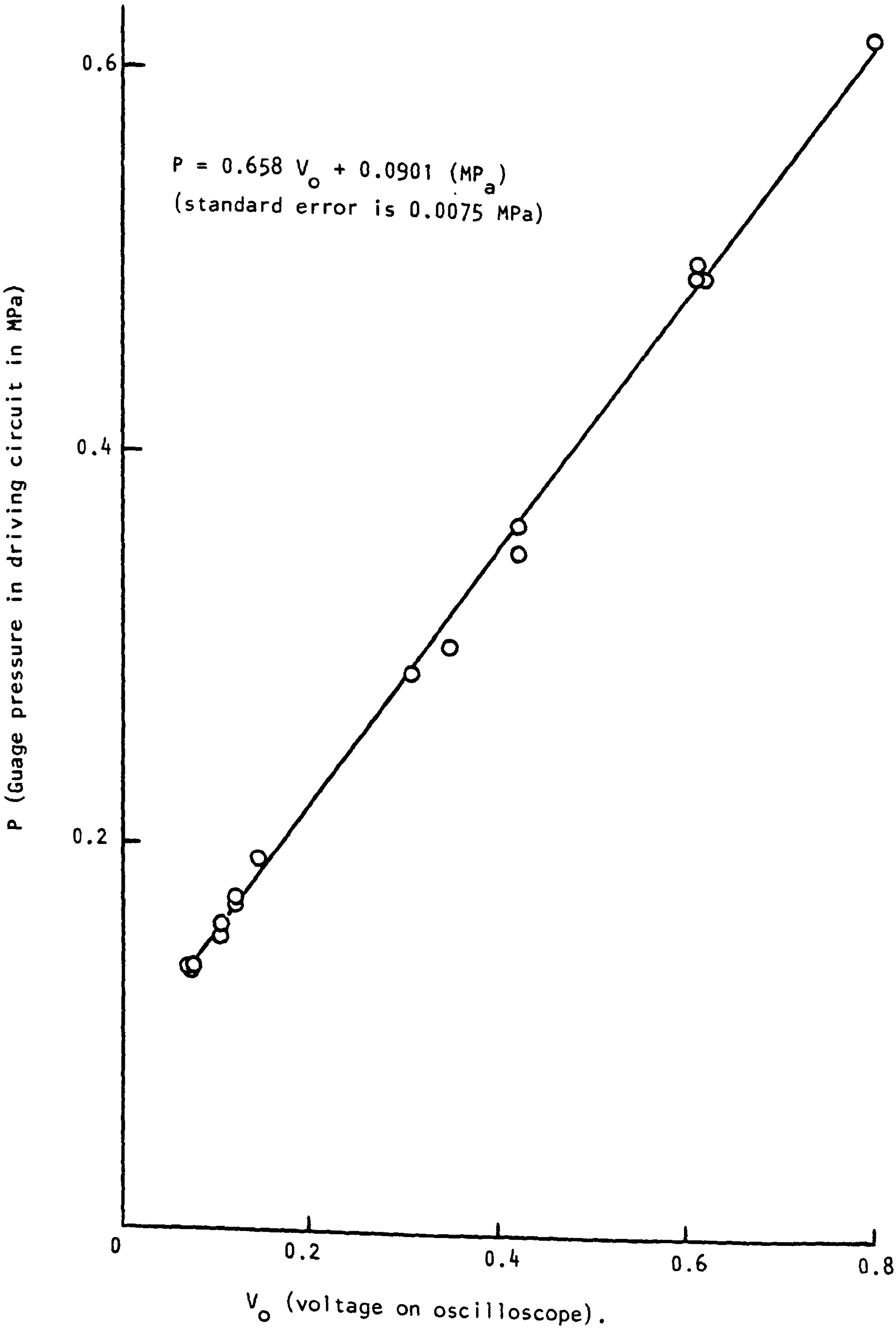

motion were not considered likely to exist and the raising and lowering of the loading assembly was probably not necessary.

In the derivation of equations (4.5.1), (4.5.2) and (4.5.3) it was stated that dynamic effects were negligible since the torque assembly was held in place by the hydrostatic bearings and the connection to the Kistler force transducer. However, during the loading cycle a slight deflection of the hydrostatic bearings occurred in the z-direction. It was considered possible that small shock loads might be recorded by the Kistler force transducer. If so, friction forces which did not exist would be predicted by equation (4.5.6.) To test this hypothesis, spacers were inserted in place of a joint specimen and the pinion gear was detached so that no oscillation occurred. Care was taken to ensure that the load line passed through the line connecting both the hydrostatic and the rolling element bearing centres. One of the spacers was made of rubber (3.5 mm thick having an elastic modulus of about 25 MPa) to approximate the compliance of the ankle joint specimens. With this test configuration, the Kistler force transducer was loaded as if a partially aligned ankle was oscillating in the simulator with zero friction between the cartilage surfaces. Both static and dynamic measurements of torque were performed as shown in Figure 4.5.7. The small recorded torque indicated that deflection of the hydrostatic bearing had occurred. The differences between static and dynamic torques shown in Figure 4.5.7 indicated that some shock loading might have occurred. However, these differences were well within the precision of the measuring procedures. For the torque values, errors up to 0.1 Nm were possible as indicated by the standard

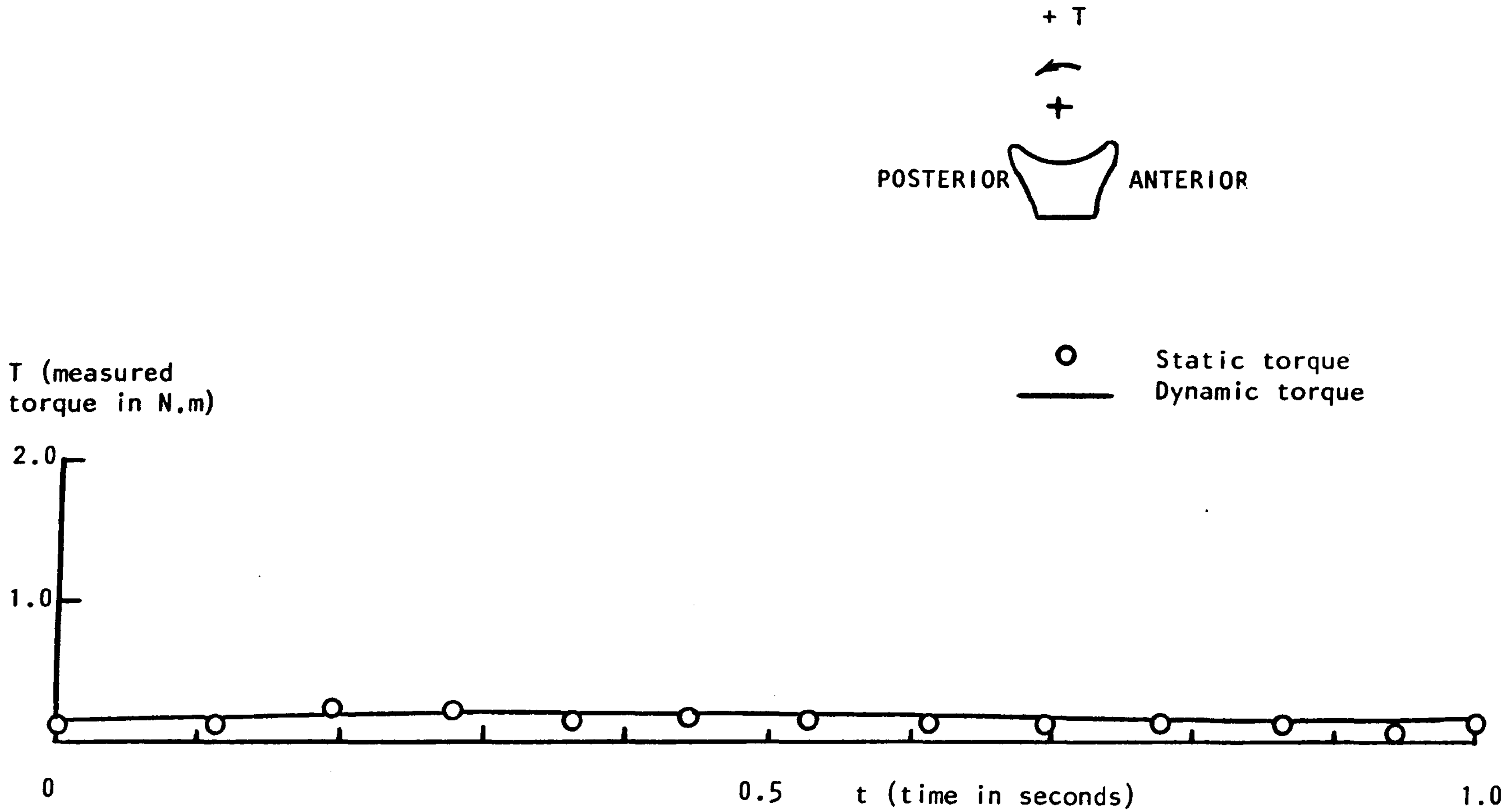

Figure 4.5.7 : Torque imposed on the torque assembly by the Kistler force transducer during static and dynamic application of load with spacers replacing the ankle specimen and without oscillation of the upper loading assembly. (The axes scales were chosen for easy comparison with subsequent plots).

error quoted in Figure 4.5.2. In addition, inaccuracy in specifying the imposed loads occurred in both static and dynamic procedures.

Larger differences of about 0.4 Nm were recorded between the static and dynamic torques when the rubber spacer was replaced by a steel one. Therefore, the stiffness of the specimen appeared to increase the shock loading on the Kistler force transducer. However, the ankle specimens were probably closer in compliance to the configuration which included the rubber spacer.

4.6 Mounting of the Joints

A total of five joints were mounted in the ankle simulator. These joints have been described in Chapter 3 and they were included in the measurements of surface radii of curvature. The tubular sleeves used to hold the joint components (shown in Figure 3.3.2) were themselves used in mounting fixtures to place the specimens in the simulator.

Joints numbers II and III were mounted and used to develop the experimental technique. The complete mounting procedure was applied to joints number 1, 2 and 3. The joint components were initially fixed in plaster of Paris using the procedure described in Section 3.3. The surface profiles had been measured and the radius of curvature of the closest profiles to both medial and lateral sides of the talus had been calculated as described in Section 3.5. Dividers were used to enable the approximate centres of the arcs representing the surfaces to be marked on the tubular sleeve containing the talus for both the medial and lateral sides. The sleeves containing the talus was then inserted into the mounting fixture shown schematically in Figure 4.6.1.

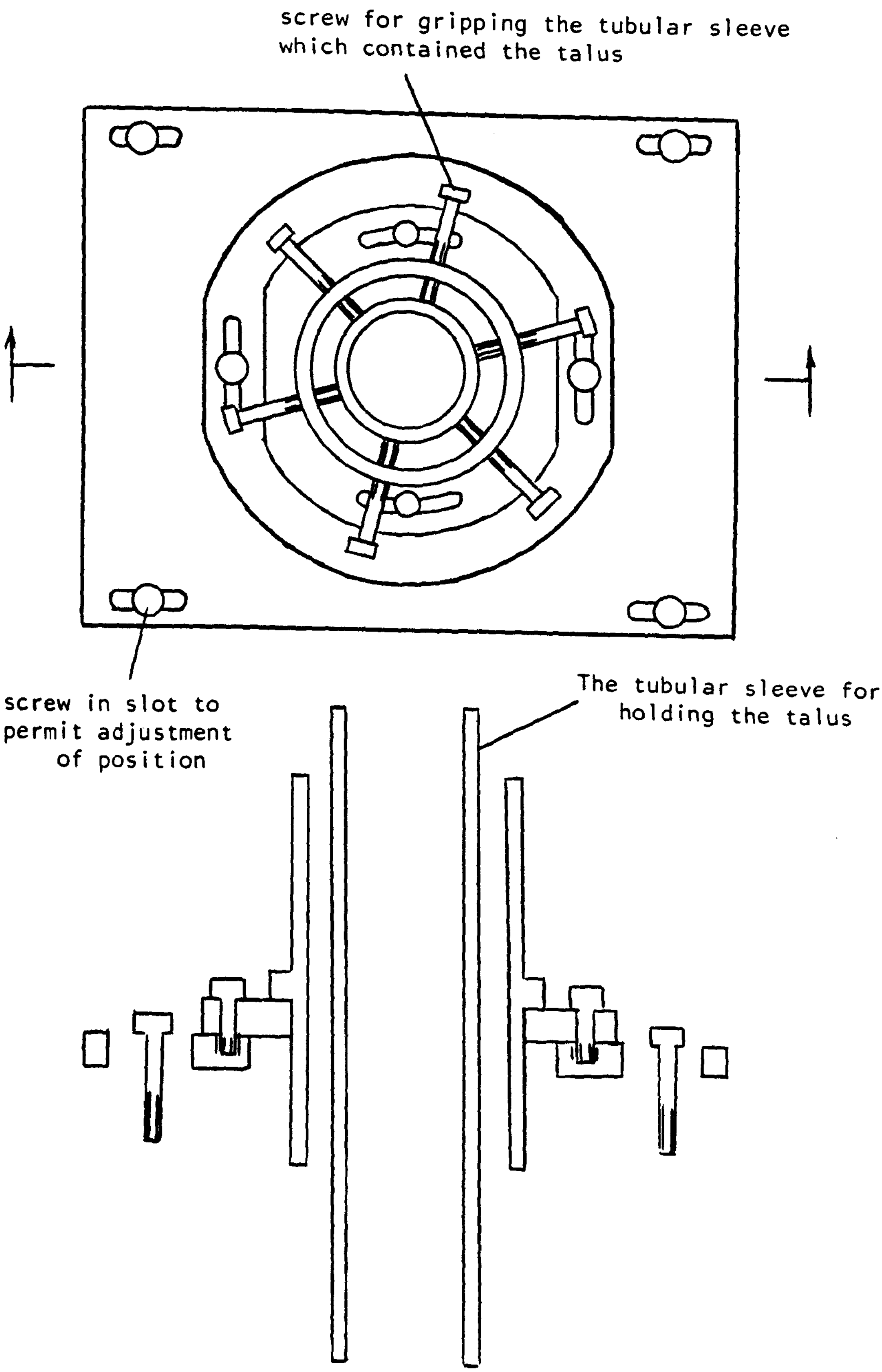

Figure 4.6.1 : Schematic of the talus fixture.

The mounting fixture could displace and rotate the sleeve which held the talus since its various connecting screws were located in slots.

The tibia and talus with some of their mounting fixtures are shown in Figure 4.6.2.

The mounting of the tube containing the tibia involved the three levelling screws shown in Figure 4.6.2 and two clamps which held the rim of the tube onto the torque assembly. A schematic representation of this mounting fixture is shown in Figure 4.6.3. The talus mounting fixture was simply attached with four screws to the top of the upper loading assembly. A mounted ankle specimen is shown in Figure 4.6.4. Aligning pins were attached to the inside of the torque assembly as shown in Figure 4.6.4.

Gauge blocks were placed under the base of the loading assembly so that the centres of the rolling element bearings and the hydrostatic bearings were aligned. The joint components and mounting fixtures were placed into the simulator. The talus mounting fixture was fastened to the upper loading assembly but the tubular sleeve which held the talus remained loose. The sleeve was then positioned by hand until the aligning pins touched the marked centres mentioned previously. The six screws in the talus fixture which held the talus sleeve were carefully tightened. Since these screws were position on two horizontal planes, the sleeve could be tilted from the vertical, if required. The tubular sleeve containing the tibia was then raised using the levelling screws until it made nominal contact with the talus. Once again the tibia could be tilted slightly by setting each levelling screw at a different height. Once in position the tibia sleeve was clamped to the torque assembly.

Figure 4.6.2 : The tibia and talus with some of their mounting fixtures.

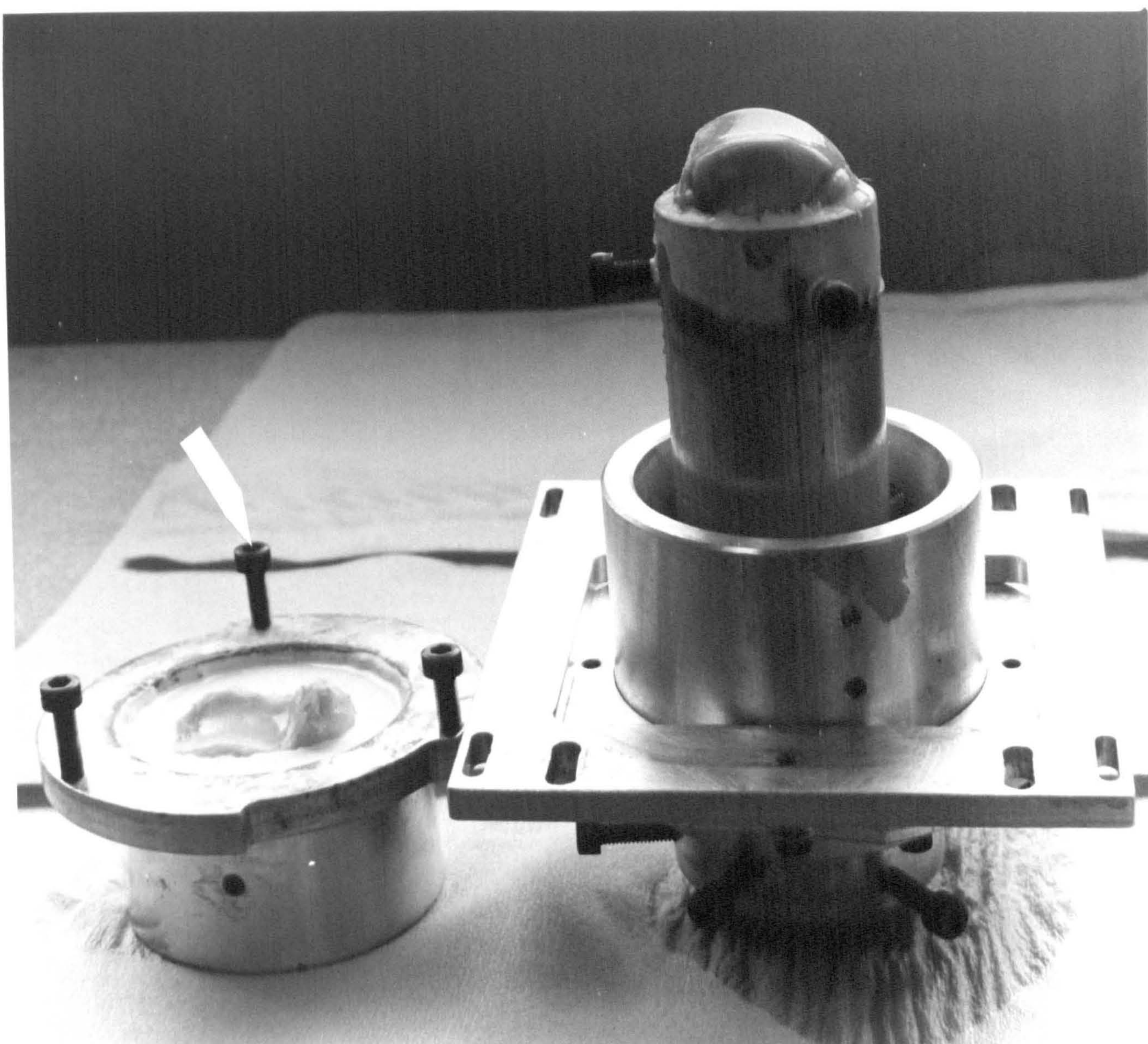

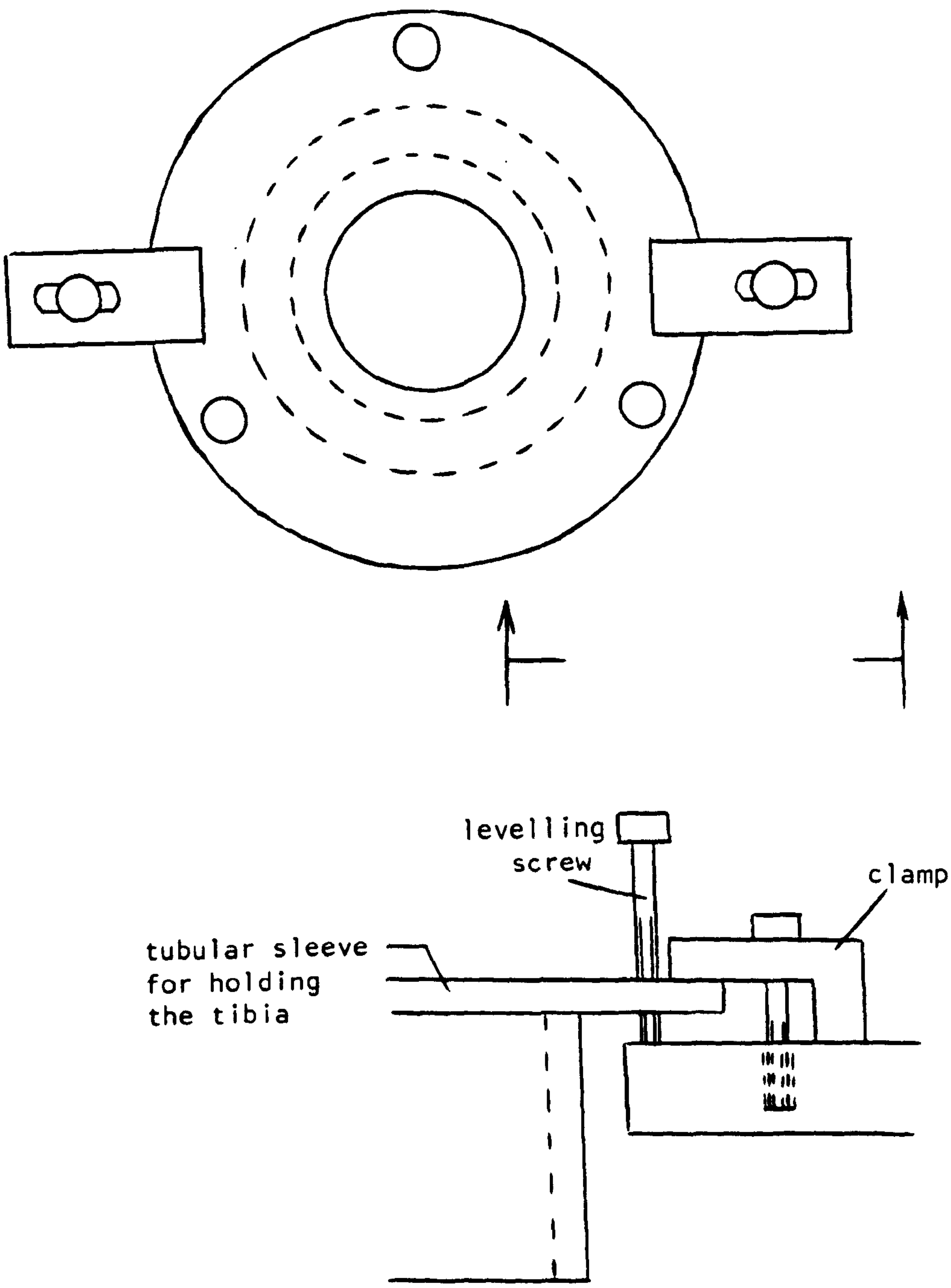

Figure 4.6.3 : Schematic of the tibia mounting fixture.

Figure 4.6.4 : A mounted ankle specimen.

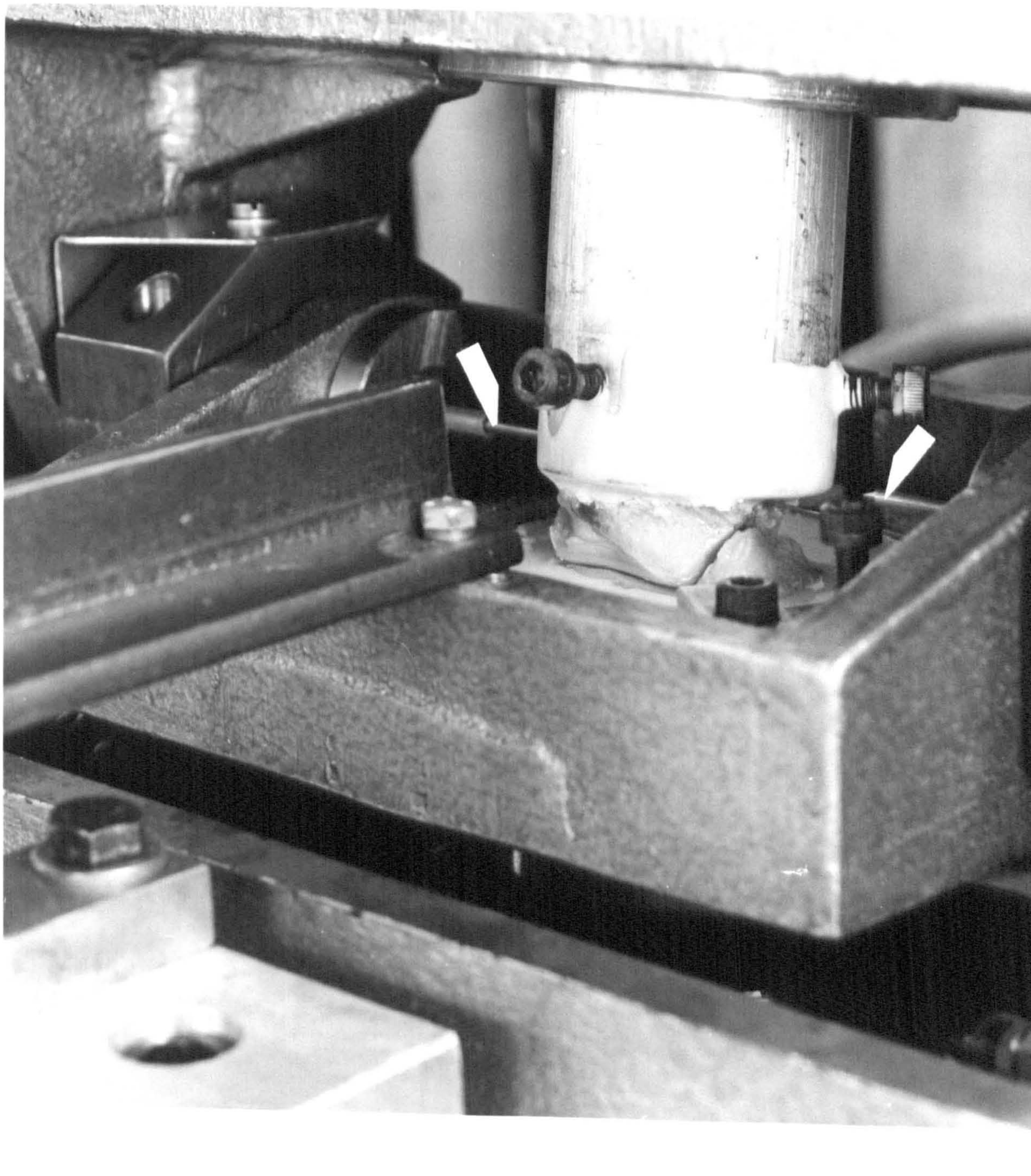

Having completed a trial mounting of the ankle specimen, the various screws were tightened and a low load applied. With the pinion gear detached, it was possible to oscillate the upper loading assembly by hand. In general, the joint seized up at some point in the oscillation. If this occurred various small adjustments were made to the position until the torque imposed during the oscillation by hand was small. Trials under full load were then conducted with the pinion gear in place. Again adjustments were made until the measured torque was minimized. It was also important to keep the tibia located in the centre of the talus with respect to the anterior-posterior dimensions of the contact region. The mounting procedure could take from half an hour to four hours depending on the conformity of the particular joint specimen.

The complexity of the mounting procedure meant that a minimum of two days was required to test a particular ankle joint. On the first day the specimen which had been thawed out overnight, was dissected, fixed in the tubular sleeves and measured using the Talycontor instrument as described in Chapter 3. The joint components were then stored overnight in a refrigerator while keeping the surfaces soaked in saline. The mounting and friction experiments were performed on the second day.

4.7 General Experimental Procedure:

Certain general procedures adopted in the operation of the simulator must be considered in addition to the detailed factors described earlier.

The minimum driving pressure (p_M) had to be set prior to each test session. This involved inserting the special force transducer, disconnecting the pinion gear and running the simulator for about ten minutes. The minimum driving pressure was then adjusted until the peak load specified for the friction experiments was attained. If the simulator was used continuously, the load pattern remained stable. However, if the simulator was left for about twenty minutes, the load had to be re-checked. Also, if the static loading procedure was introduced the minimum driving pressure had to be set again.

In general, the torque changed little when the simulator was running with an ankle joint in place. However, the torque values recorded in the present study were all obtained after about three minutes of running at the specified conditions. This helped to avoid the possibility of friction transients (Linn, 1967) which would have influenced the measured torque.

Two lubricants were used in all the experiments. Initially, saline solution (0.9% NaCl) was used with a cycle period of 1.0 s. Next, bovine synovial fluid replaced all the saline and was allowed to soak the surfaces for a minimum of about twenty minutes.

The ankle joint simulator and associated instrumentation are shown in Figure 4.7.1. Some of the equipment mentioned in previous sections is also visible.

4.8 Results of a Preliminary Study with Ankle Joint I:

When the cam had been fabricated and the limit switch installed, joint number I was tested in the simulator. The joint fixtures had been fabricated but only three screws existed in the talus fixture for gripping the talus holder and the alignment pins had not been constructed. The friction experiment with joint number I had a torque measuring system similar to that used by

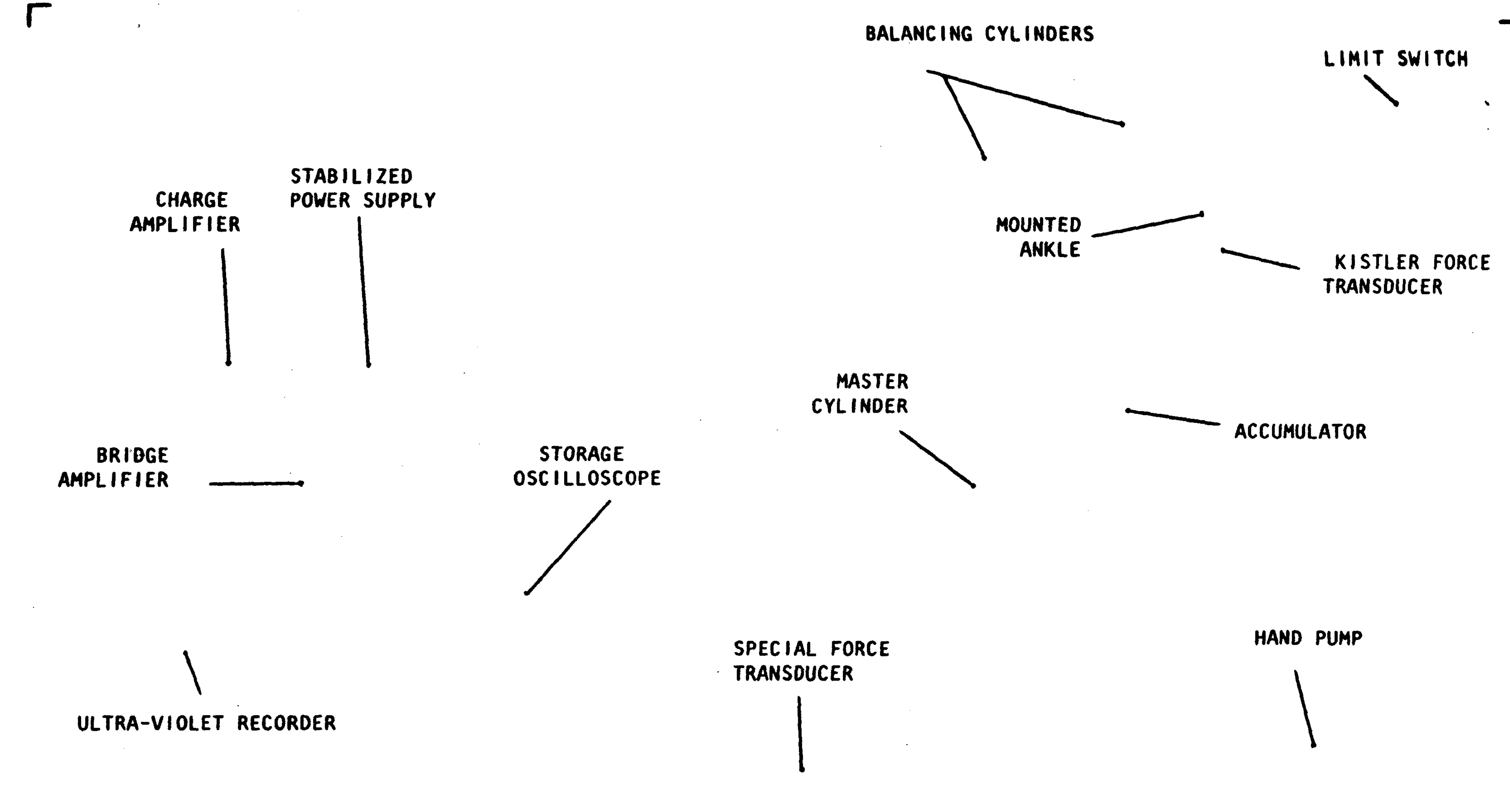

Figure 4.7.1 : The ankle joint simulator and associated instrumentation

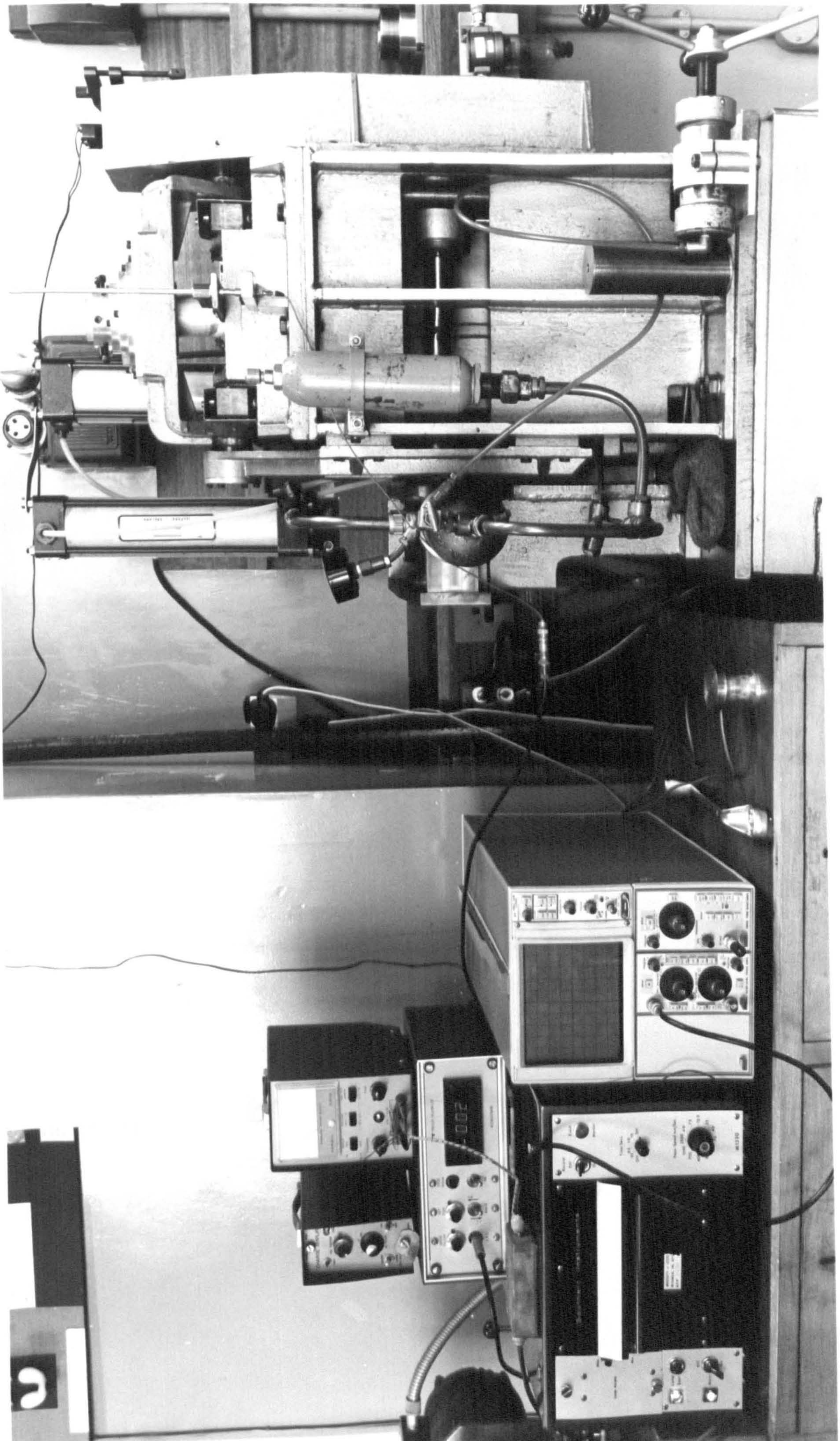

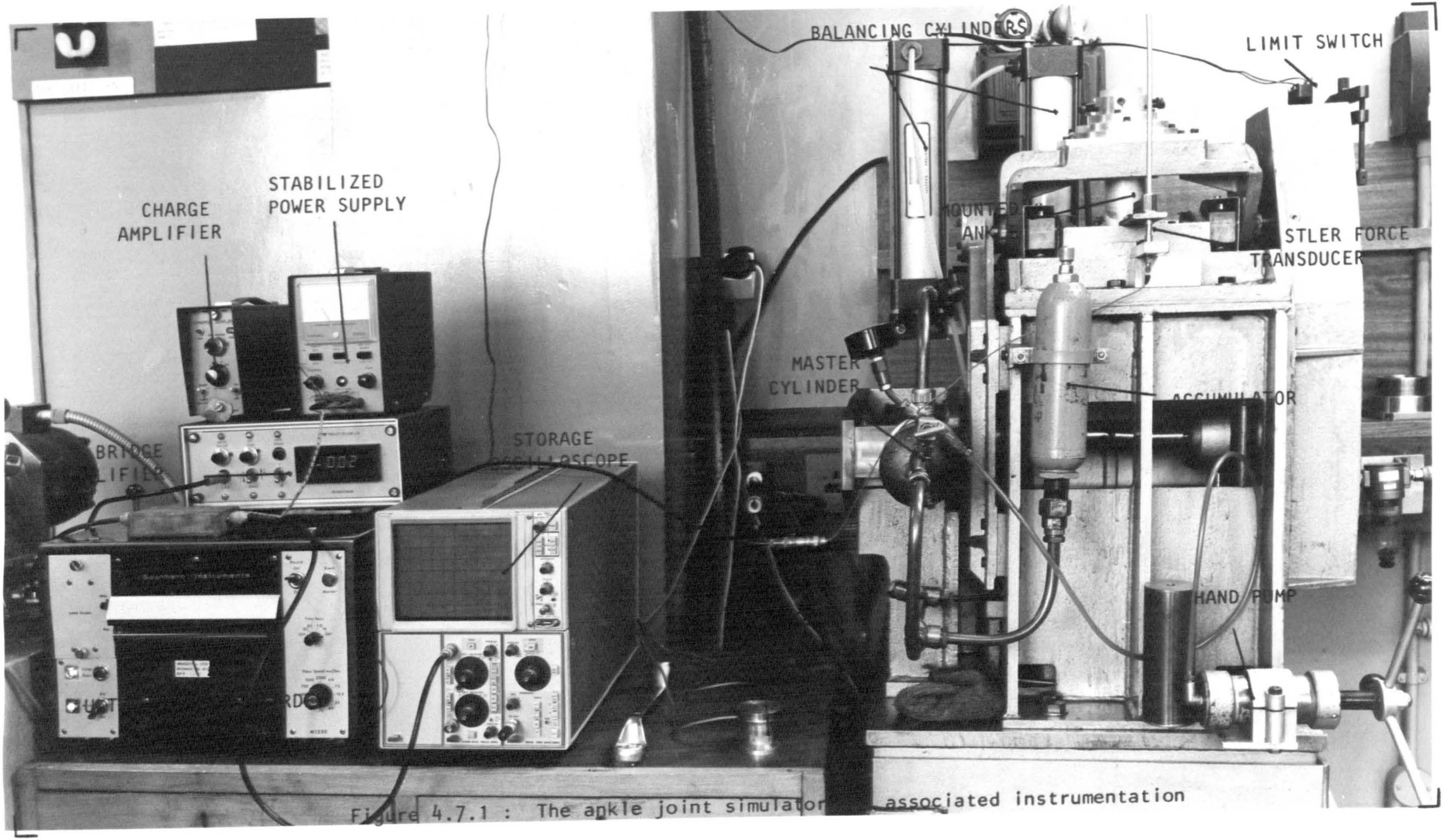

Figure 4.7.1 : The ankle joint simulator and associated instrumentation

O'Kelly (1977) and it is possible that hysteresis in the transducer might have affected the measured torque at high loads. Also, for this experiment, the oil flow rate to the hydrostatic bearings was reduced because of vibration from the pump which seriously distorted the measured torques. As a result, contact may have occurred in the hydrostatic bearings leading to the recording of reduced torques. In addition, the static loading procedure described in Section 4.6 was not applied in this experiment.

Despite the many limitations, the results of the friction experiment on joint number 1 have been included in this thesis. However, since it was considered a preliminary study its main purpose was to guide the development of the more elaborate procedures for testing further joints such as those numbered 2 and 3.

The dynamic torque was measured as shown in Figure 4.8.1. Small changes appeared in the torque curve when saline was used as a lubricant instead of bovine synovial fluid and when the period of the cycle (t_p) was altered. Also, the position of the joint was adjusted in an attempt to improve the alignment. This caused a change in the shape of the torque curve as well as increases in the magnitude of the torque shown in Figure 4.8.1.

It was not possible to locate the point of zero torque in Figure 4.8.1 since the Kistler force transducer output drifted significantly in about 60 seconds. This problem was solved in the investigations of O'Kelly (1977) and Linn (1967) by applying the same load pattern for clockwise and counter-clockwise rotation. The zero point was then located by a "folding" method. However, in the present experiment, in which an attempt was made to simulate swing phase loading, this technique could not be applied.

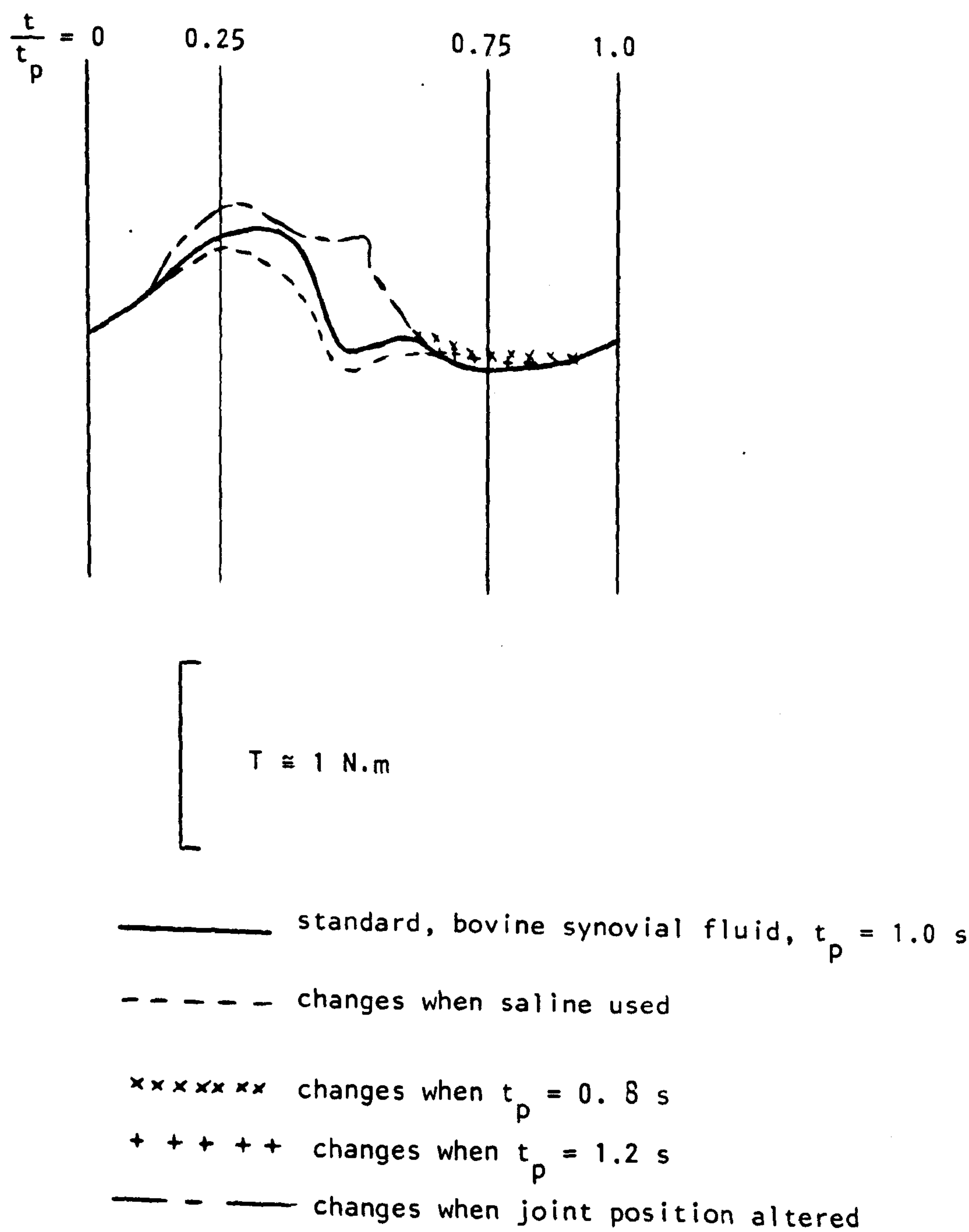

Figure 4.8.1 : Measured torque (T) versus dimensionless time (t/t_p) for joint number 1

After the dynamic torques had been measured, a constant load was applied and the static torques measured at various positions in the cycle. This was an earlier version of the static loading procedures described in Section 4.6. Since the load was not constant, the static torques could not be compared directly with the correponding dynamic values. However, significant static torque values were recorded and it became clear that the dynamic torque values alone could not be used directly to determine friction in the ankle joint.

4.9 Results for Ankle Joints 2 and 3:

The full experimental procedure was employed in testing ankle joints 2 and 3. The dynamic torque was measured as outlined in Figure 4.9.1 and 4.9.2. The torque curves for different cycle periods and lubricants were identical. However, the range of torques recorded for joint 2 was much smaller than that for joint 3.

The dynamic torque curves are also shown in Figures 4.9.3 and 4.9.4 along with the static torque values. The zero positions for the dynamic torque curves were established by using the static torque values which had accurate zero values. Considering Figure 4.5.5 and equation (4.5.6), it was noted that for the frictional torque (T_f) to oppose the motion, the static torque (T_S) must have exceeded the dynamic torque (T_D) for $0.25 < t/t_p < 0.75$. For all other portions in the cycle $T_D > T_S$. Thus, during the swing phase the dynamic torque T_D had a magnitude which was less than T_S until $t/t_p = 0.75$ and then greater than T_S for the remainder of the cycle. The dynamic torque curve was relocated until it satisfied this

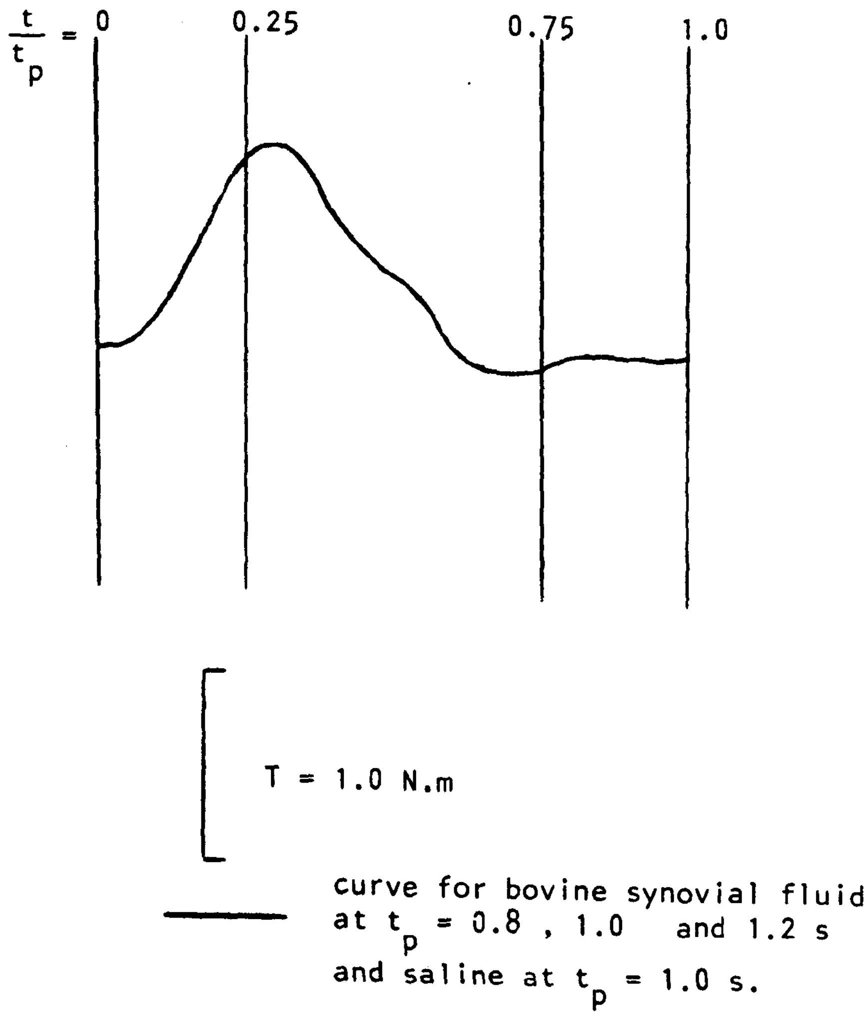

Figure 4.9.1 : Measured torque (T) versus dimensionless time (t/t_p) for joint number 2.

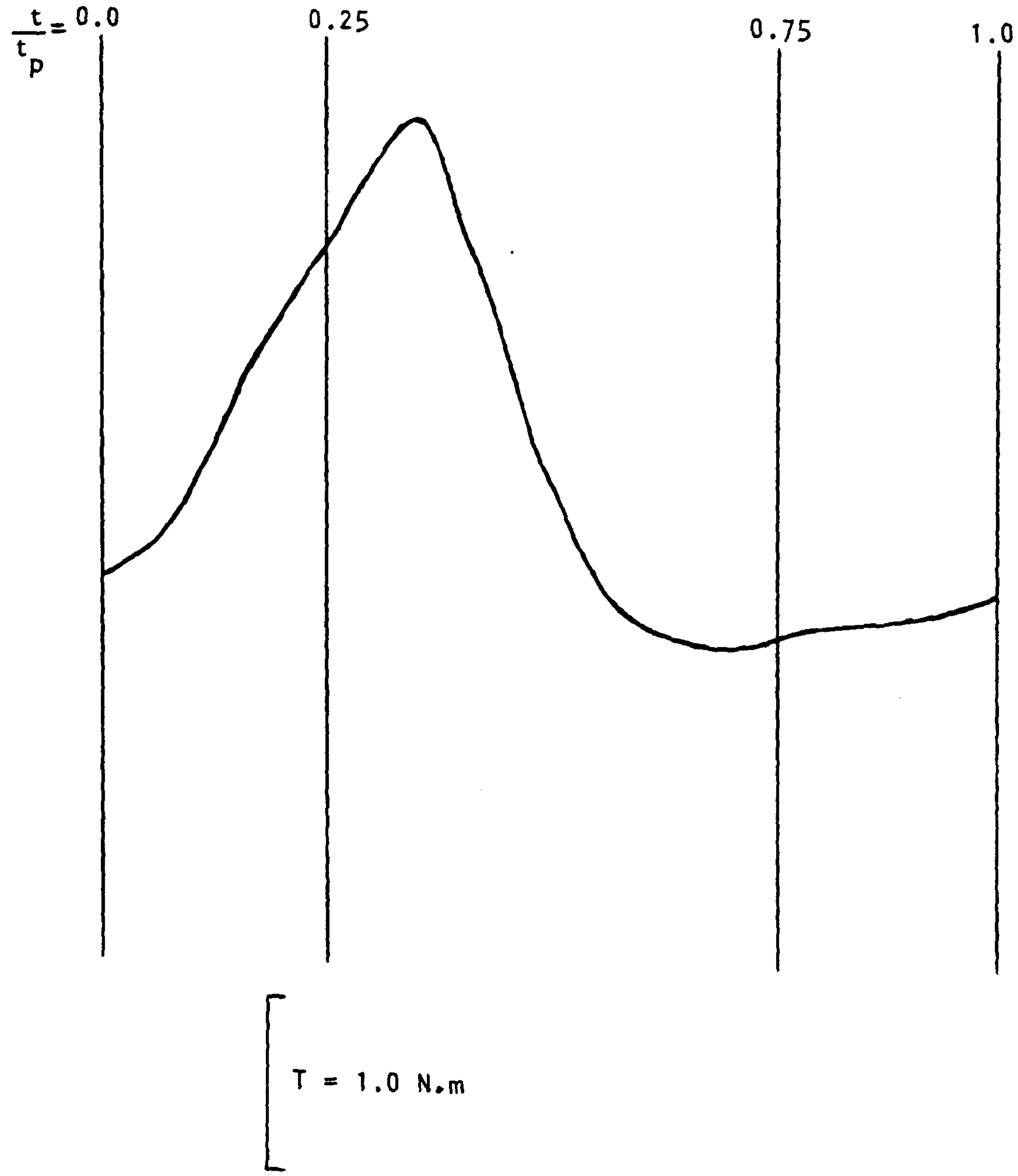

———— curve for bovine synovial fluid at t_p = 0.8 s, 1.0 s and 1.2 s and saline at t_p = 1.0s.

Figure 4.9.2 : Measured torque (T) versus dimensionless time (t/t_p) for joint number 3.

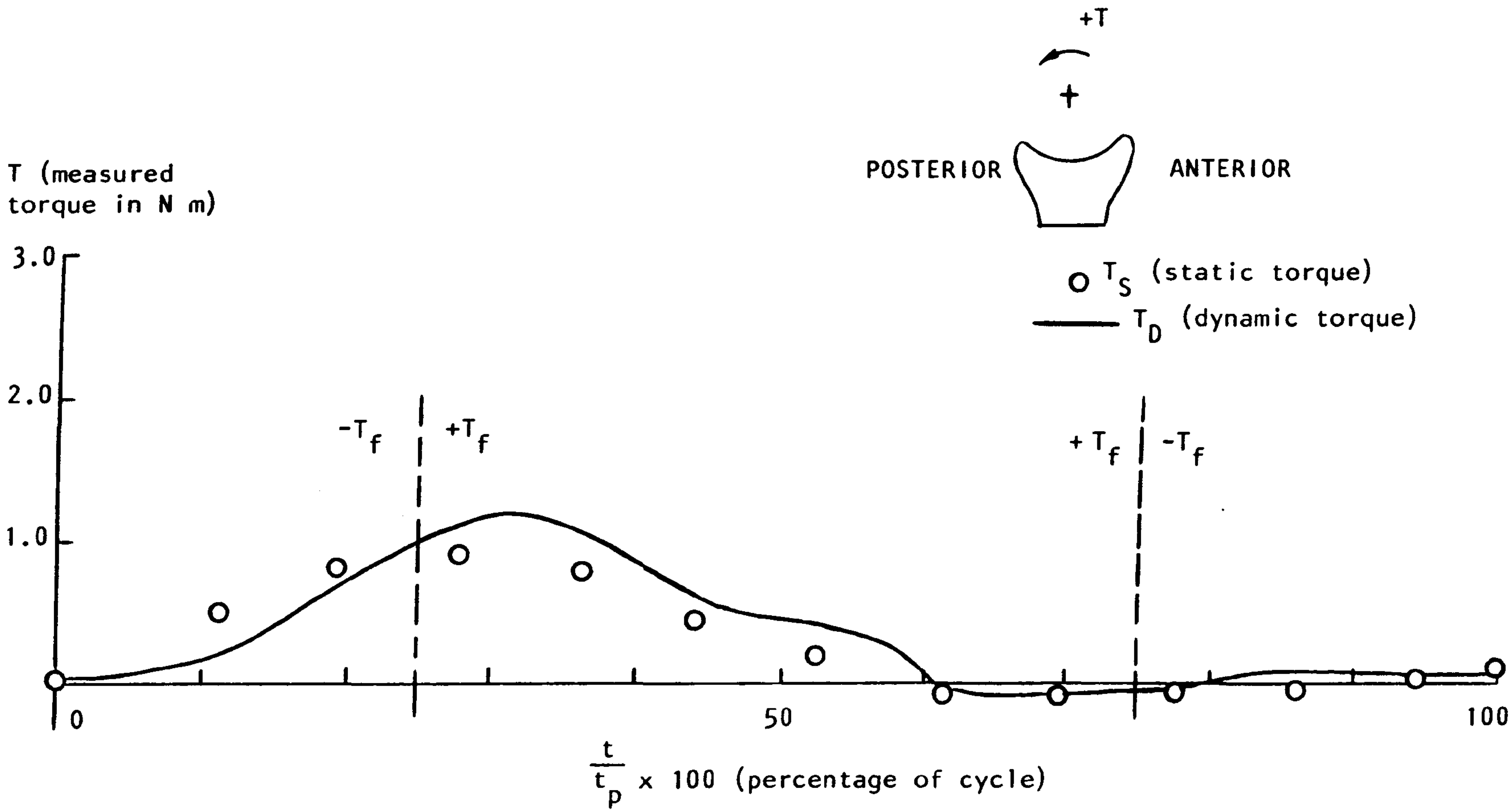

Figure 4.9.3 : Torque imposed on the torque assembly by the Kistler force transducer during static and dynamic application of load for joint number 2. If a frictional torque (T_f) existed, then $T_f = T_S - T_D$. To oppose the sliding motion

i) $T_f < 0$ for $0 < \frac{t}{t_p} < 0.25$ and $0.75 < \frac{t}{t_p} < 1.0$.

ii) $T_f > 0$ for $0.25 < \frac{t}{t_p} < 0.75$.

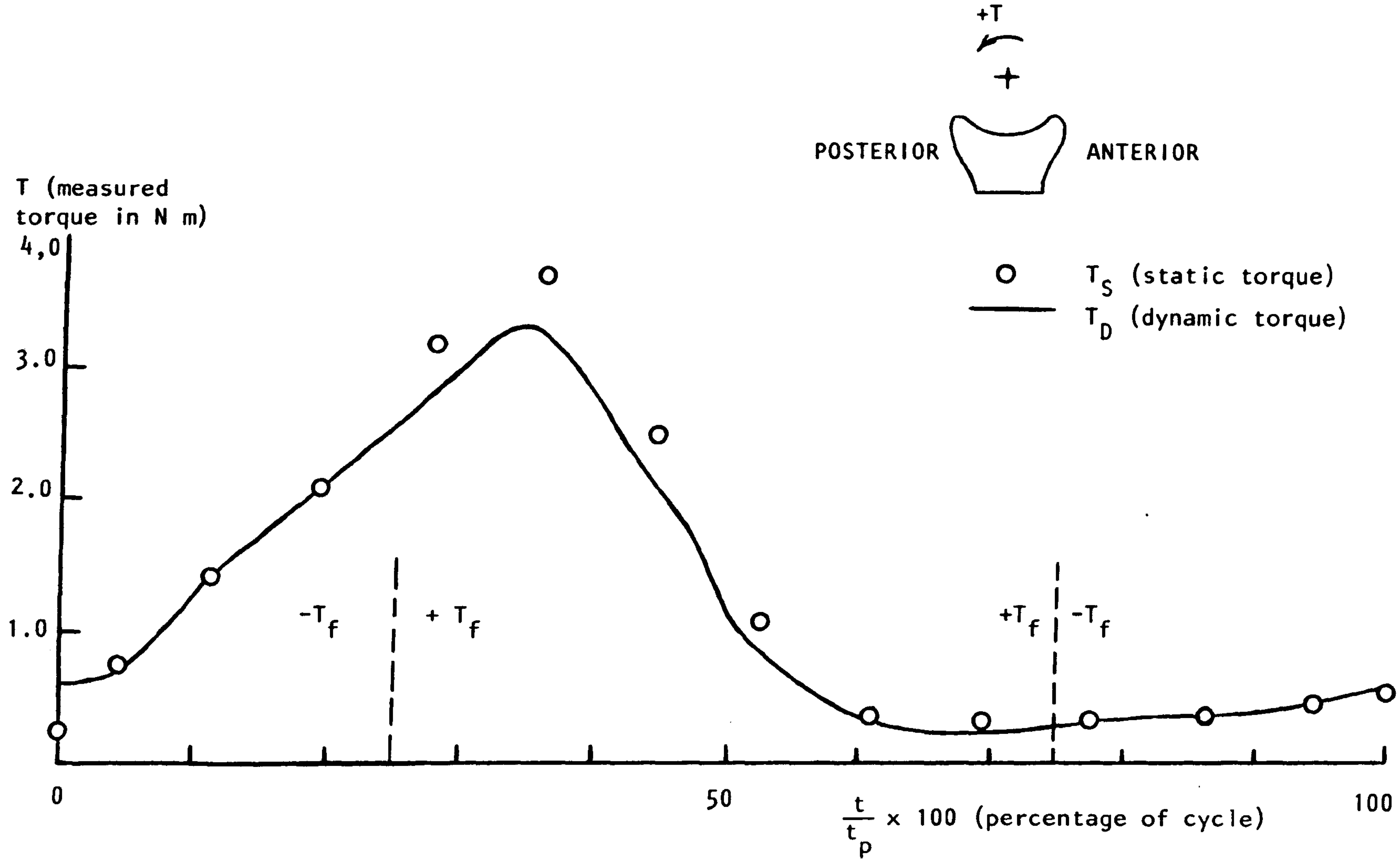

Figure 4.9.4 : Torque imposed on the torque assembly by the Kistler force transducer during static and dynamic application of load for joint number 3. If a frictional torque (T_f) existed, the $T_f = T_S - T_D$. To oppose the sliding motion

i) $T_f < 0$ for $0 < \frac{t}{t_p} < 0.25$ and $0.75 < \frac{t}{t_p} < 1.0$.

ii) $T_f > 0$ for $0.25 < \frac{t}{t_p} < 0.75$.

criterion as closely as possible and by this means the commom zero for dynamic and static torque curves were established. This procedure produced good agreement between static and dynamic torque throughout the cycle as shown in Figure 4.9.3 and 4.9.4. This clearly suggested that frictional torques were small compared with the torques arising from the alignment of the joint specimen.

4.10 Discussion of the Results:

The present study was intended to follow and extend the work of O'Kelly (1977). The magnitude of load and velocity applied in the present study to human ankle joint specimens were similar to those applied by O'Kelly and the resulting measured torques were also about the same. However, the present study did not yield the variation of friction between the cartilage surfaces throughout the applied cycle observed by O'Kelly.

The measured dynamic torque curves shown in Figures 4.8.1, 4.9.1 and 4.92 all exhibited a striking similarity to the loading curves. The effect of load on the Kistler force transducer measurements was small when the load axis was aligned as shown in Figure 4.5.7. Thus, it appeared that misalignment of the joint components had occurred in the cycle. The mounting procedure could not eliminate this misalignment. This suggested that the centre of rotation moved during the oscillation. This view was supported by the higher torque values measured for joint 3 compared with joint number 2. In Chapter 3, much poorer conformity of the surfaces of joint 3 (R = 0.19 m) were recorded. On the other hand joint 2 had excellent conformity (R = 1.00 m).

The measured torques changed when the position of the joint components was altered by a small amount as illustrated in Figure 4.8.1. Thus, the torque measurements from the present study were not unique for a particular ankle joint specimen.

When the accuracy of the measuring system was considered, it was clear that no significant differences existed between the static and dynamic torque measurements recorded in Figures 4.9.3 and 4.9.4. The rather large apparent difference between peak static and dynamic torque shown in Figure 4.9.4 was believed to result from setting the centre of rotation of the upper loading assembly lower than its position during the setting of the minimum driving pressure. This would have caused lower applied loads as discussed in Section 4.4 and thus lower dynamic torques.

By carefully considering Figures 4.9.3 and 4.9.4 it was possible to select maximum possible friction coefficients which applied to both the peak and the swing phase load regions. Friction co-efficients of up to 0.01 would have remained undetected due to the difficulties in measurement associated with the present experiments. Friction coefficient of this magnitude have been recorded for the cartilage surfaces of synovial joints in many previous investigations as discussed in Section 4.2.

4.11 Concluding Remarks:

The experimental procedures outlined earlier were not capable of detecting and recording the low coefficients of friction for cartilage surfaces from human ankle joint specimens. It can, however, be stated that friction coefficients lower than about 0.01 must have occurred.

The present study did show the difficulties involved in testing a joint with a changing centre of rotation in a simulator of the present form. Obviously, a much more sophisticated machine is required to overcome this limitation.

The load, velocity and angular displacement of the ankle joint have been described in this chapter. These conditions will be applied in subsequent theoretical studies. Both the present experimental situation and conditions similar to those occurring in the ankle during walking will be modelled.

CHAPTER 5

THEORETICAL MODEL FOR ANKLE JOINT LUBRICATION

5.1 INTRODUCTION

A number of different approaches have been employed in theoretical studies of synovial joint lubrication. Each of these approaches makes an initial assumption concerning the lubrication of synovial joints in vivo. In some investigations boundary lubrication was assumed to occur (Radin and Paul, 1972). In others it was assumed that the surface asperities of cartilage were in close proximity, and this formed the basis of both the weeping (McCutchen, 1978) and boosted (Dowson et al, 1970) lubrication theories as discussed in Section 2.4. The concepts of boosted and weeping lubrication were extended in elaborate studies of the flow of the interstitial fluid within and across the surface of cartilage (Torzilli, 1976). However, if full fluid film lubrication exists in synovial joints in vivo, the models involving close proximity of the cartilage asperities may not apply.

Human synovial joints have compliant surface layers (cartilage) on a relatively rigid backing (subchondral bone). The converging-diverging surface geometry and oscillating motion are capable of entraining the surrounding lubricant (synovial fluid). It is known that bearings with these characteristics can generate self-acting fluid films (Tanner, 1966; Dowson, 1967; Bennett and Higginson, 1970). In assessing the mode of lubrication in a bearing it is customary to assume that fluid film lubrication occurs and then to compare the predicted film thickness generated between smooth surfaces with the composite surface roughness of the bearing surfaces. If the calculated film thickness is large enough to separate the surface asperities, full fluid film lubrication can be anticipated. Elastohydrodynamic lubrication occurs when the film pressures are sufficient to deform the compliant surfaces, as described in Section 2.4.

A considerable simplification of the analysis occurs if it is assumed that the cartilage can be treated as a simple elastic material. Studies of the properties of cartilage have shown that it behaves essentially like an elastic solid when subject to cyclic loading patterns (Johnson et al, 1977; Higginson and Snaith, 1978). Investigation of squeeze film lubrication for a bearing which modelled the synovial joint and included porous elastic surfaces, indicated that the porosity had a small effect on full fluid film lubrication (Higginson and Norman, 1974a).

Thus the theoretical model developed in this thesis considers the cartilage to be an elastic surface layer exhibiting converging-diverging surfaces. The entraining action of such a bearing lubricated by a fluid lubricant was then considered and the details of the model were based on the human ankle. A representative geometry was obtained as outlined in Chapter 3, along with load and velocity conditions for walking similar to those described in Chapter 4. The cartilage surfaces were assumed to be perfectly smooth and to be held apart by synovial fluid. A similar approach was used by Higginson (1978), Rybicki et al (1979) and Dowson (1980).

The predicted fluid film thicknesses will be compared with the surface roughnesses for cartilage quoted by Clarke (1979) and Sayles et al (1979). If the estimated film thicknesses are much smaller than the heights of the surface asperities, other lubrication mechanisms must also act. In this case, the present theoretical model would identify imposed conditions contributing to the breakdown of full fluid film lubrication. However, if the predicted fluid film thicknesses exceed the heights of the surface asperities, the present theroretical model may provide a detailed description of the lubrication mechanics of the human ankle during walking.

5.2 An Equivalent Bearing for the Ankle

In Figure 3.7.1 a partial journal bearing with compliant surface layers was used to represent the geometry of the ankle joint. The theoretical modelling required a further geometrical transformation to an equivalent bearing. This facilitated the application of a standard form of the Reynolds equation and allowed comparison with the theory developed by other investigators. The equivalent bearing is shown in Figure 5.2.1 and the following standard, reduced form of the Reynolds equation was adopted.

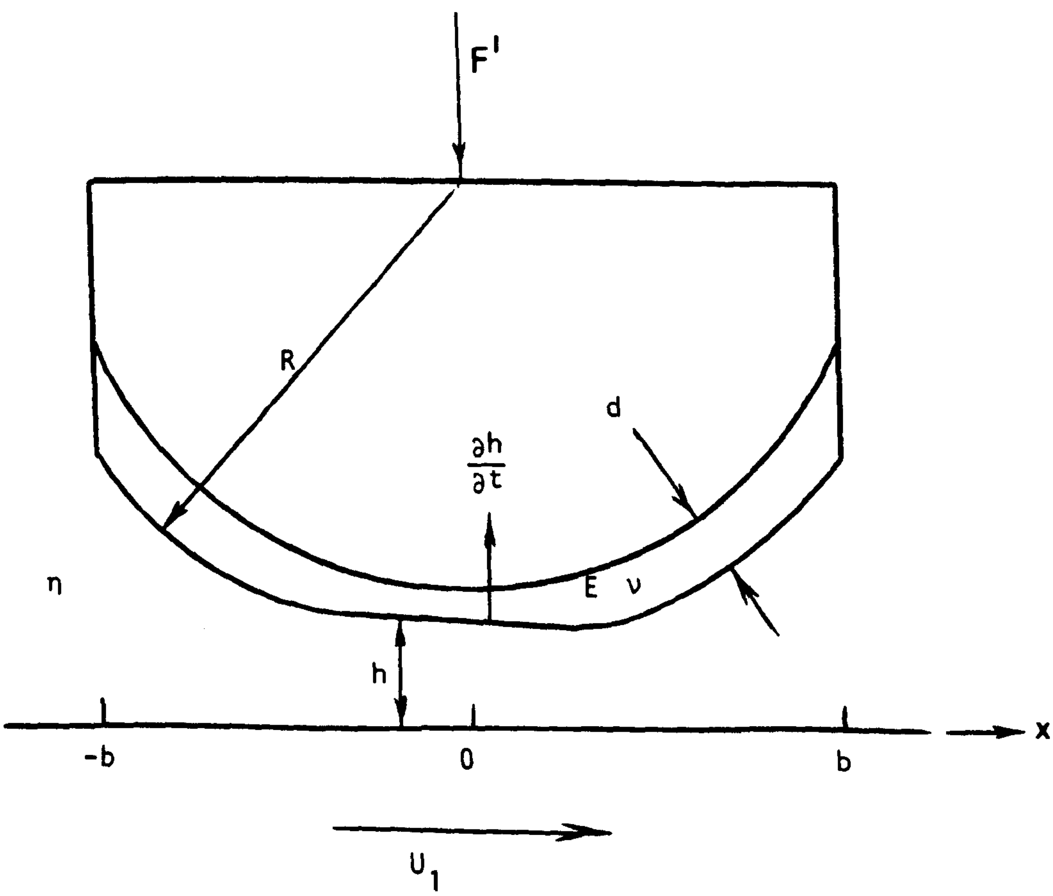

Figure 5.2.1 : An equivalent bearing for the ankle.

$$\frac{\partial}{\partial x}\left(h^3 \frac{\partial p}{\partial x}\right) = 12\eta \left(u \frac{\partial h}{\partial x} + \frac{\partial h}{\partial t}\right) \qquad (5.2.1)$$

The entrainment velocity $u = \frac{U_1 + U_2}{2}$ where U_1 and U_2 are the surface velocities of the bearing, and in the present case $u = \frac{U_1}{2}$. The derivation of the Reynolds equation in this form required the following assumptions:

i) The fluid was Newtonian.

ii) The flow was laminar and inertial forces could be neglected.

iii) Body forces (e.g. gravity) were negligible.

iv) The film thickness (h) was small compared to the radii of curvature of the surfaces and the contact dimensions.

v) The lubricant was incompressible.

vi) There was negligible variation in pressure (p) and viscosity (η) through the thickness of the film.

vii) There was no slip at the surface-fluid interface.

viii) The lubricant flow occurred in the x-direction only (i.e. the equivalent bearing was infinitely wide).

ix) The surfaces were impermeable and thus only the entrainment velocity (u) could draw lubricant into the contact.

x) The surfaces did not stretch in the x-direction.

The assumption of a Newtonian lubricant can often be relaxed in lubrication theory while still using equation (5.2.1). However, in the present analysis the lubricant was assumed Newtonian in spite of contrary finding at low shear rates by investigators such as Cooke et al (1974).

The results of Cooke et al indicated that the assumption was reasonably accurate for shear rates greater than 10^3 1/s.

The assumption that lubricant flow took place only in the x-direction was particularly important in the theoretical analysis, since it simplified the entire solution. It was supported by the possible sealing effects of the contact in the medial and lateral malleoli regions of the ankle joint. Greenwald et al (1976) reported that contact initiated in these regions as static loading was increased from zero. However, if the length of the contact was long compared to the width and the side regions were not sealed, the possibility of significant side leakage and thus two dimensional flow existed (Dowson and Whomes, 1967; Roberts and Swales, 1969). In any case, it was anticipated that the assumption of one dimensional flow would yield film thickness predictions which would give a good indication of the potential of fluid-film lubrication in the ankle joint. If the present analysis does not yield encouraging values of film thickness from the point of view of fluid-film lubrication, consideration of side-leakage will lead to less optimistic predictions.

The assumption of impermeable surfaces was discussed in Section 5.1, and the assumption of the lack of surface stretching has been supported by Linn (1967), He estimated that shearing of the cartilage surfaces in canine ankles was too small to stretch the surfaces enough to enhance fluid film lubrication.

5.3 Values of the Governing Parameters:

Two sets of values of the governing parameters were considered for the equivalent bearing shown in Figure 5.2.1. The first set, designated case A, was chosen to represent the ankle during the friction experiments. The second set, designated case B, was chosen to represent the ankle in vivo during walking. The sensitivity of calculated film thickness and coefficient of friction to variations in the chosen parameters will be considered in Chapter 8. Cases A and B will be used as basic reference conditions throughout the remainder of this thesis.

A reduced radius of curvature (R) of 0.35 m was chosen and calculated using the average values for talus and tibia radii of curvature listed in Table 3.7.2. This value was used in both cases A and B. The calculation of a reduced radius of curvature for the equivalent cylindrical geometry was described by Dowson and Higginson (1966). It was noted that errors in geometric equivalence occurred when the contact length approached the individual component radii. This condition was possible for the ankle geometry if contact existed over the entire tibia as shown in Figure 3.7.1. However, it should be noted that the selected component radii for the ankle were themselves approximations. Furthermore, it has been suggested by Dowson and Higginson (1966) that the effect on estimated film thickness of errors caused by the reduced radius approximation is often quite small. Thus, the value for reduced radius of curvature of 0.35 m was used throughout the analysis, although alternative values can readily be introduced.

The x-axis for the equivalent bearing shown in Figure 5.2.1 was a geometric transformation of the curved surface of the tibia. Thus, the bearing length (2b) must follow the arc of the tibia profile. A value for b of 15.2 mm was calculated using the average length of the tibia listed in Table 3.7.2. This value was used in both cases A and B.

The thicknesses (d) of the elastic layer for the equivalent bearing was chosen as 2.4 mm by summing the average cartilage thicknesses listed in Table 3.7.2. The validity of simply adding the two cartilage layers will be discussed further in Chapter 7. This value was also used in both cases A and B.

The entrainment velocity, $\dot{u}$, for case A was chosen for a period, t_p, of 1 s. Since only the tibia moved in the friction experiments the entrainment velocity was half the surface velocity. Using the average talus radius listed in Table 3.7.2 and equation (4.4.1) the following expression was derived for entrainment velocity;

$$u = 10.3 \left|\cos 6.28\, t\right| \text{ (mm/s)} \qquad (5.3.1)$$

The entrainment velocity was always positive because the direction from which fluid was entrained did not matter to the theoretical formulation. For case B, a somewhat higher entrainment velocity was derived for the ankle joint during walking. Both Stauffer et al (1977) and Murray et al (1964) recorded relative angular displacemnt when both surfaces of the ankle were moving. From these measurements relative surface velocities were estimated as shown in Figure 4.4.4. Unfortunately, the entrainment velocity could not be determined from relative velocity unless one surface was stationary. Thus, without a better alternative, it seemed logical to assume that for case B one surface remained stationary while the other had a velocity with the same functional form as that used in the friction experiment. The entrainment velocity for case B was again half the velocity of the moving surface. Returning to Figure 4.4.4 the chosen entrainment velocity was;

$$u = 30.0 \left|\cos 6.28\, t\right| \text{ (mm/s)} \qquad (5.3.2)$$

which acted over a period of 1s.

The loading cycle applied in the friction experiments is shown in Figure 4.4.2. The load pattern only approximated that predicted during walking as discussed in Section 4.4. However, the proportion of the load which would be transmitted by the talus-fibula contact was not known with certainty. Thus, for both cases A and B the load per unit width (F') was calculated by dividing the load applied by the simulator by the average ankle width of 25 mm shown in Table 3.7.2. The values for the chosen load per unit width are listed in Table 5.3.1 for a cycle period (t_p) of 1s.

The lubricant viscosity chosen for case A was 5×10^{-3} Ns/m^2 which corresponded to that found by Cooke et al (1978) for bovine synovial fluid. The shear rate for this value of viscosity was 10^3 1/s. However. the shear thinning found by Cooke et al had a decreasing rate and thus the chosen constant value should be a reasonable approximation when higher shear rates exist. For case B, a viscosity of 1×10^{-2} Ns/m^2 was chosen which corresponded to that found by Cooke et al (1978) for human synovial fluid at a shear rate of 10^3 1/s.

The selection of higher viscosity values for synovial fluid will be discussed in the subsequent chapters of this thesis.

The selection of the elastic modulus (E) for the equivalent bearing shown in Figure 5.2.1 required careful consideration. The characterization of cartilage as a linear elastic material at a given creep strain was accomplished by Johnson et al (1977) and Higginson and Snaith (1979). Thus, if the creep of a synovial joint during walking was known and remained reasonably constant, it would be possible to specify the effective elastic modulus.

t_p(s)	Load (kN)	F' (load per unit width kN/m)
0	0.392	15.08
0.05	0.561	21.58
0.1	0.798	30.69
0.15	1.061	40.81
0.2	1.203	46.27
0.25	1.541	59.27
0.3	1.939	74.58
0.35	2.277	87.58
0.4	2.155	82.88
0.45	1.628	62.62
0.5	1.169	44.96
0.55	0.777	29.88
0.6	0.325	12.50
0.65	0.250	9.62
0.7	0.190	7.31
0.75	0.190	7.31
0.8	0.244	9.38
0.85	0.190	7.31
0.9	0.291	11.19
0.95	0.325	12.50
1.0	0.392	15.08

Table 5.3.1 : The loads and loads per unit width (F') for both cases A and B.

However, Johnson et al tested small cartilage specimens in unconfined compression with a non-porous platen pushing on the cartilage surface. They recorded elastic moduli for cartilage in the range 10 - 20 MN/m^2 for creep strains up to 0.3. On the other hand, Higginson and Snaith tested small cartilage specimens in confined compression with a porous platen pushing on the cartilage surface. They recorded much higher elastic moduli in the range 50 - 150 MN/m^2 for creep strains up to 0.3.

It was necessary to decide which values to use in the present analysis for a whole joint surface. Freeman et al (1975) applied cyclic loading (46 - 2237 N at 0.33 Hz) to entire hip joint specimens After 2000 cycles creep strains were about 0.16 and values of the average stress divided by the strain occurring in one cycle gave an elastic modulus of about 10 MN/m^2. Thus, a representative elastic modulus of 16 MN/m^2 was chosen for both cases A and B.

Finally it was necessary to select a value of Poisson's ratio, (ν), for the equivalent bearing. Estimates of Poisson's ratio in compression have been made by a number of investigators as shown in Table 5.3.2. It was convenient for modelling purposes to select a value of 0.5 for both cases A and B. However, theoretical calculations will also be performed for a Poisson's ratio of 0.4 in Chapter 7 to enable an estimate to be made of the significance of this parameter.

Investigator	Year	ν (Poisson's ratio)
Hayes and Mockros	1971	0.37 - 0.42
Hori and Mockros	1976	0.44 - 0.49
Johnson et al	1977	0.50

Table 5.3.2 : Estimates for Poisson's ratio in compression.

5.4 The Selection of Dimensionless Groups:

The following dimensionless groups were selected for the theoretical analysis:

$$H = \frac{h}{R}, \quad \mu, \quad H_o = \frac{h_o}{R}, \quad P = \frac{p}{E'}$$

$$T = \frac{t}{t_p}, \quad X = \frac{x}{r}$$

$$U = \frac{\eta u_A}{E'R} \quad W = \frac{F_A'}{E'R} \quad S = \frac{E't_p}{\eta}$$

$$D = \frac{d}{R} \quad B = \frac{b}{R} \quad \nu$$

where h = film thickness

R = reduced radius of curvature

μ = coefficient of friction

h_o = minimum film thickness at a particular instant in time

t = time

t_p = period for cyclic loads and velocities

x = spacial co-ordinate

η = dynamic viscosity

u_A = time averaged entrainment velocity for one cycle

$E' = \frac{2E}{1 - \nu^2}$ reduced modulus where E is the elastic modulus and ν is Poisson's ratio, both for the layer.

F_A' = time averaged load per unit width for one cycle

d = thickness of effective layer of elastic bearing material

b = half bearing length in direction of motion

ν = Poisson's ratio

It was convenient to identify each dimensionless group by name and to state whether it was a variable or a fixed parameter as shown in Table 5.4.1.

Dimensionless group	Designation
H	Film thickness (variable)
μ	Coefficient of friction (variable)
H_0	Minimum film thickness (variable)
P	Pressure (variable)
T	Time (variable)
X	Co-ordinate in direction of surface motion (variable)
U	Speed (fixed parameter)
W	Load (fixed parameter)
S	Squeeze factor (fixed parameter)
D	Layer thickness (fixed parameter)
B	Starvation factor (fixed parameter)
ν	Poisson's ratio (fixed parameter)

Table 5.4.1 : Identification of the dimensionless groups.

5.5 Concluding Remarks:

The various assumptions involved in the theoretical analysis presented in this thesis have been outlined. This included the introduction of an appropriate form of the Reynolds equation and the designation of an equivalent bearing for the ankle joint. Two main sets of conditions have been considered in this analysis of the ankle joint. They were designated as case A, representing the ankle joint in the friction experiments, and case B, representing the ankle joint in vivo during walking. The representative parameters defining conditions in each of these cases are listed in Table 5.5.1, along with the values for the dimensionless groups which had fixed values in the two cases.

Parameter	Dimension	Case A (representing the friction experiments)	Case B (representing the ankle joint in vivo during walking)
R	m	0.35	0.35
b	mm	15.1	15.2
d	mm	2.4	2.4
t_p	s	1.0	1.0
u_A	mm/s	6.5572	19.099
F'_A	kN/m	33.726	33.726
η	Ns/m^2	0.005	0.01
E'	MN/m^2	42.667	42.667
U	-	2.195×10^{-12}	1.279×10^{-11}
W	-	2.258×10^{-3}	2.258×10^{-3}
S	-	8.533×10^{9}	4.267×10^{9}
D	-	6.857×10^{-3}	6.857×10^{-3}
B	-	4.343×10^{-2}	4.343×10^{-2}
ν	-	0.5	0.5

Table 5.5.1 : Parameter values for the two basic cases (A and B) considered in subsequent analysis.

CHAPTER 6

THE PLANE INCLINED SURFACE BEARING MODEL

6.1 INTRODUCTION

The full analysis of the lubrication of ankle joints taking account of the compliant layers of bearing material and the cyclic nature of the loads and speed is a formidable task. In the study of piston ring lubrication, equation (5.2.1) has been solved for rigid parabolic surfaces using an implicit numerical procedure (Dowson et al, 1979). The lubrication of the equivalent bearing shown in Figure 5.2.1 for conditions of constant load and velocity has been considered in a number of recent studies (Hooke and O'Donoghue, 1972; Cudworth and Higginson, 1976; Gupta, 1976; Varnum and Hooke, 1977; Cudworth, 1978). Reasonable agreement between theory and experimental results has been obtained in these studies. However, it appears that no analysis has been undertaken for the lubrication of bearings consisting of layers of compliant material on a hard backing subjected to time varying loads and velocities.

It was therefore decided to approach the problem in two ways. In the first case deformation in the cartilage was modelled by representing the bearing by a simple, rigid plane inclined surface bearing subjected to cyclic, time dependent loads and velocities. In a subsequent analysis account was taken directly of surface deformation in the compliant layer. In this chapter the first approach is considered in some detail. The different approximation of surface deformation will be adopted in Chapter 7.

6.2 Simplifying Assumptions For Surface Deformation:

A full solution procedure would have to consider the generation of thicker or thinner films of lubricant within the contact as imposed conditions changed with time. This situation has been described by Gibson et al (1972) in the study of start up friction of O-ring seals. However, their analysis was not extended to cyclic time varying conditions.

In the present analysis, the assumed plane profile was permitted to adjust itself immediately throughout the cycle to accommodate changes in load and velocity. Thus, the procedure required some estimation of the surface profiles which occurred for various conditions of steady state sliding. When the entrainment velocity was zero a condition of pure squeeze film lubrication existed. Once again a profile for pure squeeze film lubrication was required.

In the theoretical analysis of the lubrication of compliant solids under conditions of steady state sliding and pure squeezing, the surface profile has often been approximated by a plane configuration. Baglin and Archard (1972) examined a cylinder sliding under steady state conditions over a half space of low elastic modulus. They assumed a plane inclined surface profile for the Hertzian region of the contact and obtained excellent agreement with the full numerical solution of Swales et al (1972). For pure squeeze film lubrication of a cylinder approaching a compliant layer, Cudworth and Mykura (1980) also assumed a plane surface profile. The theroretical predictions for a Hertzian contact were similar to those obtained in the theoretical analysis of Herrebrugh (1970). However, the experimental results of Cudworth and Mykura showed much thicker films than predicted for both Hertzian and layered contacts.

As mentioned previously, a plane surface configuration was assumed to approximate the profiles for steady state sliding and pure squeezing. This simplifying assumption allowed the lubrication of the equivalent bearing shown in Figure 5.2.1 to be approximated by the cyclic time varying lubrication of a plane inclined surface. The length and inclination of this surface was allowed to vary throughout the cycle. This type of problem has also been solved by Ruddy et al (1979) for a piston ring with a profile which changed with time as a result of ring twist effects.

When pure squeezing motion occurred, the plane surface was assumed to extend over the dry contact zone which was calculated without including surface traction effects. The same approximation for the dimensions of the plane surface was assumed by Cudworth and Mykura (1980). The required dry contact length was obtained from the data presented by Gupta and Walowit (1974).

When a non-zero entrainment velocity occurred, a method of estimating both the length and inclination of the equivalent plane inclined surface bearing was required. This was accomplished by considering the published solutions for the steady state sliding of a cylinder on a compliant surface layer. The following formulae were developed from the results of Varnum and Hooke (1977) and of Hooke and O'Donoghue (1972) for minimum film thickness under steady state conditions:

$$\frac{h_o}{R} = 1.159 \left(\frac{d}{a}\right)^{0.4875} \cdot K \qquad (6.2.1)$$

$$\text{for } \frac{a}{d} \geqslant 2$$

$$\frac{h_o}{R} = 1.335\, e^{-0.2396(\frac{a}{d})} \cdot K \qquad (6.2.2)$$

for $\frac{a}{d} < 2$

where $$K = \frac{\left(\frac{2\eta u}{ER}\right)^{0.6}}{\left(\frac{F'}{ER}\right)^{0.2}}$$

The half length of the dry contact (a) was again obtained from the data presented by Gupta and Walowit (1974). Equations (6.2.1) and (6.2.2) required that the pressures in the lubricant film were close to the dry contact stresses.

The length of the plane inclined surface was initially chosen to be equal to the length of the dry contact zone. An iterative procedure was used to select a slope which gave a steady state film thickness for the plane inclined surface bearing equal to that predicted by equation (6.2.1) or (6.2.2). The following equation was used for the steady state film thickness of the plane inclined surface:

$$\frac{F'M^2}{12\eta u} = \ln\left(1 + \frac{ML}{h_o}\right) - \frac{2ML}{2h_o + ML} \qquad (6.2.3)$$

where M is the slope of the plane surface and L is the length in the direction of motion. In general, such a solution could not be obtained. Thus, the plane inclined surface was extended in length until the gradient of the film pressure distribution became zero at a distance of half the dry contact length from the point of minimum film thickness. The result was a plane inclined surface bearing with a pressure distribution similar to the dry contact stress and a steady state film thickness equal to that predicted for a cylinder sliding on a compliant layer. The features of the assumed plane inclined surface are illustrated in Figure 6.2.1.

The network of simplifying assumptions which were adopted in the present study effectively reduced the procedure for allowing for the effects of surface deformation to an easily implemented iterative procedure. It was then necessary to incorporate this procedure into a solution for the cyclic time varying film thickness.

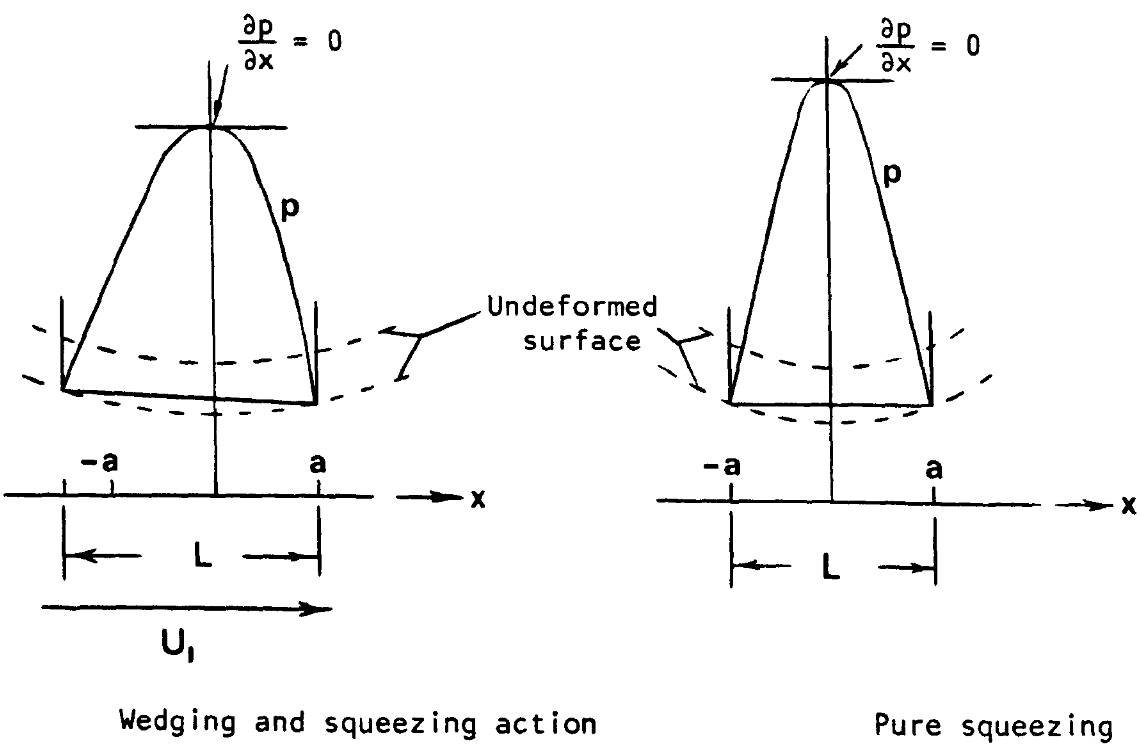

Figure 6.2.1 : The features of the assumed plane inclined surface for approximating deformation.

6.3 Lubrication Analysis:

For the analytical formulation it was convenient to describe the geometry of the equivalent plane inclined surface bearing as shown in Figure 6.3.1.

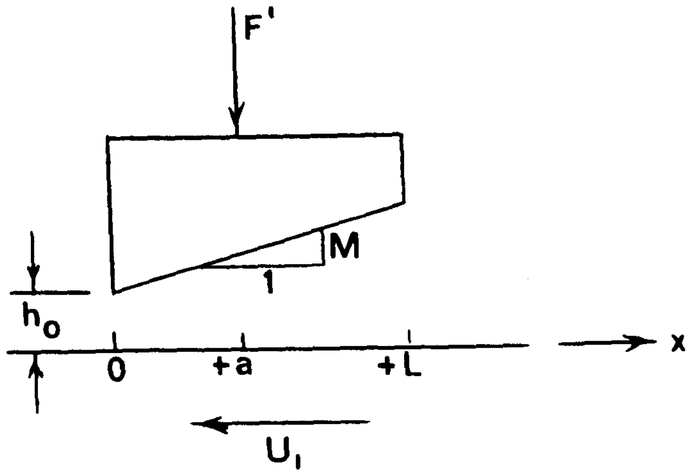

Figure 6.3.1 : The geometry of the plane inclined surface adopted for Section 6.3 only.

For this geometry equation (5.2.1) became:

$$\frac{\partial}{\partial x}\left(h^3 \frac{\partial p}{\partial x}\right) = 12\eta\left(\frac{\partial h}{\partial t} - u \frac{\partial h}{\partial x}\right) \qquad (6.3.1)$$

where the entraining velocity $u = U_1/2$ in this case. The film thickness (h) for the assumed geometry of a plane inclined surface bearing is given by:

$$h = h_o + Mx \qquad (6.3.2)$$

The slope (M) of the equivalent plane inclined surface bearing was assumed to change immediately at each instant in time as discussed in Section 6.2. However, the actual bearing surface would change much more slowly. The representation of the bearing geometry by a plane inclined surface was thus expected to give a reasonable prediction of changes in minimum film thickness (h_o) without necessarily representing fully the details of film geometry. These observations were particularly important in determining an expression for squeeze film velocity.

Equation (6.3.2) implies that,

$$\frac{\partial h}{\partial t} = \frac{dh_o}{dt} + \frac{\partial}{\partial t}(Mx)$$

and that any location (x),

$$\frac{\partial h}{\partial t} = \frac{dh_o}{dt} + x\frac{dM}{dt}$$

In a full squeeze-film analysis involving changes in the film profile throughout the cycle, it would be necessary to take account of both terms on the right hand side of the equation. However, this introduces considerable complexity into the analytical formulation. Also difficulty is introduced into the numerical procedures since the current value of $\left(\frac{dM}{dt}\right)$ is not known until the solution is obtained. Furthermore, forward extrapolation for $\left(\frac{dM}{dt}\right)$ would add considerably to the numerical effort and computing time and hence it was decided to approximate the squeeze-film velocity by the following expression and to see how rapidly the film thickness changed with time in the final solutions.

$$\frac{\partial h}{\partial t} = \frac{dh_o}{dt} \qquad (6.3.3)$$

In the event, the effect of combined entraining and squeeze-film action was found to maintain a remarkably small cyclic variation of minimum film thickness and hence it was concluded that the approximation to squeeze-film velocity represented by equation (6.3.3) would be adequate for the present purpose. The approximation of the squeeze film velocities will be discussed further in Chapter 7.

The following standard boundary conditions for a plane inclined surface bearing were applied:

$$p = 0 \quad \text{at } x = 0$$

$$p = 0 \quad \text{at } x = L$$

Substituting equations (6.3.2) and (6.3.3) into equation (6.3.1), integrating the resulting expression twice with respect to x and applying these boundary conditions yielded the following expression for pressure distribution:

$$p = \frac{12\eta\, x(L - x)\left(Mu - \frac{dh_o}{dt}\right)}{(2h_o + ML)(h_o + Mx)^2} \qquad (6.3.4)$$

Considering the following expression for applied load,

$$F' = \int_0^L p\, dx \ ,$$

equation (6.3.4) was integrated and re-arranged to give the following first order differential equation:

$$\frac{dh_o}{dt} = \frac{\frac{F'M^3}{12\eta}}{\frac{2ML}{2h_o + ML} - \ln\left(1 + \frac{ML}{h_o}\right)} + Mu \qquad (6.3.5)$$

The adoption of equations (6.3.2) and (6.3.4) in the derivation of an expression for the coefficient of friction (μ) of a fluid film bearing yielded the following expression:

$$\mu = \frac{\eta u}{MF'}\left[8 \ln\left(1 + \frac{ML}{h_o}\right) - \frac{12\, ML}{2h_o + ML}\right] - \frac{\eta}{F'M^2}\,\frac{dh_o}{dt}\left[6 \ln\left(1 + \frac{ML}{h_o}\right) - \frac{12\, ML}{2h_o + ML}\right] \qquad (6.3.6)$$

FIGURE 6.4.1 : FLOWCHART FOR THE SOLUTION PROCEDURE

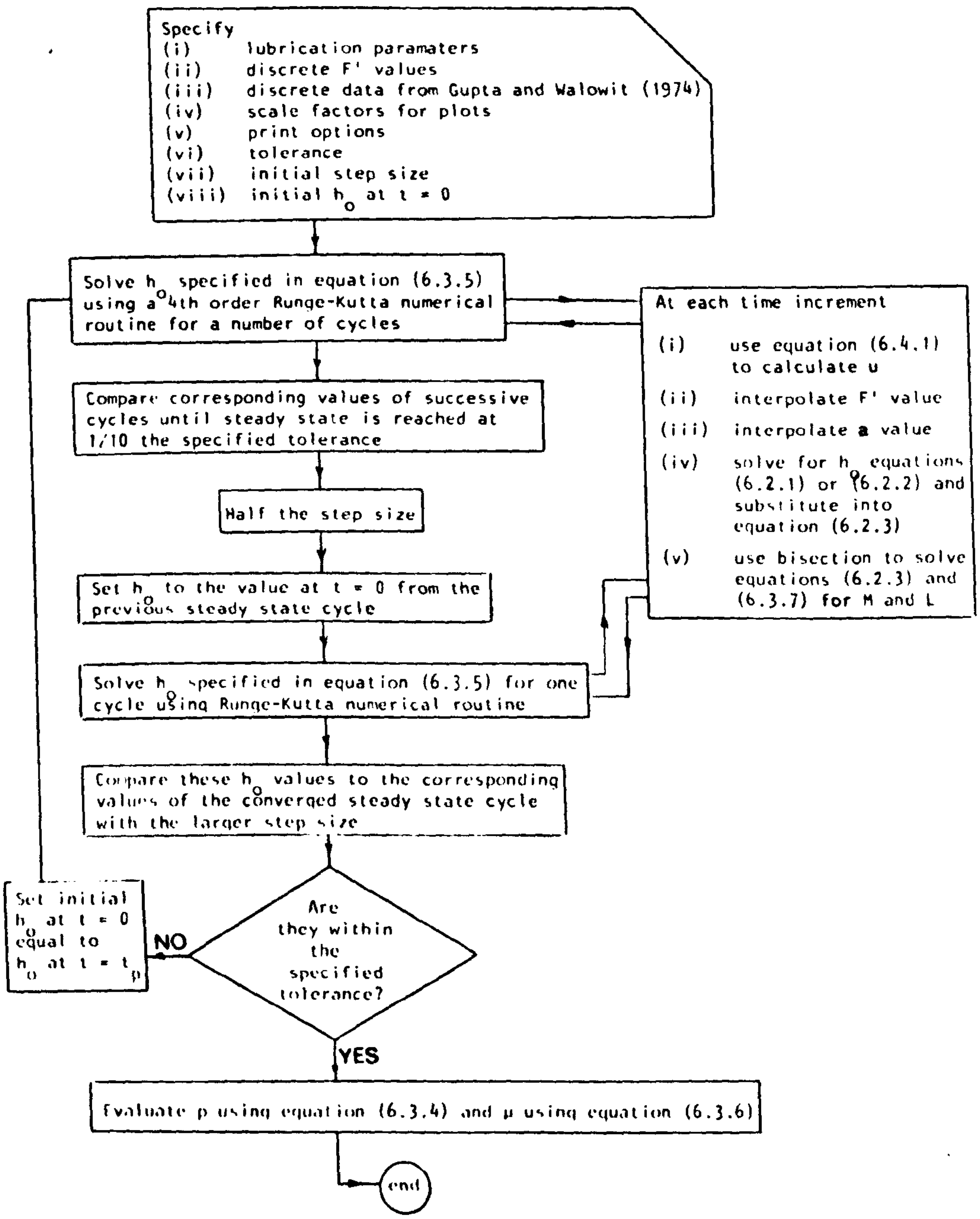

In Section 6.2, the iterative procedure for determing the slope (M) of the plane inclined surface required that;

$$\frac{\partial p}{\partial x} = 0 \quad \text{at } x = a \ .$$

Equation (6.3.4) implied that:

$$L = \frac{2h_o a}{h_o - Ma} \qquad (6.3.7)$$

6.4 The Solution Procedure:

The general form of equation (6.3.5) is as follows:

$$\frac{dh_o}{dt} = f\ (h_o\ ,\ t)$$

Equations of this form can be solved by using standard numerical routines for first order differential equations (Hornbeck, 1975). In the present study, solutions were computed using a fourth order Runge-Kutta routine. The following entrainment velocity function was incorporated into the solution procedure;

$$u = \frac{\pi u_A}{2} \left| \cos \frac{2\pi t}{t_p} \right| \qquad (6.4.1)$$

Values of the load per unit width (F') were required in the solution procedure and a cubic spline interpolation routine (Numerical Algorithms Group - E01ADF) was implemented to obtain values of F' at any instant. The half length (a) was also evaluated using the same interpolation routine on the data of Gupta and Walowit (1974).

The slope (M) and length (L) of the equivalent plane inclined surface were calculated at each instant in time by evaluating (h_o) using equations (6.2.1) and (6.2.2). Equation (6.3.7) was then substituted into equation (6.2.3) and a simple bisection routine was used to iterate for the value of M.

It was important to notice that h_o in equation (6.2.3) represented a steady state value, while h_o in equation (6.3.7) represented the value of the current time step. After M had been calculated, equation (6.3.7) was used to evaluate L. It was noted that the solution of equation (6.3.7) required a knowledge of the current value of (h_o) which itself required the value of L to be known. The previous value of (h_o) was thus adopted in the current evaluation of L.

The absolute minimum film thickness (h_o) encountered during a complete cycle was given an arbitrary value at $t = 0$. The Runge-Kutta routine was applied by dividing the cycle into a number of equal time steps. The solution was then marched out until corresponding values of successive cycles agreed within a specified tolerance. In this manner a steady but cyclic solution was calculated for the variation of h_o with time. The step size was then halved and the final cycle re-calculated. If corresponding values agreed within a specified tolerance the cycle was accepted as an accurate solution for h_o. Automatic step size halving was employed as a standard method to control round-off and truncation errors (Hornbeck, 1975).

Once the cyclic variation of minimum film thickness (h_o) had been ascertained the pressure distributions (p) and coefficients of friction (μ) were determined using equations (6.3.4), (6.3.5) and (6.3.6).

When the entrainment velocity was zero, the slope (M) was zero and the length L was equal to the dry contact length (2a). Furthermore, equation (6.3.5) reduced to,

$$\frac{dh_o}{dt} = - \frac{F' h_o^3}{\eta L^3}$$

equation (6.3.4) reduced to,

$$p = - \frac{6 \eta x (2a - x)}{h_o^3} \frac{dh_o}{dt}$$

and finally, equation (6.3.6) indicated that

$$\mu = 0$$

The entire solution procedure is summarized by the flowchart shown in Figure 6.4.1. The procedure was implemented using the computer program listed in Appendix E.

6.5 Comparison with the Analysis of Modest and Tichy:

Modest and Tichy (1979) developed approximate closed form expressions for load capacity when sinusoidal normal motions and constant sliding velocity were imposed on a plane inclined surface bearing of infinite width. Their solution included fluid inertia effects and was restricted to normal motions which were small compared with the film thickness.

A check on the derivation of equation (6.3.5) and the magnitude of numerical errors was achieved by solving a case which allowed direct comparison with predictions based upon the analysis of Modest and Tichy. Fluid film thicknesses were ascertained using the solution procedure outline in the present chapter with the following imposed conditions:

η = 0.1 Pa s

u = 0.1/π m/s

F' = 318.31 (1 - 0.1 sin(0.4 π t)) N/m

L = 0.05 m

M = 0.0002

t_p = 5 s

From the analysis of Modest and Tichy it was clear that fluid inertia effects were negligible for this case. The solution was obtained by slightly modifying the computer program listed in Appendix E. The tolerance for convergence was set at 0.0001. The variation with dimensionless time (T) of the coefficient of friction (μ) and minimum film thickness (h_o) are shown in Figure 6.5.1 (included at the end of this chapter), along with a sample pressure distribution and the surface shape at T = 0. The load function (F'/F_A') and the velocity function (u/u_A) are also shown.

The amplitudes of the fluctuations in film thickness were obtained from the computed results. These values were used in the expressions derived by Modest and Tichy to yield:

$$F' = 318.25\ (1 - 0.097\ \sin(0.4\ \pi\ t))\ \text{N/m}$$

This expression for load was compared to the imposed load and a maximum difference of 0.3% was calculated. This suggested that the sections of the solution procedure involving the time varying behaviour of the plane inclined surface configuration had been correctly formulated. Also for this case the numerical errors were probably small.

6.6 Comparison with the Analysis of Hirano and Murakami:

It was possible to perform a further check on the simplifying assumptions concerning surface deformation which were considered in Section 6.2. Hirano and Murakami (1975) performed a series of experiments in which a compliant Hertzian contact was subjected to cyclic, time varying entrainment velocities. The cyclic variation of the coefficient of friction was recorded as a function of time. The compliant bearing surfaces were photoelastic and thus the stress distribution within them could be monitored. Asperity contact during sliding caused asymmetry in the observed stress distribution because of the large surface tractions developed. Therefore, for each set of lubrication conditions, Hirano and Murakami were able to ascertain whether or not a fluid film separated the surfaces.

The geometry of the experimental apparatus was that of a nominal line contact, and the entrainment velocity was sinusoidal with the following general form:

$$u = \frac{u_A \pi}{2} \left| \cos \frac{2\pi t}{t_p} \right| \tag{6.6.2}$$

A constant load per unit width was applied.

Four cases were selected to check the solution procedure used in the present study. The details of the lubrication parameters which describe these cases are listed in Table 6.6.1 and include the composite surface roughness value (σ) of the surfaces. The value of composite surface roughness will be compared to film thickness predicted by the present solutions procedure to indicate whether fluid film lubrication was likely to have occurred. The findings of Hirano and Murakami (1975) are summarized in Table 6.6.2.

Table 6.6.1 : The lubrication parameters for the cases selected from the analysis of Hirano and Murakami (1975).

Case	R (mm)	F' (kN/m)	E (MN/m²)	ν	t_p (s)	u_A (mm/s)	σ (u_M)	η (N.s/m²)
1	30	20	3200	0.425	0. 5	60.0	0.19	1.5
2	30	20	3200	0.425	0.5	20.0	0.19	1.8
3	30	20	3200	0.425	2.08	14.4	0.19	1.35
4	30	20	3200	0.425	0.2	15.0	0.19	1.35

Table 6.6.2 : A summary of the findings for the selected cases of Hirano and Murakami (1975).

Stroke length (mm)	Hertzian length (mm)	Asperity contact	Peak friction	Reason for film breakdown
30	1.25	No	0.0104	-
10	1.25	No	0.0079	-
30	1.25	Yes	0.033	Asperity contact
3	1.25	Yes	0.01 → .12	"Film instability"

Modifications were made to the program listed in Appendix E to allow the four cases selected from the work of Hirano and Murakami (1975) to be solved. The tolerance for convergence was set at 0.001. The formula of Swales et al (1972) was used in place of equations (6.2.1) and (6.2.2), with the recognition that it did not apply when,

$$\frac{F'}{(2\ \eta\ u\ E'R)^{0.5}} < 5$$

However, it was found that this term was never less than 5 for cases 1 to 4.

The results are shown in Figure 6.6.1 (included at the end of this chapter) and include some experimental data from the work of Hirano and Murakami (1975),

Good agreement was shown between the results in Figure 6.6.1, which were calculated using the present solution procedure, and those of Hirano and Murakami. The coefficients of friction measured by Hirano and Murakami had peak values similar to those predicted by the present analysis. If fluid film breakdown was assumed to occur when the film thickness fell to about three times the composite roughness value (Johnson et al, 1972), the fluid film thickness predicted for case 3 indicated regions where asperity contact might have occurred. Case 4 was described by Hirano and Murakami as exhibiting "film instability". The similarity between the film thickness predicted by the present analysis and the measure of the composite roughness suggested that a breakdown in the lubricant film may have occurred in both cases 3 and 4. It was also noted that the peak pressures for all cases were quite close to the Hertzian maximum. This suggested that the equivalent plane inclined surface configuration adopted here gave a pressure distribution similar to that occurring under dry contact conditions.

6.7 Application to the Ankle Joint:

The solution procedure developed in this chapter was applied to the conditions described in Table 5.5.1 for cases A and B. Case A represented the ankle joint in the friction experiments described in Chapter 4 and case B represents the ankle joint in vivo during walking. The conjunction was assumed to be fully flooded for the present solution procedure.

The computer program listed in Appendix E was used with a convergence tolerance of 0.0001. The results are shown in Figure 6.7.1 (included at the end of this chapter).

In Figure 6.7.1, the inlet extent of the plane inclined surface was always less than the starvation parameter (B). Thus, the assumption of a fully flooded inlet zone was not contradicted. Starvation will be discussed further in Chapter 7.

The film thickness predicted for the ankle joint during the friction experiments were about 0.2 μm. When this value was compared with the estimated values of surface roughness (Ra) of articular cartilage 2-6 μm quoted in Chapter 2, it was deemed unlikely that continuous fluid films could be sustained. It was recognized, however, that increases in a parameter such as the reduced radius of curvature (R) might dramatically increase the predicted film thickness. This will be discussed in Chapter 8.

The conditions adopted for case B gave rise to film thickness predictions of about 0.7 μm. This value was still much smaller than the estimated height of the surface asperities and hence boundary or perhaps mixed lubrication was considered to be likely.

A full discussion of the role of elastohydrodynamic lubrication in ankle joint lubrication will be presented in Chapter 8.

6.8 Concluding Remarks:

The equivalent bearing representing the ankle described in Chapter 5 has been analysed. A number of simplifying assumptions have been made concerning the surface deformation and in the present analysis the ankle joint was represented by a form of plane inclined slider bearing. A solution procedure was developed and implemented on the computer. The results for various cases were generated in a computing time of about 20 sec of Central Processing Unit (CPU) time. The analytical formulation has been checked directly by comparing the theoretical predictions with the results of previous investigators. It was concluded that the present analytical procedure offered a reasonable approach to the solution of a very complex situation in elastohydrodynamic lubrication with considerable uncertainty in the geometry, material properties and imposed conditions for the film conjunction. However, it was deemed to be necessary to investigate further some of the assumptions involved in the plane inclined surface model. This will be accomplished in the next chapter.

Figure 6.5.1 : Results for Comparison with the Work of Modest and Tichy.

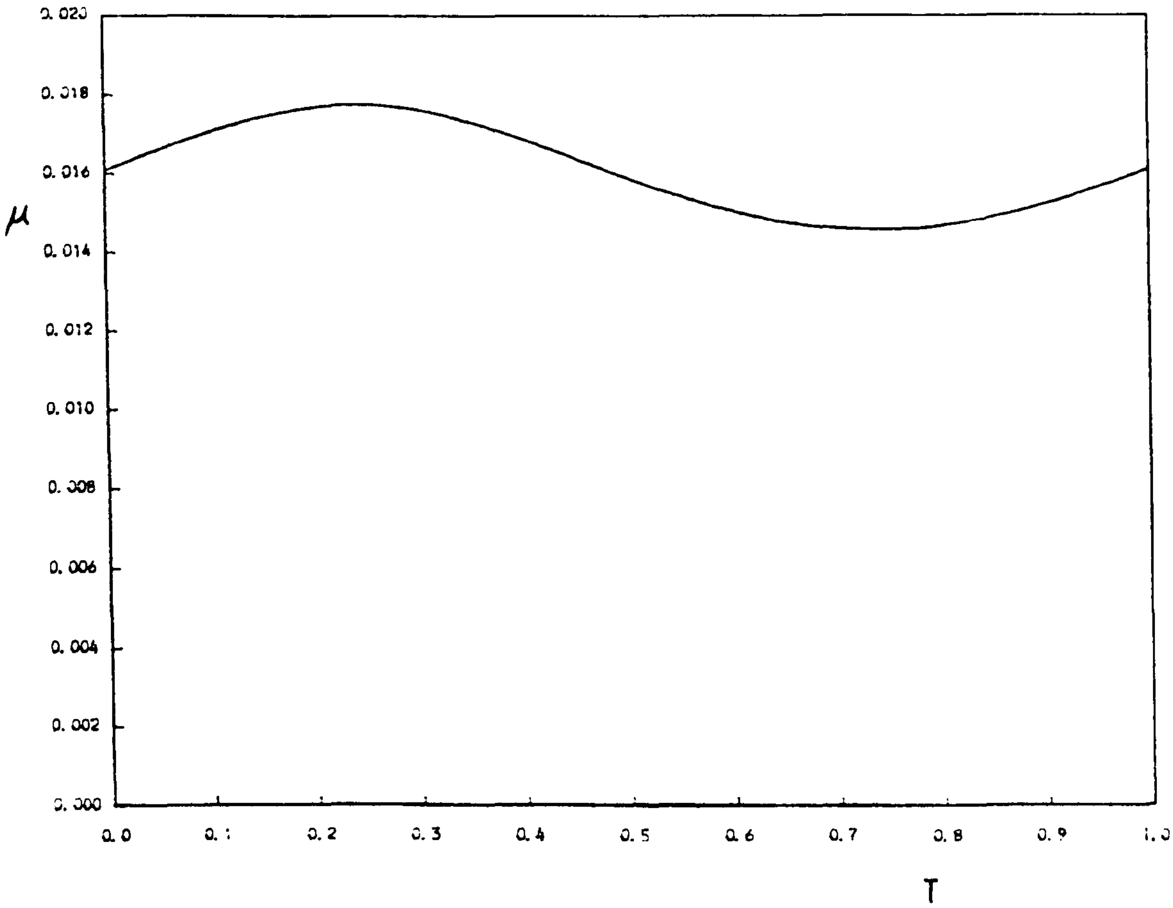
0.020
0.018
0.016
μ
0.014
0.012
0.010
0.008
0.006
0.004
0.002
0.000
0.0
0.1
0.2
0.3
0.4
0.5
0.6
0.7
0.8
0.9
1.0
T

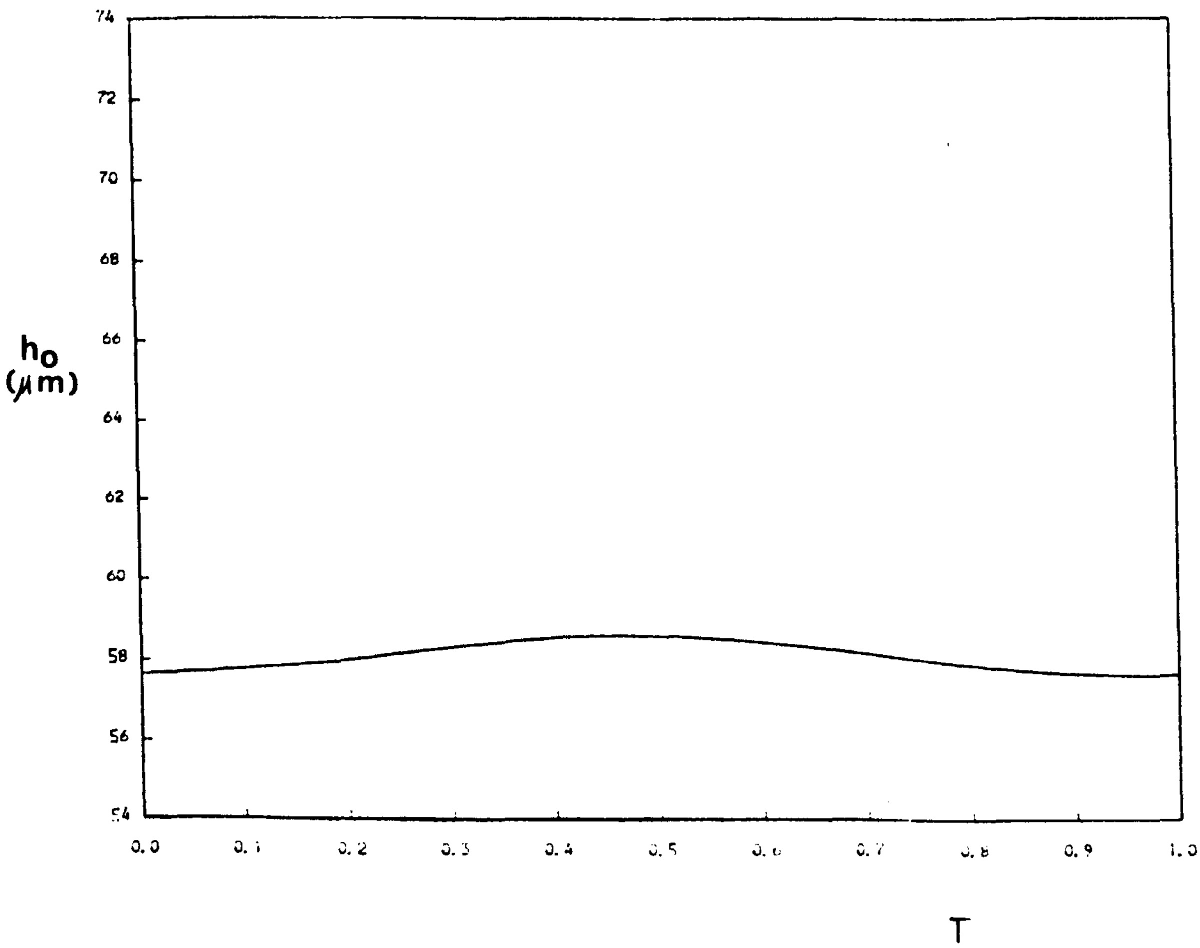
74
72
70
68
66
h_o
(μm)
64
62
60
58
56
54
0.0
0.1
0.2
0.3
0.4
0.5
0.6
0.7
0.8
0.9
1.0
T

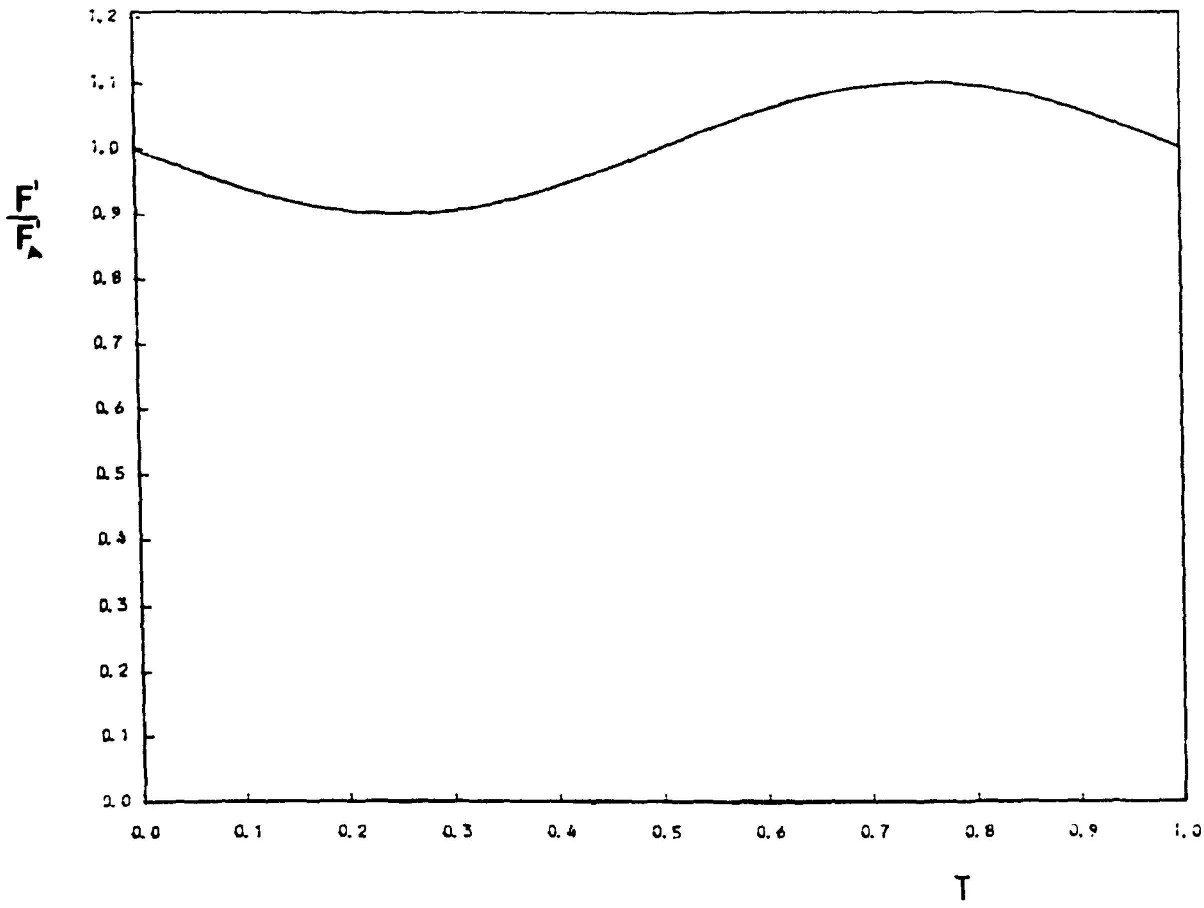

F'/F'A
1.2
1.1
1.0
0.9
0.8
0.7
0.6
0.5
0.4
0.3
0.2
0.1
0.0
0.0
0.1
0.2
0.3
0.4
0.5
0.6
0.7
0.8
0.9
1.0
T

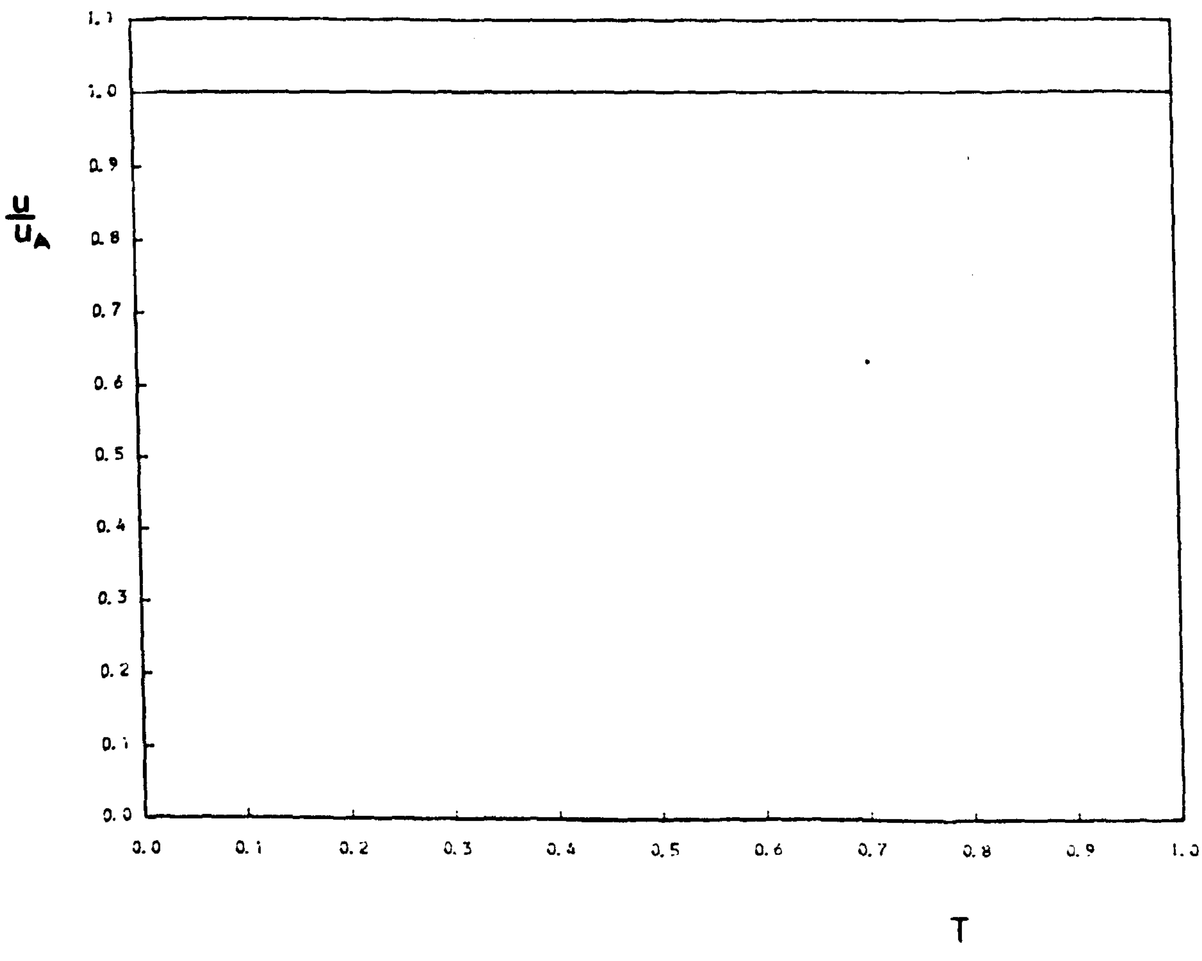

u/uA
1.1
1.0
0.9
0.8
0.7
0.6
0.5
0.4
0.3
0.2
0.1
0.0
0.0
0.1
0.2
0.3
0.4
0.5
0.6
0.7
0.8
0.9
1.0
T

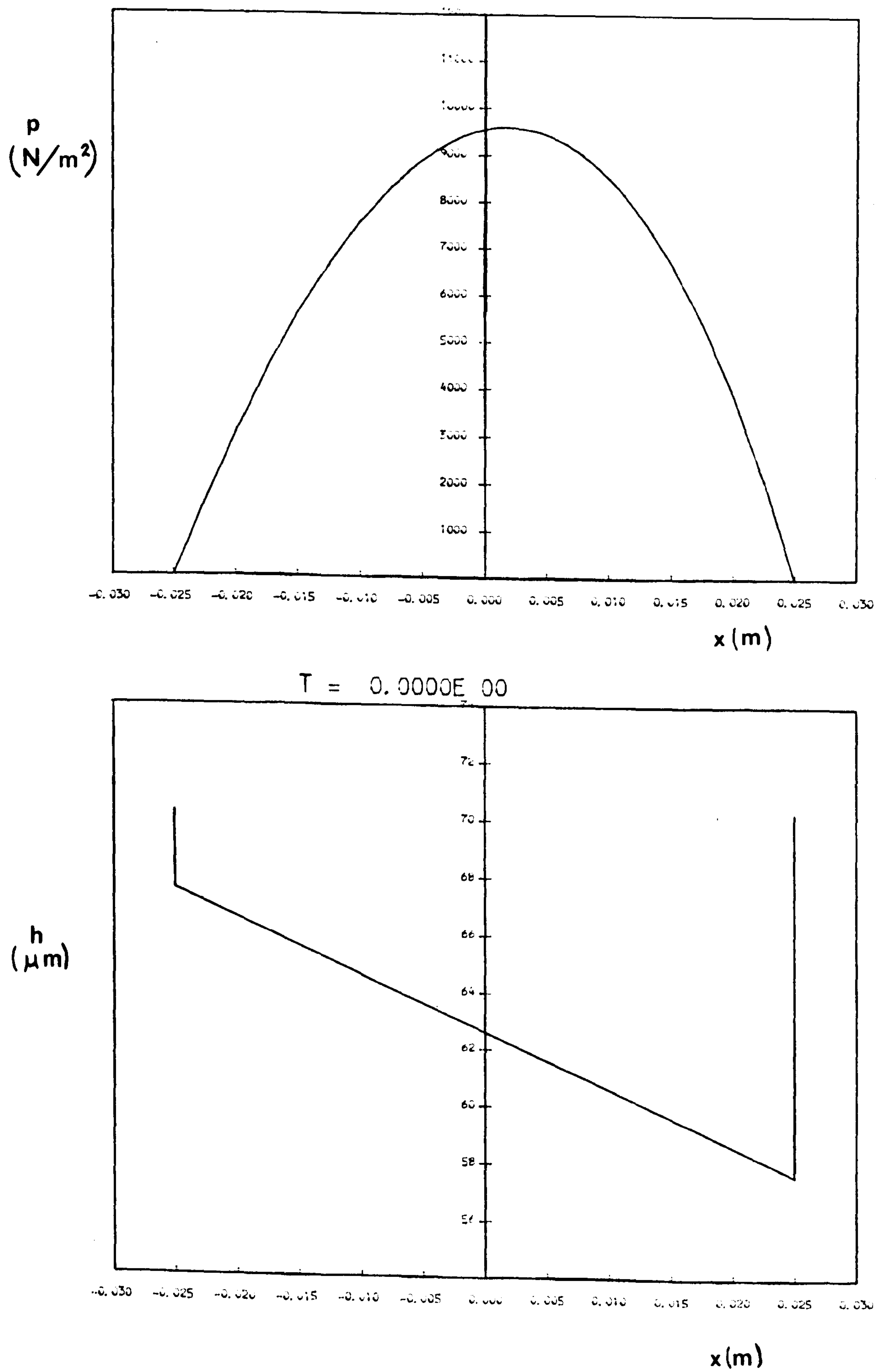
p
(N/m²)
8000
7000
6000
5000
4000
2000
1000
-0.030
-0.025
-0.020
-0.015
-0.005
0.000
0.005
0.010
0.015
0.020
0.025
0.030
x (m)
T = 0.0000E 00
h
(μm)
72
70
68
66
64
62
60
58
x (m)

Figure 6.6.1 : The results from using the present solution procedure on the cases listed in Table 6.6.1 and selected from the work of Hirano and Murakami (1975).

$3 \times \sigma$

Case 1 (standard conditions)

Case 2 (low u_A)

Case 3 (low u_A and η , high t_p)

Case 4 (low u_A, t_p and η)

o Results of Hirano and Murakami for Case 1

\+ Results of Hirano and Murakami for Case 2

▲ Maximum Hertzian pressure

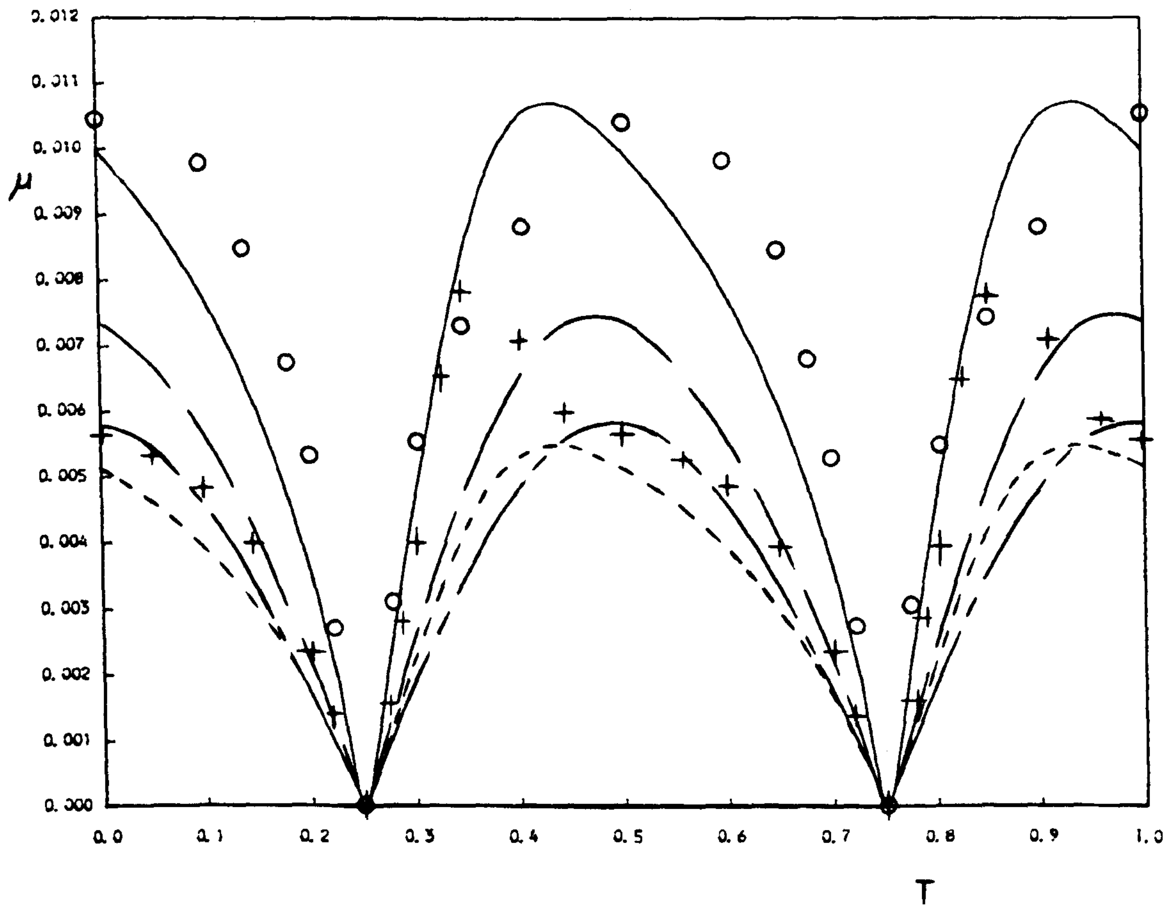

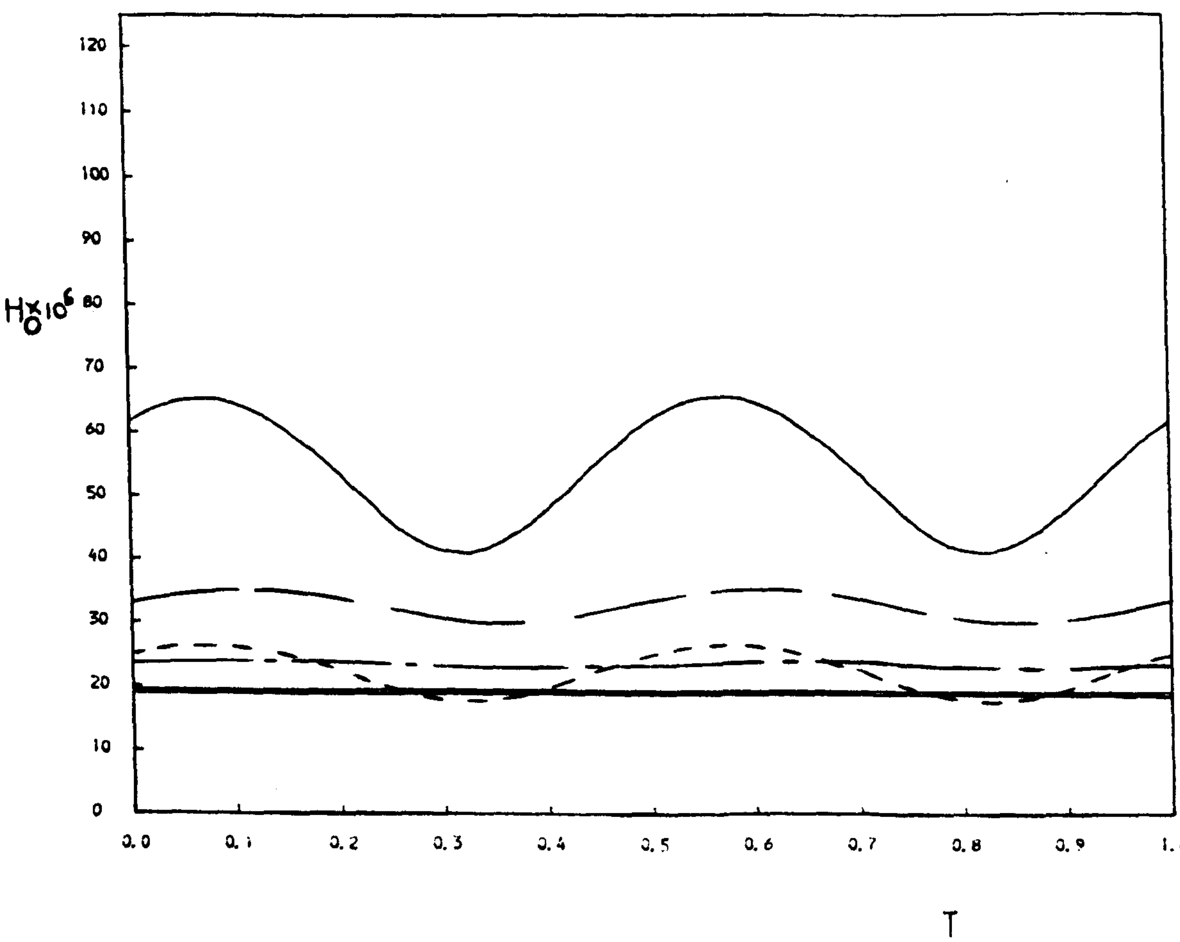

For key see page 185

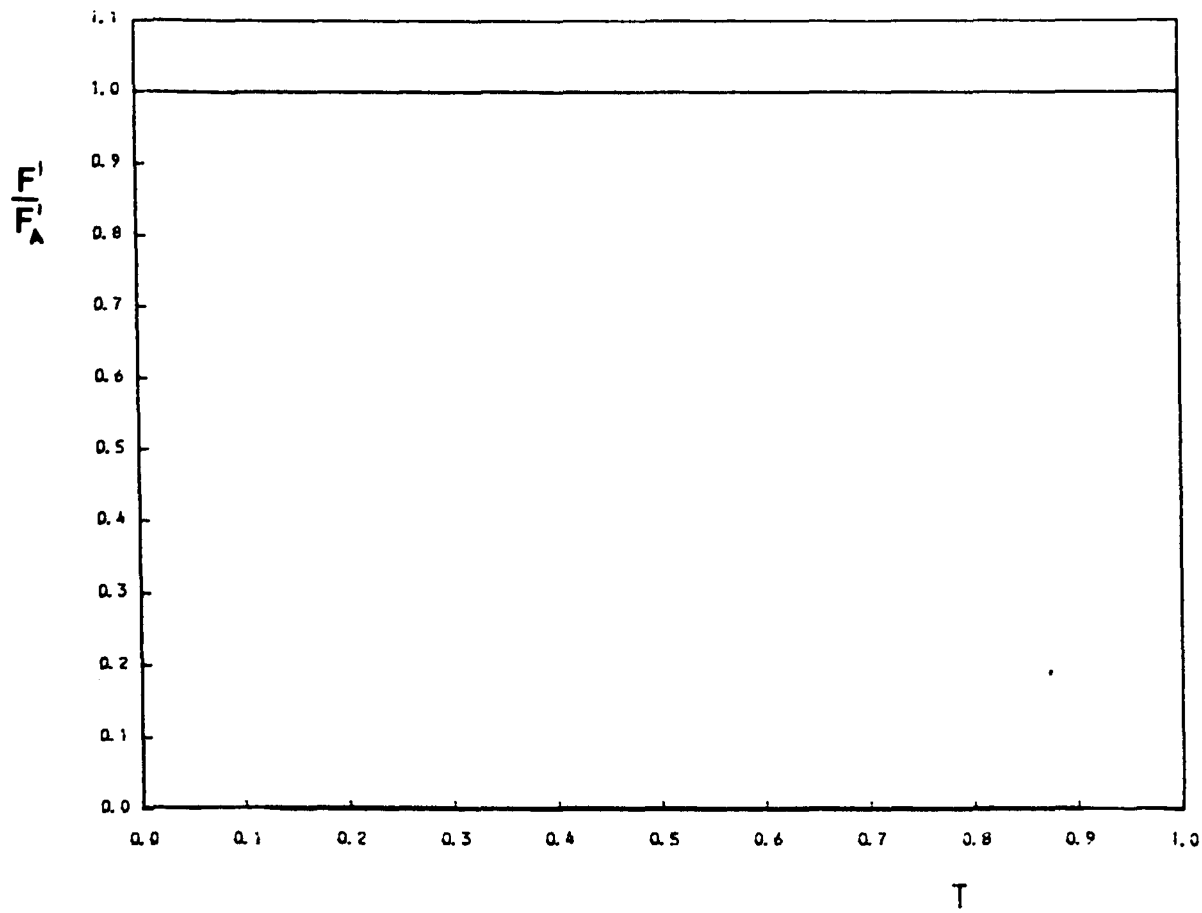

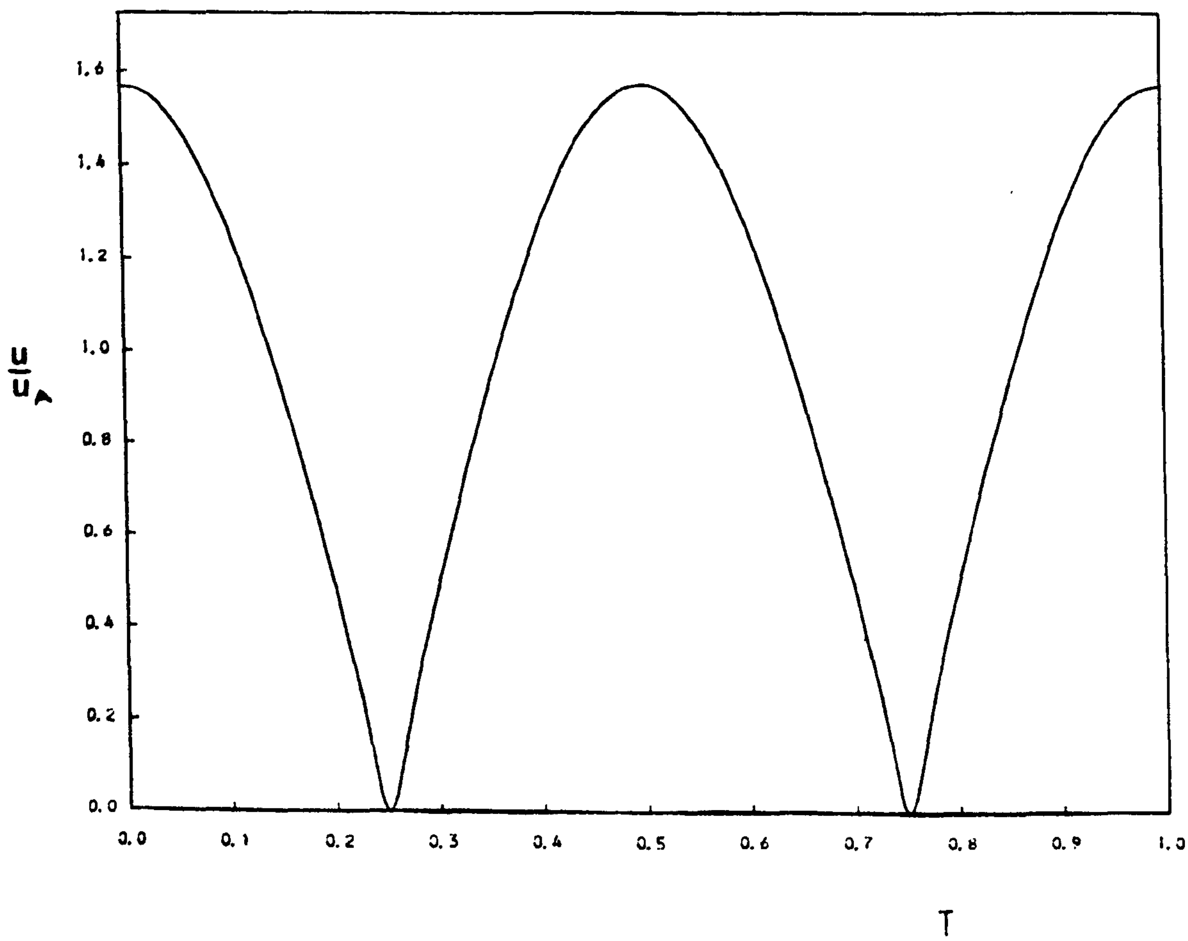

For key see page 185

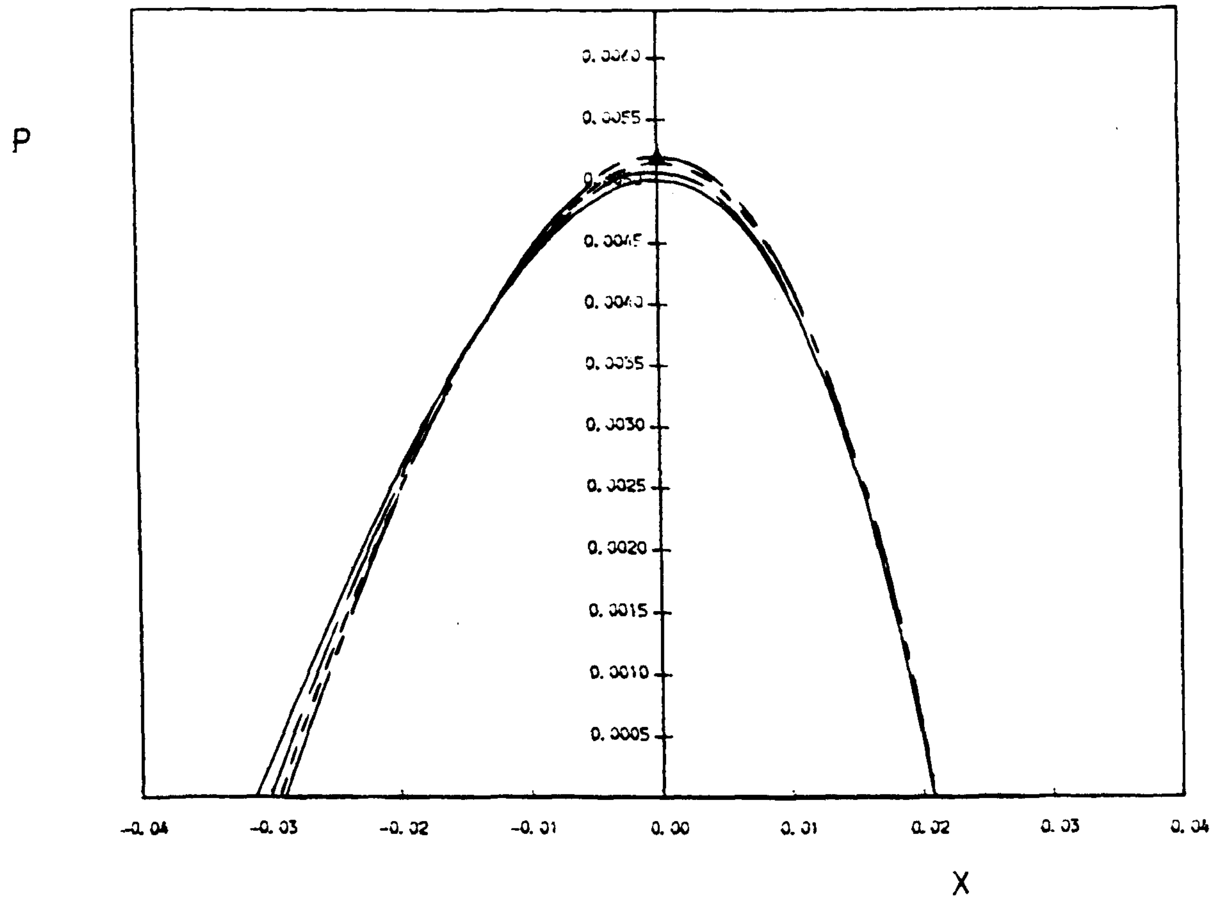

T = 0.0000E 00

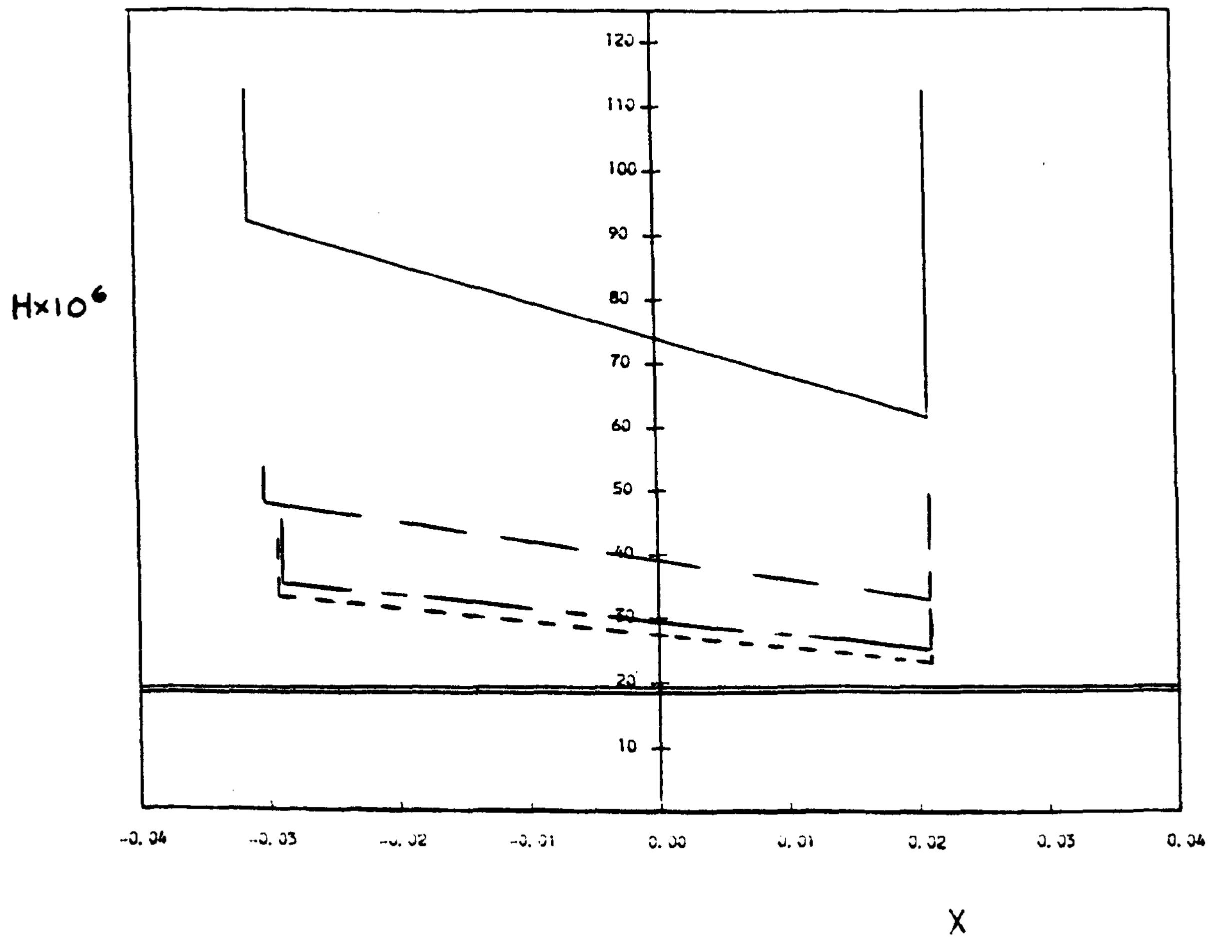

For key see page 185

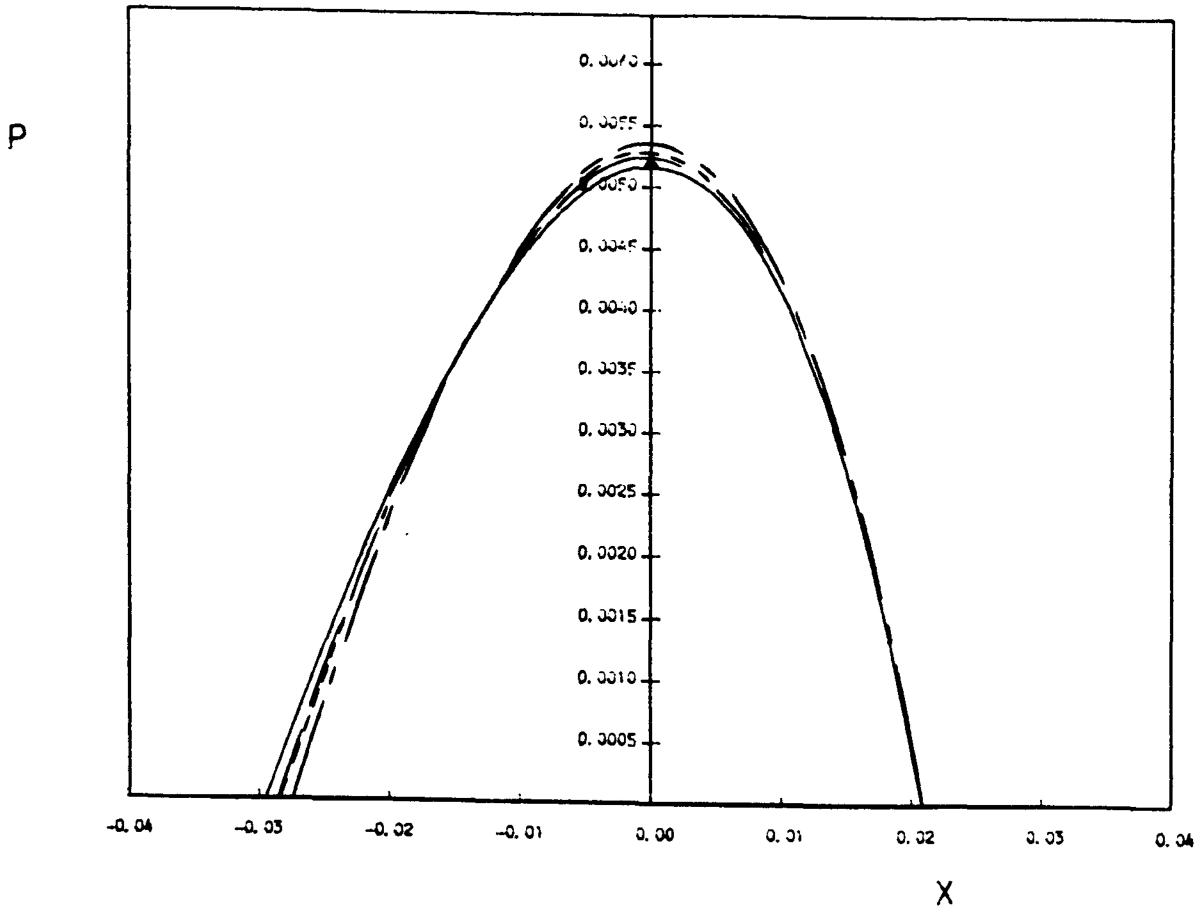

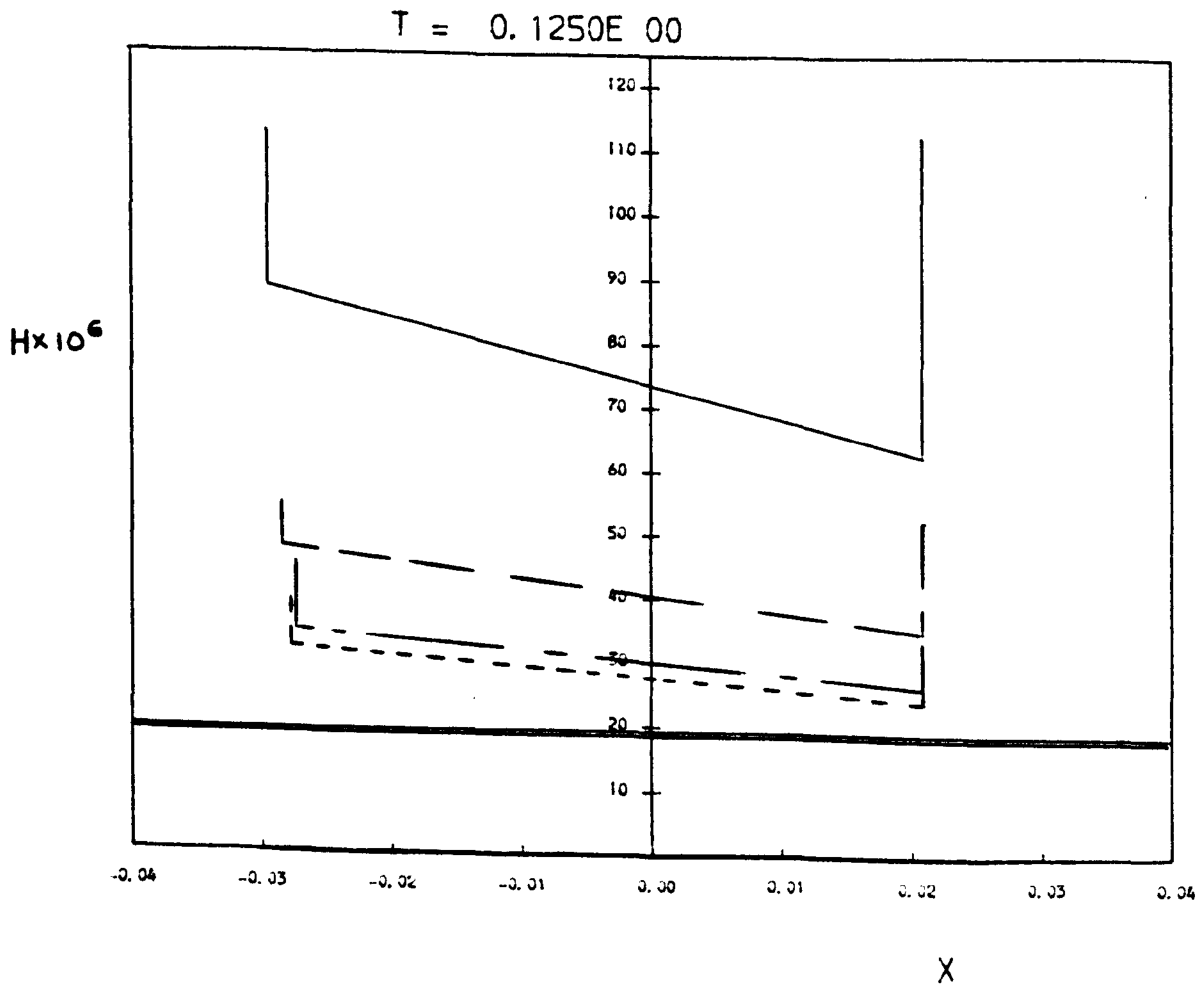

For key see page 185

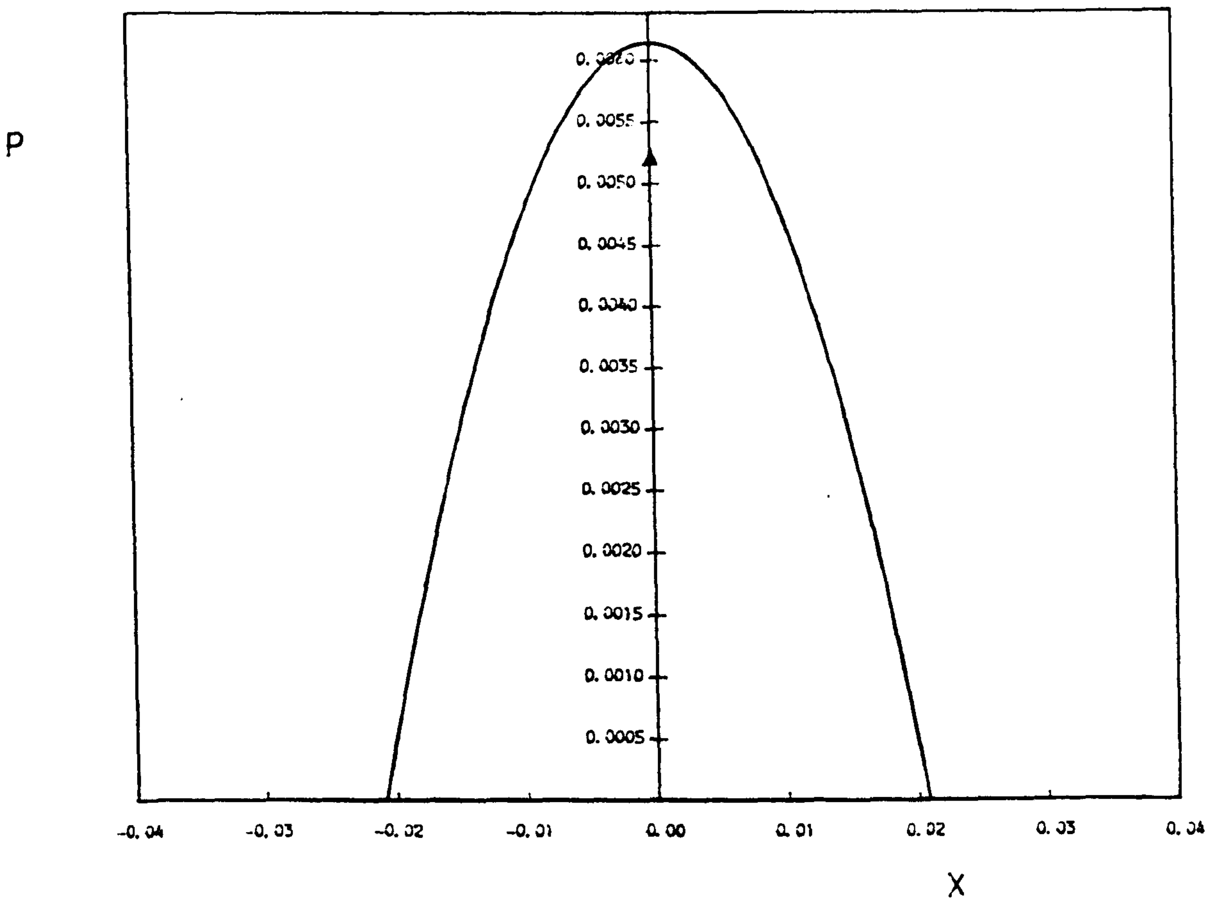

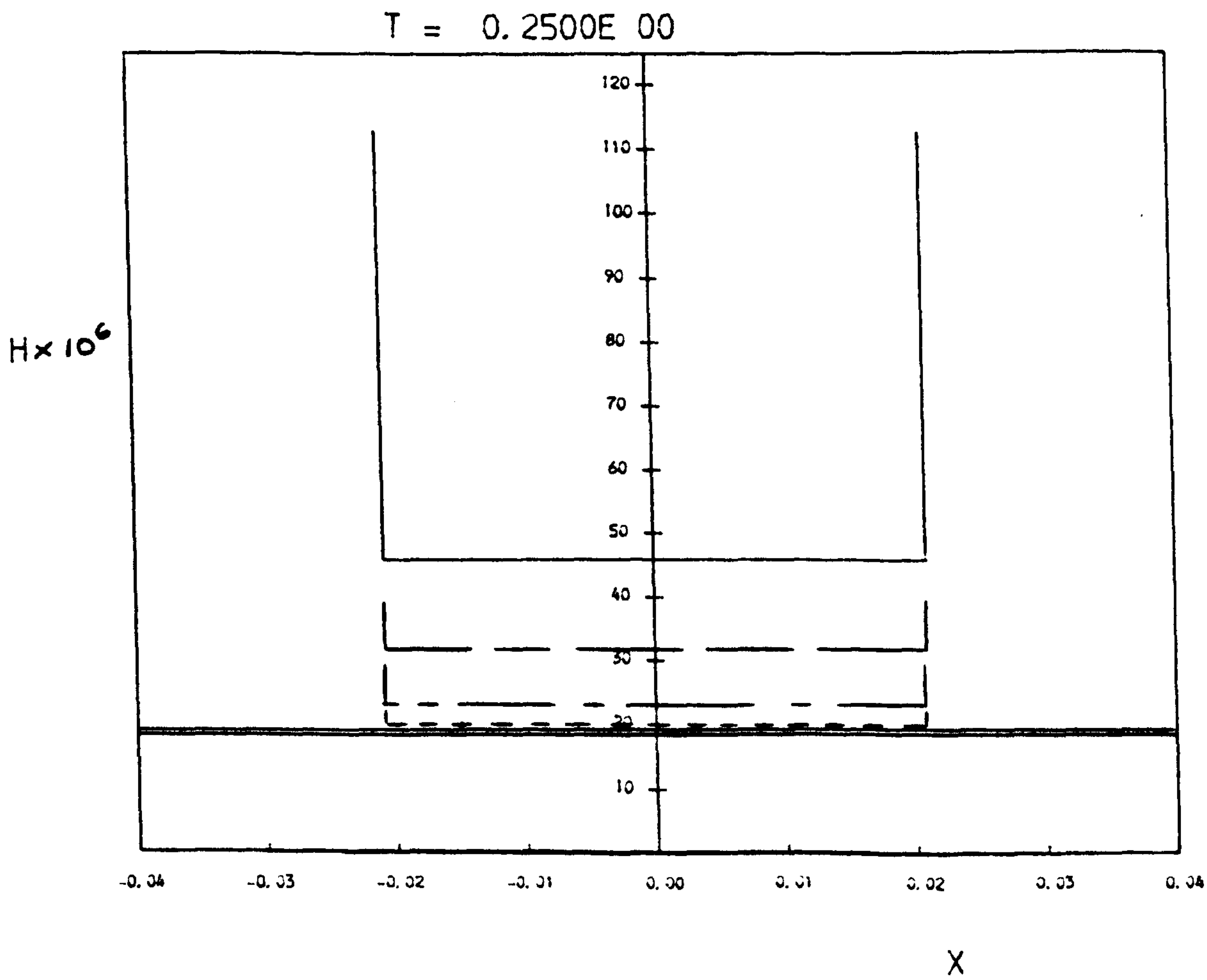

For key see page 185

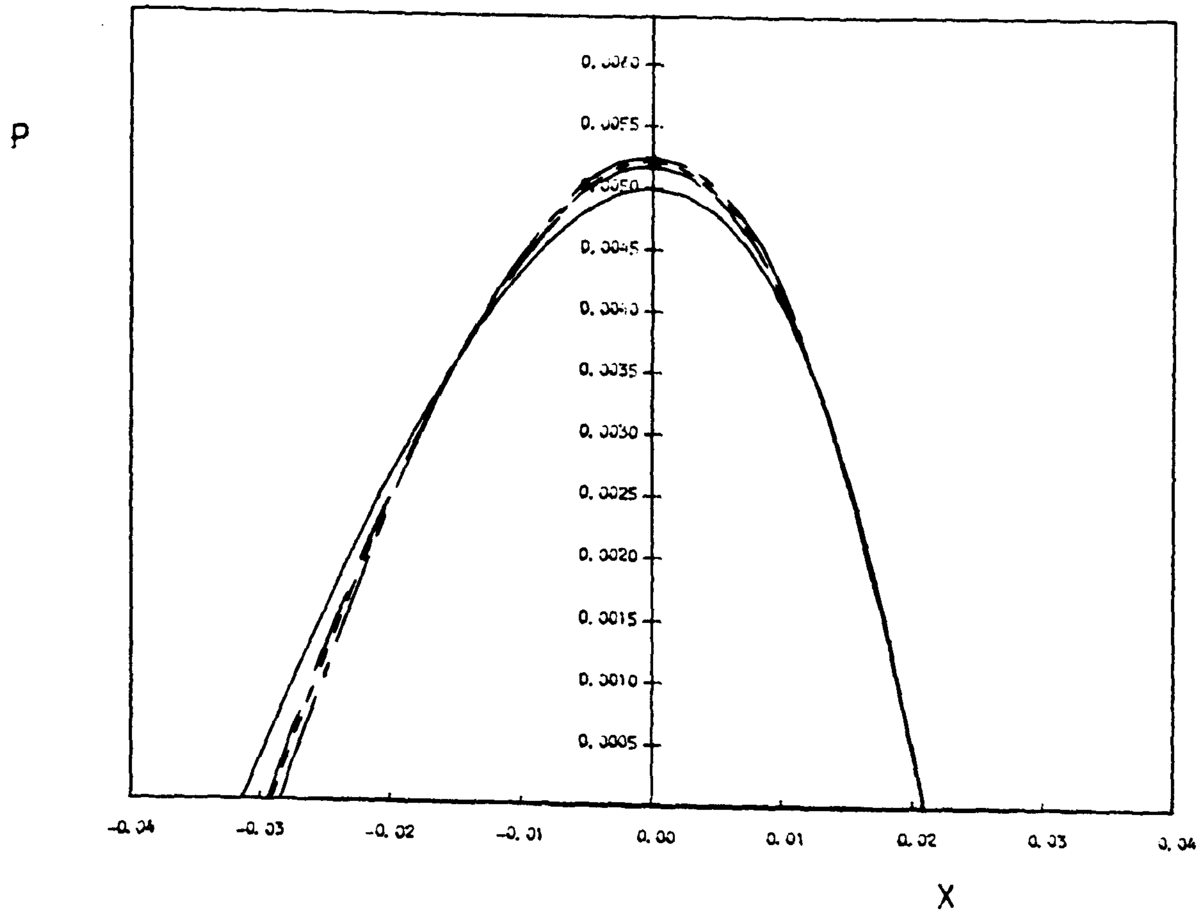

T = 0.3750E 00

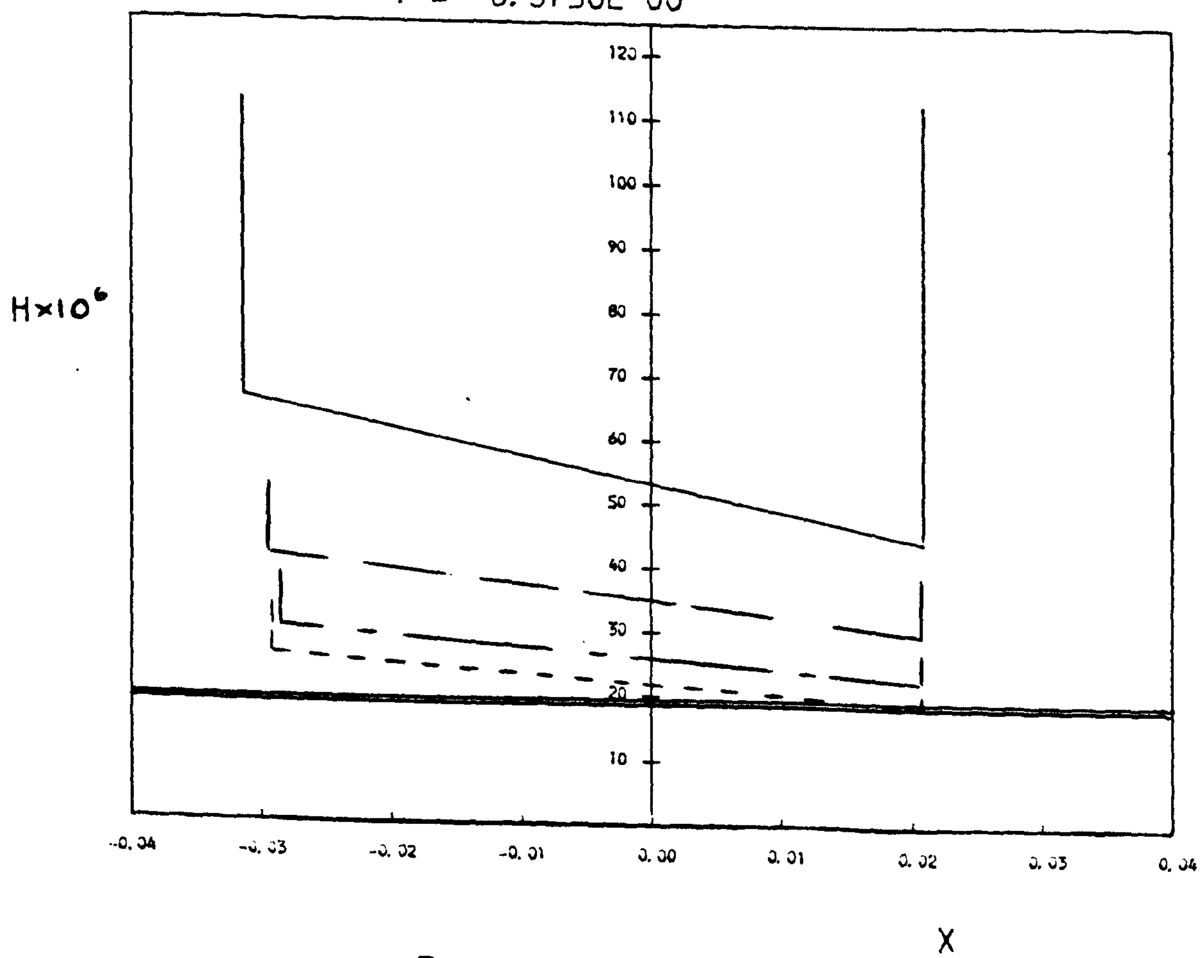

For key see page 185

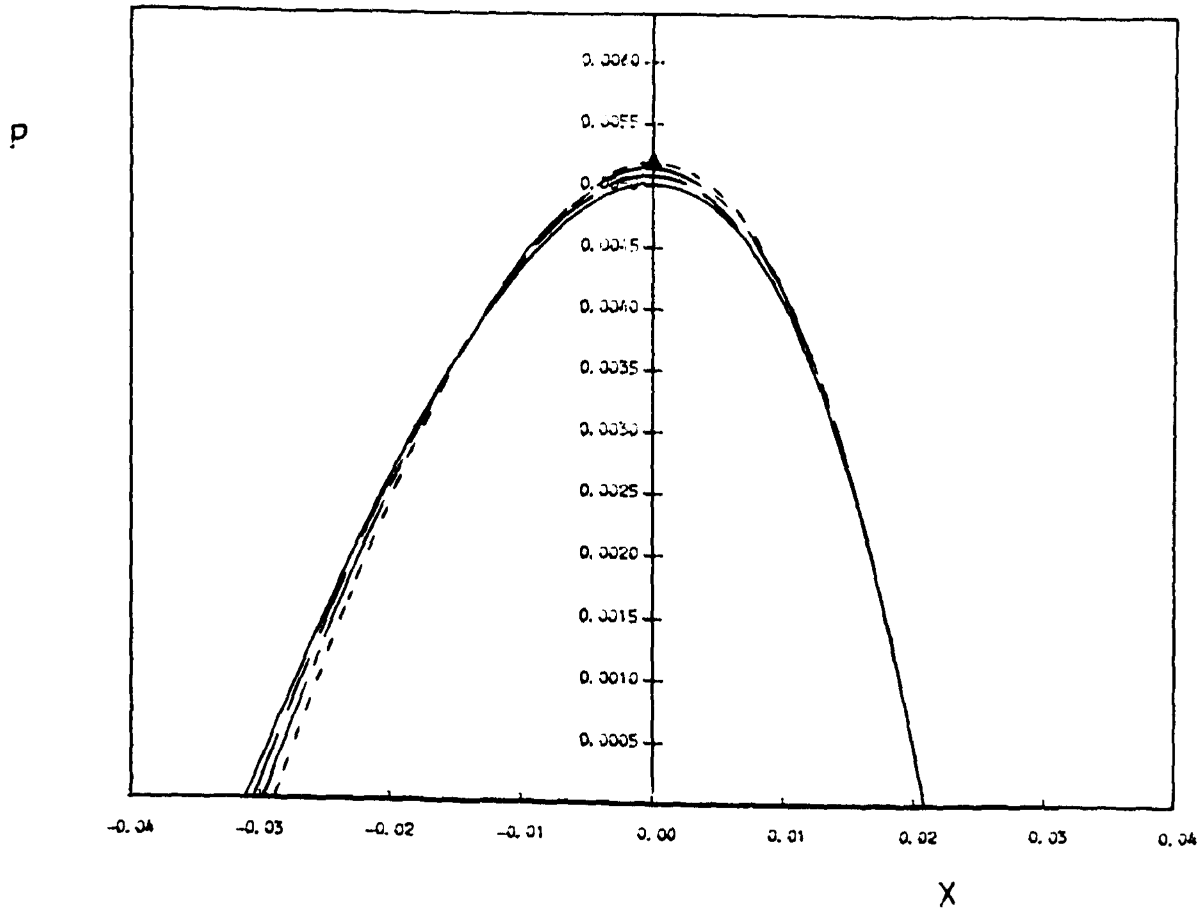

T = 0.5000E 00

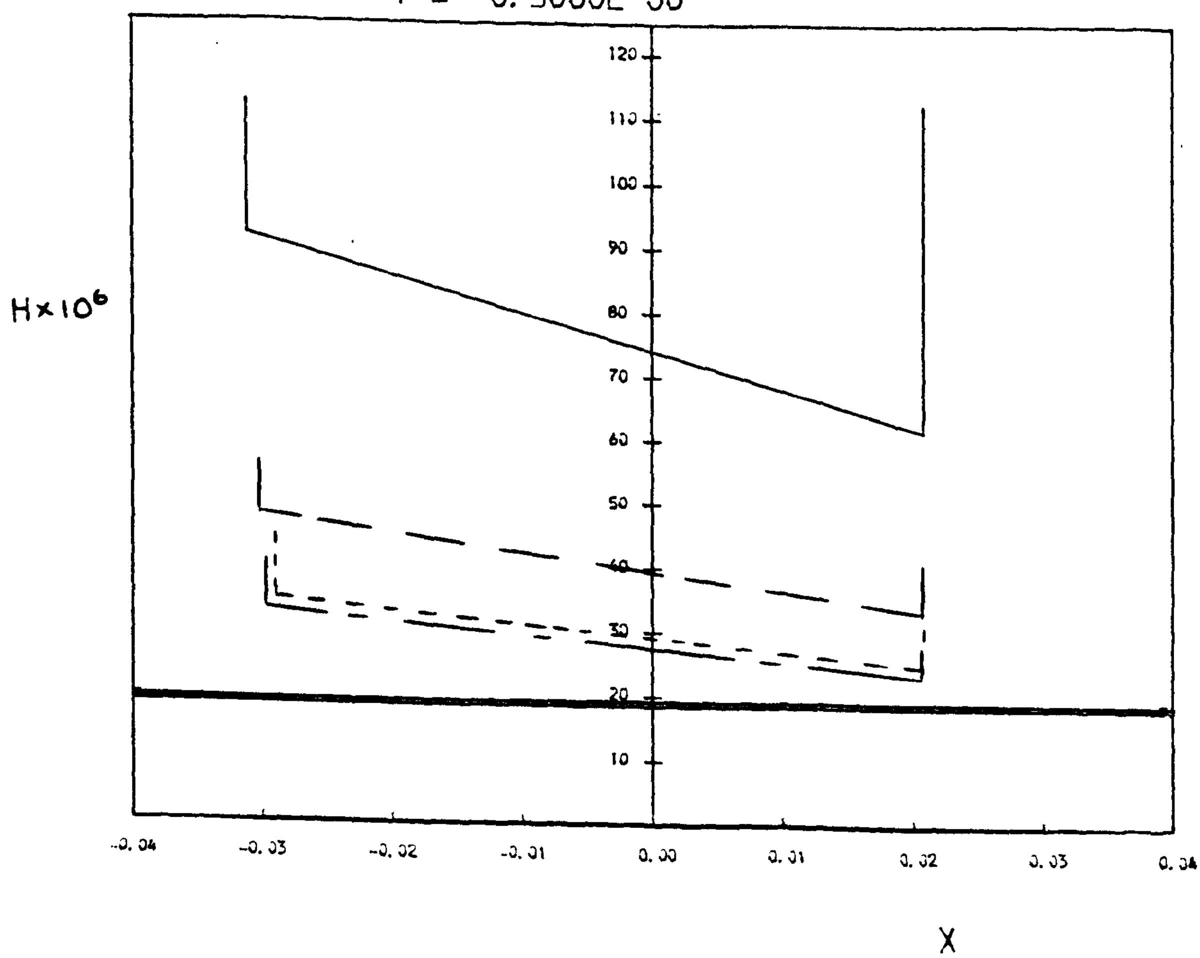

For key see page 185

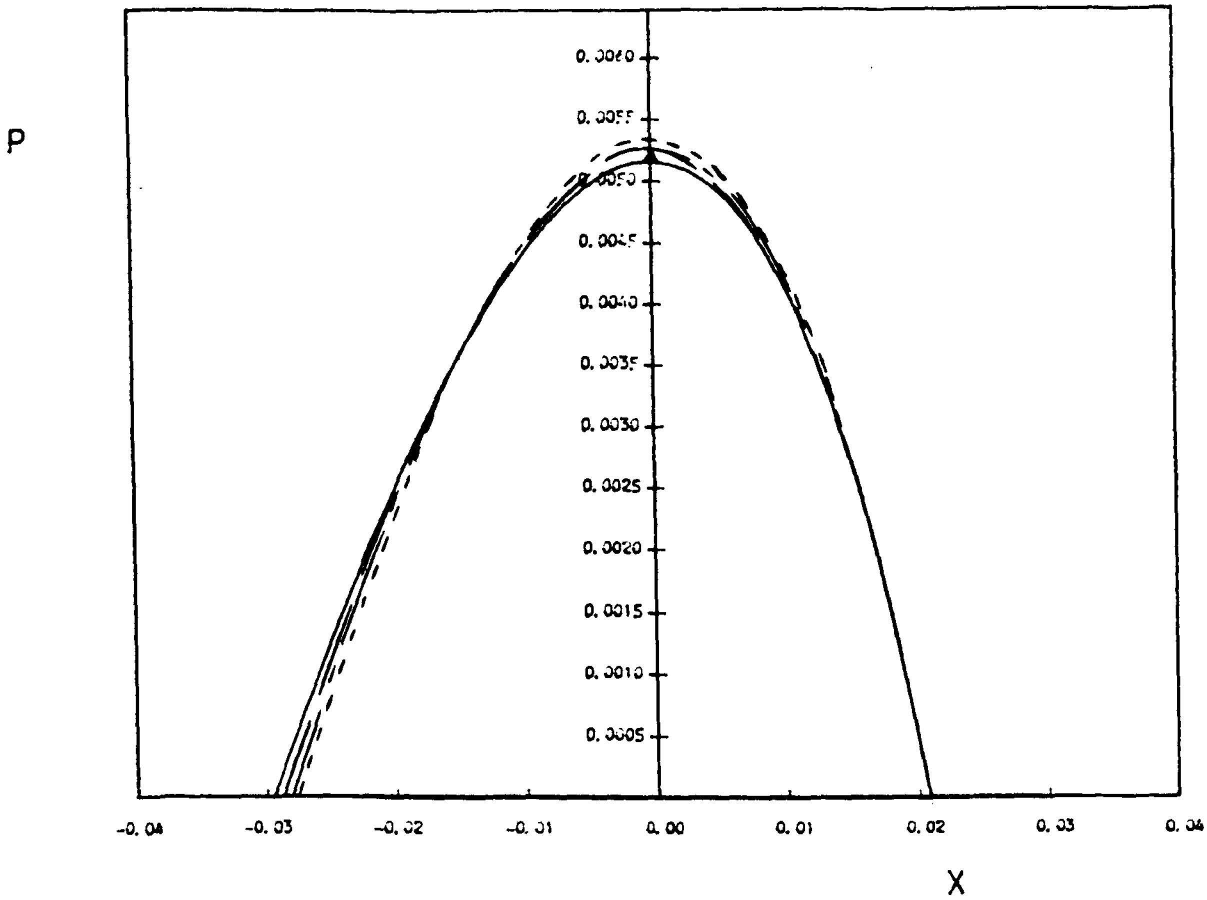

T = 0.6250E 00

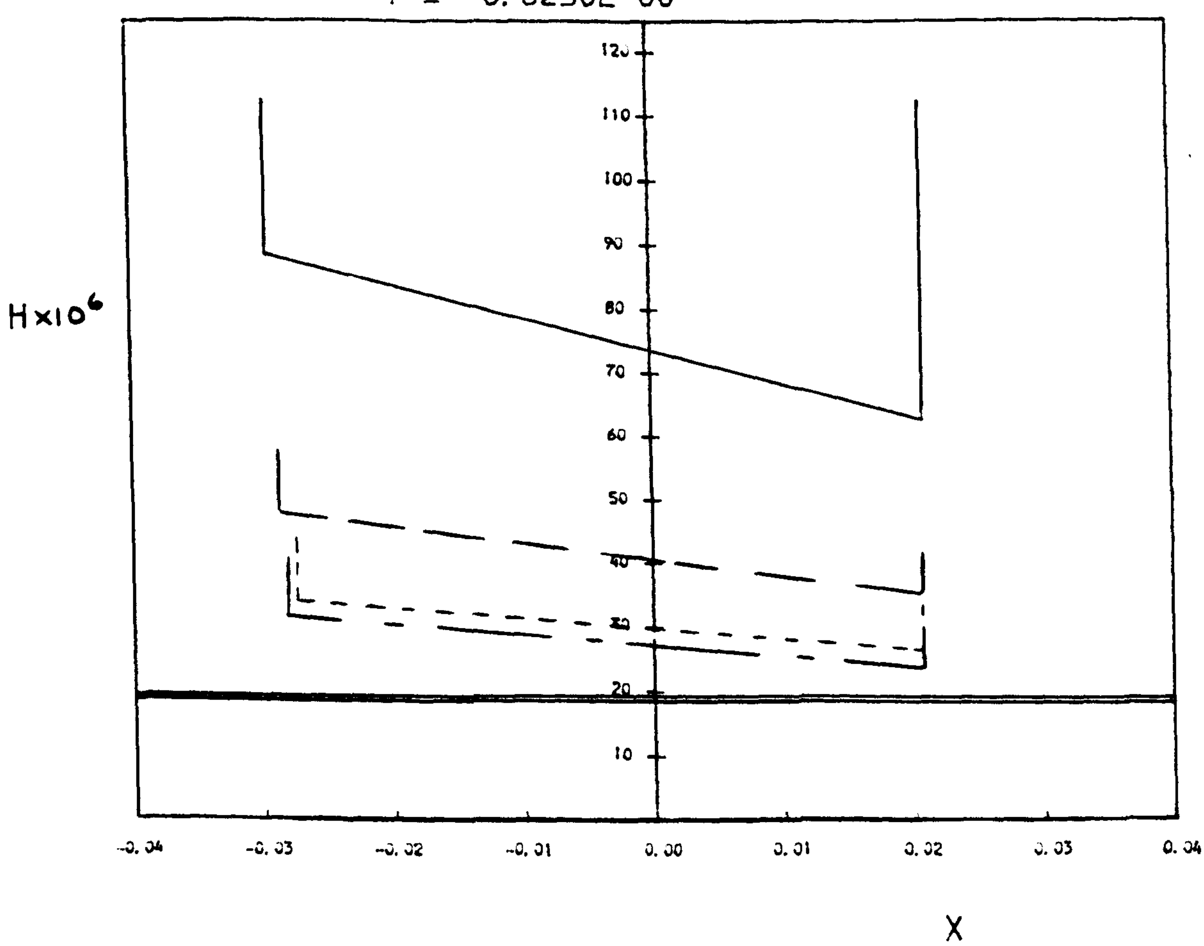

For key see page 185

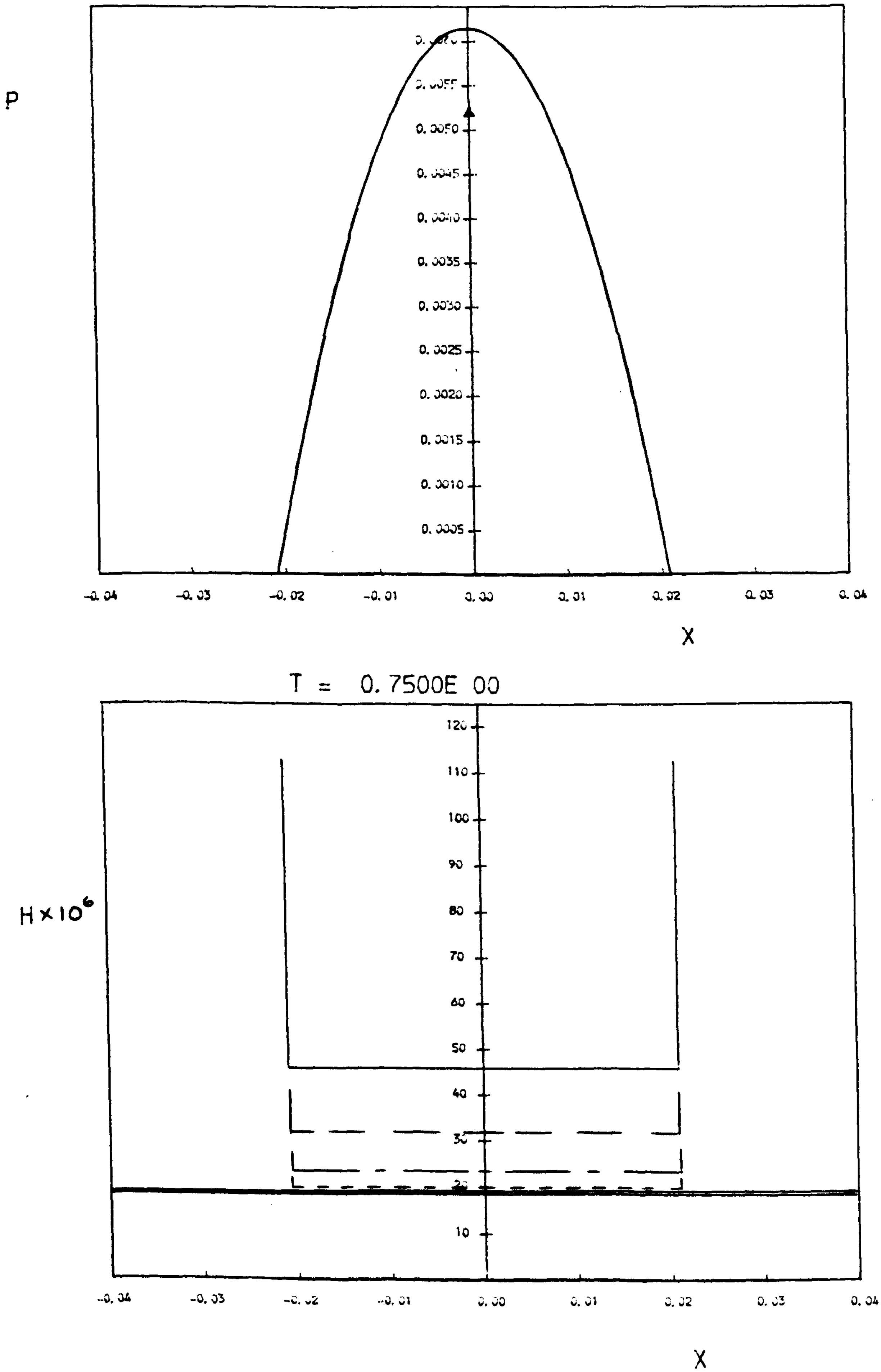

For key see page 185

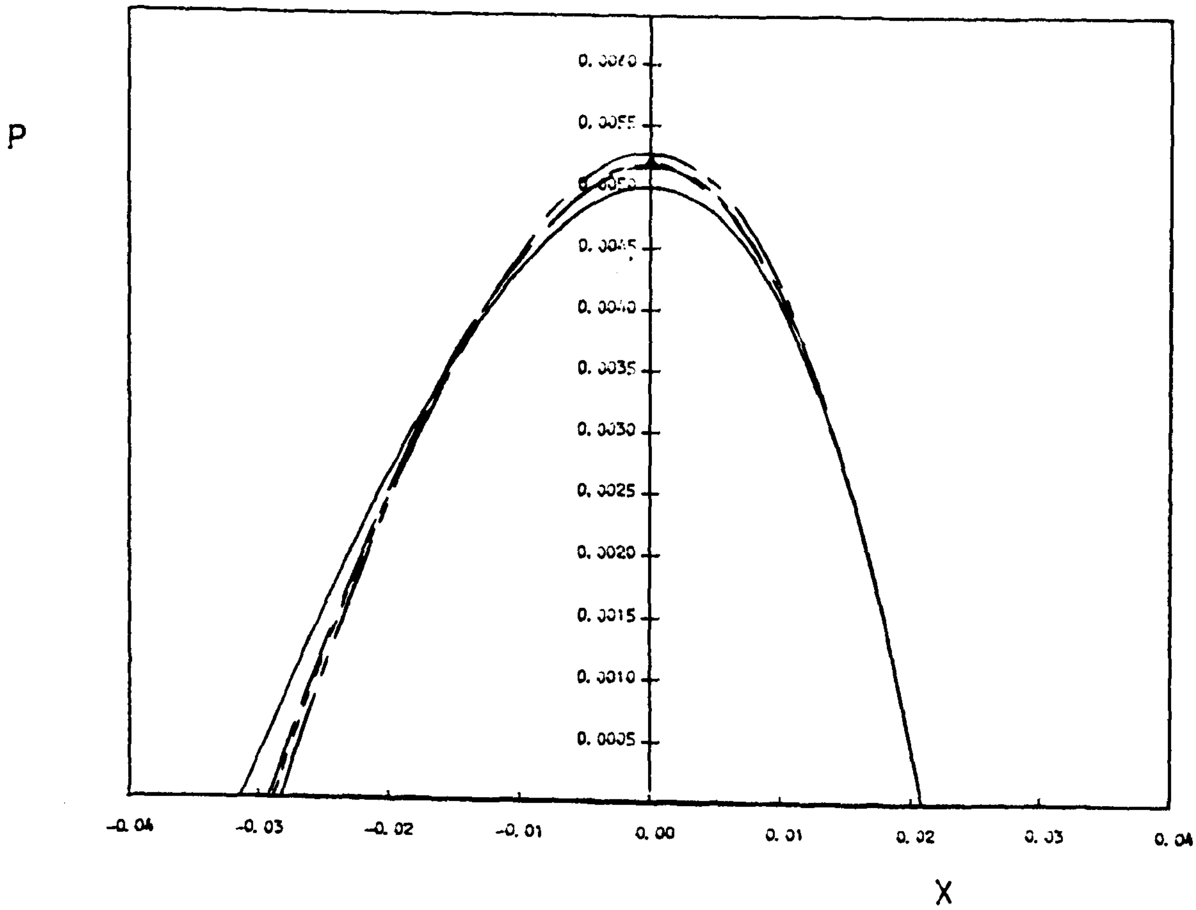

T = 0.8750E 00

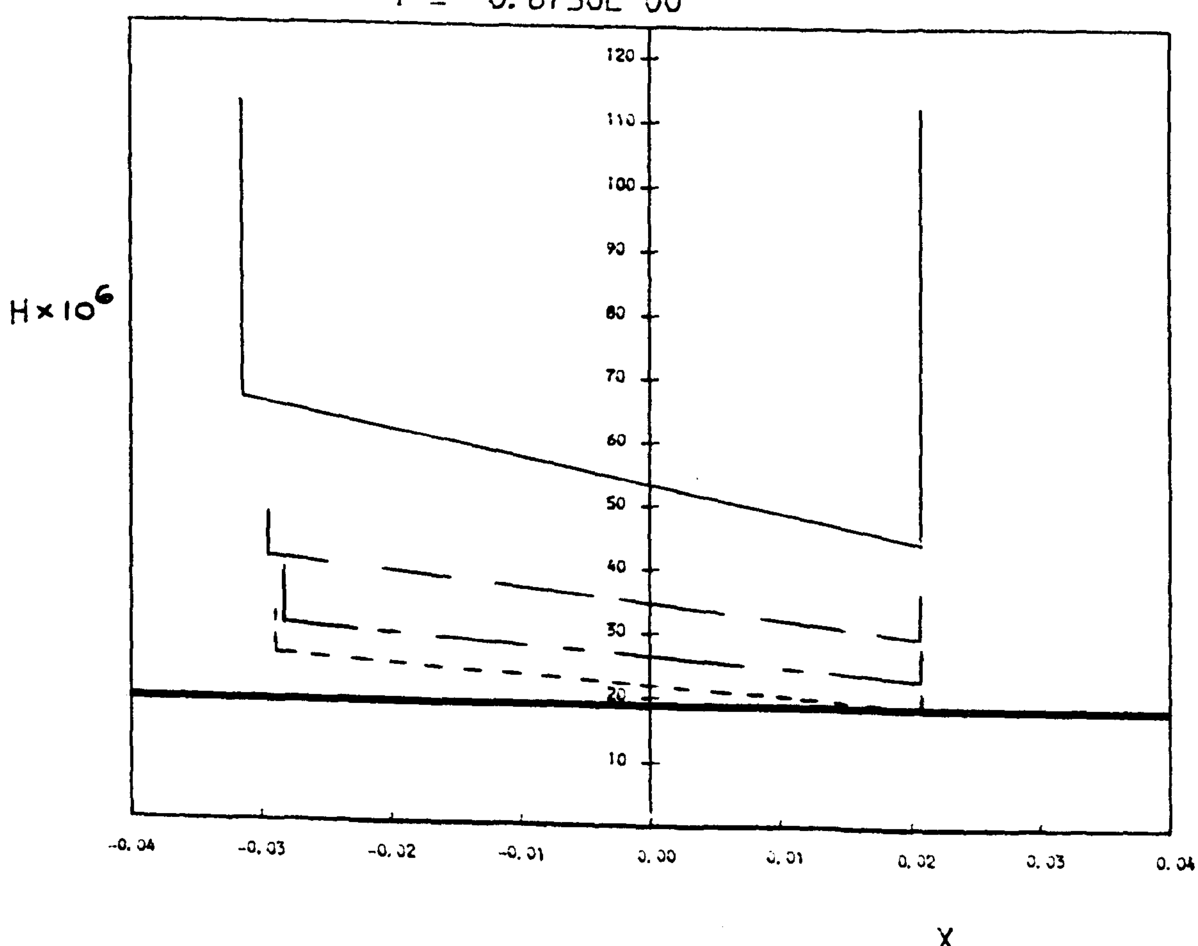

For key see page 185

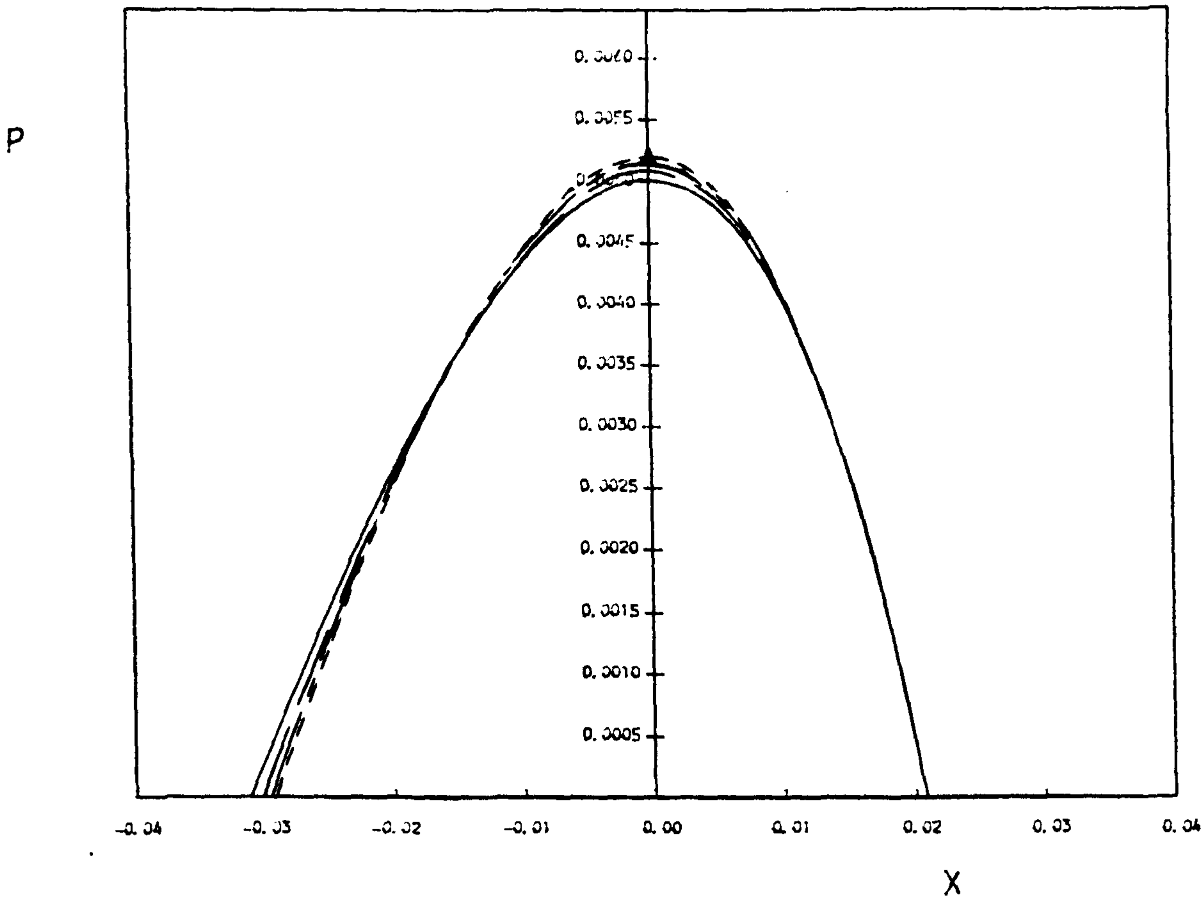

T = 0.1000E 01

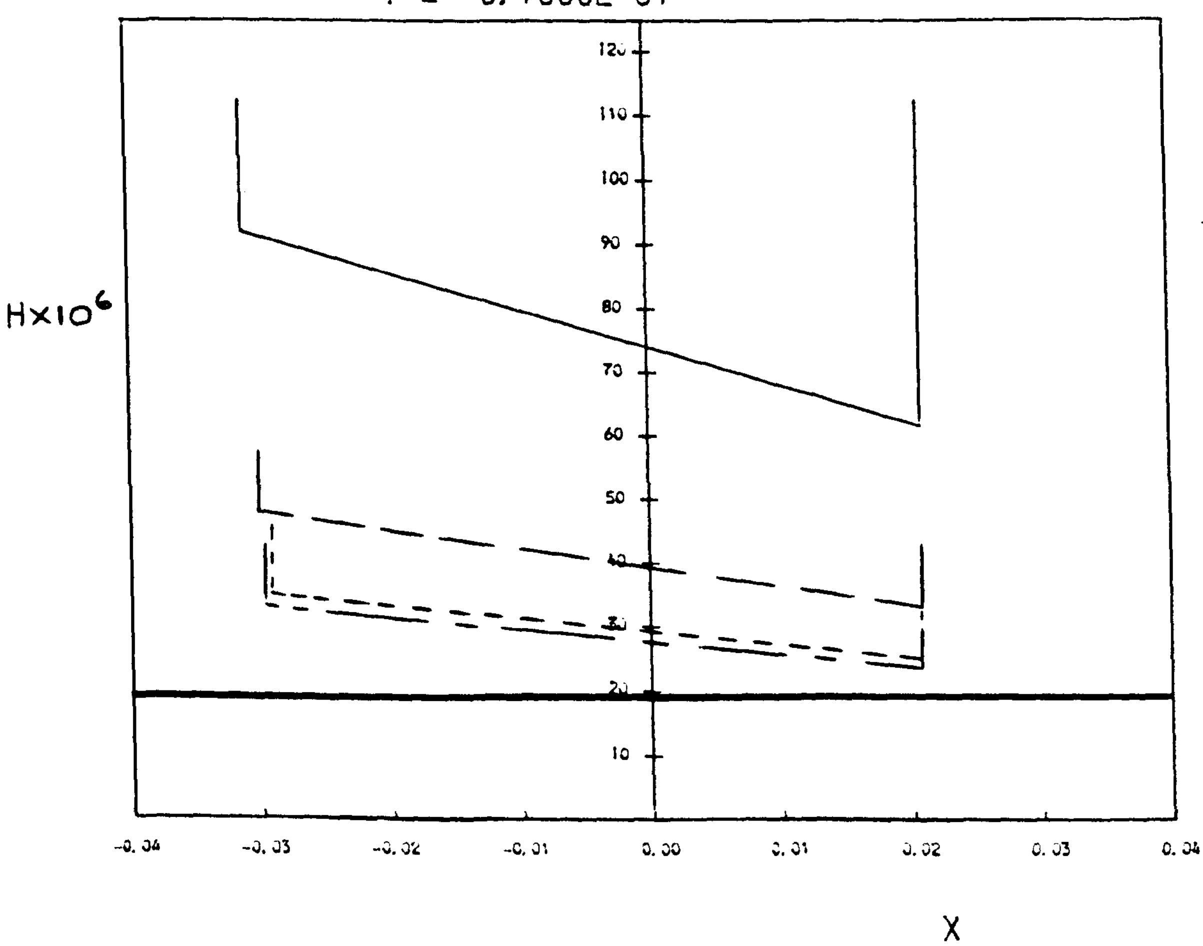

For key see page 185

Figure 6.7.1 : The solution for the conditions listed in Table 5.5.1 for Cases A and B.

—— —— Case A (for ankle joints during friction experiments).

———— Case B (for ankle joint in vivo during walking).

▲ Maximum dry contact stress in the absence of surface tractions.

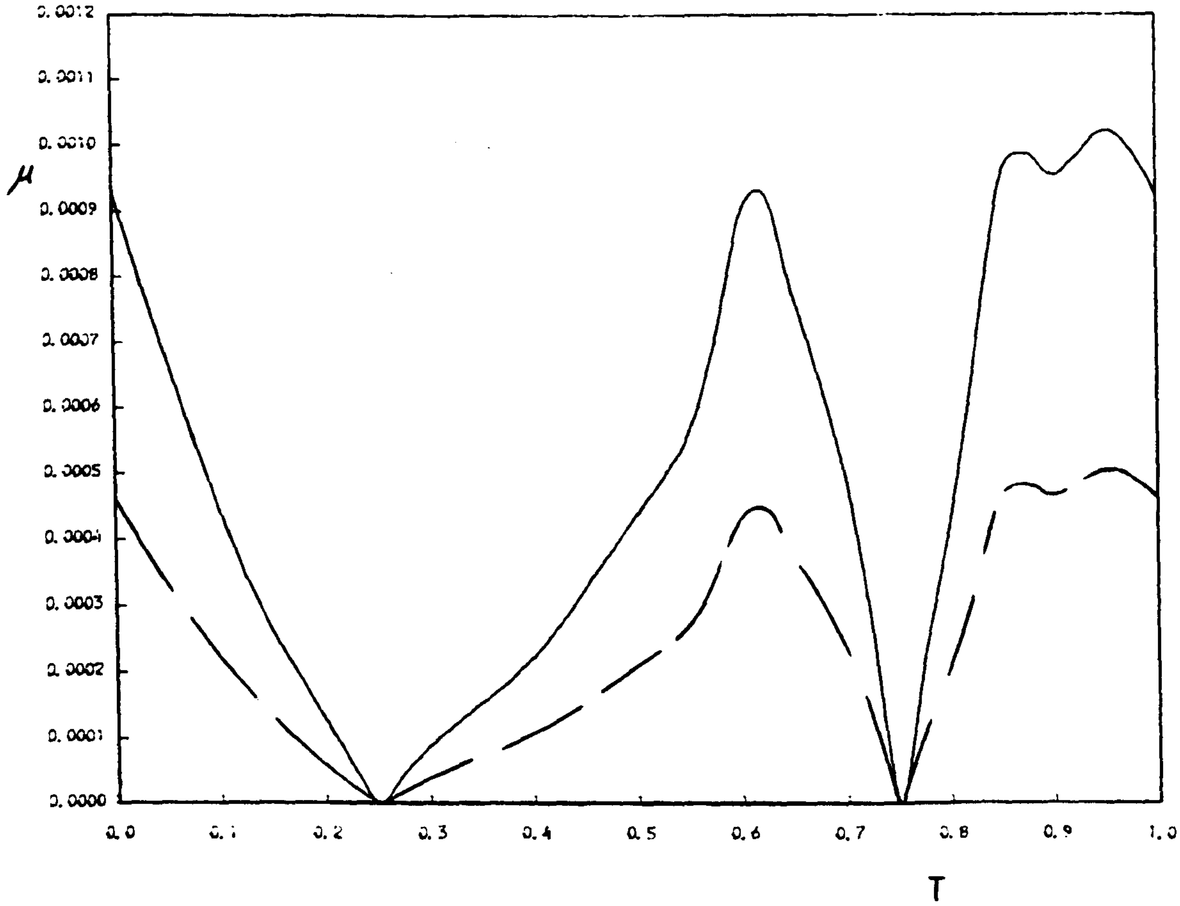

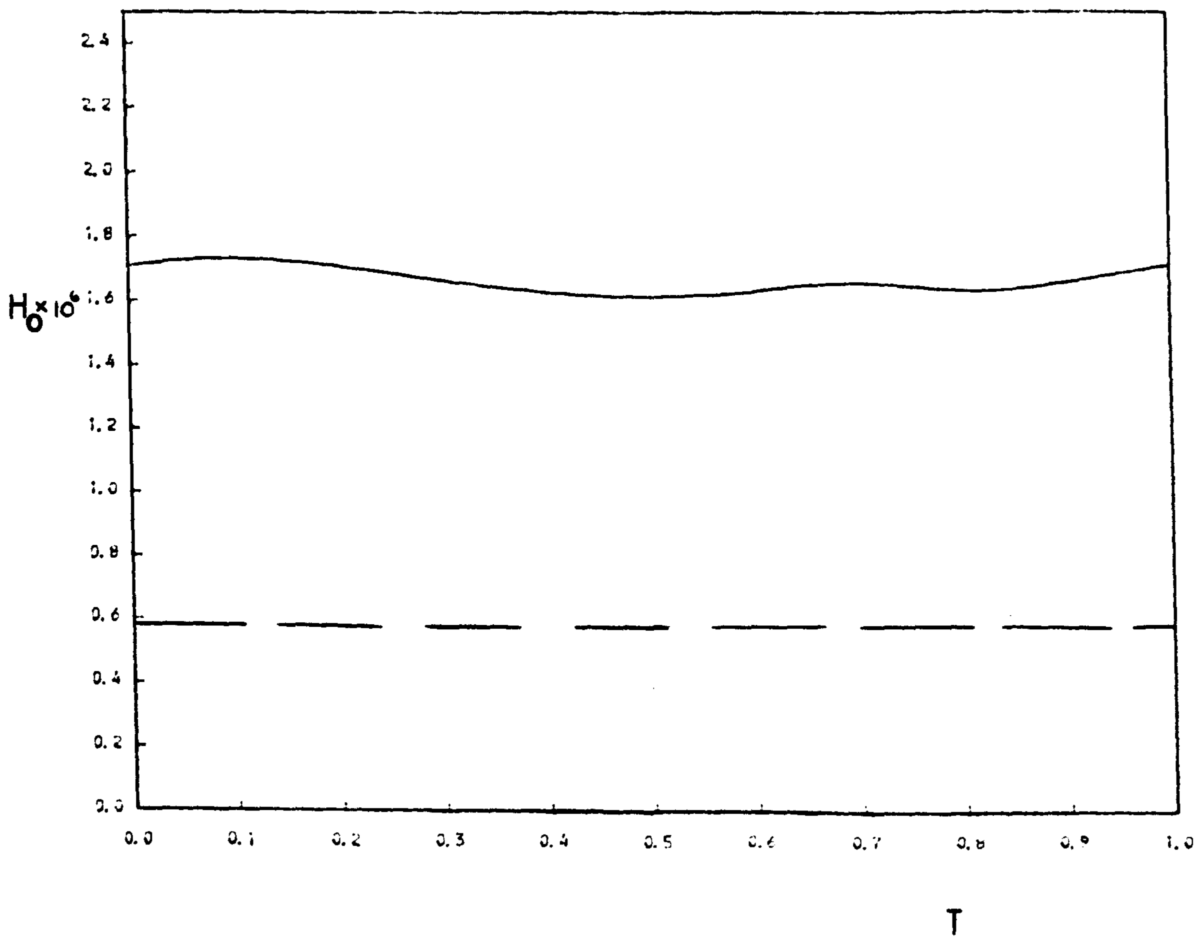

For key see page 197

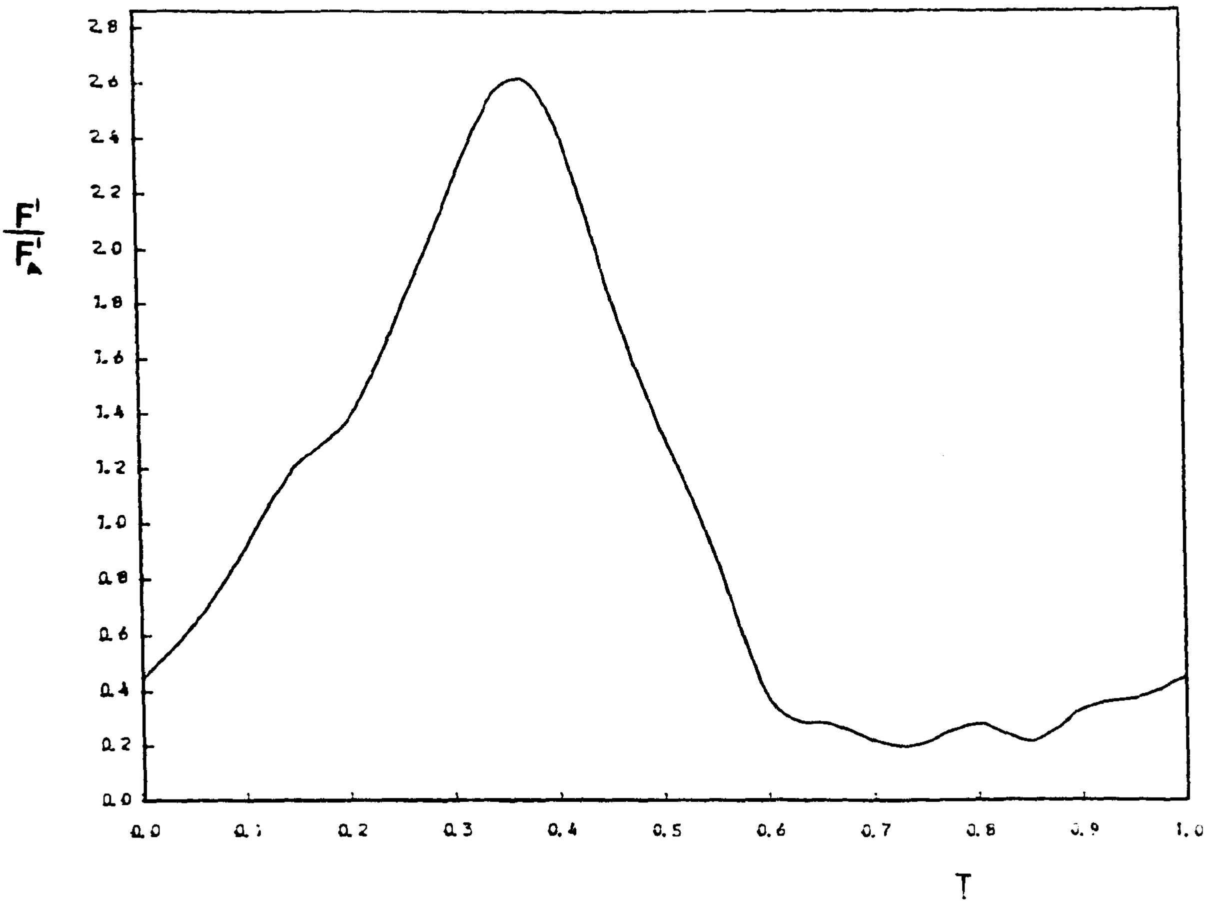

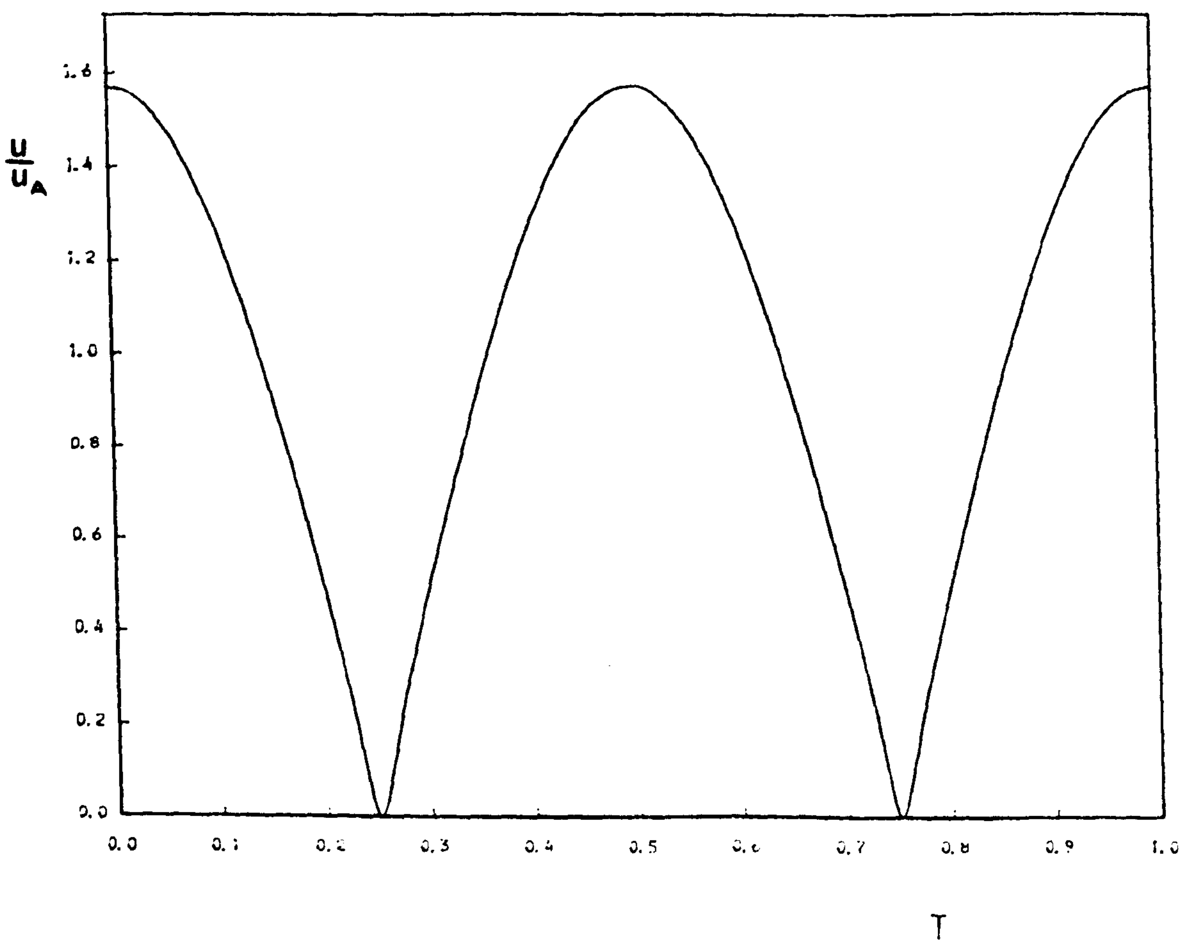

For key see page 197

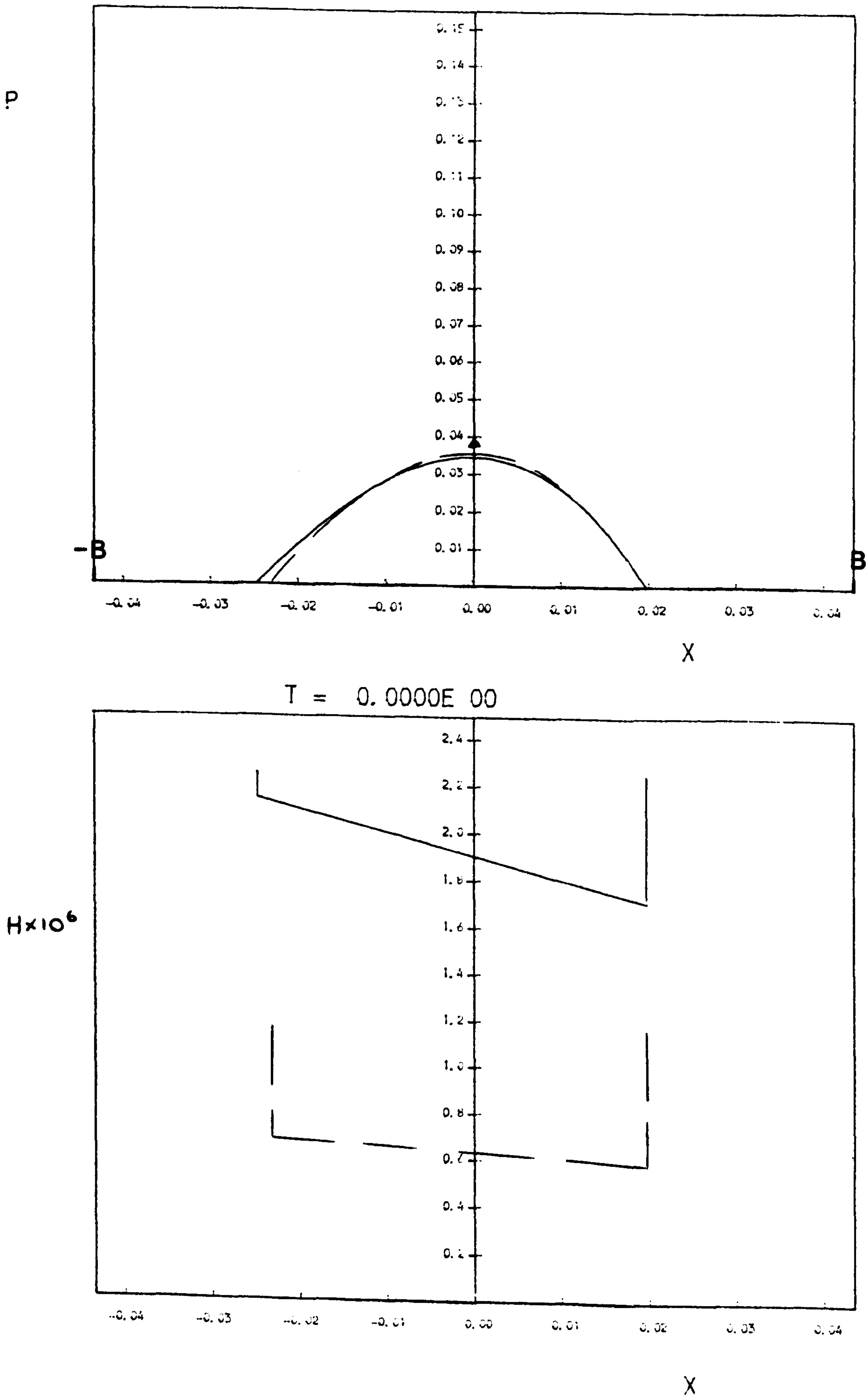

For key see page 197

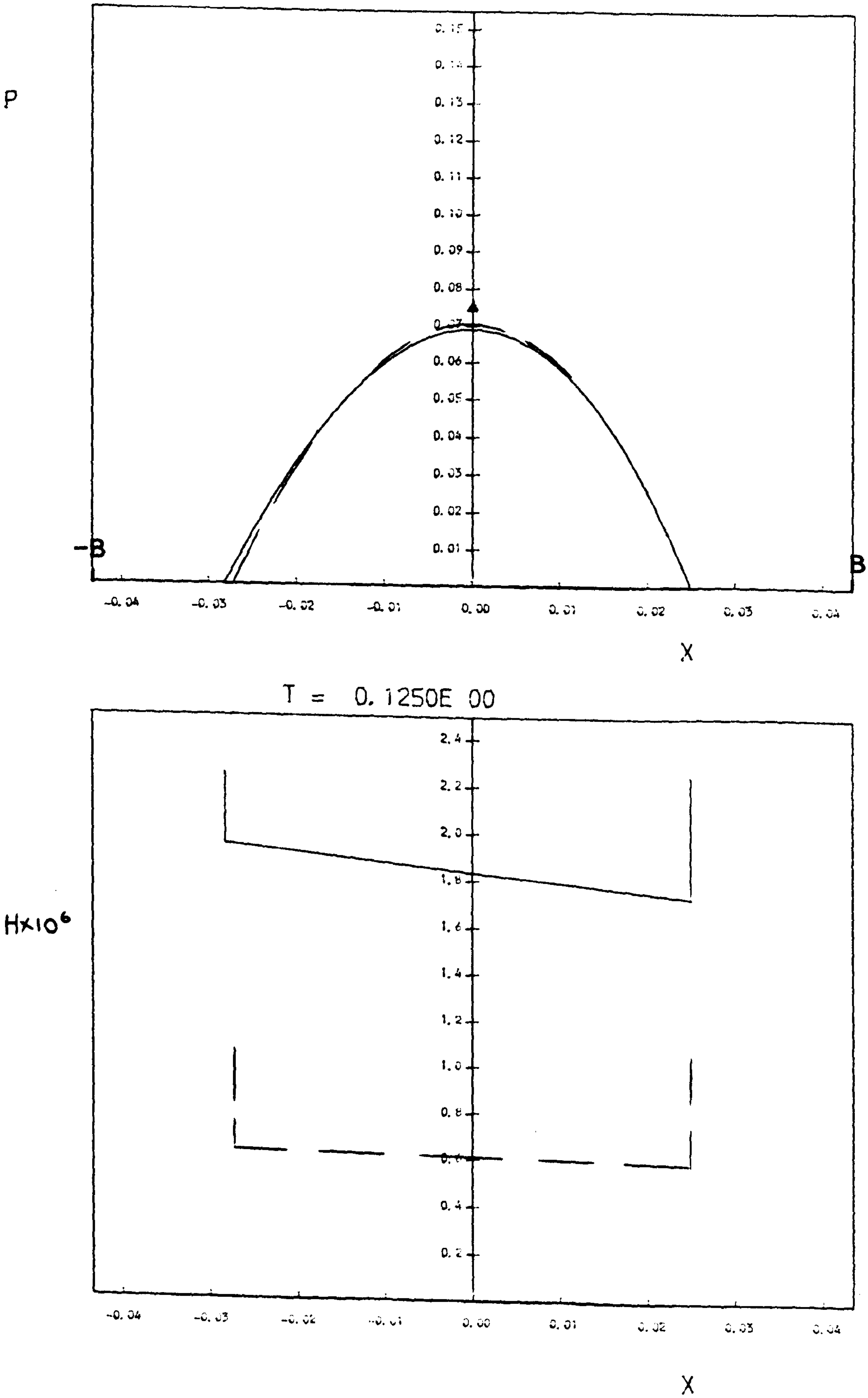

For key see page 197

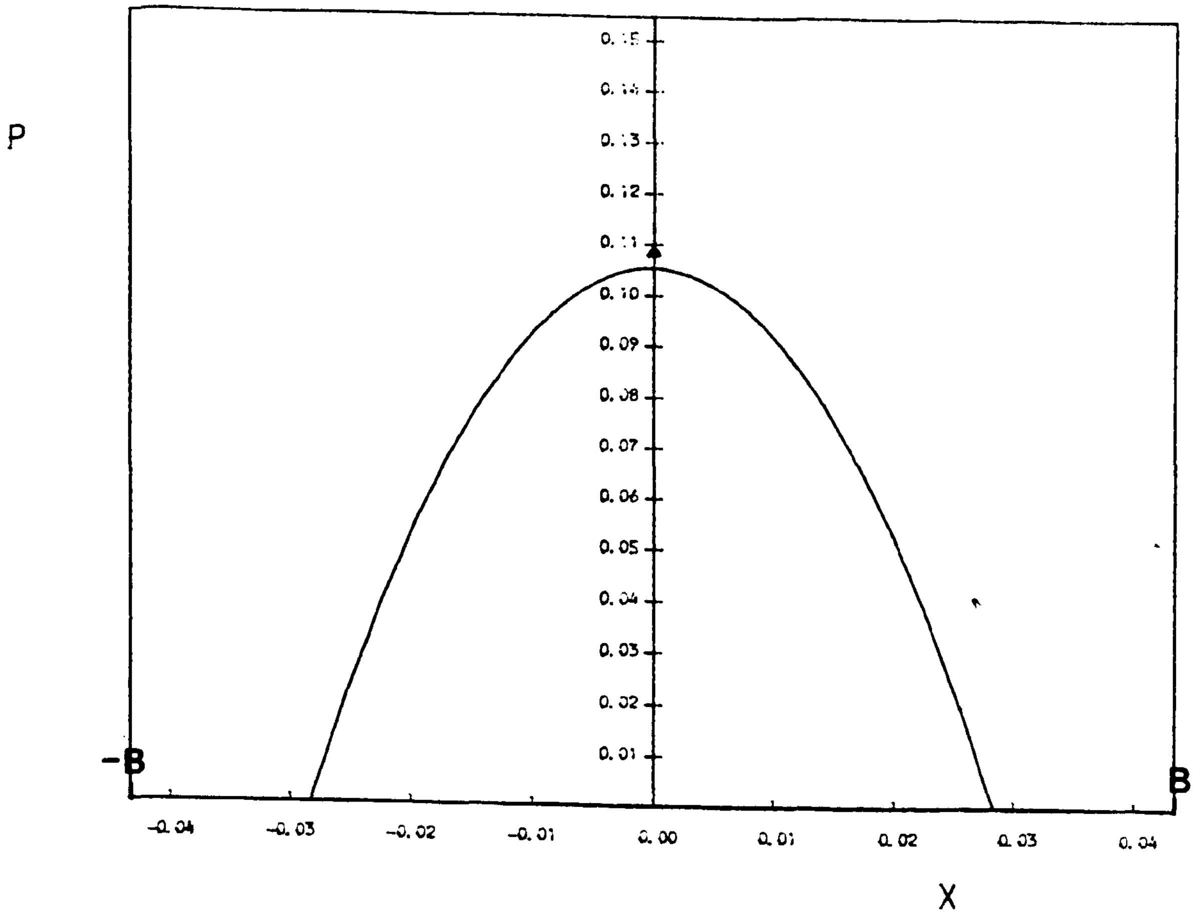

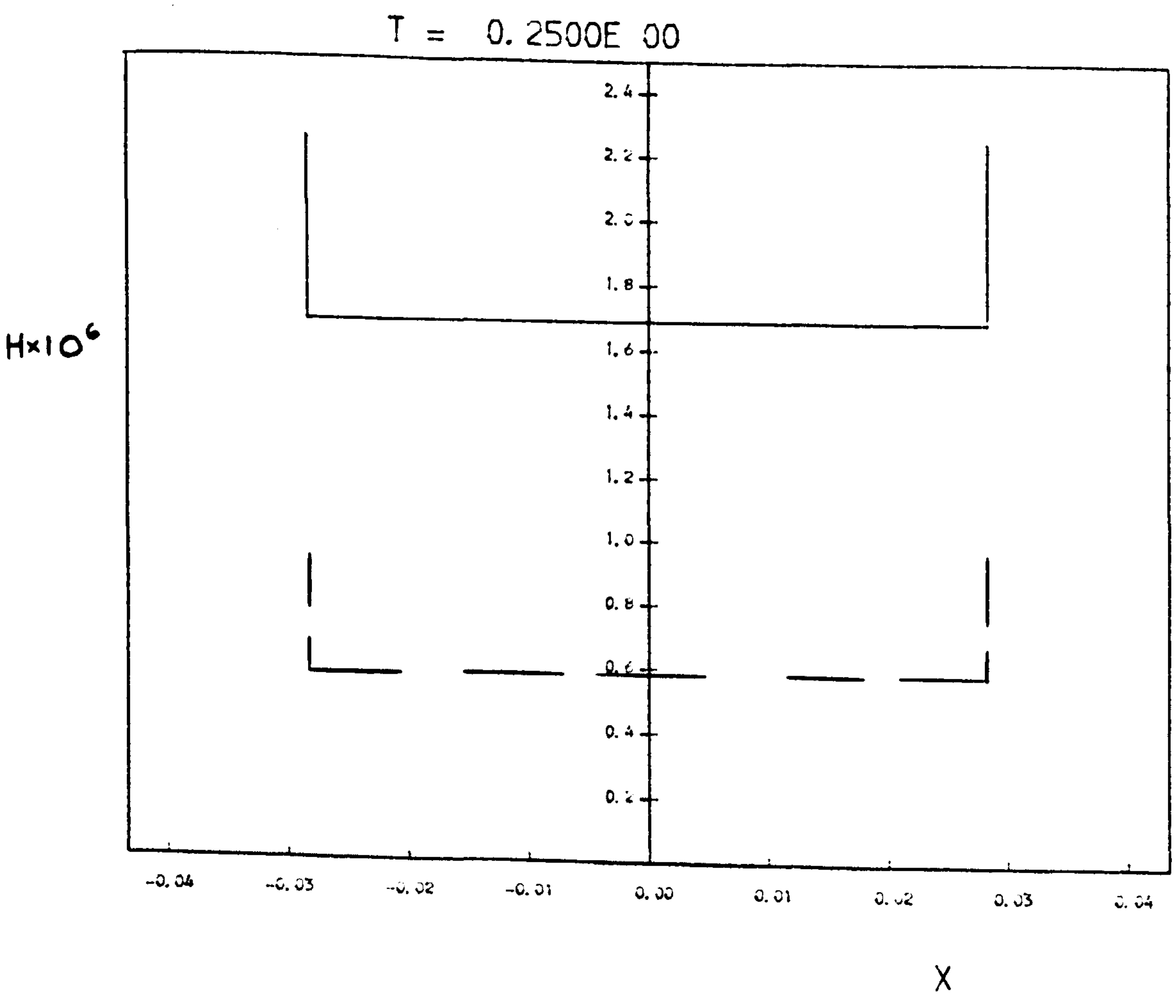

For key see page 197

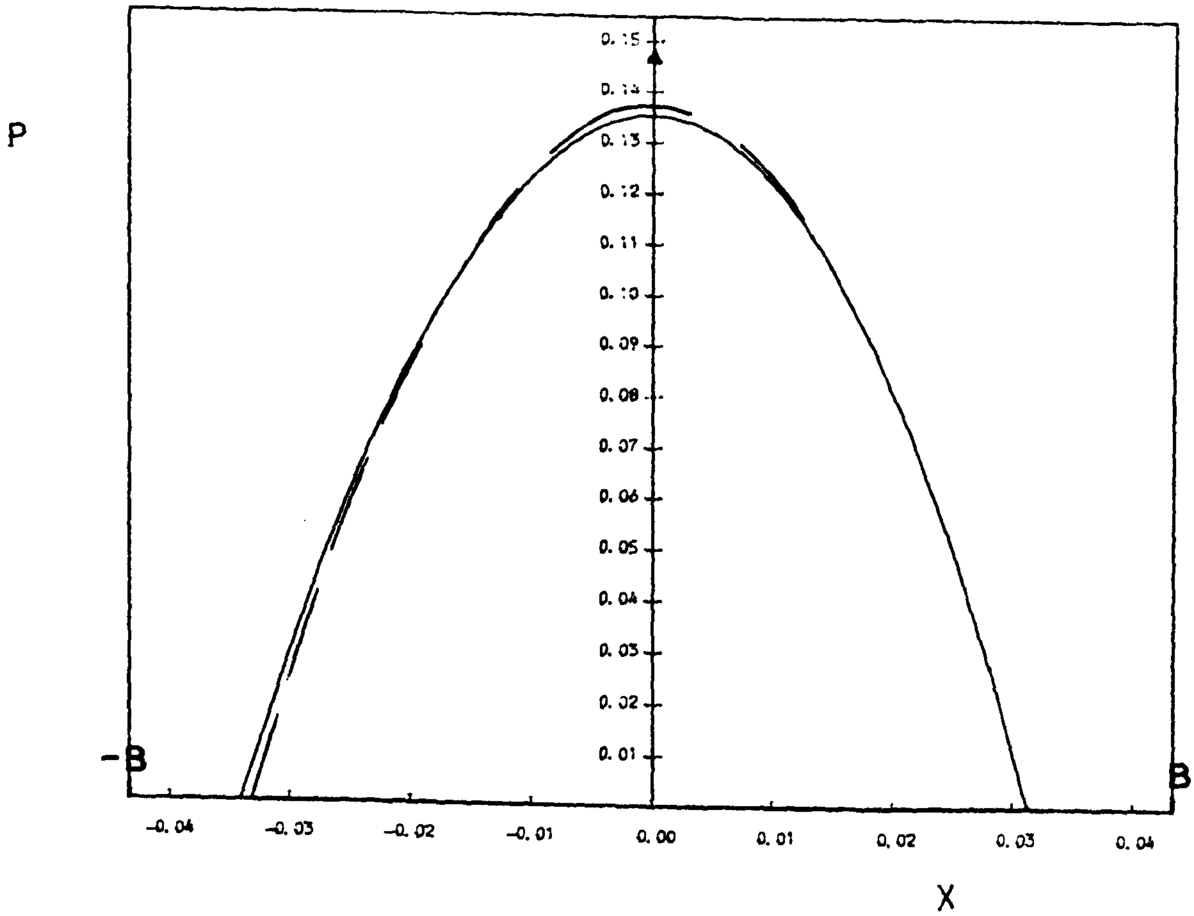

T = 0.3750E 00

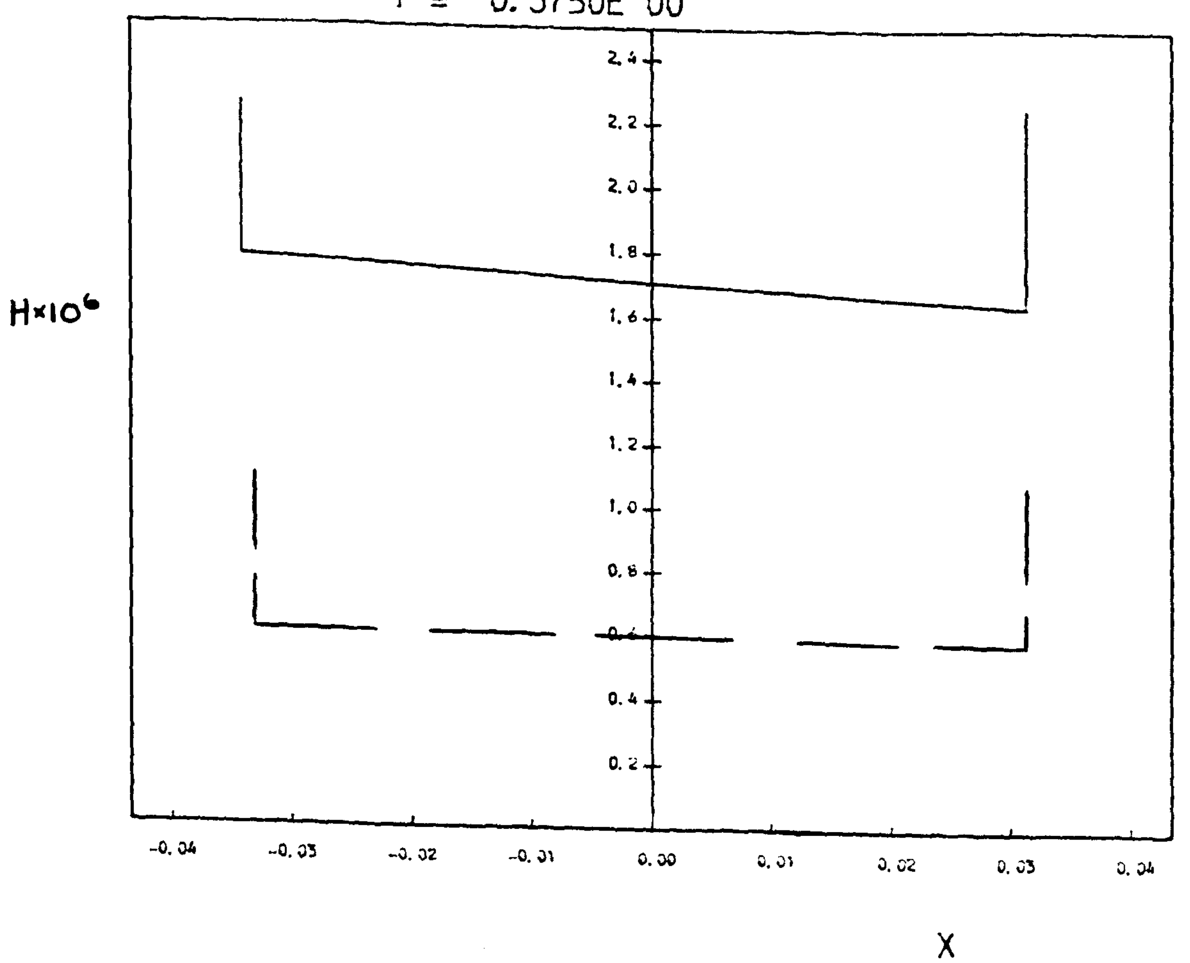

For key see page 197

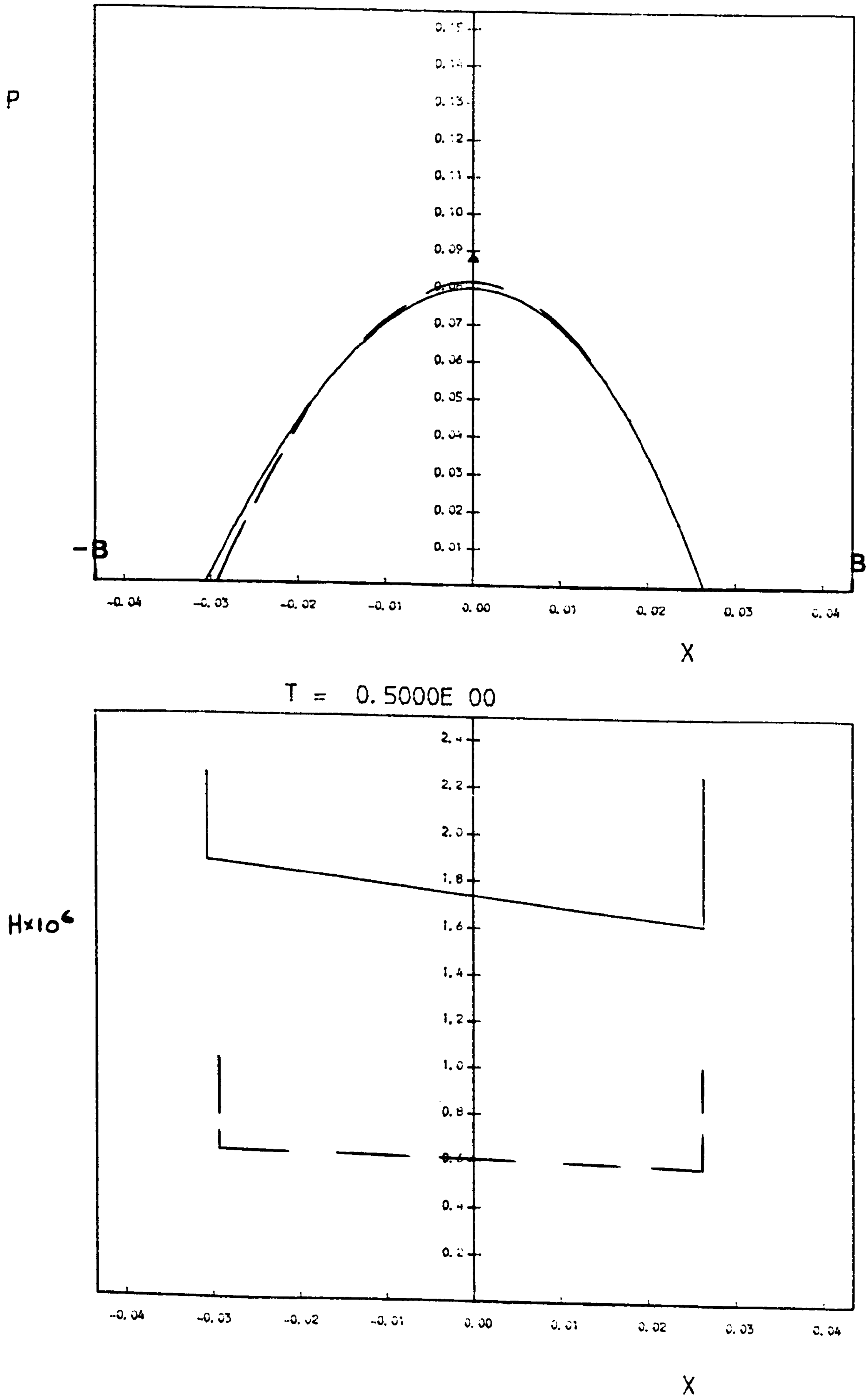

For key see page 197

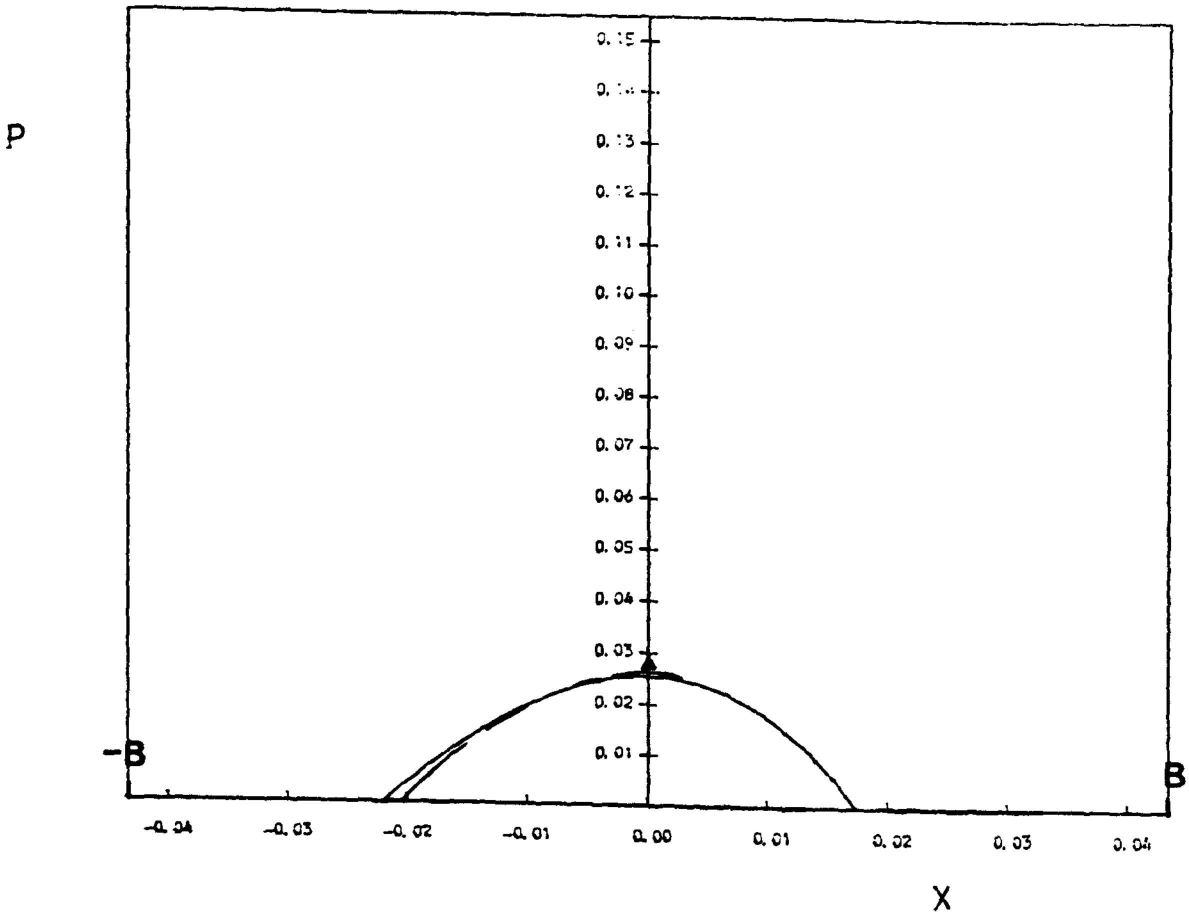

T = 0.6250E 00

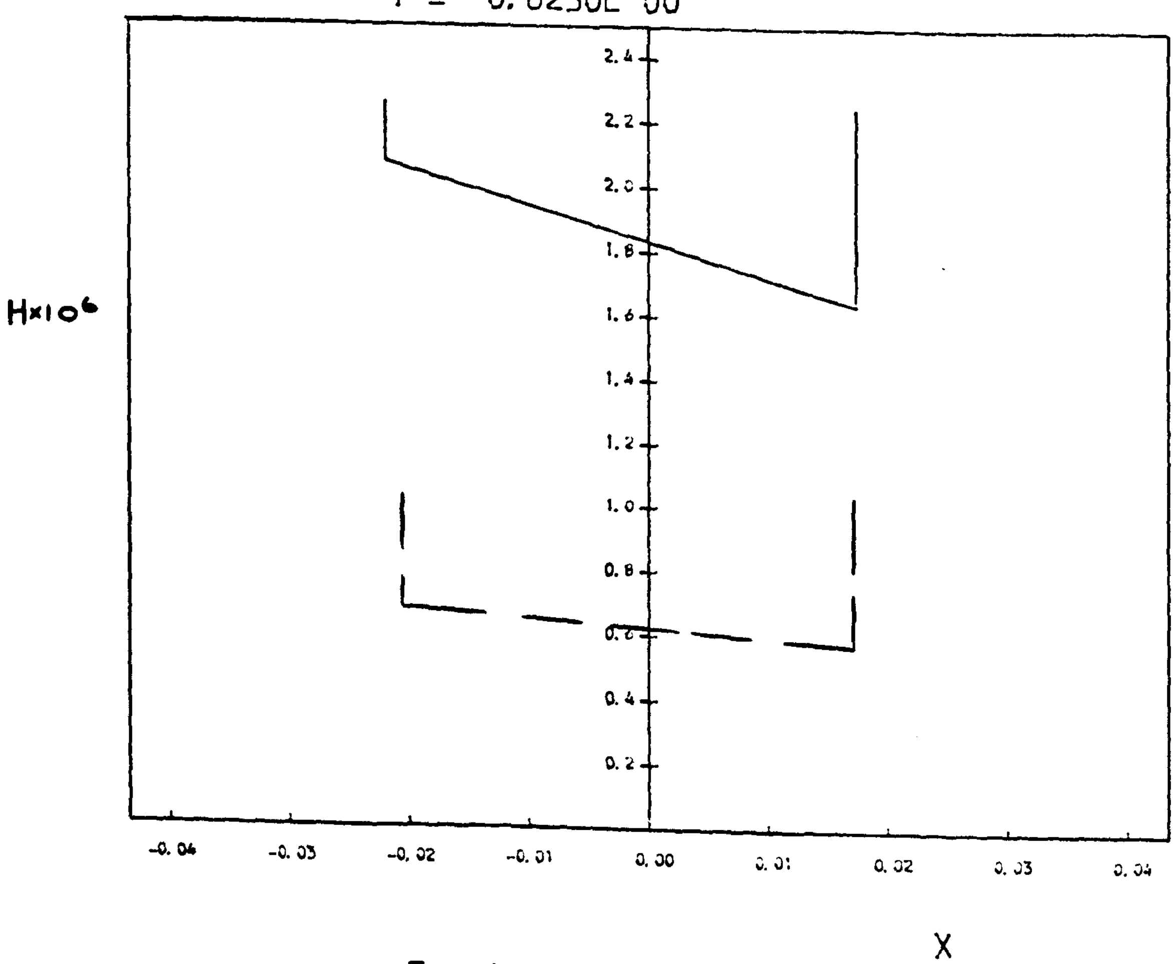

For key see page 197

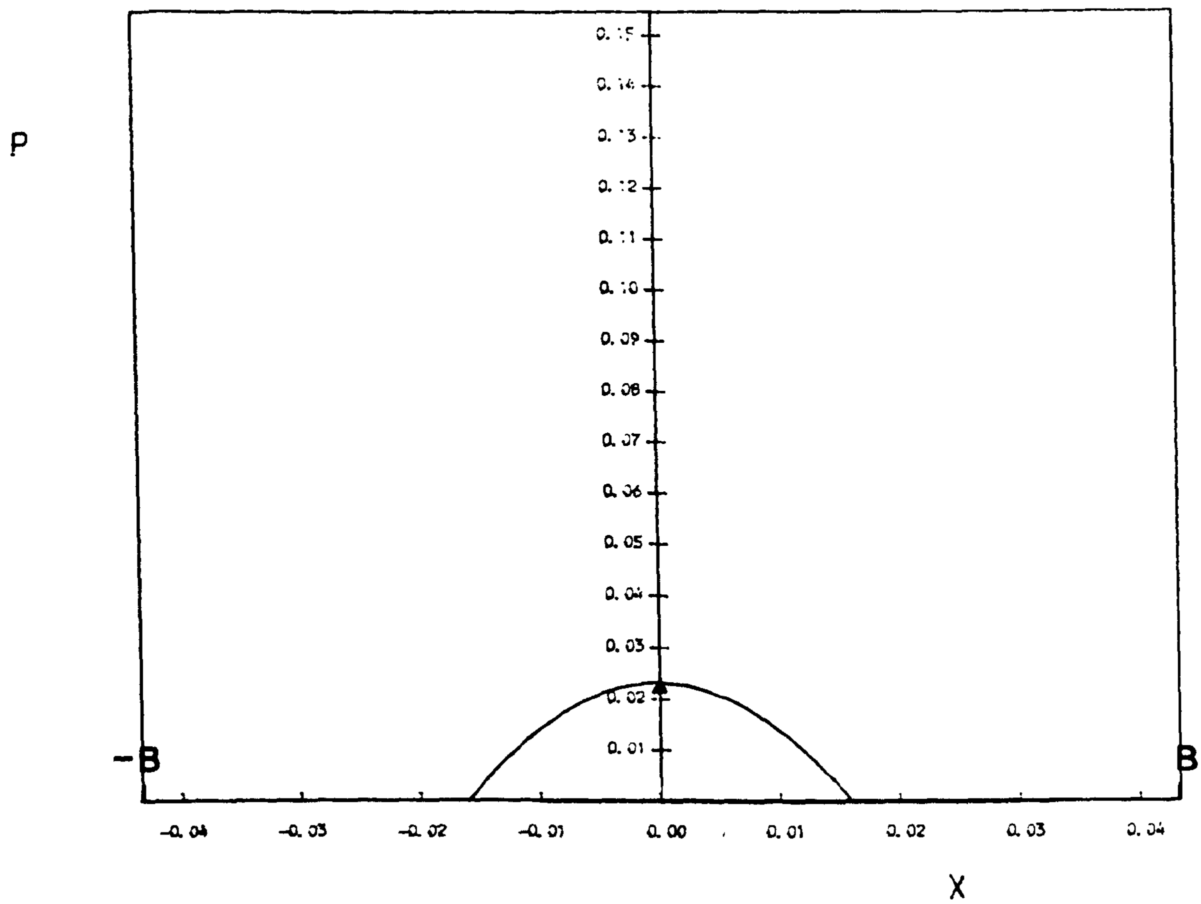

T = 0.7500E 00

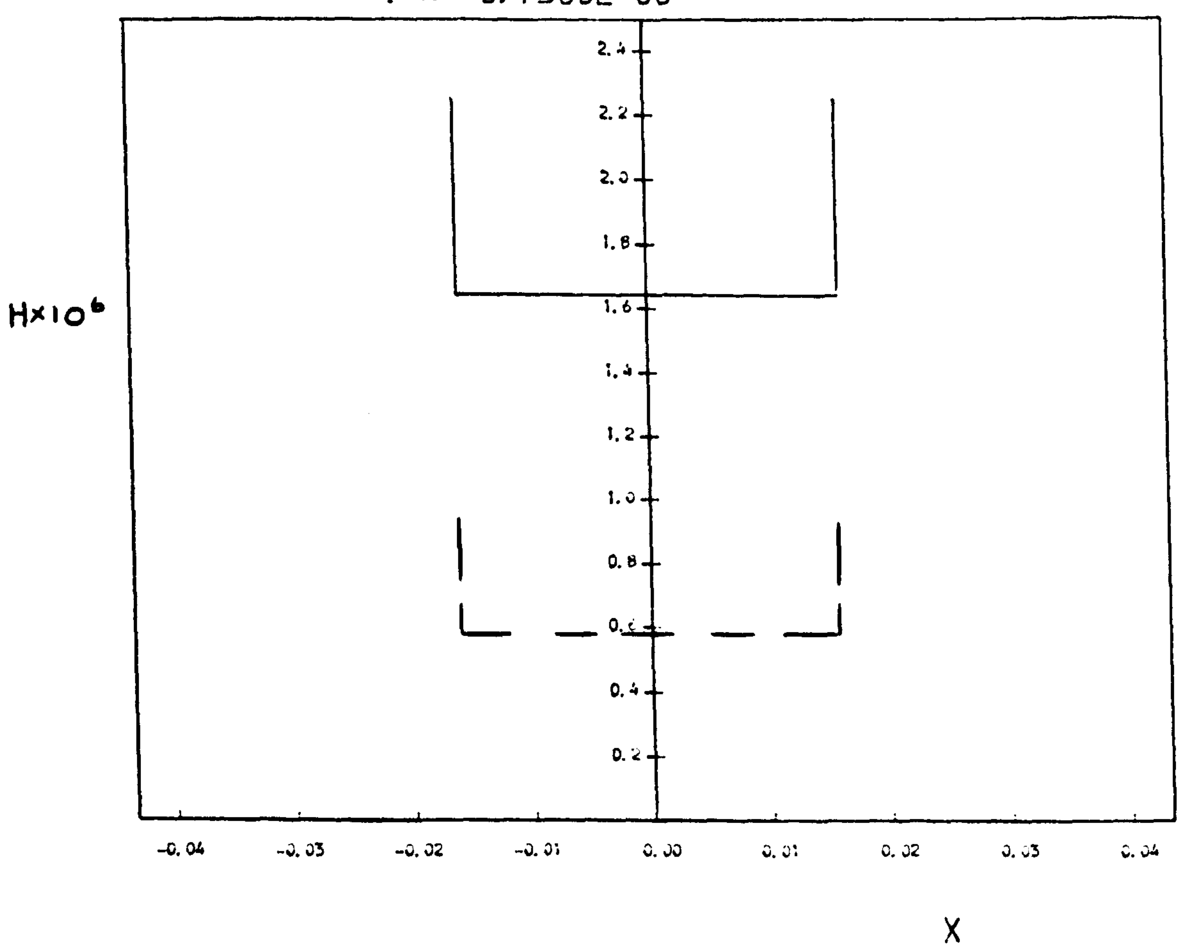

For key see page 197

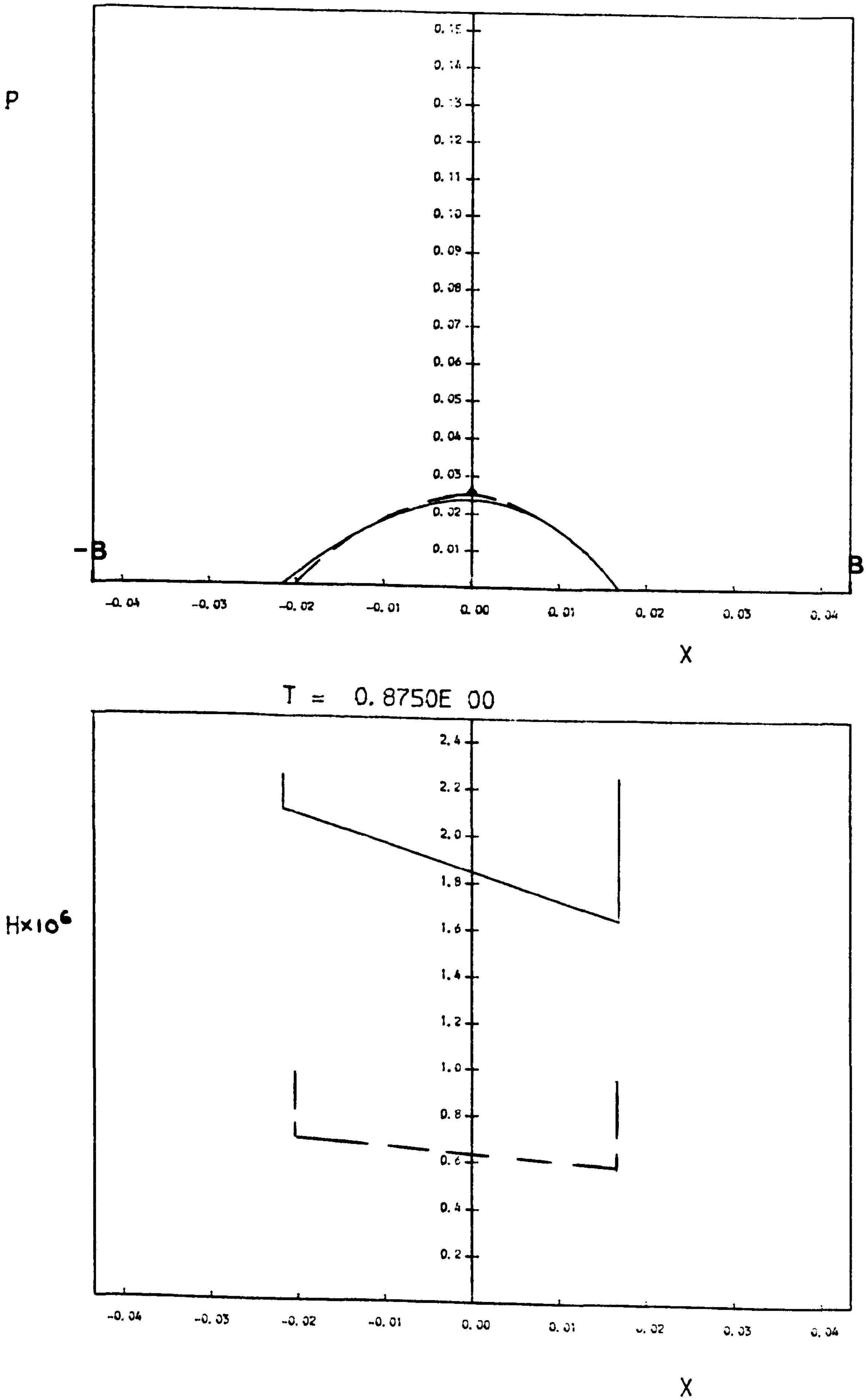

For key see page 197

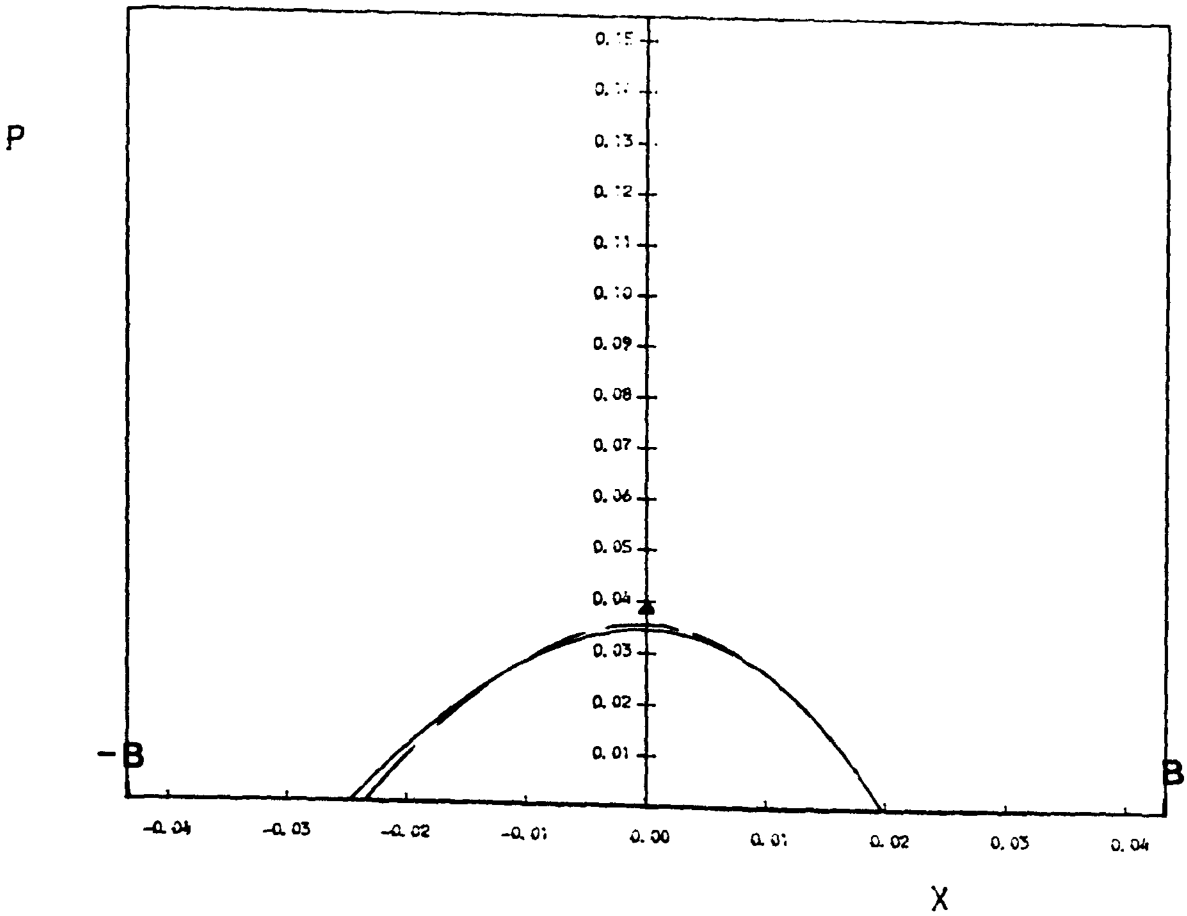

T = 0.1000E 01

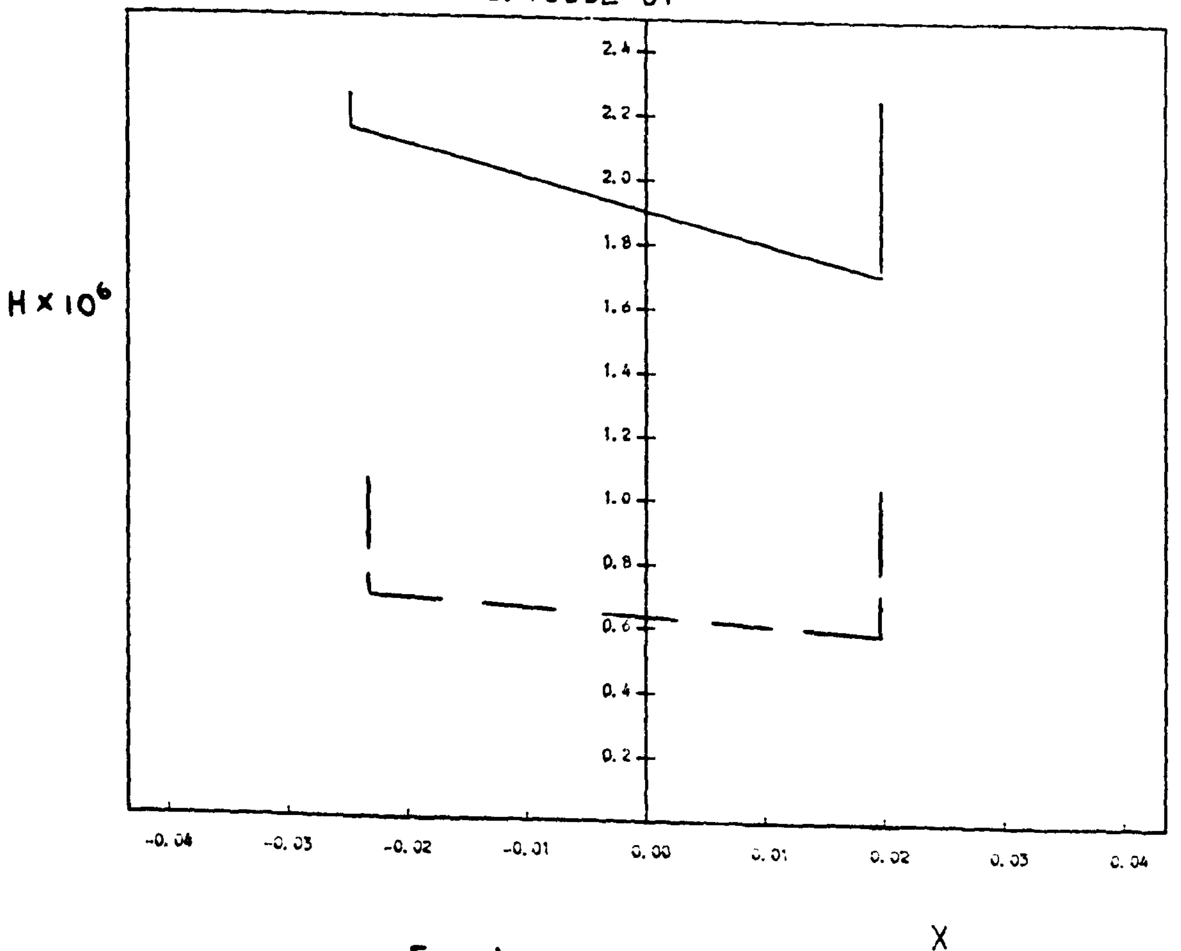

For key see page 197

CHAPTER 7

THE CONSTRAINED COLUMN DEFORMATION MODEL

7.1 INTRODUCTION

The plane inclined surface bearing model showed reasonable agreement with the investigation of Hirano and Murakami (1975). However, the equivalent bearing which represented the ankle joint was subject to widely varying loads and had a totally different geometry to that considered by Hirano and Murakami. Thus, it was deemed to be necessary to examine the assumptions made in developing the plane inclined surface bearing model. In particular the following assumptions were examined:

(i) The pressure distribution corresponded closely with the dry contact pressure which would act when surface tractions were absent.

(ii) The inlet zone was fully flooded.

(iii) Poisson's ratio of cartilage was chosen to be 0.5 and formulae based on the published data for elastic layers with this value for Poisson's ratio were employed.

(iv) The cylindrical geometry of the equivalent bearing which represented the ankle joint was approximated as a plane inclined surface configuration.

(v) Steady state profiles were adopted at each instant in time.

(vi) The squeeze film velocity at all points on the bearing surface was assumed to equal the squeeze film velocity at the point of minimum film thickness.

(vii) In Chapter 5 a single surface layer which was equal in thickness to the combined cartilage thickness was used in the equivalent bearing to represent the compliant material in the ankle joint.

The analytical complexity which led to the original formulation of the plane inclined surface bearing model prevented a rigorous examination of all these assumptions.

The basic cylindrical geometry of the ankle joint was preserved in the lubrication analysis presented in this chapter by employing a simple deformation model. This model was first suggested by Higginson (1966) in a study of journal bearings with compliant surface layers. The deformation model considered the surface layer to act as a constrained column. In other words, deformation could only occur in a direction normal to the layer surface. When Poisson's ratio of the layer approached 0.5 the deformations predicted by this model become increasingly inaccurate.

Dowson and Taylor (1967) studied thrust bearings with compliant layers and showed that the constrained column model remained reasonably accurate for a Poisson's ratio of about 0.45. This was also found by Castelli et al (1967) in a similar study of thrust bearings.

Bennett and Higginson (1970) investigated the lubrication of a cylinder sliding on a compliant layer. The constrained column model was employed and the effectiveness of a thin compliant layer in generating lubricant films was noted. Both Dowson and Taylor (1967) and Bennet and Higginson (1970) made reference to synovial joint lubrication in their investigations.

In this chapter the constrained column model was employed with a Poisson's ratio (ν) of 0.4. This value was at the low end of the range of Poisson's ratio measured for cartilage in compression as listed in Table 5.3.2.

7.2 Formulation of the Constrained Column Model:

The expression for surface deformation (δ) of a surface layer modelled as a constrained column was derived by Higginson (1966) and Dowson and Taylor (1967), and hence the derivation will not be repeated here. The following expression for surface deformation was used:

$$\delta = \frac{p.d}{E}\left[1 - \frac{2\nu^2}{1 - \nu}\right] \qquad (7.2.1)$$

The constrained column model is shown in Figure 7.2.1. It was noted that $\delta = 0$ if $\nu = 0.5$, irrespective of the applied pressure (p). However, for $\nu < 0.5$, the deflection was directly proportional to the applied pressure. Also no lateral deformation could occur and thus the deformed surface did not bulge upwards at the edges of the contact as shown in Figure 7.2.1.

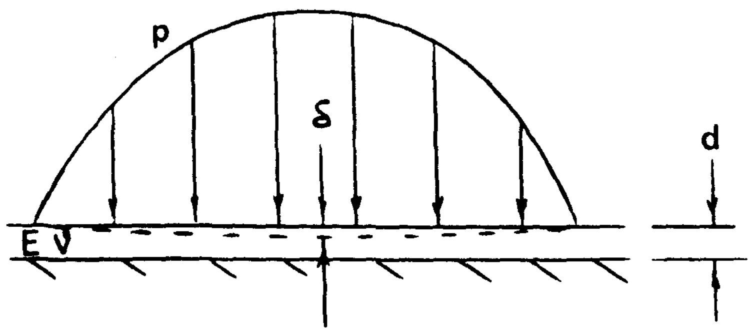

Figure 7.2.1 : The constrained column deformation model.

Expressions were developed by Bental and Johnson (1968) for a cylinder with an attached elastic layer making contact with a rigid plane without generating any surface tractions. These expressions allowed the half contact length (a) and dry contact stress distribution (p_D) to be calculated and were used in the following form in the present study:

$$\frac{a}{R} = \left[1.5\,\frac{d}{R}\,\frac{F'}{ER}\,\frac{(1 + \nu)(1 - 2\nu)}{1 - \nu}\right]^{1/3} \qquad (7.2.2)$$

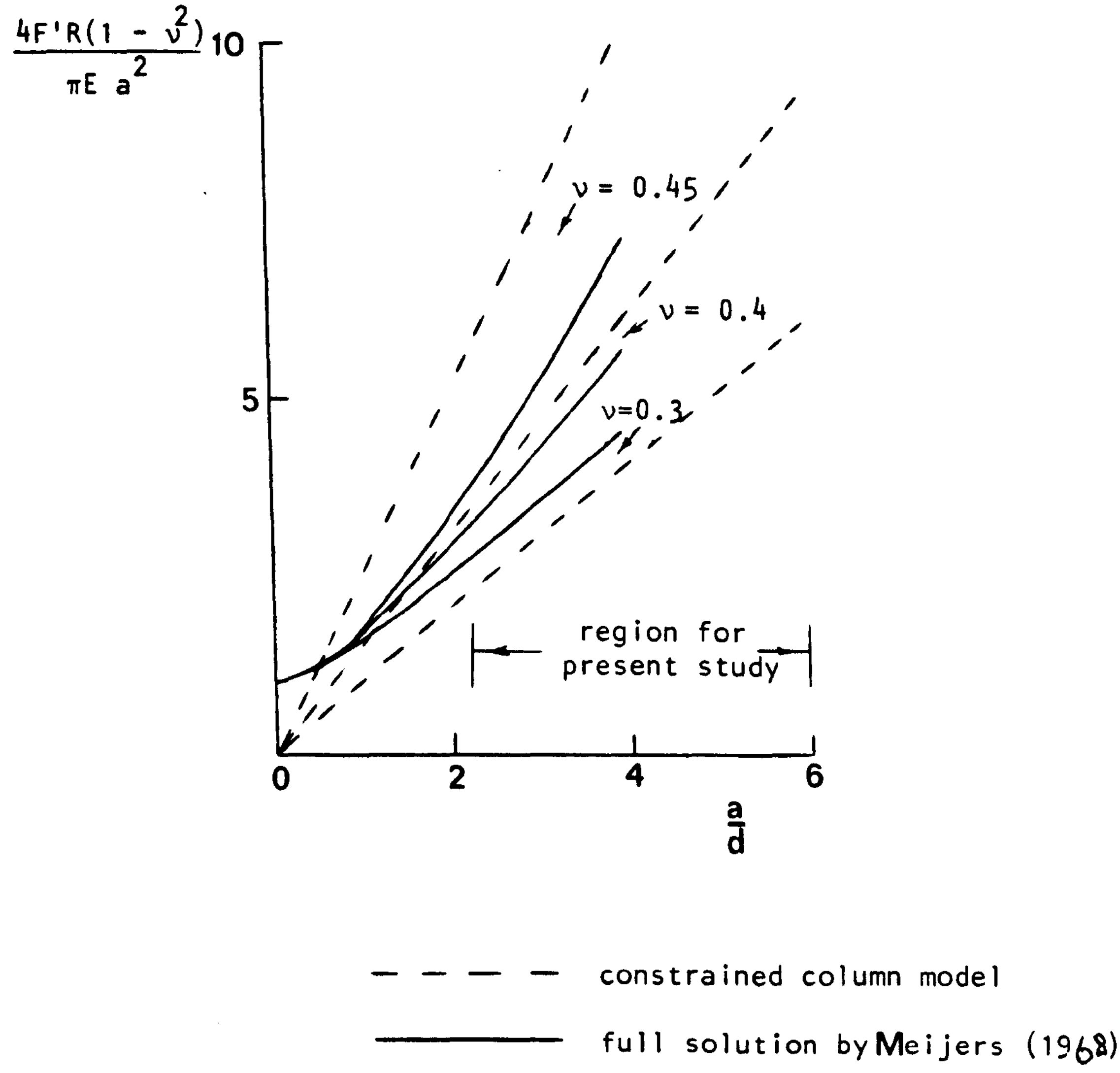

Figure 7.2.2 : Comparison of the constrained column deformation model to the full solution of Meijers (1968).

$$\frac{P_D}{E} = 0.5 \left(\frac{a}{d}\right) \left(\frac{a}{R}\right) \frac{(1 - \nu)}{(1 + \nu)(1 - 2\nu)} \left[1 - \left(\frac{x}{a}\right)^2\right] \qquad (7.2.3)$$

As stated previously, a Poisson's ratio of 0.4 was adopted in this chapter. The constrained column deformation model provided an approximation for the surface deformation and the accuracy of this approximation was indicated by the graph in Figure 7.2.2 which was developed by Meijers (1968) in his comprehensive study of the deformation of surface layers. The graphs shown in Figure 7.2.2 indicated that the approximation of the constrained column model for $\nu = 0.4$ was as good as that for $\nu = 0.3$ for the range of a/d in the present study and better than that for $\nu = 0.45$.

In the study of elastohydrodynamic lubrication, the following expression has been widely used for the film thickness of a cylinder on a plane configuration,

$$h = h_c + \frac{x^2}{2R} + \delta \qquad (7.2.4)$$

where h_c is the central film thickness excluding deformation.

For the present analysis equation (7.2.1) implied;

$$h = h_c + \frac{x^2}{2R} + \frac{p.d}{E}\left[1 - \frac{2\nu^2}{1 - \nu}\right] \qquad (7.2.5)$$

When the squeeze film velocity was zero, this expression was directly substituted into the Reynolds equation and the subsequent solution involved a single equation.

The conventional method of iterating between the elasticity and Reynolds equations sometimes causes numerical instability when solving for compliant materials subjected to high loads (Swales et al, 1972; Cudworth and Higginson, 1976). Recently Ruskell (1980). developed a procedure in which the elasticity equations were combined directly with the Reynolds equation. The procedure did not exhibit numerical instability for the range of values considered by Ruskell in a study of rectangular rubber seals. Thus, one advantage of adopting the constrained column model to approximate surface deformation lay in the possibility of avoiding numerical instability by solving a single equation which directly combined the elasticity and Reynolds equations.

7.3 The Dynamic Solution Procedure

The strategy for the dynamic solution procedure is outlined in this Section. As in Chapter 6 the squeeze film velocity was approximated by:

$$\frac{\partial h}{\partial t} = \frac{dh_o}{dt}$$

Also the surface profile at any instant in time was assumed to be that which would result if the instantaneous load and velocity were held constant. However, in the present analysis, the steady state profiles were determined by using the column deformation model and the Reynolds equation with the appropriate boundary conditions. The exact profiles, rather than a plane inclined surface approximation, were then substituted into the dynamic solution procedure.

Initial values for the dynamic routine were supplied by a variation of the plane inclined surface bearing model described in Chapter 6. This was very important since the dynamic solution procedure was very expensive in computer time and thus convergence in as few cycles as possible was desirable.

The dynamic solution procedure is shown in Figure 7.3.1. Parts 1, 2 and 3 correspond to the three main computer programs listed in Appendix F. The use of the data bank, shown in Figure 7.3.1, was particularly important. Key parameters for the steady state profiles which were computed in Part 1, were

FIGURE 7.3.1 : FLOWCHART OF THE DYNAMIC SOLUTION PROCEDURE

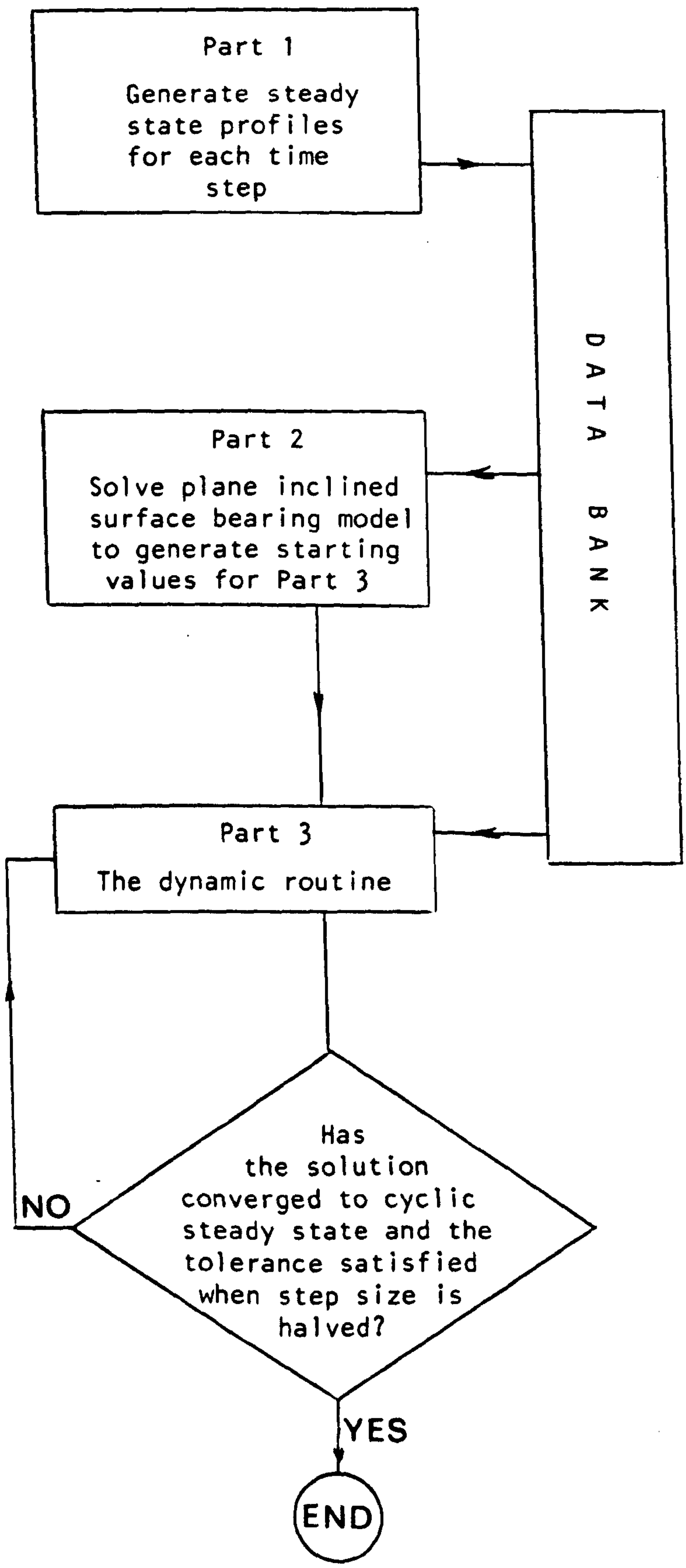

transferred to the dynamic solution of Part 3. The steady state profiles were then reconstructed in Part 3 and used in the solution. The uncoupling of the solutions for steady state profiles allowed more computer time to be available for the dynamic routine. A number of interpolation routines were included in the coding of Part 3 to select values at time steps for which Part 1 had not been solved. However, the dynamic solution procedure did not actually require them for the case considered in this chapter, since convergence occurred with a small number of time steps.

7.4 Implementation on the Computer:

The design of a complex numerical solution procedure was accomplished by following certain guidelines in much the same way as strategic axioms are followed in the game of chess. It will be shown that substituting the constrained column deformation model into the Reynolds equation yielded a first order differential equation with specified boundary conditions which could be solved for pressure. Bearing in mind that instability could occur at high loads, it was decided to use a "shooting" code instead of a finite difference solution procedure. The shooting code involved solving the specified boundary value problem as an initial value problem. Initial value routines were then used to solve the equation repeatedly as a characteristic parameter within the equation was adjusted until the boundary conditions were satisfied. In the text by Gladwell and Sayers (1980), the advantages of shooting codes were considered to include sophisticated error analysis and the availability of higher order methods. Higginson (1966) reached a similar conclusion when he used a shooting code with a fourth order Runge-Kutta numerical routine to solve a similar equation. However, Higginson noted that numerical instability still occurred at high loads. In the present study a fourth order Runge-Kutta numerical routine was initially employed. It was found that considerable computing time and an excessive number of steps across the contact were required (up to 10,000). Also, the instability noted by Higginson occurred when single precision (7 digit) arithmetic was used.

In this situation, Hornbeck (1975) recommended that a numerical package routine be incorporated and hence the NAG (Numerical Algorithm Group -Oxford) library routines were used. The danger of introducing error at a particular time step was recognized and thus the NAG libraries were used for all the numerical integrations involved in the overall solution procedure as well as for solving the first order differential equation which arose in the solution of steady state profiles.

The rationale behind this major strategic decision was described by Shampine (1980) who wrote,

> "Physical scientists are often so conscious of the defects in their crude models that they presume that crude methods will suffice for the solution of the models. Quite the contrary. Crude accuracy suffices, but the solution must be reliable. This requires very good codes because reliability is difficult to achieve at crude accuracies".

Throughout the numercial analysis in this chapter, step size halving was employed whenever the NAG library for integration (D01GAF) was used. When the routine for solving first order differential equations (D02EBF) was used the tolerance was reduced by 1/10 and the solution repeated until corresponding points agreed to a specified tolerance.

The NAG library routines employed in this chapter are listed in Figure 7.4.1. Also the interpolation routine used in Chapter 6 is included.

A Runge-Kutta-Merson routine (D02BDF) was used to ascertain whether the equation solved for the steady state profiles was stiff. It was found to be stiff, especially so near the exit boundary. A stiff equation has rapidly changing transient terms in the general solution which explode if the numerical solution strays slightly from the true solution (Hornbeck, 1975). Stiffness has been described in some detail by current texts on numerical methods (Hall and Watt, 1976; Gladwell and Sayers, 1980).

The dynamic routine used a fourth order Adams predictor-corrector pair to solve for each time step. A modifier equation was applied to the predictor equation and the corrector equation was iterated until the film thickness converged. A final evaluation of the squeeze film velocity was then obtained. This mode of operation is known as $PM(EC)^nE$ where P is the predictor equation, M is the modifier equation, E is the evaluation equation, C is the corrector equation and n is the number of iterations of EC. Details of this numerical routine were described by Lambert (1973). The local truncation error was also estimated based on the P and final C values.

7.5 The Lubrication Parameters for Case C:

The full dynamic solution procedure was solved for a single case in this chapter, which was designated as case C. The parameters are listed in Table 7.5.1 and the discrete values for the applied load per unit width (F') are listed in Table 7.5.2. A

Figure 7.4.1 Numerical Algorithm Group (NAG) library routines employed in the computer programs of this thesis

Code	General Operation	Brief Description
E01ADF	Interpolation	-interpolates by fitting cubic spline functions (simplified form of E01BAF combined with E02BBF)
E01BAF	Interpolation	-determines cubic spline interpolant to a given set of data
E02BBF	Curve Fitting	-evaluates a cubic spline from its B-spline representation
D01GAF	Quadrature	-integrates a numerically supplied function using third-order finite difference formulae with error estimates according to method of Gill and Miller (1972)
D02BDF	Ordinary Differential Equations	-solves first-order ordinary differential equation using a Runge-Kutta-Merson method -a stiffness check is available
D02EBF	Ordinary Differential Equations	-solves a stiff first-order ordinary differential equation using a variable order, variable step Gear method and returns the solution at points specified by the user.

Table 7.5.1 Parameter Values for cases C and C1

Parameter	Dimension	Case C	Case C1
R	m	0.30	0.30
b	mm	16.0	16.0
d	mm	2.4	2.4
t_p	s	1.0	1.0
u_A	mm/s	6.9382	6.9382
F'_A	kN/m	35.083	35.083
η	Pa.s	0.01	0.01
E'	MPa	38.095	38.095
U	-	6.071×10^{-12}	6.071×10^{-12}
W	-	3.070×10^{-3}	3.070×10^{-3}
S	-	3.810×10^{9}	3.810×10^{9}
D	-	8.000×10^{-3}	8.000×10^{-3}
B	-	5.333×10^{-2}	5.333×10^{-2}
μ	-	0.4	0.5

Table 7.5.2 The load per unit width (F')

Cases C and C1

t (s)	F' (kN/m)
0	12.79
0.05	18.94
0.1	27.40
0.15	37.62
0.2	49.13
0.25	60.64
0.3	78.57
0.35	93.92
0.4	94.19
0.45	81.13
0.5	49.13
0.55	35.06
0.6	13.32
0.65	6.91
0.7	5.66
0.75	4.38
0.8	6.42
0.85	6.42
0.9	6.91
0.95	9.47
1.0	12.79

second set of parameters, designated as case C1, was also considered by using the program listed in Appendix E, which had been applied to generate results in Chapter 6. Case C1 had a Poisson's ratio of 0.5, but in all other respects it was identical to case C. As mentioned previously, the dynamic procedure for the constrained column model adopted a Poisson's ratio of 0.4.

The plane inclined surface bearing model was modified for the case C conditions. Instead of using data from the literature, the results from steady state solutions of the constrained column model were taken from the data bank as shown in Figure 7.3.1. In Chapter 6, the dry contact length was found to be too short to give an iterative solution for the slope (M). Thus the condition $\frac{\partial p}{\partial x} = 0$ at $x = a$ was specified and the contact length extended maintaining this specification. However, for the constrained column model the bearing length was always long enough to achieve an iterative solution for the slope. Thus $\frac{\partial p}{\partial x} = 0$ at $x = a$ was not imposed. This was considered a minor change in procedure. The computer program which implemented the procedure is listed in Part 2 of Appendix F.

Figure 7.5.3 (included at the end of this chapter) shows results for cases C and C1. In addition, the first four graphs include cases A and B for reference.

In Figure 7.5.3, the variation of H_o with T for case C1 was in the same range as those for cases A and B. The coefficients of friction (μ) also showed a similar variation with time. Since the results for case C1 were in the range of those for cases A and B, it was clear that the conditions described by case C1 were not much different from those for cases A and B. As mentioned previously case C was the same as case C1 except for the Poisson ratio value. Thus, case C which will be used to generate a full dynamic solution in this chapter, imposed conditions quite similar to cases A and B.

However, case C which adopted a lower Poisson's ratio (ν = 0.4) than case C1 (ν = 0.5) exhibited a film thickness some sixty percent larger than that predicted for case C1. This was apparently a consequence of the larger dry contact zone which occurred for case C (ν = 0.4) as shown in the plots of pressure distribution in Figure 7.5.3. However, the minimum film thickness of about 0.54 μm remained much smaller than for the heights of the surface asperities of cartilage. This indicated that the selection of a Poisson's ratio in the range of 0.4 - 0.5 was unlikely to change the findings of this thesis significantly.

The results for case C provided a set of starting values for the dynamic routine as shown in Figure 7.3.1.

7.6 Generation of the Surface Profiles:

The surface profiles required at each time step were generated by performaing a solution of the combined Reynolds and elasticity equations for the constant load and entraining velocity. The co-ordinate system adopted for this analysis is shown in Figure 7.6.1. For this situation equation (5.2.1) became:

$$\frac{d}{dx}\left(h^3 \frac{dp}{dx}\right) = 12\eta u \frac{dh}{dx} \tag{7.6.1}$$

where $u = \frac{U_1}{2}$

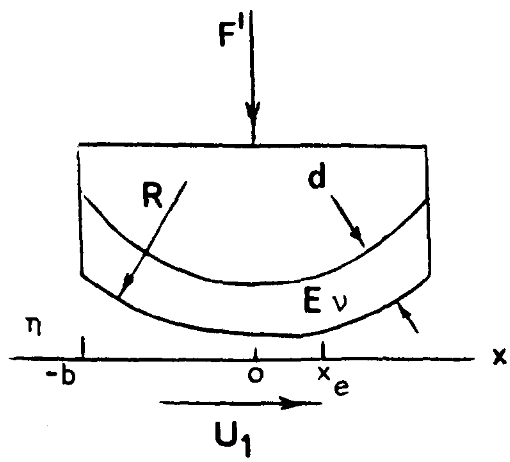

Figure 7.6.1 : Geometry for steady state solution using constrained column model.

The following boundary conditions were specified

$$p = 0 \quad \text{at } x = -b \tag{7.6.2}$$

$$p = 0 \quad \text{at } x = x_e \tag{7.6.3}$$

$$\frac{dp}{dx} = 0 \quad \text{at } x = x_e \tag{7.6.4}$$

$$p > 0 \text{ for } -b < x < x_e \tag{7.6.5}$$

$$F' = \int_{-b}^{x_e} p \, dx \tag{7.6.6}$$

When combined with equation (7.2.5) equations (7.6.1), (7.6.3) and (7.6.4) reduced to

$$\frac{dp}{dx} = \frac{12\eta u\left(\dfrac{x^2 - x_e^2}{2R} + A.p\right)}{\left(h_c + \dfrac{x^2}{2R} + A.p\right)^3} \tag{7.6.7}$$

where $A = \frac{d}{E}\left(1 - \frac{2\nu^2}{1 - \nu}\right)$

The numerical solution procedure consisted of the following five steps for a specified load (F') and velocity (u):

(i) specify x_e

(ii) specify h_c

(iii) solve equation (7.6.7) for p

(iv) iterate until equations (7.6.2) and (7.6.5) are satisfied.
(i.e. $p = 0$ at $x = -b$
$p = 0$ for $-b < x < x_e$)

(v) iterate until the specified F' approximately equals that computed from equation (7.6.6).

The initial specification for x_e and h_c were obtained from equations (6.2.1) or (6.2.2) and (7.2.4) along with an interpolation (NAG E01BAF, E02BBF) of the data from Gupta and Walowit (1974). Unfortunately, the author was initially unaware of the study by Bentall and Johnson (1968), otherwise equations (7.2.2) and (7.2.3) would have been used to specify initial values much closer to the required solution.

The solution of equation (7.6.7) required the use of the Gear method for solving stiff differential equations (NAG D02EBF) as discussed briefly in Section 7.5. This method was variable-step, variable-order and employed backward differentiation (BDF) or Adams predictor-corrector pairs, depending on local stiffness. When local stiffness was severe, as it was near $x = x_e$, the BDF formulae were required and the Jacobian expression for equation (7.6.7) was used in a Newton iteration at each step.

The iteration for h_c was performed with a bisection routine. Coupled with the Gear method, the coding constitutes a "shooting" code for solving equation (7.6.7) subject to the conditions imposed by equations (7.6.2) and (7.6.5).

The integration of the pressure distribution was accomplished using the method of Gill and Miller (1972) (NAG D01GAF). This method involved using four point finite difference formulae and resulted in a cubic interpolation of the integrand. An indication of the reliability of the answer was achieved by comparing it with the corresponding answer obtained from a process of piecewise quartic interpolation of the integrand.

The iteration for x_e was performed with a bisection routine. Reliability checks were performed by automatically reducing both tolerances and step size within the computer program as outlined in Section 7.4.

The program which solved for the steady state profiles is listed in Part 1 of Appendix F. The results for various points in the cycle for Case C is shown in Figure 7.6.2 (included at the end of this chapter).

The profiles shown for T = 0.25 and 0.75 corresponded to $u = 0.0157\ u_A$ rather than zero. Thus, these profiles had a slight inclination which would not occur during pure squeezing action.

The almost vertical rise of all the profiles at $x = x_e$ was a consequence of the large expansion of the vertical scale compared to the horizontal one which thus distorted the cylindrical geometry.

The dry contact stress from equation (7.2.3) was included in Figure 7.6.2 and coincided exactly with the computed hydrodynamic film pressures except for a very slight deviation in the inlet pressure sweep. This deviation was so small that it could not be shown in Figure 7.6.2. This supports the assumption that the steady state pressure curve was close to the dry contact stress for the solutions of cases A and B in Chapter 6. Also, the lubrication solution would have the same formulation for layers of half the thickness on both surfaces. However, equation (7.2.3) had the layer on one surface only. Since the contact dimensions and pressures coincided, it was demonstrated that for the constrained column model, two surface layers can be simply added to give a single layer on one surface. One would not expect thin layers with $\nu = 0.5$ to behave much differently from those with $\nu = 0.4$ and therefore the assumption made in Chapter 5 concerning the construction of an equivalent bearing layer thickness was supported.

Finally, by carefully observing the inlet pressure sweep, it was observed that unless the contact zone approached quite closely to the bearing length (b), lubricant starvation would be avoided.

7.7 The Dynamic Routine:

The co-ordinate system shown in Figure 7.6.1 was again adopted to formulate the dynamic routine. However, for this situation the squeeze film term in the Reynolds equation must be included. Thus equation (5.2.1) became:

$$\frac{\partial}{\partial x}\left[h^3 \frac{\partial p}{\partial x}\right] = 12\eta \left(u \frac{\partial h}{\partial x} + \frac{\partial h}{\partial t}\right)$$

subject to the same boundary conditions as imposed in Section 7.6. However, the surface profile at an instant in time was,

$$h = h_o + f(x)$$

where f(x) was the profile from the steady state solutions of Section 7.6.

For the same reasons as specified in Chapter 6, the squeeze film velocity was approximated as

$$\frac{\partial h}{\partial t} = \frac{dh_o}{dt}$$

The set of equations describing the dynamic situation simplified to:

$$\frac{\partial p}{\partial x} = \frac{12\eta}{(h_o + f(x))^3}\left[u\ (f(x) - f(x_e)) + \frac{dh_o}{dt}\ (x - x_e)\right] \qquad (7.7.1)$$

subject to the conditions imposed by equations (7.6.2), (7.6.5) and (7.6.6).

The following expression for coefficient of friction was developed from the formulation of Cudworth and Higginson (1976).

$$\mu = \frac{1}{F'}\int_{-b}^{x_e}\left(\frac{2\eta u}{h} - \frac{h}{2}\frac{\partial p}{\partial x}\right) dx + \frac{1}{F'}\int_{x_e}^{b} \frac{2\eta u h_c}{h^2}\ dx \qquad (7.7.2)$$

and this was evaluated using numerical integration within the computer program listed in Part 3 of Appendix F.

The numerical solution procedure consisted of the following steps:

(a) specify h_o at $t = 0$

(b) solve h_o for one cycle using the following procedure at each time step

(i) specify h_o

(ii) specify x_e

(iii) specify $\frac{dh_o}{dt}$

(iv) solve equation (7.7.1) for p

(v) iterate until equations (7.6.2) and (7.6.5) are satisfied (i.e. $p = 0$ at $x = -b$ and $p = 0$ for $-b < x < x_e$)

(vi) iterate until specified F' approximately equals that computed from equation (7.6.6)

(vii) iterate until h_o converges.

(c) iterate until h_o converges for the cycle.

The initial specification for h_o was obtained from a solution generated by the plane inclined surface bearing model. At each time step the intial specification of h_o was calculated by a fourth order Adam — Bashforth formula. This formula required $(\frac{dh_o}{dt})$ values to be supplied from previous time steps and initially these were supplied by the plane inclined surface bearing model.

The initial specification of x_e was set equal to x_e derived from the steady state solution required to generate the surface profile, and that of dh_o/dt from the previous time step. For the first time step this was obtained from the plane inclined surface bearing model.

The solution of equation (7.7.1)was accomplished by numerical integration using the method of Gill and Miller (1972) (NAG D01GAF) which was described in Section 7.6. The first step which occurred at x_e was subdivided to cope with the rapidly changing pressure gradient.

The surface profile required in equation (7.7.1) was obtained from the steady state solution. The present dynamic routine contained steady state solution coding and obtained initial h_o and x_e specifications from a data bank, the latter being generated by separate runs of the program listed in Part 1 of Appendix F. The built in interpolation routine of the Gear method (NAG D02EBF) was used to generate a large number of surface profile points. Further interpolation was accomplished by a simple linear routine. Thus, although f(x) was a numerically specified function, it was available to equation (7.7.1) at any position (x) and time (t).

The iteration for $(\frac{dh_o}{dt})$ was performed with a bisection routine. Coupled with the numerical integration of the pressure gradient, the coding constituted the evaluator step for the numerical method used to solve h_o for the cycle.

The integration of the pressure distribution was accomplished by a second application of the method of Gill and Miller. The iteration for x_e was performed with a bisection routine.

The solution of h_o for each time step was performed using a fourth order Adams predictor-corrector pair. This routine has been discussed in Section 7.4. Step size halving was used to check reliability and the local truncation error was monitored. The convergence to a cyclic steady state was accomplished in the same fashion as described in Chapter 6.

The entire dynamic solution procedure was run for the conditions designated as case C. In general, the tolerances employed in the dynamic solution procedure were set at 0.001. However, to avoid excessive computing times the tolerance for the step size halving employed for the fourth order Adams predictor-corrector pair was increased to 0.0075. The number of lines of coding and the Central Processing Unit (CPU) times for the various parts are shown in Table 7.7.1. The CPU time required for Part 3 was drastically increased if the starting values were not accurate or if some of the internal convergence factors were not optimal. Thus, general use of this procedure would involve enormous computing expense.

Program	Lines	CPU time (s)
Part 1 - generation of steady state profiles	783	568
Part 2 - plane inclined surface bearing model	722	20
Part 3 - dynamic routine	1551	3415
TOTALS:	3056	4003

Table 7.7.1 : The computer resources required for the full dynamic solution procedure.

The results for case C are shown in Figure 7.7.1 (included at the end of this chapter) along with those generated by the plane inclined surface bearing model of Part 2 in Appendix F. It was necessary to impose a small entrainment velocity at T = 0.25 and 0.75 for the full dynamic procedure to converge as shown in the entrainment velocity graph of Figure 7.7.1.

The minimum film thickness calculated by the plane inclined surface bearing model was almost identical to that calculated by the full dynamic procedure throughout the cycle. Thus, the plane inclined surface bearing model provided a reasonable approximation for the more realistic cylindrical geometry.

The assumption that the squeeze film velocity could be approximated by

$$\frac{\partial h}{\partial t} = \frac{dh_o}{dt}$$

was made for both sets of results shown in Figure 7.7.1. As mentioned previously this assumption was made in order to reduce the analytic and numerical complexity of the solution. In the results shown in Figure 7.7.1, the assumption that the steady state profile existed at each instant in time caused the shape to change rather rapidly throughout the cycle. In Table 7.7.2, the central and minimum film thickness values are listed for various points within the cycle.

A first order backward difference formula was used to estimate squeeze film velocity in Table 7.7.2. It was clear that considerably largervalues for squeeze film velocity occurred at the centre of the contact than at the point of minimum film thickness. The approximation adopted for the squeeze film velocity was only exactly correct at the point of minimum film thickness. However, to determine whether the approximation caused significant errors in the calculated film thickness, the role of squeeze film lubrication was examined. In Figure 7.7.2 the dimensionless film thickness is shown for the dynamic solution. Also, the dimensionless film thickness is shown which would occur if squeeze film velocities were neglected. In

Table 7.7.2 : Estimated squeeze film velocities (dh_c/dt) at x = 0 for the solution shown in Figure 7.7.1.

t s	h_o μm	h_c μm	$\frac{dh_o}{dt}$ μm/s	$\frac{dh_c}{dt}$ μm/s
0	0.538	0.633	0.090	0.144
0.125	0.542	0.597	-0.025	-0.288
0.25	0.535	0.541	-0.064	-0.392
0.375	0.528	0.578	-0.044	0.296
0.5	0.525	0.594	0.006	0.128
0.625	0.529	0.598	0.044	0.032
0.75	0.527	0.536	-0.063	-0.496
0.875	0.525	0.615	0.084	0.632
1.0	0.538	0.633	0.090	0.144

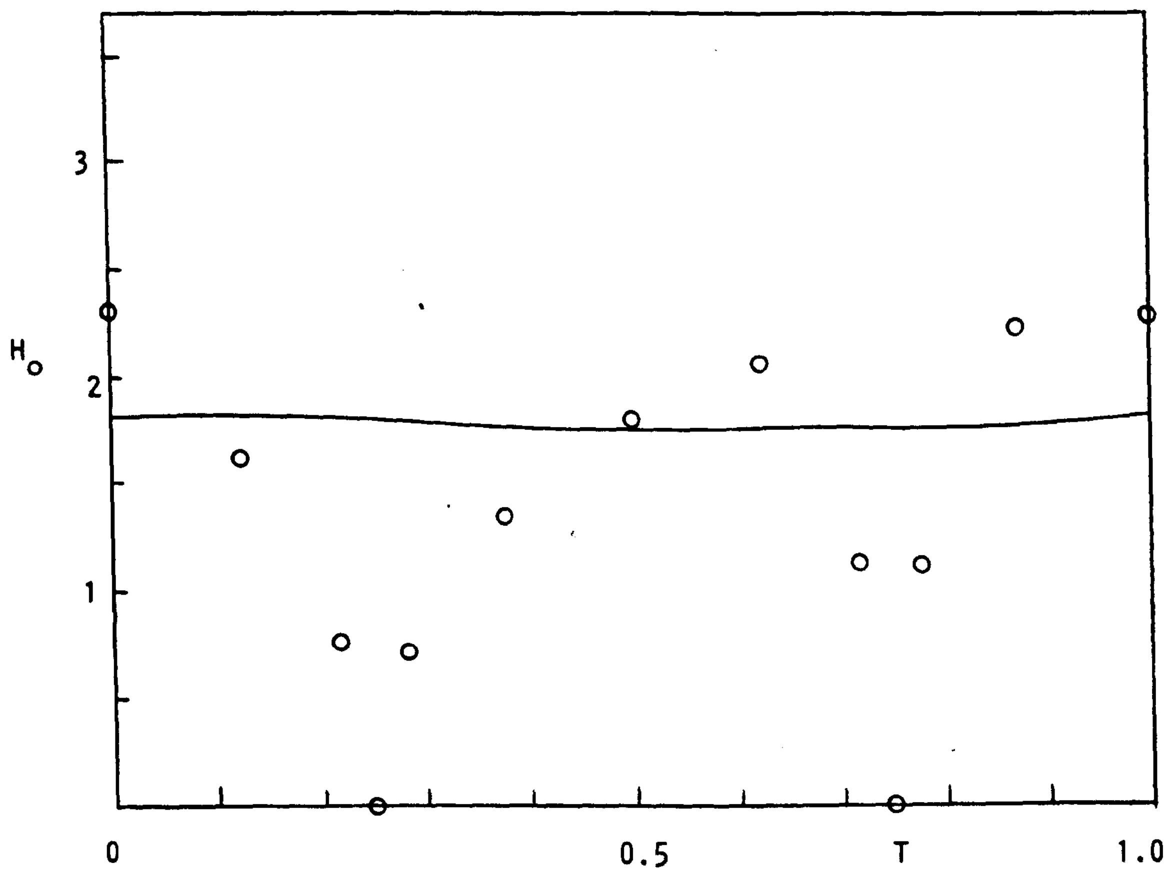

o h_o for steady state solutions as previously shown in Figure 7.6.2.

——— h_o for dynamic solution procedure.

Figure 7.7.2 : The dynamic and steady state solutions at various points in the cycle.

other words, the values for steady state film thickness calculated in Section 7.6 are plotted at various points in the cycle.

The squeeze velocity occurring at T = 0.75 was then set equal to -0.496×10^{-6} m/s, which was estimated in Table 7.7.2 to occur at the centre of the contact for the present dynamic solution. This value was large compared with the value of -0.063×10^{-6} m/s occurring at the point of minimum film thickness. Allowing the higher squeeze velocity to occur for 1 /8 of the cycle would cause the minimum film thickness to decrease by

$$\Delta h_o = h_o - \frac{dh_c}{dt} \cdot \Delta t$$

Using the values listed in Table 7.7.2 for T = 0.75 gave a decrease in minimum film thickness of about 12 percent. Thus, it was considered unlikely that the approximation adopted for the squeeze film velocity would significantly affect the accuracy of the computed results in the present models.

Finally, a comment can be made concerning the assumption that the surface profiles at each instant in the cycle had the shape that resulted when a steady state solution was performed with the constant load and velocity. The extent to which this would occur was not known. However, in Figure 7.7.1 it was shown that the minimum film thickness throughout the cycle was not particularly sensitive to change in the profile shape, since both plane inclined and cylindrical geometry gave a similar result. This indicated that the assumption concerning the profile shape may have a small effect on the accuracy of the dynamic model.

7.8 Concluding Remarks:

A dynamic solution procedure was developed in this chapter for cylindrical geometry. The procedure was applied to the case C conditions which were similar to those considered for the ankle joint in Chapter 6. The film thickness remained reasonably constant throughout the cycle and had magnitudes approximately equal to those calculated for case B in Chapter 6. Results for case C were also calculated using the plane inclined surface bearing model. The remarkable similarity, especially for minimum film thickness, indicated that the plane inclined surface could be used to approximate the true cylindrical geometry.

A number of the assumptions involved in the theoretical models were discussed. Based on the findings of the present chapter it was considered reasonable to assume that the lubrication of the ankle joint was described adequately by the plane inclined surface bearing model developed in Chapter 6.

Figure 7.5.3 : Results for cases C and C1, with cases A and B also shown on the first two plots.

Case B (for ankle joint in vivo during walking)

Case A (for ankle joint during the friction experiment)

Case C1 (similar to case C except $\nu = 0.5$)

Case C (special case for Chapter 7 with $\nu = 0.4$)

▲ Maximum dry contact stress for $\nu = 0.5$ and no surface traction

● Maximum dry contact stress for $\nu = 0.4$ solved using the column model.

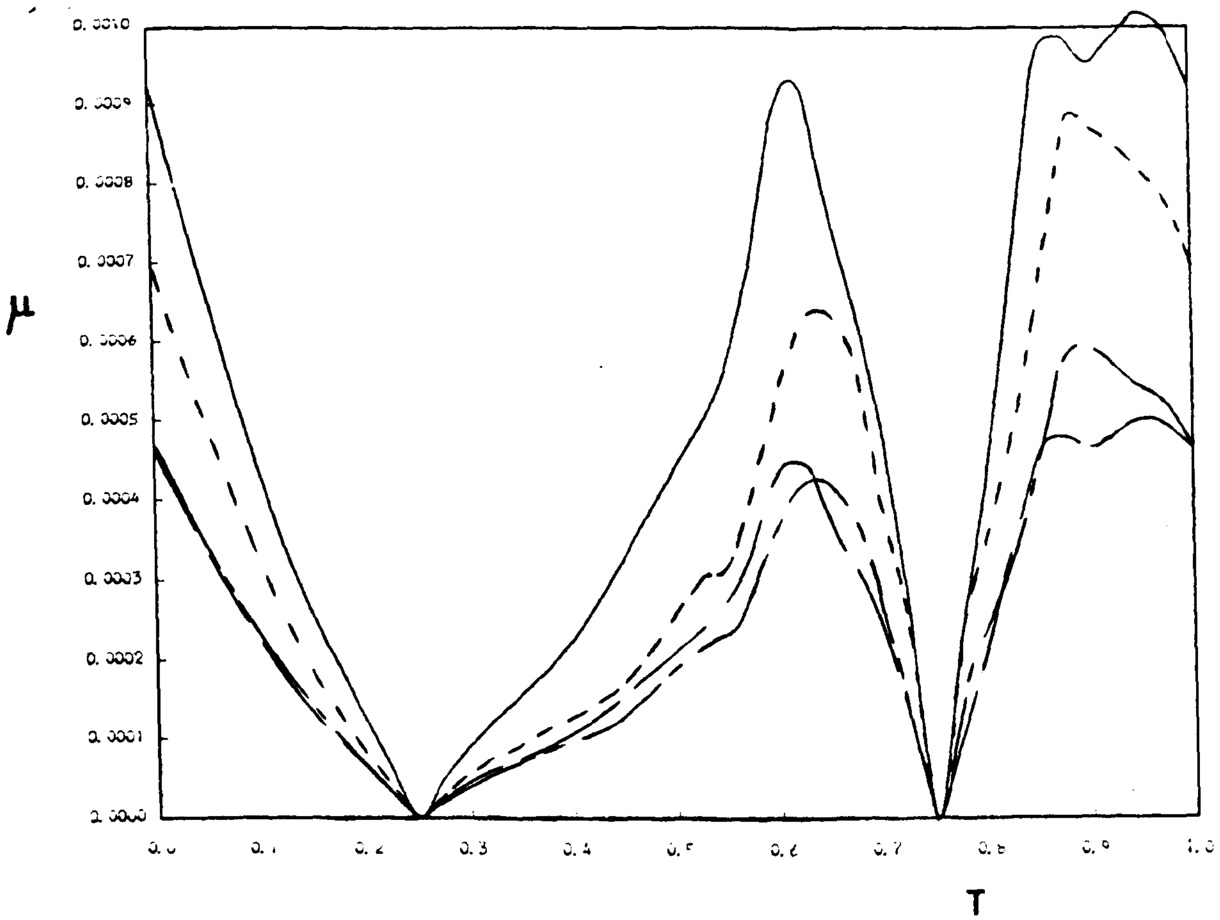

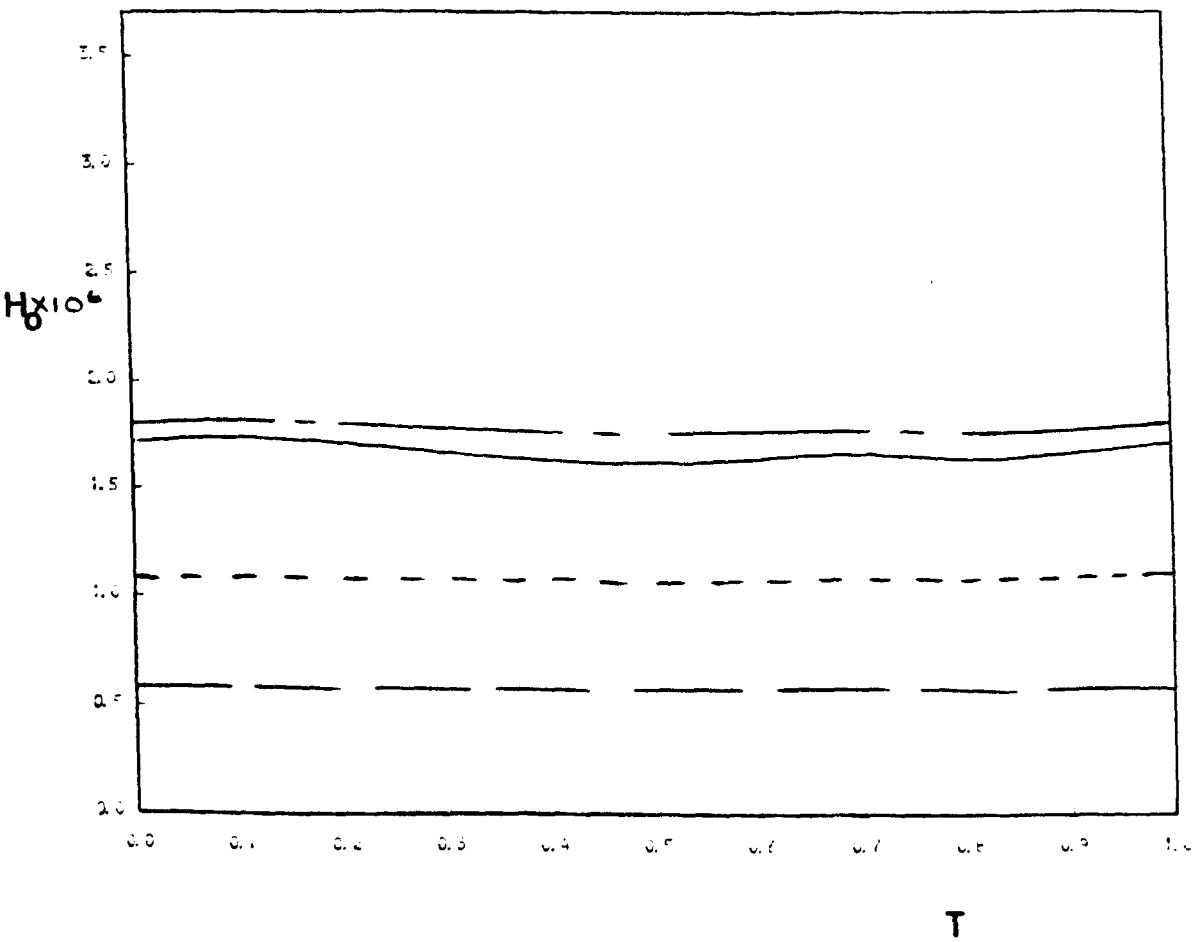

For key see page 237

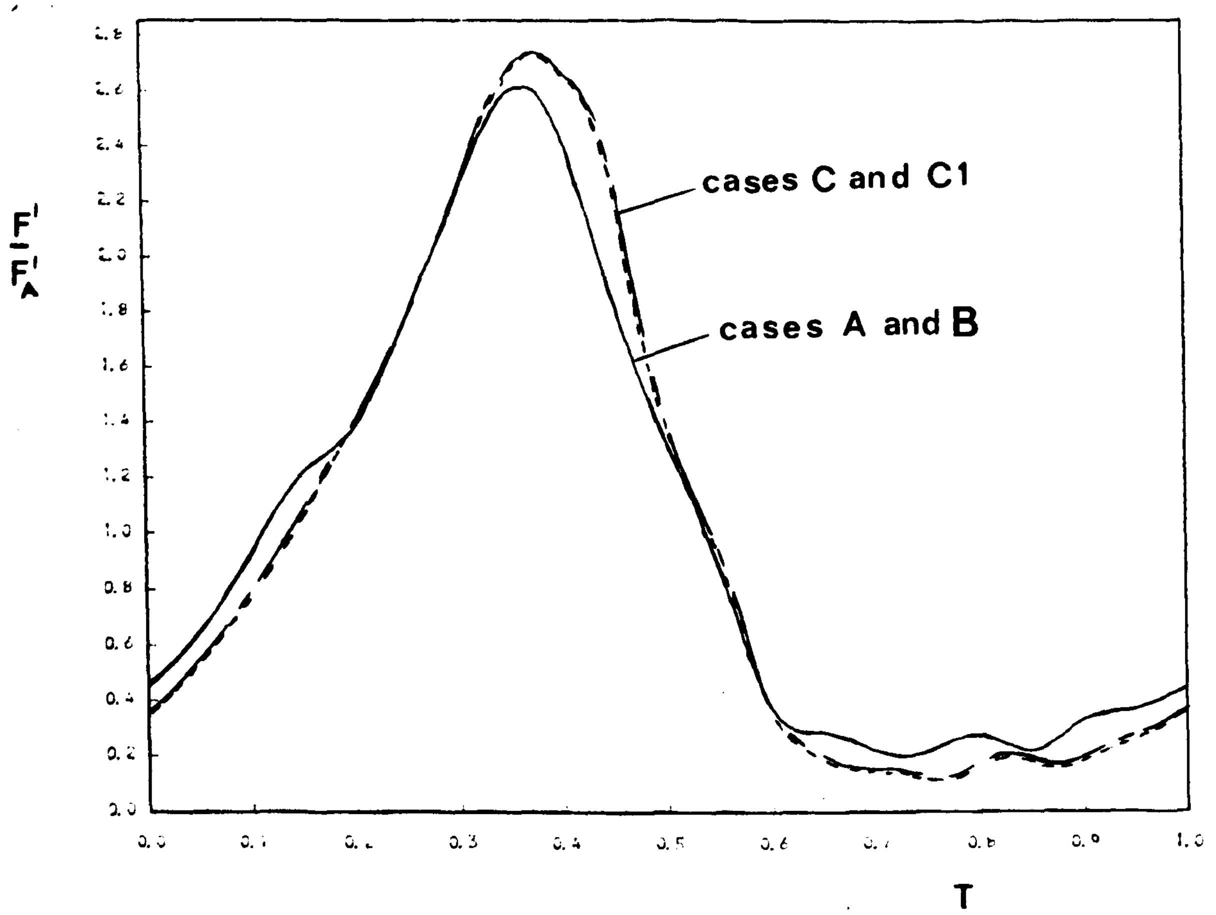

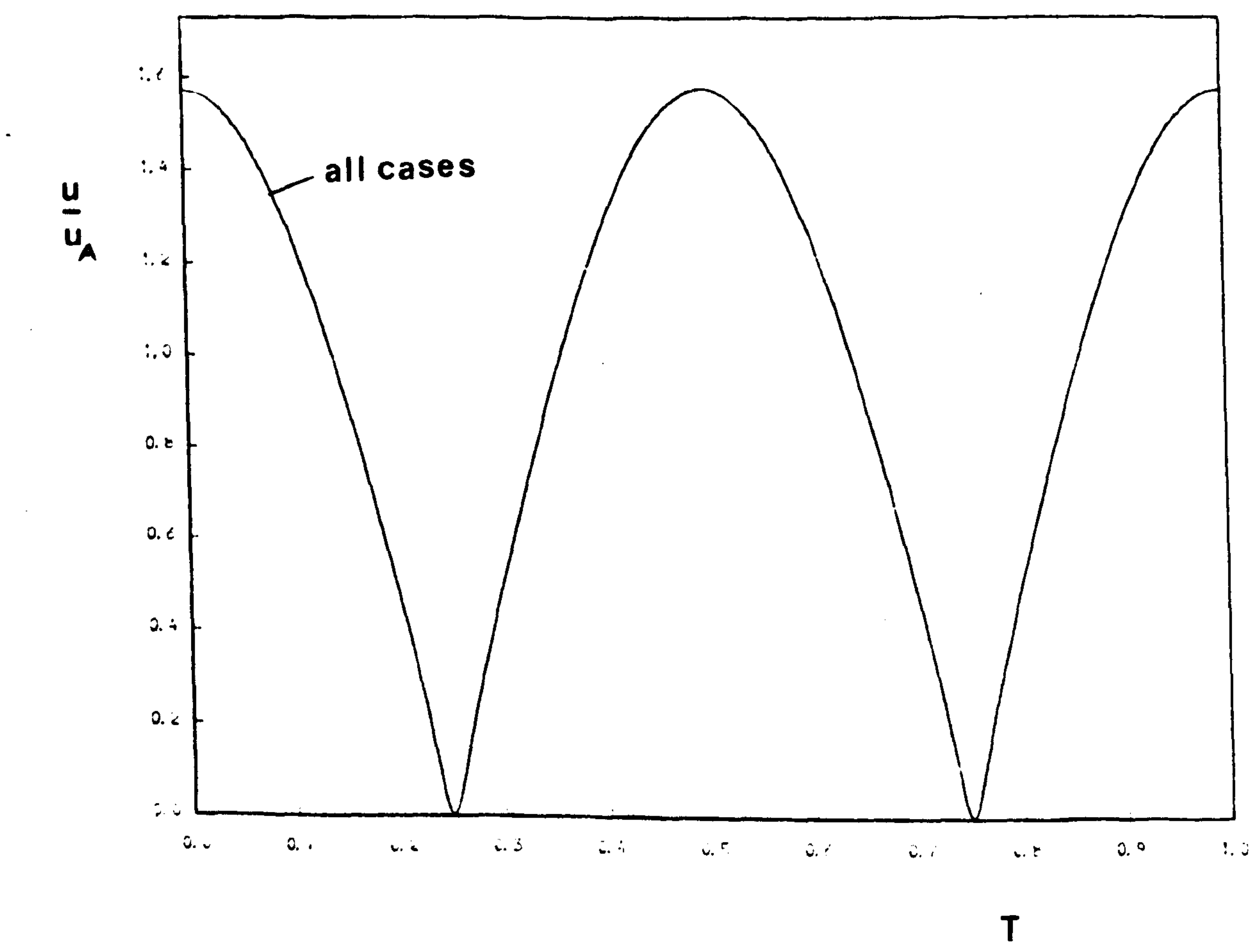

For key see page 237

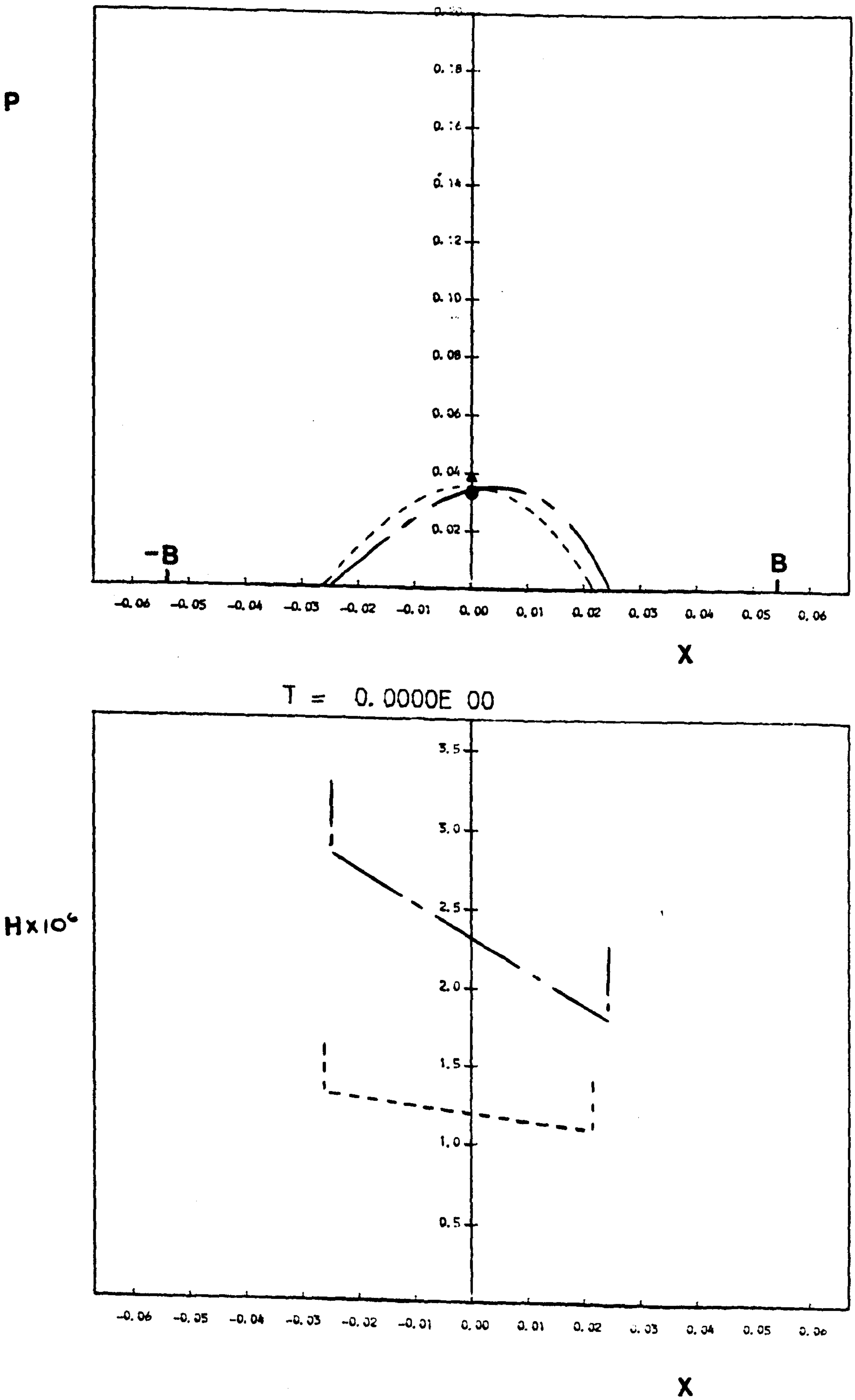

For key see page 237

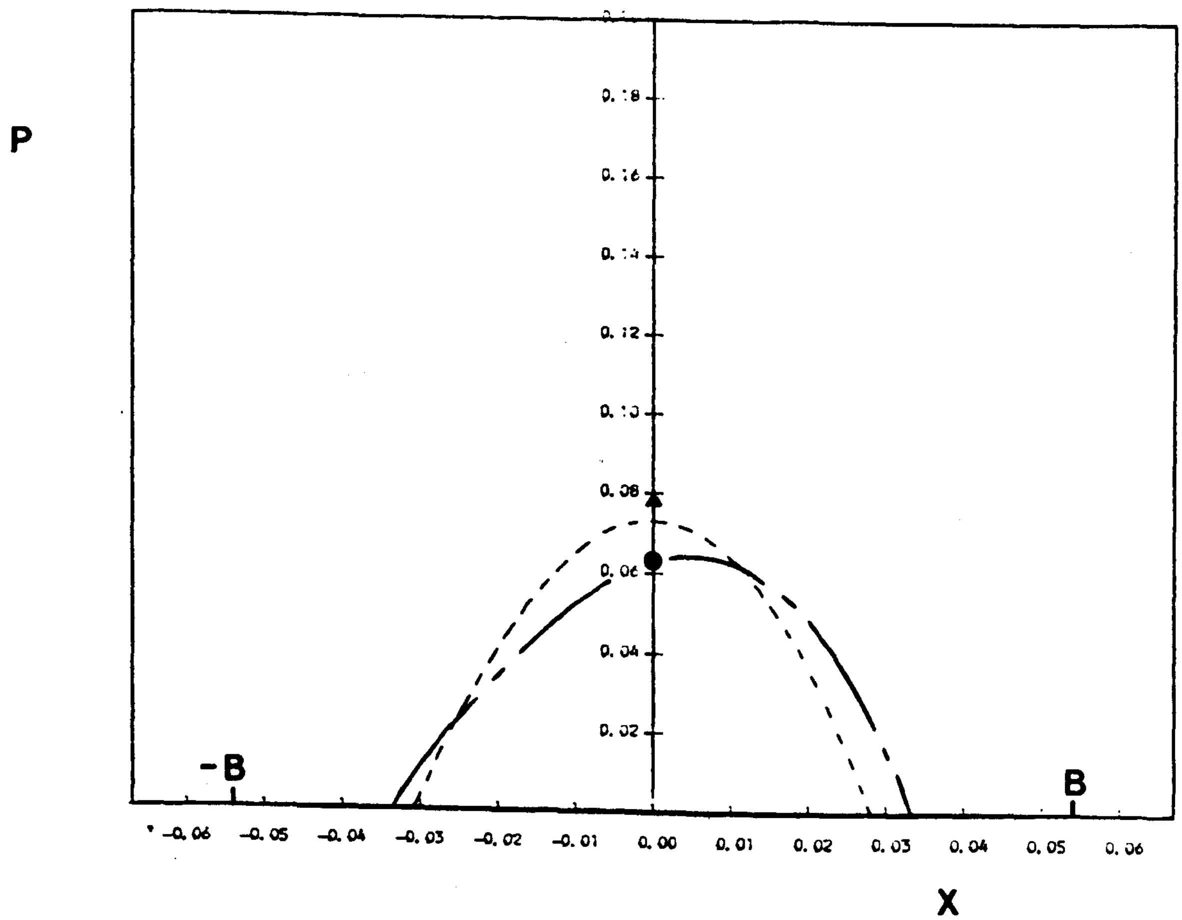

T = 0.1250E 00

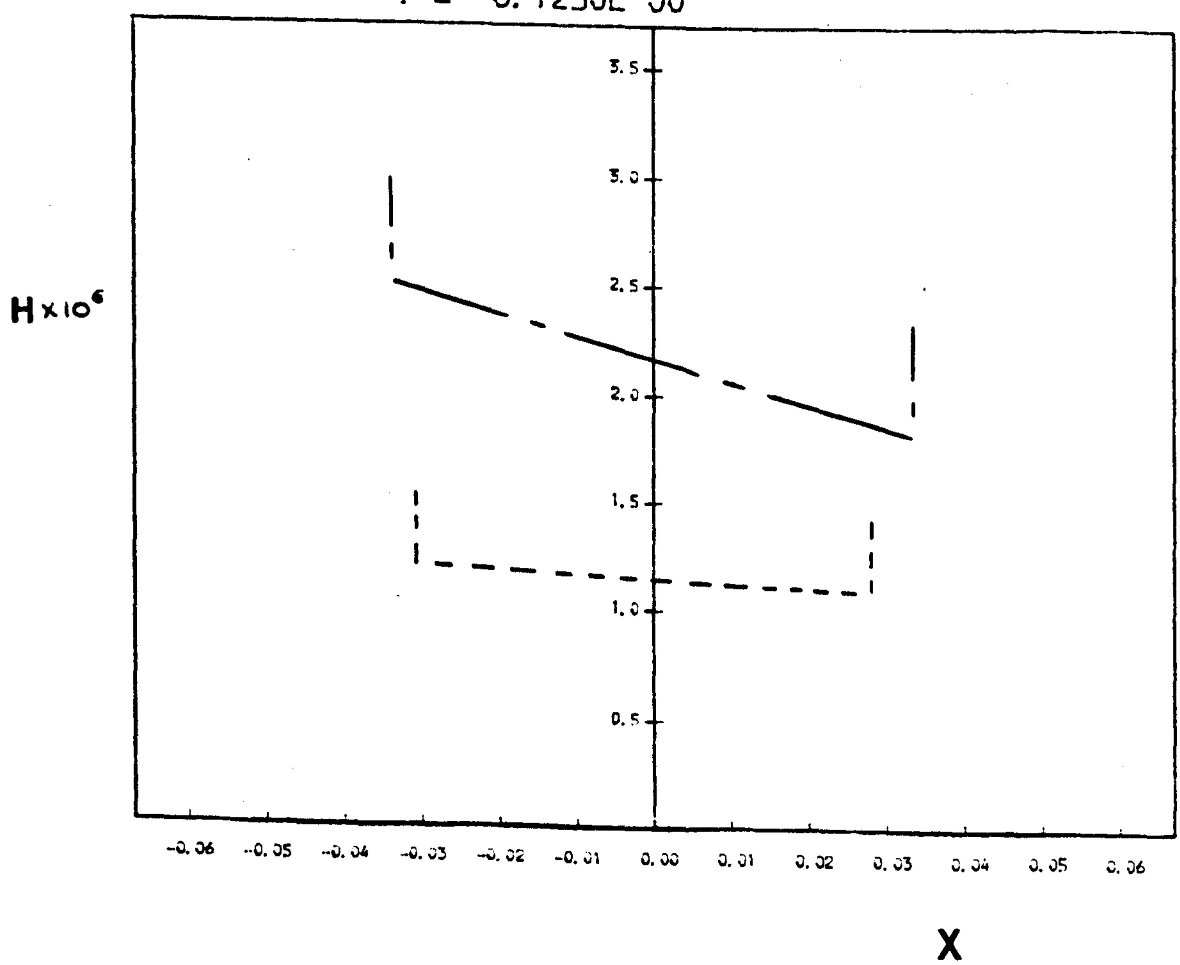

For key see page 237

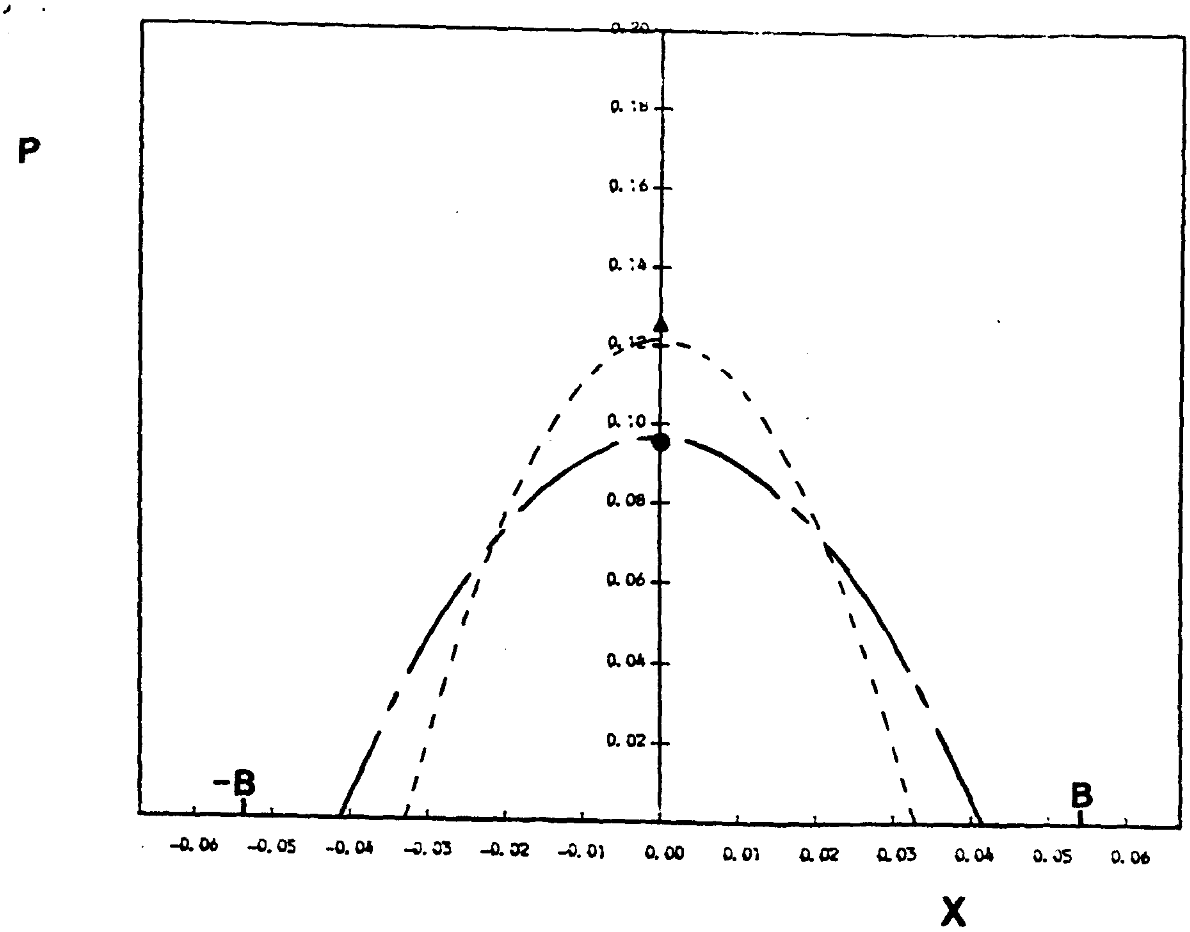

T = 0.2500E 00

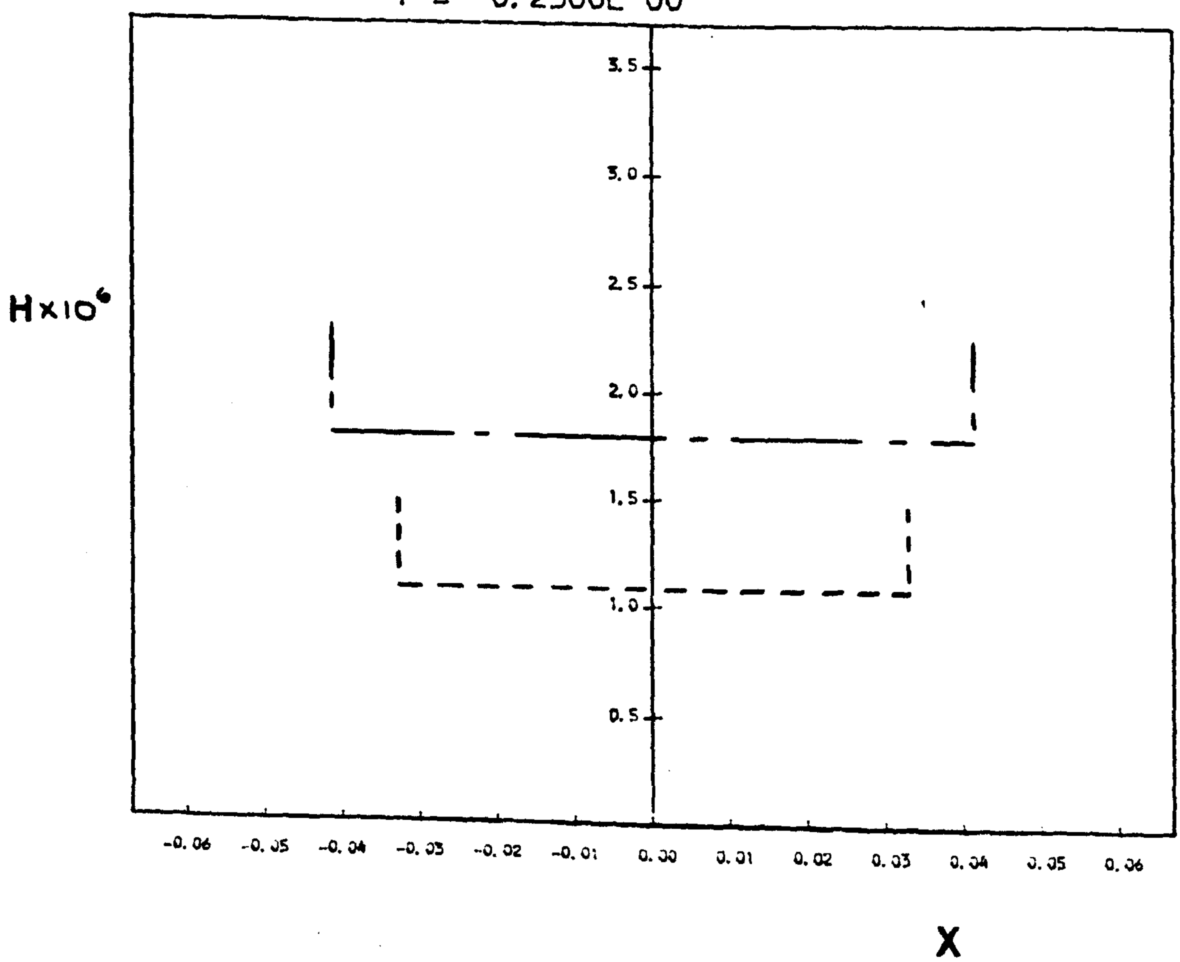

For key see page 237

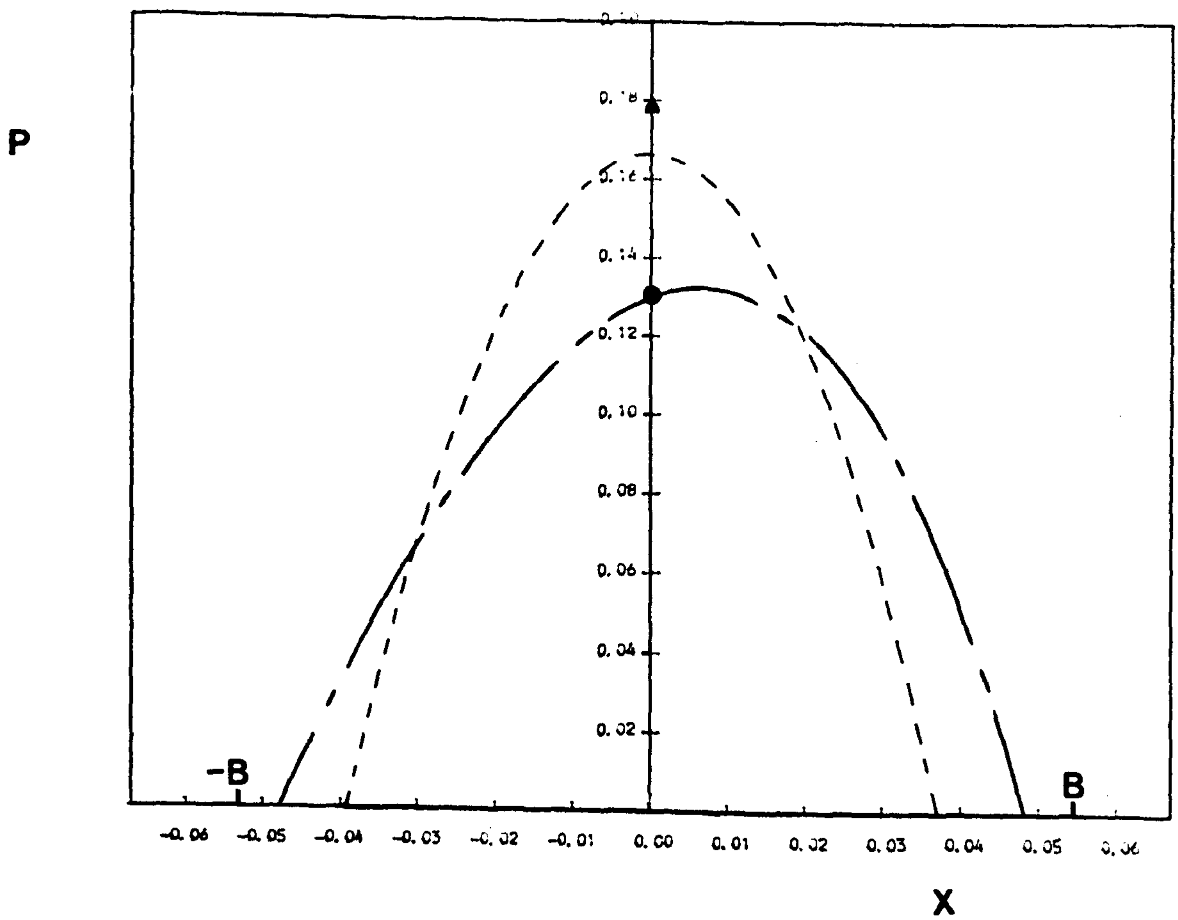

T = 0.3750E 00

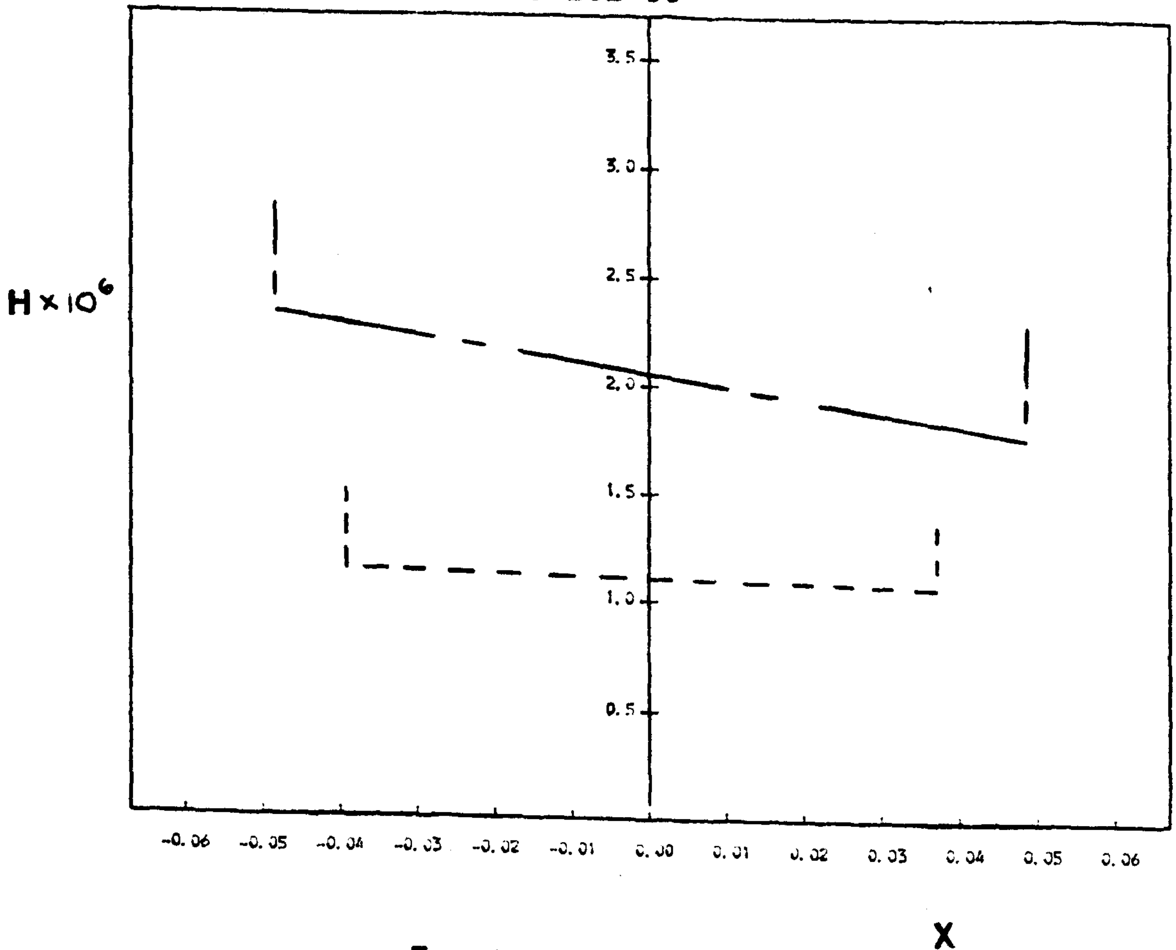

For key see page 237

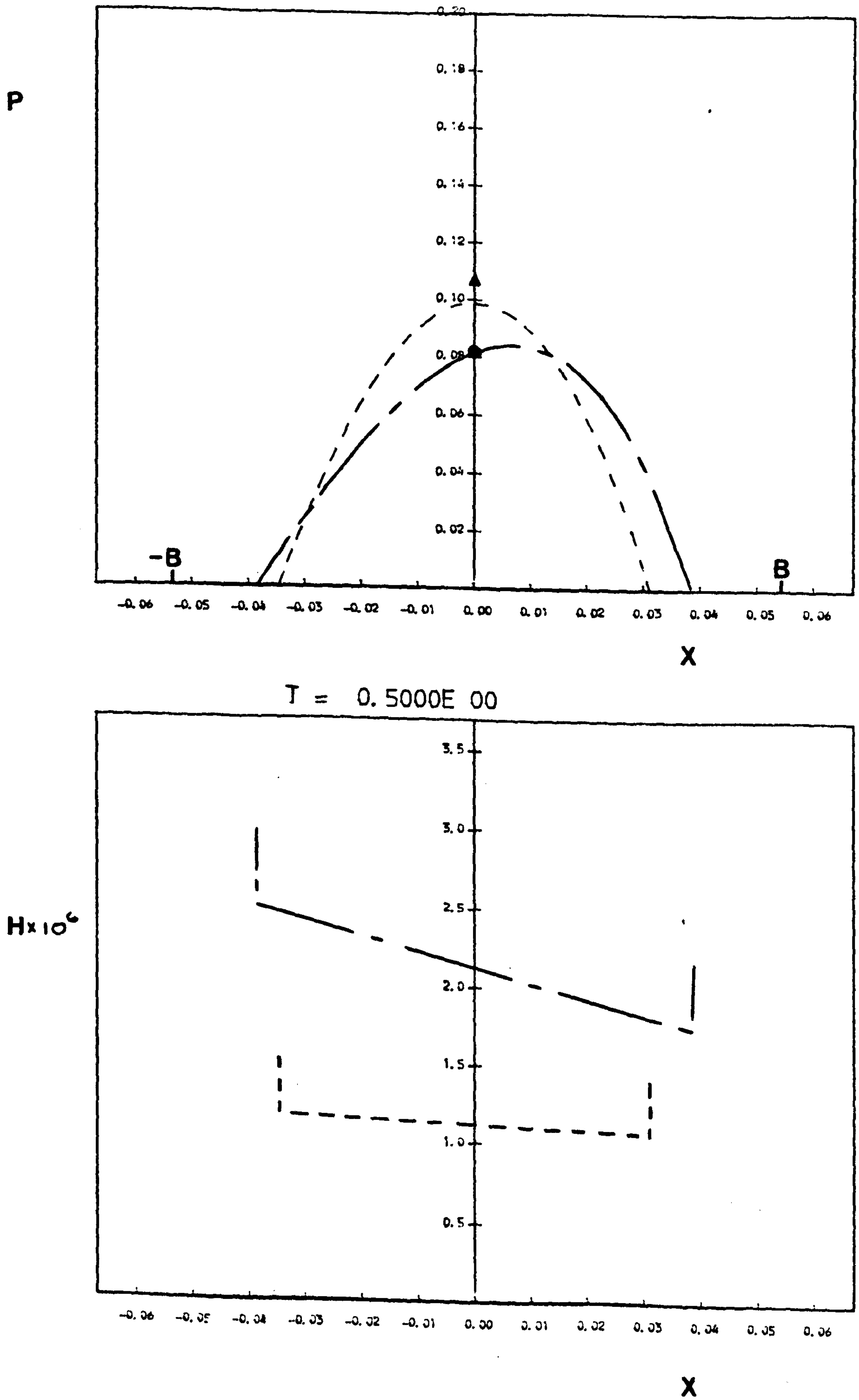

For key see page 237

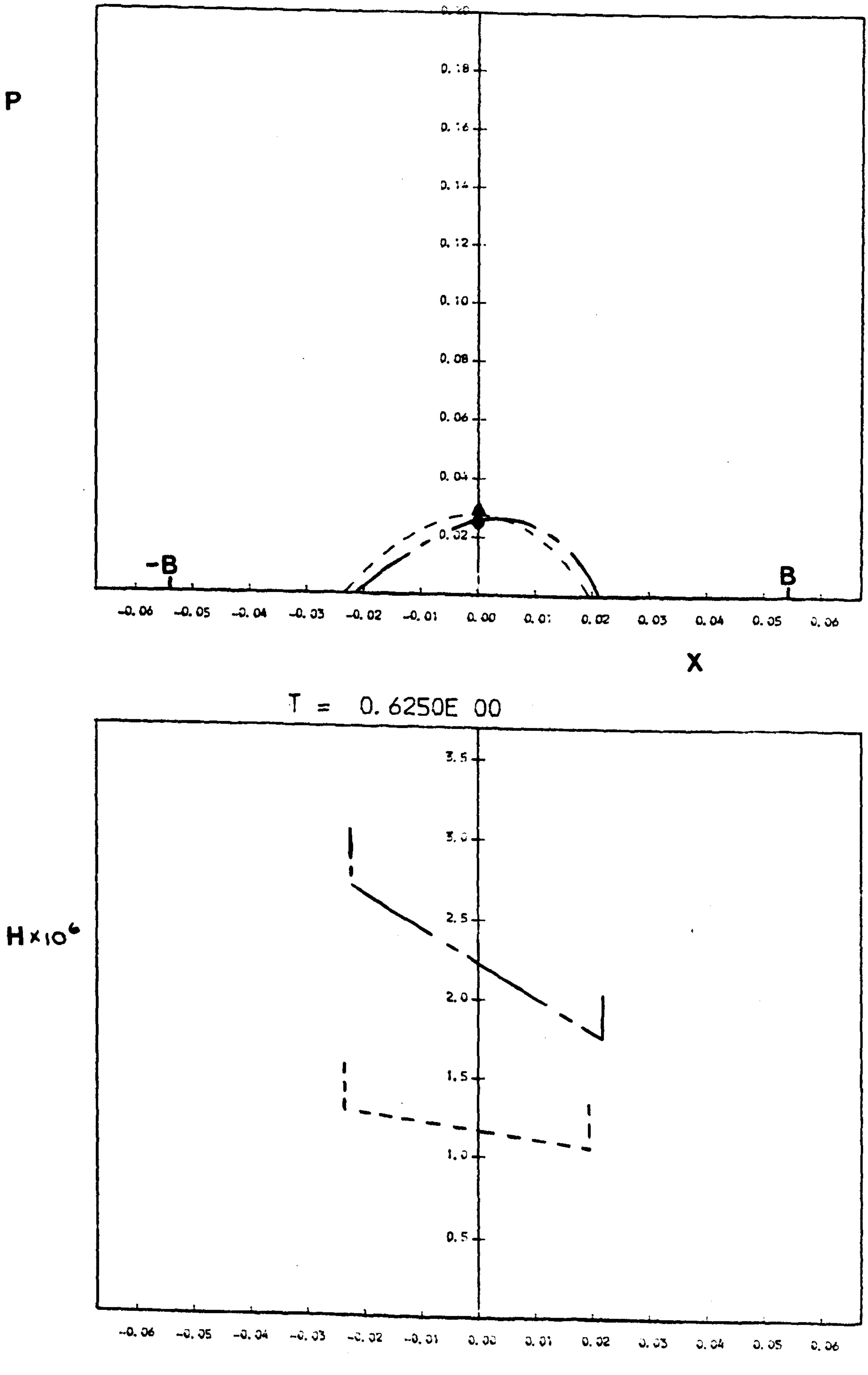

For key see page 237

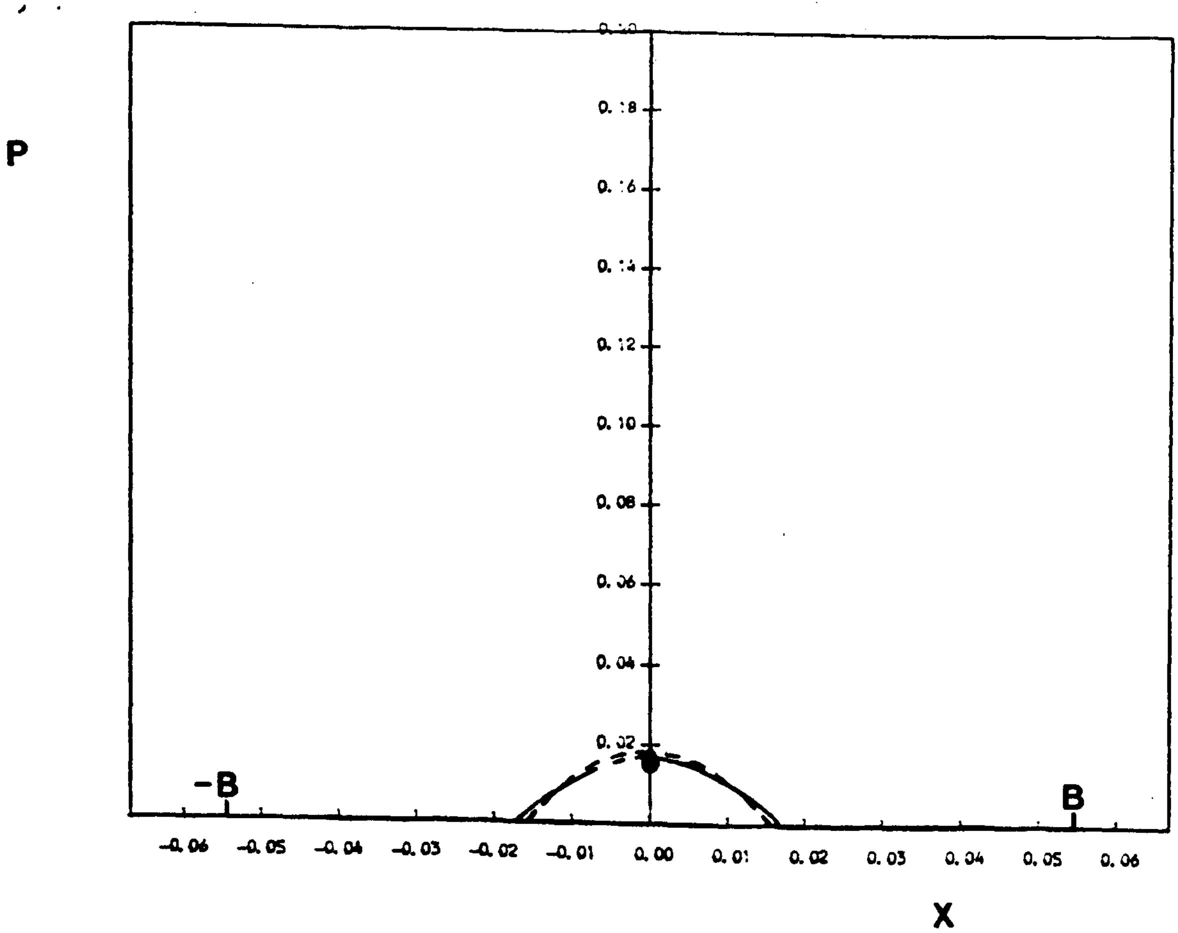

T = 0.7500E 00

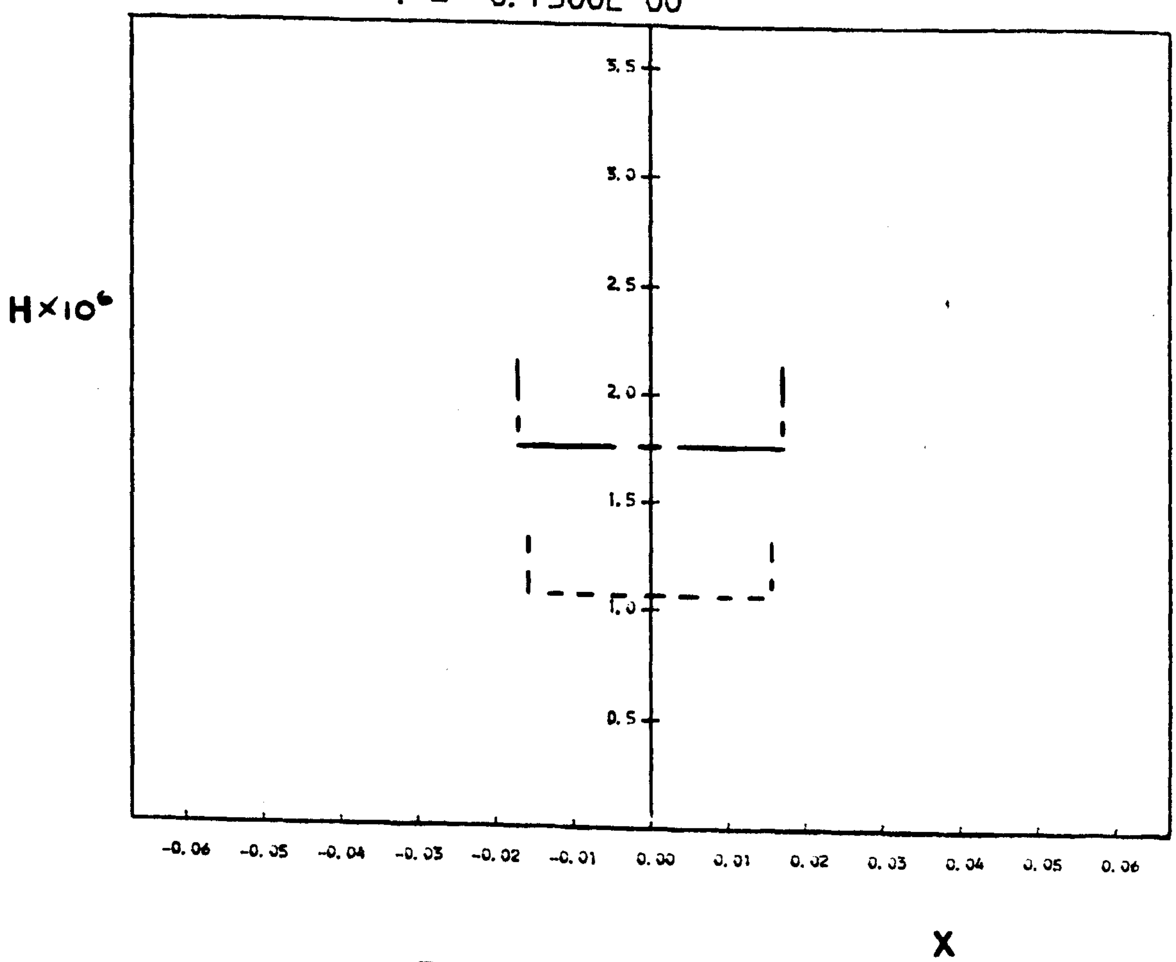

For key see page 237

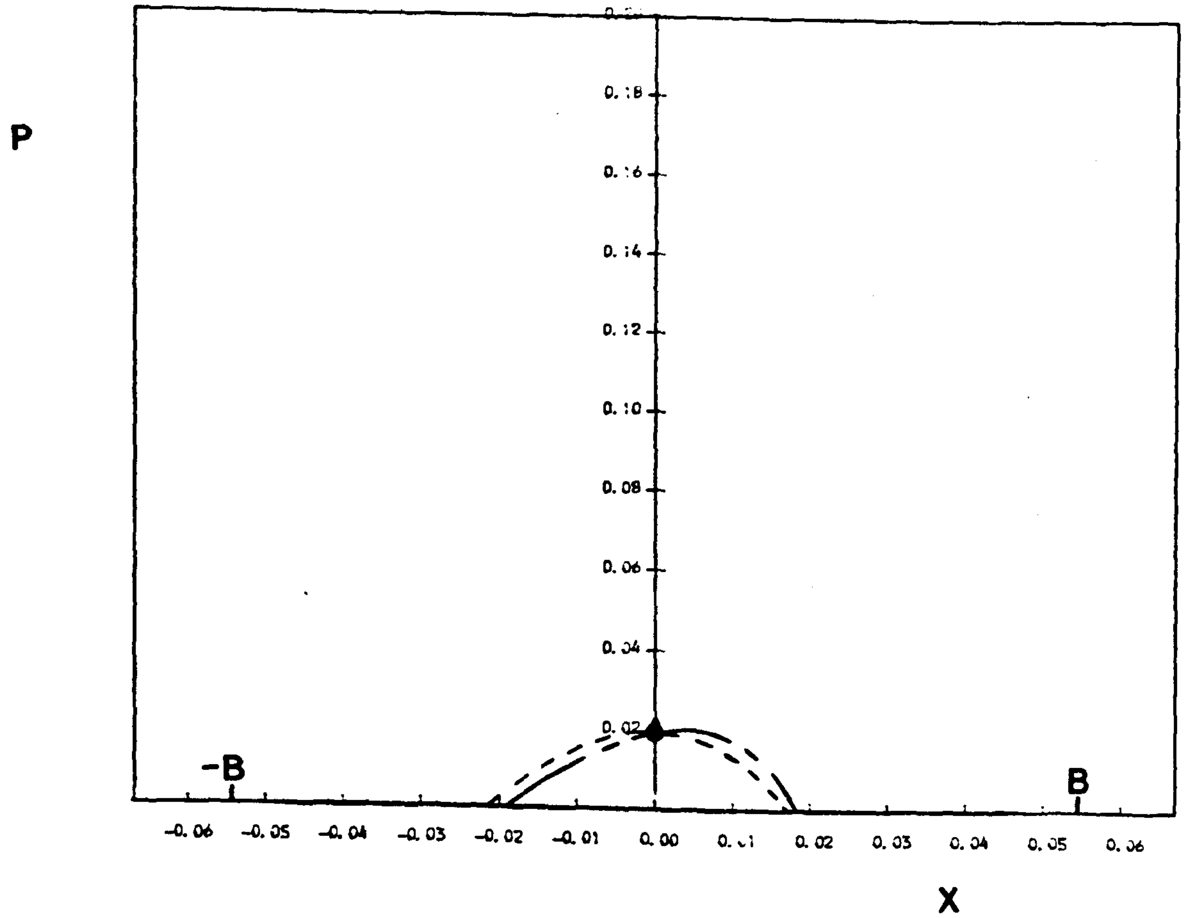

T = 0.8750E 00

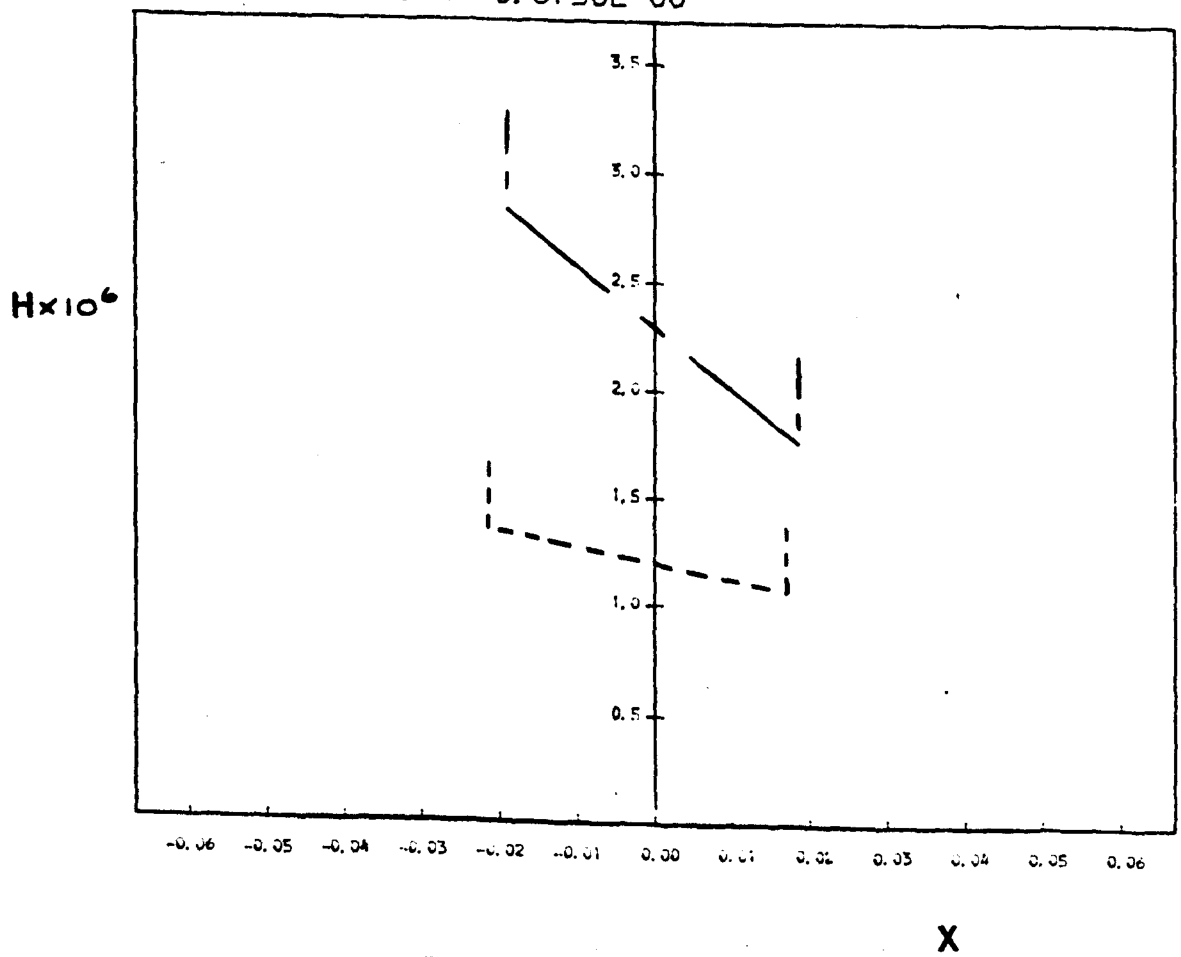

For key see page 237

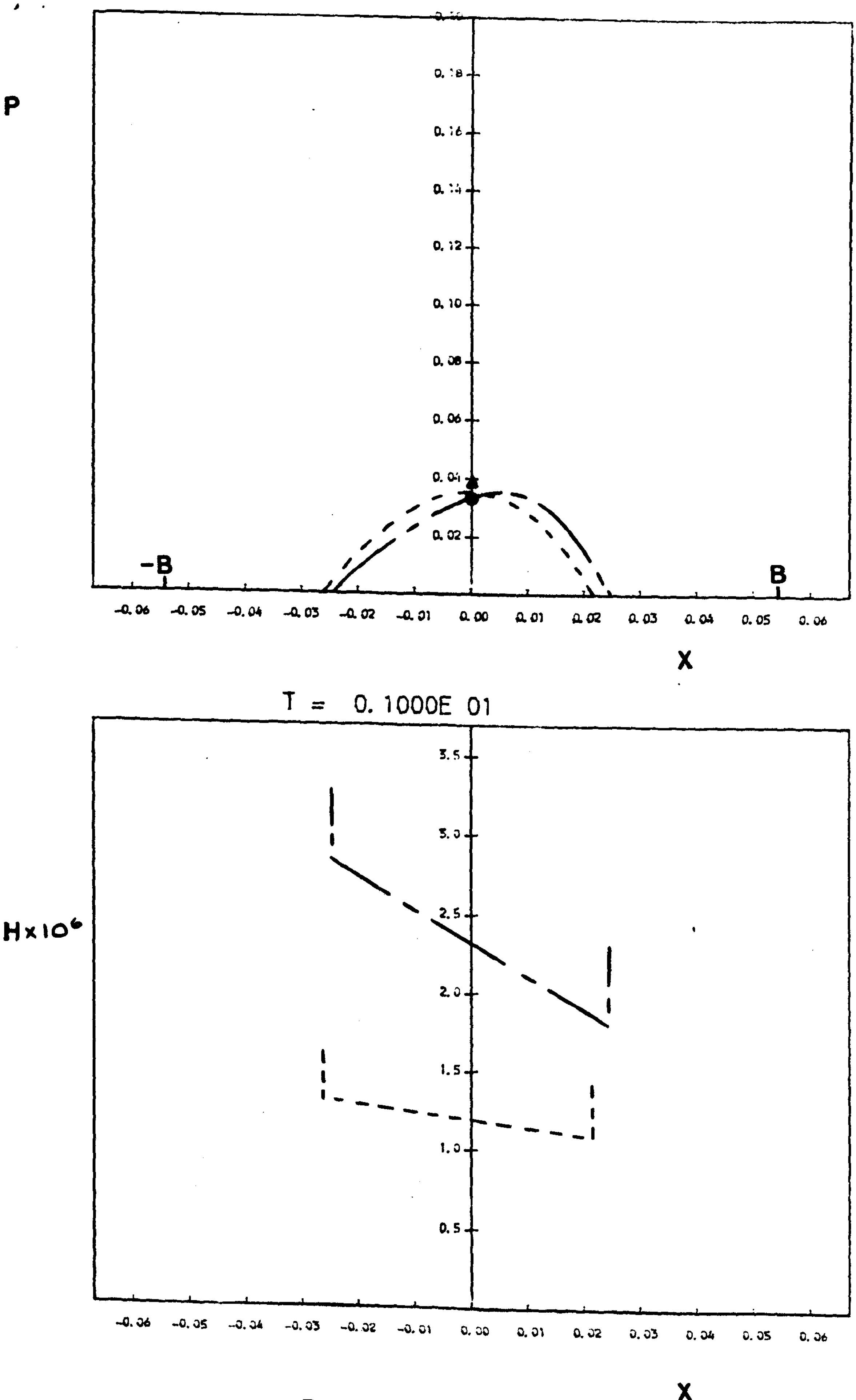

For key see page 237

Figure 7.6.2 : The steady state profiles solved by applying load and velocity equal to the instantaneous values at various points in the cycle.

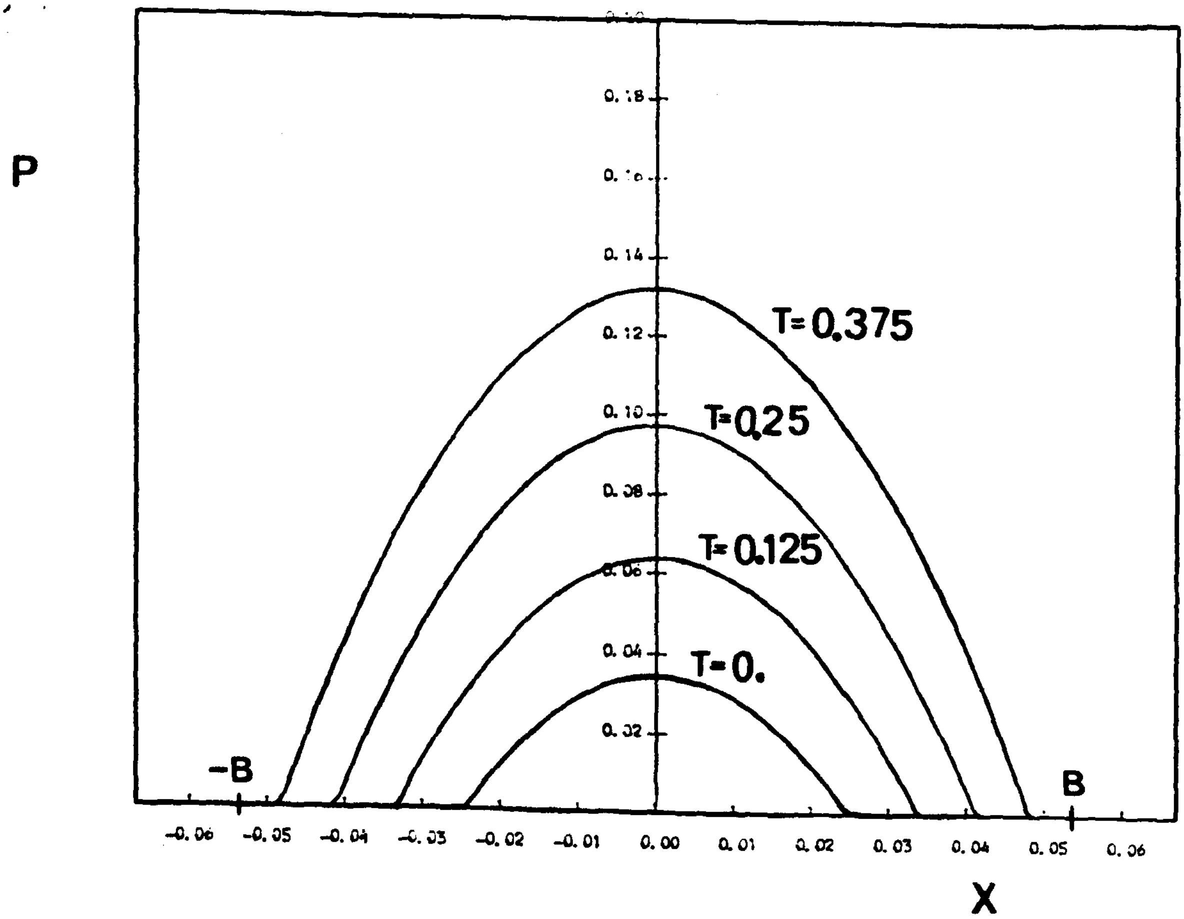
P
0.18
0.16
0.14
0.12
0.10
0.08
0.06
0.04
0.02
T=0.375
T=0.25
T=0.125
T=0.
-B
B
-0.06 -0.05 -0.04 -0.03 -0.02 -0.01 0.00 0.01 0.02 0.03 0.04 0.05 0.06
X

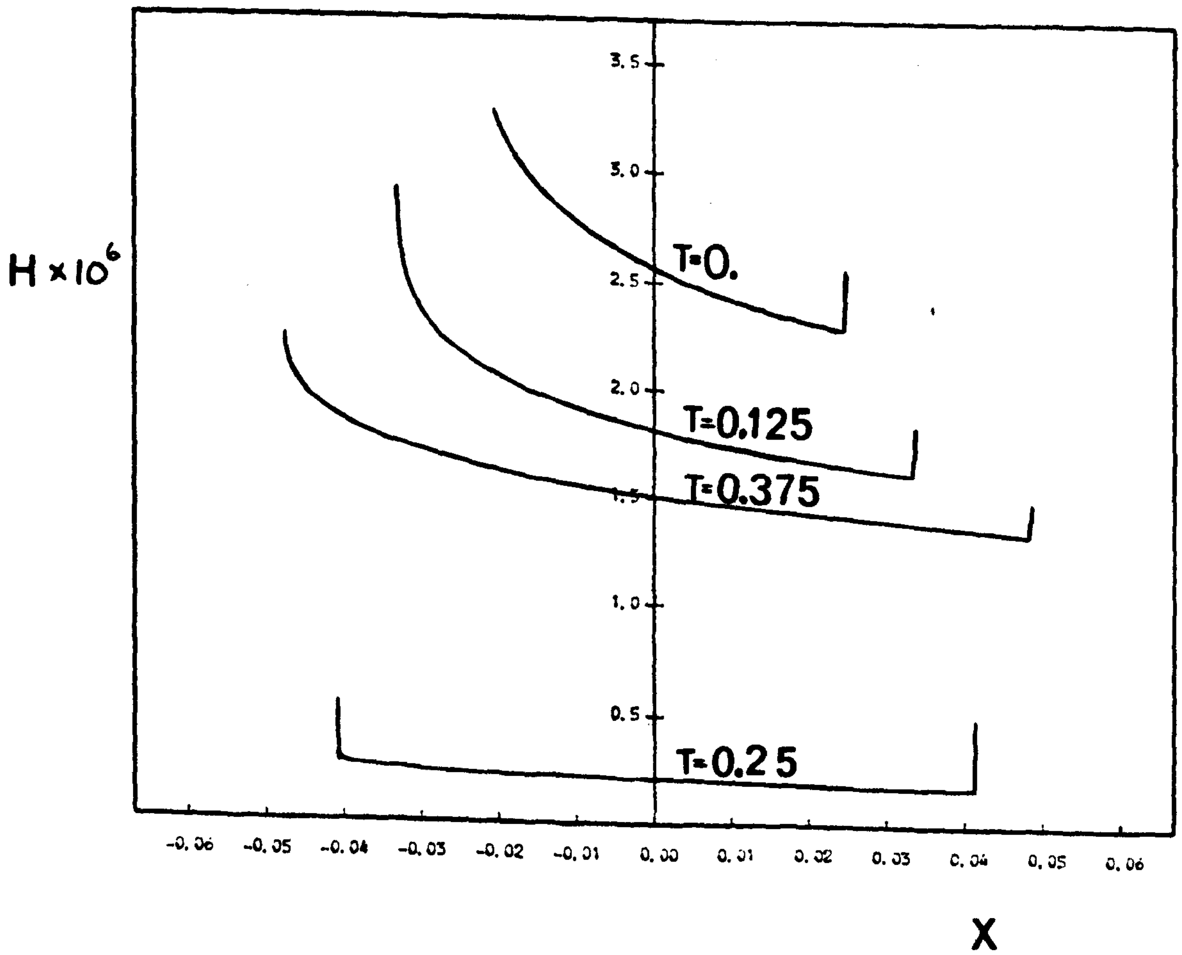
H × 10^6
3.5
3.0
2.5
2.0
1.5
1.0
0.5
T=0.
T=0.125
T=0.375
T=0.25
-0.06 -0.05 -0.04 -0.03 -0.02 -0.01 0.00 0.01 0.02 0.03 0.04 0.05 0.06
X

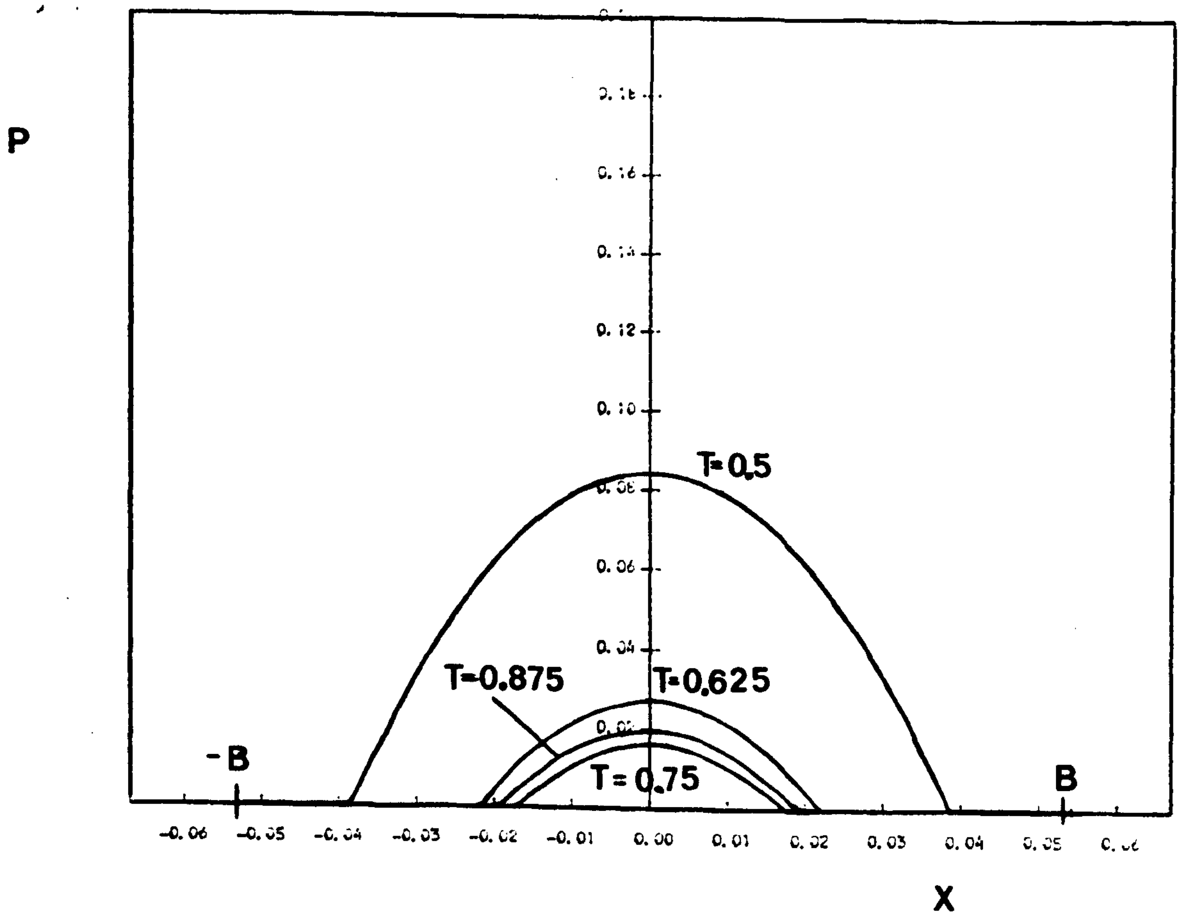
P
T=0.5
T=0.875
T=0.625
T=0.75
-B
B
0.12
0.10
0.06
0.04
-0.06
-0.05
-0.04
-0.03
-0.02
-0.01
0.00
0.01
0.02
0.03
0.04
0.05
X

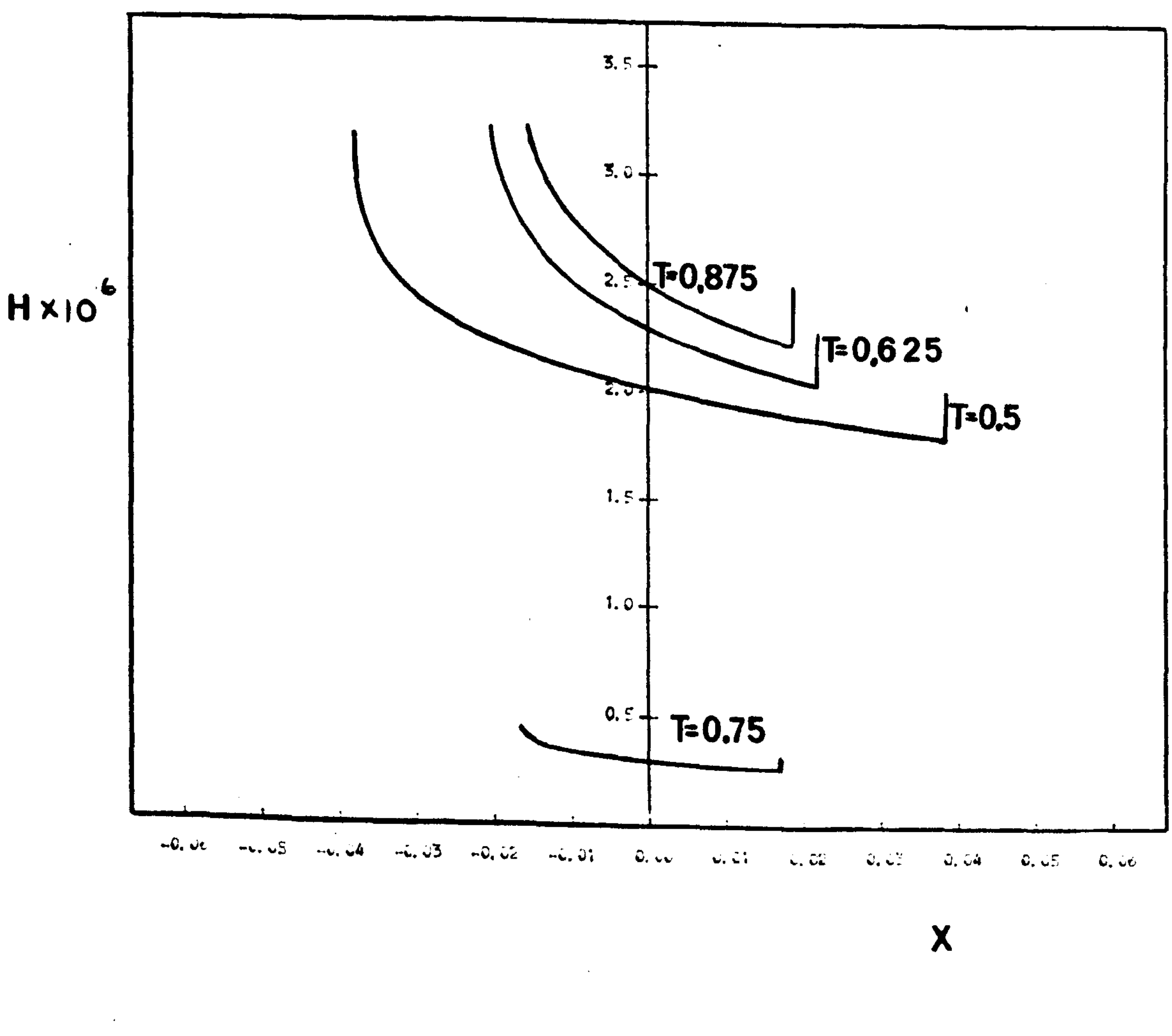
H x10^6
3.5
3.0
1.5
1.0
T=0.875
T=0.625
T=0.5
T=0.75
-0.03
-0.02
0.04
0.05
0.06
X

Figure 7.7.1 : The full dynamic solution procedure for case C.

– – – – – – – full dynamic solution

——————— plane inclined surface bearing model

▲ maximum dry contact stress for the constrained column model

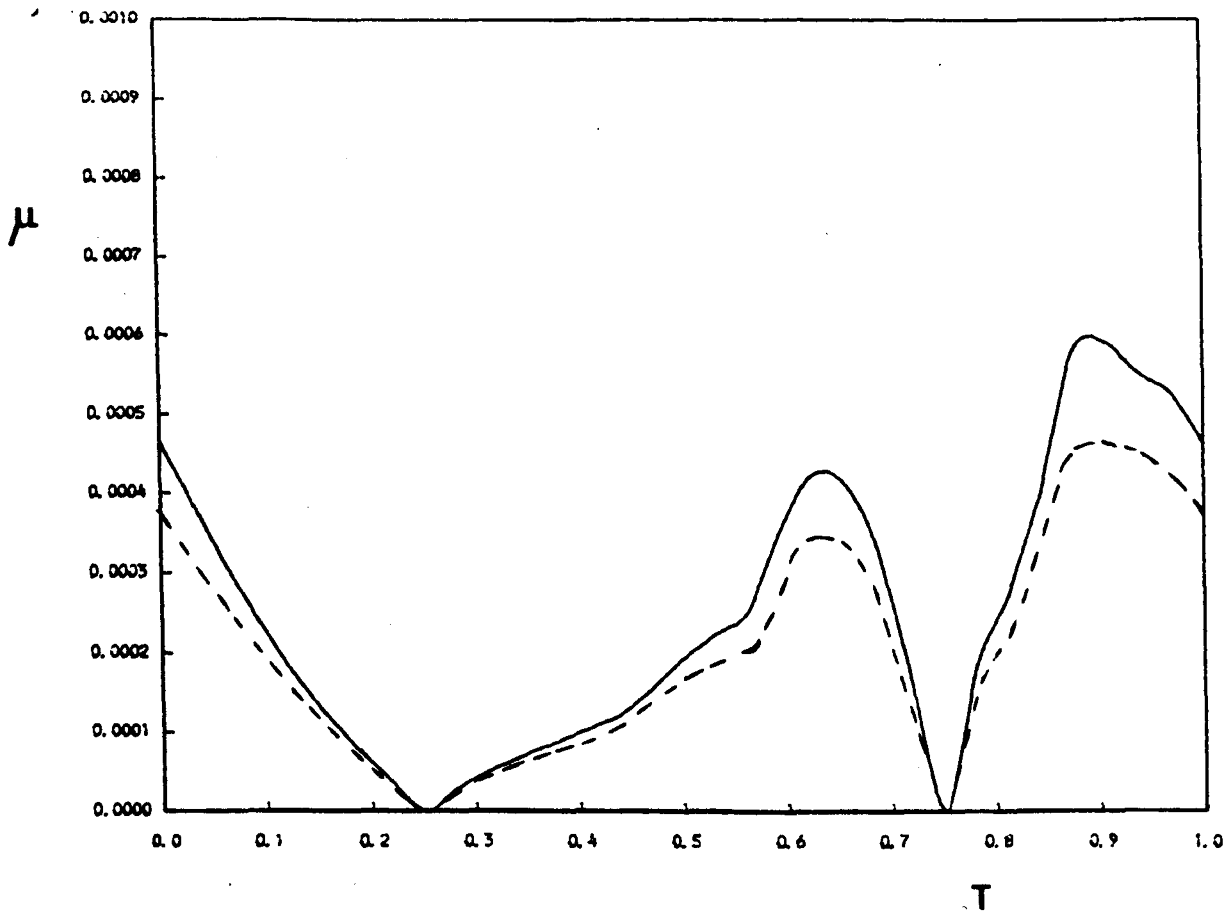

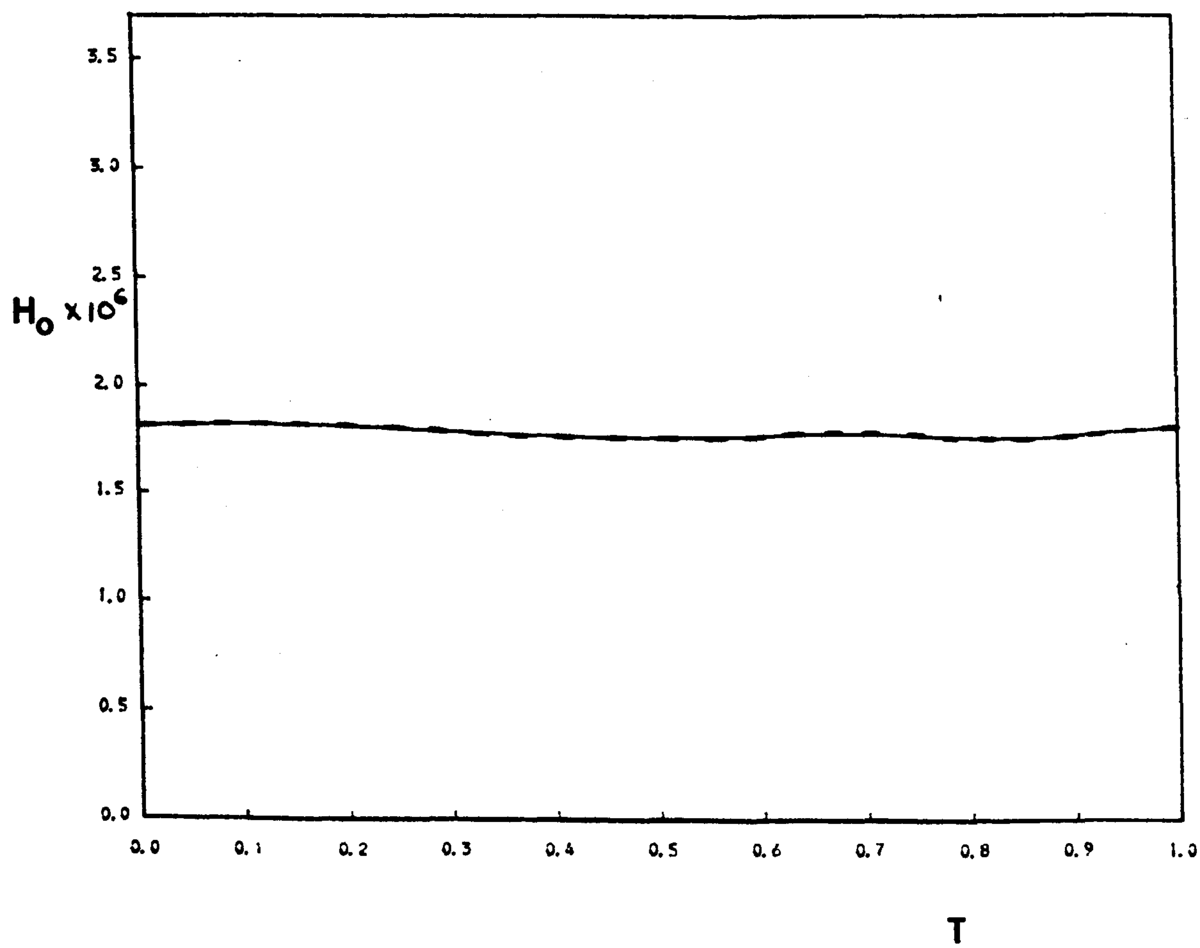

For key see page 252

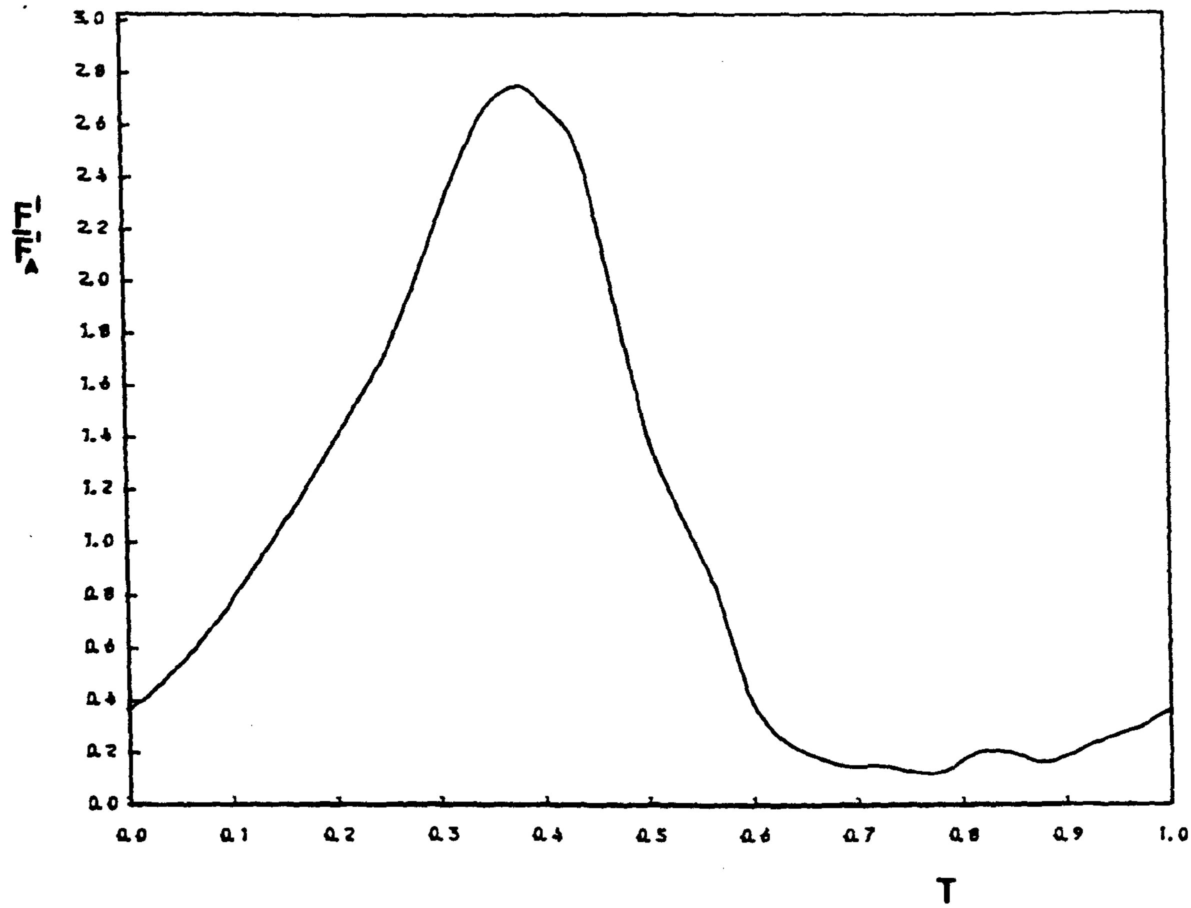

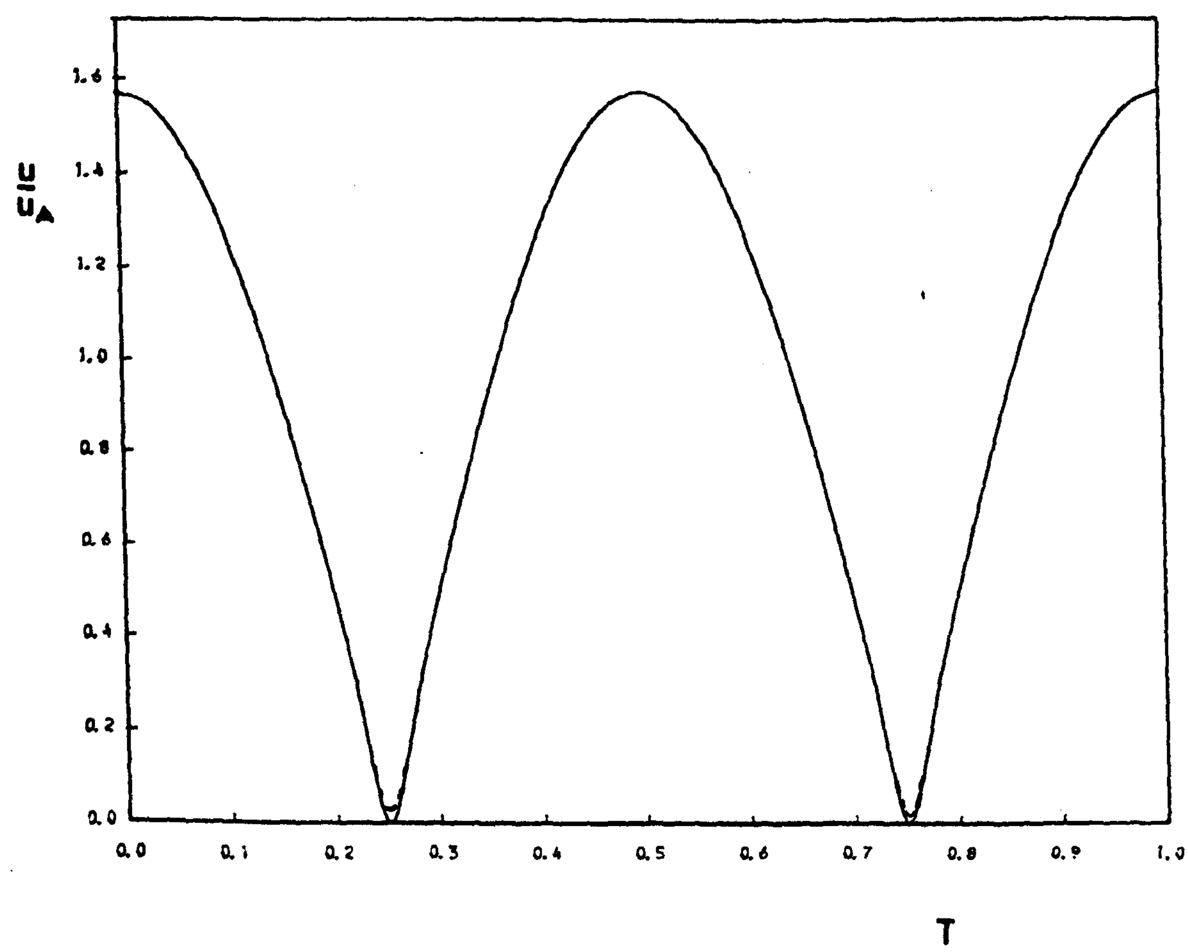

For key see page 252

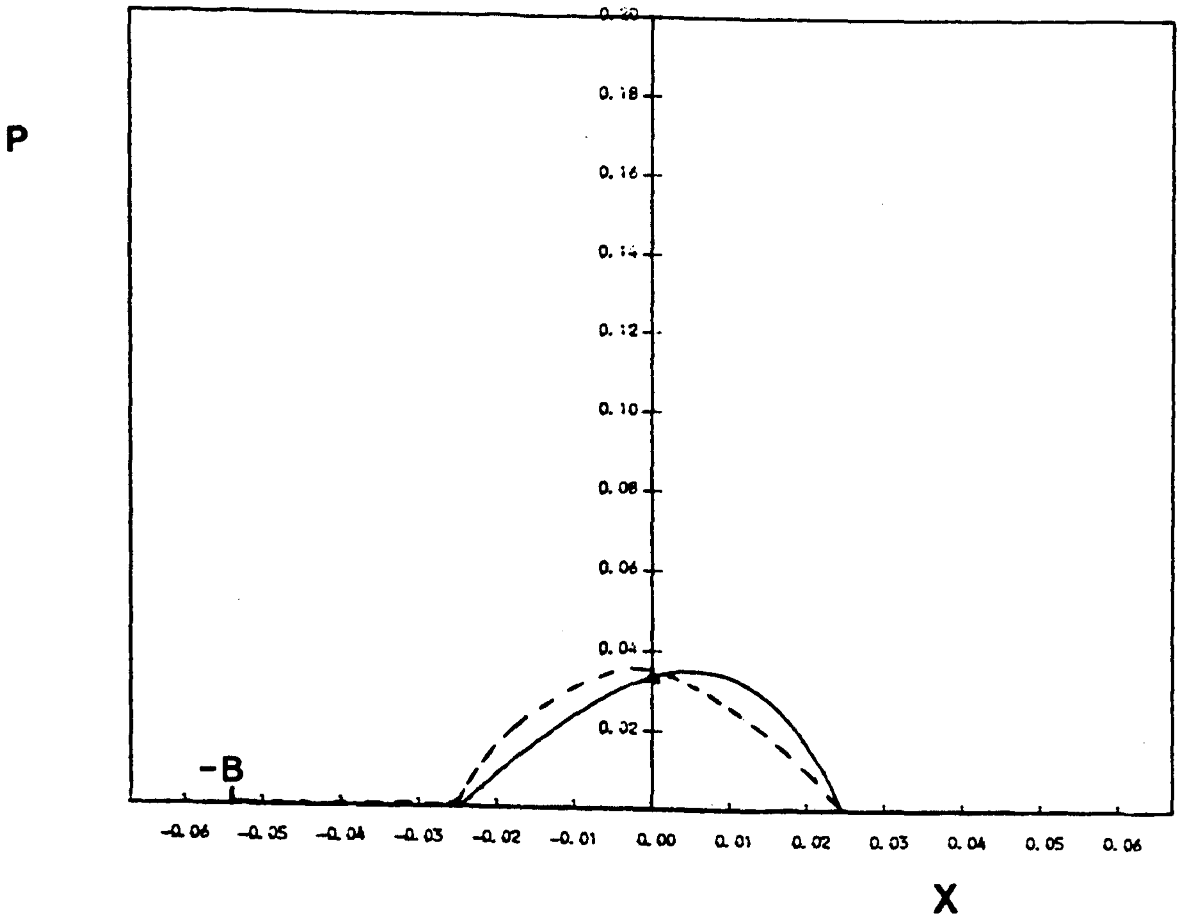

T = 0.0000E 00

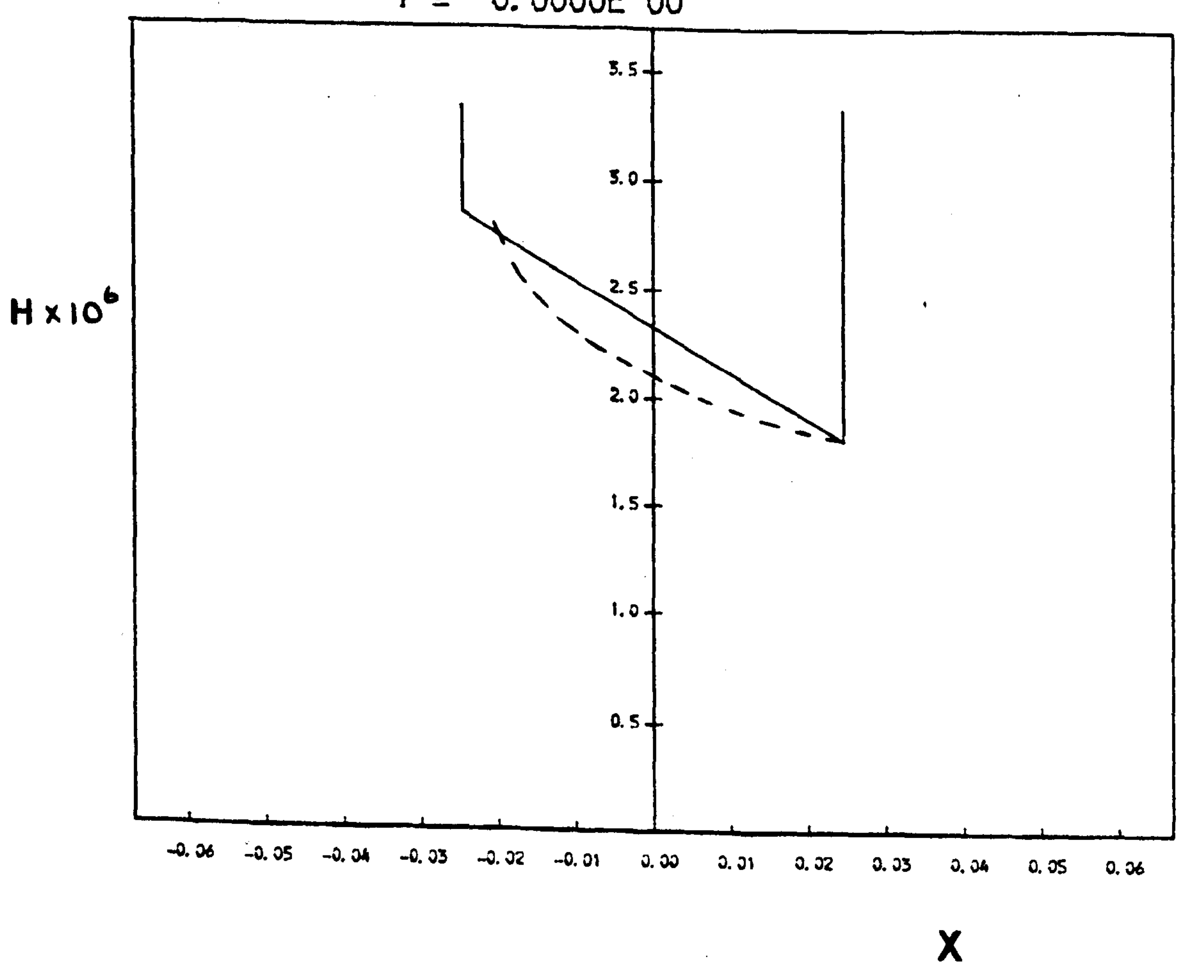

For key see page 252

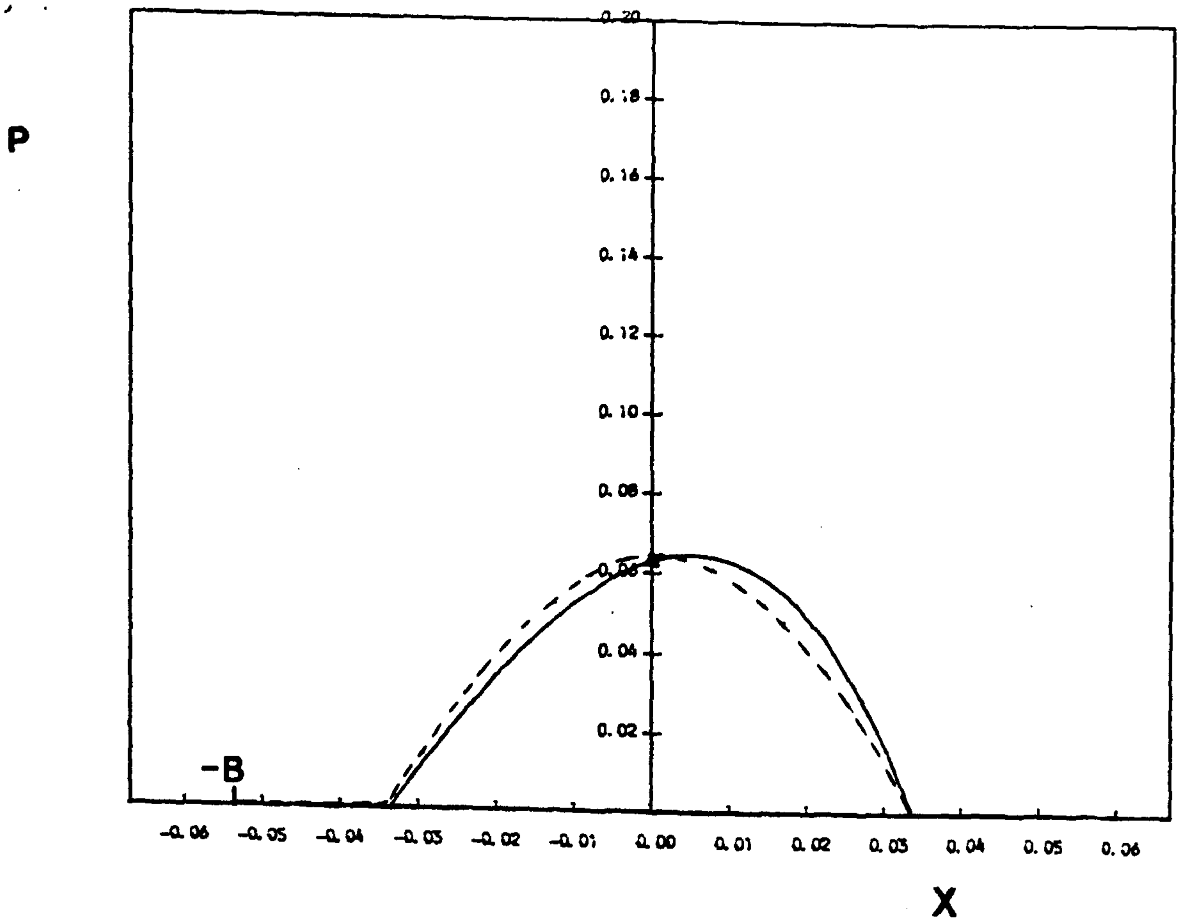

T = 0.1250E 00

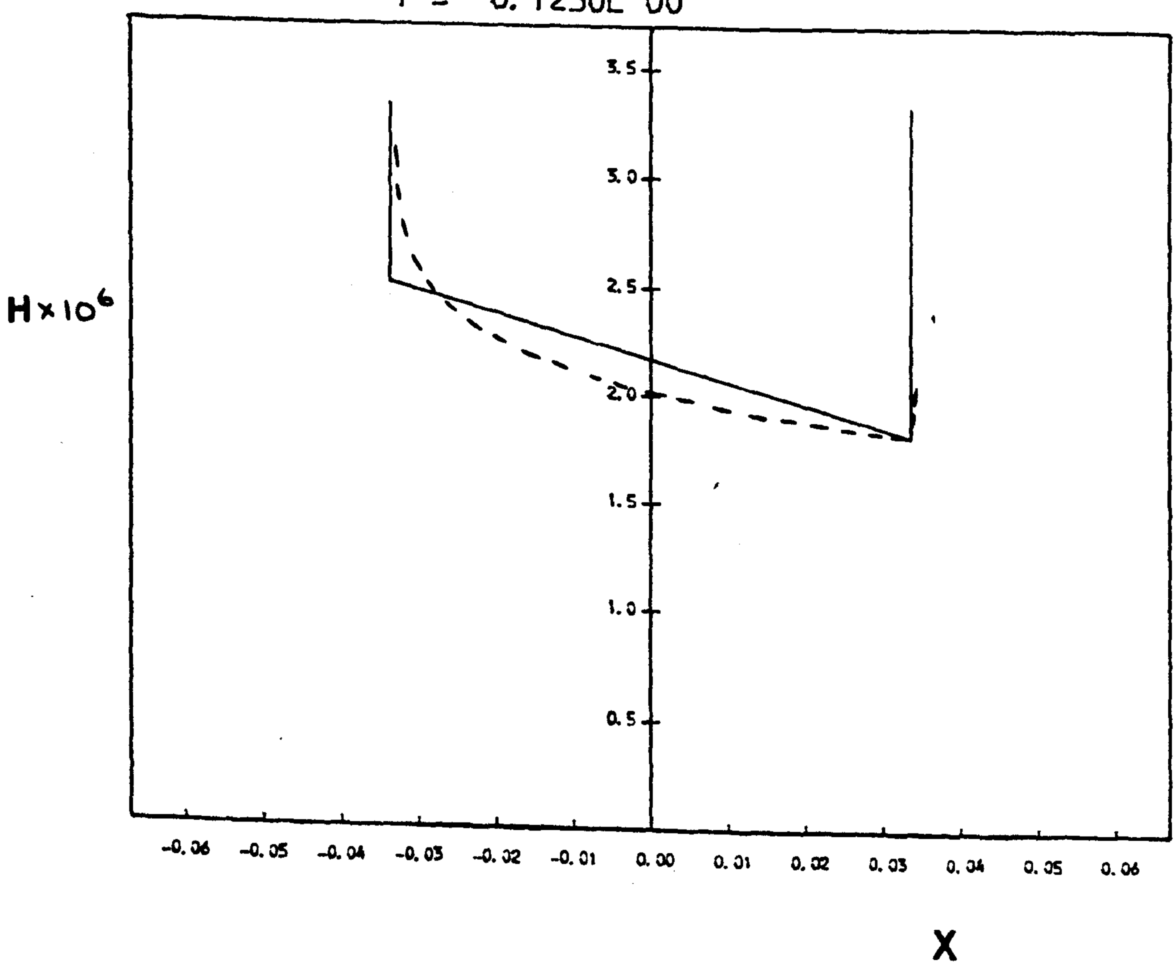

For key see page 252

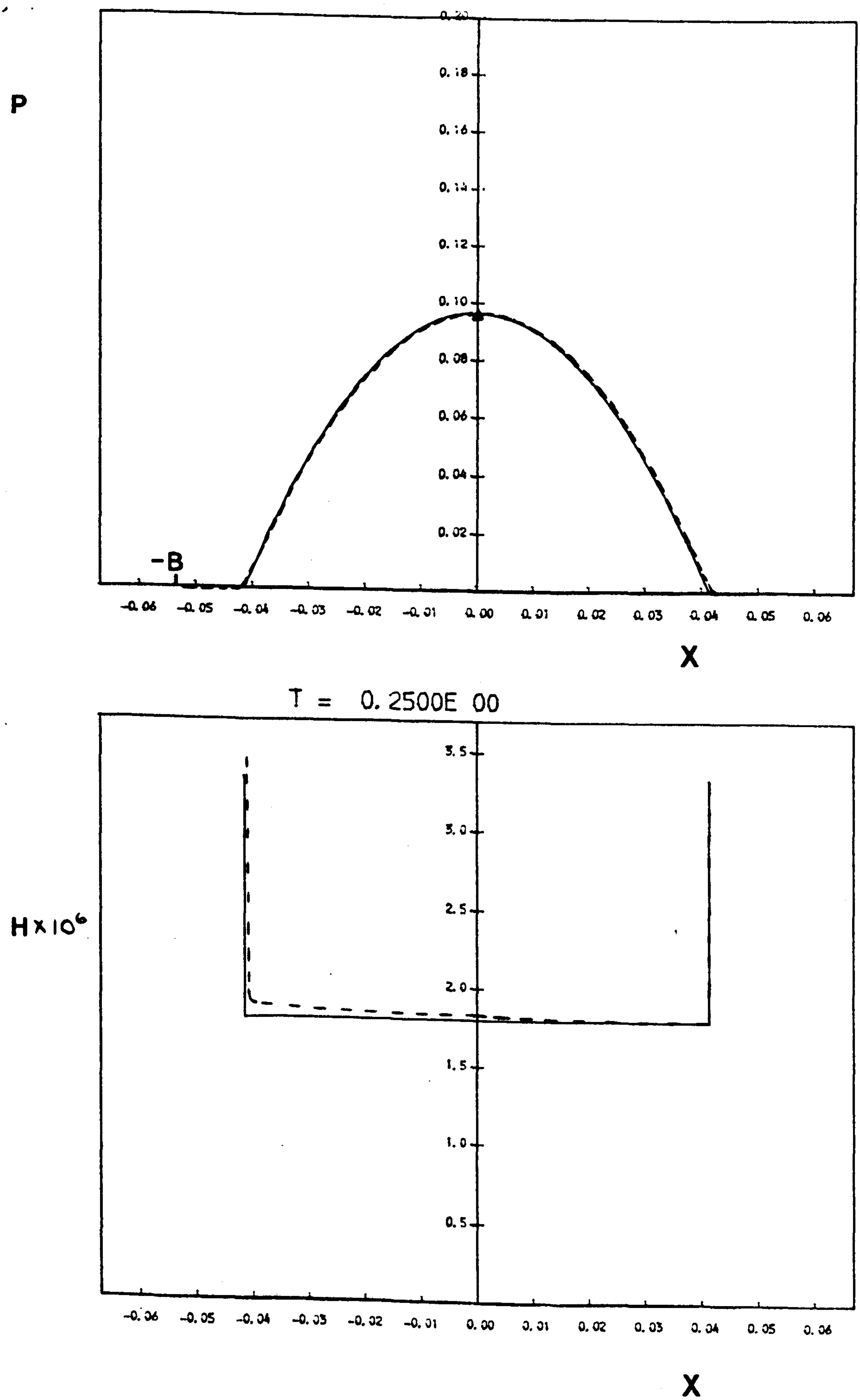

For key see page 252

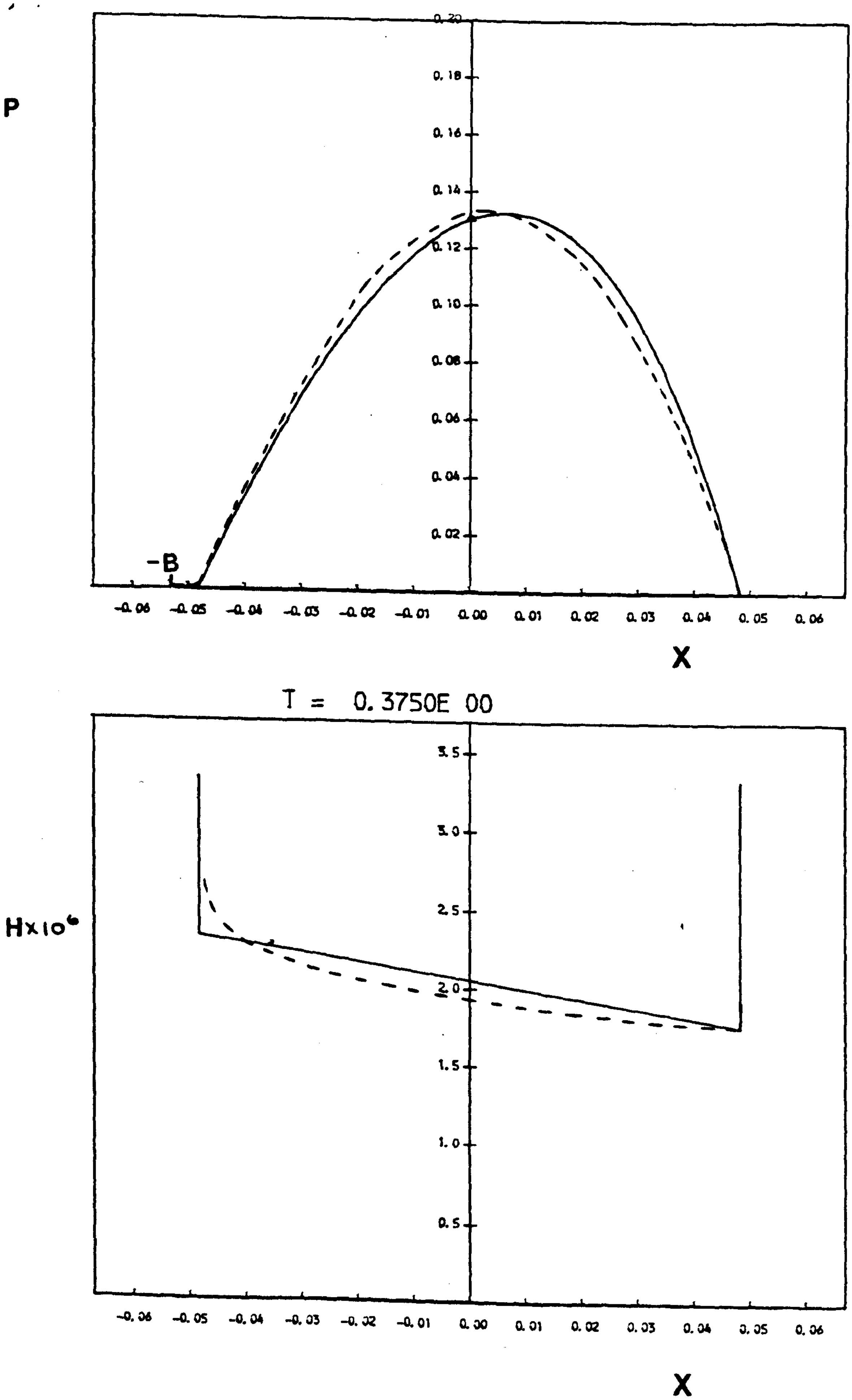

For key see page 252

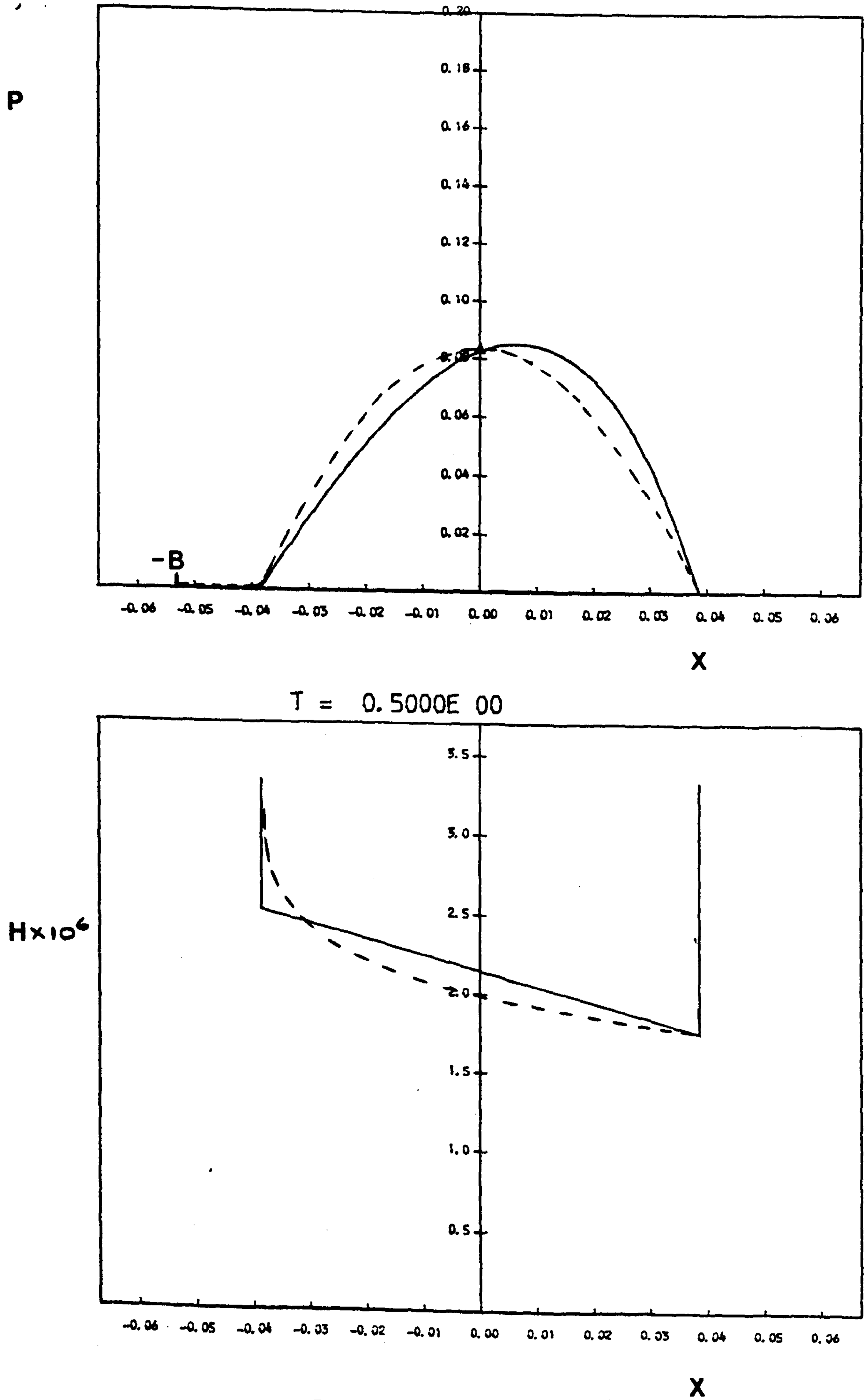

For key see page 252

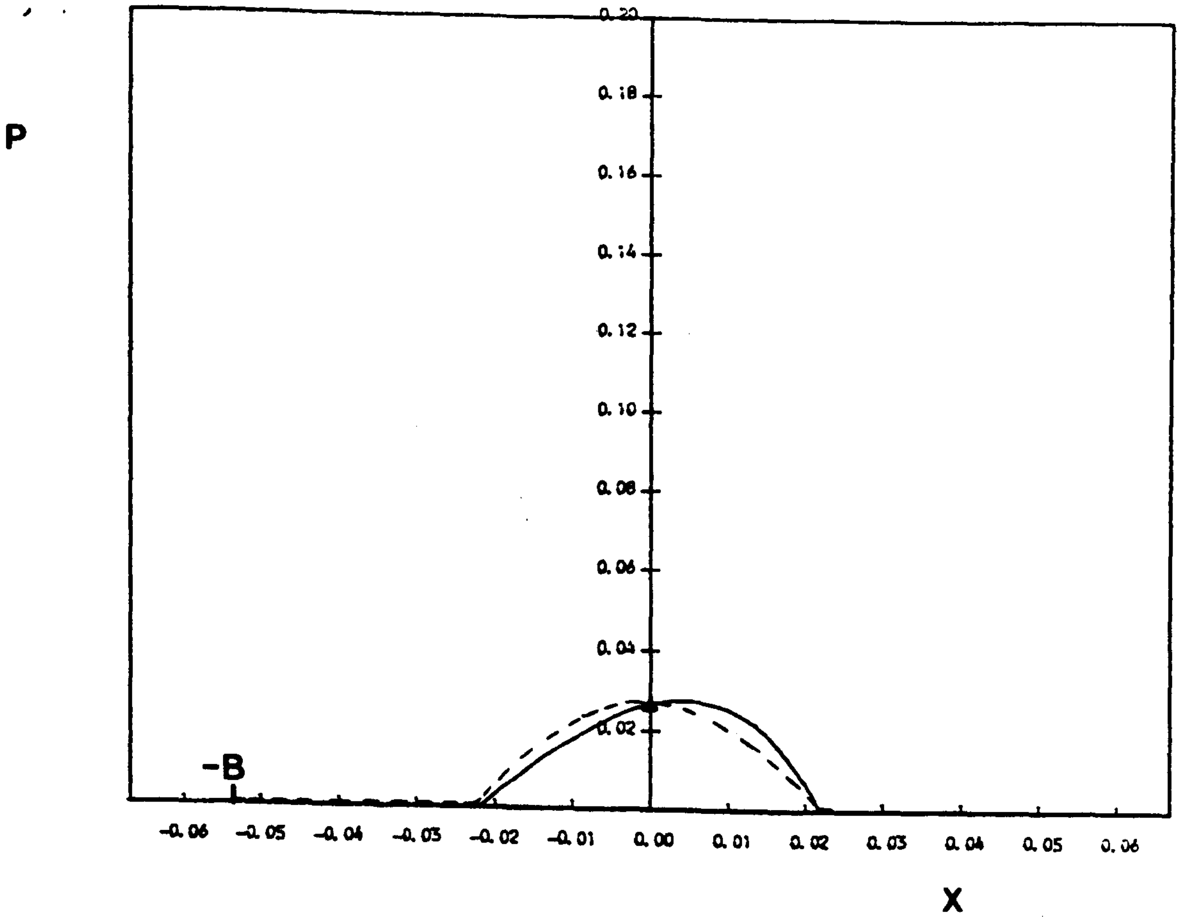

T = 0.6250E 00

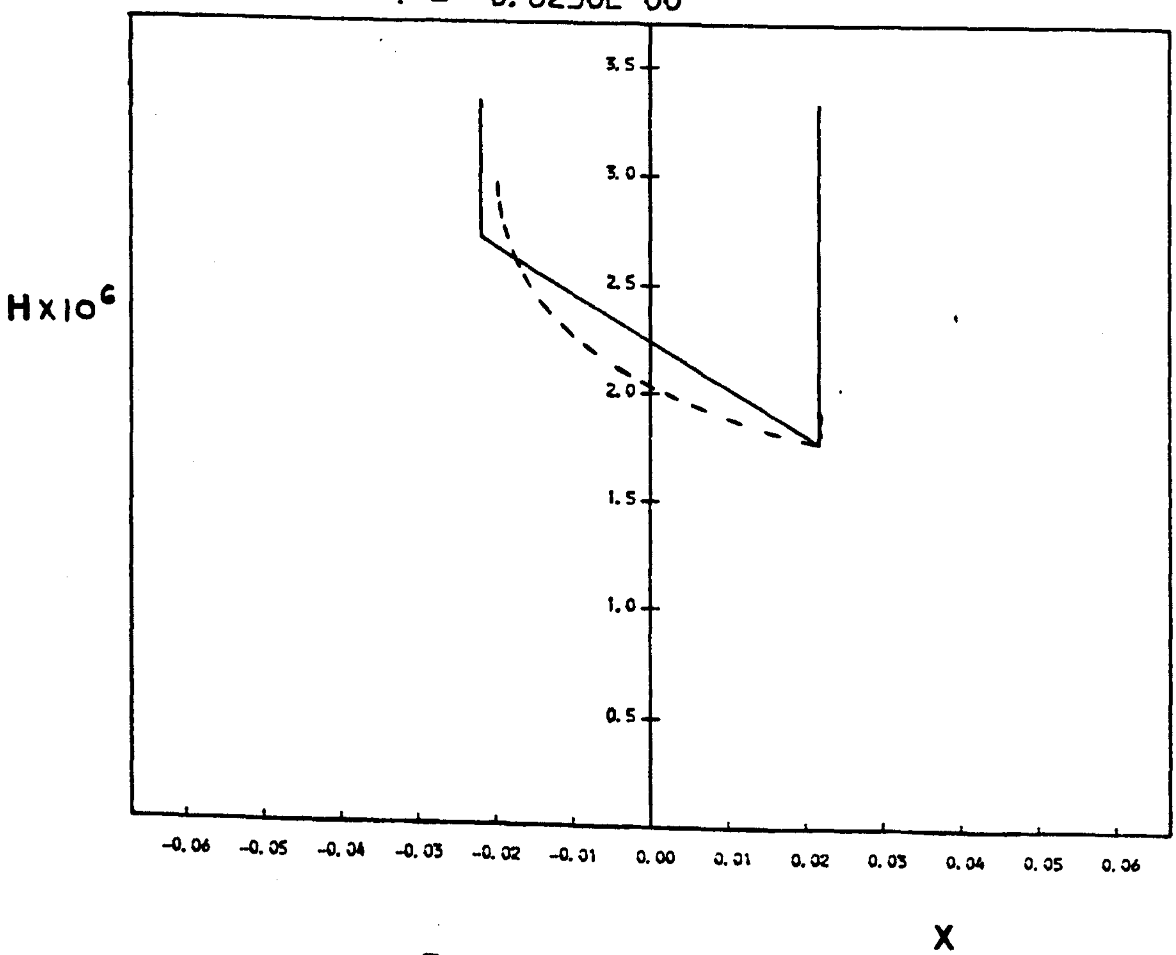

For key see page 252

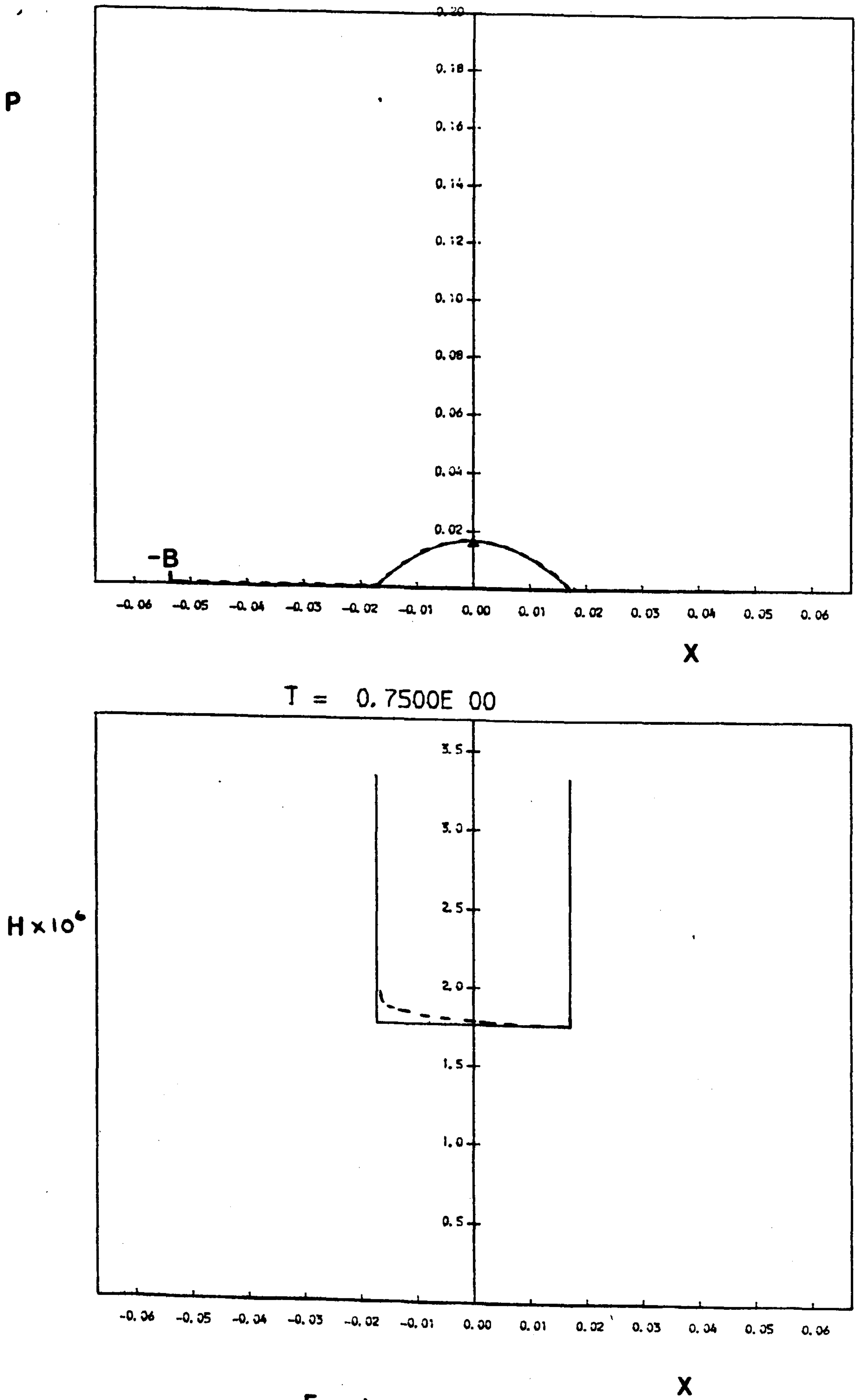

For key see page 252

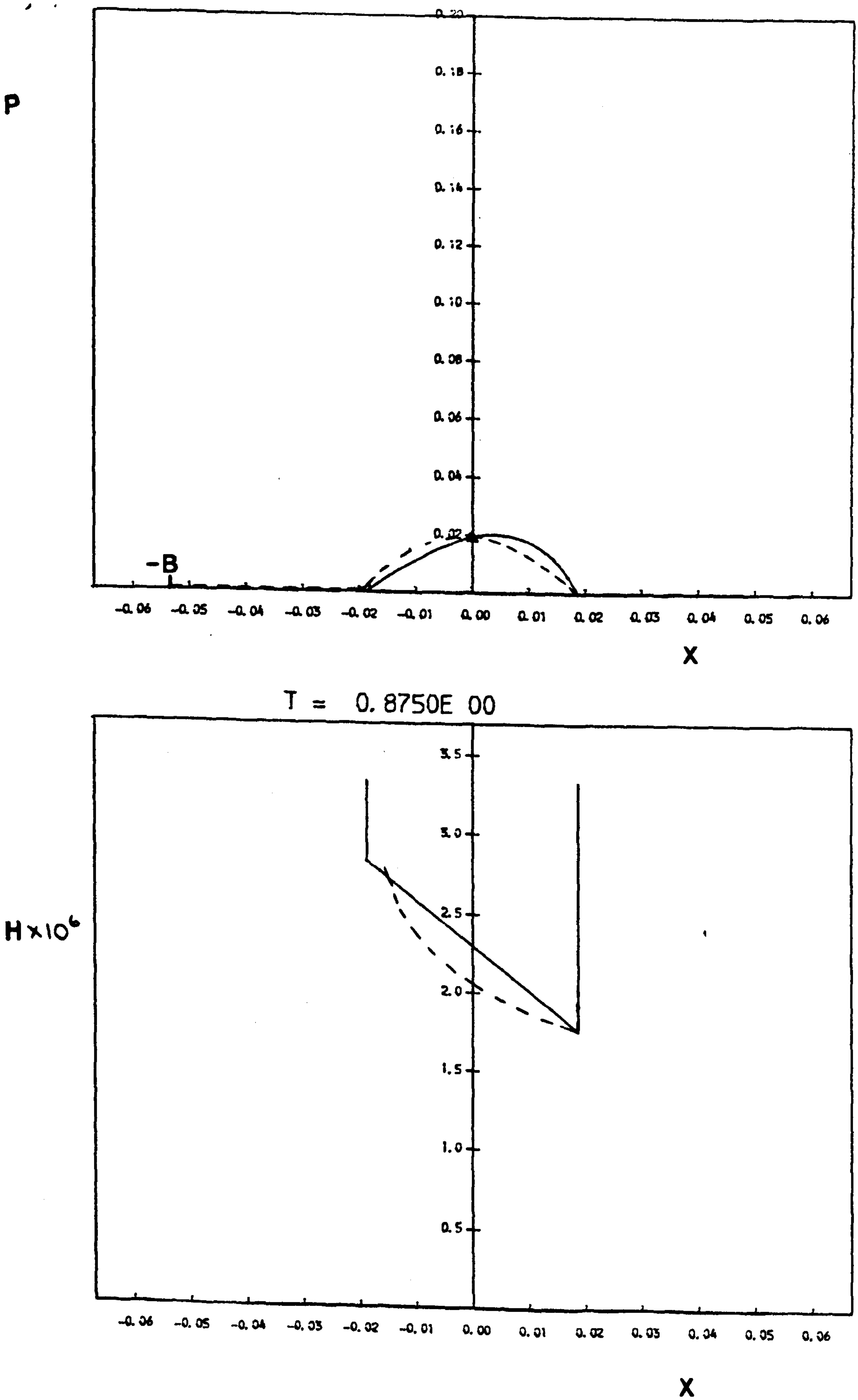

For key see page 252

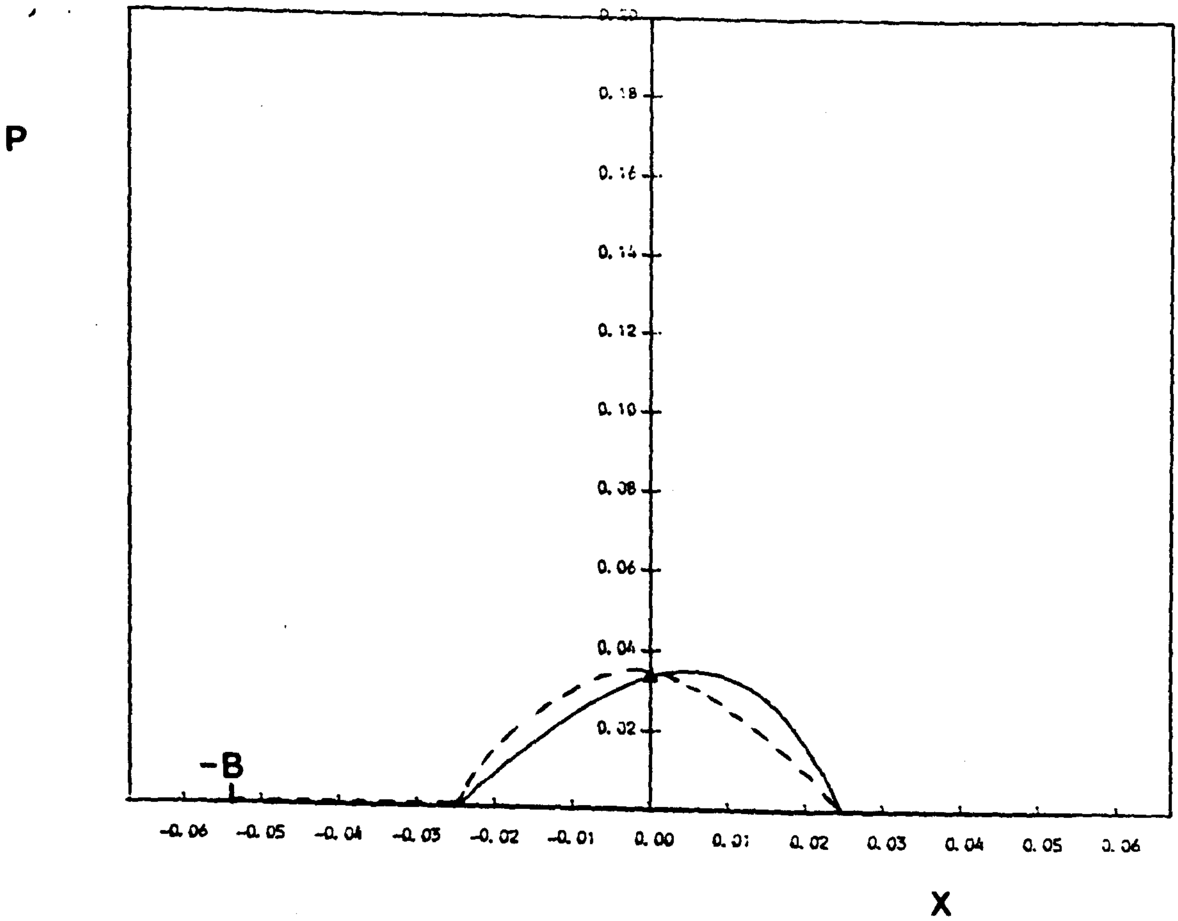

T = 0.1000E 01

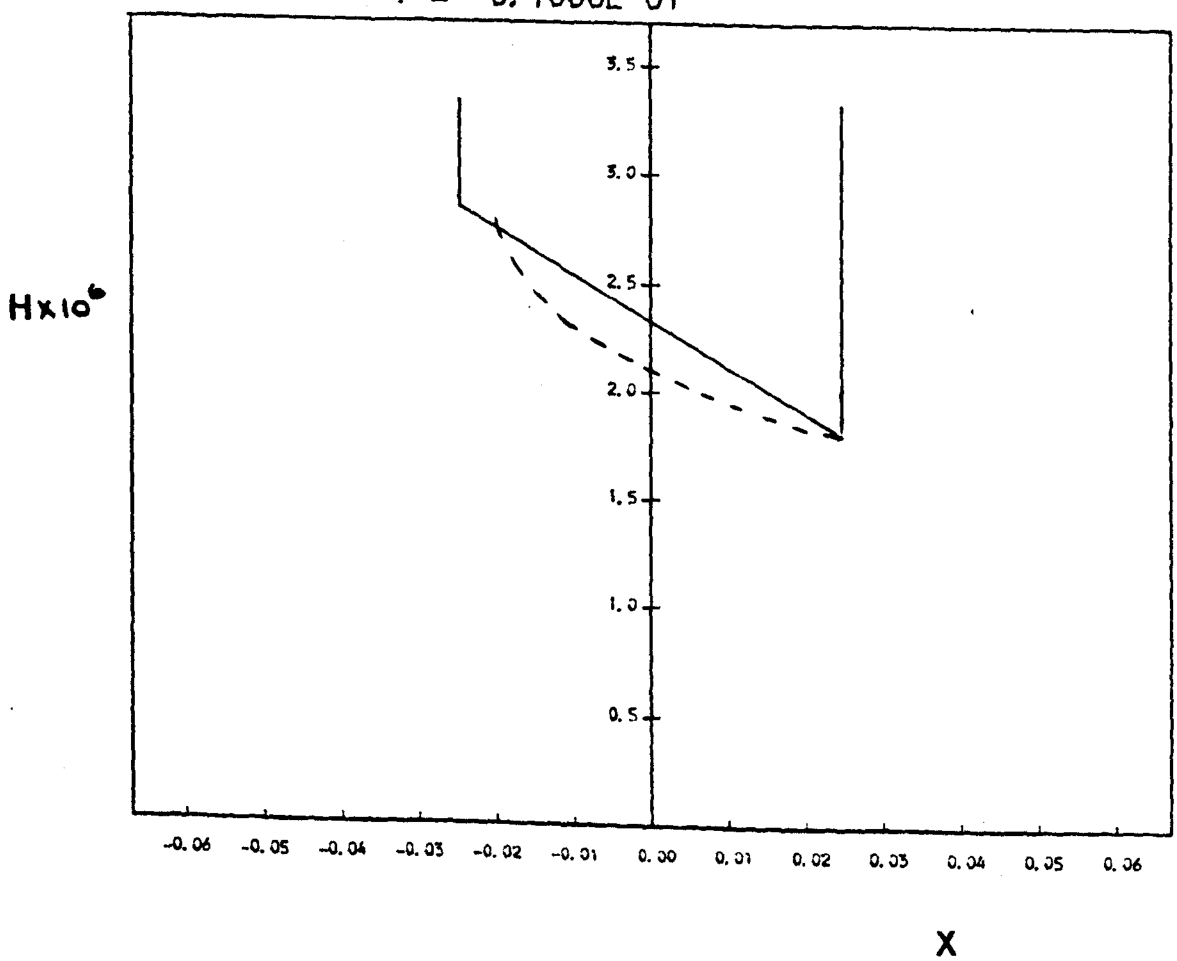

For key see page 252

CHAPTER 8

THEORETICAL PREDICTIONS OF FEATURES OF ANKLE JOINT LUBRICATION.

8.1 INTRODUCTION

The plane inclined surface bearing model was developed in Chapter 6 and applied to case B which represented the ankle joint in vivo during walking. The calculated minimum film thickness remained essentially constant throughout the cycle at a value of about 0.6 μm. The more comprehensive study of Chapter 7 provided support for many of the assumptions made in developing the plane inclined surface bearing model. It was also shown in Chapter 7 that decreasing the Poisson's ratio to 0.4, which was at the lower end of the range reported in the literature and specified in Table 5.3.2, resulted in increases of about sixty percent in minimum film thickness. Therefore, if the Poisson's ratio of 0.4 existed and the other conditions specified in case B were applied, the minimum film thickness might increase to about 1 μm. This indicated that changes in some of the assumed parameters for case B, within approximate physiological limits, could significantly influence the estimates for film thickness.

Seven cases are examined in the present chapter in which various groups of parameters in case B are altered to represent individual variations in physiology, activities other than walking and various theories of previous investigators. Film thickness, pressure distributions and coefficients of friction were calculated using the plane inclined surface bearing model described in Chapter 6. The calculated film thicknesses were compared to the measured Ra roughness of 2-6 μm for cartilage quoted in Chapter 2. The coefficients of friction were also compared to the value of 0.01 which was measured in various studies as described in Chapter 4.

8.2 Description of the Specified Cases:

The cases considered in this chapter were designated as B1, B2, ... B7, and a brief descriptive title was specified for each case along with the parameter changes compared with the standard case B, as shown in Table 8.2.1. The exact details of the parameter values are listed in Table 8.2.2 and the corresponding values of the dimensionless groups are listed in Table 8.2.3 for each case.

Cases B1 and B2 were selected to represent in an approximate fashion athletic actions such as running. The value of effective modulus (E') adopted for case B3 was at the lower limit of the measured values of Johnson et al (1977). The changes in cartilage thickness (d) and reduced radius of curvature, R, were within the ranges specified in the results presented in Chapter 3.

The values assumed for viscosity (η) in cases B4 and B5 were chosen based on investigations into the "boosted" lubrication theory for synovial joints (Walker et al, 1970; Unsworth, 1972; Walker and Gold, 1973) which has been described in Chapter 2. In these experiments a flat ended cylindrical section of a human joint surface was subjected to reciprocating motion. Synovial fluid was introduced between the flat cartilage surface and a glass counterface. After a few second the cartilage surface was quickly frozen and studies with the scanning electron microscope revealed lubricant layers a few microns thick on the surface. Using the squeeze film relationship for a circular plate (Higginson, 1978a) an apparent viscosity of 2 to 3 $N.s/m^2$ was calculated. While it cannot be ascertained whether effective viscosities of this magnitude occur in whole joint lubrication, it is considered important to examine

Table 8.2.1: General description of cases B1 to B7 considered in this chapter compared to case B

Case	Description
B	ankle joint in vivo during walking
B1	running lightly (u_Ax2, t_px0.5)
B2	running heavily (u_Ax2, t_px0.5, F_A'x2)
B3	soft conforming joint (E'x0.5, dx1.25, Rx2)
B4	enhanced viscosity (ηx300)
B5	enhanced viscosity (ηx100)
B6	squeezing with low shear rates (h_ox10 at t=0, ηx2)
B7	squeezing with high shear rates (h_ox10 at t=0)

Table 8.2.2 Parameter values for cases B and B1 to B7

Case	R (m)	b (mm)	d (mm)	t_p (s)	u_A (mm/s)	F' (kN/m)	η ($N.s/m^2$)	E' (MN/m^2)
B	0.35	15.2	2.4	1.0	19.099	33.726	0.01	42.667
B1	0.35	15.2	2.4	0.5	38.197	33.726	0.01	42.667
B2	0.35	15.2	2.4	0.5	38.197	67.452	0.01	42.667
B3	0.70	15.2	3.0	1.0	19.099	33.726	0.01	21.333
B4	0.35	15.2	2.4	1.0	19.099	33.726	3.00	42.667
B5	0.35	15.2	2.4	1.0	19.099	33.726	1.00	42.667
*B6	0.35	15.2	2.4	1.0	19.099	33.726	0.02	42.667
*B7	0.35	15.2	2.4	1.0	19.099	33.726	0.01	42.667

* h_o = 5.986 μm at t=0 for each cycle

Table 8.2.3 Values of the dimensionless groups for cases B and B1 to B7

Case	$U \times 10^{11}$	$W \times 10^{3}$	$S \times 10^{-9}$	$D \times 10^{3}$	$B \times 10^{2}$	ν
B	1.279	2.258	4.267	6.857	4.343	0.5
B1	2.558	2.258	2.133	6.857	4.343	0.5
B2	2.558	4.517	2.133	6.857	4.343	0.5
B3	1.279	2.258	2.133	4.286	2.171	0.5
B4	383.7	2.258	0.01422	6.857	4.343	0.5
B5	127.9	2.258	0.04267	6.857	4.343	0.5
B6	2.558	2.258	2.133	6.857	4.343	0.5
B7	1.279	2.258	4.267	6.857	4.343	0.5

this effect in the model adopted in the present study. Finally, the concept of squeeze film lubrication for synovial joints (Higginson, 1978) was examined for cases B6 and B7.

8.3 Results:

The results were generated for cases B and B1 using the computer program listed in Appendix E. The tolerance was specified as 0.001 and in general computing times were about 20 s (CPU). The characteristic load and velocity curves for all cases are shown in Figure 8.3.1. The variation of dimensionless minimum film thickness (H_o) and coefficient of friction (μ) with time (T) are shown in Figure 8.3.2. The minimum value of h_o and the maximum value of μ for the cycle are listed for each case in Table 8.3.1.

8.4 Discussion:

The variation of h_o throughout the cycle was small, except in cases B6 and B7 which examined the squeeze film mechanism, as shown in Figures 8.3.2 and 8.3.3. Thus, for the purposes of general discussion the minimum h_o which occurred in the cycle was considered. From the values listed in Table 8.3.1 it was clear that only massive increases in viscosity gave film thicknesses larger than the estimated Ra roughness of 2-5 μm quoted in Chapter 2. However, it is still possible that the thin film lubrication mechanism described in Chapter 2 may be invoked, or even micro-elastohydrodynamic lubrication associated with asperities on the 'soft' cartilage layers to facilitate effective lubrication.

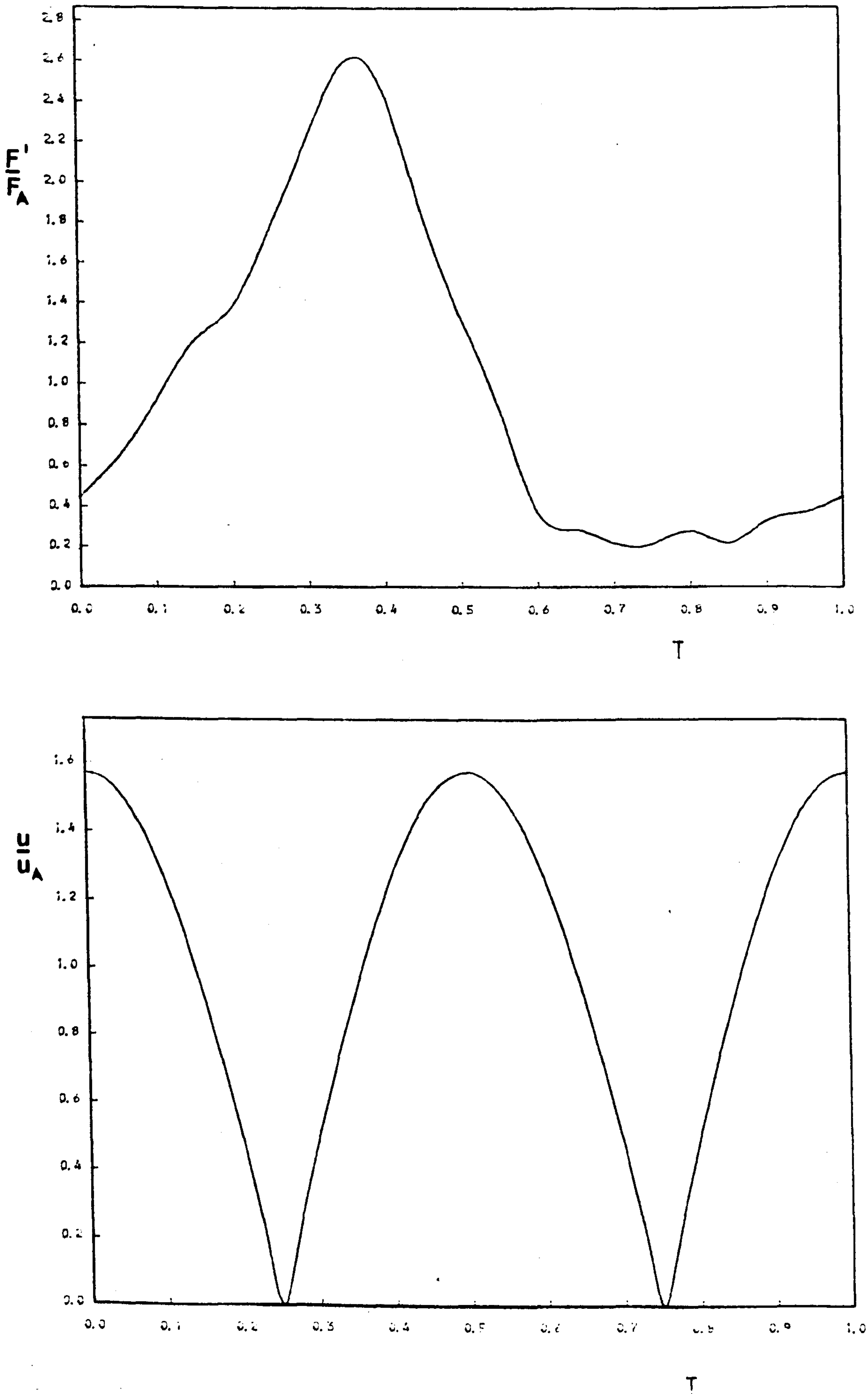

Figure 8.3.1 : Characteristic load and velocity curves for all cases.

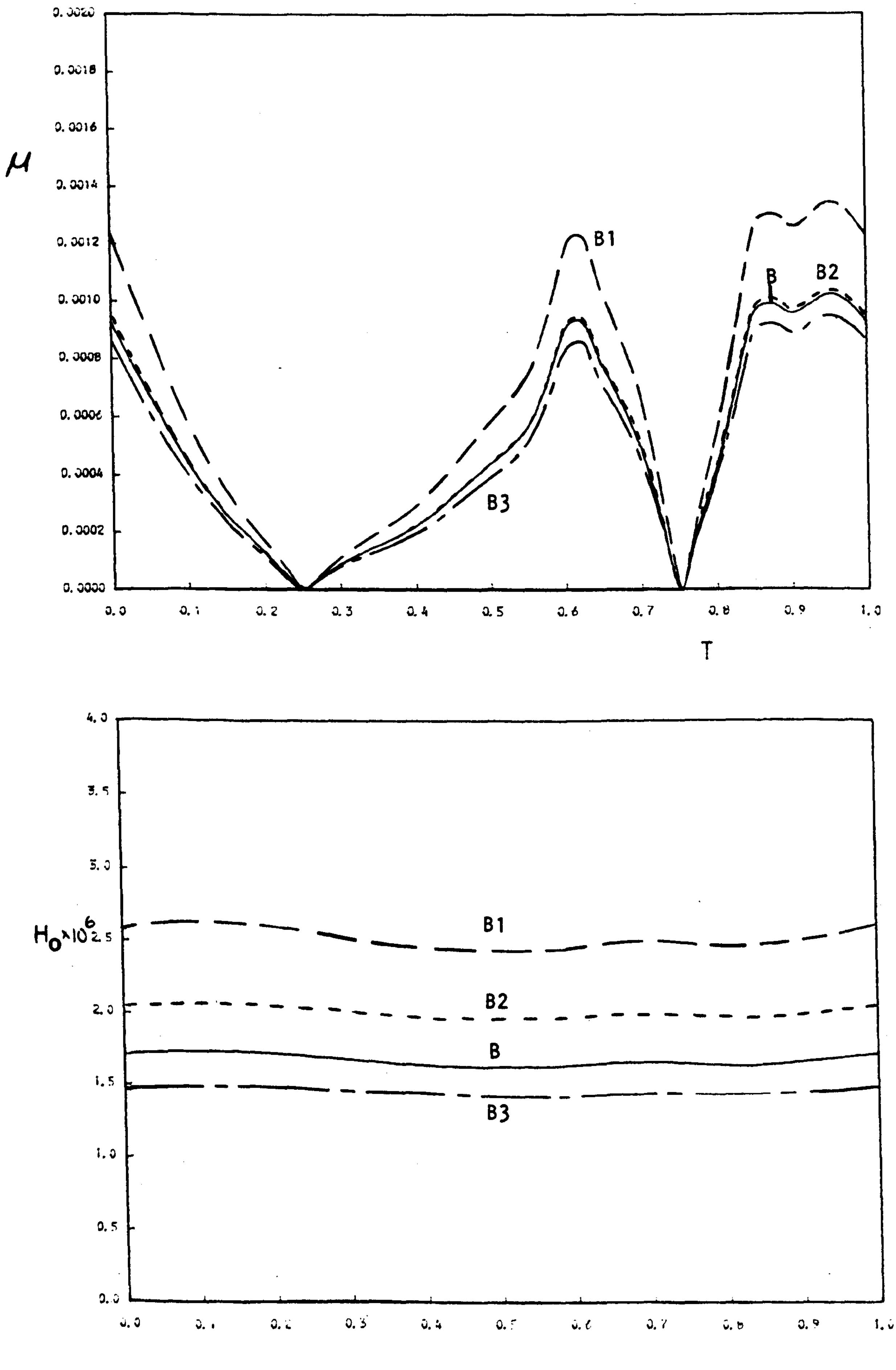

Figure 8.3.2 : Results for cases B, B1, B2 and B3.

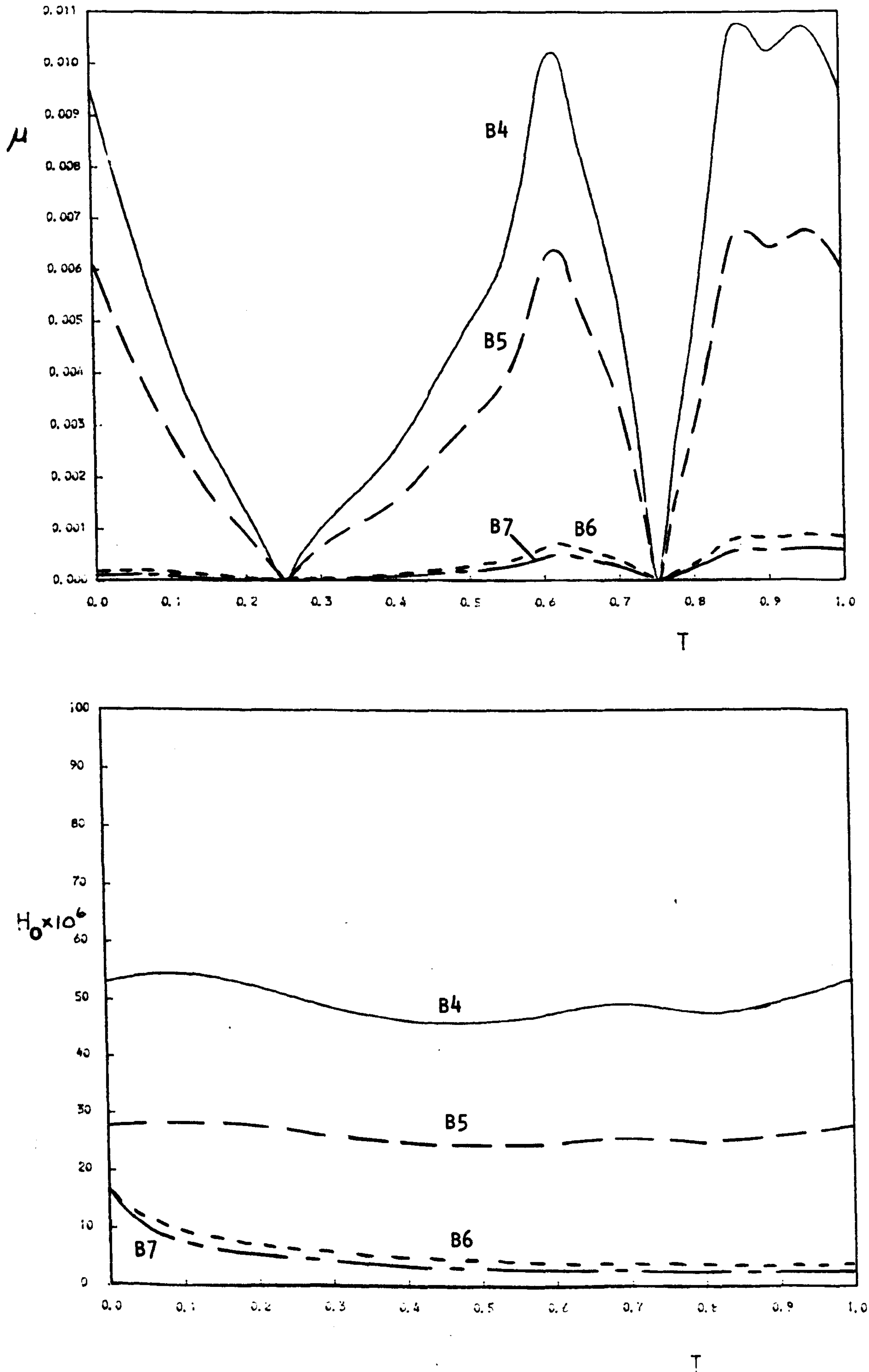

Figure 8.3.3 : Results for cases B4, B5, B6 and B7

Table 8.3.1 : Values of minimum h_o and maximum μ occurring during the cycle.

Case	Minimum h_o for the cycle (μm)	Maximum μ for the cycle
B	0.566	0.00102
B1	0.852	0.00135
B2	0.690	0.00104
B3	0.998	0.000952
B4	16.0	0.0107
B5	8.69	0.00675
B6	1.36	0.000890
B7	0.948	0.000631

The squeeze film mechanism described by Higginson (1978a) does not appear at first glance to be very effective in increasing film thickness values. However, as shown by comparing the minimum values of h_o for cases B6 and B7, viscosity increases enhance the ability of the squeeze film mechanism to preserve fluid films. Also, reasonably thick films are shown in Figure 8.3.3 throughout the stance phase for cases B6 and B7. Thus, if joint surfaces were pulled apart to create thick films during the swing phase, squeeze film lubrication might be effective. It was noted that for the swing phase loading assumed in the present study, thick films were not generated.

The various values for the dimensionless groups which describe the cases considered have been listed in Table 8.2.3. Although considerable variation occurred in the squeeze factor dimensionless group (S) the maximum coefficient of friction which occurred in a cycle could be correlated with $(\frac{U}{W})$ as shown in Figure 8.4.1. Cases B6 and B7 were excluded from Figure 8.4.1 because a special condition had been imposed on the steady state cycle. The results shown in Figure 8.4.1 suggested that the ability of the ankle joint to entrain lubricant with high viscosities or entrainment velocities would be an important factor in its potential to sustain fluid film lubrication.

The pressure distributions calculated in the solution of case B3 showed that lubrication starvation would occur. Thus, the film thicknesses calculated were probably not very realistic. In the solution for case B4 the peak pressure was always considerably less than the maximum dry contact stress. This suggested that the viscosity of 3 $N.s/m^2$ might have been too

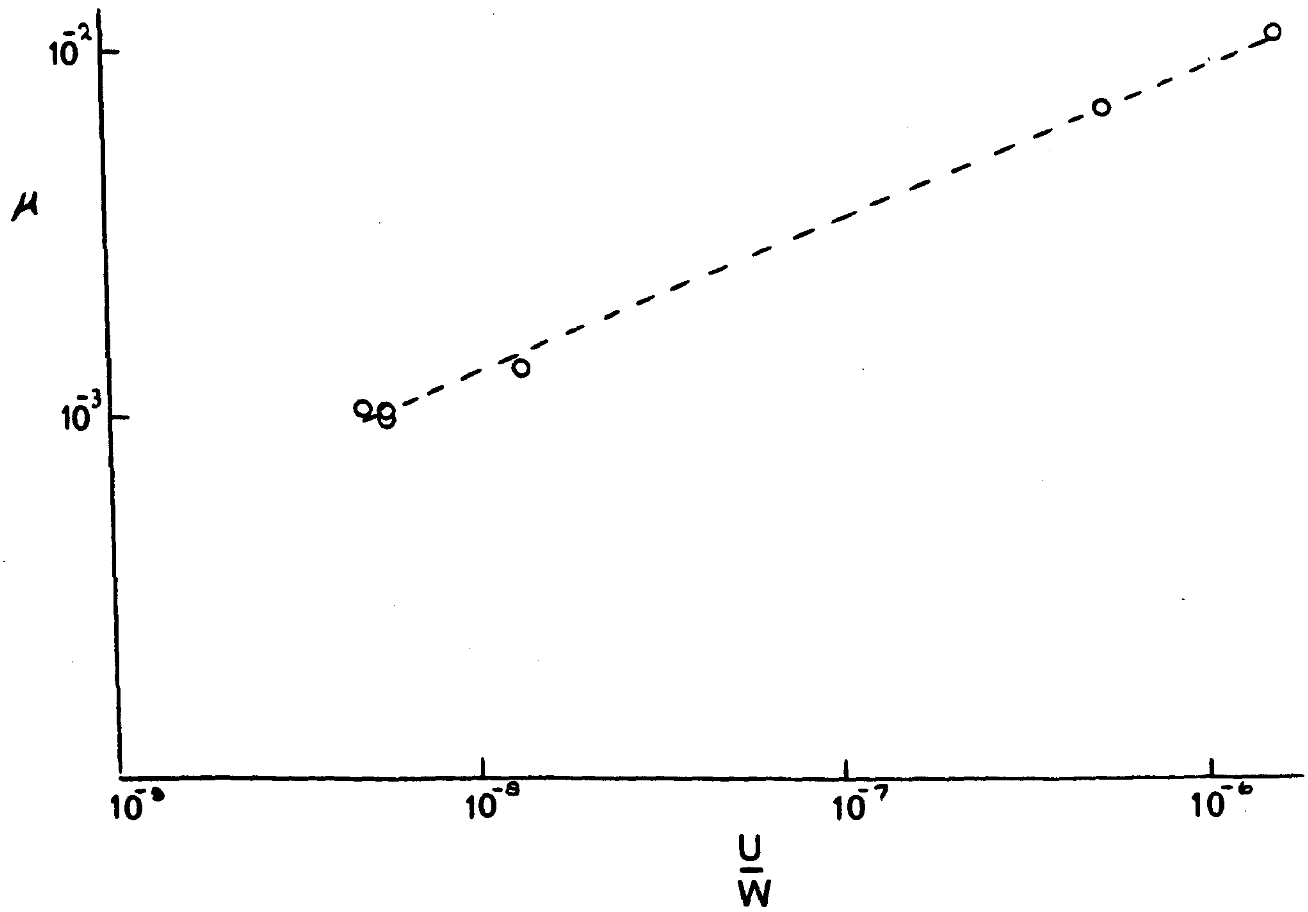

Figure 8.4.1 : The maximum coefficient of friction (μ) occurring in a cycle vs U/W.

high for the plane inclined surface model to provide accurate results.

8.5 Concluding Remarks:

Unless special thin film lubrication mechanisms act, it appears that the ankle joint cannot sustain full fluid film lubrication. The ability to develop and sustain fluid films is greatly enhanced by elastohydrodynamic and squeeze-film action. However, the role of micro-elastohydrodynamic mechanisms has yet to be fully explored. Fluid films in the order of 1.0 μm have been estimated and this value was certainly not entirely negligible compared to the surface roughness of cartilage. The advantages of an increased lubricant viscosity have been clearly demonstrated. Therefore, if synovial joints do experience fluid film lubrication a viscosity enhancing process in combination with conventional and local elastohydrodynamic action may provide the mechanism.

CHAPTER 9

OVERALL CONCLUSIONS AND RECOMMENDATIONS FOR FUTURE WORK

A wide ranging study has been performed on the lubrication of normal human ankle joints. The overall conclusions of this study now follow:

(i) The surfaces of human ankle joints in a relaxed state exhibit a converging-diverging configuration. Profiles of dissected ankle joints were measured in the direction of motion and found to be essentially circular in the central zone. When other dimensions of the articulating surfaces were considered, it was possible to represent the ankle joint with the geometry of a partial journal bearing with good accuracy. An average reduced radius of curvature of 0.35 m was deduced based upon the measured profiles.

(ii) Experiments were performed with ankle joints mounted in the simulator used by O'Kelly (1977). Great difficulty was encountered in measuring the friction forces. However, the coefficients of friction which occurred during the experiments were estimated to have been less than 0.01.

(iii) It was possible to specify an equivalent bearing consisting of a rigid cylinder with an attached compliant layer sliding on a rigid plane to represent the ankle joint for elastohydrodynamic lubrication analysis. Specific values for the dimensions of this bearing were based on the measurements recorded in this thesis.

(iv) In the lubrication analysis, the elastic deformation of the surface was initially taken into account by assuming that the deformed bearing shape could be represented by a plane inclined surface configuration. A simple solution procedure was developed for the lubrication of compliant cylindrical surfaces subjected to cyclic time varying load and velocity conditions. The accuracy of this procedure was supported by the agreement with specific cases from the work of Modest and Tichy (1979) and the work of Hirano and Murakami (1975). When the uncertainty in geometry, material properties and imposed conditions for the ankle was considered, the plane inclined surface bearing model was deemed to provide a reasonable approach to a very complex situation in elastohydrodynamic lubrication.

(v) Further support for the plane inclined surface bearing model was achieved by the implementation of a dynamic solution procedure which included a more complete, constrained column model of the elastic deformation of soft layers on cylindrical solids. This dynamic solution procedure required large computer resources. However, a solution for a single case with specified parameters which represented the ankle joint gave remarkable agreement with the results of the simple plane inclined surface bearing model.

(vi) Solutions were generated for a range of parameters, representing the normal human ankle joint. For the standard set of parameters, chosen to represent the ankle joint during walking, the minimum film thickness throughout the cycle remained reasonably constant at about 0.7 µm. This was considerably less than the Ra roughness estimated for cartilage of 2 - 6 µm (Walker et al, 1968; Clarke, 1973; Sayles et al, 1979; Thomas et al, 1980). The maximum coefficient of friction occurring in the cycle was found to be 0.001. Changes in selected groups of parameters failed to increase the film thickness and coefficients of friction significantly from those calculated for the standard case. When a large film thickness was introduced at the start of the cycle, it decreased rapidly to about 1 µm. Thus, in the present model, squeeze-film action was not capable of preserving thick films which might be generated during the swing phase in walking.

(vii) In the theoretical investigation only one change in the standard set of parameters gave thick films compared with the surface roughness of cartilage and coefficients of friction similar to those measured by previous investigators. When, in an extreme case the viscosity was increased from 0.01 to 3 $N.s/m^2$, film thicknesses of about 18 µm and coefficients of friction up to 0.01 were calculated. The massive increase in viscosity was based on apparent viscosities estimated from the results of Walker et al (1970) and Unsworth (1972).

Recommendations for Future Work:

The theoretical models developed in the present thesis have not been verified with experiments for a compliant layered geometry subjected to both dynamic loads and velocities. Friction experiments could be conducted with the appropriate cylindrical geometry. Assuming a reasonable agreement with the theory developed in this thesis, it is further proposed that small cylindrical sections should be shaped from ankle joint surfaces for similar friction experiments. It would be of particular interest to investigate the breakdown of fluid film lubrication for the natural surfaces in the presence of synovial fluid.

This proposed programme is a return to the approach of Walker et al (1970), except that a cylindrical geometry would be used as well as theory for combined entrainment and squeeze film action which is now available. The study could then be extended to the testing of whole joints in a simulator apparatus.

REFERENCES

Allen, S.J. and Kline, K.A. (1971). Lubrication theory for micropolar fluids. J. Appl. Mech., 38, 646-650.

Askew, M.J. and Mow, V.C. (1978). The biomechanical function of the collagen fibril ultrastructure of articular cartilage. J. Biomech. Eng., 100, 105-115.

Baglin, K.P. and Archard, J.F. (1972). An analytical solution of the elastohydrodynamic lubrication of materials of low elastic modulus. Instn. Mech. Engrs., C3/72, 13-21.

Barnett, C.H. and Napier, J.R. (1952). The axis of rotation at the ankle joint in man. Its influence upon the form of the talus and the mobility of the fibula. Anatomy, 86, 1-9.

Barnett, C.H. and Cobbold, A.F. (1962). Lubrication within living joints. J. Bone and Jt. Surg., 44-B, 662-674.

Behrens, J.C., Walker, P.S. and Shoji, H. (1974). Variations in strength and structure of cancellour bone at the knee. J. Biomechanics., 7, 201-207.

Bennett, A. and Higginson, G.R. (1970). Hydrodynamic lubrication of soft solids. J. Mech. Eng., Sci., 12, 218-222.

Bentall, R.H. and Johnson, K.L. (1968). An elastic strip in plane rolling contact. Int. J. Mech. Sci., 10, 637-663.

Bullough, P.G., Muneura, L., Murphy, J. and Weinstein, A.M. (1970). The strength of the menisci of the knee as it relates to their fine structure. J. Bone Jt. Surg., 52B, 564-570.

Cameron, H.U. and MacNab, I. (1972). The structure of the meniscus of the human knee joint. Clin. Orthop., 89, 215-219.

Cameron, H.U., Pilliar, R.M. and MacNab, I. (1975). The micro-hardness of articular cartilage. Clin. Orthop., 108,

Castelli, V., Rightmire, G.K. and Fuller, D.D. (1967). On the analytical and experimental investigation of a hydrostatic, axisymmetric compliant-surface thrust bearing. Trans. ASME J. Lub. Techn., Oct. 1967, 510-520.

Caygill, J.C. and West, G.H. (1969). The rheological behaviour of synovial fluid and its possible relation to joint lubrication. Med. & Biol. Eng., 7, 507-516.

Charnley, J. (1960). The lubrication of animal joints in relation to surgical reconstruction by arthroplasty. Annals. Rheum. Diseases, 19, 10-19.

Clarke, I.C. (1973). Quantitative measurement of human articular surface topography in vitro by profile recorder and stereo-microscopy techniques. J. Microsc., 97, 309-314.

Clarke, I.C., Contini, R. and Kenedi, R.M. (1975). Friction and wear studies of articular cartilage: a scanning electron microscope study. J. of Lubr. Tech., 97, 358-368.

Cooke, A.F., Dowson, D. and Wright, V. (1978). The rheology of synovial fluid and some potential synthetic lubricants for degenerate synovial joints. Engng. in Med., 7, 66-72.

Cudworth, C.J. and Higginson, G.R. (1976). Friction of lubricated soft surface layers. Wear, 37, 299-312.

Cudworth, C.J. and Mykura, J.F. (1980). Normal approach of a cylinder towards an elastic layer. J. Mech. Eng. Sci., 22, 65-70.

Cudworth, C.J. (1978). Finite element solution of the elastohydrodynamic lubrication of a compliant layer in pure sliding. Elastohydro-dynamics and Related Topics, (Edited by Dowson, D., Taylor, C.M., Godet, M. and Berthe, D.), Mechanical Engineering Publications, Suffolk, England.

D'Ambrosia, R.D., Shoji, H. and Van Meter, J. (1976). Rotational axis of the ankle joint: comparison of normal and pathological states. Surgical Forum, 27, 507-508.

Davies, D.V. (1967). Properties of synovial fluid. Proc. Instn. Mech. Engrs., 181, (3F), 25-29.

Davies, D.V. and Palfrey, J. (1969). Physical properties of synovial fluid. Lubrication and wear in joints, Edited by V. Wright, Sector, London, 20-28.

Davis, W.H., Lee, S.L. and Sokoloff, L. (1978). Boundary lubricating ability of synovial fluid in degenerative joint disease. Arth. & Rheum., 21, 754-760.

Davis, W.H., Lee, S.L. and Sokoloff, L. (1979). A proposed model of boundary lubrication by synovial fluid : structuring of boundary water. J. Biomech. Eng., 101, 185-192.

Day, W.H., Swanson, S.A.V. and Freeman, M.A.R. (1975). Contact pressures in the loaded human cadaver hip, J. Bone Jt. Surg., 57B, 3-2-313.

Dimnet, J., Carret, J.P., Gonon, G. and Fischer, L.P. (1976). A technique for joint center analysis using a stored program calculator. J. Biomechanics, 9, 771-778.

Dintenfass, L. (1963). Lubrication in synovial joints: a theoretical analysis. J. Bone Jt. Surg., 45A, 1241-1256.

Dowling, J.M., Atkinson, J.R., Dowson, D. and Charnley, J. (1978). The characteristics of acetabular cups worn in the human body. J. Bone Jt. Surg., 60B, 375-382.

Dowson, D. and Whomes, T.L. (1967). Side-leakage factors for a rigid cylinder lubricated by an isoviscous fluid. Proc. Instn. Mech. Engrs., 181 Pt 3 0, 165-176.

Dowson, D. (1967), Modes of lubrication in human joints. Proc. Instn. Mech. Engrs., 181 (3F), 45-54.

Dowson, D. and Taylor, C.M. (1967). Elastohydrostatic lubrication of circular plate thrust bearings. Trans. ASME J. Lub, Techn., July 1967, 237-244.

Dowson, D., Longfield, M.D., Walker, P.S. and Wright, V. (1968). An investigation of the friction and lubrication in human joints. Proc. Instn. Mech. Engrs., 182, (3N), 68-76.

Dowson, D., Unsworth, A. and Wright, V. (1970). Analysis of boosted lubrication in human joints. J. Mech. Eng. Sci., 12, 364-369.

Dowson, D., Economou, P.N., Ruddy, B.L., Strachan, P.J. and Baker, A.J.S. (1979). Piston ring lubrication - Part II. Theoretical analysis of a single ring and a complete ring pack, Energy conservation through fluid film technology: Frontiers in Research and Design, Edited by Rhodes, S.M., Wilcok, D.F. and Cheng, H.S. ASME Publications, 23-52.

Dowson, D. (1980). Lubrication of joints. A. Natural joints. An introduction to the biomechanics of joints and joint replacements, Edited by D. Dowson and V. Wright, Mechanical Engineering Publications Limited, Suffolk.

Ducheyne, P., Heymans, L., Martens, M., Aernoudt, E., DeMeester, P. and Mulier, J.C. (1977). The mechanical behaviour of intracondylar cancellous bone of the femur ad different loading rates. J. Biomechanics, 10, 747-762.

Edwards, J. (1967). Physical characteristics of articular cartilage. Proc. Instn. Mech. Engrs., 181, (3F), 16-24.

Ekholm, R. and Ingelmark, B.E. (1952). Functional thickness variations of human articular cartilage. Acta Soc. Med. Upsal., 57, 39-59.

Evangelista, J.J., Davies, W.H., Lee, S.L. and Sokoloff, L. (1978). Technical note: an improved McCutchen mini-viscometer for connective tissue fluids. Connective Tissue Research, 6, 109-113.

Faber, J.J., Williamson, G.R. and Feldman, N.T. (1967). Lubrication of joints. J. Appl. Physiol., 22, 793-799.

Fein, R.S. (1967). Are synovial joints squeeze film lubricated? Proc. Instn. Mech. Engrs., 181, (3F), 125-128.

Findlay, J.B. and Repo, R.U. (1978). Cartilage impact in vitro: effect of bone cement. J. Biomechanics, 11, 379-388

Freeman, M.A.R., Swanson, S.A.V. and Manley, P.T. (1975). Stress-lowering function of articular cartilage. Med. & Biol. Engng., 13, 245-251.

Freeman, M.A.R. (1979). Adult articular cartilage. Pitman Medical, London.

Gaman, I.D.C., Higginson, G.R. and Norman, R. (1974). Fluid entrapment by a soft surface layer. Wear, 28, 345-352.

Gibson, I.A., Hooke, C.J. and O'Donoghue, J.P. (1972). The frictional behaviour of reciprocating O-ring seals under starting conditions. Instn. Mech. Engrs., C13/72, 77-82.

Gill, P.E. and Miller, G.F. (1971). An algorithm for the integration of unequally spaced data. The Computer J., 15, 80-83.

Gladwell, I. and Sayers, D.K. (1980). Computational techniques for ordinary differential equations. Academic Press Inc., (London) Ltd., London.

Goldsmith, H.L. (1971). Red cell motion and wall interactions in tube flow. Fed. Proc., 30, 1578-1590.

Greenwald, A.S. and O'Connor, J.J. (1971). The transmission of load through the human hip joint. J. Biomechanics, 4, 507-528.

Greenwald, A.S. Matejczyk, M.B., Keppler, K., Black, J.D., Morgan, J.M., Porritt, D., Beck, R.D. and Wilde, A.H. (1976). Preliminary observations on the weight-bearing surfaces of the human ankle joint. Surg. Forum., 27, 505-506.

Gupta, P.K. and Walowit, J.A. (1974). Contact stresses between an elastic cylinder and a layered elastic solid. Trans.ASME J. Lub. Techn., April, 250-257.

Gupta, P.K. (1976). On the heavily loaded elastohydrodynamic contacts of layered solids. Trans. ASME J. Lub. Techn., July 1976, 367-374.

Hall, G. and Watt, J.M. (1976). Modern numerical methods for ordinary differential equations. Oxford University Press, London.

Hayes, W.C. and Mockros, L.F. (1971). Viscoelastic properties of human articular cartilage. J. Appl. Physiol., 41, 562-568.

Hayes, W.C., Keer, L.M., Herrmann, G. and Mockros, L.F. (1972). A mathematical analysis for indentation tests of articular cartilage. J. Biomechanics, 5, 541-551.

Hayes, W.C. and Carter, D.R. (1976). Post yield behaviour of subchondral trabecular bone. J. Biomed Mater. Research Symposium, 7, 537-544.

Hayes, W.C. and Bodine, A.J. (1978). Flow-independent visco-elastic properties of articular cartilage matrix. J. Bio-mechanics, 11, 407-419.

Hayes, W.C., Swenson, L.W. and Schurman, D.J. (1978). Axisymmetric finite element analysis of the lateral tibial plateau. J. Biomechanics, 11, 21-22.

Herrebrugh, K. (1970). Elastohydrodynamic squeeze films between two cylinders in normal approach. Trans. ASME J. Lub. Techn., Apr. 1970, 292-302.

Hicks, J.H. (1953). The mechanics of the foot, I: the joints. J. Anat., 87, 345-357.

Higginson, G.R. (1966). The theoretical effects of elastic deformation of the bearing liner on journal bearing performance. Proc. Instn. Mech. Engrs., 180 Pt 3B, 31-38.

Higginson, G.R. and Norman, R. (1974a). The lubrication of porous elastic solids with reference to the functioning of human joints. J. Mech. Eng. Sci., 16, 250-257.

Higginson, G.R. and Norman, R. (1974b). A model investigation of squeeze-film lubrication in animal joints. Phys. Med. Biol., 19, 785-792.

Higginson, G.R., Litchfield, M.R. and Snaith, J. (1976). Load displacement-time characteristics of articular cartilage. Int. J. Mech. Sci., 18, 481-486,

Higginson, G.R. (1978). Elastohydrodynamic lubrication in human joints. Engng. in Med., 7, 35-41.

Higginson, G.R. (1978a). Squeeze films between compliant solids, Wear, 46, 387-395.

Higginson, G.R. and Snaith, J.E. (1979). The mechanical stiffness of articular cartilage in confined oscillating compression. Engng. in Med., 8, 11-14.

Hirano, F. and Murakami, T. (1975). Photoelastic study of elasto-hydrodynamic contact condition in reciprocating motion. BHRA Fluid Engineering, 7th International Conference on Fluid Sealing, (C4-51)-(C4-70).

Hooke, C.J. and O'Donoghue, J.P. (1972). Elastohydrodynamic lubrication of soft highly deformed contacts. J. Mech. Eng. Sci., 14, 34-48.

Hori, R.Y. and Mockros, L.F. (1976). Indentation tests of human articular cartilage. J. Biomechanics, 9, 259-268.

Hornbeck, R.W. (1975). Numerical methods. Quantum Publishers Inc., New York.

Huskinsson, E.C., Dieppe, P.A., Tucker, A.K. and Cannell, L.B. (1979). Another look at osteoarthritis. Annals. Rheum. Diseases, 38, 423-428.

Ingelmark, B.E. and Ekholm, R. (1948). A study in variations in the thickness of articular cartilage in association with rest and periodic load. Acta. Soc. Med. Upsal., 53, 61-74.

Jacob, H.A.C., Huggler, A.H., Dietschi, C. and Schreiber, A. (1976). Mechanical function of subchondral bone as experimentally determined on the acetabulum of the human pelvis. J. Biomechanics, 9, 625-627.

Jamison, W.E., Lee, C.C. and Kauzlarich, J.J. (1978). Elasticity effects on the lubrication of point contacts. ASLE Trans., 21, 299-306.

Johnson, G.R., Dowson, D. and Wright, V. (1977). The elastic behaviour of articular cartilage under sinusoidally varying compressive stress. Int. J. Mech. Sci., 19, 301-308.

Johnson, K.L., Greenwood, J.A. and Poon, S.Y. (1972). A simple theory of asperity contact in elastohydrodynamic lubrication. Wear, 19, 91-108.

Jones, E.S. (1934). Joint Lubrication. The Lancet, 1426-1427.

Jones, E.S. (1936). Joint Lubrication. The Lancet, 1043-1044.

Kempson, G.E., Freeman, M.A.R. and Swanson, S.A.V. (1968). Tensile properties of articular cartilage. Nature, 220, 1127-1128.

Kempson, G.E., Spivey, C.J., Swanson, S.A.V. and Freeman, M.A.R. (1971). Patterns of cartilage stiffness on normal and degenerate human femoral heads. J. Biomechanics, 4, 597-609.

Kempson, G.E., Muir, H., Pollard, C. and Tuke, M. (1973). The tensile properties of the cartilage of human femoral condyles related to the content of collagen and glycosaminoglycans. Biochimica et Biophysica Acta, 297. 456-472.

Kempson, G.E., Freeman, M.A.R. and Tuke, M.A. (1975). Engineering considerations in the design of an ankle joint. Biomed. Engng., 166-175.

Kline, S.J. and McClintock, F.A. (1953). Describing uncertainties in single-sample experiments. Mech. Engrng., 3-8.

Lai, W.M., Kuei, S.C. and Mow, V.C. (1977). Computation of stress relaxation function and apparent viscosity from dynamic data of synovial fluids. Biorheology, 14, 229-236.

Lai, W.M., Kuei, S.C. and Mow, V.C. (1978). Rheological equations for synovial fluids. J. Biomech. Eng., 100, 169-186.

Lambert, J.D. (1973). Computational methods in ordinary differential equations. John Wiley and Sons Ltd., London.

Lambert, K.L. (1971). The weight-bearing function of the fibula. J. Bone and Jt. Surgery, 53-A, 507-513.

Lewis, P.R. and McCutchen, C.W. (1959). Sponge-hydrostatic and weeping bearings. Nature, 184, 1284-1285.

Ling, F.F. (1974). A new model of articular cartilage in human joints. J. Lubr. Tech., 96, 449-454.

Linn, F.C. and Sokoloff, L. (1965). Movement and composition of interstitial fluid of cartilage. Arth. & Rheum., 8, 481-494.

Linn, F.C. (1967). Lubrication of animal joints I: the arthrotripsometer. J. Bone and Jt. Surg., 49-A, 1079-1098.

Linn, F.C. (1968). Lubrication of animal joints II: the mechanism. J. Biomechanics, 1, 193-205.

Linn, F.C. and Radin, E.L. (1968). Lubrication of animals joints, III. The effect of certain chemical alterations of the cartilage and lubricant. Arth. & Rheum., 11, 674-682.

Little, T., Freeman, M.A.R. and Swanson, S.A.V. (1969). Experiments on friction in the human hip joint. Lubrication and wear in joints, Edited by V. Wright, Sector, London, 110-116.

Longfield, M.D., Dowson, D., Walker, P.S. and Wright, V. (1969). Boosted lubrication of human joints by fluid enrichment and entrapment. Bio-medical Eng., 4, 517-522.

Mansour, J.M. and Mow, V.C. (1976). The permeability of articular cartilage under compressive strain and at high pressures. J. Bone Jt. Surg., 58A, 509-516.

Mansour, J.M. and Mow, V.C. (1977). On the natural lubrication of synovial joints: normal and degenerate. J. Lubr. Tech., 99, 163-173.

Maquet, P.G., Van De Berg, A.J. and Simonet, J.C. (1975). Femorotibial weight-bearing areas. J. Bone Jt. Surg., 57A, 766-771.

Marnell, P. and White, R.K. (1980). Quantitative analysis of joint lubrication. Wear, 61, 203-208.

Maroudas, A. (1967). Hyaluronic acid films. Proc. Instn. Mech. Engrs., 181, (3F), 122-124.

Maroudas, A. and Bullough, P. (1968). Permeability of articular cartilage. Nature, 219, 1260-1261.

Maroudas, A., Bullough, P., Swanson, S.A.V. and Freeman, M.A.R. (1968). The permeability of articular cartilage. J. Bone Jt. Surg., 50B, 166-177.

Maroudas, A. (1969). Studies on the formation of hyaluronic acid films. Lubrication and wear in joints, Edited by V. Wright, Sector, London, 124-133.

Maroudas, A. (1979). Physico-chemical properties of articular cartilage. Adult articular cartilage, edited by M.A.R. Freeman, Pitman Medical, London 215-290.

McCall, J. (1969). Load deformation response of the microstructure of articular cartilage. Lubrication and wear in joints, Edited by V. Wright, Sector, London, 39-48.

McCutchen, C.W. (1962). The frictional properties of animal joints, Wear, 5, 1-17.

McCutchen, C.W. (1966). Boundary lubrication by synovial fluid: demonstration and possible osmotic explanation. Fed. Proc., 25, 1061-1068.

McCutchen, C.W. (1967). Physiological lubrication. Proc. Inst. Mech. Engrs., 181, (3F), 55-62.

McCutchen, C.W. (1969). More on weeping lubrication experiments with hydron, a microporous polyhydroxyalkylacrylic ester resin. Lubrication and wear in joints, Edited by V. Wright, Sector, London, 117-123.

McCutchen, C.W. (1978). Lubrication in joints. The joints and synovial fluid, Edited by L. Sokoloff, Academic Press, New York, 437-482.

Medley, J.B., Pilliar, R.M., Wong, E.W. and Strong, A.B. (1980). Hydrophilic polyurathane elastomers for hemiarthroplasty: a preliminary in vitro wear study. Eng. in Med., 9, 59-65.

Meijers, P. (1968). The contact problem of a rigid cylinder on an elastic layer . Appl. Sci. Res., 18, 353-383.

Modest, M.F. and Tichy, J.A. (1979). The slider bearing with small superimposed normal oscillations, including the effect of fluid inertia, ASLE Trans., 22, 358-360.

Moore, D.F. (1980). Friction and wear in rubbers and tyres. Wear, 61, 273-282.

Morris, J.M. (1977), Biomechanics of the foot and ankle. Clin. Orthop. Rel. Res., 122, 10-17.

Mow, M.C. and Ling, F.F. (1969). On weeping lubrication theory. Z. Angew Math. Phys., 20, 156-166.

Mow, V.C. and Mansour, J.M. (1977). The nonlinear interaction between cartilage deformation and interstitial fluid flow. J. Biomechanics, 10, 31-39.

Mow, V.C., Kuei, S.C., Lai, W.M. and Armstrong, C.G. (1980). Biphasic creep and stress relaxation of articular cartilage in compression: theory and experiment. J. Biomech. Eng., 102, 73-84.

Murray, M.P., Drought, A.B. and Kory, R.C., (1964). Walking patterns of normal men. J. Bone and Jt. Surg., 46-A, 335-360.

Negami, S. (1964). Dynamic mechanical properties of synovial fluid. M.Sc. thesis, Lehigh Univ., Penn., U.S.A.

Oberlander, W. (1978). On biomechanics of joints. The influence of functional cartilage swelling on the congruity of regularly curved joints. J. Biomechanics, 11, 151-153.

Ogston, A.G. and Stanier, J.E. (1953). The physiological function and hyaluronic acid in synovial fluid; viscous, elastic and lubricant properties. J. Physiol., 119, 244-252.

O'Kelly, J. (1977). A study of the friction of natural and artificial hip joints with an interpretation of the modes of lubrication, Ph.D. thesis, University of Leeds.

O'Kelly, J., Unsworth, A., Dowson, D., Hall, D.A. and Wright, V. (1978). A study of the role of synovial fluid and its constituents in the friction and lubrication of hip joints. Engng. in Med., 7, 73-83.

Pagowski, S., Munro, M. and Piekarski, K. (1976). A concept of lubrication in finger joints. J. of Appl. Physics, 47, 2156-2160.

Palfrey, A.J. and White, J.B. (1948). The viscosity of synovial fluid during oscillatory movement. Biorheology, 5, 189-198.

Pappas, M., Beuchel, F.F. and De Palma, A.F. (1976). Cylindrical total ankle joint replacement. Clin. Orthop. Rel. Res., 118, 82-92.

Parlasca, R., Shoji, H. and D'Ambrosia, R.D. (1979). Effects of ligamentous injury on ankle and subtalar joints: a kinematic study. Clin. Orthop. Rel. Res., 140, 266-272.

Parsons, J.R. and Black, J. (1977). The viscoelastic shear behaviour of normal rabbit articular cartilage. J. Biomechanics, 10. 21-29.

Parsons, J.R. and Black, J. (1979). Mechanical behaviour of articular cartilage: quantitative changes with alteration of ionic environment. J. Biomechanics, 12, 765-773.

Paul, J.P. (1967). Forces transmitted by joints in the human body. Proc. Instn. Mech.Engrs., 181,(3F), 8-15.

Paul, J.P. (1976). Loading on normal hip and knee joints and on joint replacements. Engineering in medicine 2: advances in artificial hip and knee joint technology, D. Hohmann, R. Thull and F. Hein, Springer-Verlag, Berlin, 53-70.

Peters, T.J. and Smillie, I.S. (1972). Studies on the chemical composition of the menisci of the knee joint with special reference to the horizontal cleavage lesion. Clin. Orthop., 86, 245-252.

Piotrowski, G. (1975). Non-Newtonian lubrication of synovial joints. Ph.D. thesis, Case Western Reserve, Cleveland, Ohio.

Pugh, J.W., Rose, R.M. and Radin, E.L. (1973a). Elastic and viscoelastic properties of trabecular bone: dependence on structure. J. Biomechanics, 6, 475-485.

Pugh, J.W., Rose, R.M. and Radin, E.L. (1973b). A structural model for the mechanical behaviour of trabecular bone. J. Biomechanics, 6, 657-670.

Radin, E.L. and Paul, I.L. (1969). Failure of synovial fluid to cushion. Nature, 222, 999-1000.

Radin, E.L. and Paul, I.L. (1970a). Does cartilage compliance reduce skeletal impact loads? The relative force-attenuating properties of articular cartilage, synovial fluid, peri-articular soft tissues and bone. Arth. & Rheum., 13, 139-144.

Radin, E.L., Paul, I.L. and Lowy, M. (1970b). A comparison of the dynamic force transmitting properties of subchondral bone and articular cartilage. J. Bone Jt. Surg., 52A, 444-456.

Radin, E.L., Paul, I.L. and Pollock, D. (1970c). Animal joint behaviour under excessive loading. Nature, 226, 554-555.

Radin, E.L., Swann, D.A. and Weisser, P.A. (1970d). Separation of a hyaluronate-free lubricating fraction from synovial fluid. Nature, 228, 377-378.

Radin, E.L. and Paul, I.L. (1971a). Importance of bone in sparing articular cartilage from impact. Clin Orthop., 78, 342-344.

Radin, E.L. and Paul, I.L. (1971b). Response of joints to impact loading. Arth. & Rheum., 14, 356-362.

Radin, E.L. and Paul, I.L. (1972). A consolidated concept of joint lubrication. J. Bone and Jt. Surg., 54-A, 607-616.

Radin, E.L., Parker, H.G., Pugh, J.W., Steinburg, R.S., Paul, I.L. and Rose, R.M. (1973). Response of joints to impact loading III. Relationships between trabecular microfractures and cartilage degeneration. J. Biomechanics, 6, 51-57.

Radin, E.L. (1974). Nature of mechanical factors causing degeneration of joints. Proc. Hip Soc., ch4, 76-80.

Rastegar, J., Miller, N. and Barmada, R. (1980). An apparatus for measuring the load displacement and load-dependent kinematic characteristics of articulating joints - application to the human ankle joint. Trans. ASME J. Biomech. Engng., 102, 208-213.

Raux, P., Townsend, P.R., Miegel, R., Rose, R.M. and Radin, E.L. (1975). Trabecular architecture of the human patella. J. Biomechanics, 8, 1-7.

Rhode, S.M., Whicker, D. and Browns, A.L. (1976). Dynamic analysis of elastohydrodynamic squeeze films. J. Lubr. Tech., 98, 401-408.

Rhode, S.M., Whicker, D. and Booker, J.F. (1979). Elastohydrodynamic squeeze films: effects of viscoelasticity and fluctuating load. J. Lubr. Tech., 101, 1, 74-80.

Roberts, A.D. and Swales, P.D. (1969). The elastohydrodynamic lubrication of a highly elastic cylindrical surface. Brit. J. Appl. Phys. (J. Phys. D), 2, 1317-1326,

Roberts, A.D. (1971). Role of electrical repulsive forces in synovial fluid. Nature, 231, 434-436.

Ruddy, B.L., Dowson, D., Economou, P.N. and Baker, A.J.S. (1979). Piston ring lubrication - Part III. The influence of ring dynamics and ring twist. Energy Conservation Through Fluid Film Technology: Frontiers in Research and Design, edited by Rhode, S.M., Wilcock, D.F. and Cheng, H.S., ASME Publications, 23-52.

Ruskell, L.E.C. (1980). A rapidly converging theoretical solution of the elastohydrodynamic problem for rectangular rubber seals. J. Mech. Eng. Sci., 22, 9-16.

Rybicki, E.F., Strenkowski, J.S., Tamm, M.A. and Glaeser, W.A. (1978). A finite element model for compliant bearing lubrication using a minimization algorithm. Wear, 47, 279-292.

Rybicki, E.F., Glaeser, W.A., Strenkowski, J.S. and Tamm, M.A. (1979). Effects of cartilage stiffness and viscosity on a non-porous compliant bearing lubrication model for living joints. J. Biomechanics, 12, 403-403.

Sammarco, G.J., Burstein, A.H. and Frankel, V.H. (1973). Biomechanics of the ankle: a kinematic study. Proc. Am. Orthop. Foot Soc., 4, 75-97.

Sayles, R.S., Thomas, T.R., Sanderson, J., Haslock, I. and Unsworth, A. (1979). Measurement of the surface microgeometry of articular cartilage. J. Biomechanics, 12, 257-267.

Scherrer, P.K. and Hillberry, B.M. (1979). Piecewise mathematical representation of articular surfaces. J. Biomechanics, 12, 301-311.

Seedhom, B.B., Dowson, D. and Wright, V. (1974). The load-bearing function of the menisci: a preliminary study. The knee joint, edited by O.S. Ingwersen, B. Van Linge, Th. J.G. Van Rens, G.E. Rosingh, B.E.E.E.M.J. Veraart and D. Le Vay, Excerpta Medica, Amsterdam and American Elsevier, New York, 37-42.

Seedhom, B.B. (1979). Transmission of the load in the knee joint with special reference to the role of the menisci. Part I: anatomy, analysis and apparatus. Engng. in Med., 8, 207-219.

Seedhom, B.B. and Hargreaves, D.J. (1979). Transmission of the load in the knee joint with special reference to the role of the menisci. Part II: experimental results, discussion and conclusions. Engng. in Med., 8, 220-228.

Seireg, A. and Arvikar, R.J. (1975). The prediction of muscular load sharing and joint forces in the lower extremities during walking. J. Biomechanics, 8, 89-102.

Selby, S.M. (1974) C.R.C. Standard Mathematical Tables, edited by S.M. Selbey, CRC Press, Cleveland, Ohio.

Shampine, L.F. (1980). What everyone solving differential equations numerically should know. Computation Techniques for Ordinary Differential Equations, edited by Gladwell, I. and Sayers, D.K., Academic Press, London.

Shrive, N.G., O'Connor, J.J. and Goodfellow, J.W. (1978). Load-bearing in the knee joint. Clin. Orthop., 131, 279-287.

Stauffer, R.N. (1976). Total ankle joint replacement as an alternative to arthrodesis. Geriatrics, 79-85.

Stauffer, R.N., Chao, E.Y.S. and Brewster, R.C. (1977). Force and motion analysis of the normal, diseased and prosthetic ankle joint. Clin. Orthop. Rel. Res., 127, 189-196.

Swales, P.D., Dowson, D. and Latham, J.L. (1972). Theoretical and experimental observations of the behaviour of soft elastic materials under elastohydrodynamic conditions. Instn. Mech. Engrs., C4/72, 22-28.

Swann, D.A., Radin, E.L., Nazimiec, M., Weisser, P.A., Curran, N. and Lewinnek, G. (1974). Role of hyaluronic acid in joint lubrication. Annals. Rheum. Diseases, 33, 318-326.

Swann, D. (1978). Macromoleculaes of synovial fluid. The joints and synovial fluid. Edited by L. Sokoloff, 407-435.

Swanson, S.A.V. and Freeman, M.A.R. (1966). Is bone hydraulically strenghthened? Med. & Biol. Engng., 4, 433-438.

Swanson, S.A.V. and Freeman, M.A.R. (1970). The mechanics of synovial joints. Modern Trends in Biomechanics I, edited by D.C. Simpson, Ch.II, Butterworths, London.

Swanson, S.A.V. (1979). Friction, wear and lubrication. Adult articular cartilage, edited by M.A.R. Freeman, Pitman, Medical, London, 415-460.

Tandon, P.H. and Jaggi, S. (1979). A polar model for synovial fluid with reference to human joints. Int. J. Mech. Sci., 21, 161-169.

Tanner, R.I. (1966). An alternative mechanism for the lubrication of synovial joints. Phys. Med. Biol., 11, 119-127.

Terayama, K., Takeda, T. and Nakada, K. (1980). Joint space of the human knee and hip joint under a static load. Engng. in Med., 9, 67-74.

Thomas, T.R., Sayles, R.S. and Haslock, I. (1980). Human joint performance and the roughness of cartilage. J. Biomech. Eng., 102, 50-56.

Timoshenko, S. and Goodier, J.N. (1951). Theory of Elasticity, McGraw-Hill, New York, 375.

Torzilli, P.A. (1976). The lubrication of human joints; a review. C.R.C. Handbook of Engineering in Medicine and Biology, 225-251.

Townsend, P.R., Rose, R.M. and Radin, E.L. (1975). Buckling studies of single human trabeculae. J. Biomechanics, 8, 199-201.

Uezaki, N., Kobayashi, A. and Matsushige, K. (1979). The visco-elastic properties of the human semilinar cartilage. J. Biomechanics, 12, 65-73.

Unsworth, A. (1972). A study of some physical and tribological characteristics of human joints. Ph.D. thesis, University of Leeds.

Unsworth, A., Dowson, D. and Wright, V. (1975). The frictional behaviour of human synovial joints - Parts I and II. Trans. ASME J. Lub. Techn., 97, 369-382.

Unsworth, A., Roberts, B. and Thompson, J.C. (1980). The application of soft layer lubrication to hip prostheses. British Orthop. Res. Soc. Meeting, Edinburgh, Scotland.

Varnam, C.J. and Hooke, C.J. (1977). Non-Hertzian elastohydro-dynamic contacts: an experimental investigation. J. Mech. Eng. Sci., 19, 189-192.

Walker, P.S., Dowson, D., Longfield, M.D. and Wright, V. ((1968). Boosted lubrication in synovial joints by fluid entrapment and enrichment. Ann. Rheum.Dis., 27, 512-520.

Walker, P.S.,Sikorski, J., Dowson, D., Longfield, M.D. Wright, V. and Buckley, T. (1969). Behaviour of synovial fluid surfaces of articular cartilage - a scanning electron microscope study. Ann Rheum. Dis., 28, 1-14.

Walker, P.S., Unsworth, A., Dowson, D., Sikorski, J. and Wright, V. (1970). Mode of aggregation of hyaluronic acid protein complex on the surface of articular cartilage. Ann. Rheum. Dis., 29, 591-602.

Walker, P.S., and Gold, B.L. (1973). Comparison of the bearing performance of normal and artificial human joints. J. Lubr. Tech., 95, 333-341

Walker, P.S. and Erkman, M.J. (1975). The role of the menisci in force transmission across the knee. Clin. Orthop., 109, 184-192.

Walker, T.W., Graham, J.D. and Mills, R.H. (1976). Changes in the mechanical behaviour of the human femoral head associated with arthritic pathologies. J. Biomechanics, 9, 615-624.

Weightman, B., Chappell, D.J. and Jenkins, E.A. (1978). A second study of tensile fatigue properties of human articular cartilage. Annals Rheu. Diseases, 37, 58-63.

Weightman, B. and Kempson, G.E. (1979), Load carriage. Adult articular cartilage, Edited by M.A.R. Freeman, Pitman Medical, London, 291-331.

Wilkins, J. (1968). Proteolytic destruction of synovial boundary lubrication. Nature, 219, 1050-1051.

Woo, S L.Y., Akeson, W.H. and Jemmott, G.F. (1976). Measurements of nonhomogeneous directional mechanical properties of articular cartilage in tension. J.Biomechanics, 9, 785-791.

Woo, S.L.Y., Lubock, P., Gomez, M.A., Jemmott, G.F., Kuei, S.C. and Akeson, W.H. (1979). Large deformation nonhomogeneous and directional properties of articular cartilage in uniaxial tension. J. Biomechanics, 12, 437-446.

Wright, V. and Johns, R.J. (1960). Physical factors concerned with the stiffness of normal and diseased joints. Bull. J. Hopkins Hosp., 106, 215-231.

Wright, V., Dowson, D. and Kerr, J. (1973). The structure of joints. International Review of Connective Tissue Research, 6, 105-125.

Wright, V. and Medley, J.B. (in the press). The mechanics of normal synovial joints. Animal Models in Physiology and Pathology: The Articular System, Edited by Dr. J.T. Dingle, Dr. N.C. Phillips and Dr. D.P. Page Thomas, Elsevier-North Holland Biomedical Press.

APPENDIX A

THE COMPUTER PROGRAM FOR CURVE FITTING THE SURFACE PROFILE DATA

An outline of the curve fitting procedure for the ankle joint surfaces was described in Section 3.5 of Chapter 3. The procedure requires the mathematical development of a circle fitting method to use on the data points from each of the profiles. The mathematical development of a circle fitting method was accomplished by Dr. R.D. Pollard (Department of Electrical and Electronics Engineering, Leeds University) and computer coding for it was written by Dr. D.E. Newland (Department of Mechanical Engineering, Leeds University). The present Appendix summarizes their work and incorporates it into a computer program written specifically for the ankle joint surfaces.

The graphical output from the Talycontor was digitized with respect to an arbitrarily selected origin. Consider N data points and let (x_i, y_i) be the co-ordinates of the i^{th} data point. It was useful to apply the following linear transformation to the data.

$$x_i' = x_i - \frac{\Sigma x_i}{N} \qquad (A.1)$$

$$y_i' = y_i - \frac{\Sigma y_i}{N} \qquad (A.2)$$

Note that

$$\Sigma x_i' = \Sigma x_i - N\frac{\Sigma x_i}{N} = 0 \qquad (A.3)$$

and

$$\Sigma y_i' = \Sigma y_i - N\frac{\Sigma y_i}{N} = 0 \qquad (A.4)$$

The surface profile data obtained from the Talycontor included small amounts of error in both x and y co-ordinates. Furthermore, the radius of the circle of best fit was the quantity required, thus a suitable least squares criterion was

$$E = \Sigma\ [(x_i' - A')^2 + (y_i' - B')^2 - R^2]^2 \qquad (A.5)$$

where (A', B') are the centre point co-ordinates in terms of the x' - y' co-ordinate system and R was the radius for the circle of best fit. It was convenient to find eventually the circle of best fit in terms of the original x - y co-ordinate system. This was accomplished using the following reverse transformations.

$$A = A' + \frac{\Sigma x_i}{N} \qquad (A.7)$$

$$B = B' + \frac{\Sigma y_i}{N} \qquad (A.8)$$

where (A, B) are the centre point co-ordinates in terms of the x - y co-ordinate system for the circle of best fit. The various geometrical terms are shown in Figure A.1.

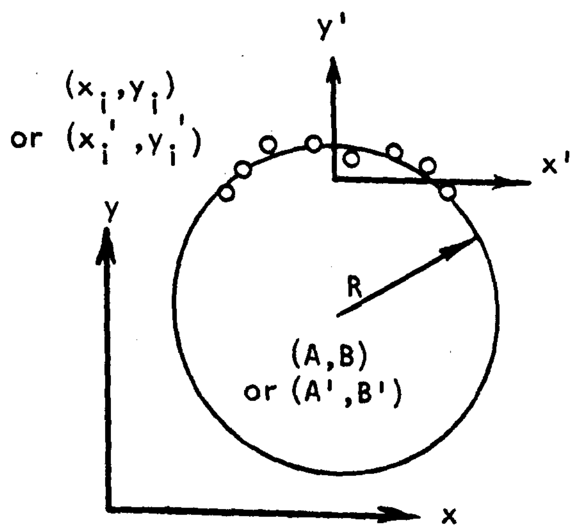

Figure A.1 : The geometrical terms involved in the circle fitting method.

The standard least square derivation may proceed as follows:

To minimize E set

$$\frac{\partial E}{\partial R} = \frac{\partial E}{\partial A'} = \frac{\partial E}{\partial B'} = 0$$

Equation A.5 implies

$$\Sigma z_i = 0 \qquad (A.9)$$

$$\Sigma z_i x_i' - A'\Sigma z_i = 0 \qquad (A.10)$$

$$\Sigma z_i y_i' - B\Sigma z_i = 0 \qquad (A.11)$$

where $z_i = (x_i' - A')^2 + (y_i' - B')^2 - R^2$

Substituting equation (A.9) into equations (A.10) and (A.11) yields

$$\Sigma z_i x_i' = 0 \qquad (A.12)$$

and $\Sigma z_i y_i' = 0$ (A.13)

Substituting equations (A.3) and (A.4) into the expanded form of equations (A.9), (A.12) and (A.13) yields

$$R^2 = (A')^2 + (B')^2 + \frac{1}{N}\Sigma\,[(x_i')^2 + (y_i')^2] \qquad (A.14)$$

$$2A'\,\Sigma(x_i')^2 + 2B'\,\Sigma x_i'y_i' = \Sigma[(x_i')^3 + x_i'(y_i')^2] \qquad (A.15)$$

$$2A'\,\Sigma x_i y_i + 2B'\,\Sigma(y_i')^2 = \Sigma[(x_i')^2\,y_i' + (y_i')^3] \qquad (A.16)$$

Equations (A.15) and (A.16) can be solved for A' and B' as follows:

$$A' = \frac{\Sigma(y_i')^2\Sigma[(x_i')^3 + x_i'(y_i')^2] - \Sigma x_i'y_i'\Sigma[(x_i')^2 y_i' + (y_i')^3]}{2[\Sigma(x_i')^2\,\Sigma(y_i')^2 - \Sigma x_i'y_i'\,\Sigma x_i'y_i']} \qquad (A.17)$$

$$B' = \frac{\Sigma(x_i')^2\Sigma[(x_i')^2 y_i' + (y_i')^3] - \Sigma x_i'y_i'\Sigma[(x_i')^3 + x_i'(y_i')^2]}{2[\Sigma(x_i')^2\,\Sigma(y_i')^2 - \Sigma x_i'y_i'\,\Sigma x_i'y_i']} \qquad (A.18)$$

Equations (A.1), (A.2), (A.7),(A.8), (A.14), (A.17) and (A.18) constitute the required mathematical method yielding A, B and R for the circle of best fit.

A computer program was written to find the circle of best fit. A listing of the program and sample output are included at the end of this Appendix. The computer program has the following features specifically suited to the ankle joint measurements and the curve fitting procedure described in Section 3.5.

(i) A spherically tipped pin was fabricated for use on the cartilage surfaces as described in Section 3.4. For the convex talus surfaces, the radius of the circle of best fit, R, was found for the output from the Talycontor. However, the actual radius of curvature for the surface was,

$$R_{talus} = R - R_{pin} \tag{A.20}$$

For the concave tibia surfaces the actual radius of curvature was,

$$R_{tibia} = R + R_{pin} \tag{A.21}$$

The geometrical basis for these relationships is demonstrated by exaggerating the pin size as show in Figure A.2.

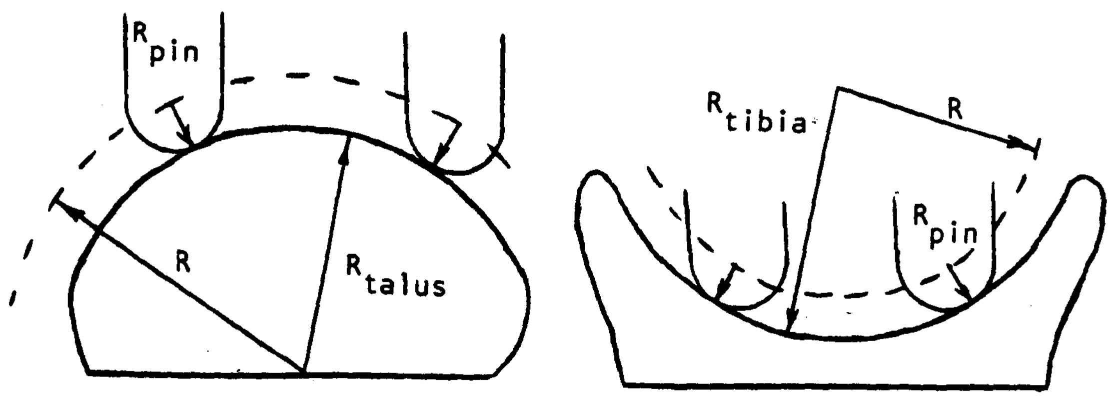

Figure A.2 : The geometry of the pin tip correction for talus and tibia surfaces.

(ii) The required input values were defined in the computer coding (format statements 901-909) and again at the beginning of the output data file. Those values which remained constant throughout the present study were specified in the program rather than being read from the input data file. All the input values were printed at the beginning of the output data file to permit identification and checking of each run. A specified number of data points at the beginning and the end of the input data sequence could be omitted from the circle fit calculation. If the "% DIFF" value (defined and listed in the output file) for one of the points used in the circle fit exceeded the value of "PREC" specified in the input, a message (format statement 801) was printed at the end of the output file. This was an important part of the curve fitting procedure described in Section 3.5.

(iii) The computer program as listed gave a multi-coloured graphical output. The graph included in this Appendix is the same as the one generated by the listed program, except for the lack of colour. The data points excluded from the circle fit were adjusted for the pin tip radius as if the calculated radis of curvature applied to them and they were plotted in the output graph. This meant that they were not completely accurate but this error was sufficiently small to ensure that the profiles of the joint surface outside the fitted region were as shown in the output graph.

```
C
C   LEAST SQUARES CURVE FIT FOR ANKLE PROFILES
C
C-----------------------------------------------------------------------
C
C
      DIMENSION X(100),Y(100),RD(100),E(100),XI(100),YI(100)
      DIMENSION XC(100),YC(100)
C-----------------------------------
C
C          INPUT
C
C-----------------------------------
      READ(5,*) NT,NS,NF
      READ(5,*) K
      READ(5,*) (YC(I),I=1,NT)
      DO 401 I=1,100
      XC(I)=20.*(I-1)
 401  CONTINUE
      RP=.79375
      MAGX=20
      MAGY=20
      CMAX=23.
      PREC=.25
C-----------------------------------
C          CHECK
C-----------------------------------
  98  FORMAT(' ******  I N P U T   D A T A  ******'///)
 100  FORMAT(5X,'NO.',6X,'X',12X,'Y'/)
 101  FORMAT(' ',I6,3X,E10.3,3X,E10.3)
 102  FORMAT(' ',///)
C
```

```
C
 901  FORMAT(' NT (NUMBER OF DATA POINTS) .................. ',I8)
 902  FORMAT(' NS (ARRAY POSITION FOR IST LS FIT DATA PT) ... ',I8)
 903  FORMAT(' NF (ARRAY POSITION FOR LAST LS FIT DATA PT) .. ',I8)
 904  FORMAT(' K (EQUALS 0 OR 1 FOR TALUS OF TIBIA) ........ ',I8)
 905  FORMAT(' RP (PIN TIP RADIUS) ......................... ',E14.7)
 906  FORMAT(' MAGX (MAGNIFICATION OF XC) .................. ',I8)
 907  FORMAT(' MAGY (MAGNIFICATION OF YC) .................. ',I8)
 908  FORMAT(' CMAX (MAXIMUM RADIUS ALLOWED IN PLOTS) ....... ',E14.7)
 909  FORMAT(' PREC (% RANGE FOR INCLUDING DATA IN LS FIT) .. ',E14.7)
C
C
 606  FORMAT(//' NOTES:'/)
 103  FORMAT(' (1.) XC IS THE X CO-ORDINATE')
 603  FORMAT(' (2.) YC IS THE Y CO-ORDINATE')
 104  FORMAT(' (3.) XC AND YC IN EXPANDED FORM MUST BE ')
 804  FORMAT('      IN SAME UNITS AS RP.'//)
 106  FORMAT(//' **** THE FOLLOWING POINTS ARE TRANSFORMED AND ',
     +        'PLOTTED ****'//)
      WRITE(6,98)
      WRITE(6,901) NT
      WRITE(6,902) NS
      WRITE(6,903) NF
```

```
      WRITE(6,904) K
      WRITE(6,905) RP
      WRITE(6,906) MAGX
      WRITE(6,907) MAGY
      WRITE(6,908) CMAX
      WRITE(6,909) PREC
      WRITE(6,606)
      WRITE(6,103)
      WRITE(6,603)
      WRITE(6,104)
      WRITE(6,804)
      WRITE(6,106)
      WRITE(6,100)
      DO 1 I=1,NT
      WRITE(6,101)I,XC(I),YC(I)
    1 CONTINUE
      WRITE(6,102)
C-----------------------------------
C
C            PREP
C
C-----------------------------------
      DO 10 I=1,NT
      XC(I)=XC(I)/MAGX
      YC(I)=YC(I)/MAGY
   10 CONTINUE
      N=0
      DO 50 I=NS,NF
      N=N+1
      X(N)=XC(I)
      Y(N)=YC(I)
   50 CONTINUE
C-----------------------------------
C
C            LEAST
C            (SUPPLIED BY DR. D.E. NEWLAND)
C
C-----------------------------------
      SIGX=0.
      SIGY=0.
      DO 2 I=1,N
      SIGX=SIGX+X(I)
      SIGY=SIGY+Y(I)
    2 CONTINUE
      AVX=SIGX/N
      AVY=SIGY/N
      DO 3 I=1,N
      XI(I)=X(I)-AVX
      YI(I)=Y(I)-AVY
    3 CONTINUE
      SIGSQ=0.
      DO 4 I=1,N
      SIGSQ=SIGSQ+XI(I)**2+YI(I)**2
    4 CONTINUE
      CI=SIGSQ/N
```

```
      DATA T1/0./,T2/0./,T2/0./,T4/0./,T5/0./
      DO 5 I=1,N
      T1=T1+YI(I)**2
      T2=T2+XI(I)**3+XI(I)*YI(I)**2
      T3=T3+XI(I)*YI(I)
      T4=T4+XI(I)**2*YI(I)+YI(I)**3
      T5=T5+XI(I)**2
    5 CONTINUE
      DENOM=2.*(T5*T1-T3*T3)
      AI=(T1*T2-T3*T4)/DENOM
      BI=(T5*T4-T3*T2)/DENOM
      A=AI+AVX
      B=BI+AVY
      R=SQRT(CI+AI*AI+BI*BI)
      ERR=0.
      KD=0
      DO 11 I=1,N
      XR=X(I)
      YR=Y(I)
      RD(I)=SQRT((XR-A)**2+(YR-B)**2)
      E(I)=100.*(RD(I)-R)/R
      EC=ABS(E(I))
      IF(EC.GT.PREC) KD=1
      ERR=ERR+(RD(I)-R)**2
   11 CONTINUE
      STDERR=SQRT(ERR/(N-3))
      PERERR=300.*STDERR/R
      RSQ=R*R
```

```
C-----------------------------------------
C
C          ADJUST
C
C-----------------------------------------
      IF(K.EQ.0) RA=R-RP
      IF(K.EQ.1) RA=R+RP
C-----------------------------------------
C
C          OUTPUT
C
C-----------------------------------------
 196  FORMAT(' CONCAVE TIBIA SURFACE PROFILE MEASURED'///)
 197  FORMAT(' CONVEX TALUS SURFACE PROFILE MEASURED'///)
 198  FORMAT(' ******  O U T P U T   D A T A  ******'///)
 200  FORMAT(' ( X - ',E14.7,2X,') ** 2 + ( Y - ',E14.7,2X,') ** 2 = ',
     +       E14.7///)
 201  FORMAT(' SURFACE RADIUS =',E14.7,1X,
     +       '   WHEN ADJUSTED FOR PIN TIP RADIUS.'/)
 202  FORMAT(5X,'NO.',7X,'X-A',15X,'Y-B',14X,'RD',11X,'% DIFF'//)
 203  FORMAT(' ',I6,4(3X,E14.7))
 204  FORMAT(' R =',E14.7,2X,'WITH A STANDARD ERROR OF ',E10.3///)
 205  FORMAT(' AN ESTIMATE OF THE UNCERTAINTY IN THE RADIUS',
     +       ' EVALUATION =',E10.3,' %')
 206  FORMAT(' THE BEST FIT CIRCLE IS'/)
 207  FORMAT(' RD=SQRT((X-A)**2+(Y-B)**2)'/)
 208  FORMAT(' % DIFF=100.*(RD-R)/R'/)
```

```
209   FORMAT(' R = BEST FIT RADIUS'/)
210   FORMAT(' A = BEST FIT X CO-ORD FOR CENTRE'/)
211   FORMAT(' B = BEST FIT Y CO-ORD FOR CENTRE'///)
212   FORMAT(//' **** THE FOLLOWING POINTS ARE USED IN THE LS FIT ',
     +        '*****'//)
801   FORMAT(/' DATA IN LS FIT EXCEEDS PREC')
811   FORMAT(/'   WHERE % UNCERTAINTY = 300. * STANDARD ERROR / R'/)
      WRITE(6,198)
      IF(K.EQ.0) WRITE(6,197)
      IF(K.EQ.1) WRITE(6,196)
      WRITE(6,207)
      WRITE(6,208)
      WRITE(6,209)
      WRITE(6,210)
      WRITE(6,211)
      WRITE(6,212)
      WRITE(6,202)
      DO 12 I=1,N
      X(I)=X(I)-A
      Y(I)=Y(I)-B
      WRITE(6,203) I,X(I),Y(I),RD(I),E(I)
12    CONTINUE
      WRITE(6,102)
      WRITE(6,206)
      WRITE(6,200) A,B,RSQ
      WRITE(6,204) R,STDERR
      WRITE(6,201) RA
      WRITE(6,205) PERERR
      WRITE(6,811)
      IF(KO.EQ.1) WRITE(6,801)
```

```
C-----------------------------------
C
C           VISUAL
C
C-----------------------------------
C
C    WARNING ... IN PRESENT FORM GRAPHICS REQUIRES DIMENSIONS IN MM
C
      DO 51 I=1,NT
      XC(I)=XC(I)-A
      YC(I)=YC(I)-B
   51 CONTINUE
      DO 52 I=1,NT
      XR=XC(I)
      YR=YC(I)
      IF(XR.EQ.0.) GOTO 71
      THETA=ATAN(ABS(YR/XR))
      GOTO 72
   71 THETA=ASIN(1.)
   72 CONTINUE
      IF(K.EQ.1) GOTO 53
      IF(XR.LE.0.) XC(I)=XR+RP*COS(THETA)
      IF(XR.GT.0.) XC(I)=XR-RP*COS(THETA)
      YC(I)=YR-RP*SIN(THETA)
      GOTO 52
```

```
53    IF(XR.LE.0.) XC(I)=XR-RP*COS(THETA)
      IF(XR.GT.0.) XC(I)=XR+RP*COS(THETA)
      YC(I)=YR+RP*SIN(THETA)
52    CONTINUE
      CMAXN=-1.*CMAX
      CALL PAPER(1)
      CALL CTRFNT(1)
      CALL BLKPEN
      CALL PSPACE(0.,1.,0.,1.)
      CALL MAP(0.,1.,0.,1.)
      IF(K.EQ.0) CALL PLOTCS(.13,.3,'TALUS',5)
      IF(K.EQ.1) CALL PLOTCS(.13,.3,'TIBIA',5)
      CALL PLOTCS(.13,.275,'RADIUS =',8)
      CALL TYPENF(RA,2)
      CALL PLOTCS(.28,.275,'% UNCERTAINTY =',15)
      CALL TYPENF(PERERR,2)
      CALL PLOTCS(.13,.255,'(ALL DIMENSIONS IN MM)',23)
      CALL BLUPEN
      CALL PSPACE(.01,.51,.35,.6)
      CALL MAP(CMAXN,CMAX,0.,CMAX)
      CALL AXES
      CALL GRNPEN
      IF(NS.EQ.1) GOTO 61
      NSM=NS-1
      CALL PTPLOT(XC,YC,1,NSM,248)
      CALL PTPLOT(2.,3.,1,1,248)
61    CONTINUE
      CALL REDPEN
      CALL PTPLOT(XC,YC,NS,NF,227)
      CALL PTPLOT(2.,5.,1,1,227)
      CALL GRNPEN
      IF(NF.EQ.NT) GOTO 62
      NFP=NF+1
      CALL PTPLOT(XC,YC,NFP,NT,249)
      IF(NS.EQ.1) CALL PTPLOT(2.,3.,1,1,249)
62    CONTINUE
      CALL BLKPEN
      CALL POSITN(0.,0.)
      CALL CIRCLE(RA)
      CALL CIRCLE(RA)
      CALL BLKPEN
      CALL CTRSIZ(.8)
      IF((NS.EQ.1).AND.(NF.EQ.NT)) GOTO 86
      CALL PLOTCS(4.,3.,'NOT USED IN LS FIT',15)
86    CONTINUE
      CALL PLOTCS(4.,5.,'USED IN LS FIT',14)
      CALL PSPACE(0.,1.,0.,1.)
      CALL MAP(0.,1.,0.,1.)
      CALL CTRSIZ(.007)
      CALL PLOTCS(.08,.53,'POSTERIOR',9)
      CALL PLOTCS(.38,.58,'ANTERIOR',8)
      CALL GREND
C-------------------------------------------------------------------
      STOP
      END
```

Executive

```
FILE: J6        EXEC     A   LEEC

EXEC SETUP FORTRAN NAGF CCGHOST
FI 5 DISK &2 DATA
FI 6 DISK &3 DATA
LOAD &1(CLEAR
EXEC PLOTFILE &4
SET BLIP *
START
```

Input

```
FILE: XC        DATA     A   LEEDS UNIVERSITY VM/BSE 6.16

30 6 25
0
-53. -30.5 -11.8 3.4 16.8 28.4 39.8 49.1 57.3 64.8 70.4 75.2 79.
81.5 83. 83.5 83.5 82. 79. 74.8 69. 62.5 54.7 45. 34.4 21. 5.7
-12.5 -34.3 -63.0
```

Output

```
FILE: YC        DATA     A   LEEDS UNIVERSITY VM/ESE 6.16

NT (NUMBER OF DATA POINTS) ..................              30
NS (ARRAY POSITION FOR IST LS FIT DATA PT) ...              6
NF (ARRAY POSITION FOR LAST LS FIT DATA PT) ..             25
K (EQUALS 0 OR 1 FOR TALUS OR TIBIA) .........              0
RP (PIN TIP RADIUS) ..........................   0.7937500E+00
MAGX (MAGNIFICATION OF XC) ...................             20
MAGY (MAGNIFICATION OF YC) ...................             20
CMAX (MAXIMUM RADIUS ALLOWED IN PLOTS) .......   0.2800000E+02
PREC (X RANGE FOR INCLUDING DATA IN LS FIT) ..   0.2500000E+00

NOTES:

(1.) XC IS THE X CO-ORDINATE
(2.) YC IS THE Y CO-ORDINATE
(3.) XC AND YC IN EXPANDED FORM MUST BE
     IN SAME UNITS AS RP.



**** THE FOLLOWING POINTS ARE TRANSFORMED AND PLOTTED ****

      NO.         X             Y

       1     0.0            -0.530E+02
       2     0.200E+02      -0.305E+02
       3     0.400E+02      -0.119E+02
       4     0.600E+02       0.340E+01
       5     0.800E+02       0.169E+02
       6     0.100E+03       0.284E+02
       7     0.120E+03       0.393E+02
       8     0.140E+03       0.491E+02
       9     0.160E+03       0.573E+02
      10     0.180E+03       0.648E+02
      11     0.200E+03       0.704E+02
      12     0.220E+03       0.752E+02
      13     0.240E+03       0.790E+02
      14     0.260E+03       0.815E+02
      15     0.280E+03       0.830E+02
      16     0.300E+03       0.835E+02
      17     0.320E+03       0.835E+02
      18     0.340E+03       0.820E+02
      19     0.360E+03       0.790E+02
      20     0.380E+03       0.748E+02
      21     0.400E+03       0.690E+02
      22     0.420E+03       0.625E+02
      23     0.440E+03       0.547E+02
      24     0.460E+03       0.459E+02
      25     0.480E+03       0.344E+02
```

26	0.500E+03	0.210E+02
27	0.520E+03	0.570E+01
28	0.540E+03	-0.125E+02
29	0.560E+03	-0.343E+02
30	0.580E+03	-0.630E+02

****** O U T P U T   D A T A ******

CONVEX TALUS SURFACE PROFILE MEASURED

RD=SQRT((X-A)**2+(Y-B)**2)

% DIFF=100.*(RD-R)/R

R = BEST FIT RADIUS

A = BEST FIT X CO-ORD FOR CENTRE

B = BEST FIT Y CO-ORD FOR CENTRE

**** THE FOLLOWING POINTS ARE USED IN THE LS FIT ****

NO.	X-A	Y-B	RO	% DIFF
1	-0.9811195E+01	0.1577335E+02	0.1857574E+02	0.1981538E+00
2	-0.8811195E+01	0.1624334E+02	0.1856721E+02	0.1521845E+00
3	-0.7811195E+01	0.1690835E+02	0.1853470E+02	-0.2321041E-01
4	-0.6811195E+01	0.1721834E+02	0.1851657E+02	-0.1209904E+00
5	-0.5811195E+01	0.1759334E+02	0.1852823E+02	-0.5810833E-01
6	-0.4811195E+01	0.1787334E+02	0.1850955E+02	-0.1588514E+00
7	-0.3811195E+01	0.1811334E+02	0.1850995E+02	-0.1567114E+00
8	-0.2811195E+01	0.1830334E+02	0.1851796E+02	-0.1135005E+00
9	-0.1811195E+01	0.1842834E+02	0.1851714E+02	-0.1179451E+00
10	-0.8111954E+00	0.1850334E+02	0.1852110E+02	-0.9654540E-01
11	0.1888046E+00	0.1852835E+02	0.1852931E+02	-0.5226458E-01
12	0.1188805E+01	0.1852835E+02	0.1856644E+02	0.1479969E+00
13	0.2188805E+01	0.1845334E+02	0.1858269E+02	0.2356433E+00
14	0.3188805E+01	0.1830334E+02	0.1857904E+02	0.2159720E+00
15	0.4188805E+01	0.1809334E+02	0.1857197E+02	0.1772880E+00
16	0.5188805E+01	0.1780334E+02	0.1854407E+02	0.2732573E-01
17	0.6188805E+01	0.1747835E+02	0.1854167E+02	0.1440362E-01
18	0.7188805E+01	0.1708835E+02	0.1853889E+02	-0.6584513E-03
19	0.8188805E+01	0.1660335E+02	0.1851291E+02	-0.1407440E+00
20	0.9188805E+01	0.1607335E+02	0.1851450E+02	-0.1321841E+00

THE BEST FIT CIRCLE IS

(X - 0.1481120E+02) ** 2 + (Y - -0.1435335E+02) ** 2 = 0.3436943E+03

R = 0.1853900E+02 WITH A STANDARD ERROR OF 0.271E-01

SURFACE RADIUS = 0.1774524E+02 WHEN ADJUSTED FOR PIN TIP RADIUS.

AN ESTIMATE OF THE UNCERTAINTY IN THE RADIUS EVALUATION = 0.439E+00 %

WHERE % UNCERTAINTY = 300. * STANDARD ERROR / R

PC PLOT

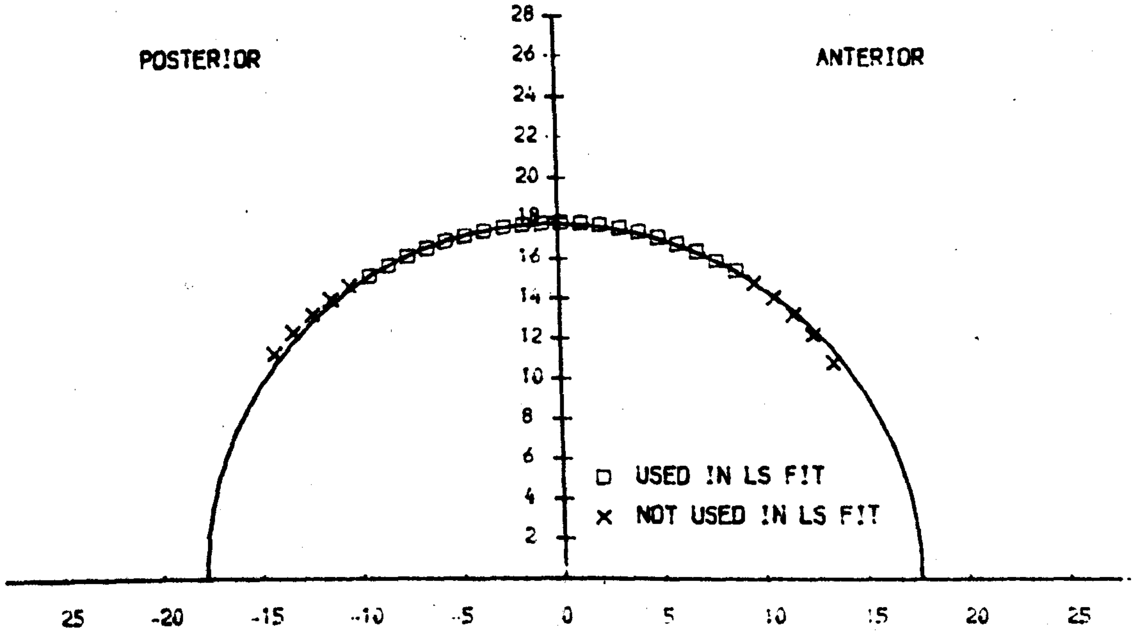

TALUS

RADIUS = 17.75 % UNCERTAINTY = 0.44

(ALL DIMENSIONS IN MM)

APPENDIX B

EFFECT OF MISALIGNMENT ON SURFACE CURVATURE MEASUREMENTS OF A CYLINDER USING A TALYCONTOR

The Talycontor instrument, made by Rank Taylor Hobson measures surface shape by traversing a lightly loaded stylus across a surface. Vertical and horizontal co-ordinates are recorded graphically. If the axis of a cylinder is placed perpendicular to the direction of stylus motion, the radius of the cylinder can be evaluated from the graphical output. However, if the axis of the cylinder is not perpendicular to the direction of stylus motion and a short distance is traversed, an inaccurate cylinder radius would be evaluated. Equations relating this source of error to misalignment angles are developed in this Appendix. These equations are required in Section 3.6 of Chapter 3 in which an estimate is provided of the accuracy of the surface curvature evaluation for ankle joints.

Two types of misalignment can occur as illustrated in Figure B.1. It is convenient to consider a "tilt" angle in the y-z plane and a "twist" angle in the x-y plane. The stylus is shown in Figure B.1 at point A which is the position of the maximum vertical or z co-ordinate. If the surface slope becomes very steep, the Talycontor cannot function properly. Thus, traversals can be considered as symmetric about point A and over distances of approximately one quarter the circumference of the cylinder.

When the cylinder of radius, r_c is tilted with angle θ, the measured surface profile is part of an ellipse as shown in Figure B.2. The smallest possible evaluation for radius equals the radius of curvature at point A. The radius of curvature at point A can be found using the following standard equation (Tuma, 1970).

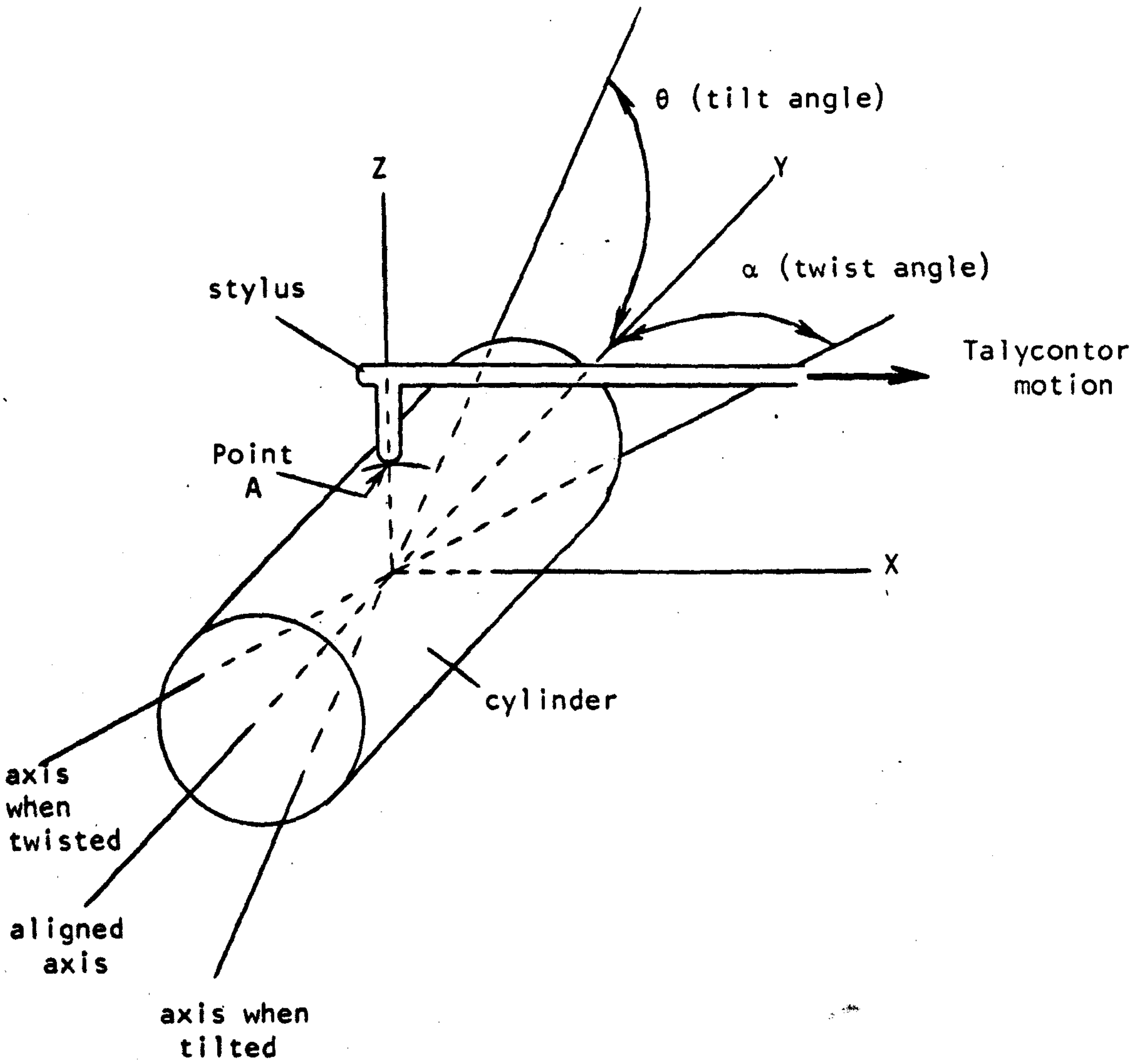

Figure B.1 : Geometric definitions for tilt and twist.

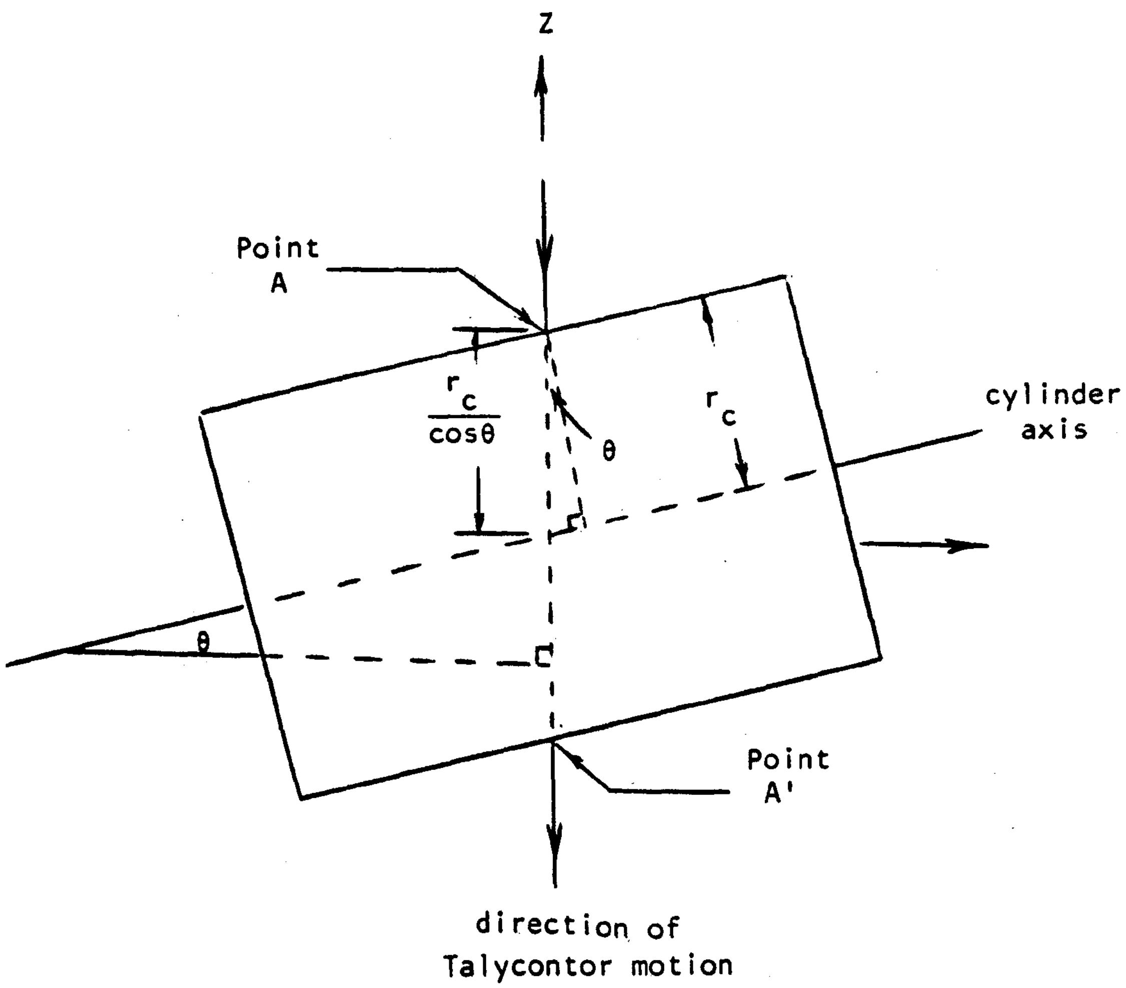

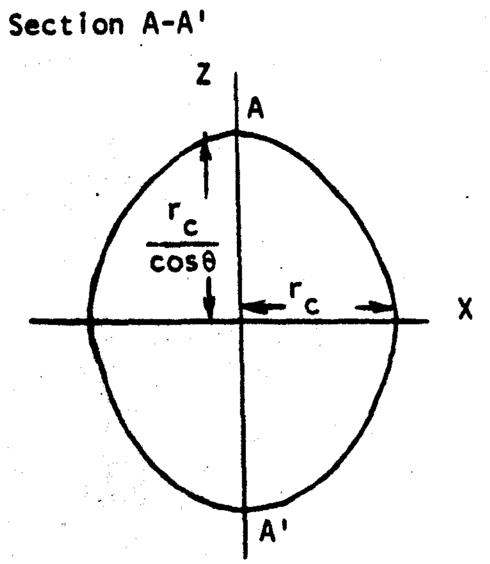

Figure B.2 : Surface geometry when tilt occurs.

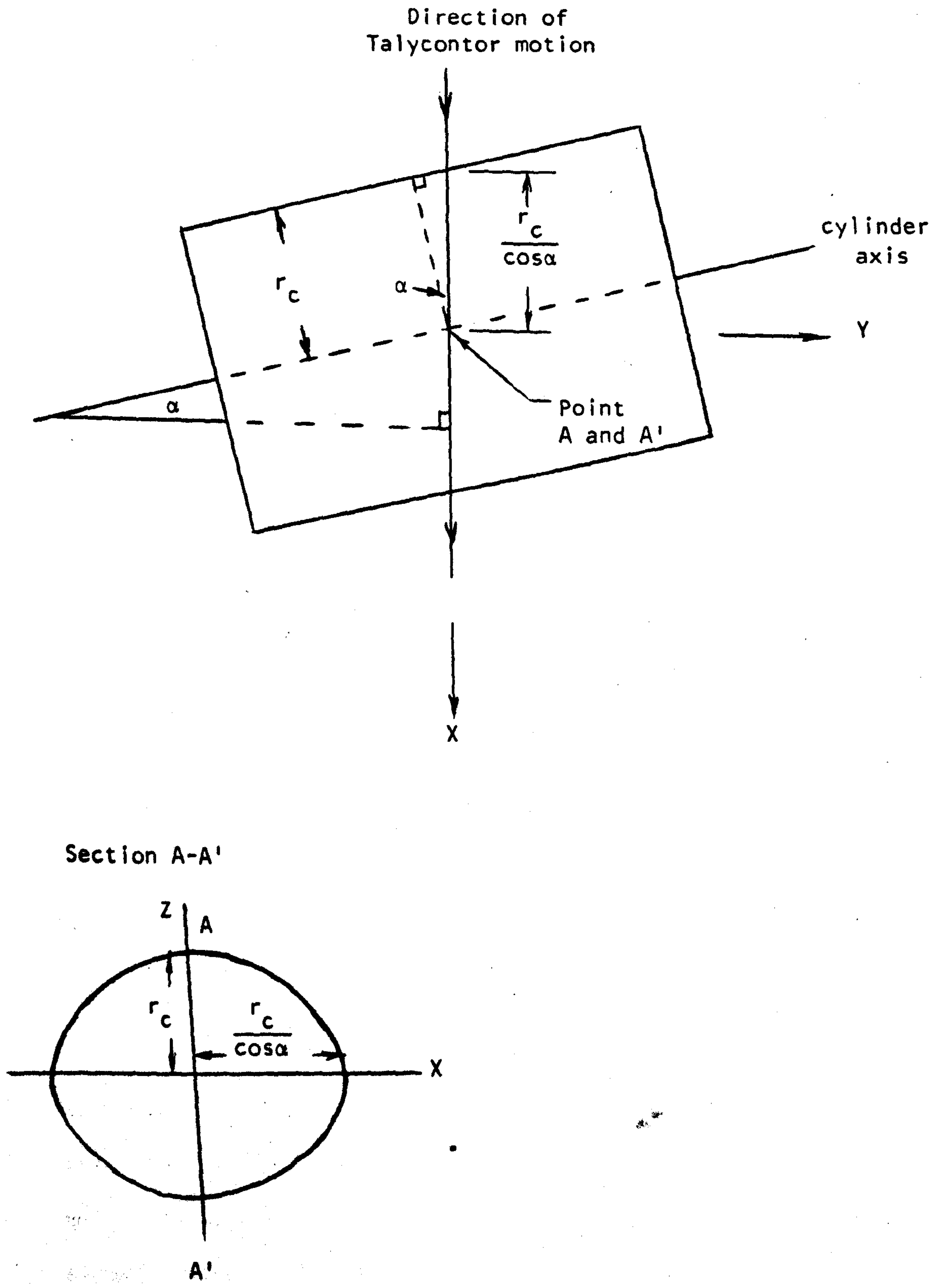

Figure B.3 : Surface geometry when twist occurs.

$$r = \frac{\left[1 + \left(\frac{dz}{dx}\bigg|_{x=0}\right)^{2}\right]^{3/2}}{-\frac{d^2z}{dx^2}\bigg|_{x=0}}$$

For the ellipse shown in Figure B.2

$$z = (r_c^{\,2} - x^2)^{1/2} \quad \frac{1}{\cos\theta}$$

which implied

$$\frac{dz}{dx}\bigg|_{x=0} = 0$$

and $$\frac{d^2z}{dx^2}\bigg|_{x=0} = \frac{-1}{r_c\cos\theta}$$

Thus, when the tilt angle is θ, the measured radius of curvature r_{TI} is

$$r_{TI} = r_c \cos\theta \qquad (B.1)$$

When the cylinder of radius r_c is twisted with angle α the measured surface profile is again part of an ellipse as shown in Figure B.3. In this case, the largest rather than the smallest possible radius equals the radius of curvature at point A. In a similar manner to the derivation of equation (B.1) the measured radius at point A, when twist occurs is,

$$r_{TW} = \frac{r_c}{\cos\alpha} \qquad (B.2)$$

Equation (B.1) indicated that tilt causes the measured radius to be smaller than the actual cylinder radius. However, equation (B.2) indicates that twist causes the opposite effect. Thus, when both tilt and twist occur together the measured radius may be estimated as

$$r_M = \frac{r_{TI} + r_{TW}}{2}$$

Equations (B.1) and (B.2) imply

$$r_M = \frac{r_c}{2}\left(\cos\theta + \frac{1}{\cos\alpha}\right) \tag{B.3}$$

which is used in Section 3.6.

APPENDIX C

THE COMPUTER PROGRAM FOR LINEAR REGRESSION

The computer program listed in this Appendix performs linear regression using a least squares criterion. The equations involved in evaluating the least squares terms are found in a standard mathematics handbook (Selby, 1974). The value for standard error is calculated using the following equation:

$$S_E = \sqrt{\frac{\Sigma(y_i - B_o - B_1 x_i)^2}{N - 2}}$$

where x_i and y_i are the independent and dependent values for a single data point, B_o and B_1 are the y-intercept and slope of the best fit line and N is the number of data points. The sample output includes a graph which differs from the one which would be generated by the listed program simply by not having multiple colours.

```
FILE: LSQ      FORTRAN  A   LEEDS UNIVERSITY VM/BSE 5.16

C
C   LEAST SQUARES CURVE FITS FOR LINEAR, POWER AND EXPONENTIAL CURVES.
C
C
C-----------------------------------------------------------------------
C
C              K.........EQUALS 0,1,2 FOR LINEAR, POWER OR EXPONENTIAL
C                        CURVES RESPECTIVELY.
C              N.........NUMBER OF DATA POINTS.
C              N2........NUMBER OF FITTED CURVE POINTS USED IN PLOT.
C              X.........INDEPENDENT VARIABLE.
C              Y.........DEPENDENT VARIABLE.
C
C-----------------------------------------------------------------------
C
C
      IMPLICIT REAL*8(A-H,O-Z)
      DIMENSION X(600),Y(600)
      REAL*4 XX(600),YY(600),XF(601),YF(601),XMAX,XMIN,YMAX,YMIN
C---------------------------------------
C
C         INPUT
C
C---------------------------------------
      READ(5,*) K,N,N2
      READ(5,*) (X(I),I=1,N)
      READ(5,*) (Y(I),I=1,N)
```

```
C-----------------------------------------------
C
C          CHECK
C
C-----------------------------------------------
  98   FORMAT(' K =',I3,5X,' N =',I5,4X,'N2 =',I5//)
 100   FORMAT(5X,'NO.',6X,'X',12X,'Y'//)
 101   FORMAT(' ',I6,3X,D10.3,3X,D10.3)
 102   FORMAT(' ',//)
       WRITE(6,98) K,N,N2
       WRITE(6,100)
       DO 2 I=1,N
       WRITE(6,101) I,X(I),Y(I)
  2    CONTINUE
       WRITE(6,102)
C-----------------------------------------------
C
C          PREP
C
C-----------------------------------------------
       XMAX=X(1)
       XMIN=X(1)
       YMAX=Y(1)
       DO 1 I=1,N
       IF(X(I).GT.XMAX) XMAX=X(I)
       IF(X(I).LT.XMIN) XMIN=X(I)
       IF(Y(I).GT.YMAX) YMAX=Y(I)
       XX(I)=X(I)
```

```
      YY(I)=Y(I)
 1    CONTINUE
      DX=(XMAX-XMIN)/N2
      IF(K.EQ.0) GOTO 11
      IF(K.EQ.2) GOTO 21
      DO 3 I=1,N
      XC=X(I)
      YC=Y(I)
      X(I)=DLOG10(XC)
      Y(I)=DLOG10(YC)
 3    CONTINUE
      GOTO 11
 21   CONTINUE
      DO 4 I=1,N
      YC=Y(I)
      Y(I)=DLOG10(YC)
 4    CONTINUE
 11   CONTINUE
C-----------------------------------------
C
C           LEAST
C
C-----------------------------------------
      DATA SUM1/0.D0/,SUM2/0.D0/,SUM3/0.D0/,SUM4/0.D0/,SUM5/0.D0/
      DATA SUM6/0.D0/
      DO 5 I=1,N
      XT=X(I)
      YT=Y(I)
      SUM1=SUM1+XT*YT
      SUM2=SUM2+YT
      SUM3=SUM3+XT
      SUM4=SUM4+XT**2
      SUM6=SUM6+YT**2
 5    CONTINUE
      B1=(N*SUM1-SUM2*SUM3)/(N*SUM4-SUM3**2)
      B0=SUM2/N-B1*SUM3/N
      F1=N*SUM4-SUM3**2
      F2=N*SUM6-SUM2**2
      CCOEF=B1*DSQRT(F1/F2)
      DO 5 I=1,N
      XT=X(I)
      YT=Y(I)
      SUM5=SUM5+(YT-B0-B1*XT)**2
 6    CONTINUE
      STDERR=DSQRT(SUM5/(N-2))
C-----------------------------------------
C
C           OUTPUT
C
C-----------------------------------------
 200  FORMAT(//5X,'Y = ',D14.7,2X,'+ (',D14.7,') * X'//)
 201  FORMAT(11X,'STANDARD ERROR =',D14.7//)
 202  FORMAT(11X,'CORRELATION COEFFICIENT =',D14.7//)
 203  FORMAT(5X,'Y = ',D14.7,2X,'* X ** ',D14.7//)
 204  FORMAT(5X,'Y = ',D14.7,2X,'* ',D14.7,'**X'//)
```

```
205   FORMAT(' ASSUMES POINT (0.,0.) IS ON THE FITTED CURVE')
206   FORMAT(' CANNOT HAVE Y = 0. IN THE INPUT DATA')
888   FORMAT(' ----------------------------------------------')
889   FORMAT(/' SPECIAL CHECK FOR MAVERICK POINTS'//)
890   FORMAT(//' ',2X,'NO.',7X,'X',9X,'Y',9X,'YCAL',9X,'YDIFF'/)
891   FORMAT(' ',I3,3X,4(D10.3,2X))
892   FORMAT(//' LOOK CLOSER IF YDIFF EXCEEDS    ',D10.3//)
      IF(K.EQ.1) GOTO 42
      IF(K.EQ.2) GO TO 46
      WRITE(6,888)
      WRITE(6,889)
      WRITE(6,890)
      DO 81 I=1,N
      XC=X(I)
      YCAL=B0+B1*XC
      YC=Y(I)
      YDIFF=DABS(YCAL-YC)
      WRITE(6,891) I,XC,YC,YCAL,YDIFF
 81   CONTINUE
      EMAX=3.D0*STDERR
      WRITE(6,892) EMAX
      WRITE(6,888)
      WRITE(6,200) B0,B1
      WRITE(6,201) STDERR
      WRITE(6,202) CCOEF
      GOTO 44
 42   CONTINUE
      B0=10.D0**B0
      WRITE(6,203) B0,B1
      WRITE(6,201) STDERR
      WRITE(6,202) CCOEF
      WRITE(6,205)
      GOTO 44
 46   CONTINUE
      B0=10.D0**B0
      B1=10.D0**B1
      WRITE(6,204) B0,B1
      WRITE(6,201) STDERR
      WRITE(6,202) CCOEF
      WRITE(6,206)
 44   CONTINUE
C-------------------------------------
C
C          VISUAL
C
C-------------------------------------
      N1=N2+1
      DO 7 I=1,N1
      XF(I)=XMIN+(I-1)*DX
 7    CONTINUE
      IF(K.EQ.1) GOTO 52
      IF(K.EQ.2) GOTO 55
      DO 8 I=1,N1
      YF(I)=B0+B1*XF(I)
      IF(YF(I).GT.YMAX) YMAX=YF(I)
```

```
8     CONTINUE
      GOTO 57
52    CONTINUE
      DO 9 I=1,N1
      YP(I)=B0*XP(I)**B1
      IF(YP(I).GT.YMAX) YMAX=YP(I)
9     CONTINUE
      GOTO 57
56    CONTINUE
      DO 10 I=1,N1
      YP(I)=B0*B1**XP(I)
      IF(YP(I).GT.YMAX) YMAX=YP(I)
10    CONTINUE
57    CONTINUE
      CALL PAPER(1)
      CALL CTRPNT(1)
      XMAX=XMAX*1.1
      XMIN=XMIN*.9
      XMIN=XMIN*1.1
      YMAX=YMAX*1.1
      CALL BLKPEN
      CALL PSPACE(0.,1.,0.,1.)
      CALL MAP(0.,1.,0.,1.)
      CALL PLOTCS(.5,.02,'X',1)
      CALL PLOTCS(.02,.55,'Y',1)
      CALL PSPACE(.1,.5,.1,.9)
      CALL MAP(0.,XMAX,0.,YMAX)
      CALL BORDER
      CALL AXES
      CALL REDPEN
      CALL CURVED(XP,YP,1,N1)
      CALL BLUPEN
      CALL PTPLOT(XX,YY,1,N,224)
      CALL GREND
      STOP
      END
```

Executive

FILE: J6 EXEC A LEEDS

```
EXEC SETUP FORTRAN NAGF CCGHOST
FI 5 DISK &2 DATA
FI 6 DISK &3 DATA
LOAD &1(CLEAR
EXEC PLOTFILE &4
SET BLIP *
START
```

Input

FILE: XLSQ DATA A LEE

```
0 6 100
4.21 7.46 10.7 13.9 16.2 20.1
6. 9.75 14.5 19.1 21.9 25.3
```

Output

FILE: YLSQ DATA A LEEDS UNIVERSITY VM/BSE 6.16

K = 0 N = 6 N2 = 100

NO.	X	Y
1	0.421D+01	0.600D+01
2	0.746D+01	0.975D+01
3	0.107D+02	0.145D+02
4	0.139D+02	0.181D+02
5	0.162D+02	0.219D+02
6	0.201D+02	0.253D+02

SPECIAL CHECK FOR MAVERICK POINTS

NO.	X	Y	YCAL	YDIFF
1	0.421D+01	0.600D+01	0.606D+01	0.628D-01
2	0.746D+01	0.975D+01	0.101D+02	0.378D+00
3	0.107D+02	0.145D+02	0.142D+02	0.320D+00
4	0.139D+02	0.181D+02	0.182D+02	0.826D-01
5	0.162D+02	0.219D+02	0.211D+02	0.841D+00
6	0.201D+02	0.253D+02	0.259D+02	0.637D+00

LOOK CLOSER IF YDIFF EXCEEDS 0.175D+01

Y = 0.7971097D+00 + (0.1250756D+01) * X

STANDARD ERROR = 0.5549305D+00

CORRELATION COEFFICIENT = 0.9974337D+00

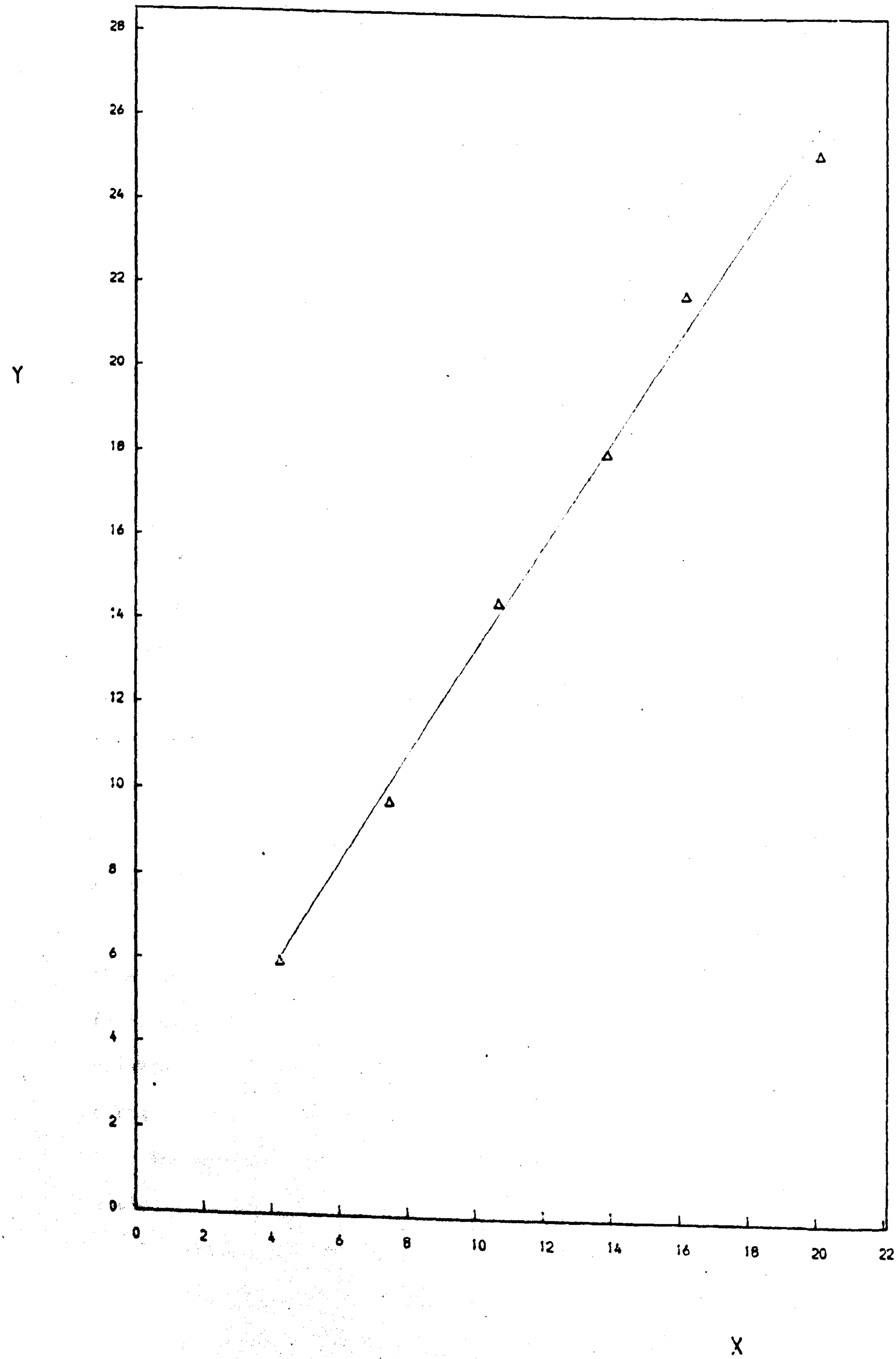
Y
28
26
24
22
20
18
16
14
12
10
8
6
4
2
0
0
2
4
6
8
10
12
14
16
18
20
22
X

APPENDIX D

DESIGN OF THE CAM FOR THE ANKLE JOINT SIMULATOR

The ankle joints in the simulator were subject to dynamic loads imposed by the cam driven hydraulic circuit shown in Figure D.1. When the cam rotated the follower was displaced in a linear fashion from the position corresponding to contact with the minimum cam radius (r_M). The magnitude of displacement can be written as ($r - r_M$), where r is the instantaneous cam radius. This displacement caused a compression of the nitrogen bag in the accumulator from a minimum gauge pressure (p_M) to an instantaneous gauge pressure (p) in the driving circuit. Balancing cylinder I applied a gauge pressure (p_I) to the piston area (A_{MB}) of the master cylinder to reduce the oil leakage from the driving circuit. In a similar fashion,balancing cylinder II applied a gauge pressure (p_{II}) to the piston area (A_{LF}) of the loading cylinder to reduce oil leakage from the driving circuit and also to balance the weight of the loading assembly.

The gauge pressure (p) in the driving circuit could be set to a specific value (p_M) when the cam was stationary and the follower touched at the minimum radius (r_M). This was accomplished by opening the valve and forcing oil into the driving circuit with the hand pump.

The dynamic load (F) was estimated by applying a simple analysis to the driving circuit. The original design notes of Mr. B. Jobbins (Department of Mechanical Engineering, Leeds University) formed a basis for the present analysis. Hydrostatic equations were applied in the analysis of the hydraulic circuit and simple thermodynamics was used to describe the compression of the nitrogen.

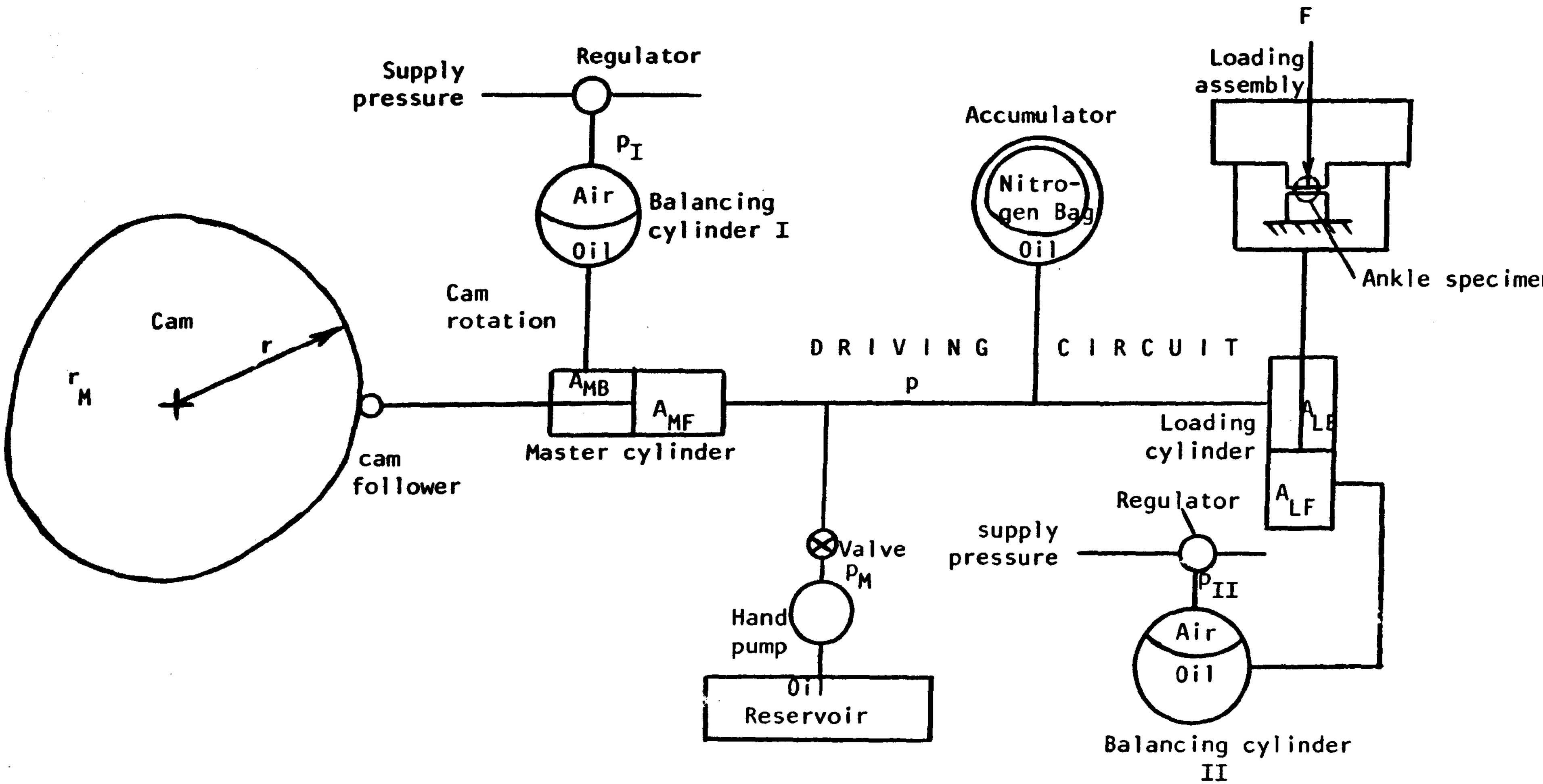

Figure D.1 : The hydraulic circuits of the joint simulator for applying dynamic loads to the ankle specimen.

When the nitrogen bag completely filled the accumulator it had a volume of V_o and a gauge pressure of p_o. As mentioned previously, the hand pump was used to force oil into the driving circuit. The volume of nitrogen at another gauge pressure (p_m) is given by;

$$V_M = \frac{V_o\,(p_o + p_A)}{p_M + p_A} \qquad (D.1)$$

where p_A is the atmospheric pressure. However, once the valve in the driving circuit was closed and cam rotation began, the nitrogen was subjected to cyclic compression and expansion. With an instantaneous gauge pressure of p and an instantaneous volume of V, this process was assumed to be adiabatic, to yield;

$$(p + p_A)V^{1.4} = (p_M + p_A)V_M^{\,1.4} \qquad (D.2)$$

A force balance on the loading cylinder yields:

$$F = p\,A_{LB} - p_{II}\,A_{LF} + W \qquad (D.3)$$

The terms in this equation are shown in Figure D.1, except for (W) which is the weight of the loading assembly. Finally the continuity equation was applied to the hydraulic oil to yield the following expression for the instantaneous volume of nitrogen.

$$V = V_M - (r - r_M)\,A_{MF} \qquad (D.4)$$

Equations (D.1), (D.2), (D.3) and (D.4) were combined to yield:

$$F = \left[\left(\frac{1}{p_M+p_A}\right)^{0.4}\left(\frac{p_M + p_A}{1 - \left(\frac{p_M + p_A}{p_o + p_A}\right)\frac{(r - r_M)\,A_{MF}}{V_o}}\right)^{1.4} - p_A\right]A_{LB} + W - p_{II}A_{LF} \qquad (D.5)$$

The various parameters required to evaluate equation (D.5) are listed in Table D.1. When values of these parameters are

Table D.1 : Parameters for the Cam Design.

Parameter type	Symbol	Definition	Value
Not easily changed	P_A	Standard atmospheric pressure	1.01×10^5 N/m^2
	W	Weight of loading assembly	418 N
	V_o	Volume of accumulator	1.80×10^{-4} m^3
	A_{MF}	Piston area for the front face of the master cylinder	4.56×10^{-3} m^2
	A_{LB}	Piston area for the back face of the loading cylinder	4.36×10^{-3} m^2
	A_{LF}	Piston area for the front face of the loading cylinder	4.56×10^{-3} m^2
Can be altered	r_M	Minimum cam radius	0.0593 m
	P_M	Gauge pressure of nitrogen when $r = r_M$ and cam stationary	1.45×10^5 N/m^2
	P_{II}	Gauge pressure in balancing cylinder II	1.68×10^5 N/m^2

substituted into equation (D.5) a non-linear relationship emerges between the force (F) on the ankle specimen and the cam radius (r).

The design of the cam used for the experiments described in Chapter 4 was accomplished by an iterative procedure. The required force pattern was first used to generate cam radius values predicted by equation (D.5). This was accomplished by using the first computer program listed at the end of this Appendix. The cam was then cut and attached to the joint simulator. A force transducer was used in place of an ankle specimen to record the dynamic load generated by the simulator.

Various dynamic effects caused higher forces than those predicted by equation (D.5) to be developed by the simulator. Thus, small portions of the cam were removed and pressures p_M and p_{II} adjusted until an acceptable load pattern was recorded. The second computer program listed at the end of this Appendix was used to evaluate the forces predicted by equation (D.5) for a proposed change in cam radius. This ensured that the loading pattern was not altered too drastically.

The second computer program was used to calculate the force pattern predicted by equation (D.5). This is compared with the actual measured forces in Figure D.3. The simple analysis developed in this Appendix provided a useful guide for the cam design. The final cam shape is shown in Figure D.2.

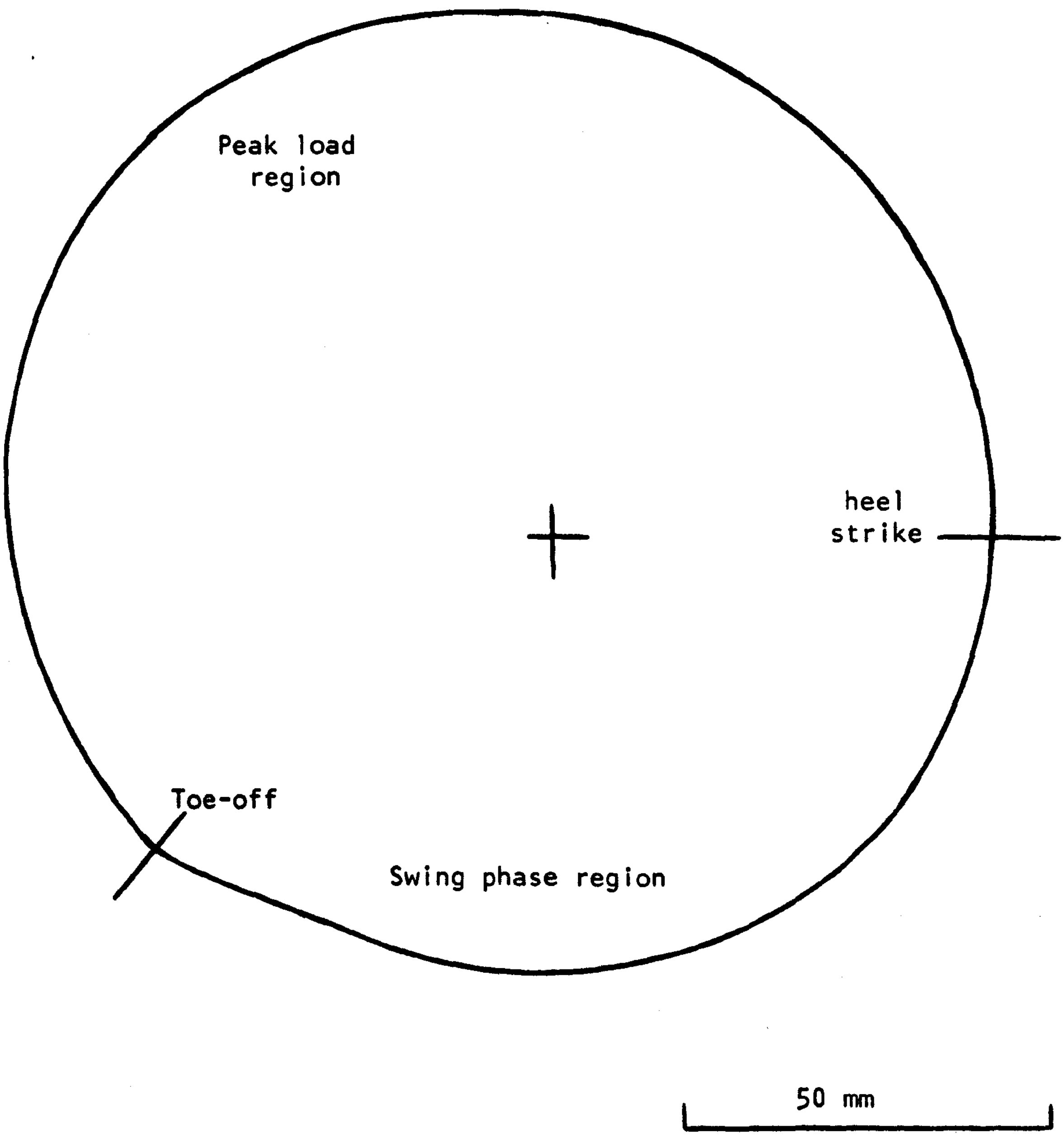

Figure D.2 : The final cam shape.

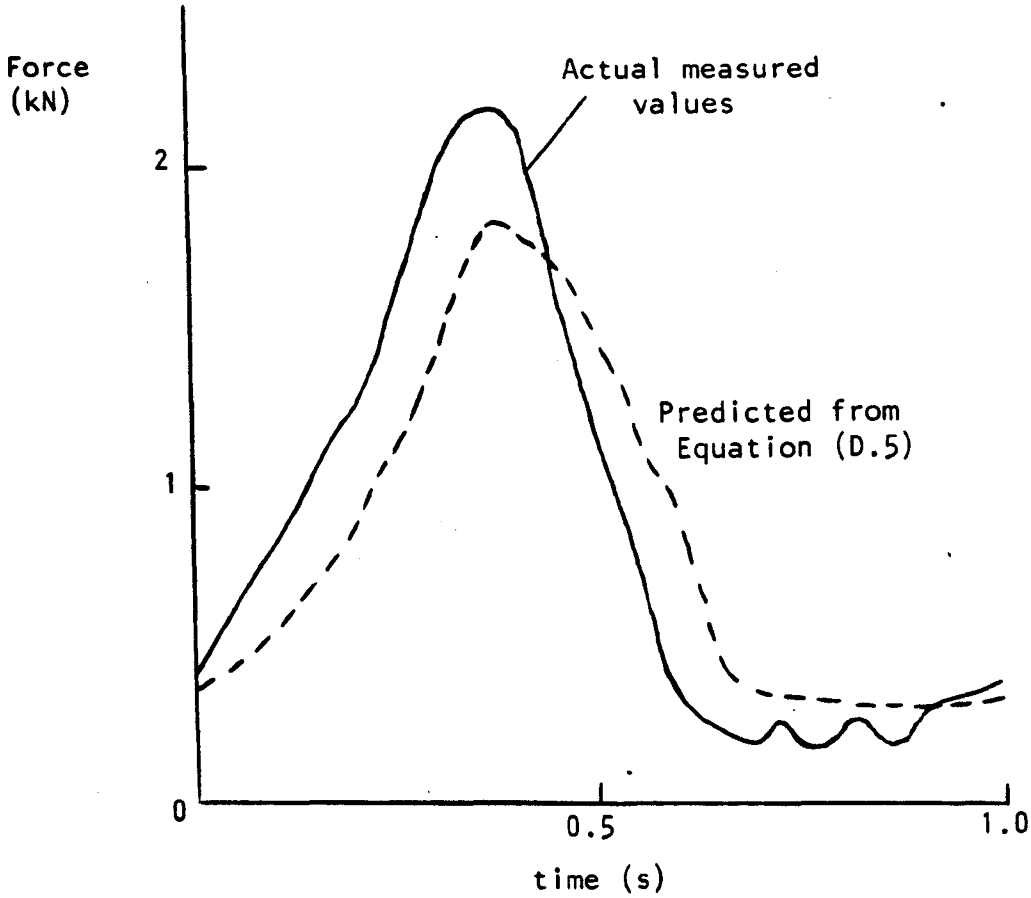

Figure D.3 : A comparison of the measured and predicted forces caused by the final cam shape.

```
      DIMENSION T(200),F(200),R(200),X(200),Y(200)
   98 FORMAT(' RM =',E10.3/)
   99 FORMAT(' R,X AND Y ARE IN MM'/)
   91 FORMAT(' F IS IN KN.'//)
  100 FORMAT(' ',5X,'T/TP',9X,'F',10X,'R',11X,'X',11X,'Y'/)
  101 FORMAT(' ',1X,5(E10.3,2X))
      READ(5,*) N
      READ(5,*) (T(I),I=1,N)
      READ(5,*) (R(I),I=1,N)
      READ(5,*) RM
      PI=3.14159
      RMM=-RM
      WRITE(6,98) RM
      WRITE(6,99)
      WRITE(6,91)
      WRITE(6,100)
      TM=0.
      FM=0.
      DO 1 I=1,N
      RX=R(I)/1000.-.059
      F(I)=1.0737*(1./(1.-26.027*RX))**1.4-.78798
      X(I)=R(I)*COS(2.*PI*T(I))
      Y(I)=R(I)*SIN(2.*PI*T(I))
      IF(T(I).GT.TM) TM=T(I)
      IF(F(I).GT.FM) FM=F(I)
      WRITE(6,101) T(I),F(I),R(I),X(I),Y(I)
    1 CONTINUE
      FM=1.1*FM
      CALL PAPER(1)
      CALL CTRFNT(1)
      CALL PSPACE(0.,1.,0.,1.)
      CALL MAP(0.,1.,0.,1.)
      CALL PLOTCS(.2,.3,'CAM (ACTUAL SIZE)',17)
      CALL GRNPEN
      CALL PSPACE(.05,.6221,.35,.9221)
      CALL MAP(RMM,RM,RMM,RM)
      CALL AXES
      CALL BLKPEN
      CALL PTPLOT(X,Y,1,N,248)
      CALL CURVEC(X,Y,1,N)
      CALL CURVEC(X,Y,1,N)
      CALL PSPACE(0.,1.,0.,1.)
      CALL MAP(0.,1.,0.,1.)
      CALL PLOTCS(.75,.28,'F',1)
      CALL PLOTCS(1.,.05,'T/TP',4)
      CALL PSPACE(.8,1.158,.1,.382)
      CALL MAP(0.,TM,0.,FM)
      CALL AXES
      CALL REDPEN
      CALL PTPLOT(T,F,1,N,248)
      CALL CURVEC(T,F,1,N)
      CALL CURVEC(T,F,1,N)
      CALL GREND
      STOP
      END
```

NO. 1

Input

(see program NO.2 for Executive)

```
38
0. .0248 .0528 .0806 .108 .136 .164 .192 .220 .247 .275 .303
.331 .359 .386 .417 .442 .470 .497 .525 .553 .581 .608 .636
.664 .692 .720 .747 .775 .803 .831 .859 .886 .914 .942
.970 .997 1.
60.2 60.9 61.8 63. 64.1 65.8 67.2 68. 70.2 71.2 72.7 73.9 75.1 76.5
76.9 76.7 76.3 76. 75. 73.8 72.1 70.9 69. 64.5 61.5 60.4 60. 59.7
59.4 59.1 59. 59.2 59.8 59.6 59.3 59.5 60. 60.2
80.
```

RM = 0.800E+02

R,X AND Y ARE IN MM

Output

F IS IN KN.

T/TP	F	R	X	Y
0.0	0.334E+00	0.602E+02	0.602E+02	0.0
0.248E-01	0.365E+00	0.609E+02	0.602E+02	0.945E+01
0.528E-01	0.406E+00	0.618E+02	0.584E+02	0.201E+02
0.806E-01	0.464E+00	0.630E+02	0.551E+02	0.306E+02
0.108E+00	0.523E+00	0.641E+02	0.499E+02	0.402E+02
0.136E+00	0.622E+00	0.658E+02	0.432E+02	0.496E+02
0.164E+00	0.715E+00	0.672E+02	0.346E+02	0.576E+02
0.192E+00	0.772E+00	0.680E+02	0.242E+02	0.635E+02
0.220E+00	0.951E+00	0.702E+02	0.132E+02	0.690E+02
0.247E+00	0.105E+01	0.712E+02	0.134E+01	0.712E+02
0.275E+00	0.120E+01	0.727E+02	-0.114E+02	0.718E+02
0.303E+00	0.135E+01	0.739E+02	-0.242E+02	0.698E+02
0.331E+00	0.151E+01	0.751E+02	-0.366E+02	0.656E+02
0.359E+00	0.173E+01	0.765E+02	-0.484E+02	0.592E+02
0.386E+00	0.180E+01	0.769E+02	-0.580E+02	0.505E+02
0.417E+00	0.176E+01	0.767E+02	-0.665E+02	0.382E+02
0.442E+00	0.169E+01	0.763E+02	-0.713E+02	0.272E+02
0.470E+00	0.164E+01	0.760E+02	-0.747E+02	0.142E+02
0.497E+00	0.149E+01	0.750E+02	-0.750E+02	0.141E+01
0.525E+00	0.133E+01	0.739E+02	-0.729E+02	-0.115E+02
0.553E+00	0.114E+01	0.721E+02	-0.681E+02	-0.236E+02
0.581E+00	0.102E+01	0.709E+02	-0.619E+02	-0.345E+02
0.608E+00	0.850E+00	0.690E+02	-0.537E+02	-0.433E+02
0.636E+00	0.545E+00	0.645E+02	-0.423E+02	-0.486E+02
0.664E+00	0.392E+00	0.615E+02	-0.316E+02	-0.527E+02
0.692E+00	0.343E+00	0.604E+02	-0.215E+02	-0.564E+02
0.720E+00	0.326E+00	0.600E+02	-0.112E+02	-0.589E+02
0.747E+00	0.314E+00	0.597E+02	-0.113E+01	-0.597E+02
0.775E+00	0.302E+00	0.594E+02	0.929E+01	-0.597E+02
0.803E+00	0.290E+00	0.591E+02	0.193E+02	-0.559E+02
0.831E+00	0.286E+00	0.590E+02	0.287E+02	-0.515E+02
0.859E+00	0.294E+00	0.592E+02	0.374E+02	-0.459E+02
0.886E+00	0.318E+00	0.598E+02	0.451E+02	-0.393E+02
0.914E+00	0.310E+00	0.596E+02	0.511E+02	-0.307E+02
0.942E+00	0.298E+00	0.593E+02	0.554E+02	-0.211E+02
0.970E+00	0.306E+00	0.599E+02	0.584E+02	-0.111E+02
0.997E+00	0.326E+00	0.600E+02	0.600E+02	-0.113E+01
0.100E+01	0.334E+00	0.602E+02	0.602E+02	-0.305E-03

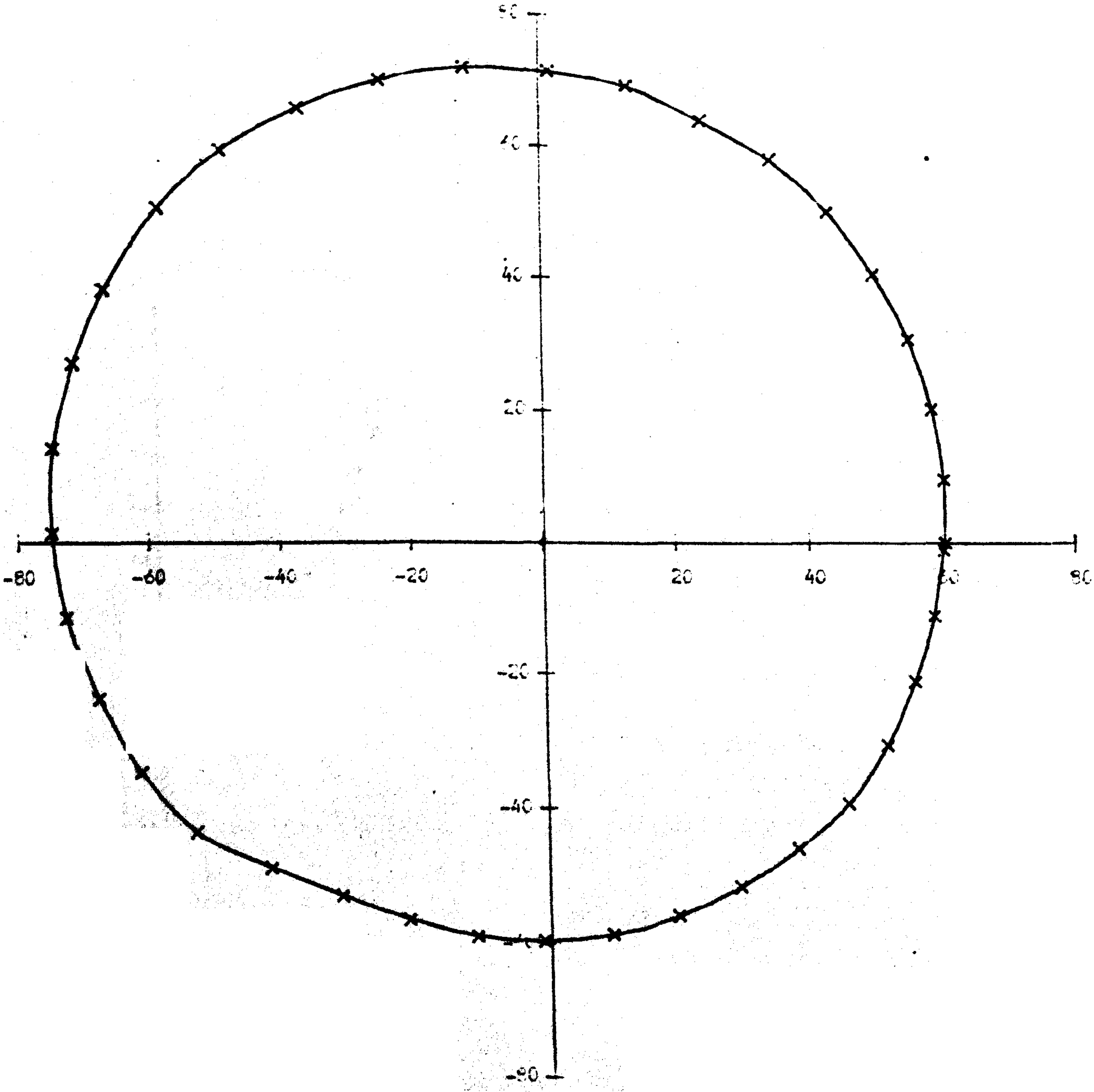

CAM (ACTUAL SIZE)

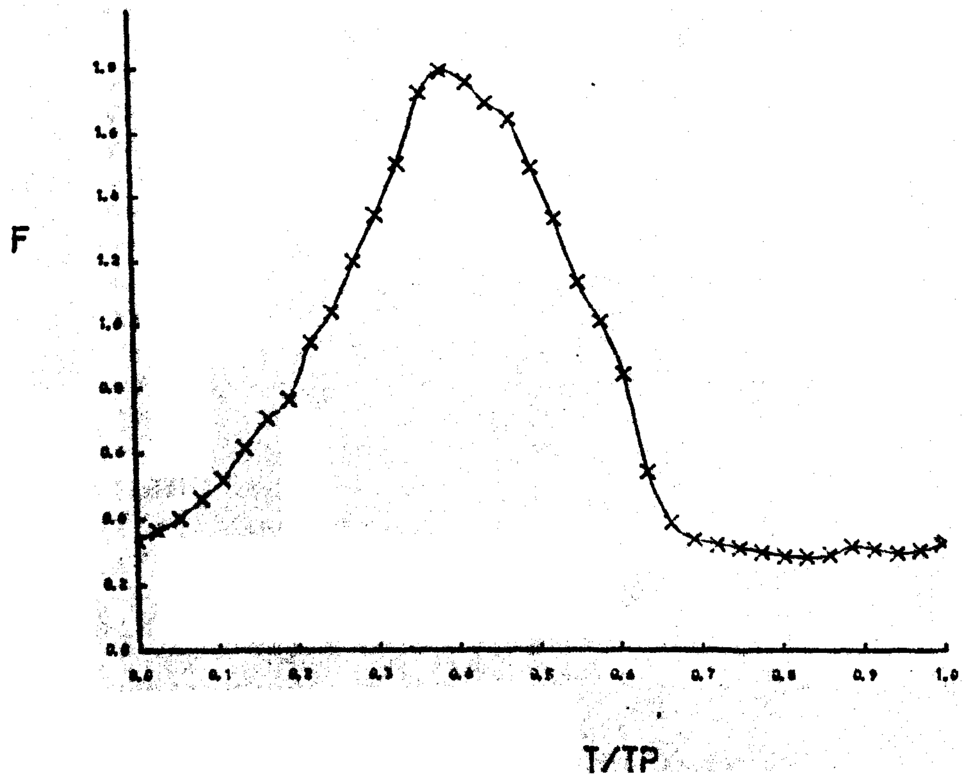

F
1.8
1.6
1.4
1.2
1.0
0.8
0.6
0.4
0.2
0.0
0.0
0.1
0.2
0.3
0.4
0.5
0.6
0.7
0.8
0.9
1.0
T/TP

FILE: CAM FORTRAN A LEEDS UNIVERSITY VM/BSE 6.16

NO. 2

```
      DIMENSION T(200),F(200),R(200),X(200),Y(200)
   98 FORMAT(' RM =',E10.3/)
   99 FORMAT(' R,X AND Y ARE IN MM'/)
   91 FORMAT(' F IS IN KN.'//)
  100 FORMAT(' ',5X,'T/TP',9X,'F',10X,'R',11X,'X',11X,'Y'/)
  101 FORMAT(' ',1X,5(E10.3,2X))
      READ(5,*) N
      READ(5,*) (T(I),I=1,N)
      READ(5,*) (F(I),I=1,N)
      READ(5,*) RM
      PI=3.14159
      RMM=-RM
      WRITE(6,98) RM
      WRITE(6,99)
      WRITE(6,91)
      WRITE(6,100)
      TM=0.
      FM=0.
      DO 1 I=1,N
      R(I)=59.+38.4216*(1.-(1.0737/(F(I)+.78798))**.714286)
      X(I)=R(I)*COS(2.*PI*T(I))
      Y(I)=R(I)*SIN(2.*PI*T(I))
      WRITE(6,101) T(I),F(I),R(I),X(I),Y(I)
      IF(T(I).GT.TM) TM=T(I)
      IF(F(I).GT.FM) FM=F(I)
    1 CONTINUE
      FM=FM*1.1
      CALL PAPER(1)
      CALL CTRFNT(1)
      CALL PSPACE(0.,1.,0.,1.)
      CALL MAP(0.,1.,0.,1.)
      CALL PLOTCS(.2,.3,'CAM (ACTUAL SIZE)',17)
      CALL GRNPEN
      CALL PSPACE(.05,.6221,.35,.9221)
      CALL MAP(RMM,RM,RMM,RM)
      CALL AXES
      CALL BLKPEN
      CALL PTPLOT(X,Y,1,N,248)
      CALL CURVEC(X,Y,1,N)
      CALL CURVEC(X,Y,1,N)
      CALL PSPACE(0.,1.,0.,1.)
      CALL MAP(0.,1.,0.,1.)
      CALL PLOTCS(.75,.2 ,'F',1)
      CALL PLOTCS(1.,.05,'T/TP',4)
      CALL PSPACE(.6,1.156,.1,.382)
      CALL MAP(0.,TM,0.,FM)
      CALL AXES
      CALL REDPEN
      CALL PTPLOT(T,F,1,N,248)
      CALL CURVEC(T,F,1,N)
      CALL CURVEC(T,F,1,N)
      CALL GREND
      STOP
      END
```

Executive

```
EXEC SETUP FORTRAN NAGF CCGHOST
FI 5 DISK &2 DATA
FI 6 DISK &3 DATA
LOAD &1(CLEAR
EXEC PLOTFILE &4
SET BLIP *
START
```

Input

```
28
0. .01 .025 .05 .1 .15 .2 .25 .3 .35 .4 .45 .5 .55 .6 .625 .65
.66 .675 .685 .7 .75 .8 .85 .9 .95 .975 1.
.1 .15 .24 .4 .7 1. 1.33 1.64 1.9 2. 1.95 1.8 1.38 .95 .52 .305
.1 .06 .04 .04 .04 .04 .04 .04 .04 .04 .04 .1
80.
```

RM = 0.800E+02 **Output**

R,X AND Y ARE IN MM

F IS IN KN.

T/TP	F	R	X	Y
0.0	0.100E+00	0.534E+02	0.534E+02	0.0
0.100E-01	0.150E+00	0.551E+02	0.550E+02	0.345E+01
0.250E-01	0.240E+00	0.578E+02	0.571E+02	0.904E+01
0.500E-01	0.400E+00	0.617E+02	0.587E+02	0.191E+02
0.100E+00	0.700E+00	0.670E+02	0.542E+02	0.394E+02
0.150E+00	0.100E+01	0.707E+02	0.416E+02	0.572E+02
0.200E+00	0.133E+01	0.738E+02	0.228E+02	0.702E+02
0.250E+00	0.164E+01	0.760E+02	0.963E-04	0.760E+02
0.300E+00	0.190E+01	0.775E+02	-0.239E+02	0.737E+02
0.350E+00	0.200E+01	0.780E+02	-0.458E+02	0.631E+02
0.400E+00	0.195E+01	0.777E+02	-0.629E+02	0.457E+02
0.450E+00	0.180E+01	0.769E+02	-0.732E+02	0.238E+02
0.500E+00	0.138E+01	0.742E+02	-0.742E+02	0.199E-03
0.550E+00	0.950E+00	0.702E+02	-0.667E+02	-0.217E+02
0.600E+00	0.520E+00	0.641E+02	-0.518E+02	-0.376E+02
0.625E+00	0.305E+00	0.595E+02	-0.421E+02	-0.421E+02
0.650E+00	0.100E+00	0.534E+02	-0.314E+02	-0.432E+02
0.660E+00	0.600E-01	0.519E+02	-0.278E+02	-0.439E+02
0.675E+00	0.400E-01	0.512E+02	-0.232E+02	-0.456E+02
0.685E+00	0.400E-01	0.512E+02	-0.203E+02	-0.470E+02
0.700E+00	0.400E-01	0.512E+02	-0.158E+02	-0.487E+02
0.750E+00	0.400E-01	0.512E+02	-0.195E-03	-0.512E+02
0.800E+00	0.400E-01	0.512E+02	0.158E+02	-0.487E+02
0.850E+00	0.400E-01	0.512E+02	0.301E+02	-0.414E+02
0.900E+00	0.400E-01	0.512E+02	0.414E+02	-0.301E+02
0.950E+00	0.400E-01	0.512E+02	0.487E+02	-0.159E+02
0.975E+00	0.400E-01	0.512E+02	0.505E+02	-0.800E+01
0.100E+01	0.100E+00	0.534E+02	0.534E+02	-0.271E-03

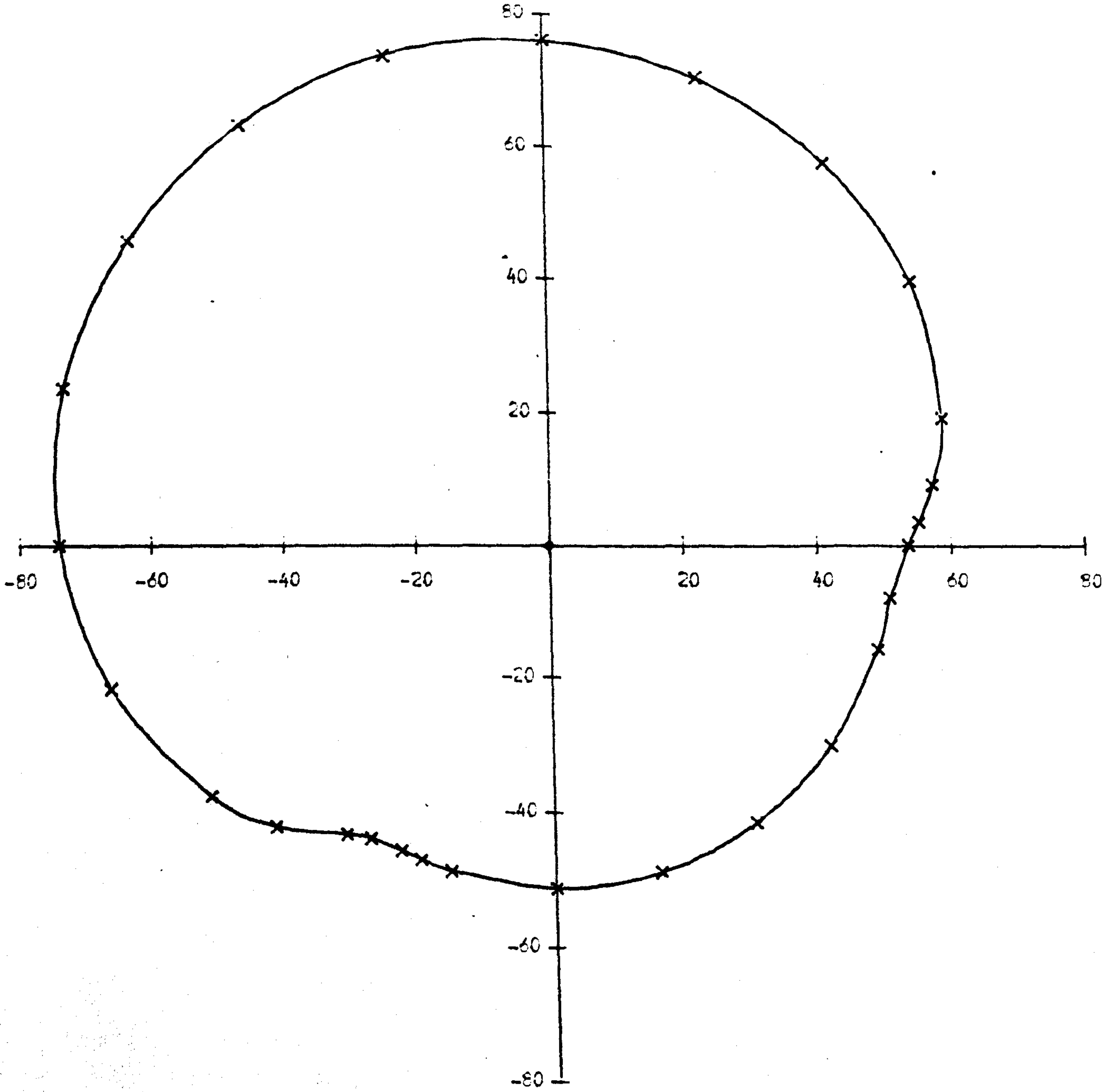

CAM (ACTUAL SIZE)

D/17

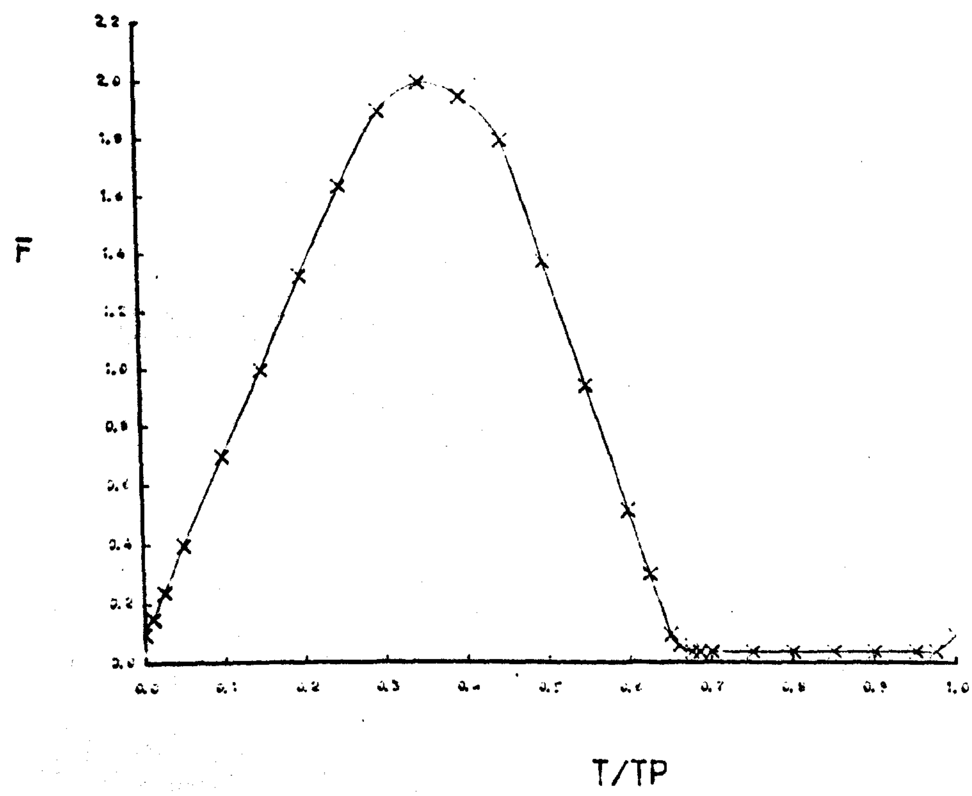

APPENDIX E

COMPUTER PROGRAM FOR THE PLANE INCLINED SURFACE BEARING MODEL

```
C*****************************************************************
C
C       PLANE INCLINED SURFACE MODEL
C       ----------------------------
C
C          THE GEOMETRY OF A RIGID CYLINDER SLIDING ON A LUBRICATED
C        ELASTIC LAYER (PR=.5) BONDED TO A RIGID PLANE IS APPROXIMATED
C        AS A PLANE INCLINED SURFACE.  THE LUBRICANT IS ISOVISCOUS.
C        THE LOAD AND VELOCITY ARE CYCLIC TIME VARYING.
C          IT IS ASSUMED THAT THE FILM THICKNESS VARIATION WITH TIME
C        CAN BE APPROXIMATED AS DH0/DT.   THE LENGTH OF THE PLANE
C        SURFACE IS CHOSEN SUCH THAT  DP/DX = 0.  AT  X = BDRY/2.
C        THE INCLINATION OF THE PLANE SURFACE IS CHOSEN SUCH THAT
C        FOR THE INSTANTANEOUS CONDITIONS OF LOAD AND VELOCITY
C        THE MINIMUM STEADY STATE FILM THICKNESS EQUALS THAT
C        PREDICTED BY AN APPROPRIATE FORMULA IN THE LITERATURE
C        FOR THE CYLINDRICAL GEOMETRY.
C
C*****************************************************************
C
      IMPLICIT REAL*8(A-H,O-Z)
      REAL*8 XXDE,XMPH,TP1,HMAX,FMAX,TT(4001),HH(4001),FF(4001),
     *        XPR(201),XPHZ(901),XX(801),PMAX(41),BB(4001),FCC(4001),
     *        XM,FPMAX,FPP(4001),UMAX,UU(4001),TPL1,XFACT,XXIP
     *        X1,X2,X3,X4,Y1,Y2,Y3,Y4,XFACT,HFACT,FFACT,PMAX1,XPHZ1
      COMMON TOL,TOL1,H0,VI,TP,E,R,TH,WD,UAMP
      COMMON PR(201,41),PHZ(201),BH(400),BFF(401),BHP(401)
      COMMON A(15),A1(15),PD(15),AH(15),W1(15),D1(15)
      COMMON TF(100),FE(100),FP(100),W11(100),D11(100),TP(100)
      COMMON T2,H2,U2,FP2,F2,B2,XM2,XP02,FR2,CH1,CH2,DT,BH2,XM
      COMMON UE(400),FPR(400),FU(400),BF(400),XMI(400),XPM(401)
      COMMON FRI(400),H(400),HST(200),UC,FPT, BC,BDRY,T1,HH
      COMMON NPER,NHALF,NSPTP,NPRT,IPRT,NPX,NPT,NP,NA,NF
      FR(VI)=((VI*UG)/(FPG*XMG))*(8.D0*DLOG(1.D0+XMG*BG/HG)
     A       -12.D0*XPG*BG/(2.D0*HG+XMG*BG))-((6.D0*VI)/(FPG*XPG**2))
     A       *(DLOG(1.D0+XMG*BG/HG)-2.D0*XPG*BG/(2.D0*HG+XMG*BG))*FG
      V(VI)=2.D0*VI*UG*BG/(HG*FPG)
      P(X,HG,BG,XMG,FG,UG)=12.D0*VI*(BE-X)*X*(XMG*UG-FG)/
     A                    ((2.D0*HG+XPG*BG)*(HG+XPG*X)**2)
C-----------------------------------
C          INPUT
C-----------------------------------
      READ(5,*) TOL,H0,NPER,NHALF,NSPTP,NPRT,IPRT,NPX,NPT,NP
      READ(5,*) VI,TP,E,R,TH,WD
      READ(5,*) UAMP
      READ(5,*) XFACT,HFACT,FFACT,PFACT
      READ(5,*) NA
      READ(5,*) (A(I),I=1,NA)
      READ(5,*) (A1(I),I=1,NA)
      READ(5,*) (PD(I),I=1,NA)
      READ(5,*) NF
      READ(5,*) (TM(I),I=1,NF)
      READ(5,*) (FE(I),I=1,NF)
C-----------------------------------
C          CHECK
```

FILE: M FORTRAN A LEEDS UNIVERSITY VM/ESE 6.16

```
C-----------------------------------------------
   99 FORMAT(' ')
  101 FORMAT(' ---------------------------------------------------',
     *'-----------------------------------------------------------')
C
C
 1400 FORMAT(' TOL (TOLERANCE FOR SS AND STEP SIZE) .......... ',D14.7)
 1401 FORMAT(' H0 (INITIAL GUESS FOR H0 AT TIME ZERO) ........ ',D14.7)
 1402 FORMAT(' NPER (MAX. NO. OF CYCLES AT SAME STEP SIZE) .. ',I5)
 1403 FORMAT(' NHALF (MAX. NO. OF STEP SIZE HALVINGS) ....... ',I8)
 1404 FORMAT(' NSPTP (INITIAL NO. OF STEPS PER CYCLE) ....... ',I8)
 1405 FORMAT(' NPRT (NO. OF STEPS PRINTED PER CYCLE) ........ ',I8)
 1406 FORMAT(' IPRT (CONVERGENCE PRINT OPTION) .............. ',I8)
 1407 FORMAT(' NPX (NO. OF PRESS. PTS. PRINTED PER DIST.) ... ',I8)
 1408 FORMAT(' NPT (NO. OF PRESS. DIST. PRINTED) ............ ',I8)
 1409 FORMAT(' NP (PRINT OPTIONS FOR PRESS. DIST.) .......... ',I8)
 1410 FORMAT(' VI (ABSOLUTE VISCOSITY) ........................ ',D14.7)
 1411 FORMAT(' TP (CYCLE PERIOD) .............................. ',D14.7)
 1412 FORMAT(' E (ELASTIC MODULUS OF LAYER) ................... ',D14.7)
 1413 FORMAT(' R (REDUCED RADIUS) ............................. ',D14.7)
 1414 FORMAT(' TH (LAYER THICKNESS) ........................... ',D14.7)
 1415 FORMAT(' WD (WIDTH OF CONTACT) .......................... ',D14.7)
 1416 FORMAT(' UAMP (AMPLIT. OF ENT.VEL.) ..................... ',D14.7)
 1418 FORMAT(' XFACT (SCALE FACTOR FOR PLOTS) ................. ',D14.7)
 1419 FORMAT(' HFACT (SCALE FACTOR FOR PLOTS) ................. ',D14.7)
 1420 FORMAT(' FFACT (SCALE FACTOR FOR PLOTS) ................. ',D14.7)
 1421 FORMAT(' PFACT (SCALE FACTOR FOR PLOTS) ................. ',D14.7)
C
C
 1599 FORMAT(/' NOTE : FOR SS TOLERANCE EQUALS .1*TOL'/)
  111 FORMAT(' ',6X,'A/TH',12X,'A/AH',12X,'P/PH')
  112 FORMAT(' ',1X,3(D14.7,2X),I8)
  114 FORMAT(' ',6X,'T/TP',12X,'TIME',12X,'LOAD',13X,'FP'/)
  115 FORMAT(' ',1X,4(D14.7,2X),I8)
  116 FORMAT(' ****   I N P U T    D A T A    ****'/)
  117 FORMAT(' ****    O U T P U T    D A T A    ****'/)
      WRITE(6,101)
      WRITE(6,116)
      WRITE(6,101)
      WRITE(6,1400) TOL
      WRITE(6,1401) H0
      WRITE(6,1402) NPER
      WRITE(6,1403) NHALF
      WRITE(6,1404) NSPTP
      WRITE(6,1405) NPRT
      WRITE(6,1406) IPRT
      WRITE(6,1407) NPX
      WRITE(6,1408) NPT
      WRITE(6,1409) NP
      WRITE(6,1410) VI
      WRITE(6,1411) TP
      WRITE(6,1412) E
      WRITE(6,1413) R
      WRITE(6,1414) TH
      WRITE(6,1415) WD
```

```
      WRITE(6,1016) LAMP
      WRITE(6,1018) XFACT
      WRITE(6,1019) HFACT
      WRITE(6,1020) FFACT
      WRITE(6,1021) PFACT
      WRITE(6,1999)
      WRITE(6,99)
      WRITE(6,101)
      WRITE(6,99)
      WRITE(6,111)
      WRITE(6,99)
      DO 1000 I=1,NA
      WRITE(6,112) A(I),A1(I),PD(I),I
 1000 CONTINUE
      WRITE(6,99)
      WRITE(6,101)
      DO 1001 I=1,MF
      TF(I)=TM(I)*TP
      FP(I)=FE(I)/WO
 1001 CONTINUE
      WRITE(6,99)
      WRITE(6,114)
      DO 1002 I=1,MF
      WRITE(6,115) TM(I),TF(I),FE(I),FP(I),I
 1002 CONTINUE
      WRITE(6,99)
      WRITE(6,101)
      WRITE(6,117)
C-------------------------------------
C          FILM
C-------------------------------------
  200 FORMAT(' ****** DOES NOT CONVERGE TO SPECIFIED TOLERANCE ******')
  201 FORMAT(' ***** DOES NOT REACH STEADY STATE *****')
  203 FORMAT(' STEP SIZE IS HALVED')
      CH1=1.D6
      DT=TP/NSPTP
      NS=NSPTP
      TOL1=TOL
      DT1=DT
      DO 2000 I=1,NA
      AM(I)=A(I)/A1(I)
 2000 CONTINUE
      DO 2002 J=1,NHALF
      TOL=TOL1
      CH2=1.D6
      IF(IPRT.EQ.1) WRITE(6,101)
      IF((IPRT.EQ.1).AND.(J.NE.1))WRITE(6,203)
      DO 2003 M=1,NPER
      H1=H0
C     ----------
      CALL NUMRT
C     ----------
C                                              ----------
      IF((J.EQ.1).AND.(M.EQ.1).AND.(IPRT.EQ.1)) CALL CVCLT
C                                              ----------
```



```
      TOL=.1D0*TOL1
      IF(CH1.LE.TOL) TOL=TOL1
      IF(CH1.LE.TOL) GOTO 3
      IF(M.EQ.1) GOTO 4
      TOL=.1D0*TOL1
    3 CH2=CH1
      DF1=-1.D0
      IF(J.NE.1) NS=NSPTP/2
      IF(M.NE.1) NS=NSPTP
      DO 2004 L=1,NS
      L1=L
      IF((J.NE.1).AND.(M.EQ.1)) L1=2*L
      DF=DABS((H(L1)-HST(L))/H(L1))
      IF(DF.GT.DF1) DF1=DF
 2004 CONTINUE
      CH1=DF1
      IF((CH2.LE.TOL).AND.(CH1.LE.TOL)) GOTO 6
C                        ----------
      IF(IPRT.EQ.1) CALL CVOUT
C                        ----------
    4 CONTINUE
      DO 2005 N=1,NSPTP
      HST(N)=H(N)
 2005 CONTINUE
      IF(CH2.LE.TOL) GOTO 8
      IF(M.EQ.1) GOTO 2003
    8 CONTINUE
      IF(CH1.LE.TOL) GOTO 9
 2003 CONTINUE
      IF(IPRT.EQ.1) WRITE(6,201)
      IF(J.EQ.NHALF) GOTO 2002
      GOTO 10
    9 H0=H1
   10 DT=DT1/(2.D0**J)
      NSPTP=2*NSPTP
 2002 CONTINUE
      WRITE(6,200)
    6 CONTINUE
C          -----
      CALL CVOUT
C          -----
C-------------------------------------
C          FCOEFF
C-------------------------------------
      HG=HZ
      UG=UZ
      FPG=FPZ
      FG=FZ
      BG=BZ
      XMG=XMZ
      IF(XMG.EQ.0.D0) FRZ=Y(VI)
      IF(XMG.GT.0.D0) FRZ=FR(VI)
      DO 3000 I=1,NSPTP
      HG=H(I)
      UG=UE(I)
```

```
      FRG=FPP(I)
      FG=FU(I)
      BG=UF(I)
      XMG=XMI(I)
      IF(XMG.EQ.0.D0) FRI(I)=Y(VI)
      IF(XMG.GT.0.D0) FRI(I)=FR(VI)
 3000 CONTINUE
C---------------------------------------
C             PRESS
C---------------------------------------
      PI=3.14159265358979312D0
      NA1=NA-1
      N1=NPX+1
      DO 4000 I=1,N1
      X=(I-1)*(BZ/NPX)
      PR(I,1)=P(X,HZ,BZ,XMZ,FZ,UZ)
 4000 CONTINUE
      AX=BHZ/(2.D0*TH)
      CALL E01ACF(NA1,AX,A,PD,W1,C1,NA,PDY)
      PHZ(1)=PDY*4.D0*DSQRT(FPZ*E/(12.D0*PI*R))
      N2=NPT+1
      DO 4001 J=2,N2
      I=(J-1)*NSFTP/NPT
      HG=H(I)
      UG=UE(I)
      FPG=FPF(I)
      FG=FU(I)
      BG=BF(I)
      BHG=BH(I)
      XMG=XMI(I)
      DO 4002 K=1,N1
      X=(K-1)*(BG/NPX)
      PR(K,J)=P(X,HG,BG,XMG,FG,UG)
 4002 CONTINUE
      AX=BHG/(2.D0*TH)
      CALL E01ACF(NA1,AX,A,PD,W1,C1,NA,PDY)
      PHZ(J)=PDY*4.D0*DSQRT(FPG*E/(12.D0*PI*R))
 4001 CONTINUE
C---------------------------------------
C             OUTPUT
C---------------------------------------
  300 FORMAT(' ---------------------------------------------------------')
  301 FORMAT(' ',6X,'TIME',13X,'HC',11X,'F COEFF'/)
  302 FORMAT(' ',1X,3(D14.7,2X),I8)
  303 FORMAT(' TIME =',D14.7/)
  304 FORMAT(' ',7X,'X',11X,'PRESSURE'/)
  305 FORMAT(' ',1X,2(D14.7,2X),I8)
  306 FORMAT(' ----------------------------------------------------------',
     *      '-------------------------')
  307 FORMAT(' MAXIMUM DRY CONTACT STRESS =',D14.7//)
  308 FORMAT(' FF =',D14.7/)
  309 FORMAT(' DRY CONTACT LENGTH =',D14.7/)
 7999 FORMAT(' $$$$  DIMENSIONLESS PARAMETERS $$$$'/)
 7980 FORMAT(' U =',D11.4)
 7981 FORMAT(' W =',D11.4)
```



```
 7982 FORMAT(' S =',D11.4)
 7983 FORMAT(' D =',D11.4)
      DO 5000 I=1,10
      WRITE(6,99)
 5000 CONTINUE
      WRITE(6,300)
      WRITE(6,99)
      WRITE(6,301)
      HCZ=HZ+XMZ*(BHZ/2.D0)
      LL=1
      WRITE(6,302) TZ,HCZ,FPZ,LL
      DO 5001 J=1,NPRT
      LL=J+1
      I=J*NSPTP/NPRT
      TPL=I*DT
      XHC=H(I)
      XHC=H(I)+XMI(I)*(BH(I)/2.D0)
      XFR=FRI(I)
      WRITE(6,302) TPL,XHC,XFR,LL
 5001 CONTINUE
      WRITE(6,99)
      WRITE(6,300)
C
C    DIMENSIONLESS PARAMETERS
C
      EP=2.D0*E/.75D0
      UAA=UAPP*2.D0/PI
      UUU=VI*UAA/(EP*R)
      EVEN=0.D0
      ODD=0.D0
      NFMI=NF-1
      DO 7979 I=2,NFMI
      J=I-1
      JF=(J/2)*2
      IF(JF.EQ.J) EVEN=EVEN+FP(I)
      IF(JF.NE.J) ODD=ODD+FP(I)
 7979 CONTINUE
      FAP=((1.DC/NFMI)/3.D0)*(2.D0*FP(1)+4.D0*ODD+2.D0*EVEN)
      WWW=FAP/(EP*R)
      SSS=EP*TP/VI
      DDD=TH/R
      WRITE(6,99)
      WRITE(6,7999)
      WRITE(6,7980) UUU
      WRITE(6,7981) WWW
      WRITE(6,7982) SSS
      WRITE(6,7983) DDD
C
C
      WRITE(6,99)
      WRITE(6,300)
      IF(NP.EQ.0) GOTO 17
      DO 5002 I=1,10
      WRITE(6,99)
 5002 CONTINUE
```

```
      WRITE(6,306)
      WRITE(6,99)
      WRITE(6,302) TZ
      WRITE(6,308) FRZ
      WRITE(6,305) BHZ
      WRITE(6,307) PHZ(1)
      WRITE(6,304)
      N1=NPX+1
      DO 5003 I=1,N1
      X=-1.D0+(I-1)*(BZ/NPX)+BHZ/2.D0
      XP=P(I,1)
      WRITE(6,305) X,XP,I
 5003 CONTINUE
      N2=NPT+1
      DO 5004 J=2,N2
      TPL=(J-1)*(TF/NPT)
      KK=(J-1)*(NSPTP/NPT)
      WRITE(6,99)
      WRITE(6,306)
      WRITE(6,99)
      WRITE(6,302) TPL
      WRITE(6,99)
      WRITE(6,308) FPR(KK)
      WRITE(6,305) BH(KK)
      WRITE(6,307) PHZ(J)
      WRITE(6,304)
      N1=NPX+1
      DO 5005 K=1,N1
      X=-1.D0+(K-1)*(BF(KK)/NPX)+BH(KK)/2.D0
      XP=P(K,J)
      WRITE(6,305) X,XP,K
 5005 CONTINUE
 5004 CONTINUE
      WRITE(6,99)
      WRITE(6,308)
   17 CONTINUE
C---------------------------------------
C            VISUAL
C---------------------------------------
      CALL PAPER(1)
      CALL CTRFNT(1)
      CALL BLKPEN
      TP1=1.
      TT(1)=TZ
      HH(1)=HZ*1.E6/R
      FF(1)=FRZ
      BFP(1)=BZ
      BHP(1)=BHZ
      XMM(1)=XMZ
      FPP(1)=FPZ/FAP
      UU(1)=UZ/UAA
      DO 6000 I=1,NSPTP
      K=I+1
      TT(K)=I*DT/TP
      HH(K)=H(I)*1.E6/R
```



```
      FF(K)=FRI(I)
      BHP(K)=BH(I)
      BFP(K)=BF(I)
      XMM(K)=XMI(I)
      FPP(K)=FPR(I)/FAP
      UU(K)=UI(I)/UAA
 6000 CONTINUE
      FPMAX=0.
      UMAX=0.
      N=NSPTP+1
      DO 6001 I=1,N
      IF(FPP(I).GT.FPMAX) FPMAX=FPP(I)
      IF(UU(I).GT.UMAX) UMAX=UU(I)
 6001 CONTINUE
      FPMAX=FPMAX*1.1
      UMAX=UMAX*1.1
      CALL PSPACE(0.,1.,0.,1.)
      CALL MAP(0.,1.,0.,1.)
      CALL PLOTCS(.06,.37,'H',1)
      CALL PLOTCS(.47,.1,'T',1)
C     CALL PLOTCS(.06,.87,'F',1)
      CALL PLOTCS(.47,.54,'T',1)
      CALL PSPACE(.11,.57,.15,.5)
      CALL MAP(0.,TP1,0.,HFACT)
      CALL BORDER
      CALL AXES
      CALL BLKPEN
      CALL CURVEC(TT,HH,1,N)
      CALL BLKPEN
      CALL PSPACE(.11,.57,.58,.93)
      CALL MAP(0.,TP1,0.,FFACT)
      CALL BORDER
      CALL AXES
      CALL BLKPEN
      CALL CURVEC(TT,FF,1,N)
      CALL FRAME
      CALL BLKPEN
      CALL PSPACE(0.,1.,0.,1.)
      CALL MAP(0.,1.,0.,1.)
      CALL PLOTCS(.06,.37,'VF',2)
      CALL PLOTCS(.47,.1,'T',1)
      CALL PLOTCS(.06,.97,'LF',2)
      CALL PLOTCS(.47,.54,'T',1)
      CALL PSPACE(.11,.57,.15,.5)
      CALL MAP(0.,TP1,0.,UMAX)
      CALL BORDER
      CALL AXES
      CALL BLKPEN
      CALL CURVEC(TT,UU,1,N)
      CALL BLKPEN
      CALL PSPACE(.11,.57,.58,.93)
      CALL MAP(0.,TP1,0.,FPMAX)
      CALL BORDER
      CALL AXES
      CALL BLKPEN
```

```
      CALL CURVE(TT,FPP,1,N)
      IF(NR.EQ.0) GOTO 29
      CALL BLKPEN
      N1=NPX+1
      N2=NPT+1
      DO 6002 J=1,N2
      TPL=(J-1)*(TF/NPT)
      TPL1=TPL/TF
      IT=(J-1)*NSPTP/NPT+1
      HX=HM(IT)
      XM=XM*(IT)
      K=(J-1)*(NSPTP/NPT)+1
      BFPX=BFP(K)
      BMPX=BMP(K)
      DO 6003 I=1,N1
      XX(I)=-1.D0+(I-1)*BFPX/NPX+BMPX/2.D0
      XX(I)=XX(I)/R
      XPR(I)=PR(I,J)/EP
 6003 CONTINUE
      XPHZ1=PHZ(J)/EP
      X1=XX(1)
      Y1=.3*HFACT
      X2=X1
      Y2=HX
      X3=XX(N1)
      Y3=HX+XXP*BFPX*1.E6/R
      X4=X3
      Y4=Y1
      XXIP=-1.D0*XFACT
      CALL FRAME
      CALL PSPACE(0.,1.,0.,1.)
      CALL MAP(0.,1.,0.,1.)
      CALL PLOTCS(.06,.37,'H',1)
      CALL PLOTCS(.47,.1,'X',1)
      CALL PLOTCS(.06,.87,'P',1)
      CALL PLOTCS(.47,.54,'X',1)
      CALL PLOTCS(.23,.51,'T =',4)
      CALL TYPENE(TPL1,4)
      CALL PSPACE(.11,.57,.58,.93)
      CALL MAP(XFACT,XXIP,0.,PFACT)
      CALL BORDER
      CALL AXES
      CALL BLKPEN
      CALL CURVEC(XX,XPR,1,N1)
      CALL CURVEC(XX,XPR,1,N1)
      CALL BLKPEN
      CALL PTPLOT(0.,XPHZ1,1,1,226)
      CALL BLKPEN
      CALL PSPACE(.11,.57,.15,.5)
      CALL MAP(XFACT,XXIP,0.,HFACT)
      CALL BORDER
      CALL AXES
      CALL BLKPEN
      CALL POSITN(X1,Y1)
      CALL JOIN(X2,Y2)
```



```
      CALL JOIN(X3,Y3)
      CALL JOIN(X4,Y4)
      CALL BLKPEN
 6002 CONTINUE
   29 CONTINUE
      CALL GREND
      STOP
      END
C---------------------------------------------------------------------
C
      SUBROUTINE CVOUT
C
C---------------------------------------------------------------------
      IMPLICIT REAL*8(A-H,O-Z)
      COMMON TOL,TOL1,H0,VI,TP,E,R,TM,WD,LAMP
      COMMON PR(201,41),PHZ(201),BM(400),BFP(401),BMP(401)
      COMMON A(15),A1(15),PD(15),AM(15),W1(15),D1(15)
      COMMON TF(100),FE(100),FP(100),W11(100),D11(100),TM(100)
      COMMON TZ,HZ,UZ,FPZ,FZ,BZ,XMZ,XMCZ,FRZ,CH1,CH2,DT,EMZ,XM
      COMMON UE(400),FPP(400),FU(400),BF(400),XMI(400),XPP(401)
      COMMON FRI(400),H(400),MST(200),UC,FPY, BC,BCRY,T1,HM
      COMMON NPER,NHALF,NSPTP,NPRT,IPRT,NPX,NPT,NP,NA,NF
   98 FORMAT(' ',/)
   99 FORMAT(' ')
  100 FORMAT(' ',6X,'TIME',13X,'H0',11X,'ENT VEL',12X,
     *       'FP',12X,'SQ VEL',10X,'LENGTH',11X,'SLOPE'/)
  101 FORMAT(' ',1X,6(D14.7,2X),D14.7)
  102 FORMAT(' ***** CONVERGES TO SPECIFIED TOLERANCE *****')
  103 FORMAT(' ***** MAXIMUM RELATIVE DIFFERENCE =',D14.7)
  104 FORMAT(' ***** NUMBER OF STEPS PER CYCLE =',I4)
  105 FORMAT(' ***** DOES NOT CONVERGE TO SPECIFIED TOLERANCE *****')
      WRITE(6,98)
      WRITE(6,100)
      WRITE(6,101) TZ,HZ,UZ,FPZ,FZ,BZ,XMZ
      DO 1 J=1,NPRT
      I=J*NSPTP/NPRT
      TPL=DT*I
      XH0=H(I)
      XU=UE(I)
      XFP=FPP(I)
      XF=FU(I)
      XB=BF(I)
      XM=XMI(I)
      XFR=FRI(I)
      WRITE(6,101) TPL,XH0,XU,XFP,XF,XB,XM
    1 CONTINUE
      IF(IPRT.EQ.1) GOTO 4
      IF((CH1.GT.TOL).OR.(CH2.GT.TCL)) GOTO 2
      WRITE(6,99)
      WRITE(6,102)
    4 CONTINUE
      IF(CH1.EQ.1.D6) GOTO 3
      WRITE(6,99)
      WRITE(6,103) CH1
      WRITE(6,104) NSPTP
```

```
      GOTO 3
    2 CONTINUE
      WRITE(6,105)
    3 RETURN
      END
C------------------------------------------------------------------------
C
      SUBROUTINE NUPRT
C
C------------------------------------------------------------------------
      IMPLICIT REAL*8(A-H,O-Z)
      COMMON TOL,TOL1,HO,VI,TP,E,R,TM,WO,UAMP
      COMMON PR(201,401),PHZ(201),BH(400),PFF(401),BHP(401)
      COMMON A(15),A1(15),PO(15),AM(15),W1(15),D1(15)
      COMMON TF(100),FE(100),FP(100),W11(100),D11(100),TM(100)
      COMMON TZ,HZ,UZ,FPZ,FZ,BZ,XMZ,XPDZ,FRZ,CH1,CH2,DT,BHZ,XM
      COMMON UE(400),FPR(400),FU(400),BF(400),XMI(400),XPP(401)
      COMMON FPI(400),H(400),HST(200),UC,FPY, BC,BDRY,T1,HV
      COMMON NPER,NHALF,NSPTP,NPRT,IPRT,NPX,NPT,NP,NA,NF
      U(T)=UAMP*DABS(DCOS((2.D0*PI/TP)*T))
      B(T)=4.D0*DSQRT(FPY*R*.75D0/(E*FI))
      F(T,HO,BC,UC,FPY,XM)=XM*U(T)*FPY*BC**3/(12.D0*VI)/
     A     (2.D0*(XM*BC)/(2.D0*HO*XP*BC)-DLOG(1.D0+XP*BC/HO))
      Y(HO,BC,FPY)=-1.D0*(FPY*HO**3)/(VI*BC**3)
      PI=3.14159265358979312D0
      NFI=NF-1
      NAI=NA-1
      TZ=0.D0
      HZ=HO
      UZ=U(TZ)
      UC=UZ
      TX=TZ
      CALL E01ADF(NFI,TX,TF,FP,W11,D11,NF,FPY)
      FPZ=FPY
      AHX=B(TZ)/(2.D0*TH)
      CALL E01ADF(NAI,AHX,AM,A,W1,C1,NA,AY)
      BHZ=2.D0*AY*TH
      BDRY=BHZ
      T1=DT
C     -----------
      CALL INCLIN
C     -----------
      XPZ=XP
      BZ=BC
      IF(XMZ.EQ.0.D0) FZ=Y(HO,BC,FPY)
      IF(XMZ.GT.0.D0) FZ=F(TZ,HZ,BZ,UZ,FPZ,XMZ)
      T=TZ
      FC=FZ
      DO 1 I=1,NSPTP
      HV=HO
      G1=FC
      T1=T+DT/2.D0
      UC=U(T1)
      CALL E01ADF(NFI,T1,TF,FP,W11,D11,NF,FPY)
      AHX=B(T1)/(2.D0*TH)
```



```
      CALL E01ACF(NAI,AHX,AM,A,W1,C1,NA,AY)
      BDRY=2.D0*AY*TH
      HO=HV+(DT/2.D0)*G1
C     -----------
      CALL INCLIN
C     -----------
      IF(XM.EQ.0.D0) G2=Y(HO,BC,FPY)
      IF(XM.GT.0.D0) G2=F(T1,HO,BC,UC,FPY,XP)
      HO=HV+(DT/2.D0)*G2
C     -----------
      CALL INCLIN
C     -----------
      IF(XM.EQ.0.D0) G3=Y(HO,BC,FPY)
      IF(XM.GT.0.D0) G3=F(T1,HO,BC,UC,FPY,XP)
      T2=T+DT
      UC=U(T2)
      CALL E01ADF(NFI,T2,TF,FP,W11,D11,NF,FPY)
      AHX=B(T2)/(2.D0*TM)
      CALL E01ACF(NAI,AHX,AM,A,W1,C1,NA,AY)
      BDRY=2.D0*AY*TH
      HO=HV+DT*G3
C     -----------
      CALL INCLIN
C     -----------
      IF(XM.EQ.0.D0) G4=Y(HO,BC,FPY)
      IF(XM.GT.0.D0) G4=F(T2,HO,BC,UC,FPY,XM)
      HO=HV+(DT/6.D0)*(G1+2.D0*G2+2.D0*G3+G4)
      T=I*DT
      UC=U(T)
      CALL E01ADF(NFI,T,TF,FP,W11,D11,NF,FPY)
      AHX=B(T)/(2.D0*TH)
      CALL E01ACF(NAI,AHX,AM,A,W1,C1,NA,AY)
      BDRY=2.D0*AY*TH
C     -----------
      CALL INCLIN
C     -----------
      IF(XM.EQ.0.D0) FC=Y(HO,BC,FPY)
      IF(XM.GT.0.D0) FC=F(T,HO,BC,UC,FPY,XM)
      H(I)=HO
      UE(I)=UC
      FPR(I)=FPY
      BH(I)=BDRY
      BF(I)=BC
      XMI(I)=XM
      FU(I)=FC
    1 CONTINUE
   60 RETURN
      END
C------------------------------------------------------------------------
C
      SUBROUTINE INCLIN
C
C------------------------------------------------------------------------
      IMPLICIT REAL*8(A-H,O-Z)
      COMMON TOL,TOL1,HO,VI,TP,E,R,TM,WO,UAMP
```

```
FILE: M        FORTRAN  A   LEEDS UNIVERSITY VM/BSE 6.16

      COMMON PR(201,41),PHZ(201),UM(400),MFP(401),XMP(401)
      COMMON A(15),A1(15),PO(15),AM(15),W1(15),D1(15)
      COMMON TF(100),FE(100),FP(100),W11(100),D11(100),TP(100)
      COMMON TZ,PZ,UZ,FPZ,FZ,BZ,XPZ,XMDZ,FR2,CH1,CH2,DT,EHZ,XM
      COMMON UE(400),FPR(400),FU(400),BF(400),XMI(400),XPP(401)
      COMMON FRI(400),H(400),HST(200),UC,FPY, BC,BDRY,T1,HM
      COMMON NPER,NHALF,NSPTP,NPRT,IPRT,NPX,NFT,NP,NA,NF
 100  FORMAT(' **** D HAS NOT ACHIEVED BUILT IN RELATIVE TOLERANCE')
      PI=3.14159265358979312D0
      UCH=UA*P*1.D-6
      IF(UC.LE.UCH) GOTO 8
      UU=2.D0*VI*LC/(E*R)
      WW=FPY/(E*R)
      AY=BDRY/(2.D0*TH)
      IF(AY.GE.2.D0) HP=1.1590D0*(1.D0/AY)**.4875D0*R*(UU**.6D0)/
     A                  (WW**.2D0)
      IF(AY.LT.2.D0) HP=1.3350D0*(1.D0/(DEXP(.2396D0*AY)))*R*(UU**.6D0)/
     A                  (WW**.2D0)
      D=0.D0
      ADD=1.D-3*HP
      DO 1 I=1,50000
      D=D+ADD
      BC=BDRY*(1.D0+D/(2.D0*HD))
      XLS=(FPY*HP**2)/(12.D0*VI*UC*BC**2)
      RS=((HM/D)**2)*(DLOG(1.D0+D/HM)-2.D0*D/(2.D0*HM+D))
      DIFF=XLS-RS
      IF(DIFF.LT.0.D0) GOTO 2
      GOTO 1
 2    RE=ADD/D
      XK=D/HM
      IF(XK.GE.1.1000D0) GOTO 12
      IF(RE.LT.1.D-12) GOTO 9
      D=D-ADD
      ADD=ADD/4.D0
 1    CONTINUE
 12   CONTINUE
      D=1.D6
      WRITE(6,100)
      GOTO 9
 8    XM=0.D0
      BC=BDRY
      GOTO 44
 9    XM=D/BC
 44   CONTINUE
      RETURN
C**********************************************************************
      END
```

```
FILE: J5        EXEC      A   LEEDS UNIVERSITY VM/BSE 6.16

EXEC SETUP FORTRAN NAGF CCGHOST
FI 5 DISK 62 DATA
FI 6 DISK 63 DATA
LOAD $1CCLEAR
EXEC PLOTFILE 69
SET BLIP *
START
```

INPUT

```
FILE: XMB        DATA      A   LEEDS UNIVERSITY VM/BSE 6.16

.0001 .5986140D-6 20 5 20 20 1 20 8 1
.01 1. 16.06 .35 .0024 .026
.03
-.04343 2.5 1.25-3 .155
13
0. .1 .2 .25 .5 1. 2. 4. 6. 8. 10. 20. 30.
1. .995 .9904 .9697 .8553 .725 .4579 .29 .1556 .1430
.11 .04591 .02677
1. 1.005 1.020 1.031 1.126 1.449 2.292 4.281 6.470 9.099
12.06 30.17 52.63
21
0. .05 .1 .15 .2 .25 .3 .35 .4 .45 .5 .55 .6 .65 .7 .75 .8 .85 .9
.95 1.
392. 561. 798. 1061. 1203. 1541. 1939. 2277. 2155. 1628. 1169. 777.
325. 250. 190. 150. 244. 190. 291. 325. 392.
```

FILE: YMB DATA A LEEDS UNIVERSITY VM/BSE 6.16

OUTPUT

**** I N P U T D A T A ****

TOL (TOLERANCE FOR SS AND STEP SIZE)	0.10000000D-03
H0 (INITIAL GUESS FOR H0 AT TIME ZERO)	0.59861980D-06
NPER (MAX. NO. OF CYCLES AT SAME STEP SIZE) ..	20
NHALF (MAX. NO. OF STEP SIZE HALVINGS)	5
NSPTP (INITIAL NO. OF STEPS PER CYCLE)	20
NPRT (NO. OF STEPS PRINTED PER CYCLE)	20
IPRT (CONVERGENCE PRINT OPTION)	1
NPX (NO. OF PRESS. PTS. PRINTED PER DIST.) ...	20
NPT (NO. OF PRESS. DIST. PRINTED)	8
NP (PRINT OPTIONS FOR PRESS. DIST.)	1
VI (ABSOLUTE VISCOSITY)	0.10000000D-01
TP (CYCLE PERIOD)	0.10000000D+01
E (ELASTIC MODULUS OF LAYER)	0.16000000D+09
R (REDUCED RADIUS)	0.35000000D+00
TH (LAYER THICKNESS)	0.24000000D-02
WD (WIDTH OF CONTACT)	0.26000000D-01
UAMP (AMPLIT. OF ENT.VEL.)	0.30000000D-01
XFACT (SCALE FACTOR FOR PLOTS)	-0.43430000E-01
HFACT (SCALE FACTOR FOR PLOTS)	0.25000000E+01
FFACT (SCALE FACTOR FOR PLOTS)	0.12000000E-02
PFACT (SCALE FACTOR FOR PLOTS)	0.15500000D+00

NOTE : FOR SS TOLERANCE EQUALS .1*TOL

A/TH	A/AH	P/PH	
0.0	0.10000000D+01	0.10000000D+01	1
0.10000000D+00	0.99500000D+00	0.10050000D+01	2
0.20000000D+00	0.98046000D+00	0.10200000D+01	3
0.25000000D+00	0.96570000D+00	0.10310000D+01	4
0.50000000D+00	0.85530000D+00	0.11260000D+01	5
0.10000000D+01	0.72500000D+00	0.14490000D+01	6
0.20000000D+01	0.49780000D+00	0.22820000D+01	7
0.40000000D+01	0.29000000D+00	0.42010000D+01	8
0.60000000D+01	0.19560000D+00	0.64780000D+01	9
0.80000000D+01	0.14300000D+00	0.50990000D+01	10
0.10000000D+02	0.11000000D+00	0.12060000D+02	11
0.20000000D+02	0.45910000D-01	0.30170000D+02	12
0.30000000D+02	0.26770000D-01	0.52630000D+02	13

T/TP	TIME	LOAD	FP

0.0	0.0	0.39200000D+03	0.15076920D+05	1
0.50000000D-01	0.50000000D-01	0.56100000D+03	0.21576920D+05	2
0.10000000D+00	0.10000000D+00	0.79800000D+03	0.30692310D+05	3
0.15000000D+00	0.15000000D+00	0.10610000D+04	0.40807690D+05	4
0.20000000D+00	0.20000000D+00	0.12030000D+04	0.46269230D+05	5
0.25000000D+00	0.25000000D+00	0.15410000D+04	0.59269230D+05	6
0.30000000D+00	0.30000000D+00	0.19390000D+04	0.74576920D+05	7
0.35000000D+00	0.35000000D+00	0.22770000D+04	0.87576920D+05	8
0.40000000D+00	0.40000000D+00	0.21550000D+04	0.82884620D+05	9
0.45000000D+00	0.45000000D+00	0.16280000D+04	0.62615380D+05	10
0.50000000D+00	0.50000000D+00	0.11690000D+04	0.44961540D+05	11
0.55000000D+00	0.55000000D+00	0.77700000D+03	0.29884620D+05	12
0.60000000D+00	0.60000000D+00	0.32500000D+03	0.12500000D+05	13
0.65000000D+00	0.65000000D+00	0.25000000D+03	0.96153850D+04	14
0.70000000D+00	0.70000000D+00	0.19000000D+03	0.73076920D+04	15
0.75000000D+00	0.75000000D+00	0.19000000D+03	0.73076920D+04	16
0.80000000D+00	0.80000000D+00	0.24400000D+03	0.93846150D+04	17
0.85000000D+00	0.85000000D+00	0.19000000D+03	0.73076920D+04	18
0.90000000D+00	0.90000000D+00	0.29100000D+03	0.11192310D+05	19
0.95000000D+00	0.95000000D+00	0.32500000D+03	0.12500000D+05	20
0.10000000D+01	0.10000000D+01	0.39200000D+03	0.15076920D+05	21

**** O U T P U T   D A T A ****

TIME	HO	SAT VEL	FP	SQ VEL	LENGTH	SLOPE
0.0	0.59861480D-06	0.30000000D-01	0.15076920D+05	0.17204710D-06	0.15521300D-01	0.98356530D-05
0.50000000D-01	0.60480100D-06	0.28531700D-01	0.21576920D+05	0.75101370D-07	0.16770840D-01	0.73538480D-05
0.10000000D+00	0.60612330D-06	0.24270510D-01	0.30692310D+05	-0.20586280D-07	0.18009540D-01	0.51483160D-05
0.15000000D+00	0.60311730D-06	0.17633560D-01	0.40807690D+05	-0.93545610D-07	0.18964970D-01	0.33728600D-05
0.20000000D+00	0.59731470D-06	0.92705100D-02	0.46269230D+05	-0.13552270D-06	0.19166700D-01	0.19121930D-05
0.25000000D+00	0.58598520D-06	0.10462610D-15	0.59269230D+05	-0.15652790D-06	0.19807850D-01	0.0
0.30000000D+00	0.58223820D-06	0.92705100D-02	0.74576920D+05	-0.14616640D-06	0.21533740D-01	0.13467150D-05
0.35000000D+00	0.57543640D-06	0.17633560D-01	0.87576920D+05	-0.12442040D-06	0.22740410D-01	0.19508200D-05
0.40000000D+00	0.57000900D-06	0.24270510D-01	0.82884620D+05	-0.90181700D-07	0.22689170D-01	0.25612470D-05
0.45000000D+00	0.56666880D-06	0.28531700D-01	0.62615380D+05	-0.40739520D-07	0.21411990D-01	0.34874460D-05
0.50000000D+00	0.56587960D-06	0.30000000D-01	0.44961540D+05	0.61740420D-09	0.19926290D-01	0.45082610D-05
0.55000000D+00	0.56712680D-06	0.28531700D-01	0.29884620D+05	0.45547040D-07	0.18138600D-01	0.57462670D-05
0.60000000D+00	0.57141330D-06	0.24270510D-01	0.12500000D+05	0.13464890D-06	0.14659300D-01	0.98454500D-05
0.65000000D+00	0.57745110D-06	0.17633560D-01	0.96153850D+04	0.72107900D-07	0.13490910D-01	0.10008030D-04
0.70000000D+00	0.57861240D-06	0.92705100D-02	0.73076920D+04	-0.24648010D-07	0.12107760D-01	0.83627500D-05
0.75000000D+00	0.57504090D-06	0.15695410D-15	0.73076920D+04	-0.10070730D-06	0.11133590D-01	0.0
0.80000000D+00	0.57123930D-06	0.92705100D-02	0.93846150D+04	-0.38678770D-07	0.12904850D-01	0.67355190D-05
0.85000000D+00	0.57301690D-06	0.17633560D-01	0.73076920D+04	0.12005900D-06	0.12659760D-01	0.12409050D-04
0.90000000D+00	0.58025200D-06	0.24270510D-01	0.11192310D+05	0.15365990D-06	0.14306270D-01	0.10766800D-04
0.95000000D+00	0.58905390D-06	0.28531700D-01	0.12500000D+05	0.19765390D-06	0.14839510D-01	0.10929990D-04
0.10000000D+01	0.59861250D-06	0.30000000D-01	0.15076920D+05	0.17204820D-06	0.15521310D-01	0.99356420D-05

E11

FILE: YMB DATA A LEEDS UNIVERSITY VM/RSE 6.16

TIME	MO	EAT VEL	FP	SQ VEL	LENGTH	SLOPE
0.0	0.5986125D-06	0.3000000D-01	0.1507692D+05	0.1720482D-06	0.1552131D-01	0.9835642D-05
0.5000000D-01	0.6047988D-06	0.2853170D-01	0.2157692D+05	0.7510264D-07	0.1677985D-01	0.7353841D-05
0.1000000D+00	0.6061211D-06	0.2427051D-01	0.3065231D+05	-0.2058484D-07	0.1800954D-01	0.5148312D-05
0.1500000D+00	0.6031152D-06	0.1763356D-01	0.4080769D+05	-0.9354409D-07	0.1896497D-01	0.3372859D-05
0.2000000D+00	0.5973127D-06	0.9270510D-02	0.4626923D+05	-0.1355211D-06	0.1916678D-01	0.1912193D-05
0.2500000D+00	0.5898033D-06	0.1046361D-16	0.5926923D+05	-0.1565364D-06	0.1980785D-01	0.0
0.3000000D+00	0.5822363D-06	0.9270510D-02	0.7457692D+05	-0.1461645D-06	0.2153375D-01	0.1346715D-05
0.3500000D+00	0.5754347D-06	0.1763356D-01	0.8757692D+05	-0.1244185D-06	0.2274041D-01	0.1950819D-05
0.4000000D+00	0.5700073D-06	0.2427051D-01	0.8288462D+05	-0.9018038D-07	0.2268918D-01	0.2561245D-05
0.4500000D+00	0.5666872D-06	0.2853170D-01	0.6261538D+05	-0.4073837D-07	0.2141198D-01	0.3487444D-05
0.5000000D+00	0.5658780D-06	0.3000000D-01	0.4496154D+05	0.6175824D-08	0.1992629D-01	0.4503258D-05
0.5500000D+00	0.5671252D-06	0.2853170D-01	0.2588462D+05	0.4554789D-07	0.1813860D-01	0.5746264D-05
0.6000000D+00	0.5714118D-06	0.2427051D-01	0.1250000D+05	0.1346495D-06	0.1469430D-01	0.9845442D-05
0.6500000D+00	0.5774497D-06	0.1763356D-01	0.9615385D+04	0.7210856D-07	0.1345092D-01	0.1000803D-04
0.7000000D+00	0.5786110D-06	0.9270510D-02	0.7307692D+04	-0.2464730D-07	0.1210776D-01	0.8362785D-05
0.7500000D+00	0.5750795D-06	0.1569541D-16	0.7307692D+04	-0.1007866D-06	0.1113359D-01	0.0
0.8000000D+00	0.5712370D-06	0.9270510D-02	0.9384615D+04	-0.3067608D-07	0.1290485D-01	0.6735515D-05
0.8500000D+00	0.5730156D-06	0.1763356D-01	0.7307692D+04	0.1200595D-06	0.1265976D-01	0.1240904D-04
0.9000000D+00	0.5802507D-06	0.2427051D-01	0.1115231D+05	0.1536603D-06	0.1430627D-01	0.1076599D-04
0.9500000D+00	0.5890527D-06	0.2853170D-01	0.1250000D+05	0.1976845D-06	0.1483951D-01	0.1092858D-04
0.1000000D+01	0.5986113D-06	0.3000000D-01	0.1507692D+05	0.1720487D-06	0.1552131D-01	0.9835635D-05

***** MAXIMUM RELATIVE DIFFERENCE = 0.3629870D-05
***** NUMBER OF STEPS PER CYCLE = 20

STEP SIZE IS HALVED

TIME	MO	EAT VEL	FP	SQ VEL	LENGTH	SLOPE
0.0	0.5986125D-06	0.3000000D-01	0.1507692D+05	0.1720482D-06	0.1552131D-01	0.9835642D-05
0.5000000D-01	0.6047976D-06	0.2853170D-01	0.2157692D+05	0.7510335D-07	0.1677085D-01	0.7353837D-05
0.1000000D+00	0.6061202D-06	0.2427051D-01	0.3065231D+05	-0.2059419D-07	0.1800954D-01	0.5149310D-05
0.1500000D+00	0.6031153D-06	0.1763356D-01	0.4080765D+05	-0.9354413D-07	0.1896497D-01	0.3372859D-05
0.2000000D+00	0.5973116D-06	0.9270510D-02	0.4626923D+05	-0.1355202D-06	0.1916670D-01	0.1912193D-05
0.2500000D+00	0.5898825D-06	0.1046361D-16	0.5926923D+05	-0.1565357D-06	0.1980785D-01	0.0
0.3000000D+00	0.5822348D-06	0.9270510D-02	0.7457692D+05	-0.1461636D-06	0.2153375D-01	0.1346714D-05
0.3500000D+00	0.5754329D-06	0.1763356D-01	0.8757692D+05	-0.1244175D-06	0.2274041D-01	0.1950819D-05
0.4000000D+00	0.5700053D-06	0.2427051D-01	0.8288462D+05	-0.9017883D-07	0.2268918D-01	0.2561244D-05
0.4500000D+00	0.5666862D-06	0.2853170D-01	0.6261538D+05	-0.4073764D-07	0.2141198D-01	0.3497443D-05
0.5000000D+00	0.5658769D-06	0.3000000D-01	0.4496154D+05	0.6175716D-08	0.1992630D-01	0.4509256D-05
0.5500000D+00	0.5671212D-06	0.2853170D-01	0.2588462D+05	0.4555014D-07	0.1813961D-01	0.5746254D-05
0.6000000D+00	0.5714309D-06	0.2427051D-01	0.1250000D+05	0.1346415D-06	0.1469426D-01	0.9845546D-05
0.6500000D+00	0.5774527D-06	0.1763356D-01	0.9615385D+04	0.7210719D-07	0.1345091D-01	0.1000804D-04
0.7000000D+00	0.5786106D-06	0.9270510D-02	0.7307692D+04	-0.2464712D-07	0.1210776D-01	0.8362783D-05
0.7500000D+00	0.5750763D-06	0.1569541D-16	0.7307692D+04	-0.1007052D-06	0.1113359D-01	0.0
0.8000000D+00	0.5712206D-06	0.9270510D-02	0.9384615D+04	-0.3866975D-07	0.1290488D-01	0.6735474D-05
0.8500000D+00	0.5730323D-06	0.1763356D-01	0.7397692D+04	0.1200527D-06	0.1265973D-01	0.1240917D-04
0.9000000D+00	0.5902776D-06	0.2427051D-01	0.1115231D+05	0.1536452D-06	0.1430621D-01	0.1076616D-04
0.9500000D+00	0.5890803D-06	0.2853170D-01	0.1250000D+05	0.1976733D-06	0.1483845D-01	0.1092876D-04
0.1000000D+01	0.5986388D-06	0.3000000D-01	0.1507692D+05	0.1720360D-06	0.1552125D-01	0.9835773D-05

FILE: YMB DATA A LEEDS UNIVERSITY VM/BSE 6.16

***** MAXIMUM RELATIVE DIFFERENCE = 0.46826510-04
***** NUMBER OF STEPS PER CYCLE = 40

TIME	HC	F COEFF	
0.0	0.66631110-06	0.92401460-03	1
0.50000000-01	0.66075790-06	0.67108470-03	2
0.10000000+00	0.64918340-06	0.43581940-03	3
0.15000000+00	0.63349770-06	0.25997580-03	4
0.20000000+00	0.61509130-06	0.12574980-03	5
0.25000000+00	0.59998250-06	0.11956430-19	6
0.30000000+00	0.59636240-06	0.90406520-04	7
0.35000000+00	0.59679080-06	0.15429080-03	8
0.40000000+00	0.55765220-06	0.22326540-03	9
0.45000000+00	0.60171490-06	0.32521350-03	10
0.50000000+00	0.60749030-06	0.43839530-03	11
0.55000000+00	0.61484980-06	0.56351620-03	12
0.60000000+00	0.63563940-06	0.69501650-03	13
0.65000000+00	0.63789530-06	0.77502820-03	14
0.70000000+00	0.62516460-06	0.45344410-03	15
0.75000000+00	0.57507690-06	0.83163320-19	16
0.80000000+00	0.61160880-06	0.41884440-03	17
0.85000000+00	0.64211220-06	0.94844690-03	18
0.90000000+00	0.64826600-06	0.95370680-03	19
0.95000000+00	0.66035300-06	0.10212180-02	20
0.10000000+01	0.66632830-06	0.92397420-03	21

$$$$ DIMENSIONLESS PARAMETERS $$$$

U = 0.12790-10
W = 0.22580-02
S = 0.42670+10
D = 0.68570-02

FILE: YMB DATA A LEEDS UNIVERSITY VM/BSE 6.16

TIME = 0.0

FP = 0.15876920+05

DRY CONTACT LENGTH = 0.13765970-01

MAXIMUM DRY CONTACT STRESS = 0.16641590+07

X	PRESSURE	
0.68829830-02	0.0	1
0.61369170-02	0.34049940+06	2
0.53309520-02	0.62521250+06	3
0.45547970-02	0.86562270+06	4
0.37787210-02	0.10649730+07	5
0.30026560-02	0.12182740+07	6
0.22265900-02	0.13323340+07	7
0.14505250-02	0.14097670+07	8
0.67445950-03	0.14530080+07	9
-0.10160590-03	0.14643310+07	10
-0.87767130-03	0.14458560+07	11
-0.16537370-02	0.13995630+07	12
-0.24298020-02	0.13273000+07	13
-0.32058670-02	0.12307960+07	14
-0.39819330-02	0.11116670+07	15
-0.47579980-02	0.97142520+06	16
-0.55340640-02	0.81148430+06	17
-0.63101290-02	0.63316930+06	18
-0.70861940-02	0.43772060+06	19
-0.78622600-02	0.22630100+06	20
-0.86383250-02	0.26085230-09	21

TIME = 0.12500000+00

FP = 0.36241130+05

DRY CONTACT LENGTH = 0.17468970-01

MAXIMUM DRY CONTACT STRESS = 0.32120290+07

X	PRESSURE	
0.87344970-02	0.0	1
0.78049880-02	0.61385240+06	2
0.68754740-02	0.11596280+07	3

CONTINUES ....

APPENDIX F

THE CONSTRAINED COLUMN DEFORMATION MODEL

```
C-----------------------------------------------------------------------
C             PART 1
C     THE STEADY STATE COLUMN MODEL
C
C             SOLVED USING GEAR NUMERICAL ROUTINE
C
C-----------------------------------------------------------------------
      IMPLICIT REAL*8(A-H,O-Z)
      REAL*4 XX(800),XX1(800),PP(800),HH(800),PMAX,HFACT,XXE,XFACT
      DIMENSION A(64),A1(64),AM(64),PCP(64)
      DIMENSION AK(68),AC(68),AM(400),PKI(68),PCI(68)
      DIMENSION TP(100),FE(100),FPI(100),TM(100),FKI(104),FCI(104)
      DIMENSION FW(616)
      DIMENSION FCS(1),W2(1,19),FR2(7000),PPD(4500)
      COMMON X(9000),PSTORE(9000)
      COMMON VI,UM,H0,R,AM,XE,XI,CX,JI,NST
      EXTERNAL FCN,PEDERV,OUTPUT
      CALL SETTIP
      PI=3.14159265358979312D0
C
C-------------------------
C          INPUT
C-------------------------
      READ(4,*) NTIME
      READ(4,*) UM0
      READ(4,*) VI,TP,E,R,TH,WD,PR
      READ(4,*) RT,THETA
      READ(4,*) XI,NST
      READ(4,*) DTCL
      READ(4,*) PTCL,FPTOL
      READ(4,*) FRTOL
      READ(4,*) HFACT,XFACT
      READ(4,*) F1,F2,F3,F4
      READ(4,*) I1,I2
      READ(4,*) IPT,MAGN
      READ(4,*) NA
      READ(4,*) (A(I),I=1,NA)
      READ(4,*) (A1(I),I=1,NA)
      READ(4,*) (FCR(I),I=1,NA)
      READ(4,*) NF
      READ(4,*) (TP(I),I=1,NF)
      READ(4,*) (FE(I),I=1,NF)
C-------------------------
C          CHECK
C-------------------------
  99  FORMAT(' ')
 100  FORMAT(' ----------------------------------------------------',
     +      '-------------------------------'/)
 101  FORMAT(' ----------------------------------------------------',
     +'-------------------------------------------------------'/)
6928  FORMAT(/' ********  CPU =',D11.3/)
 114  FORMAT(' ',6X,'T/TP',12X,'TIME',12X,'LOAD',13X,'F'/)
 115  FORMAT(' ',1X,4(D14.7,2X),I8)
 116  FORMAT(' ****  I N P U T   D A T A   ****'/)
 117  FORMAT(' ****   O U T P U T   D A T A   ****'/)
C
C
 1396 FORMAT(' NTIME (NO. OF TIME STEPS) ..................... ',I8)
 1397 FORMAT(' UM0 (LOWER LIMIT FOR UM) ........................ ',D14.7)
 1400 FORMAT(' VI (ABSOLUTE VISCOSITY) ......................... ',D14.7)
 1700 FORMAT(' TP (PERIOD OF CYCLE) ............................ ',D14.7)
 1401 FORMAT(' E (ELASTIC MODULUS OF LAYER) .................... ',D14.7)
 1701 FORMAT(' R (REDUCED RADIUS) .............................. ',D14.7)
 1702 FORMAT(' TH (LAYER THICKNESS) ............................ ',D14.7)
 1703 FORMAT(' WD (WIDTH OF BEARING) ........................... ',D14.7)
 1402 FORMAT(' PR (POISSONS RATIO) ............................. ',D14.7)
 1712 FORMAT(' RT (TALUS RADIUS) ............................... ',D14.7)
 1713 FORMAT(' THETA (ANGULAR AMPLITUDE IN DEGREES) ............ ',D14.7)
 1407 FORMAT(' XI (INLET BOUNDARY) ............................. ',D14.7)
 1408 FORMAT(' NST (INITIAL NUMBER OF STEPS) ................... ',I8)
 1409 FORMAT(' DTCL (INITIAL RELATIVE TOLERANCE FOR CO2EEF) .. ',D14.7)
 1410 FORMAT(' PTOL (RELATIVE INLET PRESSURE TOLERANCE) ...... ',D14.7)
 1411 FORMAT(' FPTOL (RELATIVE LOAD CAPACITY TOLERANCE) ...... ',D14.7)
 1414 FORMAT(' FRTCL (TOLERANCE FOR FR STEP DEPENDENCE) ...... ',D14.7)
 1514 FORMAT(' HFACT (SCALE FACTOR FOR FILM PLOTS) ........... ',E14.7)
 1614 FORMAT(' XFACT (SCALE FACTOR FOR PLOTS) ................ ',E14.7)
 1416 FORMAT(' F1 (XA=XE*F1, INITIAL XE INCREMENT) ........... ',D14.7)
 1417 FORMAT(' F2 (XE=XE*F2, INITIAL XE GUESS) ............... ',D14.7)
 1418 FORMAT(' F3 (HA=H0*F3, INITIAL H0 INCREMENT) ........... ',D14.7)
 1419 FORMAT(' F4 (HMGU=HM*F4, INITIAL H0 GUESS) ............. ',D14.7)
 1421 FORMAT(' I1 (NUMBER OF POINTS PLOTTED) ................. ',I9)
 1422 FORMAT(' I2 (NUMBER OF POINTS PRINTED) ................. ',I8)
 1423 FORMAT(' IPT (PRINT OPTION FOR CONVERGENCE DATA) ....... ',I8)
 1523 FORMAT(' MAGN (PRINT OPTION FOR 1 CYCLE) ............... ',I8)
C
C
 132  FORMAT(' ',6X,'AH/TH',11X,'A/TH',12X,'A/AH',12X,'P/PM')
 133  FORMAT(' ',1X,4(D14.7,2X),I8)
      WRITE(5,101)
      WRITE(5,116)
      WRITE(5,101)
      WRITE(5,99)
      WRITE(5,1396) NTIME
      WRITE(5,1399) UM0
      WRITE(5,1400) VI
      WRITE(5,1700) TP
      WRITE(5,1401) E
      WRITE(5,1701) R
      WRITE(5,1702) TH
      WRITE(5,1703) WD
      WRITE(5,1402) PR
      WRITE(5,1712) RT
      WRITE(5,1713) THETA
      WRITE(5,1407) XI
      WRITE(5,1408) NST
      WRITE(5,1409) DTCL
      WRITE(5,1410) PTCL
      WRITE(5,1411) FPTCL
      WRITE(5,1414) FRTCL
      WRITE(5,1514) HFACT
```

```
      WRITE(5,1616) XFACT
      WRITE(5,1916) F1
      WRITE(5,1917) F2
      WRITE(5,1918) F3
      WRITE(5,1919) F4
      WRITE(5,1921) I1
      WRITE(5,1922) I2
      WRITE(5,1923) IPT
      WRITE(5,1523) MAGN
      WRITE(5,99)
      WRITE(5,100)
      WRITE(5,99)
      WRITE(5,132)
      WRITE(5,99)
      DO 467 I=1,NA
      AM(I)=A(I)/A1(I)
      WRITE(5,133) AM(I),A(I),A1(I),PCR(I),I
  467 CONTINUE
      WRITE(5,100)
      DO 1010 I=1,NF
      TF(I)=TM(I)*TP
      FPI(I)=FE(I)/WD
 1010 CONTINUE
      WRITE(5,99)
      WRITE(5,114)
      DO 1011 I=1,NF
      WRITE(5,115) TM(I),TF(I),FE(I),FPI(I),I
 1011 CONTINUE
      WRITE(3,99)
      WRITE(5,101)
      WRITE(5,117)
      WRITE(5,101)
      WRITE(5,99)
C-------------------------
C         CCNO
C-------------------------
 4779 FORMAT(' IACEX NO. (NT) =',I6/)
 4780 FORMAT(' ENTRAINMENT VELOCITY (UM)  =  ',D14.7/)
 4781 FORMAT(' LOAD PER UNIT WIDTH  (FP)  =  ',D14.7/)
 4782 FORMAT(' TIME (TC) =',D14.7/)
      NF4=NF+4
      NA4=NA+4
      LWRK=6*NA+16
      LWRK1=6*NF+16
      CALL PAPER(1)
      CALL CTRFNT(1)
      AM=(TM/E)*(1.D0-2.D0*(PR**2)/(1.D0-PR))
      CALL E01BAF(NF,TF,FFI,FKI,FCI,NF4,FW,LWRK1,0)
      CALL E01BAF(NA,AM,A,AK,AC,NA4,AW,LWRK,0)
      CALL E01BAF(NA,A,PCR,PKI,PCI,NA4,AW,LWRK,0)
      NST1=NST
      IPTS=IPT
      DTOL1=DTOL
      DT=TP/NTIME
      NTMP=NTIME+1
```



```
C
C=====================================================================
C
      DO 1067 NT=1,NTMP
C
C=====================================================================
C
      IF(NT.EQ.MAGN) IPT=1
      TC=(NT-1)*DT
      NST=NST1
      DTOL=DTOL1
      CALL E02BBF(NF4,FKI,FCI,TC,FP,0)
      UM=(PI**2*THETA*RT/(TP*180.D0))*DABS(DCOS((2.D0*PI/TP)*TC))
      WRITE(5,100)
      WRITE(5,99)
      WRITE(5,4779) NT
      WRITE(5,4782) TC
      WRITE(5,4780) UM
      WRITE(5,4781) FP
      WRITE(5,100)
C-------------------------
C         LIMIT
C-------------------------
      IF(UM.LT.UM0) UM=UM0
C-------------------------
C         COMPARISONS
C-------------------------
  501 FORMAT(' VARIOUS ESTIMATES FOR POISSONS RATIO OF .5'/)
  701 FORMAT(' ',5X,'HMIN =',D14.7,4X,'HCEN =',D14.7/)
  789 FORMAT(' ',5X,'A =',D14.7,7X,'PMAX =',D14.7/)
  604 FORMAT(' (1.) FOR SURFACE LAYER USING DATA BY GUPTA')
  605 FORMAT(' (2.) FOR SURFACE LAYER USING FORMULAS BY HOOKE AND',
     C' VARNUM')
  606 FORMAT(' (3.) FOR RIGID SURFACE USING FORMULA BY MARTIN')
  431 FORMAT(' (4.) FOR ELASTIC SURFACES USING HERTZIAN FORMULAS')
  607 FORMAT(' (5.) FOR ELASTIC SURFACES USING FORMULA BY SWALES')
  608 FORMAT(' ',5X,'HMIN = HCEN =',D14.7/)
  609 FORMAT(' (6.) FOR ELASTIC SURFACES USING FORMULA BY VARNUM')
  610 FORMAT(' (7.) FOR ELASTIC SURFACES USING FORMULA BY HERREBRUGH')
      AMX=(2.D0/TM)*DSQRT(FP*R*.75D0/(E*PI))
      CALL E02BBF(NA4,AK,AC,AMX,AY,0)
      AYX=AY
      CALL E02BBF(NA4,PKI,PCI,AYX,PDY,0)
      XE=AY*TM
      PDRY=PDY*4.D0*DSQRT(FP*E/(12.D0*PI*R))
      UU=2.D0*VI*UM/(E*R)
      WW=FP/(E*R)
      IF(AY.GE.2.D0) HM=1.159D0*(1.D0/AY)**.4875D0*R*(UU**.6D0)/
     C(WW**.2D0)
      IF(AY.LT.2.D0) HM=1.335D0*(1.D0/(DEXP(.2396D0*AY)))*R*(UU**.6D0)/
     C(WW**.2D0)
      HCM=HM/.795D0
      HRIGID=1.224D0*VI*UM*R/FP
      EP=E/.75D0
      UX=VI*UM/(EP*R)
```

```
      UM=FP/(EP*F)
      HMMZ=2.30*R*(UX**.5790)/(UM**.1300)
      HCMZ=HMMZ/.7000
      HMV=1.7120*R*(UU**.6D0)/(UW**.2D0)
      HCV=HMV/.7550D0
      HMM=3.1870D*R*(UX**.6D0)/(UW**.2D0)
      HCMM=HMM/.7000
      AMZ=AMX*TH
      PMZ=PCRY/PCY
C     IF(IPT.EQ.0) GOTO 1868
      WRITE(5,501)
      WRITE(5,604)
      WRITE(5,705) XE,PCRY
      WRITE(5,605)
      WRITE(5,701) HM,HCH
      WRITE(5,606)
      WRITE(5,608) HRIGID
      WRITE(5,431)
      WRITE(5,709) AMX,PMZ
      WRITE(5,607)
      WRITE(5,701) HMMZ,HCMZ
      WRITE(5,609)
      WRITE(5,701) HMV,HCV
      WRITE(5,610)
      WRITE(5,701) HMM,HCMM
      WRITE(5,100)
      WRITE(5,99)
C1868 CONTINUE
C---------------------------
C          PREP
C---------------------------
      XE=XE*F2
      HMGU=HM*F4
      ICOUNT=2
      KL1=0
      KL3=0
      XA=XE*F1
      PT=PTOL*PCRY
      DTL=DTOL*PCRY
C---------------------------
C          PRESSURE
C---------------------------
  118 FORMAT(' H0 =',D14.7,I9)
   84 CONTINUE
      H0=HMGU-1.D0*(XE**2)/(2.D0*R)
      HA=H0*F3
      JCOUNT=2
      KL2=1
    8 CONTINUE
      IF(IPT.EQ.1) WRITE(5,118) H0,KL2
C
C   SOLVING PRESSURE FOR TRIAL H0 USING D02EBF
C
      PCS(1)=0.D0
      XC=XE
```



```
      DX=XI-XE
      JI=0
      CALL D02EBF(XC,XI,1,PCS,DTL,1,FCN,1,PEDERV,OUTPUT,W2,19,0)
      KL2=KL2+1
      KL3=KL3+1
      PC=PCS(1)
      IF(PC.LT.0.D0) GOTO 5
      IF(PC.GT.PT) GOTO 6
      GOTO 9
C
C   DETERMINING THE REQUIRED H0 USING BISECTION
C
    5 IF(JCOUNT.EQ.0) HA=HA/2.D0
      JCOUNT=1
      H0=H0-HA
      GOTO 8
    6 IF(JCOUNT.EQ.1) HA=HA/2.D0
      JCOUNT=0
      H0=H0+HA
      GOTO 8
    9 CONTINUE
C-------------------------
C          LOAD
C-------------------------
  120 FORMAT(' ...CALCULATED FP = ',D14.7,3X,'FOR XE =',D14.7,3X,
     *'( EE =',D10.3,' % )',I9)
  119 FORMAT(' ...SPECIFIED FP =',D14.7)
C
C   SOLVING LOAD CAPACITY FOR TRIAL XE USING D02EBF AND D01GAF
C
      PCS(1)=0.D0
      XC=XE
      DX=(XI-XE)/NST
      JI=0
      CALL D02EBF(XC,XI,1,PCS,DTL,1,FCN,1,PEDERV,OUTPUT,W2,19,0)
      KL3=KL3+1
      NPLUS=NST+1
      CALL D01GAF(X,PSTORE,NPLUS,FPC,EE,0)
      KL1=KL1+1
      FPC=-FPC
      IF(IPT.EQ.0) GOTO 1597
      EE=100.D0*DABS(EE)/FPC
      WRITE(5,120) FPC,XE,EE,KL1
      WRITE(5,119) FP
 1597 CONTINUE
      DIFF=DABS(FP-FPC)/FP
      IF(DIFF.LE.FPTOL) GOTO 81
      IF(FP.GT.FPC) GOTO 82
      IF(FP.LT.FPC) GOTO 83
C
C   DETERMINING THE REQUIRED XE USING BISECTION
C
   82 IF(ICOUNT.EQ.1) XA=XA/2.D0
      ICOUNT=0
      XE=XE+XA
```

```
      GOTO 84
   83 IF(ICOUNT.EQ.0) XA=XA/2.D0
      ICOUNT=1
      XE=XE-XA
      GOTO 89
   81 CONTINUE
C-------------------------
C          FRICTION
C-------------------------
  497 FORMAT(' *****H0 ERROR IN FRICTION SECTION')
      PMXD=0.D0
      HXE=H0+XE**2/(2.D0*R)
      FX2(1)=2.D0/HXE
      DO 890 I=1,NST
      J8=I+1
      XC=X(J8)
      PC=PSTORE(J8)
      HX=H0+(XC**2)/(2.D0*R)+AM*PC
      IF(PC.GT.PMXD) PMXD=PC
      FX2(J8)=6.D0*HXE/(HX**2)-4.D0/HX
  890 CONTINUE
C
C   SOLVING INTEGRALS FOR FRICTION CALCULATION USING D01GAF
C
      CALL D01GAF(X,FX2,NPLUS,FR2,ER2,0)
      FR2=-FR2
      IF(H0.LT.0.D0) XV=DSQRT(-H0/(2.D0*R))
      IF(H0.GT.0.D0) XV1=DSQRT(2.D0*H0*R)
      IF(H0.EQ.0.D0) WRITE(5,497)
      DEN1=H0+(XI**2)/(2.D0*R)
      DEN2=H0+(XE**2)/(2.D0*R)
      IF(H0.LT.0.D0) XINT=(1.D0/(2.D0*H0))*(.5D0*(1.D0/XV)*
     C(DLOG((H0-XI*XV)*(H0-XE*XV)/((H0+XI*XV)*(H0+XE*XV))))-
     C(XI/DEN1+XE/DEN2))
      IF(H0.GT.0.D0) XINT=(1.D0/(2.D0*H0))*(DSQRT(2.D0*R/H0)*
     C(DATAN(-XI/XV1)-DATAN(XE/XV1))-(XI/DEN1+XE/DEN2))
      FR=(VI*UM/FPC)*(FR2+2.D0*HXE*XINT)
C-------------------------
C          RELIABILITY
C-------------------------
  662 FORMAT(' DTL DECREASED FOR GLOBAL PRESSURE RELIABILITY CHECK'/)
  721 FORMAT(' NO. OF STEPS DOUBLED FOR FP RELIABILITY CHECK'/)
  948 FORMAT(' NO. OF STEPS DOUBLED FOR FR RELIABILITY CHECK'/)
  941 FORMAT(' ',7X,'POLD',12X,'PNEW',13X,'X',12X,'A.DIFF.'/)
  942 FORMAT(' ',1X,4(D14.7,2X)/)
  943 FORMAT(' ',6X,'FPOLD',11X,'FPNEW',10X,'P.DIFF.'/)
  751 FORMAT(' ',6X,'FROLD',11X,'FRNEW',10X,'R.DIFF.'/)
  944 FORMAT(' ',1X,3(D14.7,2X)/)
  999 FORMAT(' RELIABILITY CHECKS CONVERGE TO SPECIFIED TOLERANCES'/)
  951 FORMAT(' ABSOLUTE INLET PRESSURE TOLERANCE ADJUSTED'/)
  952 FORMAT(' ',7X,'PTOLD',11X,'PTNEW',11X,'R.DIFF.'/)
  953 FORMAT(' ',1X,3(D14.7,2X)/)
  983 FORMAT(' FINAL DTL FOR RELIABILITY CHECKS =',D14.7/)
  984 FORMAT(' FINAL NO. OF STEPS FOR RELIABILITY CHECKS =',I6/)
  985 FORMAT(' TOTAL NUMBER OF CALLS TO D02EBF =',I6/)
```



```
C
C   STORE CURRENT PRESSURE VALUES
C
      PPD(1)=PSTORE(1)
      DO 4567 I=1,NST
      J8=I+1
      PPD(J8)=PSTORE(J8)
 4567 CONTINUE
      J=1
      DTL=DTL*.1D0
      NST=2*NST
      NPLUS=NST+1
      DX=(XI-XE)/NST
      XC=XE
      PCS(1)=0.D0
      HXE=H0+XE**2/(2.D0*R)
      FX2(1)=2.D0/HXE
      HX1=0.D0
      PC1=0.D0
      JI=0
      CALL D02EBF(XC,XI,1,PCS,DTL,1,FCN,1,PEDERV,OUTPUT,W2,19,0)
C
C   GLOBAL PRESSURE RELIABILITY CHECK
C
      SPTOL=PT*.1D0
      PMXD=0.D0
      DO 76 I=1,NST
      J8=I+1
      XC=X(J8)
      PC=PSTORE(J8)
      HX=H0+(XC**2)/(2.D0*R)+AM*PC
      IF(PC.GT.PMXD) P11=PC1
      IF(PC1.EQ.PMXD) P22=PC
      IF(PC.GT.PMXD) PMXD=PC
      PC1=PC
      FX2(J8)=6.D0*HXE/(HX**2)-4.D0/HX
      IC=(I/2)*2
      IF(IC.NE.I) GOTO 76
      J=J+1
      DP=DABS(PC-PPD(J))
      IF(DP.GT.SPTOL) GOTO 77
   76 CONTINUE
      GOTO 78
   77 CONTINUE
      IF(IPT.EQ.0) GOTO 6792
      WRITE(5,100)
      WRITE(5,99)
      WRITE(5,662)
      WRITE(5,941)
      WRITE(5,942) PPD(J),PC,XC,DP
      WRITE(5,100)
 6792 CONTINUE
      NST=NST/2
      GOTO 8
   78 CONTINUE
```

```
C
C   ABSOLUTE INLET PRESSURE TOLERANCE CHECKED
C
      PTN=PMXD*PTCL
      DPT=DABS((PTN-PT)/PTN)
      IF(DPT.GT.PTOL) GOTO 723
      GOTO 722
 723  CONTINUE
      IF(IPT.EQ.0) GOTO 6321
      WRITE(5,100)
      WRITE(5,951)
      WRITE(5,952)
      WRITE(5,953) PT,PTN,DPT
      WRITE(5,100)
 6321 CONTINUE
      NST=NST/2
      DTL=DTL*10.D0*PTN/PT
      PT=PTN
      GOTO 8
 722  CONTINUE
C
C   FP RELIABILITY CHECK
C
      SFTOL=.1D0*FPTCL
      CALL D01GAF(X,PSTORE,NPLUS,FPCD,ERROR,0)
      FPCD=-FPCD
      DFP=DABS((FPCD-FPC)/FPCD)
      IF(DFP.GT.SFTOL) GOTO 719
      GOTO 720
 719  CONTINUE
      IF(IPT.EQ.0) GOTO 6322
      WRITE(5,100)
      WRITE(5,95)
      WRITE(5,721)
      WRITE(5,943)
      WRITE(5,944) FPC,FPCD,DFP
      WRITE(5,100)
 6322 CONTINUE
      DTL=DTL*10.D0
      GOTO 8
 720  CONTINUE
C
C   FR RELIABILITY CHECK
C
      NPLUS=NST+1
      CALL D01GAF(X,FX2,NPLUS,FR2,ER2,0)
      FR2=-FR2
      IF(H0.LT.0.D0) XY=DSQRT(-H0/(2.D0*R))
      IF(H0.GT.0.D0) XY1=DSQRT(2.D0*H0*R)
      IF(H0.EQ.0.D0) WRITE(5,497)
      DEN1=H0+(XI**2)/(2.D0*R)
      DEN2=H0+(XE**2)/(2.D0*R)
      IF(H0.LT.0.D0) XINT=(1.D0/(2.D0*H0))*(.5D0*(1.D0/XY)*
     C(DLOG((H0-XI*XY)*(H0-XE*XY)/((H0+XI*XY)*(H0+XE*XY))))-
     C(XI/DEN1+XE/DEN2))
```



```
      IF(H0.GT.0.D0) XINT=(1.D0/(2.D0*H0))*(DSQRT(2.D0*R/H0)*
     C(DATAN(-XI/XY1)-DATAN(XE/XY1))-(XI/DEN1+XE/DEN2))
      FRD=(VI*UM/FPCD)*(FR2+2.D0*HXE*XINT)
      DFR=DABS((FRD-FR)/FRD)
      IF(DFR.GT.FRTOL) GOTO 329
      GOTO 796
 329  CONTINUE
      IF(IPT.EQ.0) GOTO 6323
      WRITE(5,100)
      WRITE(5,99)
      WRITE(5,948)
      WRITE(5,751)
      WRITE(5,944) FR,FRD,DFR
      WRITE(5,100)
 6323 CONTINUE
      DTL=DTL*10.D0
      GOTO 8
 796  CONTINUE
      IF(IPT.EQ.0) GOTO 6324
      WRITE(5,99)
      WRITE(5,100)
      WRITE(5,97)
      WRITE(5,995)
      WRITE(5,982) DTL
      WRITE(5,984) NST
      WRITE(5,985) KL3
      WRITE(5,100)
 6324 CONTINUE
C-------------------------
C          FIXED
C-------------------------
C
C   ERROR ESTIMATE FOR MAXIMUM PRESSURE
C
      E11=DABS((F11-PMXD)/PMXD)
      E22=DABS((F22-PMXD)/PMXD)
      ERP=E11*100.D0
      IF(E22.GT.E11) ERP=E22*100.D0
C
C   MINIMUM AND CENTRAL FILM THICKNESS
C
      HMIN=H0+XE**2/(2.D0*R)
      H1=HMIN
      DO 199 I=1,NST
      J8=I+1
      XC=X(J8)
      PC=PSTORE(J8)
      HX=H0+(XC**2)/(2.D0*R)+AM*PC
      IF(H1.EQ.HMIN) HM1=HX
      IF(HM1.EQ.H1) HM2=HX
      IF(HX.LT.HMIN) XMIN=XC
      IF(HX.LT.HMIN) HMIN=HX
      H1=HX
      IF(XC.LT.0.D0) GOTO 199
      P1=PC
```

96

```
      X1=HC
      HC1=HX
      N2=J0+1
  199 CONTINUE
      X2=-1.D0*X(N2)
      P2=PSTORE(N2)
      HC2=H0+X2**2/(2.D0*R)+AM*P2
      IF(X1.LT.X2) GOTO 7521
      HC=HC2
      HC2=HC1
      GOTO 7522
 7521 CONTINUE
      HC=HC1
      HC2=HC2
 7522 CONTINUE
      EHC=100.D0*DABS((HC-HC2)/HC)
      E1=DABS((HMIN-HM1)/HMIN)
      E2=DABS((HM1-HM2)/HM1)
      EHM=E1*100.D0
      IF(E2.GT.E1) EHM=E2*100.D0
      EXMM=DABS(CX/XMMIN)*100.D0
      RATIO=HMIN/HC
C-------------------------
C           OUTPUT
C-------------------------
  107 FORMAT(' ',9X,'X',14X,'P',15X,'CP',13X,'H'/)
  108 FORMAT(' ',1X,4(D14.7,2X),I8,I8)
  109 FORMAT(' CALCULATED LOAD CAPACITY (FP) =',D14.7/)
  111 FORMAT(' H0 =',D25.18/)
  161 FORMAT(' PMAX =',D14.7,8X,'ESTIMATED % ERROR =',D14.7)
  162 FORMAT(' CAVITATION POINT (XE)  =',D25.18/)
  191 FORMAT(' HMIN =',D14.7,8X,'ESTIMATED % ERROR =',D14.7)
  192 FORMAT(' HCEN =',D14.7,8X,'ESTIMATED % ERROR =',D14.7)
  193 FORMAT(' HM/HC =',D14.7)
  397 FORMAT(' FINAL NO. OF STEPS IN CONTACT ZONE =',I6/)
 5656 FORMAT(' FINAL DTL FOR D02EBF =',D14.7/)
  622 FORMAT(' HF (HXE) =',D14.7/)
  637 FORMAT(' FRICTION COEFFICIENT (FRD) =',D14.7/)
  493 FORMAT(' XHMIN =',D14.7,7X,'ESTIMATED % ERROR =',D14.7)
  510 FORMAT(' FINAL CONVERGED VALUES'//)
  511 FORMAT(' VALUES WHICH DEPEND ON SMALL STEP SIZE'/)
C
C   CONSTRUCTING THE EXIT PROFILES
C
      NB=(XE+XI)/CX
      XXED=XE-DX*NB
      XIP=-1.D0*XI
      DO 40 I=1,NPLUS
      K=NPLUS-I+1
      J=K+NB
      X(J)=X(K)
      PSTORE(J)=PSTORE(K)
   40 CONTINUE
      DO 401 I=1,NB
      X(I)=XXED+(I-1)*DX
```

FILE: SSCB FORTRAN A LEEDS UNIVERSITY VM/BSE 6.16

```
      PSTORE(I)=0.D0
  401 CONTINUE
      NPLUS=NPLUS+NB
      NCAV=NB+1
      IF(XXED.EQ.XIP) GOTO 9928
      DO 402 I=1,NPLUS
      K=NPLUS+1-I
      J=K+1
      X(J)=X(K)
      PSTORE(J)=PSTORE(K)
  402 CONTINUE
      X(1)=XIP
      PSTORE(1)=0.D0
      NPLUS=NPLUS+1
      NCAV=NCAV+1
 9928 CONTINUE
C
C   PRINTING DATA AT SPECIFIED SPACING
C
      N2=NPLUS/I2
      JMD=0
      WRITE(5,99)
      WRITE(5,99)
      WRITE(5,107)
      DO 3 I=1,NPLUS
      ICC=(I/N2)*N2
      IF((ICC.NE.I).AND.(I.NE.NPLUS).AND.(I.NE.1).AND.(I.NE.NCAV))
     + GOTO 3
      JMD=JMD+1
      PC=PSTORE(I)
      XC=X(I)
      HX=H0+XC**2/(2.D0*R)+AM*PC
      DDPD=(12.D0*VI*UN/(H0+XC**2/(2.D0*R)+AM*PC)**3)
     C*((XC**2-XE**2)/(2.D0*R)+AM*PC)
      IF(XC.GE.XE) DDPD=0.D0
      WRITE(5,108) XC,PC,DDPD,HX,I,JMD
    3 CONTINUE
C
C   FIXED DATA
C
      WRITE(5,100)
      WRITE(5,99)
      WRITE(5,511)
      WRITE(5,161) PMXD,ERP
      WRITE(5,191) HMIN,EHM
      WRITE(5,493) XHMIN,EXMM
      WRITE(5,192) HC,EHC
      WRITE(5,193) RATIO
      WRITE(5,99)
      WRITE(5,100)
C
C   CONVERGED DATA
C
      WRITE(5,99)
      WRITE(5,510)
```

FILE: SSCB FORTRAN A LEEDS UNIVERSITY VM/BSE 6.16

```
      WRITE(5,189) FPCD
      WRITE(5,1111) H0
      WRITE(5,162) XE
      WRITE(5,622) HXE
      WRITE(5,631) FRD
      WRITE(5,397) NST
      WRITE(5,5656) DTL
C-----------------------
C       PLANE
C-----------------------
      WRITE(6,*) TC,XE,FMXD,HMIN,H0
C-----------------------
C       VISUAL
C-----------------------
C
C   CONDITIONING FOR PLOTS
C
      KK1=0
      N1=NPLUS/I1
      HTL=.9*HFACT
      NNP=0
      DO 4000 I=1,NPLUS
      ICC=(I/N1)*N1
      IF((ICC.NE.I).AND.(I.NE.NPLUS).AND.(I.NE.NCAV)
     *.AND.(I.NE.1)) GOTO 4000
      NNP=NNP+1
      XC=X(I)
      PC=PSTORE(I)
      HX=H0+XC**2/(2.D0*R)+AM*PC
      XX(NNP)=XC
      PP(NNP)=PC
      IF(HX.GE.HTL) GOTO 4000
      KK1=KK1+1
      XX1(KK1)=XC
      HH(KK1)=HX
 4000 CONTINUE
      PMAX=PMXD*1.1D0
      XXE=-1.D0*XFACT
C
C   PLOTTING USING GHOST80
C
      CALL PSPACE(0.,1.,0.,1.)
      CALL MAP(0.,1.,0.,1.)
      CALL PLOTCS(.05,.37,'H',1)
      CALL PLOTCS(.47,.01,'X',1)
      CALL PLOTCS(.05,.87,'P',1)
      CALL PLOTCS(.47,.54,'X',1)
      CALL PLOTCS(.23,.47,'TIME =',7)
      CALL TYPENE(TC,4)
      CALL PSPACE(.07,.57,.05,.4)
      CALL MAP(XFACT,XXE,0.,HFACT)
      CALL BORDER
      CALL AXES
      CALL GRNPEN
      CALL CURVEC(XX1,HH,1,KK1)
      CALL BLKPEN
      CALL PSPACE(.07,.57,.58,.93)
      CALL MAP(XXI,XXE,0.,PMAX)
      CALL BORDER
      CALL AXES
      CALL GRNPEN
      CALL CURVEC(XX,PP,1,NNP)
      CALL BLKPEN
      CALL FRAME
      CPU=CPUTIM(XDU)
      WRITE(5,6928) CPU
      IPT=IPTS
C
C=======================================================================
C
 1867 CONTINUE
C
C=======================================================================
C
      CALL GREND
      CPU=CPUTIM(XCU)
      WRITE(5,6928) CPU
      STOP
      END
C-----------------------------------------------------------------------
C
      SUBROUTINE FCN(XC,PCS,F)
C
C-----------------------------------------------------------------------
      IMPLICIT REAL*8(A-H,O-Z)
      COMMON X(9000),PSTORE(9000)
      COMMON VI,LM,H0,R,AM,XE,XI,CX,JI,NST
      DIMENSION PCS(1),F(1)
      PC=PCS(1)
      F(1)=(12.D0*VI*UM/(H0+(XC**2)/(2.D0*R)+AM*PC)**3)*((XC**2
     C-XE**2)/(2.D0*R)+AM*PC)
      RETURN
      END
C-----------------------------------------------------------------------
C
      SUBROUTINE OUTPUT(XSOL,PCS)
C
C-----------------------------------------------------------------------
      IMPLICIT REAL*8(A-H,O-Z)
      COMMON X(9000),PSTORE(9000)
      COMMON VI,LM,H0,R,AM,XE,XI,CX,JI,NST
      DIMENSION PCS(1)
      JI=JI+1
      X(JI)=XSOL
      PSTORE(JI)=PCS(1)
      XSOL=XE+JI*CX
      IF(JI.EQ.NST) XSOL=XI
      RETURN
      END
C-----------------------------------------------------------------------
```

FILE: SSCB   FORTRAN A   LEEDS UNIVERSITY VM/BSE 6.16

```
C
      SUBROUTINE PEDERV(XC,PCS,PW)
C
C---------------------------------------------------------------------
      IMPLICIT REAL*8(A-H,O-Z)
      COMMON X(3000),PSTORE(9000)
      COMMON VI,UM,HO,R,AM,XE,XI,CX,JI,NST
      DIMENSION PW(1,1),PCS(1)
      PC=PCS(1)
      PW(1,1)=12.D0*VI*UM*AM*(HO-XC**2/R+1.5D0*XE**2/R-2.D0*AM*PC)/
     C((HO+XC**2/(2.D0*R)+AM*PC)**4)
      RETURN
      END
```

FILE: JSSCB   EXEC   A   LEEDS UNIVERSITY VM/BSE 6.16

for connected running

```
EXEC SETUP FORTRAN LDSF NAGF CCGHCST
FI 4 DISK XSSCB DATA
FI 5 DISK YSSCB DATA(RECFM F LRECL 120 BLOCK 120
FI 8 DISK BANK DATA
LOAD SSCB(CLEAR
EXEC PLOTFILE PSSCB
SET BLIP *
START
```

FILE: KSSCB   EXEC   A   LEEDS UNIVERSITY VM/BSE 6.16

for batch running

```
&CONTROL ALL
&IF &READFLAG EQ STACK DESBUF
&STACK 1000 2 5000
&STACK FI 4 DISK XSSCB DATA
&STACK
&STACK FI 5 DISK YSSCB DATA (RECFM F LRECL 120 BLOCK 120
&STACK FI 8 DISK BANK DATA
&STACK FI PLOTTER DISK PSSCB PLOT A (RECFM F LRECL 129 BLOCK 129
&STACK
EXEC SETUP FORTRAN LDSF NAGF CCGHCST
LOAD SSCB
GENMOD SSCB
EXEC BATCH PENSJP RUN SSCB JD FILES
```

INPUT

FILE: XSSCB   DATA   A   LEEDS UNIVERSITY VM/BSE 6.16

```
32
.10898510-3
.01 1. 16.06 .3 .0024 .0265 .4
.022085 9.
-.016 1000
1.D-7
.001 .001
.001
1.1E-6 -.02
.1 1.25 .01 1.02
200 20
0 -1
12
.1 .2 .25 .5 1. 2. 4. 6. 8. 10. 20. 30.
 .995 .9804 .9697 .8953 .725 .4978 .29 .1956 .1430 .11 .04591 .02677
1.005 1.020 1.031 1.126 1.449 2.282 4.281 6.478 9.099 12.06 30.17 52.63
39
0. .05 .1 .15 .175 .2 .25 .3 .35 .375 .4 .425 .45 .475 .5
.525 .55 .575 .6 .625 .65 .675 .7 .71 .725 .75 .76 .775
.8 .825 .85 .865 .875 .89 .9 .925 .95 .975 1.0000000001
339. 502. 726. 957. 1133. 1302. 1607. 2082. 2489. 2557. 2496.
2408. 2150. 1675. 1302. 1051. 925. 590. 353. 230. 183. 150.
150. 170. 116. 116. 129. 116. 170. 190. 170. 129. 150. 150.
183. 217. 251. 285. 339.
```

OUTPUT

FILE: YSSCB DATA A LEEDS UNIVERSITY VM/BSE 6.15

**** I N P U T   D A T A ****

NTIME (NO. OF TIME STEPS)	32
UMB (LOWER LIMIT FOR UM)	0.1089851D-03
VI (ABSOLUTE VISCOSITY)	0.1000000D-01
TP (PERIOD OF CYCLE)	0.1000000D+01
E (ELASTIC MODULUS OF LAYER)	0.1600000D+08
R (REDUCED RADIUS)	0.3000000D+00
TH (LAYER THICKNESS)	0.2400000D-02
WD (WIDTH OF BEARING)	0.2650000D-01
PR (POISSONS RATIO)	0.4000000D+00
RT (TALUS RADIUS)	0.2209500D-01
THETA (ANGULAR AMPLITUDE IN DEGREES)	0.9000000D+01
XI (INLET BOUNDARY)	-0.1600000D-01
NST (INITIAL NUMBER OF STEPS)	1000
DTOL (INITIAL RELATIVE TOLERANCE FOR C02EBF)	0.1000000D-06
PTOL (RELATIVE INLET PRESSURE TOLERANCE)	0.1000000D-02
FPTOL (RELATIVE LOAD CAPACITY TOLERANCE)	0.1000000D-02
FRTOL (TOLERANCE FOR FR STEP DEPENDENCE)	0.1000000D-02
HFACT (SCALE FACTOR FOR FILM PLOTS)	0.1100000D-05
XFACT (SCALE FACTOR FOR PLOTS)	-0.2000000D-01
F1 (XA=XE*F1, INITIAL XE INCREMENT)	0.1800000D+00
F2 (XE=XE*F2, INITIAL XE GUESS)	0.1250000D+01
F3 (HA=HO*F3, INITIAL HO INCREMENT)	0.1000000D-01
F4 (HMGU=HM*F4, INITIAL HO GUESS)	0.1020000D+01
I1 (NUMBER OF POINTS PLOTTED)	200
I2 (NUMBER OF POINTS PRINTED)	20
IPT (PRINT OPTION FOR CONVERGENCE DATA)	0
MAGN (PRINT OPTION FOR 1 CYCLE)	-1

AM/TH	A/TH	A/AM	P/PM	
0.1005025D+00	0.1000000D+00	0.9950000D+00	0.1005000D+01	1
0.2039984D+00	0.2000000D+00	0.9804000D+00	0.1020000D+01	2
0.2579117D+00	0.2500000D+00	0.9697000D+00	0.1031000D+01	3
0.5584720D+00	0.5000000D+00	0.8953000D+00	0.1126000D+01	4
0.1379310D+01	0.1000000D+01	0.7250000D+00	0.1449800D+01	5
0.4017678D+01	0.2000000D+01	0.4978000D+00	0.2282000D+01	6
0.1379310D+02	0.4000000D+01	0.2900000D+00	0.4201000D+01	7
0.3067485D+02	0.6000000D+01	0.1956000D+00	0.6478000D+01	8
0.5594406D+02	0.8000000D+01	0.1430000D+00	0.9098000D+01	9
0.9090909D+02	0.1000000D+02	0.1100000D+00	0.1206000D+02	10
0.4356349D+03	0.2000000D+02	0.4591000D-01	0.3017000D+02	11
0.1120657D+04	0.3000000D+02	0.2677000D-01	0.5263000D+02	12

FILE: YSSCB DATA A LEEDS UNIVERSITY VM/BSE 6.16

T/TP	TIME	LOAD	FP	
0.0	0.0	0.3390000D+03	0.1275245D+05	1
0.5000000D-01	0.5000000D-01	0.5020000D+03	0.1494340D+05	2
0.1000000D+00	0.1000000D+00	0.7260000D+03	0.2735623D+05	3
0.1500000D+00	0.1500000D+00	0.9570000D+03	0.3762264D+05	4
0.1750000D+00	0.1750000D+00	0.1133000D+04	0.4275472D+05	5
0.2000000D+00	0.2000000D+00	0.1302000D+04	0.4913208D+05	6
0.2500000D+00	0.2500000D+00	0.1607000D+04	0.6064151D+05	7
0.3000000D+00	0.3000000D+00	0.2082000D+04	0.7856604D+05	8
0.3500000D+00	0.3500000D+00	0.2488000D+04	0.9392453D+05	9
0.3750000D+00	0.3750000D+00	0.2557000D+04	0.9645057D+05	10
0.4000000D+00	0.4000000D+00	0.2496000D+04	0.9418868D+05	11
0.4250000D+00	0.4250000D+00	0.2408000D+04	0.9086792D+05	12
0.4500000D+00	0.4500000D+00	0.2150000D+04	0.8113208D+05	13
0.4750000D+00	0.4750000D+00	0.1675000D+04	0.6320755D+05	14
0.5000000D+00	0.5000000D+00	0.1302000D+04	0.4913208D+05	15
0.5250000D+00	0.5250000D+00	0.1051000D+04	0.3966038D+05	16
0.5500000D+00	0.5500000D+00	0.9290000D+03	0.3505668D+05	17
0.5750000D+00	0.5750000D+00	0.5900000D+03	0.2226415D+05	18
0.6000000D+00	0.6000000D+00	0.3530000D+03	0.1332075D+05	19
0.6250000D+00	0.6250000D+00	0.2390000D+03	[illegible]	20
0.6500000D+00	0.6500000D+00	0.1830000D+03	0.6905660D+04	21
0.6750000D+00	0.6750000D+00	0.1500000D+03	0.5660377D+04	22
0.7000000D+00	0.7000000D+00	0.1500000D+03	0.5660377D+04	23
0.7100000D+00	0.7100000D+00	0.1700000D+03	0.6415094D+04	24
0.7250000D+00	0.7250000D+00	0.1160000D+03	0.4377358D+04	25
0.7500000D+00	0.7500000D+00	0.1150000D+03	0.4377358D+04	26
0.7600000D+00	0.7600000D+00	0.1290000D+03	0.4867925D+04	27
0.7750000D+00	0.7750000D+00	0.1160000D+03	0.4377358D+04	28
0.8000000D+00	0.8000000D+00	0.1700000D+03	0.6415094D+04	29
0.8250000D+00	0.8250000D+00	0.1900000D+03	0.7169811D+04	30
0.8500000D+00	0.8500000D+00	0.1700000D+03	0.6415094D+04	31
0.8650000D+00	0.8650000D+00	0.1290000D+03	0.4867925D+04	32
0.8750000D+00	0.8750000D+00	0.1500000D+03	0.5660377D+04	33
0.8900000D+00	0.8900000D+00	0.1900000D+03	0.7169811D+04	34
0.9000000D+00	0.9000000D+00	0.1830000D+03	0.6905660D+04	35
0.9250000D+00	0.9250000D+00	0.2170000D+03	0.8188679D+04	36
0.9500000D+00	0.9500000D+00	0.2510000D+03	0.9471698D+04	37
0.9750000D+00	0.9750000D+00	0.2850000D+03	0.1075472D+05	38
0.1000000D+01	0.1000000D+01	0.3390000D+03	0.1275245D+05	39

**** O U T P U T   D A T A ****

INDEX NO. (NT) = 1

TIME (TC) = 0.0

F10

ENTRAINMENT VELOCITY (UM) = 0.1089851D-01

LOAD PER UNIT WIDTH (FP) = 0.1275245D+05

VARIOUS ESTIMATES FOR POISSONS RATIO OF .5

(1.) FOR SURFACE LAYER USING DATA BY GUPTA
A = 0.6277183D-02 PMAX = 0.1528521D+07

(2.) FOR SURFACE LAYER USING FORMULAS BY MOORE AND VARNUM
HMIN = 0.4434827D-06 HCEN = 0.5577393D-06

(3.) FOR RIGID SURFACE USING FORMULA BY MARTIN
HMIN = HCEN = 0.3128355D-08

(4.) FOR ELASTIC SURFACES USING HERTZIAN FORMULAS
A = 0.6305571D+01 PMAX = 0.5381096D+06

(5.) FOR ELASTIC SURFACES USING FORMULA BY SWALES
HMIN = 0.5751007D-06 HCEN = 0.1255257D-05

(6.) FOR ELASTIC SURFACES USING FORMULA BY VARNUM
HMIN = 0.1045366D-05 HCEN = 0.1319526D-05

(7.) FOR ELASTIC SURFACES USING FORMULA BY HERREBRUGH
HMIN = 0.1054965D-05 HCEN = 0.1351879D-05

X	P	DP	H	
0.1600080D-01	0.0	0.0	0.3366461D-03	1
0.1442984D-01	0.0	0.0	0.2570134D-03	136
0.1283996D-01	0.0	0.0	0.1847533D-03	272
0.1125008D-01	0.0	0.0	0.1205201D-03	408
0.9660202D-02	0.0	0.0	0.6551190D-04	544
0.8070321D-02	0.0	0.0	0.1952963D-04	680
0.7380594D-02	0.0	0.0	0.7680951D-06	739
0.6480441D-02	0.2959628D+06	-0.3087281D+09	0.6984100D-06	916
0.4890561D-02	0.7266200D+06	-0.2330294D+09	0.7055215D-06	952
0.3300680D-02	0.1036939D+07	-0.1573402D+09	0.7226862D-06	1088
0.1710800D-02	0.1226928D+07	-0.9165939D+08	0.7425326D-06	1224
0.1209195D-03	0.1296603D+07	-0.5590562D+07	0.7660361D-06	1360
-0.1466761D-02	0.1245585D+07	0.6965596D+08	0.7794923D-06	1496
-0.3058841D-02	0.1075120D+07	0.1452701D+09	0.8320887D-06	1632
-0.4648722D-02	0.7641143D+06	0.2207715D+09	0.9551752D-06	1768
-0.6238602D-02	0.3733736D+06	0.2556850D+09	0.5925625D-06	1904
-0.7829432D-02	0.4351670D+04	0.7346487D+07	0.1242599D-04	2040
-0.9419363D-02	0.1433247D+04	0.3946428D+06	0.5792241D-04	2176
-0.1100824D-01	0.1110618D+04	0.1034953D+06	0.1120263D-03	2312
-0.1259812D-01	0.1003851D+04	0.4272572D+05	0.1745709D-03	2448
-0.1418800D-01	0.9552851D+03	0.2162340D+05	0.2455454D-03	2584
-0.1577728D-01	0.9290917D+03	0.1235648D+05	0.3245472D-03	2720
-0.1600080D-01	0.9264428D+03	0.1150912D+05	0.3367110D-03	2739

VALUES WHICH DEPEND ON SMALL STEP SIZE

PMAX = 0.1296975D+07 ESTIMATED % ERROR = 0.3676972D-03
HMIN = 0.6823041D-06 ESTIMATED % ERROR = 0.1445713D-01
XHMIN = 0.7357213D-02 ESTIMATED % ERROR = 0.1588957D+00
HCEN = 0.7679472D-06 ESTIMATED % ERROR = 0.2509879D-01
HM/HC = 0.8891250D+00

FINAL CONVERGED VALUES

CALCULATED LOAD CAPACITY (FP) = 0.1279607D+05

H0 =-0.9002051675006033310D-04

CAVITATION POINT (XE) = 0.7380593954090019190D-02

HP (HXE) = 0.7680951D-06

FRICTION COEFFICIENT (FRO) = 0.3024301D-03

FINAL NO. OF STEPS IN CONTACT ZONE = 2000

FINAL DTL FOR D02EBF = 0.1296979D-01

******** CPU = 0.135D+02

INDEX NO. (NT) = 2

TIME (TC) = 0.3125000D-01

ENTRAINMENT VELOCITY (UM) = 0.1068910D-01

LOAD PER UNIT WIDTH (FP) = 0.1638535D+05

VARIOUS ESTIMATES FOR POISSONS RATIO OF .5

(1.) FOR SURFACE LAYER USING DATA BY GUPTA

A = 0.6745C940-02 PMAX = 0.12410720+07

(2.) FOR SURFACE LAYER USING FORMULAS BY HOOKE AND VARNUM
HMIN = 0.40271640-06 HCEN = 0.50656210-06

(3.) FOR RIGID SURFACE USING FORMULA BY MARTIN
HMIN = HCEN = 0.23940780-08

(4.) FOR ELASTIC SURFACES USING HERTZIAN FORMULAS
A = 0.71376620+01 PMAX = 0.60908050+06

(5.) FOR ELASTIC SURFACES USING FORMULA BY SWALES
HMIN = 0.93763950-06 HCEN = 0.12021010-05

(6.) FOR ELASTIC SURFACES USING FORMULA BY VARNUM
HMIN = 0.58331160-06 HCEN = 0.12360780-05

(7.) FOR ELASTIC SURFACES USING FORMULA BY HERREBRUGH
HMIN = 0.99187070-06 HCEN = 0.12716290-05

X	P	DP	H	
0.16003980-01	0.0	0.0	0.32029890-03	1
0.14416750-01	0.0	0.0	0.24002690-03	133
0.12917660-01	0.0	0.0	0.16752860-03	266
0.11222570-01	0.0	0.0	0.10353250-03	399
0.96254940-02	0.0	0.0	0.49038940-04	532
0.80283950-02	0.0	0.0	0.10474600-05	665
0.80163870-02	0.0	0.0	0.72634480-06	666
0.64313050-02	0.54428330+06	-0.30636820+09	0.65022850-06	798
0.48342150-02	0.97286040+06	-0.23032590+09	0.67158130-06	931
0.32371260-02	0.12808010+07	-0.15429620+09	0.68729170-06	1064
0.16400360-02	0.14657120+07	-0.78268160+08	0.70456670-06	1197
0.42946230-04	0.15300050+07	-0.22480170+07	0.72567510-06	1330
-0.15541430-02	0.14728970+07	0.73758300+08	0.75066870-06	1463
-0.31512330-02	0.12944220+07	0.14973590+09	0.78221530-06	1596
-0.47483230-02	0.99464750+06	0.22564680+09	0.82519460-06	1729
-0.63454130-02	0.57379660+06	0.30130190+09	0.99442840-06	1862
-0.79425020-02	0.39123300+05	0.25907640+09	0.14957910-05	1995
-0.95395920-02	0.13581580+04	0.61261740+06	0.45350350-04	2128
-0.11136680-01	0.90478530+03	0.12634100+06	0.10033510-03	2261
-0.12733770-01	0.77965200+03	0.47522910+05	0.16352510-03	2394
-0.14330860-01	0.72655730+03	0.22956660+05	0.23596240-03	2527
-0.15927950-01	0.69306320+03	0.12775160+05	0.31650350-03	2660
-0.16850010-01	0.69815330+03	0.12471540+05	0.32333750-03	2666

VALUES WHICH DEPEND ON SMALL STEP SIZE

FILE: VSSCB DATA A LEEDS UNIVERSITY VM/BSE 6.16

PMAX = 0.15300580+07 ESTIMATED % ERROR = 0.25493020-03
HMIN = 0.64624540-06 ESTIMATED % ERROR = 0.13569370-01
XHMIN = 0.79923780-02 ESTIMATED % ERROR = 0.15024570+00
HCEN = 0.72635620-06 ESTIMATED % ERROR = 0.23493580-01
HM/HC = 0.88970860+00

FINAL CONVERGED VALUES

CALCULATED LOAD CAPACITY (FP) = 0.16373330+05

H0 =-0.10637774468793841D-03

CAVITATION POINT (XE) = 0.80163865734888956ID-02

HP (HXE) = 0.72634480-06

FRICTION COEFFICIENT (FRD) = 0.26727970-03

FINAL NO. OF STEPS IN CONTACT ZONE = 2000

FINAL DTL FOR D02EBF = 0.15300580-01

******** CPU = 0.335D+02

INDEX NO. (NT) = 3

TIME (TC) = 0.62500000-01

ENTRAINMENT VELOCITY (UM) = 0.10068910-01

LOAD PER UNIT WIDTH (FP) = 0.20924570+05

VARIOUS ESTIMATES FOR POISSONS RATIO OF .5

(1.) FOR SURFACE LAYER USING DATA BY GUPTA
A = 0.72136430-02 PMAX = 0.22040990+07

(2.) FOR SURFACE LAYER USING FORMULAS BY HOOKE AND VARNUM
HMIN = 0.35829370-06 HCEN = 0.45067130-06

(3.) FOR RIGID SURFACE USING FORMULA BY MARTIN
HMIN = HCEN = 0.17754520-08

(4.) FOR ELASTIC SURFACES USING HERTZIAN FORMULAS
A = 0.90456870+01 PMAX = 0.68656530+06

CONTINUES ....

F/2

OUTPUT

FILES BANK DATA A LEEDS UNIVERSITY VM/BSE 6.16

.0	.73085939540980C19195E-02	1256579.40715427518
.682904102787C17292E-06	-.90020516750086033315E-04	
.3125000000000C00000E-01	.88163865734E889561E-02	1530057.36935946495
.646245394127946266E-06	-.186377744687988410E-03	1796402.40875099852
.625000000000C000000E-01	.862613345494771616E-02	
.600413392556574830E-06	-.125073876226005587E-03	2093125.59496485605
.93750000000000000000E-01	.937618214464184179E-02	
.546427533634445493E-06	-.145505520099759953E-03	2417092.53743135976
.12500000000000000000	.100756082150560277E-01	
.484677484392216309E-06	-.166652912375531527E-03	2724481.07486385979
.15625000000000C00000	.106571157132258266E-01	
.415937731962936433E-06	-.190247479603612419E-03	3045099.35707980464
.18750000000000C00000	.113090316419249591E-01	
.334940365094305423E-06	-.212781668375213117E-03	3362690.77915116563
.21875000000000000000	.118841514600555032E-01	
.232704755901304818E-06	-.235127904892725560E-03	3664947.26204662095
.25000000000000000000	.124067655366960476E-01	
.513271032113676455E-07	-.256488956520173046E-03	4086675.57267739797
.28125000000000000000	.131001988856524641E-01	
.221368279444557329E-06	-.295777461769372819E-03	4521674.05304966099
.31250000000000C00000	.137911074114644969E-01	
.302564263629606979E-06	-.316192690158509036E-03	4659327.27965151402
.34375000000000000000	.142860702577946638E-01	
.358219780375414159E-06	-.339751791383757253E-03	4996502.52940892451
.37500000000000000000	.144863091885001731E-01	
.401554284951520915E-06	-.345305451296649493E-03	4695516.75624421914
.40625000000000C00000	.143391679250941208E-01	
.437931332711661418E-06	-.342195610725652341E-03	4668215.00827803253
.43750000000000000000	.14C6232421326352408E-01	
.467381446391183950E-06	-.326251472406229235E-03	3545013.06788602455
.46875000000000000000	.128720845435204333E-01	
.503146314463222540E-06	-.275586792017060358E-03	3186586.92733419188
.50000000000000C00000	.115608780806618202E-01	
.537049273227561411E-06	-.222458992577611464E-03	2710627.71439471332
.53125000000000C00000	.106698925173432823E-01	
.554827878035913023E-06	-.199121598585544103E-03	2251024.06298423000
.56250000000000000000	.972332394664747463E-02	
.565296673717640870E-06	-.15693730791314 7C35E-03	1441523.75689258213
.59375000000000000000	.776209342939725600E-02	
.603849840751100285E-06	-.100256029126980677E-03	1024399.45773782438
.62500000000000C00000	.655932941378033034E-02	
.610527724858580948E-06	-.710209681101600860E-04	828356.27529250204
.65625000000000C00000	.530564953525349398E-02	
.572236635190771631E-06	-.574833211169610905E-04	714189.95551321504
.68750000000000000000	.547686302922019419E-02	
.493154334863442456E-06	-.494379656727726126E-04	720930.12871174103
.71875000000000C00000	.554067539408974791E-02	
.347457312541276535E-06	-.507744603913477517E-04	624672.83449784966
.75000000000000C00000	.516297004743636323E-02	
.402209722950739055E-07	-.443371926546567264E-04	655558.50694630099
.78125000000000C00000	.524723533821934075E-02	
.357937493875107713E-06	-.454864458277265383E-04	669777.93597304356
.81250000000000C00000	.604406327764909743E-02	
.466539061505539947E-06	-.603592119553595778E-04	862631.97571716743
.84375000000000C00000	.601918375163704547E-02	

FILES BANK DATA A LEEDS UNIVERSITY VM/BSE 6.16

.566187332875036597E-06	-.597467604652105898E-04	
.97500000000000C00000	.562258295912481700E-02	752699.61073919202
.665796363711121850E-06	-.515382892843162349E-04	
.90625000000000C00000	.601738742251041892E-02	862116.03649203972
.696267111348213384E-06	-.595634970903171963E-04	
.93750000000000C00000	.654586732327767495E-02	1020198.50680407416
.700791736449171995E-06	-.706247351877252294E-04	
.96875000000000000000	.649029621847361216E-02	1127979.46261229932
.702681193289646443E-06	-.781675549022437912E-04	
1.00000000000000000000	.730859395233925441E-02	1296979.40653849160
.642804102783248392E-06	-.900205167065913742E-04	

PSSCB PLOT

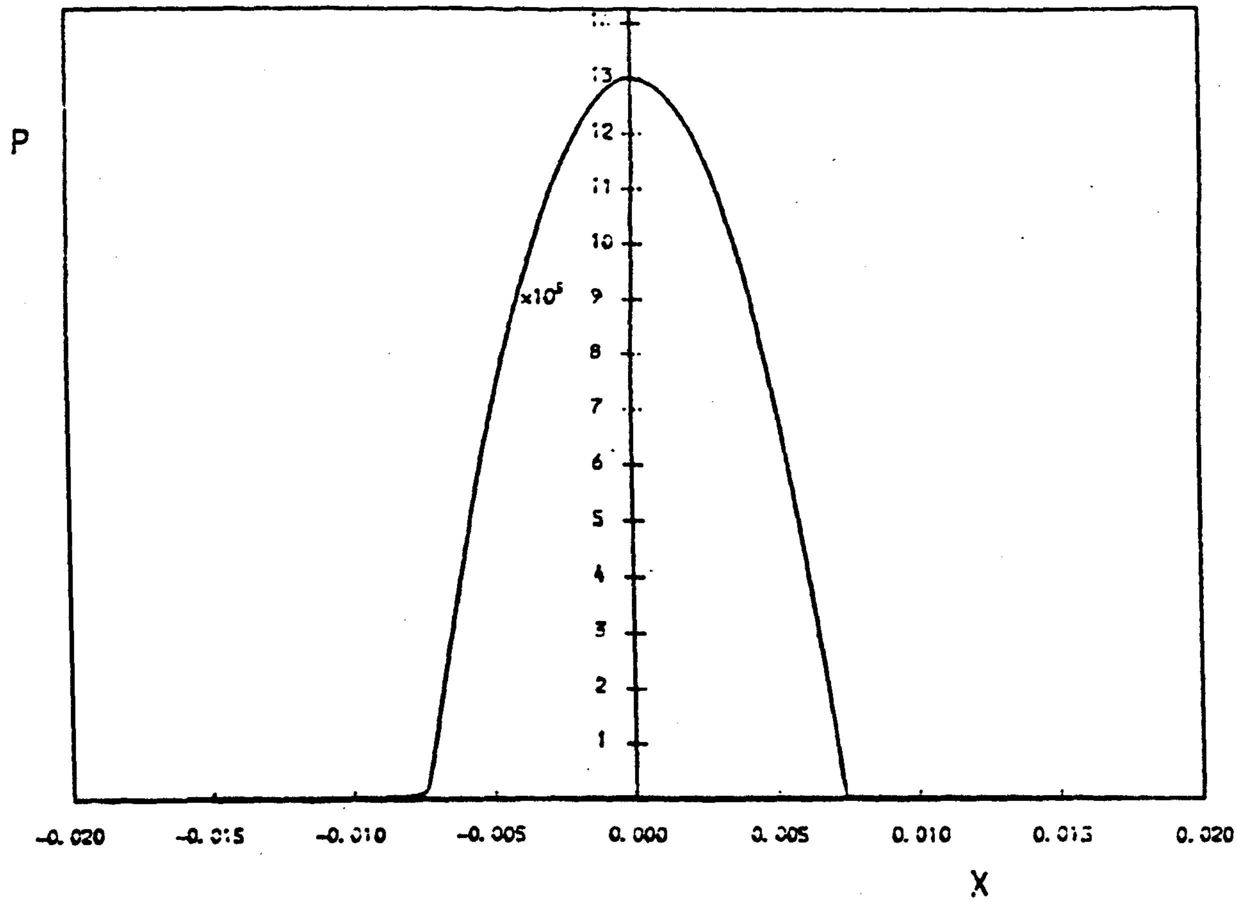

TIME = 0.0000E 00

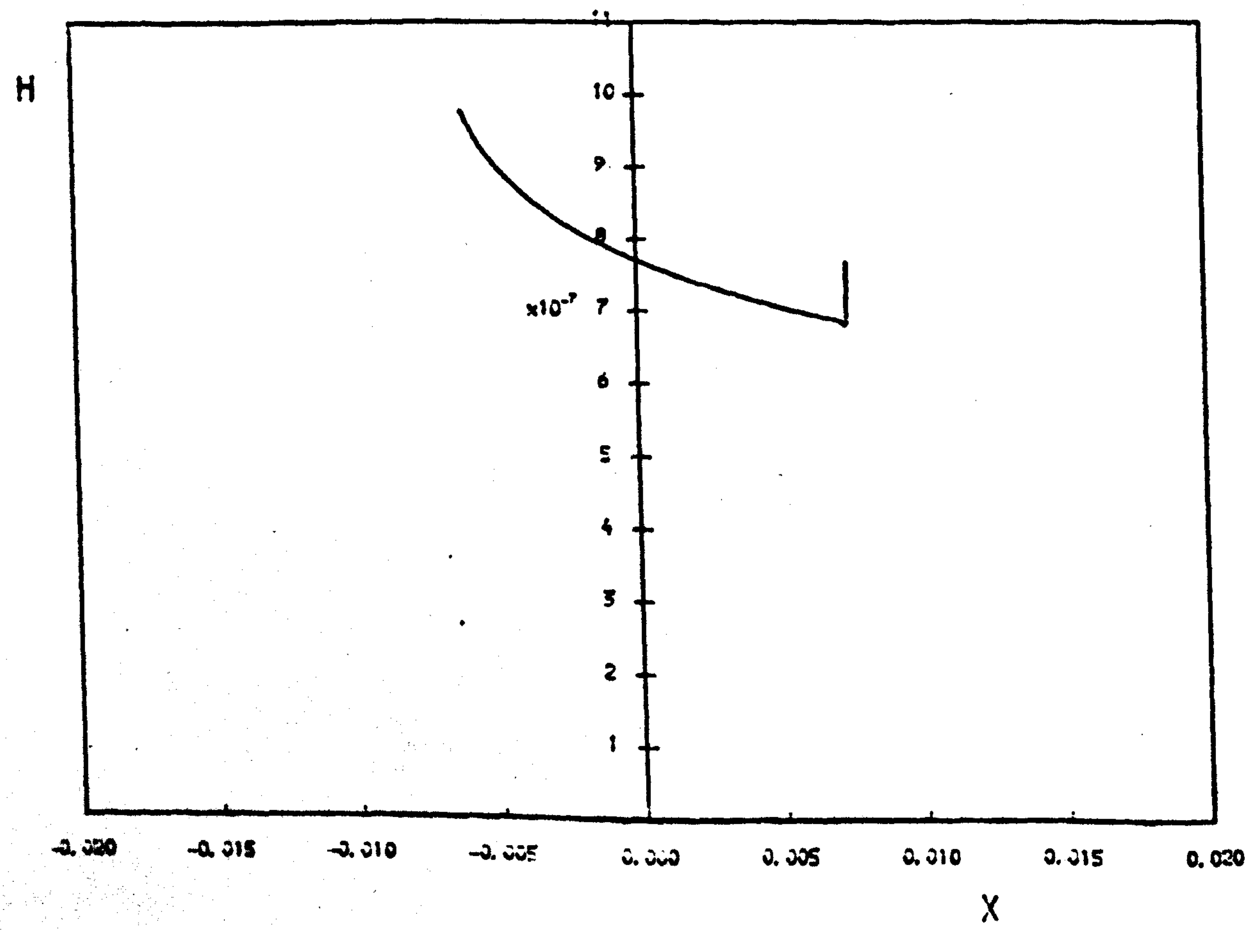

PART 2

```
FILE: PLISP    FORTRAN  A   LEEDS UNIVERSITY VM/BSE 6.16

C*************************************************************
C                  PART 2
C      PLANE INCLINED SURFACE MODEL
C      ---------------------------
C
C         THE GEOMETRY OF A RIGID CYLINDER SLIDING ON A LUBRICATED
C       ELASTIC LAYER BONDED TO A RIGID PLANE IS APPROXIMATED
C       AS A PLANE INCLINED SURFACE.  THE LUBRICANT IS ISOVISCOUS.
C       THE LOAD AND VELOCITY ARE CYCLIC TIME VARYING.
C          IT IS ASSUMED THAT THE FILM THICKNESS VARIATION WITH TIME
C       CAN BE APPROXIMATED AS DHG/DT.   THE LENGTH OF THE PLANE
C       SURFACE IS CHOSEN SUCH THAT  DP/DX = 0.  AT  X = BDRY/2.
C       THE INCLINATION OF THE PLANE SURFACE IS CHOSEN SUCH THAT
C       FOR THE INSTANTANEOUS CONDITIONS OF LOAD AND VELOCITY
C       THE MINIMUM STEADY STATE FILM THICKNESS EQUALS THAT
C       PREDICTED BY SOLUTIONS GENERATED USING THE COLUMN MODEL.
C
C*************************************************************
C
      IMPLICIT REAL*8(A-H,O-Z)
      REAL*4 PMAX,TPI,HFACT,FFACT,TT(401),HH(401),FF(401),
     *       XPR(201),XX(201),FCC(401),XPHZ,
     *       FPMAX,FPP(401),UMAX,UU(401),TPL1,XFACT,XXIP
     *       X1,X2,X3,X4,Y1,Y2,Y3,Y4
      COMMON TOL,TCL1,H0,VI,TP,E,R,TH,WD,UAMP
      COMMON PR(201,41),PHZ(201),BH(400),EFP(401),BHP(401)
      COMMON XE(64),PD(64),TO(64),HMCCL(64)
      COMMON XEK(68),XEC(68),PKI(68),PCI(68),FKI(104),FCI(104)
      COMMON AW(400),FW(616),HKI(68),HCI(68)
      COMMON TF(100),FE(100),FP(100),TP(100)
      COMMON TZ,HZ,UZ,FPZ,FZ,BZ,XMZ,XPDZ,FRZ,CH1,CH2,DT,PHZ,XM
      COMMON UE(400),FPR(400),FU(400),BF(400),XMI(400),XPP(401)
      COMMON FRI(400),H(400),HST(2000),UC,FPY,BC,BDRY,HM,UM0
      COMMON NPER,NHALF,NSPTP,NPRT,IPRT,NPX,NPT,NP,NA4,NF4,NH4
      FR(VI)=((VI*UG)/(FPG*XMG))*(8.D0*DLOG(1.D0+XMG*BG/HG)
     A      -12.D0*XMG*BG/(2.D0*HG+XMG*BG))-((6.D0*VI)/(FPG*XMG**2))
     A      *(DLOG(1.D0+XMG*BG/HG)-2.D0*XMG*BG/(2.D0*HG+XMG*BG))*FG
      Y(VI)=2.D0*VI*UG*BG/(HG*FPG)
      P(X,HG,BG,XMG,FG,UG)=12.D0*VI*(BG-X)*X*(XMG*UG-FG)/
     A                  ((2.D0*HG+XMG*BG)*(HG+XMG*X)**2)
C-----------------------------------
C          INPUT
C-----------------------------------
      READ(5,*) TOL,H0,NPER,NHALF,NSPTP,NPRT,IPRT,NPX,NPT,NP
      READ(5,*) VI,TP,E,R,TH,WD
      READ(5,*) UAMP,POIS,UM0
      READ(5,*) XFACT,HFACT,FFACT,PFACT
      READ(5,*) NF
      READ(5,*) (TF(I),I=1,NF)
      READ(5,*) (FE(I),I=1,NF)
      READ(5,*) NH
      DO 6291 I=1,NH
      READ(4,*) TO(I),XE(I),PD(I),HMCOL(I),DUMMY
 6291 CONTINUE
C-----------------------------------

FILE: PLISP    FORTRAN  A   LEEDS UNIVERSITY VM/BSE 6.16

C          CHECK
C-----------------------------------
   99 FORMAT(' ')
  101 FORMAT(' -----------------------------------------------',
     *'-----------------------------------------------'/)
C
C
 1400 FORMAT(' TOL (TOLERANCE FOR SS AND STEP SIZE) .......... ',D14.7)
 1401 FORMAT(' H0 (INITIAL GUESS FOR H0 AT TIME ZERO) ........ ',D14.7)
 1402 FORMAT(' NPER (MAX. NO. OF CYCLES AT SAME STEP SIZE) .. ',I8)
 1403 FORMAT(' NHALF (MAX. NO. OF STEP SIZE HALVINGS) ....... ',I8)
 1404 FORMAT(' NSPTP (INITIAL NO. OF STEPS PER CYCLE) ....... ',I8)
 1405 FORMAT(' NPRT (NO. OF STEPS PRINTED PER CYCLE) ........ ',I8)
 1406 FORMAT(' IPRT (CONVERGENCE PRINT OPTION) .............. ',I8)
 1407 FORMAT(' NPX (NO. OF PRESS. PTS. PRINTED PER DIST.) ... ',I8)
 1408 FORMAT(' NPT (NO. OF PRESS. DIST. PRINTED) ............ ',I8)
 1409 FORMAT(' NP (PRINT OPTIONS FOR PRESS. DIST.) .......... ',I8)
 1410 FORMAT(' VI (ABSOLUTE VISCOSITY) ...................... ',D14.7)
 1411 FORMAT(' TP (PERIOD) .................................. ',D14.7)
 1412 FORMAT(' E (ELASTIC MODULUS OF LAYER) ................. ',D14.7)
 1413 FORMAT(' R (REDUCED RADIUS) ........................... ',D14.7)
 1414 FORMAT(' TH (LAYER THICKNESS) ......................... ',D14.7)
 1415 FORMAT(' WD (WIDTH OF CONTACT) ........................ ',D14.7)
 1417 FORMAT(' UAMP (AMPLIT. OF ENT. VEL.) .................. ',D14.7)
 1418 FORMAT(' POIS (POISSONS RATIO) ........................ ',D14.7)
 1419 FORMAT(' UM0 (LOWER LIMIT FOR ENT. VEL.) .............. ',D14.7)
 1420 FORMAT(' XFACT (SCALE FACTOR FOR PLOTS) ............... ',E14.7)
 1421 FORMAT(' HFACT (SCALE FACTOR FOR FILM PLOTS) .......... ',E14.7)
 1422 FORMAT(' FFACT (SCALE FACTOR FOR FRICTION PLOTS) ...... ',E14.7)
 1423 FORMAT(' PFACT (SCALE FACTOR FOR FRICTION PLOTS) ...... ',E14.7)
C
C
 1599 FORMAT(/' NOTE : FOR SS TOLERANCE EQUALS .1*TOL'/)
 1603 FORMAT(/24X,'DATA BANK'//)
  111 FORMAT(' ',6X,'TO',15X,'XE',14X,'PD',13X,'HMCOL'/)
  112 FORMAT(' ',1X,4(D14.7,2X),I8)
  114 FORMAT(' ',4X,'T/TP',10X,'TIME',9X,'LOAD',11X,'FP'/)
  115 FORMAT(' ',1X,3(D11.4,2X),D14.7,I8)
  116 FORMAT(' ****  I N P U T   D A T A   ****'/)
  117 FORMAT(' ****   O U T P U T   D A T A   ****'/)
      WRITE(6,101)
      WRITE(6,116)
      WRITE(6,101)
      WRITE(6,1400) TOL
      WRITE(6,1401) H0
      WRITE(6,1402) NPER
      WRITE(6,1403) NHALF
      WRITE(6,1404) NSPTP
      WRITE(6,1405) NPRT
      WRITE(6,1406) IPRT
      WRITE(6,1407) NPX
      WRITE(6,1408) NPT
      WRITE(6,1409) NP
      WRITE(6,1410) VI
      WRITE(6,1411) TP
```

```
      WRITE(6,1412) E
      WRITE(6,1413) R
      WRITE(6,1414) TH
      WRITE(6,1415) WC
      WRITE(6,1417) UAMP
      WRITE(6,1418) POIS
      WRITE(6,1419) UPB
      WRITE(6,1420) KFACT
      WRITE(6,1421) MFACT
      WRITE(6,1422) FFACT
      WRITE(6,1421) MFACT
      WRITE(6,1423) PFACT
      WRITE(6,1555)
      WRITE(6,99)
      WRITE(6,101)
      WRITE(6,99)
      WRITE(6,1683)
      WRITE(6,111)
      DO 1000 I=1,NH
      WRITE(6,112) TO(I),XE(I),PC(I),HMCOL(I),I
 1000 CONTINUE
      WRITE(6,99)
      WRITE(6,101)
      DO 1001 I=1,NF
      TF(I)=TM(I)*TP
      FP(I)=FE(I)/WC
 1001 CONTINUE
      WRITE(6,114)
      DO 1002 I=1,NF
      WRITE(6,115) TM(I),TF(I),FE(I),FP(I),I
 1002 CONTINUE
      WRITE(6,99)
      WRITE(6,101)
      WRITE(6,117)
C-------------------------------------
C           FILM
C-------------------------------------
 200  FORMAT(' ****** DOES NOT CONVERGE TO SPECIFIED TOLERANCE ******')
 201  FORMAT(' ***** DOES NOT REACH STEADY STATE *****')
 203  FORMAT(' STEP SIZE IS HALVED')
      NA4=NA+4
      NF4=NF+4
      NH4=NH+4
      LWRK1=6*NF+16
      LWR=6*NH+16
      CALL E01BAF(NH,TO,XE,XEK,XEC,NH4,AW,LWR,0)
      CALL E01BAF(NH,TC,PC,PKI,PCI,NH4,AW,LWR,0)
      CALL E01BAF(NF,TF,FP,FKI,FCI,NF4,FW,LWRK1,0)
      CALL E01BAF(NH,TC,HMCOL,HKI,HCI,NH4,AW,LWR,0)
      CH1=1.D6
      DT=TP/NSPTP
      NS=NSPTP
      TOL1=TOL
      DT1=DT
      DO 2002 J=1,NHALF
```

FILE: PLISP FORTRAN A LEEDS UNIVERSITY VM/BSE 6.16

```
      TOL=TOL1
      CH2=1.D6
      IF(IPRT.EQ.1) WRITE(6,101)
      IF((IPRT.EQ.1).AND.(J.NE.1))WRITE(6,203)
      DO 2003 M=1,NPER
      H1=H0
C     ----------
      CALL NUMRT
C     ----------                                            ----------
C     IF((J.EQ.1).AND.(M.EQ.1).AND.(IPRT.EQ.1)) CALL CVCLT
C                                                           ----------
      TOL=.1D0*TOL1
      IF(CH1.LE.TOL) TOL=TOL1
      IF(CH1.LE.TOL) GOTO 3
      IF(M.EQ.1) GOTO 4
      TOL=.1D0*TOL1
    3 CH2=CH1
      DF1=-1.D0
      IF(J.NE.1) NS=NSPTP/2
      IF(M.NE.1) NS=NSPTP
      DO 2004 L=1,NS
      L1=L
      IF((J.NE.1).AND.(M.EQ.1)) L1=2*L
      DF=DABS((H(L1)-HST(L))/H(L1))
      IF(DF.GT.DF1) DF1=DF
 2004 CONTINUE
      CH1=DF1
      IF((CH2.LE.TOL).AND.(CH1.LE.TOL)) GOTO 6
C                       ----------
      IF(IPRT.EQ.1) CALL CVOUT
C                       ----------
    4 CONTINUE
      DO 2005 N=1,NSPTP
      HST(N)=H(N)
 2005 CONTINUE
      IF(CH2.LE.TOL) GOTO 8
      IF(M.EQ.1) GOTO 2003
    8 CONTINUE
      IF(CH1.LE.TOL) GOTO 9
 2003 CONTINUE
      IF(IPRT.EQ.1) WRITE(6,201)
      IF(J.EQ.NHALF) GOTO 2002
      GOTO 10
    9 H0=H1
   10 DT=DT1/(2.D0**J)
      NSPTP=2*NSPTP
 2002 CONTINUE
      WRITE(6,200)
    6 CONTINUE
C          -----
      CALL CVOUT
C          -----
C-------------------------------------
C           FCOEFF
```

F17

```
C---------------------------------------
      HG=HZ
      UG=UZ
      FPG=FPZ
      FG=FZ
      BG=BZ
      BHG=BHZ
      XMG=XMZ
      IF(XMG.EQ.0.D0) FRZ=Y(VI)
      IF(XMG.GT.0.D0) FRZ=FR(VI)
      FRZ=Y(VI)
      DO 3000 I=1,NSPTP
      HG=H(I)
      UG=UE(I)
      FPG=FPR(I)
      FG=FU(I)
      BG=BF(I)
      BG=BH(I)
      XMG=XMI(I)
      IF(XMG.EQ.0.D0) FRI(I)=Y(VI)
      IF(XMG.GT.0.D0) FRI(I)=FR(VI)
      FRI(I)=Y(VI)
 3000 CONTINUE
C---------------------------------------
C         PRESS
C---------------------------------------
      PI=3.14159265358979312D0
      N1=NPX+1
      DO 4000 I=1,N1
      X=(I-1)*(BZ/NPX)
      PR(I,1)=P(X,HZ,BZ,XMZ,FZ,UZ)
 4000 CONTINUE
      CALL E02BBF(NH4,PKI,PCI,TZ,PDY,0)
      PHZ(1)=PDY
      N2=NPT+1
      DO 4001 J=2,N2
      I=(J-1)*NSPTP/NPT
      TG=I*DT
      HG=H(I)
      UG=UE(I)
      FPG=FPR(I)
      FG=FU(I)
      BG=BF(I)
      BHG=BH(I)
      XMG=XMI(I)
      DO 4002 K=1,N1
      X=(K-1)*(BG/NPX)
      PR(K,J)=P(X,HG,BG,XMG,FG,UG)
 4002 CONTINUE
      CALL E02BBF(NH4,PKI,PCI,TG,PDY,0)
      PHZ(J)=PDY
 4001 CONTINUE
C---------------------------------------
C         OUTPUT
C---------------------------------------
```



```
  300 FORMAT(' ------------------------------------------------')
  301 FORMAT(' ',6X,'TIME',13X,'HO',14X,'HC',12X,'F COEFF'/)
  302 FORMAT(' ',1X,4(D14.7,2X),I8)
  303 FORMAT(' TIME =',D14.7/)
  304 FORMAT(' ',7X,'X',11X,'PRESSURE'/)
  305 FORMAT(' ',1X,2(D14.7,2X),I8)
  306 FORMAT(' -----------------------------------------------',
     *'------------------------')
  307 FORMAT(' MAXIMUM DRY CONTACT STRESS =',D14.7//)
  308 FORMAT(' FP =',D14.7/)
  309 FORMAT(' DRY CONTACT LENGTH =',D14.7/)
 7999 FORMAT(' $$$$ DIMENSIONLESS PARAMETERS $$$$'/)
 7980 FORMAT(' U =',D11.4)
 7981 FORMAT(' W =',D11.4)
 7982 FORMAT(' S =',D11.4)
 7983 FORMAT(' C =',D11.4)
      DO 5000 I=1,10
      WRITE(6,99)
 5000 CONTINUE
C
C     WRITING ON CHANNEL 8
C
      WRITE(8,*) HZ
      DO 5015 I=1,NSPTP
      ICC=(I/2)*2
      IF(ICC.NE.I) GOTO 5015
      WRITE(8,*) H(I)
 5015 CONTINUE
      NSQ=NSPTP-7
      DO 5016 I=NSQ,NSPTP
      ICC=(I/2)*2
      IF(ICC.NE.I) GOTO 5016
      WRITE(8,*) FU(I)
 5016 CONTINUE
C
C
      WRITE(6,300)
      WRITE(6,99)
      WRITE(6,301)
      HCZ=HZ+XMZ*(BHZ/2.D0)
      LL=1
      WRITE(6,302) TZ,HZ,HCZ,FRZ,LL
      DO 5001 J=1,NPRT
      LL=J+1
      I=J*NSPTP/NPRT
      TPL=I*DT
      XHO=H(I)
      XHC=H(I)+XMI(I)*(BH(I)/2.D0)
      XFR=FRI(I)
      WRITE(6,302) TPL,XHO,XHC,XFR,LL
 5001 CONTINUE
      WRITE(6,99)
      WRITE(6,300)
C
C     DIMENSIONLESS PARAMETERS
```

```
C
      EP=2.D0*E/(1.D0-PCIS**2)
      UAA=UAMP*2.D0/PI
      UUU=VI*UAA/(EP*R)
      FAP=35.0M3C3
      WWW=FAP/(EP*R)
      SSS=EP*TP/VI
      QQQ=TH/R
      WRITE(6,99)
      WRITE(6,7999)
      WRITE(6,7980) UUU
      WRITE(6,7981) WWW
      WRITE(6,7982) SSS
      WRITE(6,7983) QQQ
C
C
      IF(NP.EQ.0) GOTO 17
      DO 5002 I=1,10
      WRITE(6,99)
 5002 CONTINUE
      WRITE(6,306)
      WRITE(6,99)
      WRITE(6,302) TZ
      WRITE(6,308) FPZ
      WRITE(6,309) BHZ
      WRITE(6,307) PHZ(1)
      WRITE(6,304)
      N1=NPX+1
      DO 5003 I=1,N1
      X=-1.D0+(I-1)*(BZ/NPX)+BHZ/2.D0
      XP=PR(I,1)
      WRITE(6,305) X,XP,I
 5003 CONTINUE
      N2=NPT+1
      DO 5004 J=2,N2
      TPL=(J-1)*(TP/NPT)
      KK=(J-1)*(NSPTP/NPT)
      WRITE(6,99)
      WRITE(6,306)
      WRITE(6,99)
      WRITE(6,302) TPL
      WRITE(6,99)
      WRITE(6,308) FPR(KK)
      WRITE(6,309) BH(KK)
      WRITE(6,307) PHZ(J)
      WRITE(6,304)
      N1=NPX+1
      DO 5005 K=1,N1
      X=-1.D0+(K-1)*(BF(KK)/NPX)+BH(KK)/2.D0
      XP=PR(K,J)
      WRITE(6,305) X,XP,K
 5005 CONTINUE
 5004 CONTINUE
      WRITE(6,99)
      WRITE(6,330)
```



```
   17 CONTINUE
C-----------------------------------
C          VISUAL
C-----------------------------------
      CALL PAPER(1)
      CALL CTRFNT(1)
      CALL BLKPEN
      TP1=1.
      TT(1)=TZ
      HH(1)=HZ*1.E6/R
      FF(1)=FRZ
      BFP(1)=BZ
      BHP(1)=BHZ
      XMM(1)=XMZ
      FPP(1)=FPZ/FAP
      UU(1)=UZ/UAA
      DO 6000 I=1,NSPTP
      K=I+1
      TT(K)=I*DT/TP
      HH(K)=H(I)*1.E6/R
      FF(K)=FRI(I)
      BHP(K)=BH(I)
      BFP(K)=BF(I)
      XMM(K)=XMI(I)
      FPP(K)=FPR(I)/FAP
      UU(K)=UE(I)/UAA
 6000 CONTINUE
      FPMAX=0.
      UMAX=0.
      N=NSPTP+1
      DO 6001 I=1,N
      IF(FPP(I).GT.FPMAX) FPMAX=FPP(I)
      IF(UU(I).GT.UMAX) UMAX=UU(I)
 6001 CONTINUE
      FPMAX=FPMAX*1.1
      UMAX=UMAX*1.1
      CALL PSPACE(0.,1.,0.,1.)
      CALL MAP(0.,1.,0.,1.)
      CALL PLOTCS(.06,.37,'H',1)
      CALL PLOTCS(.47,.1,'T',1)
C     CALL PLOTCS(.06,.87,'F',1)
      CALL PLOTCS(.47,.54,'T',1)
      CALL PSPACE(.11,.57,.15,.5)
      CALL MAP(0.,TP1,0.,HFACT)
      CALL BORDER
      CALL AXES
      CALL BLKPEN
      CALL CURVEC(TT,HH,1,N)
      CALL BLKPEN
      CALL PSPACE(.11,.57,.58,.93)
      CALL MAP(0.,TP1,0.,FFACT)
      CALL BORDER
      CALL AXES
      CALL BLKPEN
      CALL CURVEC(TT,FF,1,N)
```

619

```
      CALL FRAME
      CALL BLKPEN
      CALL PSPACE(0.,1.,0.,1.)
      CALL MAP(0.,1.,0.,1.)
      CALL PLOTCS(.06,.37,'WF',2)
      CALL PLOTCS(.47,.1,'T',1)
      CALL PLOTCS(.06,.87,'LF',2)
      CALL PLOTCS(.47,.54,'T',1)
      CALL PSPACE(.11,.57,.15,.5)
      CALL MAP(0.,TP1,0.,UMAX)
      CALL BORDER
      CALL AXES
      CALL BLKPEN
      CALL CURVEC(TT,UL,1,N)
      CALL BLKPEN
      CALL PSPACE(.11,.57,.58,.93)
      CALL MAP(0.,TP1,0.,FPMAX)
      CALL BORDER
      CALL AXES
      CALL BLKPEN
      CALL CURVEC(TT,FPF,1,N)
      IF(NP.EQ.0) GOTO 29
      CALL BLKPEN
      N1=NPX+1
      N2=NPT+1
      DO 6002 J=1,N2
      TPL=(J-1)*(TP/NPT)
      TPL1=TPL
      IT=(J-1)*NSPTP/NPT+1
      HX=HM(IT)
      XXM=XMM(IT)
      M=(J-1)*(NSPTP/NPT)+1
      BFPX=BFP(M)
      BMPX=BMP(M)
      DO 6003 I=1,N1
      XX(I)=-1.D0*(I-1)*BFPX/NPX+BMPX/2.D0
      XX(I)=XX(I)/R
      XPR(I)=PR(I,J)/EP
 6003 CONTINUE
      XPMZ=PMZ(J)/EP
      X1=XX(1)
      Y1=.9*MFACT
      X2=X1
      Y2=HX
      X3=XX(N1)
      Y3=HX+XXM*BFPX*1.E6/R
      X4=X3
      Y4=Y1
      XXIP=-1.D0*XFACT
      CALL FRAME
      CALL PSPACE(0.,1.,0.,1.)
      CALL MAP(0.,1.,0.,1.)
      CALL PLOTCS(.06,.37,'H',1)
      CALL PLOTCS(.47,.1,'X',1)
      CALL PLOTCS(.06,.87,'P',1)
```

FILE: PLISP FORTRAN A LEEDS UNIVERSITY VM/BSE 6.16

```
      CALL PLOTCS(.47,.54,'X',1)
      CALL PLOTCS(.23,.51,'T =',4)
      CALL TYPENE(TPL1,4)
      CALL PSPACE(.11,.57,.58,.93)
      CALL MAP(XFACT,XXIP,0.,PFACT)
      CALL BORDER
      CALL AXES
      CALL BLKPEN
      CALL CURVEC(XX,XPR,1,N1)
      CALL CURVEC(XX,XPR,1,N1)
      CALL BLKPEN
      CALL PTPLOT(0.,XPMZ,1,1,226)
      CALL BLKPEN
      CALL PSPACE(.11,.57,.15,.5)
      CALL MAP(XFACT,XXIP,0.,HFACT)
      CALL BORDER
      CALL AXES
      CALL BLKPEN
      CALL POSITN(X1,Y1)
      CALL JOIN(X2,Y2)
      CALL JOIN(X3,Y3)
      CALL JOIN(X4,Y4)
      CALL BLKPEN
 6002 CONTINUE
   29 CONTINUE
      CALL GREND
      STOP
      END
C-----------------------------------------------------------------------
C
      SUBROUTINE CVOUT
C
C-----------------------------------------------------------------------
      IMPLICIT REAL*8(A-H,O-Z)
      COMMON TOL,TOL1,H0,VI,TP,E,R,TH,WD,UAPP
      COMMON PR(201,41),PMZ(201),BH(400),BFP(401),BMP(401)
      COMMON XE(64),PD(64),TO(64),HMCOL(64)
      COMMON XEK(68),XEC(68),PKI(68),FCI(68),FKI(104),FCI(104)
      COMMON AW(400),FW(616),HKI(68),HCI(68)
      COMMON TF(100),FE(100),FP(100),TM(100)
      COMMON TZ,HZ,UZ,FPZ,FZ,BZ,XMZ,XMCZ,FRZ,CH1,CH2,DT,BHZ,XM
      COMMON UE(400),FPR(400),FU(400),BF(400),XMI(400),XMM(401)
      COMMON FRI(400),H(400),HST(2000),UC,FPY,BC,BCRY,HM,UM0
      COMMON NPER,NHALF,NSPTP,NPRT,IPRT,NPX,NPT,NP,NA4,NF4,NH4
   98 FORMAT(' ',/)
   99 FORMAT(' ')
  100 FORMAT(' ',6X,'TIME',13X,'H0',11X,'ENT VEL',12X,
     +       'FP',12X,'SQ VEL',10X,'LENGTH',11X,'SLOPE'/)
  101 FORMAT(' ',1X,6(D14.7,2X),D14.7)
  102 FORMAT(' ***** CONVERGES TO SPECIFIED TOLERANCE *****')
  103 FORMAT(' ***** MAXIMUM RELATIVE DIFFERENCE =',D14.7)
  104 FORMAT(' ***** NUMBER OF STEPS PER CYCLE =',I4)
  105 FORMAT(' ***** DOES NOT CONVERGE TO SPECIFIED TOLERANCE *****')
      WRITE(6,98)
      WRITE(6,100)
```

F20

```
      WRITE(6,101) TZ,HZ,UZ,FPZ,FZ,BZ,XMZ
      DO 1 J=1,NPRT
      I=J*NSPTP/NPRT
      TPL=DT*I
      XH0=H(I)
      XU=UE(I)
      XFP=FPR(I)
      XF=FU(I)
      XB=BF(I)
      XM=XMI(I)
      XFR=FRI(I)
      WRITE(6,101) TPL,XH0,XU,XFP,XF,XB,XM
    1 CONTINUE
      IF(IPRT.EQ.1) GOTO 4
      IF((CH1.GT.TOL).OR.(CH2.GT.TOL)) GOTO 2
      WRITE(6,99)
      WRITE(6,102)
    4 CONTINUE
      IF(CH1.EQ.1.D6) GOTO 3
      WRITE(6,99)
      WRITE(6,103) CH1
      WRITE(6,104) NSPTP
      GOTO 3
    2 CONTINUE
      WRITE(6,105)
    3 RETURN
      END
C---------------------------------------------------------------------------
C
      SUBROUTINE NUMRT
C
C---------------------------------------------------------------------------
      IMPLICIT REAL*8(A-H,O-Z)
      COMMON TOL,TOL1,H0,VI,TP,E,R,TM,WD,LAMP
      COMMON PR(201,41),PMZ(201),BM(400),BFP(401),BHP(401)
      COMMON XE(64),PD(64),TO(64),HMCCL(64)
      COMMON XEK(68),XEC(68),PKI(68),PCI(68),FKI(104),FCI(104)
      COMMON AW(400),FW(816),HKI(68),HCI(68)
      COMMON TF(100),FE(100),FP(100),TM(100)
      COMMON TZ,HZ,UZ,FPZ,FZ,BZ,XMZ,XMCZ,FRZ,CH1,CH2,DT,BMZ,XM
      COMMON UE(400),FPR(400),FU(400),BF(400),XMI(400),XMM(401)
      COMMON FRI(400),H(400),MST(2000),UC,FPY,BC,BDRY,HM,UM0
      COMMON NPER,NHALF,NSPTP,NPRT,IPRT,NPD,NPT,NP,NA4,NF4,NH4
      U(T)=UAMP*DABS(DCOS((2.D0*PI/TP)*T))
      B(T)=4.D0*DSQRT(FPY*R*(1.D0-POIS**2)/(E*PI))
      F(T,H0,BC,UC,FPY,XM)=XM*U(T)*FPY*XM**3/(12.D0*VI)/
     A     (2.D0*(XM*BC)/(2.D0*H0+XM*BC)-DLOG(1.D0+XM*BC/H0))
      Y(H0,BC,FPY)=-1.D0*(FPY*H0**3)/(VI*BC**3)
      PI=3.14159265358979312D0
      TZ=0.D0
      HZ=H0
      UZ=U(TZ)
      UC=UZ
      CALL E02BBF(NF4,FKI,FCI,TZ,FPY,0)
      CALL E02BBF(NH4,XEK,XEC,TZ,AY,0)
```

FILE: PLISP FORTRAN A LEEDS UNIVERSITY VM/BSE 6.16

```
      CALL E02BBF(NH4,HKI,HCI,TZ,HM,0)
      FPZ=FPY
      BMZ=2.D0*AY
      BDRY=BMZ
C     -----------
      CALL INCLIN
C     -----------
      XMZ=XM
      BZ=BC
      IF(XMZ.EQ.0.D0) FZ=Y(HZ,BZ,FPZ)
      IF(XMZ.GT.0.D0) FZ=F(TZ,HZ,BZ,UZ,FPZ,XMZ)
      T=TZ
      FC=FZ
      DO 1 I=1,NSPTP
      HV=H0
      G1=FC
      T1=T+DT/2.D0
      UC=U(T1)
      CALL E02BBF(NF4,FKI,FCI,T1,FPY,0)
      CALL E02BBF(NH4,XEK,XEC,T1,AY,0)
      CALL E02BBF(NH4,HKI,HCI,T1,HM,0)
      BDRY=2.D0*AY
      H0=HV+(DT/2.D0)*G1
C     -----------
      CALL INCLIN
C     -----------
      IF(XM.EQ.0.D0) G2=Y(H0,BC,FPY)
      IF(XM.GT.0.D0) G2=F(T1,H0,BC,UC,FPY,XM)
      H0=HV+(DT/2.D0)*G2
C     -----------
      CALL INCLIN
C     -----------
      IF(XM.EQ.0.D0) G3=Y(H0,BC,FPY)
      IF(XM.GT.0.D0) G3=F(T1,H0,BC,UC,FPY,XM)
      T1=T+DT
      UC=U(T1)
      CALL E02BBF(NF4,FKI,FCI,T1,FPY,0)
      CALL E02BBF(NH4,XEK,XEC,T1,AY,0)
      CALL E02BBF(NH4,HKI,HCI,T1,HM,0)
      BDRY=2.D0*AY
      H0=HV+DT*G3
C     -----------
      CALL INCLIN
C     -----------
      IF(XM.EQ.0.D0) G4=Y(H0,BC,FPY)
      IF(XM.GT.0.D0) G4=F(T1,H0,BC,UC,FPY,XM)
      H0=HV+(DT/6.D0)*(G1+2.D0*G2+2.D0*G3+G4)
      T=I*DT
      UC=U(T)
      CALL E02BBF(NF4,FKI,FCI,T,FPY,0)
      CALL E02BBF(NH4,XEK,XEC,T,AY,0)
      CALL E02BBF(NH4,HKI,HCI,T,HM,0)
      BDRY=2.D0*AY
C     -----------
      CALL INCLIN
```

FILE: PLISP   FORTRAN A   LEEDS UNIVERSITY VM/BSE 6.16

```
C       ----------
        IF(XM.EQ.0.D0) FC=Y(H0,BC,FPY)
        IF(XM.GT.0.D0) FC=F(T,H0,BC,UC,FPY,XP)
        H(I)=H0
        UE(I)=UC
        FPR(I)=FPY
        BM(I)=BORY
        BF(I)=BC
        XMI(I)=XM
        FU(I)=FC
   1    CONTINUE
  60    RETURN
        END
C-------------------------------------------------------------------------
C
        SUBROUTINE INCLIN
C
C-------------------------------------------------------------------------
        IMPLICIT REAL*8(A-H,O-Z)
        COMMON TOL,TOL1,H0,VI,TP,E,R,TH,WD,UAPP
        COMMON PR(201,41),PHZ(201),BM(400),BFP(401),BMF(401)
        COMMON XE(64),PD(64),TO(64),HMCCL(64)
        COMMON XEK(68),XEC(68),PKI(68),PCI(68),FKI(104),FCI(104)
        COMMON AW(400),FW(616),HKI(68),HCI(68)
        COMMON TF(100),FE(100),FP(100),TP(100)
        COMMON TZ,HZ,UZ,FPZ,FZ,BZ,XMZ,XPCZ,FRZ,CH1,CH2,DT,BMZ,XM
        COMMON UE(400),FPR(400),FU(400),BF(400),XMI(400),XPP(401)
        COMMON FRI(400),H(400),HST(2000),UC,FPY,BC,BORY,HP,UM0
        COMMON NPER,NHALF,NSPTP,NPRT,IPRT,NPX,NPT,NP,NA4,NF4,NM4
 100    FORMAT(' **** D HAS NOT ACHIEVED BUILT IN RELATIVE TOLERANCE')
        PI=3.14159265358979312D0
        IF(UC.LT.UM0) GOTO 8
        D=0.D0
        ADD=1.D-3*HP
        DO 1 I=1,50000
        D=D+ADD
C       BC=BORY*(1.D0+D/(2.D0*H0))
        BC=BORY
        XLS=(FPY*HP**2)/(12.D0*VI*UC*BC**2)
        RS=((HM/D)**2)*(DLOG(1.D0+D/HP)-2.D0*D/(2.D0*HP+D))
        DIFF=XLS-RS
        IF(DIFF.LT.0.D0) GOTO 2
        GOTO 1
   2    RE=ADD/D
        XK=D/HM
        IF(XK.GE.1.188D0) GOTO 12
        IF(RE.LT.1.D-12) GOTO 9
        D=D-ADD
        ADD=ADD/4.D0
   1    CONTINUE
  12    CONTINUE
        D=1.D6
        WRITE(6,100)
        GOTO 9
   8    XM=0.D0
```

FILE: PLISP   FORTRAN A   LEEDS UNIVERSITY VM/BSE 6.16

```
        BC=BORY
        GOTO 44
   9    XM=D/BC
  44    CONTINUE
        RETURN
C.........................................................................
        END
```

FILE: JPSP   EXEC   A   LEEDS UNIVERSITY VM/BSE 6.16

```
EXEC SETUP FORTRAN NAGF CCGHOST
FI 4 DISK BANK DATA
FI 5 DISK XPSP DATA
FI 6 DISK YPSP DATA
FI 8 DISK STPSP DATA
LOAD PLISP(CLEAR
EXEC PLOTFILE PPSP
SET BLIP *
START
```

F22

INPUT

```
FILE: BANK     DATA     A   LEEDS UNIVERSITY VM/BSE 6.16

 .0                           .73805939540503151 9E-02   1296979.40715427510
 .60290410270761729 2E-06   -.90020516759060332 1E-04
 .31250000000000000 0E-01    .80163965734808956 1E-02   1530057.36035484495
 .64624535941378402 66E-06  -.10637774462795941 0E-03
 .62500000000000000 0E-01    .86681334589477161 6E-02   1796402.40875089052
 .60041335295697403 8E-06   -.12507307622690559 7E-03
 .93750000000000000 0E-01    .93761021496418417 0E-02   2893125.59496485605
 .54642753363449547 3E-06   -.14590552009975785 3E-03
 .12500000000000000 9        .10075600815056027 7E-01   2417092.53743135976
 .95467779843923163 09E-06  -.16865281237553152 7E-03
 .15625000000000000 0        .10697115713225926 6E-01   2724491.87498385879
 .41593777318625364 33E-06  -.19824797560361241 9E-03
 .19750000000000000 0        .11305031649192495 91E-01  3045699.35707500964
 .33494035509430942 3E-06   -.21278166837521311 7E-03
 .21375000000000000 0        .11084151460055503 2E-01   3262690.77915116563
 .23270475598130481 8E-06   -.23512780489272556 0E-03
 .25000000000000000 0        .12406765536650047 6E-01   3664947.26204662095
 .51327103211367645 5E-07   -.25648895652017304 6E-03
 .20125000000000000 0        .13100176885652464 1E-01   4886075.57267739797
 .22139927944455732 9E-06   -.29577746176937281 9E-03
 .31250000000000000 0        .13781107411464456 95E-01  4521075.05304966095
 .30256926362960699 8E-06   -.31619269015950003 6E-03
 .34375000000000000 0        .14286070257754663 0E-01   4859327.27965151402
 .35821978003754141 58E-06  -.33975175139375725 3E-03
 .37500000000000000 0        .14486305180500173 1E-01   4996502.52940892451
 .40155428495152091 5E-06   -.34930545128664949 3E-03
 .40625000000000000 0        .14339167925094129 8E-01   4855516.75624421914
 .43793133271166141 8E-06   -.34219561072565234 1E-03
 .43750000000000000 0        .14002324213263524 0E-01   4668215.00827803253
 .46738144508118395 0E-06   -.32625147240622922 5E-03
 .46875000000000000 0        .12872084543520433 35E-01  3945013.06750902459
 .50314631446332254 0E-06   -.27558698301706035 9E-03
 .50000000000000000 0        .11560780806610820 25E-01  3186586.02733419198
 .53704827322756141 1E-06   -.22245892577611446 45E-03
 .53125000000000000 0        .10669802517243282 3E-01   2710627.71439871332
 .55482787803559130 23E-06  -.19912159058554410 35E-03
 .56250000000000000 0        .97223239466474946 3E-02   2251024.06298423000
 .56529667371764097 0E-06   -.15693730791314703 5E-03
 .59375000000000000 0        .77820834253572560 05E-02  1441523.75698259213
 .60394984075110028 5E-06   -.10025602912698067 7E-03
 .62500000000000000 0        .65553294137803363 4E-02   1024399.45773702438
 .61052772485850949 8E-06   -.71020968110160086 0E-04
 .65625000000000000 0        .59056495525934939 8E-02   930356.275292502804
 .57223663519077163 1E-06   -.57483321116961080 6E-04
 .68750000000000000 0        .54768630232201941 9E-02   714189.955513215042
 .49315433636344245 6E-06   -.49437965672772612 6E-04
 .71875000000000000 0        .55406753949884747 41E-02  720930.128711741403
 .39745731254137653 5E-06   -.50774460391347751 7E-04
 .75000000000000000 0        .51625700474363632 3E-02   624672.834498848606
 .80220972295073905 5E-07   -.44337192654656726 4E-04
 .78125000000000000 0        .52472353382193407 55E-02  655556.506946300999
 .35793745938951077 13E-06  -.45496449927726528 35E-04
 .81250000000000000 0        .60440632776493097 43E-02  869777.585972043596
 .46633906150553599 47E-06  -.60355211955359577 9E-04
 .84375000000000000 0        .60151837516370494 7E-02   862631.975717167443
```

```
FILE: BANK     DATA     A   LEEDS UNIVERSITY VM/BSE 6.16

 .56618733207563659 7E-06   -.59746760465210528 05E-04
 .87500000000000000 0        .56225929591249170 05E-02  752699.610739192023
 .66578363711121850 4E-06   -.51938285284316223 40E-04
 .90625000000000000 0        .60173874225104189 2E-02   862116.836482038721
 .69626711134821358 4E-06   -.59563487090317196 3E-04
 .93750000000000000 0        .65458673232776749 5E-02   1020198.52680407416
 .70075173644417199 5E-06   -.70624735197725229 4E-04
 .96875000000000000 0        .68829621847361216 5E-02   1127979.46261229932
 .70268118328964644 5E-06   -.78167594902243791 2E-04
1.00000000000000000 0        .73805935523382544 1E-02   1296979.46653849160
 .60280410278324839 2E-06   -.90020516706591374 2E-04
```

INPUT

```
FILE: XPSP     DATA     A   LEEDS UNIVERSITY VM/BSE 6.16

.005 .54199230-6 20 5 16 16 1 20 8 1
.01 1. 16.06 .3 .0024 .0265
.01089851 .4 .10898510-3
-.067 3.7 .001 .2
39
0. .05 .1 .15 .175 .2 .25 .3 .35 .375 .4 .425 .45 .475 .5
.525 .55 .575 .6 .625 .65 .675 .7 .71 .725 .75 .76 .775
.8 .825 .85 .865 .875 .89 .9 .925 .95 .975 1.0000000001
339. 502. 726. 997. 1133. 1302. 1607. 2092. 2489. 2557. 2496.
2403. 2150. 1675. 1302. 1051. 929. 590. 353. 239. 183. 150.
150. 170. 116. 116. 129. 116. 170. 190. 170. 129. 150. 150.
183. 217. 251. 285. 339.
33
```

OUTPUT

**** I N P U T D A T A ****

TOL (TOLERANCE FOR SS AND STEP SIZE)	0.50000000-02
HO (INITIAL GUESS FOR HO AT TIME ZERO)	0.54195230-06
NPER (MAX. NO. OF CYCLES AT SAME STEP SIZE) ..	20
NHALF (MAX. NO. OF STEP SIZE HALVINGS)	5
NSPTP (INITIAL NO. OF STEPS PER CYCLE)	16
NPRT (NO. OF STEPS PRINTED PER CYCLE)	16
IPRT (CONVERGENCE PRINT OPTION)	1
NPX (NO. OF PRESS. PTS. PRINTED PER DIST.) ...	20
NPT (NO. OF PRESS. DIST. PRINTED)	8
NP (PRINT OPTIONS FOR PRESS. DIST.)	1
VI (ABSOLUTE VISCOSITY)	0.10000000-01
TP (PERIOD)	0.10000000+01
E (ELASTIC MODULUS OF LAYER)	0.16000000+08
R (REDUCED RADIUS)	0.30000000+00
TH (LAYER THICKNESS)	0.24000000-02
WD (WIDTH OF CONTACT)	0.26500000-01
UAMP (AMPLIT. OF ENT. VEL.)	0.10898510-01
POIS (POISSONS RATIO)	0.40000000+00
UMB (LOWER LIMIT FOR ENT. VEL.)	0.10899510-03
XFACT (SCALE FACTOR FOR PLOTS)	-0.66999970E-01
HFACT (SCALE FACTOR FOR FILM PLOTS)	0.37000000E+01
FFACT (SCALE FACTOR FOR FRICTION PLOTS)	0.99999995E-03
HFACT (SCALE FACTOR FOR FILM PLOTS)	0.37000000E+01
PFACT (SCALE FACTOR FOR FRICTION PLOTS)	0.20000000D+00

NOTE : FOR SS TOLERANCE EQUALS .1*TOL

DATA BANK

TO	XE	PC	HPCOL	
0.0	0.73805940D-02	0.12969790D+07	0.68280410D-06	1
0.31250000D-01	0.80163870D-02	0.15300580D+07	0.64624540D-06	2
0.62500000D-01	0.86861330D-02	0.17964020D+07	0.60041340D-06	3
0.93750000D-01	0.93761020D-02	0.20531260D+07	0.54642750D-06	4
0.12500000D+00	0.10075610D-01	0.24170930D+07	0.48467740D-06	5
0.15625000D+00	0.10697120D-01	0.27244820D+07	0.41553770D-06	6
0.18750000D+00	0.11309030D-01	0.30450990D+07	0.32454040D-06	7
0.21875000D+00	0.11884150D-01	0.33626910D+07	0.23270480D-06	8
0.25000000D+00	0.12406770D-01	0.36649470D+07	0.51327100D-07	9
0.28125000D+00	0.13100200D-01	0.40960760D+07	0.22139830D-06	10
0.31250000D+00	0.13781110D-01	0.45219780D+07	0.30256430D-06	11
0.34375000D+00	0.14286070D-01	0.48593270D+07	0.35821960D-06	12
0.37500000D+00	0.14486310D-01	0.49965030D+07	0.40155430D-06	13
0.40625000D+00	0.14335170D-01	0.48955170D+07	0.43793130D-06	14
0.43750000D+00	0.14002320D-01	0.46692150D+07	0.46730140D-06	15
0.46875000D+00	0.12972080D-01	0.35450130D+07	0.50314630D-06	16
0.50000000D+00	0.11564780D-01	0.31865070D+07	0.53704830D-06	17
0.53125000D+00	0.10669890D-01	0.27106280D+07	0.55492750D-06	18
0.56250000D+00	0.97233240D-02	0.22510240D+07	0.56529670D-06	19
0.59375000D+00	0.77820030D-02	0.14419240D+07	0.60364980D-06	20
0.62500000D+00	0.65593290D-02	0.10243990D+07	0.61052770D-06	21
0.65625000D+00	0.55056490D-02	0.83039630D+06	0.57223660D-06	22
0.68750000D+00	0.54766630D-02	0.71415000D+06	0.49315430D-06	23
0.71875000D+00	0.55406750D-02	0.73053010D+06	0.34745730D-06	24
0.75000000D+00	0.51629700D-02	0.63467280D+06	0.80220970D-07	25
0.78125000D+00	0.52472350D-02	0.65555850D+06	0.35793750D-06	26
0.81250000D+00	0.60440630D-02	0.86977800D+06	0.46653910D-06	27
0.84375000D+00	0.60191840D-02	0.86263200D+06	0.56619730D-06	28
0.87500000D+00	0.56225830D-02	0.75265560D+06	0.66578360D-06	29
0.90625000D+00	0.60173870D-02	0.86211650D+06	0.69626710D-06	30
0.93750000D+00	0.65458670D-02	0.10201950D+07	0.70079170D-06	31
0.96875000D+00	0.68829620D-02	0.11275750D+07	0.70268120D-06	32
0.10000000D+01	0.73805940D-02	0.12969790D+07	0.68280410D-06	33

T/TP	TIME	LOAD	FP	
0.0	0.0	0.33500D+03	0.12792450D+05	1
0.50000D-01	0.50000D-01	0.50200D+03	0.18943400D+05	2
0.10000D+00	0.10000D+00	0.72600D+03	0.27396230D+05	3
0.15000D+00	0.15000D+00	0.99700D+03	0.37622640D+05	4
0.17500D+00	0.17500D+00	0.11330D+04	0.42754720D+05	5
0.20000D+00	0.20000D+00	0.13020D+04	0.49132080D+05	6
0.25000D+00	0.25000D+00	0.16070D+04	0.60641510D+05	7
0.30000D+00	0.30000D+00	0.20820D+04	0.78566040D+05	8
0.35000D+00	0.35000D+00	0.24890D+04	0.93924530D+05	9
0.37500D+00	0.37500D+00	0.25570D+04	0.96490570D+05	10
0.40000D+00	0.40000D+00	0.24960D+04	0.94188680D+05	11
0.42500D+00	0.42500D+00	0.24080D+04	0.90867920D+05	12
0.45000D+00	0.45000D+00	0.21500D+04	0.81132080D+05	13
0.47500D+00	0.47500D+00	0.16750D+04	0.63207550D+05	14
0.50000D+00	0.50000D+00	0.13020D+04	0.49132080D+05	15
0.52500D+00	0.52500D+00	0.10510D+04	0.39660380D+05	16
0.55000D+00	0.55000D+00	0.92900D+03	0.35056600D+05	17
0.57500D+00	0.57500D+00	0.59000D+03	0.22264150D+05	18
0.60000D+00	0.60000D+00	0.35300D+03	0.13320750D+05	19
0.62500D+00	0.62500D+00	0.23800D+03	0.89811320D+04	20
0.65000D+00	0.65000D+00	0.18300D+03	0.69056600D+04	21
0.67500D+00	0.67500D+00	0.15000D+03	0.56603770D+04	22
0.70000D+00	0.70000D+00	0.15000D+03	0.56603770D+04	23
0.71000D+00	0.71000D+00	0.17000D+03	0.64150940D+04	24
0.72500D+00	0.72500D+00	0.11600D+03	0.43773580D+04	25
0.75000D+00	0.75000D+00	0.11600D+03	0.43773580D+04	26
0.76000D+00	0.76000D+00	0.12900D+03	0.48679250D+04	27
0.77500D+00	0.77500D+00	0.11600D+03	0.43773580D+04	28
0.80000D+00	0.80000D+00	0.17000D+03	0.64150940D+04	29

CONTINUES ....

OUTPUT

FILE: STPSP DATA A LEEDS UNIVERSITY VM/BSE 6.16

renamed START for input into Part 3

```
.542162435046369435E-06
.546256661049567535555E-06
.546298499411761396E-06
.543267733204142443E-06
.538591412120866557E-06
.534773973988321639E-06
.531254953039727849SE-06
.528989560890577301E-06
.528279145850270914E-06
.529082166316869655E-06
.531524705649660432E-06
.532710331462224073E-06
.529664563066363339E-06
.526282663261366920E-06
.527659692196895543E-06
.533607309579841072S1E-06
.543285276587659338E-06
-.256041251582353091E-07
.337923639725167262E-07
.119343514015389640E-06
.977416037998369383E-07
```

F25

PART 3

```
C-----------------------------------------------------------------
C                 PART 3
C        D Y N A M I C   C O L U M N   M O D E L
C
C-----------------------------------------------------------------
      IMPLICIT REAL*8(A-H,O-Z)
      DIMENSION TF(40),FE(40),FPI(40),TM(40),FKI(44),FCI(44)
      DIMENSION XS(16000),XSR(2000),PS(2000),HS(2000),DPS(16000)
      DIMENSION CFS1(2000),XS1(2000),FM(256),PPO(700)
      DIMENSION X2(3000),FX2(6000),FX1(16000)
      DIMENSION H(240),ETS(240),HMCS(240),FRST(240),MST(120)
      DIMENSION TCS(240),UMS(240),FPS(240)
      DIMENSION IR(4),MR(4),MRK(8),MMC(8),MRW(40)
      REAL*4 XX1(2000),XX(2000),HM(2000),PP(2000),XFACT,XXE,MFACT,PMMM
      REAL*4 TT(240),HMP(240),FRR(240),UU(240),FPP(240)
      REAL*4 UMA),FPMAX,FFACT,XJ1,XJ2,XJ3,XJ4,YJ1,YJ2,YJ3,YJ4
      COMMON X(50000),FX(50000)
      COMMON HM,FM,F1,F2,CTCL,PTCL,FPTCL
      COMMON VI,LM,H0,R,AM,XE,XI,CX,FP
      COMMON E,PR,TH,HPC,HMT,FXE,XEF,TC
      COMMON TO(64),XB(64),PB(64),HMCCL(64),HB(64),HPK(68),HMC(68)
      COMMON AM(400),XEK(68),XEC(68),PKI(68),PCI(68),HKI(68),HCI(68)
      COMMON MST,JI,MP,IPT,I2,NCAV,MS,NM4
      U(T)=(PI**2*THETA*RT/(TP*180.D0))*DABS(DCOS((2.D0*PI/TP)*T))
      CALL SETTIM
      PI=3.14159265358979312D0
C-----------------------------------
C          INPUT
C-----------------------------------
C
C   FROM CHANNEL 4
C
      READ(4,*) VI,TP,E,R,TH,WD,PR
      READ(4,*) RT,THETA,XI
      READ(4,*) HMDAI0
      READ(4,*) F1,F2,F3,F4
      READ(4,*) NX,NX1,I1,NST,I2,I3
      READ(4,*) CTCL,PTCL,FPTCL,FPTOL
      READ(4,*) TTCL,NT,MTP,NPX
      READ(4,*) CFUL
      READ(4,*) UM0
      READ(4,*) XFACT,MFACT,FFACT
      READ(4,*) IPT,MAGN
      READ(4,*) NF
      READ(4,*) (TM(I),I=1,NF)
      READ(4,*) (FE(I),I=1,NF)
      READ(4,*) NM
C
C  FROM CHANNEL 2
C
      DO 8351 I=1,NM
      READ(2,*) TC(I),XB(I),PB(I),HMCCL(I),HB(I)
 8351 CONTINUE
      TC(NM)=TO(NM)*1.000000000000100
C
C   FROM CHANNEL 3
C
      NTP=NT+1
      DO 8361 I=1,NTP
      READ(3,*) MST(I)
 8361 CONTINUE
      READ(3,*) HMD4
      READ(3,*) HMD3
      READ(3,*) HMC2
      READ(3,*) HMD1
C-----------------------------------
C          CHECK
C-----------------------------------
   99 FORMAT(' ')
  999 FORMAT(' '/)
  100 FORMAT(' ------------------------------------------------',
     *        '-----------------------------'/)
  101 FORMAT(' -----------------------------------------------------------',
     *'---------------------------------------------------------------'/)
  114 FORMAT(' ',4X,'T/TP',10X,'TIME',9X,'LOAD',11X,'FP'/)
  115 FORMAT(' ',1X,3(D11.4,2X),D14.7,I8)
  116 FORMAT(' ****  I N P U T   D A T A   ****'/)
  117 FORMAT(' ****   O U T P U T   D A T A   ****'/)
C
C
 1212 FORMAT(' HMD4 (SQ. VEL. FROM I-4 TIME STEP) ............ ',D14.7)
 1312 FORMAT(' HMD3 (SQ. VEL. FROM I-3 TIME STEP) ............ ',D14.7)
 1512 FORMAT(' HMC2 (SQ. VEL. FROM I-2 TIME STEP) ............ ',D14.7)
 1413 FORMAT(' HMD1 (SQ. VEL. FROM I-1 TIME STEP) ............ ',D14.7)
C
C
 1400 FORMAT(' VI (ABSOLUTE VISCOSITY) ....................... ',D14.7)
 1401 FORMAT(' TP (PERIOD) ................................... ',D14.7)
 1402 FORMAT(' E (ELASTIC MODULUS OF CARTILAGE) .............. ',D14.7)
 1403 FORMAT(' R (REDUCED RADIUS) ............................ ',D14.7)
 1404 FORMAT(' TH (CARTILAGE THICKNESS) ...................... ',D14.7)
 1405 FORMAT(' WD (WIDTH OF ANKLE) ........................... ',D14.7)
 1406 FORMAT(' PR (POISSONS RATIO) ........................... ',D14.7)
 1407 FORMAT(' RT (TALUS RADIUS) ............................. ',D14.7)
 1408 FORMAT(' THETA (ANGULAR AMPLITUDE IN DEGREES) .......... ',D14.7)
 1409 FORMAT(' XI (INLET BOUNDARY) ........................... ',D14.7)
 1514 FORMAT(' HMDAI0 (HMDAI IF HMD1 EQUALS ZERO) ............ ',D14.7)
 1415 FORMAT(' F1 (HA=H0*F1, INITIAL H0 INCREMENT) ........... ',D14.7)
 1416 FORMAT(' F2 (XA=XEF*F2, INITIAL XEF INCREMENT) ......... ',D14.7)
 1417 FORMAT(' F3 (HMDAI=HMD1*F3, INITIAL HMD INCREMENT) ..... ',D14.7)
 1418 FORMAT(' F4 (XA=XE*F4, INITIAL XE INCREMENT) ........... ',D14.7)
 1419 FORMAT(' NX (INIT. NO. OF STEPS AT CURRENT TIME STEP) .. ',I8)
 1519 FORMAT(' NX1 (NO. OF SUB-STEPS IN FIRST STEP) .......... ',I8)
 1420 FORMAT(' I1 (NO. OF PTS. PRINTED AT CURRENT TIME STEP) . ',I8)
 1421 FORMAT(' NST (INITIAL NO. OF STEPS FOR PROFILE ) ....... ',I8)
 1422 FORMAT(' I2 (NO. OF PTS. PRINTED FOR PROFILE) .......... ',I8)
 1522 FORMAT(' I3 (NO. OF PTS. PLOTTED) ...................... ',I8)
 1424 FORMAT(' CTCL (INITIAL ABSOLUTE TOLERANCE FOR COEEF) .. ',D14.7)
 1425 FORMAT(' PTOL (RELATIVE INLET PRESSURE TOLERANCE) ...... ',D14.7)
 1426 FORMAT(' FPTCL (RELATIVE LOAD CAPACITY TOLERANCE) ...... ',D14.7)
```

F27

```
 1526 FORMAT(' FRTOL (RELATIVE FRICTION COEFF. TOLERANCE) .... ',D14.7)
 1626 FORMAT(' TTOL (TIME STEP TOLERANCE) ..................... ',D14.7)
 1726 FORMAT(' NT (INITIAL NO. OF TIME STEPS) ................. ',I8)
 1826 FORMAT(' MTP (NO. OF TIME STEPS PRINTED) ................ ',I9)
 1926 FORMAT(' NPX (NO. OF PRESS. DIST. PRINTED) .............. ',I9)
 2026 FORMAT(' CPUL (LIMIT ON CPU TIME) ....................... ',D14.7)
 1530 FORMAT(' UM0 (LOWER LIMIT FOR ENT. VEL.) ................ ',D14.7)
 1630 FORMAT(' XFACT (SCALE FACTOR FOR PLOTS) ................. ',E14.7)
 1730 FORMAT(' HFACT (SCALE FACTOR FOR FILM PLOTS) ............ ',E14.7)
 1830 FORMAT(' FFACT (SCALE FACTOR FOR FRICTION PLOTS) ........ ',E14.7)
 1431 FORMAT(' IPT (PRINT OPTION FOR CONVERGENCE) ............. ',I9)
 1531 FORMAT(' MAGN (PRINT OPTION FOR ONE TIME STEP) .......... ',I8//)
 1432 FORMAT(' ***** NOTE :'//)
 1433 FORMAT(' (1.) NX AND NX1 SHOULD BE EVENLY DIVISIBLE BY 4'/)
 1434 FORMAT(' (2.) I1 AND I3 SHOULD NOT EXCEED NX/2'/)
 1435 FORMAT(' (3.) I2 SHOULD NOT EXCEED 2*NST'/)
 1436 FORMAT(' (4.) FOR SS TOLERANCE EQUALS .1*TTOL'/)
 1437 FORMAT(' (5.) MTP AND NPX SHOULD DIVIDE NT EVENLY'/)
C
C
 2472 FORMAT(///24X,'DATA BANK'//)
 2473 FORMAT(' ',6X,'TO',15X,'XE',14X,'PO',15X,'HM',13X,'HB'/)
 2471 FORMAT(' ',1X,5(D14.7,2X),I8)
 2477 FORMAT(///20X,'PREVIOUS CYCLE'//)
 2478 FORMAT(8X,'HO'/)
 2479 FORMAT(' ',1X,D14.7,I8)
      WRITE(5,101)
      WRITE(5,116)
      WRITE(5,101)
C
C    FROM CHANNEL 3
C
      WRITE(5,1212) HMD4
      WRITE(5,1312) HMD3
      WRITE(5,1512) HMC2
      WRITE(5,1413) HMC1
      WRITE(5,99)
      WRITE(5,100)
C
C    FROM CHANNEL 4
C
      WRITE(5,1400) VI
      WRITE(5,1401) TP
      WRITE(5,1402) E
      WRITE(5,1403) R
      WRITE(5,1404) TH
      WRITE(5,1405) WO
      WRITE(5,1406) PR
      WRITE(5,1407) RT
      WRITE(5,1408) THETA
      WRITE(5,1409) XI
      WRITE(5,1514) HMDAI0
      WRITE(5,1415) F1
      WRITE(5,1416) F2
      WRITE(5,1417) F3
```



```
      WRITE(5,1418) F4
      WRITE(5,1419) NX
      WRITE(5,1519) NX1
      WRITE(5,1420) I1
      WRITE(5,1421) NST
      WRITE(5,1422) I2
      WRITE(5,1522) I3
      WRITE(5,1424) DTOL
      WRITE(5,1425) PTOL
      WRITE(5,1426) FPTOL
      WRITE(5,1526) FRTOL
      WRITE(5,1626) TTOL
      WRITE(5,1726) NT
      WRITE(5,1826) MTP
      WRITE(5,1926) NPX
      WRITE(5,2026) CPUL
      WRITE(5,1530) UM0
      WRITE(5,1630) XFACT
      WRITE(5,1730) HFACT
      WRITE(5,1830) FFACT
      WRITE(5,1431) IPT
      WRITE(5,1531) MAGN
C
      WRITE(5,1432)
      WRITE(5,1433)
      WRITE(5,1434)
      WRITE(5,1435)
      WRITE(5,1436)
      WRITE(5,1437)
      WRITE(5,99)
      WRITE(5,101)
      DO 1001 I=1,NF
      TF(I)=TM(I)+TP
      FPI(I)=FE(I)/WO
 1001 CONTINUE
      WRITE(5,99)
      WRITE(5,114)
      DO 1002 I=1,NF
      WRITE(5,115) TM(I),TF(I),FE(I),FPI(I),I
 1002 CONTINUE
C
C    FROM CHANNEL 2
C
      WRITE(5,2472)
      WRITE(5,2473)
      DO 1003 I=1,NH
      WRITE(5,2471) TO(I),XB(I),PB(I),HMCOL(I),HB(I),I
 1003 CONTINUE
C
C    FROM CHANNEL 3
C
      WRITE(5,2477)
      WRITE(5,2478)
      DO 1004 I=1,NTP
      IMI=I-1
```

F28

```
      WRITE(5,2475) MST(I),INI
 1000 CONTINUE
      WRITE(5,995)
      WRITE(5,99)
      WRITE(5,101)
      WRITE(5,117)
      WRITE(5,101)
C-----------------------------------------
C           INITIAL
C-----------------------------------------
      CALL PAPER(1)
      CALL CTRFNT(1)
      IPTS=IPT
      HPT1=HST(NTP)
      DHMT1=0.D0
      CPU1=0.D0
      NF4=NF+4
      NH4=NH+4
      LWRK=6*NF+16
      LWR=6*NH+16
      CALL E01BAF(NF,TF,FPI,FKI,FCI,NF4,FW,LWRK,0)
      CALL E01BAF(NH,TC,XB,XEK,XEC,NH4,AW,LWR,0)
      CALL E01BAF(NH,TO,PB,PKI,PCI,NH4,AW,LWR,0)
      CALL E01BAF(NH,TO,HMCCL,HMK,HMC,NH4,AW,LWR,0)
      CALL E01BAF(NH,TO,HE,HKI,HCI,NH4,AW,LWR,0)
      NHALF=1
      ET=0.D0
      FRD=-1.D0
      NSTIN=NST
      NXIN=NX
      DT=TP/NT
      TTOL1=TTOL*.1D0
C======================================================================
C
C         T I M E   C Y C L E   L O O P   -   S T A R T
C
C======================================================================
 7550 FORMAT(/' ',6X,'TIME',9X,'MIN FILM TH',4X,'% TRUNC ERR',7X,
     *       'ENT VEL',9X,'SQ VEL',9X,'LOAD PER UW',6X,'FRIC COEFF'//)
 7551 FORMAT(' ',1X,7(D14.7,2X),I4)
 9922 FORMAT(//' ')
 9880 CONTINUE
      KT1=NT/NPX
      KMM=NT/MTP
      IF(NHALF.EQ.2) WRITE(5,101)
      IF(NHALF.EQ.2) GOTO 3060
      IF(NHALF.EQ.1) WRITE(5,9922)
      HMD44=HMD4
      HMD33=HMD3
      HMD22=HMD2
      HMD11=HMD1
      HMT11=HMT1
 3060 CONTINUE
      T0=0.D0
      UM=U(T0)
```



```
      IF(UM.LT.UM0) UM=UM0
      UMS(1)=UM
      CALL E02BBF(NF4,FKI,FCI,T0,FP,0)
      FPS(1)=FP
      ETS(1)=0.D0
      FRST(1)=FRC
      H(1)=HMT1
      HMDS(1)=HMD1
      IT=0
      IF(NHALF.NE.2) WRITE(5,7550)
      INM=(IT/KMM)*KMM
      IF(NHALF.NE.2) WRITE(5,7551) T0,HMT1,ET,UM,HMD1,FP,FRD,IT
C     ===============
      DO 9876 IT=1,NT
C     ===============
      TC=IT*DT
      IF(IT.EQ.MAGN) IPT=1
C
C======================================================================
C
C-----------------------------------------
C           PREP
C-----------------------------------------
  200 FORMAT(' TIME =',D14.7,4X,'ENT VEL =',D14.7,4X,'FP =',D14.7//)
  201 FORMAT(' **** TIME STEP ITERATION *****'/)
  202 FORMAT(' **** PROFILE ITERATION ****'/)
      UM=U(TC)
      IF(UM.LT.UM0) UM=UM0
      CALL E02BBF(NF4,FKI,FCI,TC,FP,0)
      IF(IPT.EQ.0) GOTO 7810
      WRITE(5,99)
      WRITE(5,200) TC,UM,FP
 7810 CONTINUE
      ICOUNT=2
      KL1=0
      KL3=0
      HMDAI=DABS(HMD1)*F3
      IF(HMD1.EQ.0.D0) HMDAI=HMDAI0
      IF(IPT.EQ.0) GOTO 1697
      WRITE(5,101)
      WRITE(5,202)
      WRITE(5,101)
 1697 CONTINUE
C
C   FINDING STEADY STATE PROFILE
C
      CALL SURF
C
      XE=XEF
      XA=XE*F4
      PT=PTCL*PM
      IF(IPT.EQ.0.) GOTO 1992
      WRITE(5,101)
      WRITE(5,201)
      WRITE(3,101)
```

```
 1092 CONTINUE
C------------------------------------
C           PRESSURE
C------------------------------------
 118  FORMAT(' DMP/DT =',D14.7,3X,'PXI =',D10.3,3X,'( EE =',
     +        D10.3,' % )',I8)
 1118 FORMAT(' --- HM =',D14.7,I8)
C
C     SOLVING FOR HM USING A 4TH ORDER ADAMS METHOD - PMECDE MODE
C
C
C     PREDICTOR
C
       HMTP=HMT1+(DT/24.D0)*(55.D0*HMD1-59.D0*HMD2+37.D0*HMD3-9.D0*HMD4)
C
C     MODIFIER TO PREDICTOR
C
       HMTPM=HMTP-(251.D0/270.D0)*DHMT1
C
       HMD=HMD1
  84   CONTINUE
       HMT=HMTPM
       JCOUNT=2
       HMT0=0.D0
       IADAM=0
       KL4=0
 8444  CONTINUE
  86   CONTINUE
       KL4=KL4+1
       IF(IPT.EQ.1) WRITE(5,1118) HMT,KL4
       KL2=0
C
C     EVALUATOR - START ::::::::
C
C
       HMDA=HMDAI
   8   CONTINUE
C
C     SOLVING PRESSURE DISTRIBUTION FOR TRIAL SQ VEL USING D01GAF
C
       DX=(XI-XE)/NX
       DX1=DX/NX1
       NS=NCAV
       NXP1=NX1+1
C
C     (1.) SUB-DIVIDED FIRST STEP
C
       DO 5501 I=1,NXP1
       XC=XE+(I-1)*DX1
       FXT=H0+XC**2/(2.D0*R)-HM
       IF(XC.LT.XEF) CALL INTP(XC,FXT)
       IF(I.EQ.1) FXE=FXT
       DPS1(I)=12.D0*VI*(UM*(FXT-FXE)+HMD*(XC-XE))/(HMT+FXT)**3
       XS1(I)=XC
 5501  CONTINUE
```

FILE: TCA FORTRAN A LEEDS UNIVERSITY VM/BSE 6.16

```
       CALL D01GAF(XS1,DPS1,NXP1,PC1,EE1,0)
       KL3=KL3+1
       NS=NCAV
       XEE=XE+DX
C
C     (2.) REMAINDER OF CONTACT ZONE
C
       DO 10 I=1,NX
       XC=XEE+(I-1)*DX
       FXT=H0+XC**2/(2.D0*R)-HM
       IF(XC.LT.XEF) CALL INTP(XC,FXT)
       DPS(I)=12.D0*VI*(UM*(FXT-FXE)+HMD*(XC-XE))/(HMT+FXT)**3
       XS(I)=XC
  10   CONTINUE
       CALL D01GAF(XS,DPS,NX,PC,EE2,0)
       KL3=KL3+1
       PC=PC+PC1
       EE=DABS((EE1+EE2)/PC)
       KL2=KL2+1
       IF(IPT.EQ.1) WRITE(5,118) HMD,PC,EE,KL2
       IF(PC.LT.0.D0) GOTO 5
       IF(PC.GT.PT) GOTO 6
       GOTO 9
C
C     DETERMINING THE REQUIRED SQUEEZE.VELOCITY USING BISECTION
C
   5   IF(JCOUNT.EQ.0) HMDA=HMDA/2.D0
       JCOUNT=1
       HMD=HMD+HMDA
       GOTO 8
   6   IF(JCOUNT.EQ.1) HMDA=HMDA/2.D0
       JCOUNT=0
       HMD=HMD-HMDA
       GOTO 8
C
C
C     EVALUATOR - FINISH ::::::::
C
   9   CONTINUE
       IF(IADAM.EQ.1) GOTO 1598
C
C     CORRECTOR
C
       HMT=HMT1+(DT/24.D0)*(9.D0*HMD+19.D0*HMD1-5.D0*HMD2+HMD3)
C
C     CONVERGENCE CHECK FOR CORRECTOR
C
       TTOLA=TTOL*.001D0
       DH=DABS((HMT-HMT0)/HMT)
       IF(DH.LE.TTOLA) GOTO 9090
       HMT0=HMT
       GOTO 8444
 9090  CONTINUE
       DHMT=HMT-HMTP
       ET=100.D0*19.D0*DABS(DHMT)/(270.D0*HMT)
```

```
      IADAM=1
      GOTO 96
 1590 CONTINUE
C-----------------------------------
C         LOAD
C-----------------------------------
 120  FORMAT(' .........CALCULATED FP =',D14.7,3X,'FCR XE =',D14.7,
     *       3X,'( EE =',D10.3,' % )',I5)
 119  FORMAT(' .........SPECIFIED FP =',D14.7)
      PS(1)=0.D0
      XSR(1)=XE
      JL=1
      DO 1010 I=1,NX
      ICC=(I/4)*4
      IF(ICC.NE.I) GOTO 1010
      JL=JL+1
      CALL D01GAF(XS,DPS,I,PC,EE,0)
      PC=PC+PC1
      KL3=KL3+1
      XSR(JL)=XS(I)
      PS(JL)=PC
 1010 CONTINUE
C
C     SOLVING LOAD CAPACITY FOR TRIAL XE USING D01GAF
C
      CALL D01GAF(XSR,PS,JL,FPC,EE,0)
      KL1=KL1+1
      KL3=KL3+1
      FPC=-FPC
      EE=100.D0*DABS(EE/FPC)
      IF(IPT.EQ.0) GOTO 1500
      WRITE(5,120) FPC,XE,EE,KL1
      WRITE(5,119) FP
 1500 CONTINUE
      DIFF=DABS(FP-FPC)/FP
      IF(DIFF.LE.FPTOL) GOTO 81
      IF(FP.GT.FPC) GOTO 82
      IF(FP.LT.FPC) GOTO 83
C
C     DETERMINING THE REQUIRED XE USING BISECTION
C
 82   IF(ICOUNT.EQ.1) XA=XA/2.D0
      ICOUNT=0
      XE=XE+XA
      GOTO 84
 83   IF(ICOUNT.EQ.0) XA=XA/2.D0
      ICOUNT=1
      XE=XE-XA
      GOTO 84
 81   CONTINUE
C-------------------------
C         FRICTION
C-------------------------
      NS=NCAV
      DO 7929 I=1,NX
```

FILE: TCA FORTRAN A LEEDS UNIVERSITY VM/BSE 6.16

```
      J=NX-I+1
      K=J+1
      DPS(K)=DPS(J)
      XS(K)=XS(J)
 7929 CONTINUE
      NXP=NX+1
      XS(1)=XE
      DPS(1)=0.D0
      DO 7926 I=1,NXP
      XC=XS(I)
      FXT=H0+XC**2/(2.D0*R)-HM
      IF(XC.LT.XEF) CALL INTP(XC,FXT)
      HSC=HMT+FXT
      IF(I.EQ.1) HXE=HSC
      FX1(I)=2.D0*VI*UM/HSC-HSC*DPS(I)/2.D0
 7926 CONTINUE
      DXF=DX
 8278 CONTINUE
      NBB=(XE+XI)/DXF
      XXED=XE-DXF*NBB
      NS=NCAV
      NBP=NBB+1
      IF(NBP.GE.4) GOTO 8277
      DXF=DXF/2.D0
      GOTO 8278
 8277 CONTINUE
      DO 7927 I=1,NBP
      XC=XXED+(I-1)*DXF
      FXT=H0+XC**2/(2.D0*R)-HM
      IF(XC.LT.XEF) CALL INTP(XC,FXT)
      HSC=FXT+HMT
      FX2(I)=2.D0*VI*UM*HXE/(HSC**2)
      X2(I)=XC
 7927 CONTINUE
      CALL D01GAF(XS,FX1,NXP,FR1,ER1,0)
      CALL D01GAF(X2,FX2,NBP,FR2,ER2,0)
      FR1=-FR1
      FR2=-FR2
      FRCON=FR1/FPC
      FRCAV=FR2/FPC
      FR=FRCON+FRCAV
C-------------------------
C         RELIABILITY
C-------------------------
 662  FORMAT(' NO. OF STEPS DOUBLED FOR PRESS. RELIABILITY CHECK'/)
 721  FORMAT(' NO. OF STEPS DOUBLED FOR FP RELIABILITY CHECK'/)
 948  FORMAT(' NO. OF STEPS DOUBLED FOR FR RELIABILITY CHECK'/)
 941  FORMAT(' ',7X,'POLD',12X,'PNEW',13X,'X',12X,'A.DIFF.'/)
 942  FORMAT(' ',1X,4(D14.7,2X)/)
 943  FORMAT(' ',6X,'FPCLC',11X,'FPNEW',10X,'R.DIFF.'/)
 751  FORMAT(' ',6X,'FRCLC',11X,'FRNEW',10X,'R.DIFF.'/)
 944  FORMAT(' ',1X,3(D14.7,2X)/)
 951  FORMAT(' ABSOLUTE INLET PRESSURE TOLERANCE ADJUSTED'/)
 952  FORMAT(' ',7X,'PTOLD',11X,'PTNEW',11X,'R.DIFF.'/)
 953  FORMAT(' ',1X,3(D14.7,2X)/)
```

```
C
C   STORE CURRENT PRESSURE VALUES
C
      DO 4567 I=1,JL
      PPD(I)=PS(I)
 4567 CONTINUE
C
C   DOUBLING NUMBER OF STEPS
C
      NX=NX*2
C
C   SOLVING PRESSURE DISTRIBUTION USING D01GAF
C
      DX=(XI-XE)/NX
      DX1=DX/NX1
      NXP1=NX1+1
      NS=NCAV
C
C   (1.) SUB-DIVIDED FIRST STEP
C
      DO 7000 I=1,NXP1
      XC=XE+(I-1)*DX1
      FXT=H0+XC**2/(2.D0*R)-HM
      IF(XC.LT.XEF) CALL INTP(XC,FXT)
      DPS1(I)=12.D0*VI*(UM*(FXT-FXE)+HPD*(XC-XE))/(HMT+FXT)**3
      XS1(I)=XC
 7000 CONTINUE
      CALL D01GAF(XS1,DPS1,NXP1,PC1,EE,0)
      KL3=KL3+1
      NS=NCAV
      XEE=XE+DX
C
C   (2.) REMAINDER OF CONTACT ZONE
C
      DO 7061 I=1,NX
      XC=XEE+(I-1)*DX
      FXT=H0+XC**2/(2.D0*R)-HM
      IF(XC.LT.XEF) CALL INTP(XC,FXT)
      DPS(I)=12.D0*VI*(UM*(FXT-FXE)+HPD*(XC-XE))/(HMT+FXT)**3
      XS(I)=XC
 7061 CONTINUE
      PX=0.D0
      PS(1)=0.D0
      XSR(1)=XE
      JL=1
      DO 7001 I=1,NX
      ICC=(I/4)*4
      IF(ICC.NE.I) GOTO 7001
      JL=JL+1
      CALL D01GAF(XS,DPS,I,PC,EE,0)
      PC=PC+PC1
      KL3=KL3+1
      XSR(JL)=XS(I)
      PS(JL)=PC
      IF(PC.GT.PX) PX=PC
```

FILE: TCA   FORTRAN A   LEEDS UNIVERSITY VM/ESE 6.16

```
 7001 CONTINUE
C
C   GLOBAL PRESSURE RELIABILITY CHECK
C
C     SPTOL=PT*.1D0
C     IF(UM.EQ.UP0) SPTOL=PT
      SPTOL=PT
      J=1
      JLM=JL-1
      DO 7660 I=1,JLM
      K=I+1
      XC=XSR(K)
      PC=PS(K)
      IC=(I/2)*2
      IF(IC.NE.I) GOTO 7660
      J=J+1
      DPR=DABS(PC-PPD(J))
      IF(DPR.GT.SPTOL) GOTO 77
 7660 CONTINUE
      GOTO 78
   77 CONTINUE
      IF(IPT.EQ.0) GOTO 7651
      WRITE(5,100)
      WRITE(5,99)
      WRITE(5,662)
      WRITE(5,941)
      WRITE(5,942) PPD(J),PC,XC,DPR
      WRITE(5,100)
 7651 CONTINUE
      GOTO 8
   78 CONTINUE
C
C   ABSOLUTE TOLERANCE FOR INLET PRESSURE CHECK
C
      PTN=PX*PTOL
      DPT=DABS((PTN-PT)/PTN)
      IF(DPT.GT.PTOL) GOTO 723
      GOTO 722
  723 CONTINUE
      IF(IPT.EQ.0) GOTO 7652
      WRITE(5,100)
      WRITE(5,951)
      WRITE(5,932)
      WRITE(5,953) PT,PTN,DPT
      WRITE(5,100)
 7652 CONTINUE
      NX=NX/2
      PT=PTN
      GOTO 8
  722 CONTINUE
C
C   SOLVING LOAD CAPACITY USING D01GAF
C
C     SFTOL=FPTOL*.1D0
C     IF(UM.EQ.UP0) SFTOL=FPTOL
```

```
      SFTOL=FPTOL
      CALL D01GAF(XSR,PS,JL,FPCD,ERROR,0)
      KL1=KL1+1
      KL3=KL3+1
      FPCD=-FPCD
C
C   FP RELIABILITY CHECK
C
      DFP=DABS((FPCD-FPC)/FPCD)
      IF(DFP.GT.SFTOL) GOTO 719
      GOTO 720
 719  CONTINUE
      IF(IPT.EQ.0) GOTO 7653
      WRITE(5,100)
      WRITE(5,99)
      WRITE(5,721)
      WRITE(5,943)
      WRITE(5,944) FPC,FPCD,DFP
      WRITE(5,100)
 7653 CONTINUE
      GOTO 8
 720  CONTINUE
C
C   FR RELIABILITY CHECK
C
      MS=NCAV
      DO 7928 I=1,NX
      J=NX-I+1
      K=J+1
      DPS(K)=DPS(J)
      XS(K)=XS(J)
 7928 CONTINUE
      NXP=NX+1
      XS(1)=XE
      DPS(1)=0.D0
      DO 8926 I=1,NXP
      XC=XS(I)
      FXT=H0*XC**2/(2.D0*R)-HM
      IF(XC.LT.XEF) CALL INTP(XC,FXT)
      HSC=HMT+FXT
      IF(I.EQ.1) HXE=HSC
      FX1(I)=2.D0*VI*UP/HSC-HSC*DPS(I)/2.D0
 8926 CONTINUE
      DXF=DX
 8281 CONTINUE
      NBB=(XE+XI)/DXF
      XXED=XE-DXF*NBB
      MS=NCAV
      NBP=NBB+1
      IF(NBP.GE.4) GOTO 8282
      DXF=DXF/2.D0
      GOTO 8281
 8282 CONTINUE
      DO 8927 I=1,NBP
      XC=XXED+(I-1)*DXF
```



```
      FXT=H0*XC**2/(2.D0*R)-HM
      IF(XC.LT.XEF) CALL INTP(XC,FXT)
      HSC=FXT+HMT
      FX2(I)=2.D0*VI*UP*HXE/(HSC**2)
      X2(I)=XC
 8927 CONTINUE
      CALL D01GAF(XS,FX1,NXP,FR1,ER1,0)
      CALL D01GAF(X2,FX2,NBP,FR2,ER2,0)
      FR1=-FR1
      FR2=-FR2
      FRCON=FR1/FPCD
      FRCAV=FR2/FPCD
      FRD=FRCON+FRCAV
      DFR=DABS((FRD-FR)/FRD)
      IF(DFR.GT.FRTOL) GOTO 329
      GOTO 796
 329  CONTINUE
      IF(IPT.EQ.0) GOTO 6323
      WRITE(5,100)
      WRITE(5,99)
      WRITE(5,948)
      WRITE(5,751)
      WRITE(5,944) FR,FRD,DFR
      WRITE(5,100)
 6323 CONTINUE
      GOTO 9
 796  CONTINUE
C---------------------------------------
C            OUTPUT
C---------------------------------------
 9990 FORMAT(' RELIABILITY CHECKS SATISFY SPECIFIED TOLERANCES'/)
 121  FORMAT(' FINAL NO. OF STEPS FOR PRESSURE INTEGRATIONS =',I8/)
 1277 FORMAT(' FINAL NO. OF STEPS FOR LOAD INTEGRATION =',I8/)
 985  FORMAT(' TOTAL NO. OF CALLS TO D01GAF IN TIME ITERATIONS =',I8/)
 122  FORMAT(' ',3(D14.7,2X),I8,2X,I8)
 123  FORMAT(' ',7X,'X',15X,'P',15X,'H'/)
 1233 FORMAT(/' STEP NO. =',I6/)
 1244 FORMAT(' TIME (TC) =',D14.7/)
 124  FORMAT(' MINIMUM FILM THICKNESS (HMT)  =',D14.7)
 125  FORMAT(' SQUEEZE VELOCITY (HMD) =',D14.7/)
 127  FORMAT(' MODIFIER TERM (DHMT) =',D14.7/)
 128  FORMAT(' CURRENT TIME STEP VALUES'//)
 129  FORMAT(' ESTIMATED % TRUNC. ERROR IN HMT =',D10.3/)
 159  FORMAT(' FRICTION COEFFICIENT (FRD) =',D14.7)
 875  FORMAT(/' CAVITATION BOUNDARY (XE) =',D14.7)
 976  FORMAT(' SS CAVITATION BD    (XEF) =',D14.7/)
      IF((NHALF.NE.2).AND.(IPT.EQ.0)) GOTO 9890
      ICCT=(IT/KT1)*KT1
      IF(ICCT.NE.IT) GOTO 9890
      IF(IPT.EQ.0) GOTO 1698
      WRITE(5,101)
      WRITE(5,9990)
      WRITE(5,121) NX
      WRITE(5,1277) JL
      WRITE(5,985) KL3
```

```
      WRITE(5,101)
      WRITE(5,99)
 1690 CONTINUE
      WRITE(5,123) IT
      WRITE(5,124) TC
      WRITE(5,100)
C
C     GENERATING PROFILE
C
      NS=NCAV
      DO 1102 I=1,JL
      XC=XSR(I)
      FXT=H0+XC**2/(2.D0*R)-HM
      IF(XC.LT.XEF) CALL INTP(XC,FXT)
      HS(I)=HMT+FXT
 1102 CONTINUE
C
C     CONSTRUCTING THE EXIT PROFILE
C
      DX=4.D0*DX
      NB=(XE+XI)/DX
      XXED=XE-DX*NB
      XIP=-1.D0*XI
      DO 40 I=1,JL
      K=JL-I+1
      J=K+NB
      XSR(J)=XSR(K)
      PS(J)=PS(K)
      HS(J)=HS(K)
 40   CONTINUE
      NS=NCAV
      DO 401 I=1,NB
      XC=XXED+(I-1)*DX
      XSR(I)=XC
      PS(I)=0.D0
      FXT=H0+XSR(I)**2/(2.D0*R)-HM
      IF(XC.LT.XEF) CALL INTP(XC,FXT)
      HS(I)=FXT+HMT
 401  CONTINUE
      JL=JL+NB
      NCAV=NB+1
      IF(XXED.EQ.XIP) GOTO 9928
      DO 402 I=1,JL
      K=JL+1-I
      J=K+1
      XSR(J)=XSR(K)
      PS(J)=PS(K)
      HS(J)=HS(K)
 402  CONTINUE
      XSR(1)=XIP
      PS(1)=0.D0
      HS(1)=H0+XIP**2/(2.D0*R)-HM+HMT
      JL=JL+1
      NCAV=NCAV+1
 9928 CONTINUE
```



```
C
C     PRINTING DATA AT SPECIFIED SPACING
C
      WRITE(5,123)
      N3=JL/I1
      JMD=0
      DO 2222 I=1,JL
      ICC=(I/N3)*N3
      IF((ICC.NE.I).AND.(I.NE.JL).AND.(I.NE.1).AND.(I.NE.NCAV))
     * GOTO 2222
      JMD=JMD+1
      WRITE(5,122) XSR(I),PS(I),HS(I),I,JMD
 2222 CONTINUE
      WRITE(5,99)
      WRITE(5,101)
C
C     PRINTING CURRENT TIME STEP VALUES
C
      WRITE(5,120)
      WRITE(5,125) HMD
      WRITE(5,124) HMT
      WRITE(5,125) ET
      WRITE(5,155) FRD
      WRITE(5,127) DHMT
      WRITE(5,875) XE
      WRITE(5,876) XEF
      WRITE(5,101)
C
C     CONDITIONING FOR GRAPHICS
C
      KK1=0
      N1=JL/I3
C***
C     N1=1
      IF(IT.EQ.0) N1=1
      NNP=0
      HTL=HFACT*.5
      DO 4000 I=1,JL
      ICC=(I/N1)*N1
      IF((ICC.NE.I).AND.(I.NE.JL).AND.(I.NE.NCAV)
     *.AND.(I.NE.1)) GOTO 4000
      NNP=NNP+1
      XC=XSR(I)
      XX(NNP)=XC
      PP(NNP)=PS(I)
      HX=HS(I)
      IF(HX.GE.HTL) GOTO 4000
      KK1=KK1+1
      XX1(KK1)=XC
      HH(KK1)=HX
 4000 CONTINUE
      DO 4999 I=1,NNP
 4999 CONTINUE
      PMMM=PM*1.1D0
      XXE=-1.D0*XFACT
```

```
C
C   PLOTTING USING GHOST80
C
      CALL BLKPEN
      CALL PSPACE(0.,1.,0.,1.)
      CALL MAP(0.,1.,0.,1.)
      CALL PLOTCS(.05,.27,'H',1)
      CALL PLOTCS(.47,.01,'X',1)
      CALL PLOTCS(.05,.87,'P',1)
      CALL PLOTCS(.47,.50,'X',1)
      CALL PLOTCS(.23,.47,'TIME =',7)
      CALL TYPENE(TC,4)
      CALL PSPACE(.07,.57,.05,.4)
      CALL MAP(XFACT,XRE,0.,HFACT)
      CALL BORDER
      CALL AXES
      CALL GRNPEN
      CALL CURVE(XX1,HH,1,KK1)
      XJ1=XX1(1)
      YJ1=HFACT*.990
      CALL POSITN(XJ1,YJ1)
      XJ2=XJ1
      YJ2=HH(1)
      CALL JOIN(XJ2,YJ2)
      XJ3=XX1(KK1)
      YJ3=HH(KK1)
      CALL POSITN(XJ3,YJ3)
      XJ4=XJ3
      YJ4=YJ1
      CALL JOIN(XJ4,YJ4)
      CALL BLKPEN
      CALL PSPACE(.07,.57,.58,.93)
      CALL MAP(XFACT,XRE,0.,PMMM)
      CALL BORDER
      CALL AXES
      CALL GRNPEN
      CALL CURVE(XX,PF,1,NNP)
      CALL FRAME
C=======================================================================
C
C        T I M E   C Y C L E   L O O P   -   F I N I S H
C
C=======================================================================
 9890 CONTINUE
      IMM=(IT/KMM)*KMM
      IF(NHALF.EQ.2) GOTO 6712
      IF((IMM.NE.IT).AND.(IPT.EQ.0)) GOTO 6712
      IF(IPT.EQ.1) WRITE(5,99)
      WRITE(5,7551) TC,HMT,ET,UM,FPD,FF,FRD,IT
      IF(IPT.EQ.1) WRITE(5,99)
 6712 CONTINUE
      HMD4=HMD3
      HMD3=HMD2
      HMD2=HMD1
      HMD1=HMD
```



```
      HMT1=HMT
      DHMT1=DHMT
      NST=NSTIN
      NX=NXIN
      L=IT+1
      TCS(L)=TC
      UMS(L)=UM
      FPS(L)=FP
      H(L)=HPT
      ETS(L)=ET
      HMDS(L)=HMD
      IF(UM.EQ.UP0) FRD=0.D0
      FRST(L)=FRD
      IPT=IPTS
      CPU6=CPUTIM(XDU)
      WRITE(6,*) IT,CPU6
C=============
 9876 CONTINUE
C=============
C
C=======================================================================
C
C
C-----------------------------------
C          STEADY STATE
C-----------------------------------
 7553 FORMAT(//' ********* MAXIMUM RELATIVE DIFFERENCE =',D14.7)
 4553 FORMAT('            NUMBER OF STEPS =',I6)
 3241 FORMAT(/' ****** CPU =',D11.3/)
      IF(NHALF.EQ.2) GOTO 9881
      NTP=NT+1
      DH=0.D0
      DO 9879 IT=1,NTP
      DH1=DABS((H(IT)-HST(IT))/H(IT))
      IF(DH1.GT.DH) DH=DH1
 9879 CONTINUE
      CPU=CPUTIM(XDU)
      DCPU=CPU-CPU1
      PCPU=CPU+DCPU
      CPU1=CPU
      WRITE(5,7553) DH
      WRITE(6,7553) DH
      WRITE(5,999)
      WRITE(5,4553) NT
      WRITE(5,3241) CPU
      IF(DH.LE.TTOL1) NHALF=2
      IF((DH.LE.TTOL1).AND.(PCPU.GT.CPUL)) GOTO 8988
      DO 9877 IT=1,NTP
      HST(IT)=H(IT)
 9877 CONTINUE
      IF(PCPU.GT.CPUL) GOTO 8888
      IF(DH.GT.TTOL1) GOTO 9890
C-----------------------------------
C          RELIABILITY
C-----------------------------------
 9221 FORMAT(/' STEP SIZE IS HALVED'/)
```

F35

```
 6291 FORMAT(//' * * *   D O E S   N O T   C O N V E R G E   * * *'//)
 6292 FORMAT(//' * * *   C O N V E R G E S * * *'//)
      WRITE(5,9221)
      NHALF=2
C
C   INTERPOLATION OF SQ VEL FOR TIME STEP SIZE HALVING
C
      TR(1)=TP-3.D0*DT
      TR(2)=TP-2.D0*DT
      TR(3)=TP-DT
      TR(4)=TP
      HR(1)=HMD44
      HR(2)=HMD33
      HR(3)=HMD22
      HR(4)=HMD11
      CALL E01BAF(4,TR,HR,HRK,HRC,8,HRW,40,0)
C
C   TIME STEP SIZE HALVING
C
      NT=2*NT
      DT=TP/NT
      TR4=TP-3.D0*DT
      TR2=TP-DT
      CALL E02BBF(8,HRK,HRC,TR4,HMD4,0)
      CALL E02BBF(8,HRK,HRC,TR2,HMD2,0)
      HMD3=HMD22
      HMD1=HMD11
      HMT1=HMT11
      GOTO 9880
 9881 CONTINUE
C
C   MIN FILM TH RELIABILITY CHECK
C
      NTP1=NT+1
      J=0
      DM=0.D0
      DO 9882 IT=1,NTP1
      ICT=(IT/2)*2
      IF(ICT.NE.IT) GOTO 9882
      J=J+1
      DM1=DABS((H(IT)-HST(J))/H(IT))
      IF(DM1.GT.DM) DM=DM1
 9882 CONTINUE
      CPU=CPUTIM(XCU)
      WRITE(5,7553) DM
      WRITE(5,999)
      WRITE(5,4553) NT
      WRITE(5,3241) CPU
      IF(DM.LE.TTCL) WRITE(5,6292)
      IF(DM.GT.TTCL) WRITE(5,6291)
      IF(DM.GT.TTCL) GOTO 8888
C-----------------------------------
C         OUTPUT
C-----------------------------------
 5910 FORMAT(//' ',6X,'TIME',6X,'MIN FILM TH',6X,'FRICTION'//)
```



```
 5911 FORMAT(' ',1X,3(D14.7,2X))
C
C   PRINTING FINAL CYCLE
C
      ETS(1)=0.D0
      WRITE(5,7558)
      DO 590 I=1,NTP1
      IM=I-1
      IMM=(IM/KMP)*KMP
      IF((IMM.NE.IM).AND.(I.NE.1)) GOTO 590
      WRITE(5,7551) TCS(I),H(I),ETS(I),UMS(I),HMDS(I),FPS(I),FRST(I),IM
  590 CONTINUE
C
C   FINAL GRAPHICS
C
      CALL BLKPEN
      TP1=TP
      DO 6800 I=1,NTP1
      TT(I)=TCS(I)
      HMM(I)=H(I)
      FRR(I)=FRST(I)
      UU(I)=UMS(I)
      FPP(I)=FPS(I)
 6800 CONTINUE
      UMAX=0.
      FPMAX=0.
      DO 6801 I=1,NTP1
      IF(FPP(I).GT.FPMAX) FPMAX=FPP(I)
      IF(UU(I).GT.UMAX) UMAX=UU(I)
 6801 CONTINUE
      FPMAX=FPMAX*1.1
      UMAX=UMAX*1.1
C
C   PLOTTING USING GHOST80
C
      CALL BLKPEN
      CALL FRAME
      CALL PSPACE(0.,1.,0.,1.)
      CALL MAP(0.,1.,0.,1.)
      CALL PLOTCS(.01,.37,'H',1)
      CALL PLOTCS(.47,.01,'TIME',4)
      CALL PLOTCS(.01,.97,'F',1)
      CALL PLOTCS(.47,.54,'TIME',4)
      CALL PSPACE(.07,.57,.05,.4)
      CALL MAP(0.,TP1,0.,HFACT)
      CALL BORDER
      CALL AXES
      CALL REDPEN
      CALL CURVEC(TT,HMM,1,NTP1)
      CALL BLKPEN
      CALL PSPACE(.07,.57,.58,.93)
      CALL MAP(0.,TP1,0.,FFACT)
      CALL BORDER
      CALL AXES
      CALL REDPEN
```

```
      CALL CURVE(TT,FRR,1,NTP1)
      CALL FRAME
      CALL BLKPEN
      CALL PSPACE(0.,1.,0.,1.)
      CALL MAP(0.,1.,0.,1.)
      CALL PLOTCS(.01,.37,'U',1)
      CALL PLOTCS(.47,.01,'TIME',4)
      CALL PLOTCS(.005,.37,'FP',2)
      CALL PLOTCS(.47,.54,'TIME',4)
      CALL PSPACE(.07,.57,.05,.4)
      CALL MAP(0.,TP1,0.,UMAX)
      CALL BORDER
      CALL AXES
      CALL REDPEN
      CALL CURVE(TT,UU,1,NTP1)
      CALL BLKPEN
      CALL PSPACE(.07,.57,.58,.93)
      CALL MAP(0.,TP1,0.,FPMAX)
      CALL BORDER
      CALL AXES
      CALL REDPEN
      CALL CURVE(TT,FPP,1,NTP1)
 8888 CONTINUE
C
C   WRITING NEW STARTING VALUES ON CHANNEL 7
C
      DO 8887 I=1,NTP
      WRITE(7,*) HST(I)
 8887 CONTINUE
      IF(NHALF.NE.2) GOTO 8886
      WRITE(7,*) HMD44
      WRITE(7,*) HMD33
      WRITE(7,*) HMD22
      WRITE(7,*) HMD11
      GOTO 8885
 8886 CONTINUE
      WRITE(7,*) HMD4
      WRITE(7,*) HMD3
      WRITE(7,*) HMD2
      WRITE(7,*) HMD1
 8885 CONTINUE
      CALL GREND
      STOP
      END
C-----------------------------------------------------------------------
C
C              S U B R O U T I N E S
C
C-----------------------------------------------------------------------
C-------------------------------------------
C
      SUBROUTINE SURF
C
C-------------------------------------------
      IMPLICIT REAL*8(A-H,O-Z)
```



```
      DIMENSION PCS(1),W2(1,20),PPC(8500)
      COMMON X(50000),FX(50000)
      COMMON HM,FM,F1,F2,DTOL,PTCL,FPTCL
      COMMON VI,UP,H0,R,AM,XE,XI,CX,FP
      COMMON E,PR,TH,HMC,HMT,FXE,XEF,TC
      COMMON TO(64),XB(64),PB(64),HMCAL(64),HB(64),HPK(68),HMC(69)
      COMMON AW(400),XEK(68),XEC(68),PKI(68),PCI(68),HKI(68),HCI(68)
      COMMON NST,JI,NP,IPT,I2,NCAV,MS,NM4
      EXTERNAL FCN,PEDERV,OUTPUT
   99 FORMAT(' ')
  100 FORMAT(' ---------------------------------------------------',
     *       '----------------------------'/)
C-------------------------
C          PREP
C-------------------------
      ICOUNT=2
      KL1=0
      KL3=0
      MMM=0
      CALL E02BBF(NM4,XEK,XEC,TC,XEF,0)
      CALL E02BBF(NM4,PKI,PCI,TC,FP,0)
      CALL E02BBF(NM4,HKI,HCI,TC,H0,0)
      XA=XEF*F2
      AM=(TH/E)*(1.D0-2.D0*(PR**2)/(1.D0-PR))
      PT=PTCL*PM
      DTL=DTOL*PM
C-------------------------
C          PRESSURE
C-------------------------
  118 FORMAT(' H0 =',D14.7,I8)
   84 CONTINUE
      HA=H0*F1
      JCOUNT=2
      KL2=1
    8 CONTINUE
      IF(IPT.EQ.1) WRITE(5,118) H0,KL2
C
C   SOLVING PRESSURE DISTRIBUTION FOR TRIAL H0 USING D02EBF
C
      PCS(1)=0.D0
      XC=XEF
      DX=XI-XEF
      JI=0
      CALL D02EBF(XC,XI,1,PCS,DTL,1,FCN,1,PEDERV,OUTPUT,W2,20,0)
      KL2=KL2+1
      KL3=KL3+1
      PC=PCS(1)
      IF(PC.LT.0.D0) GOTO 5
      IF(PC.GT.PT) GOTO 6
      GOTO 9
C
C   DETERMINING THE REQUIRED H0 USING BISECTION
C
    5 IF(JCOUNT.EQ.0) HA=HA/2.D0
      JCOUNT=1
```

```
      NO=NO-NA
      GOTO 9
    6 IF(JCOUNT.EQ.1) NA=NA/2.D0
      JCOUNT=0
      NO=NO+NA
      GOTO 8
    9 CONTINUE
C-------------------------
C         LOAD
C-------------------------
  120 FORMAT(' ...CALCULATED FP =',D14.7,3X,'FOR XEF =',D14.7,
     *       3X,'( EE =',D10.3,' % )',I8)
  119 FORMAT(' ....SPECIFIED FP =',D14.7)
C
C   SOLVING LOAD CAPACITY FOR TRIAL XEF USING D02EBF AND D01GAF
C
      PCS(1)=0.D0
      XC=XEF
      DX=(XI-XEF)/NST
      JI=0
      CALL D02EBF(XC,XI,1,PCS,DTL,1,FCN,1,PEDERV,OUTPUT,W2,20,0)
      KL3=KL3+1
      NPLUS=NST+1
      CALL D01GAF(X,FX,NPLUS,FPC,EE,0)
      KL1=KL1+1
      FPC=-FPC
      EE=100.D0*DABS(EE/FPC)
      IF(IPT.EQ.0) GOTO 1500
      WRITE(5,120) FPC,XEF,EE,KL1
      WRITE(5,119) FP
 1500 CONTINUE
      DIFF=DABS(FP-FPC)/FP
      IF(DIFF.LE.FPTOL) GOTO 81
      IF(FP.GT.FPC) GOTO 82
      IF(FP.LT.FPC) GOTO 83
C
C   DETERMINING THE REQUIRED XEF USING BISECTION
C
   82 IF(ICOUNT.EQ.1) XA=XA/2.D0
      ICOUNT=0
      XEF=XEF+XA
      GOTO 84
   83 IF(ICOUNT.EQ.0) XA=XA/2.D0
      ICOUNT=1
      XEF=XEF-XA
      GOTO 84
   81 CONTINUE
C-------------------------
C         RELIABILITY
C-------------------------
  662 FORMAT(' DTL DECREASED FOR GLOBAL PRESSURE RELIABILITY CHECK'/)
  721 FORMAT(' NO. OF STEPS DOUBLED FOR FP RELIABILITY CHECK'/)
  941 FORMAT(' ',7X,'POLD',12X,'PNEW',13X,'X',12X,'A.DIFF.'/)
  942 FORMAT(' ',1X,4(D14.7,2X)/)
  943 FORMAT(' ',6X,'FPOLD',11X,'FPNEW',10X,'R.DIFF.'/)
```



```
  944 FORMAT(' ',1X,3(D14.7,2X)/)
  999 FORMAT(' GLOBAL RELIABILITY AND DISCRETE ERROR CHECKED'/)
  998 FORMAT(' CONVERGES TO SPECIFIED TOLERANCES'/)
  951 FORMAT(' ABSOLUTE INLET PRESSURE TOLERANCE ADJUSTED'/)
  952 FORMAT(' ',7X,'PTOLD',11X,'PTNEW',11X,'R.DIFF'/)
  953 FORMAT(' ',1X,3(D14.7,2X)/)
  983 FORMAT(' FINAL DTL =',D14.7/)
  984 FORMAT(' NO. OF STEPS TO SATISFY SPECIFIED TOLERANCES =',I6/)
  985 FORMAT(' INCREASING NUMBER OF STEPS FOR ACCURATE',
     *       ' PROFILE INTERPOLATION'/)
C
C   STORE CURRENT PRESSURE VALUES
C
      PPO(1)=FX(1)
      DO 4567 I=1,NST
      L=I+1
      PPO(L)=FX(L)
 4567 CONTINUE
C
C   DECREASE DTL AND DOUBLE NST
C
      DTL=DTL*.1D0
      NST=2*NST
C
C   SOLVING PRESSURE DISTRIBUTION USING D02EBF
C
      NPLUS=NST+1
      DX=(XI-XEF)/NST
      XC=XEF
      PCS(1)=0.D0
      JI=0
      CALL D02EBF(XC,XI,1,PCS,DTL,1,FCN,1,PEDERV,OUTPUT,W2,20,0)
C
C   GLOBAL PRESSURE RELIABILITY CHECK
C
      PMAX=0.D0
      J=1
      SPTOL=.1D0*PT
      DO 76 I=1,NST
      L=I+1
      XC=X(L)
      PC=FX(L)
      IF(PC.GT.PMAX) PMAX=PC
      IC=(I/2)*2
      IF(IC.NE.I) GOTO 76
      J=J+1
      DPR=DABS(PC-PPO(J))
      IF(DPR.GT.SPTOL) GOTO 77
   76 CONTINUE
      GOTO 79
   77 IF(IPT.EQ.0) GOTO 1501
      WRITE(5,100)
      WRITE(5,662)
      WRITE(5,941)
      WRITE(5,942) PPO(J),PC,XC,DPR
```

F38

```
      WRITE(5,100)
 1501 NST=NST/2
      GOTO 8
 78   CONTINUE
C
C     ABSOLUTE TOLERANCE FOR INLET PRESSURE CHECK
C
      PTN=PPAX*PTCL
      DPT=DABS((PTN-PT)/PTN)
      IF(DPT.GT.PTCL) GOTO 723
      GOTO 722
 723  IF(IPT.EQ.0) GOTO 1503
      WRITE(5,100)
      WRITE(5,951)
      WRITE(5,952)
      WRITE(5,953) PT,PTN,DPT
      WRITE(5,100)
 1503 CONTINUE
      DTL=DTL*10.D0*PTN/PT
      NST=NST/2
      PT=PTN
      GOTO 8
 722  CONTINUE
C
C     SOLVING LOAD CAPACITY USING D01GAF
C
      SFTOL=.1D0*FPTOL
      CALL D01GAF(X,FX,NPLUS,FPCD,ERROR,0)
      FPCD=-FPCD
C
C     FP RELIABILITY CHECK
C
      DFP=DABS((FPCD-FPC)/FPCD)
      IF(DFP.GT.SFTOL) GOTO 719
      GOTO 720
 719  IF(IPT.EQ.0) GOTO 1502
      WRITE(5,100)
      WRITE(5,721)
      WRITE(5,943)
      WRITE(5,944) FPC,FPCD,DFP
      WRITE(5,100)
 1502 DTL=DTL*10.D0
      GOTO 8
 720  CONTINUE
C
C     PRINTING FINAL DTL AND NST TO SATISFY SPECIFIED TOLERANCES
C
      IF(MMM.EQ.1) GOTO 1569
      IF(IPT.EQ.0) GOTO 1509
      WRITE(5,99)
      WRITE(5,100)
      WRITE(5,999)
      WRITE(5,998)
      WRITE(5,983) DTL
      WRITE(5,984) NST
```



```
      WRITE(5,100)
 1509 CONTINUE
 1569 CONTINUE
C
C     INCREASING NST FOR ACCURATE PROFILE INTERPOLATION
C
      IF(MMM.EQ.1) GOTO 9461
      NST=NST*10
      IF(IPT.EQ.0) GOTO 1505
      WRITE(5,100)
      WRITE(5,985)
      WRITE(5,100)
 1505 CONTINUE
      MMM=1
      GOTO 9
 9461 CONTINUE
C
C     GENERATE PROFILE
C
      HMIN=1.D6
      DO 92 I=1,NPLUS
      XC=X(I)
      PC=FX(I)
      FXX=H0+XC**2/(2.D0*R)+AM*PC
      IF(FXX.LT.HMIN) HMIN=FXX
      FX(I)=FXX
 92   CONTINUE
      DO 797 I=1,NPLUS
      FX(I)=FX(I)-HMIN
 797  CONTINUE
C-------------------------
C            OUTPUT
C-------------------------
 600  FORMAT(' ',6X,'X',17X,'FX(I)',/)
 601  FORMAT(' ',2(D14.7,5X),I6)
 986  FORMAT(' FINAL NO. OF STEPS =',I8/)
 1301 FORMAT(' FINAL NO. OF CALLS TO D02EBF =',I8/)
      IF(IPT.EQ.0) GOTO 1507
      WRITE(5,100)
      WRITE(5,986) NST
      WRITE(5,1301) KL3
      WRITE(5,100)
 1507 CONTINUE
      HM=HMIN
      PM=PPAX
      NB=(XEF+XI)/DX
      XXED=XEF-DX*NB
      XIP=-1.D0*XI
      DO 40 I=1,NPLUS
      K=NPLUS-I+1
      J=K+NB
      X(J)=X(K)
      FX(J)=FX(K)
 40   CONTINUE
      DO 401 I=1,NB
```

F39

```
      X(I)=XXED+(I-1)*DX
      FX(I)=H0*X(I)**2/(2.D0*R)-HMIN
 401  CONTINUE
      NPLUS=NPLUS+N0
      NCAV=N0+1
      IF(XXED.EQ.XIP) GOTO 9920
      DO 402 I=1,NPLUS
      K=NPLUS+1-I
      J=K+1
      X(J)=X(K)
      FX(J)=FX(K)
 402  CONTINUE
      X(1)=XIP
      FX(1)=H0*XIP**2/(2.D0*R)-HMIN
      NPLUS=NPLUS+1
      NCAV=NCAV+1
 9920 CONTINUE
      NP=NPLUS
      X(NP)=XI
      N3=NP/I2
      IF(IPT.EQ.0) GOTO 1500
      WRITE(5,99)
      WRITE(5,600)
      DO 45 I=1,NP
      ICC=(I/N3)*N3
      IF((ICC.NE.I).AND.(I.NE.NP).AND.(I.NE.1)
     *.AND.(FX(I).NE.0.D0).AND.(I.NE.NCAV)) GOTO 45
      WRITE(5,601) X(I),FX(I),I
 45   CONTINUE
      WRITE(5,99)
      WRITE(5,100)
 1500 CONTINUE
      RETURN
      END
C----------------------------------------
C
      SUBROUTINE FCN(XC,PCS,F)
C
C----------------------------------------
      IMPLICIT REAL*8(A-H,O-Z)
      COMMON X(50000),FX(50000)
      COMMON HM,PP,F1,F2,CTOL,PTCL,FPTOL
      COMMON VI,LP,H0,R,AM,XE,XI,DX,FP
      COMMON E,PF,TH,HMC,HMT,FXE,XEF,TC
      COMMON TO(64),XB(64),PB(64),HMCCL(64),HB(64),HMK(68),HMC(68)
      COMMON AW(400),XEK(68),XEC(68),PKI(68),PCI(68),HKI(68),HCI(68)
      COMMON NST,JI,NP,IPT,I2,NCAV,MS,NN4
      DIMENSION PCS(1),F(1)
      PC=PCS(1)
      F(1)=(12.D0*VI*UM/(H0+(XC**2)/(2.D0*R)+AM*PC)**3)*((XC**2
     C-XEF**2)/(2.D0*R)+AM*PC)
      RETURN
      END
C----------------------------------------
C
      SUBROUTINE OUTPUT(XSOL,PCS)
C
C----------------------------------------
      IMPLICIT REAL*8(A-H,O-Z)
      COMMON X(50000),FX(50000)
      COMMON HM,FP,F1,F2,CTOL,PTCL,FPTCL
      COMMON VI,LP,H0,R,AM,XE,XI,DX,FP
      COMMON E,PF,TH,HMC,HMT,FXE,XEF,TC
      COMMON TO(64),XB(64),PB(64),HMCCL(64),HB(64),HMK(68),HMC(68)
      COMMON AW(400),XEK(68),XEC(68),PKI(68),PCI(68),HKI(68),HCI(68)
      COMMON NST,JI,NP,IPT,I2,NCAV,MS,NN4
      DIMENSION PCS(1)
      JI=JI+1
      X(JI)=XSOL
      FX(JI)=PCS(1)
      XSOL=XEF+JI*DX
      IF(JI.EQ.NST) XSOL=XI
      RETURN
      END
C----------------------------------------
C
      SUBROUTINE FEDERV(XC,PCS,PW)
C
C----------------------------------------
      IMPLICIT REAL*8(A-H,O-Z)
      COMMON X(50000),FX(50000)
      COMMON HM,FP,F1,F2,CTCL,PTCL,FPTOL
      COMMON VI,LP,H0,R,AM,XE,XI,DX,FP
      COMMON E,PF,TH,HMD,HMT,FXE,XEF,TC
      COMMON TO(64),XB(64),PB(64),HMCCL(64),HB(64),HMK(68),HMC(68)
      COMMON AW(400),XEK(68),XEC(68),PKI(68),PCI(68),HKI(68),HCI(68)
      COMMON NST,JI,NP,IPT,I2,NCAV,MS,NN4
      DIMENSION PW(1,1),PCS(1)
      PC=PCS(1)
      PW(1,1)=12.D0*VI*UM*AM*(H0-XC**2/R+1.5D0*XEF**2/R-2.D0*AM*PC)/
     C((H0+XC**2/(2.D0*R)+AM*PC)**4)
      RETURN
      END
C----------------------------------------
C
      SUBROUTINE INTP(XC,FXT)
C
C----------------------------------------
      IMPLICIT REAL*8(A-H,O-Z)
      COMMON X(50000),FX(50000)
      COMMON HM,FP,F1,F2,CTOL,PTCL,FPTCL
      COMMON VI,LP,H0,R,AM,XE,XI,DX,FP
      COMMON E,PR,TH,HMC,HMT,FXE,XEF,TC
      COMMON TO(64),XB(64),PB(64),HMCOL(64),HB(64),HMK(68),HMC(68)
      COMMON AW(400),XEK(68),XEC(68),PKI(68),PCI(68),HKI(68),HCI(68)
      COMMON NST,JI,NP,IPT,I2,NCAV,MS,NN4
      IF(NCAV.EQ.1) GOTO 3
      DO 1 I=MS,NF
      IF(X(I).LT.XC) GOTO 2
    1 CONTINUE
```

FILE: TCA FORTRAN A LEEDS UNIVERSITY VM/BSE 6.16

```
    2  MS=I-1                                       TCA15410
       XR=X(MS)                                     TCA15420
       XV=X(I)                                      TCA15430
       FXR=FX(MS)                                   TCA15440
       FXV=FX(I)                                    TCA15450
       FXT=FXR+((FXV-FXR)/(XV-XR))*(XC-XR)          TCA15460
       GOTO 4                                       TCA15470
    3  FXT=FX(I)                                    TCA15480
    4  CONTINUE                                     TCA15490
       RETURN                                       TCA15500
       END                                          TCA15510
```

FILE: JTCA EXEC A LEEDS UNIVERSITY VM/BSE 6.16

```
EXEC SETUP FORTRAN LOSF NAGF CCGHCST
FI 2 DISK BANK DATA
FI 3 DISK START DATA
FI 4 DISK XTCA DATA
FI 5 DISK YTCA DATA(RECFM F LRECL 120 BLOCK 120
FI 7 DISK STARTN DATA
LOAD TCA(CLEAR
EXEC PLOTFILE PTCA
SET BLIP *
START
```

INPUT

FILE: BANK DATA A LEEDS UNIVERSITY VM/BSE 6.16

.0	.7380553954090019195E-02	1296979.40715427510
.6829041027870172925E-06	-.9002051675006033215E-04	
.3125000000000000000E-01	.8016396573488895615E-02	1530057.96835484495
.6462453941378402665E-06	-.1063777446839994105E-03	
.6250000000000000000E-01	.8696133458947716165E-02	1796402.40875089052
.6004133529565748305E-06	-.1250738762268055875E-03	
.9375000000000000000E-01	.9376102144641841785E-02	2093125.59496485605
.5464275336344454935E-06	-.1459055200997598535E-03	
.1250000000000000000	.1007560881505602775E-01	2417092.53743135976
.4846774043922163095E-06	-.1688528123755315275E-03	
.1562500000000000000	.1069711571322592665E-01	2724481.87486305879
.4159377310625364335E-06	-.1902474756036124195E-03	
.1875000000000000000	.1130503164152495915E-01	3045095.35707900464
.3349403650943094235E-06	-.2127816683752131175E-03	
.2187500000000000000	.1188415146008550832E-01	3362690.77915116563
.2327047558013048185E-06	-.2351276048272556055E-03	
.2500000000000000000	.1240676553669004765E-01	3664947626204662095
.5132710321136764555E-07	-.2564089565201730465E-03	
.2812500000000000000	.1310019888565246415E-01	4086075.57267739787
.2213882794445573295E-06	-.2857774617653728195E-03	
.3125000000000000000	.1379110741146449695E-01	4521078.05304966099
.3025642636296069985E-06	-.3161526901585000365E-03	
.3437500000000000000	.1428607025779466395E-01	4659327.27965151402
.3592197803754141585E-06	-.3357517913837572535E-03	
.3750000000000000000	.1448630918050017315E-01	4996502.52940852451
.4015542849515209155E-06	-.3453054512866494935E-03	
.4062500000000000000	.1433916792509412885E-01	4895516.75624421914
.4379313327116614188E-06	-.3421956107256523415E-03	
.4375000000000000000	.1400232421326352405E-01	4668215.00827803253
.4673814460811839505E-06	-.3262514724062282255E-03	
.4687500000000000000	.1287208454352043335E-01	3545013.06780882459
.5031463144633225405E-06	-.2755869830170603585E-03	
.5000000000000000000	.1156878090661982025E-01	3186586.82733419188
.5370492732279614115E-06	-.2224589257761144645E-03	
.5312500000000000000	.1066984251732432823E-01	2710627.71439871332
.5549278780359130235E-06	-.1991215905955441035E-03	
.5625000000000000000	.9722323546647494635E-02	2251024.06298423000
.5652966737176409705E-06	-.1569373079131470355E-03	
.5937500000000000000	.7782093429397256005E-02	1441923.79688258213
.6033498407511002355E-06	-.1002560291269806775E-03	
.6250000000000000000	.6559329413780330345E-02	1024399.45773702438
.6105277248585809485E-06	-.7102086811016008605E-04	
.6562500000000000000	.5905649535253493885E-02	830396.275292502904
.5722366351807716315E-06	-.5748332111696109065E-04	
.6875000000000000000	.5476863029220194195E-02	714189.955513215042
.4931543308634424555E-06	-.4943756567277261265E-04	
.7187500000000000000	.5540675394384747415E-02	720930.129711741403
.3474573125413765355E-06	-.5077446039124775175E-04	
.7500000000000000000	.5162970047436363235E-02	634672.834498848606
.3022097229507360555E-07	-.4433719265465672645E-04	
.7812500000000000000	.5247235339219340755E-02	655559.506946300895
.3579374598951077135E-06	-.4548644982772653835E-04	
.8125000000000000000	.6044063279649087435E-02	865777.585973043586
.4665390615055397475E-06	-.6035521195535857795E-04	
.8437500000000000000	.6015193751637049475E-02	862631.975717167443

FILES: BANK   DATA   A   LEEDS UNIVERSITY VM/BSE 6.16

```
.5661873320750365597E-06  -.5974676046521058095E-04
.8750000000000000000       .5622592959124217008E-02   752699.6107391920 23
.6657436371112185045E-06  -.5192029920431621409E-04
.9062500000000000000       .6017227422510416923E-02   862116.8364820387 21
.6962671112452138849E-06  -.5956346769031719635E-04
.9375000000000000000       .6545867323277674955E-02   1020198.5868040741 6
.7007917364441719955E-06  -.7062473510772522945E-04
.9687500000000000000       .6802562184736121659E-02   1127979.4626122992 2
.7026911032095464495E-06  -.7816758490224379125E-04
1.0000000000000000000      .7368593952328354415E-02   1296979.4065384916 0
.6420041027852483925E-06  -.9002051670659137425E-04
```

INPUT

FILES: XTCA   DATA   A   LEEDS UNIVERSITY VM/BSE 6.16

```
.01 1. 16.06 .3 .0024 .0265 .4
.022085 3. -.016
1.0-8
.001 .1 1. .001
200 80 20 200 20 100
1.0-6 .001 .005 .01
.0075 16 16 8
1000.
.10898510-3
-.02 1.1E-6 1.E-3
0 -1
39
0. .05 .1 .15 .175 .2 .25 .3 .35 .375 .4 .425 .45 .475 .5
.525 .55 .575 .6 .625 .65 .675 .7 .71 .725 .75 .76 .775
.8 .825 .85 .865 .875 .89 .9 .925 .95 .975 1.0000000001
339. 502. 726. 997. 1133. 1302. 1607. 2002. 2489. 2557. 2496.
2408. 2150. 1675. 1302. 1051. 929. 590. 353. 238. 183. 150.
150. 170. 116. 116. 129. 116. 170. 190. 170. 129. 150. 150.
183. 217. 251. 285. 339.
33
```

INPUT

FILES: START   DATA   A   LEEDS UNIVERSITY VM/BSE 6.16

```
.53825370-6
.54225110-6
.54233960-6
.53953170-6
.53542160-6
.53154720-6
.52815060-6
.52607620-6
.52542980-6
.52631710-6
.52816690-6
.52974920-6
.52698580-6
.52365010-6
.52526090-6
.53209390-6
.53841830-6
-.22979860-7
.83997660-7
.10846280-6
.90085560-7
```

F42

OUTPUT


```
----------------------------------------------------------------------------

****  I N P U T   D A T A  ****

----------------------------------------------------------------------------

HMD4 (SQ. VEL. FROM I-4 TIME STEP) ............ -0.2257588D-07
HMD3 (SQ. VEL. FROM I-3 TIME STEP) ............  0.8359766D-07
HMD2 (SQ. VEL. FROM I-2 TIME STEP) ............  0.1089628D-06
HMD1 (SQ. VEL. FROM I-1 TIME STEP) ............  0.9009556D-07

----------------------------------------------------------------------------

VI (ABSOLUTE VISCOSITY) .......................  0.1000000D-01
TP (PERIOD) ...................................  0.1000000D+01
E (ELASTIC MODULUS OF CARTILAGE) ..............  0.1600000D+08
R (REDUCED RADIUS) ............................  0.2000000D+00
TH (CARTILAGE THICKNESS) ......................  0.2400000D-02
WD (WIDTH OF ANKLE) ...........................  0.2650000D-01
PR (POISSONS RATIO) ...........................  0.4000000D+00
RT (TALUS RADIUS) .............................  0.2209500D-01
THETA (ANGULAR AMPLITUDE IN DEGREES) ..........  0.5000000D+01
XI (INLET BOUNDARY) ........................... -0.1600000D-01
HMDAI0 (HMDAI IF HMD1 EQUALS ZERO) ............  0.1000000D-07
F1 (HA=H0*F1, INITIAL H0 INCREMENT) ...........  0.1000000D-02
F2 (XA=XEF*F2, INITIAL XEF INCREMENT) .........  0.1000000D+00
F3 (HMDAI=HMD1*F3, INITIAL HMD INCREMENT) .....  0.1000000D+01
F4 (XA=XE*F4, INITIAL XE INCREMENT) ...........  0.1000000D-02
NX (INIT. NO. OF STEPS AT CURRENT TIME STEP) ..      200
NX1 (NO. OF SUB-STEPS IN FIRST STEP) ..........       90
I1 (NO. OF PTS. PRINTED AT CURRENT TIME STEP) .       20
NST (INITIAL NO. OF STEPS FOR PROFILE ) .......      200
I2 (NO. OF PTS. PRINTED FOR PROFILE) ..........       20
I3 (NO. OF PTS. PLOTTED) ......................      100
DTOL (INITIAL ABSOLUTE TOLERANCE FOR C02EBF) ..  0.1000000D-07
PTOL (RELATIVE INLET PRESSURE TOLERANCE) ......  0.1000000D-02
FPTOL (RELATIVE LOAD CAPACITY TOLERANCE) ......  0.5000000D-02
FRTOL (RELATIVE FRICTION COEFF. TOLERANCE) ....  0.1000000D-01
TTOL (TIME STEP TOLERANCE) ....................  0.7500000D-02
NT (INITIAL NO. OF TIME STEPS) ................       16
MTP (NO. OF TIME STEPS PRINTED) ...............       16
NPX (NO. OF PRESS. DIST. PRINTED) .............        8
CPUL (LIMIT ON CPU TIME) ......................  0.1800000D+04
UM0 (LOWER LIMIT FOR ENT. VEL.) ...............  0.1099851D-02
XFACT (SCALE FACTOR FOR PLOTS) ................ -0.2000000D-01
HFACT (SCALE FACTOR FOR FILM PLOTS) ...........  0.1100000D-05
FFACT (SCALE FACTOR FOR FRICTION PLOTS) .......  0.5555559D-03
IPT (PRINT OPTION FOR CONVERGENCE) ............        0
MAGN (PRINT OPTION FOR ONE TIME STEP) .........       -1

***** NOTE :

(1.) NX AND NX1 SHOULD BE EVENLY DIVISIBLE BY 4
```

FILE: YTCA DATA A LEEDS UNIVERSITY VM/BSE 6.16

```
(2.) I1 AND I3 SHOULD NOT EXCEED NX/2

(3.) I2 SHOULD NOT EXCEED 2*NST

(4.) FOR SS TOLERANCE EQUALS .1*TTOL

(5.) MTP AND NPX SHOULD DIVIDE NT EVENLY

----------------------------------------------------------------------------
```

T/TP	TIME	LOAD	FP	
0.0	0.0	0.33500+03	0.12792450D+05	1
0.50000D-01	0.50000D-01	0.50200+03	0.18943400D+05	2
0.10000D+00	0.10000D+00	0.72600D+03	0.27396230D+05	3
0.15000D+00	0.15000D+00	0.99700D+03	0.37622640D+05	4
0.17500D+00	0.17500D+00	0.11330D+04	0.42754720D+05	5
0.20000D+00	0.20000D+00	0.13020D+04	0.49132080D+05	6
0.25000D+00	0.25000D+00	0.16070D+04	0.60641510D+05	7
0.30000D+00	0.30000D+00	0.20820D+04	0.78566040D+05	8
0.35000D+00	0.35000D+00	0.24890D+04	0.93924530D+05	9
0.37500D+00	0.37500D+00	0.25570D+04	0.96490570D+05	10
0.40000D+00	0.40000D+00	0.24960D+04	0.94188680D+05	11
0.42500D+00	0.42500D+00	0.24080D+04	0.90867920D+05	12
0.45000D+00	0.45000D+00	0.21500D+04	0.81132080D+05	13
0.47500D+00	0.47500D+00	0.16750D+04	0.63207550D+05	14
0.50000D+00	0.50000D+00	0.13020D+04	0.49132080D+05	15
0.52500D+00	0.52500D+00	0.10510D+04	0.39660380D+05	16
0.55000D+00	0.55000D+00	0.92900D+03	0.35056600D+05	17
0.57500D+00	0.57500D+00	0.59000D+03	0.22264150D+05	18
0.60000D+00	0.60000D+00	0.35300D+03	0.13320750D+05	19
0.62500D+00	0.62500D+00	0.23800D+03	0.89811320D+04	20
0.65000D+00	0.65000D+00	0.18300D+03	0.69056630D+04	21
0.67500D+00	0.67500D+00	0.15000D+03	0.56603770D+04	22
0.70000D+00	0.70000D+00	0.15000D+03	0.56603770D+04	23
0.71000D+00	0.71000D+00	0.17000D+03	0.64150940D+04	24
0.72500D+00	0.72500D+00	0.11600D+03	0.43773580D+04	25
0.75000D+00	0.75000D+00	0.11600D+03	0.43773580D+04	26
0.76000D+00	0.76000D+00	0.12900D+03	0.48679250D+04	27
0.77500D+00	0.77500D+00	0.11600D+03	0.43773580D+04	28
0.80000D+00	0.80000D+00	0.17000D+03	0.64150940D+04	29
0.82500D+00	0.82500D+00	0.19000D+03	0.71698110D+04	30
0.85000D+00	0.85000D+00	0.17000D+03	0.64150940D+04	31
0.86500D+00	0.86500D+00	0.12900D+03	0.48679250D+04	32
0.87500D+00	0.87500D+00	0.15000D+03	0.56603770D+04	33
0.89000D+00	0.89000D+00	0.19000D+03	0.71698110D+04	34
0.90000D+00	0.90000D+00	0.18300D+03	0.69056600D+04	35
0.92500D+00	0.92500D+00	0.21700D+03	0.81846790D+04	36
0.95000D+00	0.95000D+00	0.25100D+03	0.94716980D+04	37
0.97500D+00	0.97500D+00	0.28500D+03	0.10754720D+05	38
0.10000D+01	0.10000D+01	0.33500D+03	0.12792450D+05	39

FILE: YTCA DATA A LEEDS UNIVERSITY VM/HSE 6.16

DATA BANK

TO	XE	PC	MM	MO	
0.0	0.73805940D-02	0.12969790D+07	0.69280410D-06	-0.90020520D-04	1
0.31250000D-01	0.80163870D-02	0.15308580D+07	0.64624540D-06	-0.10637770D-03	2
0.62500000D-01	0.86961330D-02	0.17964020D+07	0.60841340D-06	-0.12507290D-03	3
0.93750000D-01	0.93761020D-02	0.20531260D+07	0.54642750D-06	-0.14590550D-03	4
0.12500000D+00	0.10075610D-01	0.24170930D+07	0.49967740D-06	-0.16965290D-03	5
0.15625000D+00	0.10697120D-01	0.27244820D+07	0.41553770D-06	-0.19024750D-03	6
0.18753000D+00	0.11309830D-01	0.30456990D+07	0.32454840D-06	-0.21278170D-03	7
0.21875090D+00	0.11854150D-01	0.33626910D+07	0.23270480D-06	-0.23512780D-03	8
0.25000080D+00	0.12406770D-01	0.36649470D+07	0.51327100D-07	-0.25648900D-03	9
0.28125000D+00	0.13108200D-01	0.40860760D+07	0.22139830D-06	-0.28577750D-03	10
0.31250000D+00	0.13731110D-01	0.45212780D+07	0.30256430D-06	-0.31619270D-03	11
0.34375000D+00	0.14296070D-01	0.48593270D+07	0.35921980D-06	-0.33975180D-03	12
0.37500000D+00	0.14456310D-01	0.45965030D+07	0.40155430D-06	-0.34930550D-03	13
0.40625000D+00	0.14339170D-01	0.48955170D+07	0.43793120D-06	-0.34215560D-03	14
0.43750800D+00	0.14002320D-01	0.46692150D+07	0.46739140D-06	-0.32625150D-03	15
0.46875000D+00	0.12872060D-01	0.39450130D+07	0.50314630D-06	-0.27558700D-03	16
0.50000000D+00	0.11568790D-01	0.31865870D+07	0.53704830D-06	-0.22495890D-03	17
0.53125000D+00	0.10663880D-01	0.27106280D+07	0.55482750D-06	-0.18912160D-03	18
0.56250000D+00	0.97233240D-02	0.22510240D+07	0.56529670D-06	-0.15693730D-03	19
0.59375000D+00	0.77820830D-02	0.14419240D+07	0.60384980D-06	-0.10025600D-03	20
0.62500000D+00	0.65593290D-02	0.10243990D+07	0.61052770D-06	-0.71020870D-04	21
0.65625000D+00	0.55056490D-02	0.83039630D+06	0.57223660D-06	-0.57483320D-04	22
0.68750000D+00	0.54768630D-02	0.71419800D+06	0.49315430D-06	-0.49437970D-04	23
0.71875000D+00	0.55406750D-02	0.73093010D+06	0.34745730D-06	-0.50774460D-04	24
0.75000000D+00	0.51629700D-02	0.63467280D+06	0.80220970D-07	-0.44337190D-04	25
0.78125000D+00	0.52472350D-02	0.65555850D+06	0.35793750D-06	-0.45486450D-04	26
0.81250000D+00	0.60440630D-02	0.86977800D+06	0.46653910D-06	-0.60359210D-04	27
0.84375000D+00	0.60191840D-02	0.86263200D+06	0.56618730D-06	-0.59746760D-04	28
0.87500000D+00	0.56225830D-02	0.75269960D+06	0.66578360D-06	-0.51938290D-04	29
0.90625000D+00	0.60173870D-02	0.86211690D+06	0.69626710D-06	-0.59563490D-04	30
0.93750000D+00	0.65458670D-02	0.10201950D+07	0.70079170D-06	-0.70624740D-04	31
0.96875000D+00	0.68829620D-02	0.11279790D+07	0.70260120D-06	-0.78167590D-04	32
0.10000000D+01	0.73805940D-02	0.12965750D+07	0.68290410D-06	-0.90020520D-04	33

PREVIOUS CYCLE

MO	
0.53525370D-06	0
0.54225110D-06	1
0.54233960D-06	2
0.53953170D-06	3
0.53542160D-06	4
0.53154720D-06	5
0.52815860D-06	6

F44

0.52607620-06	7
0.52542990-06	8
0.52631710-06	9
0.52816690-06	10
0.52974920-06	11
0.52698590-06	12
0.52365010-06	13
0.52526080-06	14
0.53289390-06	15
0.53841830-06	16

**** O U T P U T   D A T A ****

TIME	MIN FILM TH	% TRUNC ERR	ENT VEL	SQ VEL	LOAD PER UW	FRIC COEFF	
0.0	0.53841830-06	0.0	0.10898510-01	0.90085560-07	0.12792450+05	-0.10000000+01	0
0.62500000-01	0.54241670-06	0.11307790-01	0.10068910-01	0.31340800-07	0.20824570+05	0.25466390-03	1
0.12500000+00	0.54249120-06	0.12254190-01	0.77064110-02	-0.24990000-07	0.32497710+05	0.14800240-03	2
0.18750000+00	0.53965470-06	0.75607740-02	0.41706790-02	-0.60864330-07	0.45914940+05	0.66268410-04	3
0.25000000+00	0.53555140-06	0.17578670-02	0.10898510-03	-0.63932800-07	0.60641510+05	0.12012880-05	4
0.31250000+00	0.53166640-05	0.12402240-01	0.41706730-02	-0.61841250-07	0.83162960+05	0.45402920-04	5
0.37500000+00	0.52825720-06	0.12042870-01	0.77064110-02	-0.43663310-07	0.96490570+05	0.75179300-04	6
0.43750000+00	0.52617980-06	9.75099520-02	0.10068910-01	-0.23665170-07	0.87224720+05	0.10413030-03	7
0.50000000+00	0.52553230-06	0.66089630-02	0.10898510-01	.0.49687610-08	0.49132080+05	0.16268710-03	8
0.56250000+00	0.52641980-06	0.93712990-02	0.10068910-01	0.19079270-07	0.29176070+05	0.21095060-03	9
0.62500000+00	0.52826980-06	0.15154360-01	0.77064110-02	0.44046280-07	0.89811320+04	0.34233550-03	10
0.68750000+00	0.52933410-06	0.37904100-01	0.41706790-02	-0.16194750-07	0.52286590+04	0.26857110-03	11
0.75000000+00	0.52703560-06	0.60974180-01	0.10898510-03	-0.62912810-07	0.43773580+04	0.75401840-05	12
0.81250000+00	0.52370970-06	0.80624680-02	0.41706790-02	-0.22977920-07	0.70252960+04	0.22598530-03	13
0.87500000+00	0.52531830-06	0.29119860-01	0.77064110-02	0.83990580-07	0.56603770+04	0.45862840-03	14
0.93750000+00	0.53215140-06	0.40266230-01	0.10068910-01	0.10945370-06	0.89154100+04	0.44028550-03	15
0.10000000+01	0.53847530-06	0.57552150-01	0.10898510-01	0.90077960-07	0.12792450+05	0.37388710-03	16

********** MAXIMUM RELATIVE DIFFERENCE = 0.30571030-03

NUMBER OF STEPS = 16

****** CPU = 0.4550+03

STEP SIZE IS HALVED

F45

STEP NO. = 4

TIME (TC) = 0.1250000D+00

X	P	H		
0.1600000D-01	0.0	0.2580716D-03	1	1
0.1463986D-01	0.0	0.1886140D-03	12	2
0.1307527D-01	0.0	0.1163427D-03	24	3
0.1151069D-01	0.0	0.5223122D-04	36	4
0.1007647D-01	0.0	0.6304994D-06	47	5
0.9946092D-02	0.6488316D+05	0.5429177D-06	48	6
0.9301504D-02	0.7951498D+06	0.5499450D-06	60	7
0.6816915D-02	0.1371628D+07	0.5575740D-06	72	8
0.5252327D-02	0.1926994D+07	0.5659141D-06	84	9
0.3687738D-02	0.2153967D+07	0.5751076D-06	96	10
0.2123150D-02	0.2355425D+07	0.5853453D-06	108	11
0.5585614D-03	0.2434327D+07	0.5968909D-06	120	12
-0.1006027D-02	0.2393789D+07	0.6101251D-06	132	13
-0.2570616D-02	0.2237121D+07	0.6256291D-06	144	14
-0.4135204D-02	0.1967896D+07	0.6443606D-06	156	15
-0.5699792D-02	0.1590081D+07	0.6660898D-06	168	16
-0.7264381D-02	0.1108319D+07	0.7007704D-06	180	17
-0.8828969D-02	0.5287924D+06	0.7557733D-06	192	18
-0.1039356D-01	0.4248133D+04	0.1163686D-04	204	19
-0.1195815D-01	0.2444302D+04	0.6979510D-04	216	20
-0.1352273D-01	0.2250985D+04	0.1362295D-03	228	21
-0.1508732D-01	0.2240377D+04	0.2109309D-03	240	22
-0.1600000D-01	0.2224573D+04	0.2581176D-03	247	23

CURRENT TIME STEP VALUES

SQUEEZE VELOCITY (HPD) =-0.2499276D-07

MINIMUM FILM THICKNESS (HMT) = 0.5424195D-06
ESTIMATED % TRUNC. ERROR IN HMT = 0.227D-04

FRICTION COEFFICIENT (FRD) = 0.1479693D-03
MODIFIER TERM (CHMT) =-0.1627779D-11

CAVITATION BOUNDARY (XE) = 0.1007647D-01
SS CAVITATION BC (XEF) = 0.1007561D-01

F46

STEP NO. = 8

TIME (TC) = 0.2500000D+00

X	P	H		
0.1600000D-01	0.0	0.1706618D-03	1	1
0.1447392D-01	0.0	0.9315222D-04	44	2
0.1290199D-01	0.0	0.2143075D-04	88	3
0.1258045D-01	0.0	0.7775128D-05	97	4
0.1133007D-01	0.6282587D+06	0.5358307D-06	132	5
0.9759149D-02	0.1434558D+07	0.5364453D-06	176	6
0.8136214D-02	0.2115358D+07	0.5371027D-06	220	7
0.6614299D-02	0.2671395D+07	0.5378091D-06	264	9
0.5042364D-02	0.3102353D+07	0.5385725D-06	308	9
0.3470439D-02	0.3412287D+07	0.5394023D-06	352	10
0.1898513D-02	0.3595073D+07	0.5403112D-06	396	11
0.3265879D-03	0.3664688D+07	0.5413157D-06	440	12
-0.1245337D-02	0.3610959D+07	0.5424351D-06	484	13
-0.2817263D-02	0.3438942D+07	0.5437100D-06	528	14
-0.4389158D-02	0.3150514D+07	0.5451775D-06	572	15
-0.5961113D-02	0.2747947D+07	0.5469153D-06	616	16
-0.7533039D-02	0.2234131D+07	0.5490497D-06	660	17
-0.9104964D-02	0.1613389D+07	0.5519367D-06	704	19
-0.1067689D-01	0.8912446D+06	0.5559523D-06	748	19
-0.1224981D-01	0.8370821D+05	0.5661932D-06	792	20
-0.1382074D-01	-0.5322168D+03	0.6245728D-04	836	21
-0.1539267D-01	-0.5348431D+03	0.1389926D-03	880	22
-0.1600000D-01	-0.5351974D+03	0.1707690D-03	897	23

CURRENT TIME STEP VALUES

SQUEEZE VELOCITY (HPD) =-0.6394366D-07

MINIMUM FILM THICKNESS (HMT) = 0.5354331D-06
ESTIMATED % TRUNC. ERROR IN HMT = 0.100D-02

FRICTION COEFFICIENT (FRD) = 0.1190185D-05
MODIFIER TERM (CHMT) = 0.7630907D-10

CAVITATION BOUNDARY (XE) = 0.1258046D-01
SS CAVITATION BC (XEF) = 0.1240677D-01

STEP NO. = 12

TIME (TC) = 0.3750000D+00

X	P	H		
0.16000000D-01	0.0	0.77497740D-04	1	1
0.14792720D-01	0.0	0.15529460D-04	5	2
0.14497940D-01	0.0	0.65011350D-06	6	3
0.13269320D-01	0.99763090D+06	0.53109110D-06	10	4
0.11743930D-01	0.19725990D+07	0.53508950D-06	15	5
0.10219540D-01	0.27192070D+07	0.53531650D-06	20	6
0.86951480D-02	0.34302710D+07	0.54380030D-06	25	7
0.71707560D-02	0.40086870D+07	0.54957200D-06	30	8
0.56463540D-02	0.44574440D+07	0.55367070D-06	35	9
0.41219720D-02	0.47796360D+07	0.55914350D-06	40	10
0.25975910D-02	0.49784780D+07	0.56504850D-06	45	11
0.10731990D-02	0.50573190D+07	0.57146080D-06	50	12
-0.45120310D-03	0.50196670D+07	0.57847130D-06	55	13
-0.19755950D-02	0.48692180D+07	0.58620660D-06	60	14
-0.34999870D-02	0.46058970D+07	0.59493270D-06	65	15
-0.50243790D-02	0.42459130D+07	0.60459880D-06	70	16
-0.65497710D-02	0.37818430D+07	0.61592030D-06	75	17
-0.80731620D-02	0.32227610D+07	0.62507730D-06	80	18
-0.95975540D-02	0.25744730D+07	0.64530930D-06	85	19
-0.11121950D-01	0.18439690D+07	0.66641900D-06	90	20
-0.12646340D-01	0.10405940D+07	0.69742470D-06	95	21
-0.14170730D-01	0.18165700D+06	0.77223050D-06	100	22
-0.15695120D-01	0.22079590D+04	0.61636980D-04	105	23
-0.16000000D-01	0.22294830D+04	0.77738130D-04	106	24

CURRENT TIME STEP VALUES

SQUEEZE VELOCITY (HPD) =-0.43664220D-07

MINIMUM FILM THICKNESS (HMT) = 0.52806640D-06
ESTIMATED % TRUNC. ERROR IN HMT = 0.107D-02

FRICTION COEFFICIENT (FRD) = 0.75122480D-04
MODIFIER TERM (CMPT) = 0.80216390D-10

CAVITATION BOUNDARY (XE) = 0.14497940D-01
SS CAVITATION BC (XEF) = 0.14496310D-01

STEP NO. = 16

TIME (TC) = 0.50000000D+00

X	P	H		
0.16000000D-01	0.0	0.20419610D-03	1	1
0.14738940D-01	0.0	0.13959500D-03	11	2
0.13222570D-01	0.0	0.68923460D-04	22	3
0.11706310D-01	0.0	0.59254580D-05	33	4
0.11569460D-01	0.0	0.59510050D-06	34	5
0.10190840D-01	0.69889610D+06	0.53121180D-06	44	6
0.86737760D-02	0.13693630D+07	0.53805640D-06	55	7
0.71575180D-02	0.19349150D+07	0.59549580D-06	66	8
0.56412450D-02	0.23949310D+07	0.55349110D-06	77	9
0.41249790D-02	0.27487780D+07	0.56218910D-06	88	10
0.26087140D-02	0.29958140D+07	0.57170570D-06	99	11
0.10924480D-02	0.31353790D+07	0.59222750D-06	110	12
-0.42381760D-03	0.31667590D+07	0.55358410D-06	121	13
-0.19400830D-02	0.30893780D+07	0.60730180D-06	132	14
-0.34563490D-02	0.29023920D+07	0.62266420D-06	143	15
-0.49726140D-02	0.26050830D+07	0.64082970D-06	154	16
-0.64889800D-02	0.21956480D+07	0.66310310D-06	165	17
-0.80051450D-02	0.16761780D+07	0.69206680D-06	176	18
-0.95214110D-02	0.10426910D+07	0.73433160D-06	187	19
-0.11037640D-01	0.29585440D+06	0.92586320D-06	198	20
-0.12553940D-01	0.35929080D+04	0.49342500D-04	209	21
-0.14070210D-01	0.31323720D+04	0.10759240D-03	220	22
-0.15586470D-01	0.30309430D+04	0.18253100D-03	231	23
-0.16000000D-01	0.30164780D+04	0.20429970D-03	234	24

CURRENT TIME STEP VALUES

SQUEEZE VELOCITY (HMD) = 0.58752470D-08

MINIMUM FILM THICKNESS (HMT) = 0.52940160D-06
ESTIMATED % TRUNC. ERROR IN HMT = 0.521D-03

FRICTION COEFFICIENT (FRC) = 0.16409190D-03
MODIFIER TERM (CMMT) =-0.69511450D-10

CAVITATION BOUNDARY (XE) = 0.11568460D-01
SS CAVITATION BD (XEF) = 0.11568790D-01

STEP NO. = 20

TIME (TC) = 0.62500000D+00

X P H

F49

0.16000000D-01	0.0	0.35556390D-03	1	1
0.14677900D-01	0.0	0.28796510D-03	7	2
0.13098990D-01	0.0	0.21496540D-03	14	3
0.11519990D-01	0.0	0.15007660D-03	21	4
0.99408720D-02	0.0	0.93599670D-04	28	5
0.83618620D-02	0.0	0.45431680D-04	35	6
0.67829520D-02	0.0	0.55756810D-05	42	7
0.65572980D-02	0.0	0.57224620D-06	43	8
0.52033930D-02	0.34270670D+06	0.54096170D-06	49	9
0.36248330D-02	0.66407690D+06	0.55649470D-06	56	10
0.20459240D-02	0.89042530D+06	0.57517080D-06	63	11
0.46651410D-03	0.10117410D+07	0.59750850D-06	70	12
-0.11121350D-02	0.10178900D+07	0.62528140D-06	77	13
-0.26912050D-02	0.89849030D+06	0.66203160D-06	84	14
-0.42702150D-02	0.64265540D+06	0.71689910D-06	91	15
-0.58492240D-02	0.23832820D+06	0.83733110D-06	98	16
-0.74282340D-02	0.20460240D+04	0.20990430D-04	105	17
-0.90072430D-02	0.94534540D+03	0.64156820D-04	112	18
-0.10586250D-01	0.74712890D+03	0.11570690D-03	119	19
-0.12165250D-01	0.67450790D+03	0.17557660D-03	126	20
-0.13744270D-01	0.64067670D+03	0.24375990D-03	133	21
-0.15323280D-01	0.62192610D+03	0.32025510D-03	140	22
-0.16000000D-01	0.61643790D+03	0.35558310D-03	143	23

CURRENT TIME STEP VALUES

SQUEEZE VELOCITY (HMD) = 0.44060010D-07

MINIMUM FILM THICKNESS (HMT) = 0.52851950D-06
ESTIMATED % TRUNC. ERROR IN HMT = 0.799D-02

FRICTION COEFFICIENT (FRD) = 0.34254060D-03
MODIFIER TERM (CMMT) =-0.59914420D-09

CAVITATION BOUNDARY (XE) = 0.65572900D-02
SS CAVITATION BD (XEF) = 0.65593290D-02

STEP NO. = 24

TIME (TC) = 0.75000000D+00

X	P	H		
0.16000000D-01	0.0	0.38277590D-03	1	1
0.14426690D-01	0.0	0.30239140D-03	60	2

F50

0.1282669D-01	0.0	0.2303157D-03	120	3
0.1122669D-01	0.0	0.1661724D-03	180	4
0.9626680D-02	0.0	0.1105643D-03	240	5
0.8026653D-02	0.0	0.6348865D-04	300	6
0.6426692D-02	0.0	0.2494632D-04	360	7
0.5333349D-02	0.0	0.3516917D-05	401	8
0.4826691D-02	0.8721302D+05	0.5271178D-06	420	9
0.3226680D-02	0.4894053D+06	0.5295916D-06	480	10
0.1626679D-02	0.5873446D+06	0.5325624D-06	540	11
0.2667772D-04	0.6397979D+06	0.5362747D-06	600	12
-0.1573323D-02	0.5564063D+06	0.5412215D-06	660	13
-0.3173324D-02	0.3759140D+06	0.5486931D-06	720	14
-0.4773326D-02	0.8222399D+05	0.5660223D-06	780	15
-0.6373327D-02	-0.1277851D+02	0.2384557D-04	840	16
-0.7973329D-02	-0.2892139D+02	0.6218329D-04	900	17
-0.9573329D-02	-0.3224924D+02	0.1088942D-03	960	18
-0.1117333D-01	-0.3348133D+02	0.1642196D-03	1020	19
-0.1277333D-01	-0.3486385D+02	0.2280763D-03	1080	20
-0.1437333D-01	-0.3437876D+02	0.3084675D-03	1140	21
-0.1597333D-01	-0.3456664D+02	0.3813919D-03	1200	22
-0.1600000D-01	-0.3456908D+02	0.3828130D-03	1201	23

CURRENT TIME STEP VALUES

SQUEEZE VELOCITY (HMD) =-0.6291834D-07

MINIMUM FILM THICKNESS (HMT) = 0.5266541D-06
ESTIMATED % TRUNC. ERROR IN HMT = 0.358D-02

FRICTION COEFFICIENT (FRD) = 0.7520953D-05
MODIFIER TERM (CMPT) = 0.2678994D-09

CAVITATION BOUNDARY (XE) = 0.5333348D-02
SS CAVITATION BC (XEF) = 0.5162973D-02

STEP NO. = 28

TIME (TC) = 0.9750000D+00

X	P	H		
0.1600000D-01	0.0	0.3745878D-03	1	1
0.1491426D-01	0.0	0.3156465D-03	7	2
0.1340093D-01	0.0	0.2472315D-03	14	3
0.1158769D-01	0.0	0.1834478D-03	21	4
0.1037441D-01	0.0	0.1273016D-03	28	5

F57

0.8661121D-02	0.0	0.7879689D-04	35	6
0.7347939D-02	0.0	0.3790559D-04	42	7
0.5834558D-02	0.0	0.4657732D-05	49	8
0.5612366D-02	0.0	0.5567764D-06	58	9
0.4321264D-02	0.2505486D+06	0.5399775D-06	56	10
0.2887779D-02	0.4975511D+06	0.5683149D-06	63	11
0.1294693D-02	0.6744602D+06	0.5846455D-06	70	12
-0.2195928D-03	0.7601653D+06	0.6148839D-06	77	13
-0.1731978D-02	0.7337611D+06	0.6548182D-06	84	14
-0.3245164D-02	0.5743084D+06	0.7129871D-06	91	15
-0.4759458D-02	0.2602324D+06	0.8369850D-06	98	16
-0.6271735D-02	0.2892913D+04	0.1366299D-04	105	17
-0.7785021D-02	0.7728474D+03	0.4897009D-04	112	18
-0.9298307D-02	0.4600477D+03	0.9203489D-04	119	19
-0.1081159D-01	0.3530513D+03	0.1427475D-03	126	20
-0.1232448D-01	0.3041546D+03	0.2010975D-03	133	21
-0.1383816D-01	0.2780430D+03	0.2670826D-03	140	22
-0.1535145D-01	0.2626351D+03	0.3407019D-03	147	23
-0.1600000D-01	0.2579470D+03	0.3745299D-03	150	24

CURRENT TIME STEP VALUES

SQUEEZE VELOCITY (HPD) = 0.8398345D-07

MINIMUM FILM THICKNESS (HMT) = 0.5251561D-06
ESTIMATED % TRUNC. ERROR IN HMT = 0.181D-02

FRICTION COEFFICIENT (FRO) = 0.4583595D-03
MODIFIER TERM (CHMT) = 0.1347224D-09

CAVITATION BOUNDARY (XE) = 0.5619366D-02
SS CAVITATION BC (XEF) = 0.5622593D-02

STEP NO. = 32

TIME (TC) = 0.1000000D+01

X	P	H		
0.1600000D-01	0.0	0.3365016D-03	1	1
0.1485927D-01	0.0	0.2777221D-03	6	2
0.1345563D-01	0.0	0.2115913D-03	12	3
0.1205299D-01	0.0	0.1519586D-03	18	4
0.1065033D-01	0.0	0.9889404D-04	24	5
0.9247679D-02	0.0	0.5236751D-04	30	6
0.7945030D-02	0.0	0.1240907D-04	36	7

F52

0.73774800D-02	0.0	0.57016600D-06	36	8
0.64423810D-02	0.24459640D+06	0.54617940D-06	42	9
0.50397320D-02	0.53152110D+06	0.55945140D-06	48	10
0.36370930D-02	0.96956650D+06	0.57428250D-06	54	11
0.22344350D-02	0.10963500D+07	0.55107650D-06	60	12
0.83174590D-03	0.12491700D+07	0.61041850D-06	66	13
-0.57086300D-03	0.13155650D+07	0.63321050D-06	72	14
-0.19735120D-02	0.12832660D+07	0.66095510D-06	78	15
-0.33761610D-02	0.11398070D+07	0.69646250D-06	84	16
-0.47708090D-02	0.87256550D+06	0.74615600D-06	90	17
-0.61014580D-02	0.46816570D+06	0.83256530D-06	96	18
-0.75841070D-02	0.50345650D+04	0.62615720D-05	102	19
-0.89967560D-02	0.14509520D+04	0.44553020D-04	108	20
-0.10389400D-01	0.59036250D+03	0.95817540D-04	114	21
-0.11792050D-01	0.84576140D+03	0.14166210D-03	120	22
-0.13194790D-01	0.73090790D+03	0.20007030D-03	126	23
-0.14597350D-01	0.74626340D+03	0.26503970D-03	132	24
-0.16000000D-01	0.72567650D+03	0.33656620D-03	138	25

CURRENT TIME STEP VALUES

SQUEEZE VELOCITY (HPD) = 0.90071570-07

MINIMUM FILM THICKNESS (HMT) = 0.53823160-06
ESTIMATED % TRUNC. ERROR IN HMT = 0.5170-02

FRICTION COEFFICIENT (FPD) = 0.37342840-03
MODIFIER TERM (DHMT) =-0.39558580-09

CAVITATION BOUNDARY (XE) = 0.73774800-02
SS CAVITATION BC (XEF) = 0.73805940-02

********* MAXIMUM RELATIVE DIFFERENCE = 0.56711210-02

NUMBER OF STEPS = 32

****** CPU = 0.1140+04

* * * C O N V E R G E S * * *

TIME MIN FILM TH % TRUNC ERR ENT VEL SQ VEL LOAD PER UW FRIC COEFF

F53

0.0	0.53941830D-06	0.0	0.10958510D-01	0.90035560D-07	0.12792450D+05	0.37386710D-03	0
0.62500000D-01	0.54229670D-06	0.36217070D-02	0.10068910D-01	0.31352060D-07	0.20824570D+05	0.25940690D-03	2
0.12500000D+00	0.54241950D-06	0.23712550D-04	0.77064110D-02	-0.24392760D-07	0.32497710D+05	0.14776930D-03	4
0.18750000D+00	0.53962320D-06	0.40231180D-03	0.41706790D-02	-0.60952550D-07	0.45914840D+05	0.66241460D-04	6
0.25000000D+00	0.53543310D-06	0.10025070D-02	0.10958510D-03	-0.63943660D-07	0.60641510D+05	0.0	8
0.31250000D+00	0.53135620D-06	0.68098540D-02	0.41706790D-02	-0.61431300D-07	0.83162960D+05	0.45601570D-04	10
0.37500000D+00	0.52806640D-06	0.10695670D-02	0.77064110D-02	-0.43664220D-07	0.96490570D+05	0.75122480D-04	12
0.43750000D+00	0.52590830D-06	0.41799050D-03	0.10068910D-01	-0.23136660D-07	0.87224720D+05	0.10472580D-03	14
0.50000000D+00	0.52540160D-06	0.93101090D-03	0.10958510D-01	0.58752470D-08	0.49132090D+05	0.16408190D-03	16
0.56250000D+00	0.52623990D-06	0.25060490D-02	0.10068910D-01	0.19076890D-07	0.29176070D+05	0.21079110D-03	18
0.62500000D+00	0.52651450D-06	0.79773920D-02	0.77064110D-02	0.44060810D-07	0.89811320D+04	0.34254060D-03	20
0.68750000D+00	0.52573940D-06	0.30949110D-02	0.41706790D-02	-0.15478700D-07	0.52286590D+04	0.27056970D-03	22
0.75000000D+00	0.52665410D-06	0.35796120D-02	0.10958510D-03	-0.62918340D-07	0.43773590D+04	0.0	24
0.81250000D+00	0.52362820D-06	0.19633090D-02	0.41706790D-02	-0.22179610D-07	0.70252960D+04	0.22772100D-03	26
0.87500000D+00	0.52515610D-06	0.18052670D-02	0.77064110D-02	0.93993450D-07	0.56603770D+04	0.45935990D-03	28
0.93750000D+00	0.53169460D-06	0.12660460D-01	0.10068910D-01	0.10842450D-06	0.89194100D+04	0.43978520D-03	30
0.10000000D+01	0.53823160D-06	0.51728340D-02	0.10898510D-01	0.98071570D-07	0.12792450D+05	0.37342840D-03	32

F54

OUTPUT

FILES: STARTN DATA A LEEDS UNIVERSITY VM/BSE 6.16

```
 .5384193000000000001E-06
 .5424156763375600002E-06
 .5424911559944252227E-06
 .5396546792054029115E-06
 .5355513360088667346E-06
 .5316664401713489497E-06
 .5282571968624211557E-06
 .5261799440000392819E-06
 .5255323124645480043E-06
 .5264197666970223635E-06
 .5282633021414822046E-06
 .5294341223493853099E-06
 .5270355579066530537E-06
 .5237097337952088514E-06
 .5253183390333333223E-06
 .5321513607218865109E-06
 .5384752938531333332E-06
-.2297739599999599997E-07
 .8399766000000000063E-07
 .1084627999999599999E-06
 .9008555599999559555E-07
```

F56

PTCA PLOT

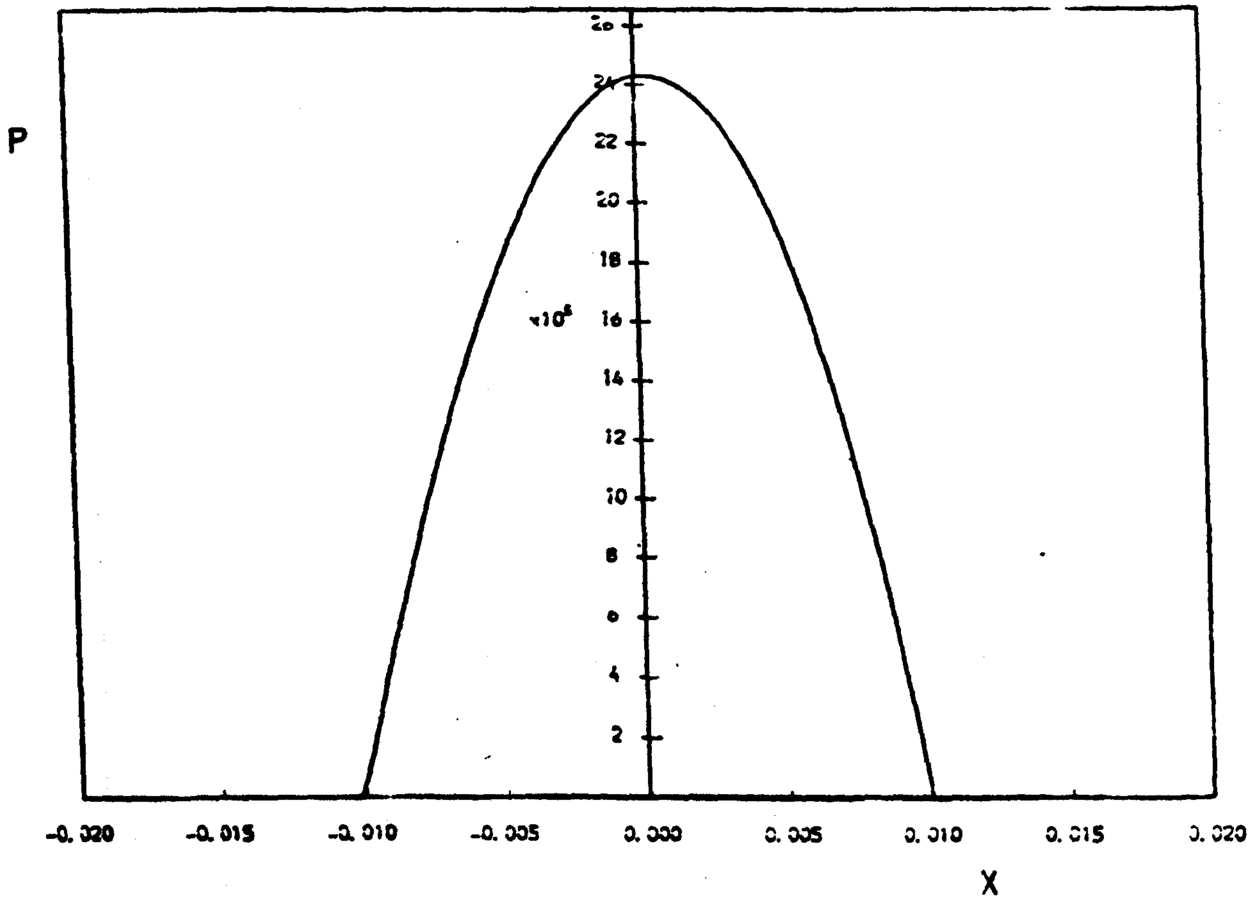

TIME = 0.1250E 00

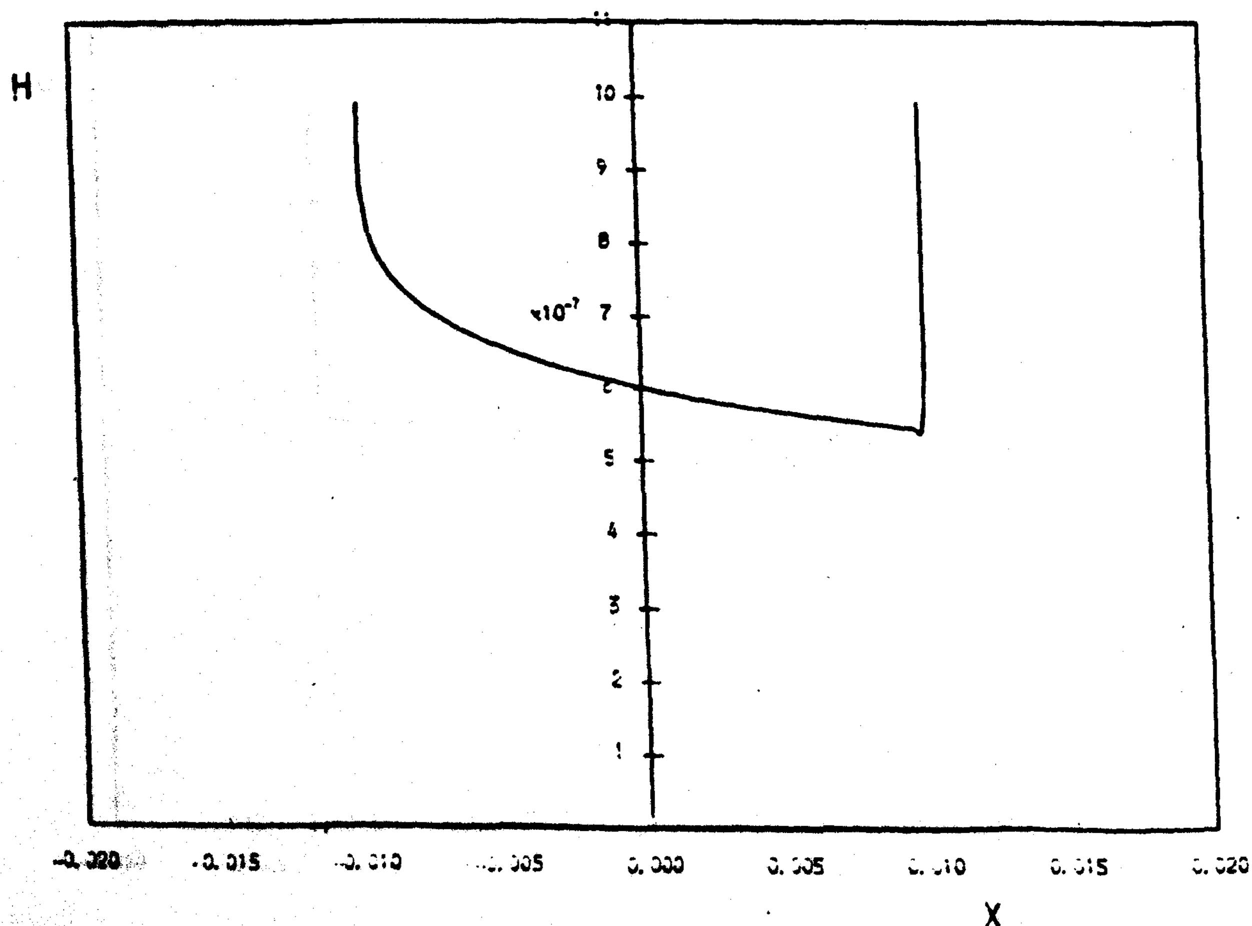

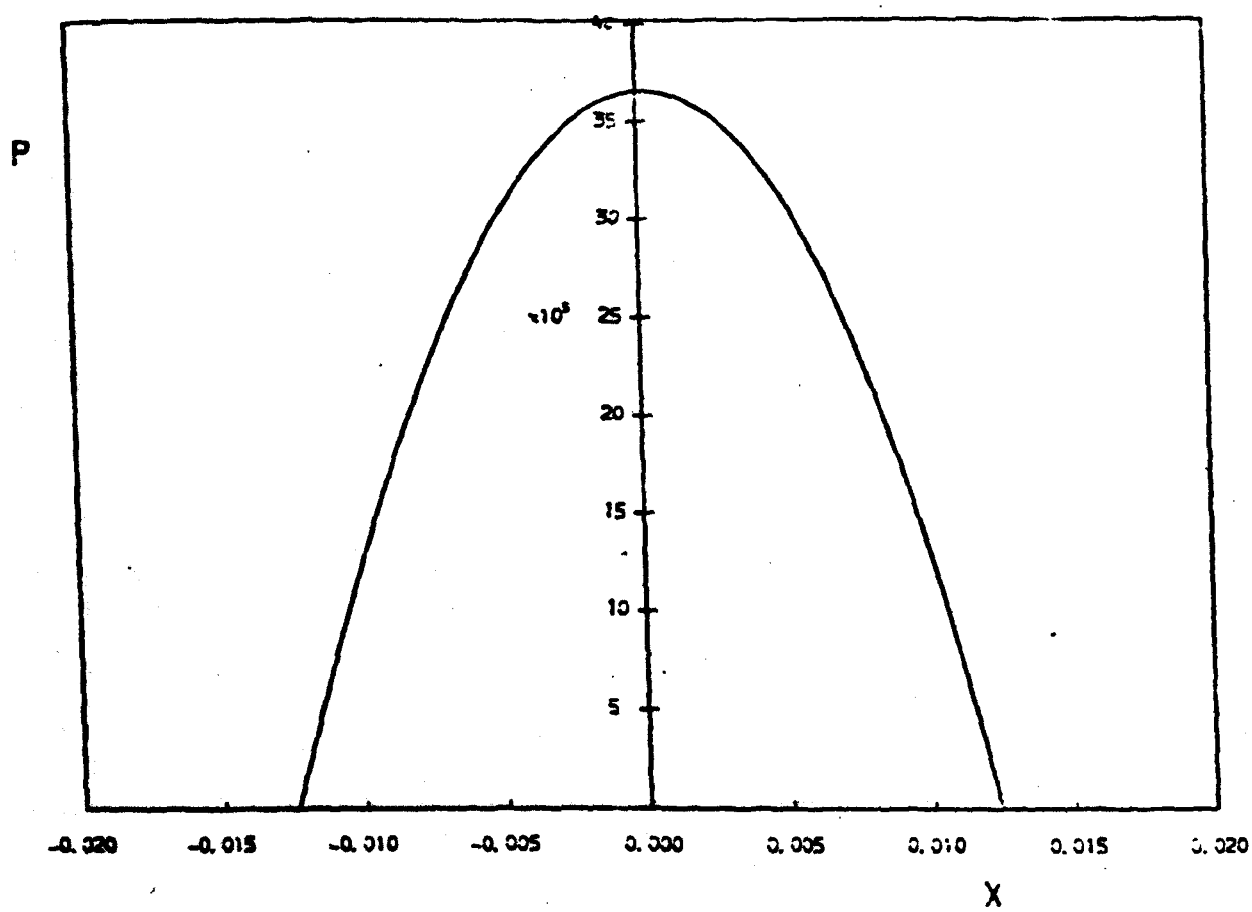

TIME = 0.2500E 00

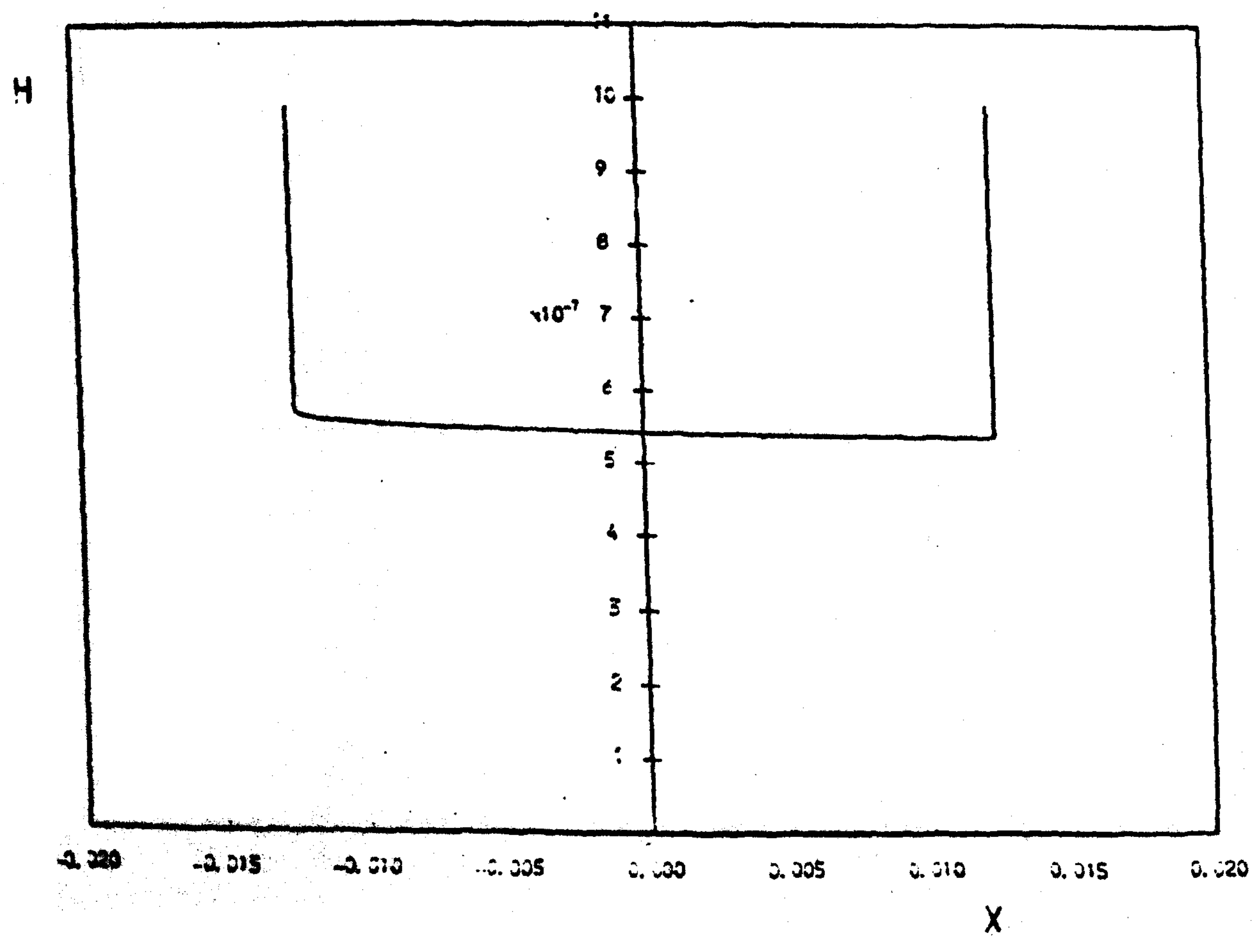

CONTINUES . . . .

F58

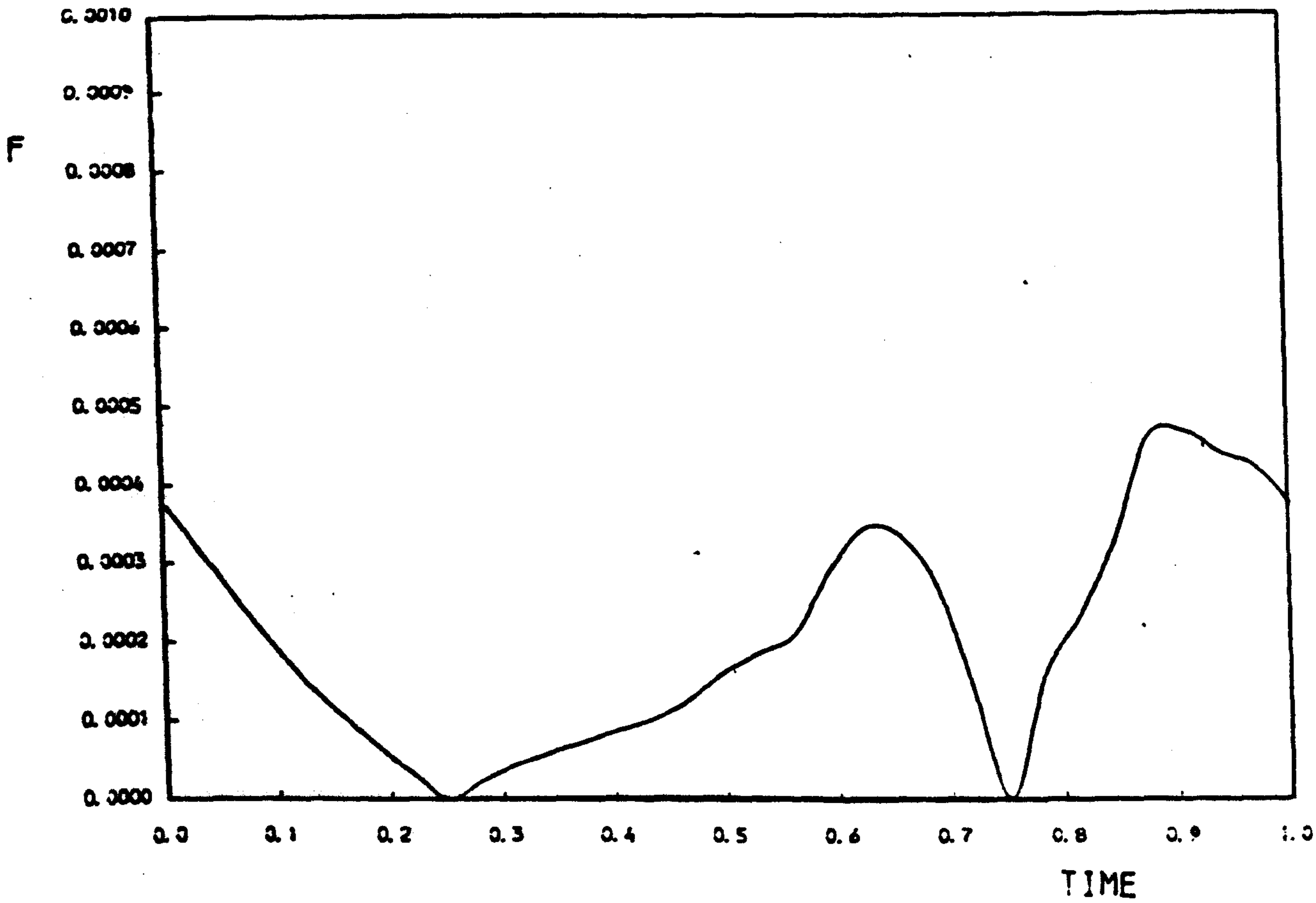
F
0.0010
0.0009
0.0008
0.0007
0.0006
0.0005
0.0004
0.0003
0.0002
0.0001
0.0000
0.0
0.1
0.2
0.3
0.4
0.5
0.6
0.7
0.8
0.9
1.0
TIME

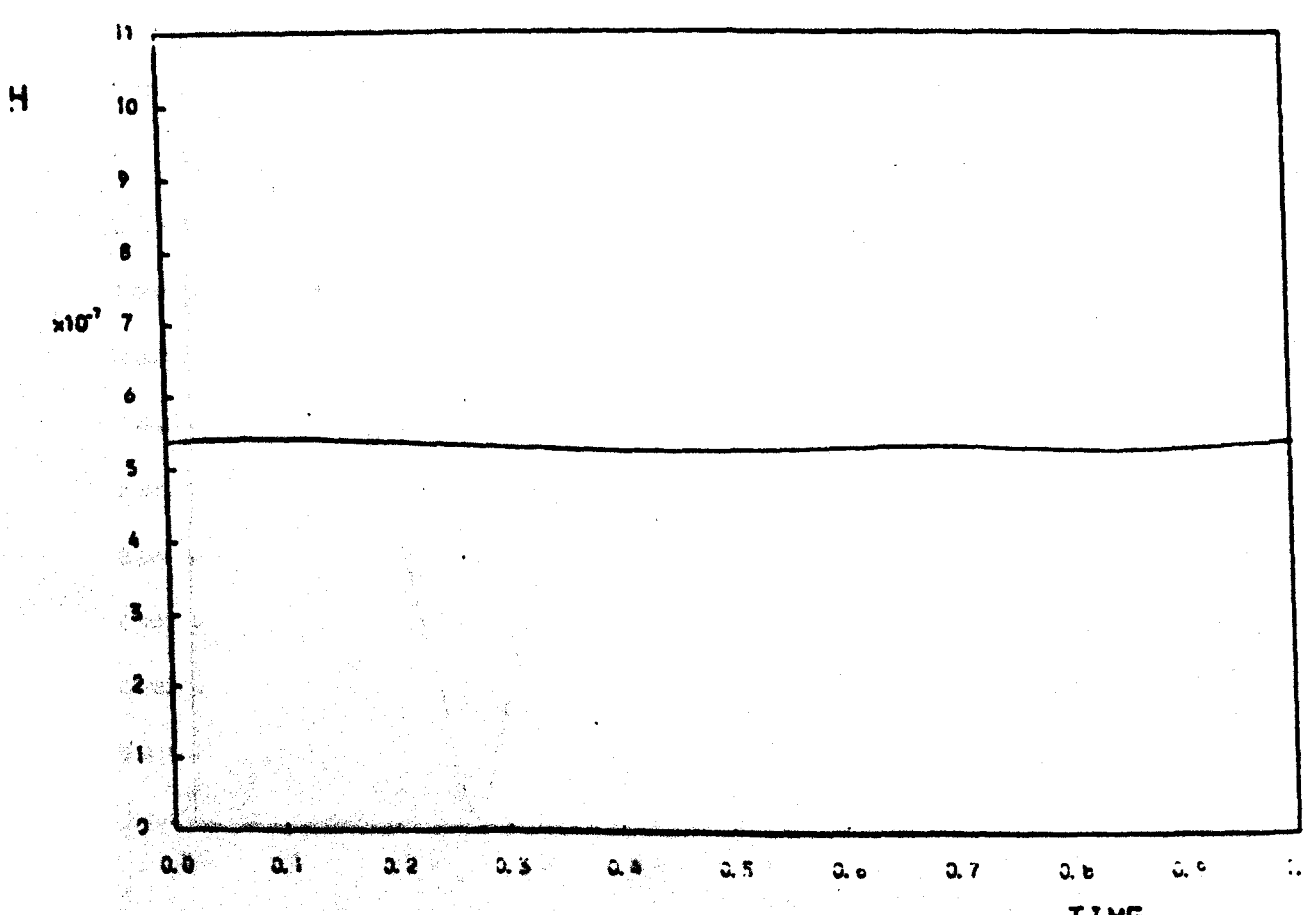
H
x10⁷
11
10
9
8
7
6
5
4
3
2
1
0
0.0
0.1
0.2
0.3
0.4
0.5
0.6
0.7
0.8
0.9
1.0
TIME

F59

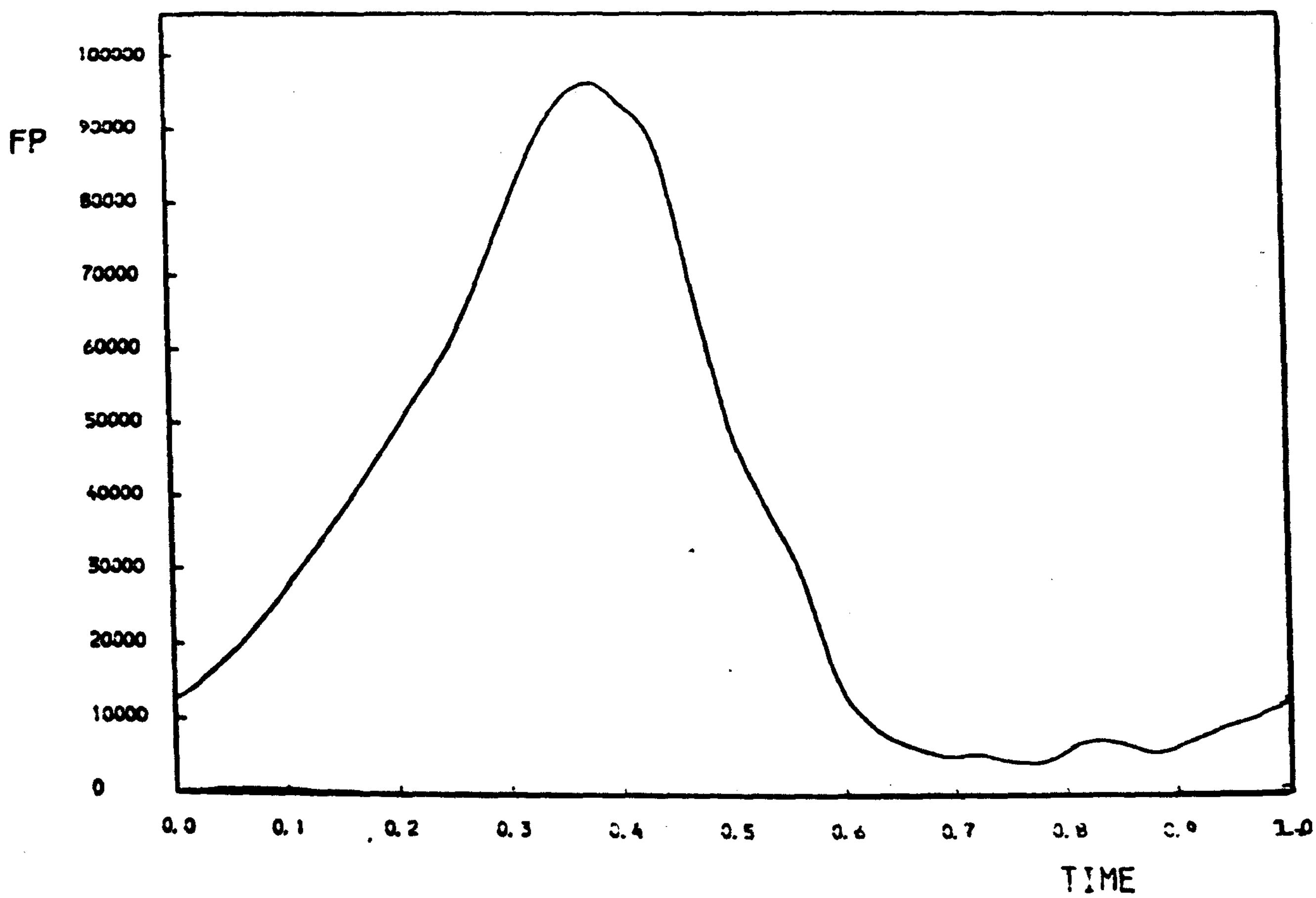
FP
100000
90000
80000
70000
60000
50000
40000
30000
20000
10000
0
0.0
0.1
0.2
0.3
0.4
0.5
0.6
0.7
0.8
1.0
TIME

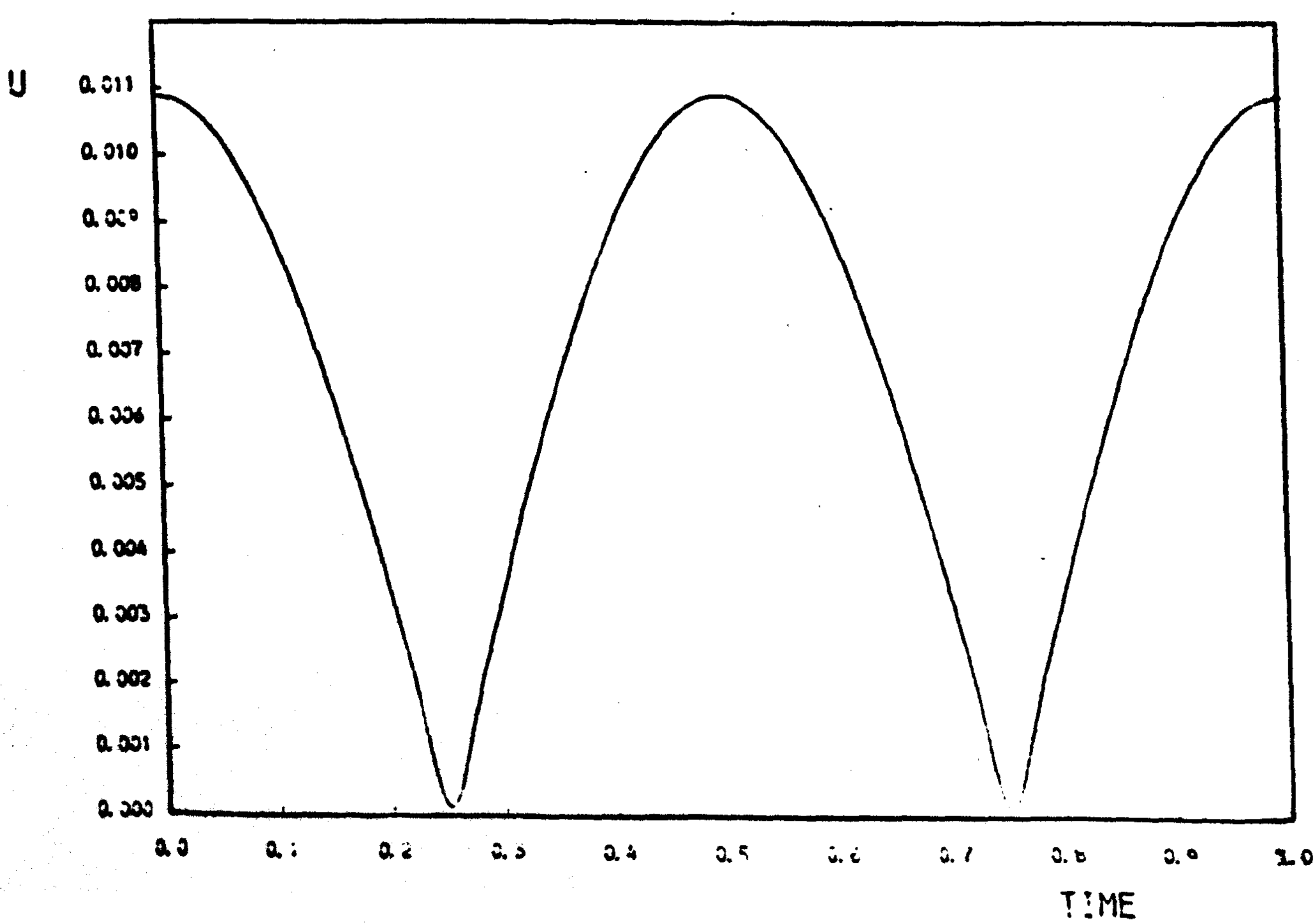
U
0.011
0.010
0.008
0.007
0.004
0.003
0.002
0.0
0.4
0.5
1.0
TIME

END